NBS SPECIAL PUBLICATION 444

U.S. DEPARTMENT OF COMMERCE / National Bureau of Standards

WIND AND SEISMIC EFFECTS

Proceedings of the Sixth Joint UJNR Panel Conference

NATIONAL BUREAU OF STANDARDS

The National Bureau of Standards [1] was established by an act of Congress March 3, 1901. The Bureau's overall goal is to strengthen and advance the Nation's science and technology and facilitate their effective application for public benefit. To this end, the Bureau conducts research and provides: (1) a basis for the Nation's physical measurement system, (2) scientific and technological services for industry and government, (3) a technical basis for equity in trade, and (4) technical services to promote public safety. The Bureau consists of the Institute for Basic Standards, the Institute for Materials Research, the Institute for Applied Technology, the Institute for Computer Sciences and Technology, and the Office for Information Programs.

THE INSTITUTE FOR BASIC STANDARDS provides the central basis within the United States of a complete and consistent system of physical measurement; coordinates that system with measurement systems of other nations; and furnishes essential services leading to accurate and uniform physical measurements throughout the Nation's scientific community, industry, and commerce. The Institute consists of the Office of Measurement Services, the Office of Radiation Measurement and the following Center and divisions:

Applied Mathematics — Electricity — Mechanics — Heat — Optical Physics — Center for Radiation Research: Nuclear Sciences; Applied Radiation — Laboratory Astrophysics [2] — Cryogenics [2] — Electromagnetics [2] — Time and Frequency [2].

THE INSTITUTE FOR MATERIALS RESEARCH conducts materials research leading to improved methods of measurement, standards, and data on the properties of well-characterized materials needed by industry, commerce, educational institutions, and Government; provides advisory and research services to other Government agencies; and develops, produces, and distributes standard reference materials. The Institute consists of the Office of Standard Reference Materials, the Office of Air and Water Measurement, and the following divisions:

Analytical Chemistry — Polymers — Metallurgy — Inorganic Materials — Reactor Radiation — Physical Chemistry.

THE INSTITUTE FOR APPLIED TECHNOLOGY provides technical services to promote the use of available technology and to facilitate technological innovation in industry and Government; cooperates with public and private organizations leading to the development of technological standards (including mandatory safety standards), codes and methods of test; and provides technical advice and services to Government agencies upon request. The Institute consists of the following divisions and Centers:

Standards Application and Analysis — Electronic Technology — Center for Consumer Product Technology: Product Systems Analysis; Product Engineering — Center for Building Technology: Structures, Materials, and Life Safety; Building Environment; Technical Evaluation and Application — Center for Fire Research: Fire Science; Fire Safety Engineering.

THE INSTITUTE FOR COMPUTER SCIENCES AND TECHNOLOGY conducts research and provides technical services designed to aid Government agencies in improving cost effectiveness in the conduct of their programs through the selection, acquisition, and effective utilization of automatic data processing equipment; and serves as the principal focus within the executive branch for the development of Federal standards for automatic data processing equipment, techniques, and computer languages. The Institute consists of the following divisions:

Computer Services — Systems and Software — Computer Systems Engineering — Information Technology.

THE OFFICE FOR INFORMATION PROGRAMS promotes optimum dissemination and accessibility of scientific information generated within NBS and other agencies of the Federal Government; promotes the development of the National Standard Reference Data System and a system of information analysis centers dealing with the broader aspects of the National Measurement System; provides appropriate services to ensure that the NBS staff has optimum accessibility to the scientific information of the world. The Office consists of the following organizational units:

Office of Standard Reference Data — Office of Information Activities — Office of Technical Publications — Library — Office of International Relations — Office of International Standards.

---

[1] Headquarters and Laboratories at Gaithersburg, Maryland, unless otherwise noted; mailing address Washington, D.C. 20234.

[2] Located at Boulder, Colorado 80302.

NATIONAL BUREAU OF STANDARDS LIBRARY
APR 7 1976

WIND AND SEISMIC EFFECTS

Proceedings of the Sixth Joint Panel Conference of the U.S. - Japan Cooperative Program in Natural Resources

May 15-17, 1974
National Bureau of Standards
Gaithersburg, Md.

H.S. Lew, Editor

Institute for Applied Technology
National Bureau of Standards
Washington, D. C. 20234

U.S. DEPARTMENT OF COMMERCE, Elliot L. Richardson, *Secretary*

James A. Baker, III, *Under Secretary*

Dr. Betsy Ancker-Johnson, *Assistant Secretary for Science and Technology*

NATIONAL BUREAU OF STANDARDS, Ernest Ambler, *Acting Director*

Issued April 1976

Library of Congress Catalog Card Number: **76-608055**

National Bureau of Standards Special Publication 444

Nat. Bur. Stand. (U.S.), Spec. Publ. 444, 462 pages (Apr. 1976)

CODEN: XNBSAV

U.S. GOVERNMENT PRINTING OFFICE
WASHINGTON: 1976

For sale by the Superintendent of Documents, U.S. Government Printing Office, Washington, D.C. 20402
(Order by SD Catalog No. C13.10:444). Price **$5.80** (Add 25 percent additional for other than U.S. mailing).

PREFACE

The Sixth Joint Meeting of the U.S. - Japan Panel on Wind and Seismic Effects was held in Washington, D.C. on May 15-17, 1974. This panel is one of the twenty panels in the U.S. - Japan Cooperative Program in Natural Resources (UJNR). The UJNR was established in 1964 by the U.S. - Japan Cabinet-level Committee on Trade and Economic Affairs. The purpose of the UJNR is to exchange scientific and technological information which will be mutually beneficial to the economics and welfare of both countries. Accordingly, the purpose of the annual joint meeting of this panel is to exchange technical information on the latest research and development activities within governmental agencies of both countries in the area of wind and seismic effects.

The proceedings include the opening remarks, the program, the formal resolutions, and the technical papers presented at the Joint Meeting. The papers were presented in the respective language of each country. The texts of the papers, all of which were prepared in English, have been edited. The remarks made by the delegates during the opening session were recorded and transcribed. The formal resolutions were drafted at the closing session of the Joint Meeting and adopted unanimously by the panels of both countries.

Pages of the technical papers are numbered with a prefix corresponding to the Theme number. The texts are consecutively numbered in each theme.

H. S. Lew, Secretary
U.S. Panel on Wind and
Seismic Effects

In view of present accepted practice in this technological area, U.S. customary units of measurements have been used throughout this report. It should be noted that the U.S. is a signatory to the General Conference on Weights and Measures which gave official status to the metric SI system of units in 1960. Conversion factors for units in this report are:

	Customary Unit	International (SI), UNIT	Conversion Approximate
Length	inch (in)	meter (m)[a]	1 in=0.0254m*
	foot (ft)	meter (m)	1 ft=0.3048m*
Force	pound (lbf)	newton (N)	1 lbf=4.448N
	kilogram (kgf)	newton (N)	1 kgf=9.807N
Pressure Stress	pound per square inch (psi)	newton/meter^2	1 psi=6895N/m^2
	Kip per square inch (ksi)	newton/meter^2	1 ksi=6895x10^{6}N/m^2
Energy	inch-pound (in-lbf)	joule (J)	1 in-lbf=0.1130 J
	foot-pound (ft-lbf)	joule (J)	1 ft-lbf=1.3558 J
Torque or Bending Moment	pound-inch (lbf-in)	newton-meter (N-m)	1 lbf-in=0.1130 N-m
	pound-foot (lbf-ft)	newton-meter (N-m)	1 lbf-ft=1.3558 N-m
Weight or Mass	pound (lbf)	kilogram (kg)	1 lb=0.4536 kg
Unit Weight	pound per cubic foot (pcf)	kilogram per cubic meter (kg/m^3)	1 pcf=16.018 kg/m^3
Velocity	foot per second (ft/sec)	meter per second (m/s)	1 fps=0.3048 m/s
Acceleration	foot per second per second (ft/sec^2)	meter per second per second (m/s^2)	1 ft/sec^2=0.3048 m/s^2

[a]Meter may be subdivided. A centimeter (cm) is 1/100 m and a millimeter (mm) is 1/1000 m.

*Exact

CONTENTS

	Page
PREFACE	iii
SI CONVERSION	iv
ABSTRACT	viii
PROGRAM OF THE JOINT MEETING	ix
OPENING SESSION	
Remarks by Dr. Ernest Ambler, Deputy Director, National Bureau of Standards	xiii
Remarks by Mr. Isao Uchida, Counselor, Embassy of Japan	xiii
Remarks by Dr. Edward O. Pfrang, Chairman, U.S. Panel	xiv
Remarks by Mr. Mitsuru Nagao, Chairman, Japan Panel	xv
LIST OF MEMBERS	xvi
PHOTOGRAPH OF PARTICIPANTS	xix
FORMAL RESOLUTIONS	xx
THEMES AND TECHNICAL PAPERS	
THEME I: EXTREME WINDS IN STRUCTURAL DESIGN	
On the Gust Response of Long Span Suspension Bridges — N. Narita and K. Yokoyama	I- 1
Extreme Winds in Hurricanes and Possibility of Modifying Them — R. C. Gentry	I- 21
Extreme Winds in the United States — A. R. Hull and P. E. Hughes	I- 34
THEME II: ASSESSMENT AND EXPERIMENTAL TECHNIQUES FOR MEASURING WIND LOADS	
Wind Tunnel Experiments for Studying a Local Wind — K. Suda, S. Soma and K. Takeuchi	II- 1
A Study of Wind Pressures on a Single-Family Dwelling in Model and Full Scale — R. D. Marshall	II- 21
THEME III: DYNAMICS OF SOIL STRUCTURES AND GROUND RESPONSE IN EARTHQUAKES	
Non-linear Calculations of Ground Response in Earthquakes — W. B. Joyner, A. T. F. Chew and P. C. Doherty	III- 1
Observation and Analysis of Ground Response in Earthquakes — S. Hayashi and H. Tsuchida	III- 13
Research Study on Liquefaction — W. F. Marcuson	III- 24

Page

Estimation of Liquefaction Potential by Means of Explosion Test
K. Yamamura and Y. Koga..... III- 38

Landslide Incidence and Mechanisms During Earthquakes
G. E. Erickson..... III- 52

Stress Condition Effects on Dynamic Properties of Soil
E. Kuribayashi and T. Iwasaki..... III- 72

Prediction of Maximum Earthquake Intensities for the San Francisco Bay Region
R. D. Borcherdt and J. F. Gibbs..... III- 84

THEME IV: STRUCTURAL RESPONSE TO WIND AND EARTHQUAKE, AND DESIGN CRITERIA

A Statistical Approach to the Loading and Failure of Structures
R. G. Merrit..... IV- 1

Synthetic Experimental Research on the Ductility of Reinforced Concrete Short Columns Under Large Deflection
K. Nakano and M. Hirosawa..... IV- 16

Non-Linear Analysis of A Guyed Tower
S. K. Takahashi and W. A. Shaw..... IV- 37

A Standard for the Structural Integrity of Prefabricated Dwellings
K. Nakano, M. Hirosawa and T. Murota..... IV- 55

An Analytical Model for Determining Energy Dissipation in Dynamically Loaded Structures
J. F. McNamara and S. K. Sharma..... IV- 70

Design of Pile Foundations Subjected to Lateral Loads
M. Nagao, T. Okubo, K. Komada and A. Yamakawa..... IV- 90

Comprehensive Seismic Design Provisions for Buildings
C. G. Culver..... IV-113

Wind Loading and Modern Building Codes
E. Simiu and R. D. Marshall..... IV-127

THEME V: DISASTER MITIGATION AGAINST NATURAL HAZARDS

Seismic Retrofitting of Existing Highway Bridges
J. D. Cooper, R. R. Robinson and A. Longinow ..... V- 1

Dynamic Tests of Structures by Use of A Large Scale Shake Table
S. Inaba..... V- 25

A Methodology for Evaluation of Existing Buildings Against Earthquakes, Hurricanes and Tornadoes
H. S. Lew and C. G. Culver..... V- 35

Experimental Research on the Aseismic Characteristics of A Spherical Steel Tank for Liquid Petroleum Gas
K. Nakano and M. Watabe..... V- 50

Page

Research on Minimizing Earthquake Structural Damage to Single-Family Dwellings
W. J. Werner..... V- 63

Earthquake Engineering Research Supported by the National Science Foundation
C. Thiel..... V- 66

The Wind Engineering Program
M. P. Gaus..... V- 80

THEME VI: TECHNOLOGICAL ASSISTANCE TO DEVELOPING COUNTRIES

Preliminary Report on Present Status and Development Project of Volcanological Observation and Research in Indonesia
A. Suwa..... VI- 1

Use of Stabilized Adobe Block and Cane in Construction of Low-Cost Housing in Peru
S. G. Fattal..... VI- 16

A Comment on the Technological Aid to Developing Countries
M. Nagao and T. Okubo..... VI- 25

ABSTRACT

The Sixth Joint Meeting of the U.S. - Japan Panel on Wind and Seismic Effects was held in Washington, D.C. on May 15-17, 1974. The proceedings of the Joint Meeting include the opening remarks, the program, the formal resolutions, and the technical papers. The subject matter covered in the papers includes extreme winds in structural design; assessment and experimental techniques for measuring wind loads; dynamics of soil structures and ground response in earthquakes; structural response to wind and earthquake and design criteria; disaster mitigation against natural hazards; and technological assistance to developing countries.

Key Words: Bridges; buildings; codes; disaster; dynamic analysis; earthquakes; modeling; soils; structural response; volcanoes; and wind.

SIXTH JOINT MEETING
PROGRAM OF THE
U.S. - JAPAN PANEL ON WIND AND SEISMIC EFFECTS
May 15-17, 1974
at
National Bureau of Standards

WEDNESDAY-May 15

OPENING SESSION (10th Floor Conf. Room, Admin., Bldg.)

1000 Call to order by Dr. H. S. Lew, Secretary, U.S. Panel

Remarks by Dr. Ernest Ambler, Deputy Director
National Bureau of Standards

Remarks by Mr. Isao Uchida, Counselor, Embassy of Japan

Remarks by Dr. Edward O. Pfrang, Chairman, U.S. Panel

Remarks by Mr. Mitsuru Nagao, Chairman, Japan Panel

1030 Introduction of U.S. Panel Members by U.S. Chairman
and Japan Panel Members by Japan Chairman

1045 Election of Conference Chairman

1100 Adoption of Agenda

1115 Adjourn

1130 Group Photograph

1145 Lunch-Dining Room C

1300 Leave for Fairbanks Highway Research Laboratories
Federal Highway Administration

THURSDAY-May 16

THEME II-ASSESSMENT AND EXPERIMENTAL TECHNIQUES FOR
MEASURING WIND LOADS

Chairman: Dr. Edward O. Pfrang

0900 Wind Tunnel Experiments for Studying a Local Wind -
K. Suda*, S. Soma and K. Takeuchi

0920 A Study of Wind Pressures on Single-Family Dwellings in
Model and Full Scale - R. D. Marshall

0940 Discussion

THEME I-EXTREME WINDS IN STRUCTURAL DESIGN

Chairman: Mr. Mitsuru Nagao

1000 The Gust Response of Long Span Suspension Bridges -
N. Narita and K. Yokoyama (Presented by T. Okubo)

*Underline designates the person presenting the paper.

1020 Extreme Winds in Hurricanes and Possibility of Modifying Them - R. C. Gentry

1040 Break

1100 Extreme Winds in the United States - A. Hull and P. Hughes

1120 Discussion

1130 A film presentation, "The Only Decision" - J. Lefter

1215 Lunch-Dining Room C

THEME IV-STRUCTURAL RESPONSE TO WIND AND EARTHQUAKE, AND DESIGN CRITERIA

Chairman: Dr. Edward O. Pfrang

1340 A Statistical Approach to the Loading and Failure of Structures - R. G. Merrit

1400 Synthetic Experimental Research on the Ductility of Reinforced Concrete Short Columns under Large Deflection - K. Nakano and M. Hirosawa

1420 Non-linear Analysis of a Guyed Tower - S. K. Takahashi and W. A. Shaw

1430 A standard for the Structural Integrity of Prefabricated Dwellings - K. Nakano, M. Hirosawa and T. Murota

1440 Break

1455 An Analytical Model for Determining Energy Dissipation in Dynamically Loaded Structures - J. F. McNamara and S. K. Sharma

1505 Design of Pile Foundations Subjected to Lateral Load - M. Nagao, T. Okubo, K. Komada and A. Yamakawa

1515 Comprehensive Seismic Design Provisions for Buildings - C. Culver

1525 Wind Loading and Modern Building Codes - E. Simiu and R. Marshall

1535 Discussion

THEME VI-TECHNOLOGICAL ASSISTANCE TO DEVELOPING COUNTRIES

Chairman: Mr. Mitsuru Nagao

1600 Preliminary Report on Present Status and Development Project of Volcanological Observation and Research in Indonesia - A. Suwa

1620 Use of Stabilized Adobe Block and Cane in Construction of Low-cost Housing in Peru - S. G. Fattal

1640 A Comment on the Technological Aid to Developing Countries - M. Nagao and T. Okubo

1715 Discussion

Adjourn

FRIDAY-May 17

THEME III-DYNAMICS OF SOIL STRUCTURES AND GROUND RESPONSE IN EARTHQUAKES

Chairman: Dr. Edward O. Pfrang

0900 Non-linear Calculations of Ground Response in Earthquakes - W. B. Joyner, A. T. F. Chew and P. C. Doherty

0920 Observation and Analysis of Ground Response in Earthquakes - S. Hayashi (Presented by H. Tsuchida)

0940 Research Study on Liquefaction - W. F. Marcuson (Presented by K. O. O'Donnell)

0950 Estimation of Liquefaction Potential by Means of Explosion Tests - K. Yamamura and Y. Koga (Presented by S. Inaba)

1000 Landslide Incidence and Mechanisms during Earthquakes - G. E. Ericksen

1010 Stress Condition Effects on Dynamic Properties of Soil E. Kuribayashi and T. Iwasaki (Presented by H. Tsuchida)

1020 Break

1040 Prediction of Maximum Earthquake Intensities for the San Francisco Bay Region - R. Brocherdt and J. F. Gibbs

1050 Discussion

1115 Tour of NBS Wind Tunnel Facilities

1215 Lunch-Dining Room C

THEME V-DISASTER MITIGATION AGAINST NATURAL HAZARDS

Chairman: Mr. Mitsuru Nagao

1340 Seismic Retrofitting of Existing Highway Bridges - J. D. Cooper, R. Robinson and A. Longinow

1400 Dynamic Tests of Structures by Use of a Large Scale Shaking Table - S. Inaba

1420 A Methodology for Evaluation of Existing Buildings against Earthquakes, Hurricanes and Tornadoes - H. S. Lew and C. Culver

1430 Experimental Research on the Aseismic Characteristics of Spherical Steel Tank for Liquid Petroleum Gas - K. Nakano and M. Watabe

1440 Research on Minimizing Earthquake Structural Damage to Single-Family Dwellings - W. J. Werner

1450 Earthquake Engineering Research Supported by the National Science Foundation - C. Thiel

1500 The Wind Engineering Program - M. Gaus

1510 Discussion

1530 Break

THEME VII-Free Discussion

Chairman: Mr. Mitsuru Nagao

1550 Discussion

CLOSING SESSION

Chairman: Dr. Edward O. Pfrang

1620 Adoption of Formal Resolution

1700 Adjourn

OPENING REMARKS BY DR. ERNEST AMBLER
DEPUTY DIRECTOR, NATIONAL BUREAU OF STANDARDS

Counselor Uchida, Mr. Nagao and distinguished guests, common interests are the bonds between individuals and between nations. We at the National Bureau of Standards, as fellow members of the scientific community and your hosts, welcome you and hope you find your stay pleasant and profitable. Our laboratories will be open to you, and the staff will be happy to talk with you about any problems that interest you.

In the pursuit of scientific information on wind and seismic effects, you are travelling like the wind to the four corners of the earth. This same pursuit of scientific knowledge has led many Bureau scientists to become world travelers as they studied, for instance, the engineering aspects of the 1964 Alaska earthquake, the 1971 San Fernando earthquake, and the 1972 Managua disaster.

Our two nations, bordering as we do on the Pacific Ocean, the borders of which show considerable seismic activity, are interested in developing design methods and criteria for building structures that will better withstand wind and shock. Both of us individually conduct research programs, but we are here today to make our programs more effective through cooperation. We think this is a very important undertaking and we are very happy that you are here today, and again, welcome you to the National Bureau of Standards.

OPENING REMARKS BY MR. ISAO UCHIDA
COUNSELOR, EMBASSY OF JAPAN

Ladies and Gentlemen,

It is my great honor to be given the opportunity to say a few words at the opening of the Sixth Joint Meeting of the UJNR panel on wind and seismic effects.

The United States and Japan have very close cooperative relations in every facet of our activities. Science and technology is not the exception. Now we have the U.S. - Japan committee on scientific cooperation and the U.S. - Japan Committee on Medical Science, as well as UJNR.

Many activities such as exchange of scientists, joint seminars and joint research are being carried out actively and effectively under these cooperative programs. We have also very close cooperative programs in the area of so called big sciences: nuclear development and space development. In addition, the new cooperative agreement on energy research and development will be signed in the near future.

The Japanese government has been making considerable advancement in research and development of science and technology by realizing that science and technology play an important role in the progress of the national economy and the improvement of the welfare of the people. At the same time, we understand that the science and technology belong to all people in the world. From this point of view, we have developed a policy to promote international cooperation in research and development of science and technology. I hope and believe that our cooperative effort in science and technology contributes not only to the prosperity of both countries but also to the welfare of all people in the world.

UJNR has already marked its ten year history and the second five year report is presently in progress. At present, we have twenty working panels under UJNR programs who are producing valuable information. I believe this is the result of the efforts by many concerned people from both countries.

In regard to the matter of wind and seismic effects, which is handled in this panel, although I am a layman in this field, I know that the U.S. and Japan are the two leading countries in the field and all members here are the experts of both countries. I believe in the success of this panel and the hope for future developments.

I should like to express my heartfelt gratitude to each and all of the participants, especially to Dr. Ambler, Dr. Pfrang and other American panel members, Dr. Lew and other secretariate staff, for their great contribution toward making the arrangements and for their warm hospitality to the Japanese members.

Thank you.

OPENING REMARKS BY DR. EDWARD O. PFRANG
CHAIRMAN, U.S. PANEL

Mr. Uchida and Mr. Fujisawa, I would like to thank you and the Japan Embassy for all the assistance you have given us, not only with respect to this panel meeting but all the past meetings. To Mr. Nagao, I would like to congratulate him on the outstanding panel which he has brought with him to the Joint Meeting. I have had a brief opportunity to begin studying the papers and I find them to have excellent technical contributions.

I don't know how many people in this room realize the fact that this meeting was almost not held. On May 9th, a Richter 6.8 earthquake took place 100 kilometers from Tokyo. Had it been on the Kanto plane, this meeting would have definitely been cancelled. This is one measure of the need for our joint study. Following the San Fernando earthquake of 1971,

Dr. Fukuoka, former chairman of the Japan Panel, led a team of distinguished Japanese engineers and scientists to the United States. I believe that you in Japan learned much from our sad experience. We look forward to learning from you, on the occasion of the 7th Joint Meeting, your lessons from the Izu earthquake.

Another area of our cooperation which needs to be mentioned regards our work with developing countries. We have scientifically cooperated in Peru. We appreciate the great kindness that you have shown to us in regard to our efforts in the Phillipines. It has been very kind of Mr. Nagao and Dr. Okubo and others to meet with our people in their efforts with regard to the Phillipines and to provide their counsel.

We have accomplished much through our UJNR Program. However, when we consider the loss of life in San Fernando and Izu, and when we also take into account the fact that on May 3rd approximately 300 people lost their lives in tornadoes within the U.S., there is much that remains to be done. Thank you very much.

OPENING REMARKS BY MR. MITSURU NAGAO
CHAIRMAN, JAPAN PANEL

Dr. Ambler, Dr. Pfrang, members of the U.S. Panel and guests, I feel very honored to have this opportunity to express my greetings on behalf of the Japan Panel. I also would like to express my appreciation for the great efforts made by Dr. Pfrang and all other U.S. Panel members preparing for the Sixth Joint Meeting.

As you know, in our past five joint meetings many topics concerning important wind and seismic problems have been presented and discussed. The valuable results from these meetings have been highly evaluated at the UJNR Conference. At this Joint Meeting, as many as thirty three technical papers have been submitted. This clearly indicated continuing tireless efforts of the members of both sides for the success of our program and I am assured that we shall end our meeting with fruitful results. The fear of wind and earthquake will not diminish from mankind. We hope that we can continue our efforts toward our mutual goals.

In closing, I would like to express my gratitude for the cooperation and the assistance of the U.S. Embassy in Tokyo and the Japan Embassy in Washington, D.C., the National Bureau of Standards, and others, expecially Dr. Pfrang and the Secretary of the U.S. Panel. Thank you for your kind attention.

U. S. Panel on Wind and Seismic Effects
Membership List
April 1974

Dr. Edward O. Pfrang, Chairman
Chief, Structures, Materials & Safety Division
Center for Building Technology, IAT
National Bureau of Standards
Washington, D.C. 20234

Dr. S. T. Algermissen
Seismicity and Risk Analysis Branch
Building 25, Denver Federal Center
Denver, Colorado 80225

Mr. Billy Bohannan
Enginerred Wood Structures
Wood Engineering Research
U. S. Forest Products Lab.
Madison, Wisconsin 53705

Dr. George Ericksen
U.S. Geological Survey
12201 Sunrise Valley Drive
Reston, Virginia 22092

Dr. Michael P. Gaus
Section Head of Engineering Mechanics
Engineering Division
National Science Foundation
1800 G Street, N.W.
Washington, D.C. 20550

Dr. R. Cecil Gentry
Director, National Hurricane Research Lab.
National Oceanic Atmospheric Administration
P.O. Box 8265, University of Miami Branch
Coral Gables, Florida 33124

Mr. Sigmund Gerber
Director for Construction Standards
and Design for Installation and Logistics
Office of the Secretary of Defense
Room 3E763, The Pentagon
Washington, D.C. 20301

Mr. Jack Healy
Chief, Material Systems & Science Division
Department of the Army
Construction Engineering Research Labs.
P.O. Box 4005
Champaign, Illinois 61820

Mr. Arnold R. Hull
Associated Director for Climatology
NOAA-EDS
Washington, D.C. 20235

Dr. William B. Joyner
U.S. Geological Survey
Office of Earthquake Research
345 Middlefield Road
Menlo Park, California 94025

Mr. John W. Kaufman
Chief, Atmospheric Dynamics Branch
Aerospace Environment Division
National Aeronautics & Space Administration
Marshall Space Flight Center
Mobile, Alabama 35812

Mr. James Lefter
Director, Civil Engineering Service
Office of Construction
Veterans Administration
Lafayette Building, Room 507
811 Vermont Avenue, N.W.
Washington, D.C. 20420

Dr. R. B. Matthiesen
Director, Seismic Engineering Branch
U.S. Geological Survey
390 Main Street
San Francisco, California 94104

Mr. Keith O. O'Donnell
Assistant Chief, Structural Branch
Engineering Division, Civil Works Directorate
Forrestal Building, ATTN: DAEN-CWE-D
Washington, D.C. 20314

Mr. Larry F. Rousch
Public Building Service
General Services Administration
18th & F Strett, N.W.
Washington, D.C. 20405

Mr. Charles Scheffey
Acting Associate Administrator
Federal Highway Administration
Washington, D.C. 20590

Dr. Warren A. Shaw
Head, Civil Engineering Department
Civil Engineering Laboratory
Naval Construction Batallion Center
Port Hueneme, California 93043

Mr. Lawrence C. Shao
Directorate of Licensing
U.S. Atomic Energy Commission
Washington, D.C. 20545

Dr. Charles T. Thiel
Program Manager, Earthquake Engineering
Division of Advanced Technology Applications
National Science Foundation
Washington, D.C. 20550

Mr. William J. Werner
Division of Building Technology and Safety
Department of Housing and Urban Development
Room 4120
451 7th Street, S.W.
Washington, D.C. 20410

Dr. Roger D. Brocherdt, Alternate
U.S. Geological Survey
National Center for Earthquake Research
345 Middlefield Road
Menlo Park, California 94025

Dr. H. S. Lew, Secretary and Alternate
Structures, Materials & Safety Division
Center for Building Technology, IAT
National Bureau of Standards
Washington, D.C. 20234

Dr. Jchn B. Scalzi, Alternate
Division of Advanced Technology & Applications
National Science Foundation
Washington, D.C. 20550

Mr. F. J. Tamanini, Alternate
Chief, Structures and Applied Mechanics Div.
HRS-10
U.S. Department of Transportation
Federal Highway Administration
Washington, D.C. 20550

Japan Panel on Wind and Seismic Effects
Membership List
April 1974

Mr. Mitsuru Nagao, Chairman
Director, Public Works Research Institute
Ministry of Construction
2-28-32- Honkomagome, Bunkyo-ku, Tokyo

Dr. Satoshi Hayashi
Head, Structure Division
Port and Harbor Research Institute, Ministry of Transport
3-1-1 Nagase, Yokosuka-shi, Kanagawa-ken

Mr. Seiichi Inaba
Chief, Earthquake Engineering Laboratory
National Research Center for Disaster Prevention
Science and Technology Agency
4489-1 Kurihara Aza, Sakuramura, Niiharigun, Ibaragin-ken

Dr. Yasunori Koizumi
Director, Building Research Institute
Ministry of Construction
3-28-2 Hyakunin-cho, Shin Juku-ku, Tokyo

Mr. Eiichi Kuribayashi
Chief, Earthquake Engineering Section
Structure and Bridge Division, Chiba Branch
Public Works Research Institute, Ministry of Construction
4-12-52 Anagawa, Chiba-shi, Chiba-ken

Dr. Kiyoshi Nakano
Head, Structural Division, Building Research Institute
Ministry of Construction
3-28-8 Hyakunin-cho, Shin Juku-ku, Tokyo

Mr. Nobuyuki Narita
Chief, Structure Section
Structure and Bridge Division, Chiba Branch
Public Works Research Institute, Ministry of Construction
4-12-52 Anagawa, Chiba-shi, Chiba-ken

Dr. Tadayoshi Okubo
Head, Structure and Bridge Division
Chiba Branch, Public Works Researcy Institute
Ministry of Construction
4-12-52 Anagawa, Chiba-shi, Chiba-ken

Mr. Tetsuo Santo
Head, International Institute of Seismology and Earthquake Engineering
Building Research Institute, Ministry of Construction
3-28-8 Hyakunin-cho, Shin Juku-ku, Tokyo

Dr. Ken Suda
Director, Meteorological Research Institute
Meteorological Agency, Ministry of Transport
4-35-8 Kita, Koenji, Suginami-ku, Tokyo

Mr. Akira Suwa
Head, Siesmological Laboratory, Meteorological Research Institute
Meteorological Agency, Ministry of Transport
4-35-8-Kita, Koenji, Suginami-ku, Tokyo

Dr. Kiyohide Takeuchi
Head, Applied Meteorological Laboratory
Meteorological Research Institute
Meteorological Agency, Ministry of Transport
4-35-8-Kita, Koenji, Suginami-ku, Tokyo

Mr. Hajime Tsuchida
Chief, Earthquake Resistant Structures Lab.
Structure Division
Building Research Institute, Ministry of Construction
3-28-8-Hyakunin-cho, Shin Juku-ku, Tokyo

Dr. Makoto Watabe
Chief, International Institute of Seismology and Earthquake Engineering
Building Research Institute, Ministry of Construction
3-28-8-Hyakunin-cho, Shin Juku-ku, Tokyo

Vacant
Chief, Soil Dynamics Section
Construction Method and Equipment Division
Chiba Branch, Public Works Research Institute
Ministry of Construction
4-12-52 Anagawa, Chiba-shi, Chiba-ken

Mr. Hiroshi Yoshimura, Secretary
Head, Planning Division
Public Works Research Institute
Ministry of Construction
2-28-32-Honkomagome, Bunkyo-ku, Tokyo

The U.S. and Japan members attending the Sixth Joint Meeting.

SIXTH JOINT MEETING PROPOSED RESOLUTIONS

Both delegations proposed the following formal resolutions at the conclusion of the Sixth Joint Meeting of the U. S. - Japan Panel.

1. That the Sixth Joint Meeting was of great value to both sides and the joint program should continue.

2. That the next Joint Meeting should be held in Tokyo in 1975, preferably in May, and that the technical sessions should be extended to three days.

3. That increased effort should be made in the near future to encourage joint research programs, expecially in the area of the mutual utilization of research facilities and the exchange of researchers.

4. That the scope of the activities of the Joint Panel should be expanded to include areas of mutual interest in seismic risk analysis as related to earthquake prediction.

5. That efforts should continue, or be implemented, to publish the proceedings of past Joint Meetings in the respective countries and make them available to the respective engineering and scientific professions at large.

ON THE GUST RESPONSE OF LONG-SPAN SUSPENSION BRIDGES

by

N. Narita
Chief, Structure Section
Public Works Research Institute
Ministry of Construction
Japan

K. Yokoyama
Research Engineer
Structure Section
Public Works Research Institute

In the design of above-ground structures it is established practice to consider the effects of wind. For some structures, like long-span suspension bridges, the influence of wind may be the primary design control which will then govern the inherent safety of the structures and the final construction cost.

This paper, therefore, will describe the required changes in design specifications to incorporate the influence of gusts on long-span suspension bridges.

The necessary numerical calculations are illustrated in addition to some long-term observations on the Kanmon Bridge. The importance and necessity of studies on gust response are emphasized.

Key Words: Bridge; design; field data; gust response; model; specifications; structure; theory; wind.

INTRODUCTION

Necessity of Study on Gust Response of a Structure

When one considers wind effects, its fluctuation must be relative to time and space. The time fluctuating wind tends to introduce forced random vibrations in above-ground structures. This necessitates consideration of some dynamic magnification effects applied to the static response of the structure. The spatial fluctuation of wind tends to decrease the probability that the wind, with mean speed, attacks the entire structure at the same time, thus some modification may also be necessary in order to include this effect.

The determination of the response of a structure to wind, as based on a statistical concept relative to a stationary time series, was introduced by A. G. Davenport in 1961. This concept has since been adopted into the design specifications for building structures in Denmark and Canada. The importance of gust response in long-span suspension bridges was also suggested by Davenport and the magnification effect due to gustiness was estimated as three or more times that of the static response.

The gust response in suspension bridges, relative to buildings, points out the following;

(i) The structural configuration of a bridge is far more complicated, as compared to a building structure, i.e., the cable and the suspended structure are composed of horizontally long elements, and the main tower is composed of vertically long elements.

(ii) The damping capacity is small, compared to a building structure.

(iii) The geographical location of the bridge inhibits one for obtaining aerodynamic characteristics by analytical methods.

Moreover, the accumulation of statistical data of natural wind is minimal and it may be dangerous to utilize a statistical theory.

In order to solve this difficult problem, it is necessary to study the following themes;

(i) To evaluate the statistical characteristics of wind, especially strong wind.

(ii) To evaluate the structural and vibrational characteristics of long-span suspension bridges.

(iii) To evaluate the aerodynamic characteristics of brige sections.

(iv) To improve the method of statistical analysis.

(v) To accumulate test data, as obtained during the observation of the gust response of real structures, and to compare these with the theoretical results.

In this paper items (ii), (iv) and (v) will be presented.

Gust Response and Design Specifications

A wind resistant design specification, for long-span suspension bridges, was first presented in 1974 for use in the design of the proposed Honshu-Shikoku Bridge. This specification was developed by a Technical Advisory Committee of the Japan Society of Civil Engineers. However, these initial design specifications, which have been applied to bridges of 150 meters in length or less, have not specified dynamic effects due to wind loading. Subsequent modifications to the specifications have since occurred through

consideration of recent research activities. The basis for the (1964) specification and subsequent revision (1972) will now be presented.

(i) Wind Resistant Design Specification (1964) for the proposed Honshu-Shikoku Bridge

In this specification the design wind load is defined as $P_d = 1/2 \times \rho V_d^2 AC_d$, where P_d denotes design wind load, ρ air density, C_d drag coefficient, and A the exposed area of the structure per unit length. The design wind speed V_d was derived relative to the basic wind speed V_{10} as given by: $V_d = V_{10} \times \gamma_1 \times \gamma_2$, where γ_1 is a modification factor for V_{10} and takes into account the altitude of the structure, and it is assumed to satisfy the power law. The second modification factor γ_2 is relative to the wind gustiness and was determined by making the following assumptions.

The instantaneous wind speed parallel to the mean flow, at an arbitrary point, is the sum of the mean wind speed ($\bar{V}_s$) and the fluctuating wind speed ($\bar{V}_t$), averaged over (s) seconds or;

$$\bar{V}_t = \bar{V}_s + V_t = \bar{V}_s + \sum_i V_i \sin (W_i t + \delta_i)$$

The wave length L_1, which corresponds to the circular frequency W_i, may then be written as $L_i = \bar{V}_s \frac{2\pi}{W_i} = \bar{V}_s T_i$, where $T_i = \frac{2\pi}{W_i}$. The lateral scale of turbulence B_i corresponding to W_i, is assumed to be 1/k times L_i and equal to the horizontal length of the structure B. Then, $s = k \times b/\bar{V}_s$.

The relation between mean wind speed and the averaging time of the wind speed is;

$$\bar{V}_s/\bar{V}_z = (S/600)^{-r} \quad , \quad r = r_o(Z/Z_o)^{-0.42}$$

where $\bar{V}_z$ is the ten minute averaged wind speed at the height of 10 meters, and the constant $r_o = 0.090$ at $Z_o = 12.2$ meters. From the above equations the gust response modification factor γ_2 can be obtained as;

$$r_2 = \bar{V}_s/\bar{V}_z = (600\ V_z/kB)^{r/1-r}$$

where $\bar{V}_z$ varies according to V_{10} and the power index p, r varies according to the altitude as noted previously. When $V_{10} = 40$ m/s, the power index p = 1/6, which are the values that are assumed in the calculation of the modification factor γ_2.

However, as mentioned above, the (1964) design specifications did not take into account the dynamic characteristics of the structure. These considerations will now be presented.

(ii) Wind Resistant Design Specification (1972) for the proposed Honshu-Shikoku Bridge

More than ten years have passed since the wind resistant design statistical concepts were first proposed by Davenport. Though the concept has been applied to the building structures in Denmark and Canada, it has not been established in Japan. In developing the 1972 specification, a preliminary study was first conducted using the stationary time series theory. The modification factor for the gust response was then evaluated and found to equal 1.3 to 1.5, for the lateral bending moment of stiffening frames of suspension bridges with center span lengths of 500 to 1,500 meters. However, there is no evidence of induced lateral vibration of real bridges, therefore, the dynamic response effect the stiffening frame of the structure was neglected in the modification factor γ_2, which gave a value between 1.14 and 1.19. This revised specification, which considered statistical characteristics of wind, still remained ambiguous.

GUST RESPONSE OF A SUSPENSION BRIDGE

Fundamental Equations and Some Remarks on the Numerical Calculations

The fundamental equations for evaluating the gust response of a suspension bridge will now be introduced without presenting the details.

(i) Structural Analysis of the System

Lateral motion of the system was analyzed by use of the so-called finite element method. The fundamental equation of the system is given by;

$$\frac{d^2}{dx^2}\left(EI\frac{d^2v}{dx^2}\right) = q_t + \frac{P_s}{k}(u + v)$$

$$H\frac{d^2u}{dx^2} = -q_c + \frac{P_s}{k}(u - v)$$

and the mechanical admittance for r^{th} mode of vibration is;

$$|H_r(n)|^2 = 1/P_r{}^4[\{1 - (P/P_r)^2\}^2 + 4\xi_r{}^2(P/P_r)^2]$$

The fraction of damping was assumed as

$$\xi_r = \xi_{r_o} + \xi_{r_{aero}}, \text{ where } \xi_{r_o} = \frac{0.03}{2\pi}, \quad \xi_{r_{aero}} = \frac{C_D B\bar{V}_z}{32\pi m n_r}$$

(ii) Spectral Density of Wind Force

The mean wind force $\bar{P}$ corresponding to the mean wind speed $\bar{V}_z$ is

$$\bar{P} = 1/2\ \rho\bar{V}_z{}^2 C_D A$$

The spectral density of the u-component was evaluated by Hino's formula, namely,

$$S_u(n) = 0.476\ \frac{6KV_{10}{}^2}{\beta}\left(1 + \frac{n^2}{\beta^2}\right)^{-5/6}$$

$$\beta = 1.169 \times 10^{-3}\ \frac{V_{10}{}^\alpha}{\sqrt{k}}\ (Z/10)^{(2m_e\alpha - 1)}$$

The cross-wind correlation spectrum was evaluated by Davenport's expression;

$$R_u(\chi_1, \chi_2, n) = \exp\left(-\frac{kn}{V_z}|\chi_1 - \chi_2|\right)$$

Then, the spectrum of the fluctuating wind force is expressed as;

$$S_p(n) = 4\ \bar{P}^2|\chi_u(n)|^2\ \frac{S_u(n)}{V_z{}^2}$$

The aerodynamic admittance equation is given by Vickery's formula and is;

$$|\chi_u(n)|^2 = \left\{1 + 2\left(\frac{nD}{V_z}\right)^{4/3}\right\}^{-1}$$

(iii) Aerodynamic Response

The response spectrum of the lateral bending moment of the stiffening frames is;

$$S_m(\chi, n) = \sum_r M_r{}^2(\chi)|H_r(n)|^2|J_r(n)|^2\ S_p(n)$$

where the joint acceptance $J_r(n)$ is given in the following form;

$$|J_r(n)|^2 = \iint \gamma_r(\lambda_1)\, \gamma_r(\lambda_2)\, R_u(\lambda_1, \lambda_2, n)\, d\lambda_1 d\lambda_2$$

The variance and effective frequency for the bending moment are given as;

$$\sigma_m^2(\lambda) = \int_0^\infty S_m(\lambda, n)\, dn = \sum_r M_r^2(\lambda) \int_0^\infty |H_r(n)|^2 |J_r(n)|^2 S_p(n)\, dn$$

$$\gamma_m^2(\lambda) = \int_0^\infty m^2 P_m(\lambda, n)\, dn / \sigma_m^2(\lambda)$$

The expected value of the maximum response is $g_{rm}(\lambda)\sigma_m(\lambda)$, where

$$g_{Tm}(\lambda) = [2\ln\{\gamma_m(\lambda)T\}]^{1/2} + \frac{0.5772}{[2\ln\{\gamma_m(\lambda)T\}]^{1/2}}$$

Finally, the modification factor for the wind speed relative to bending moment is expressed as;

$$G_{Tm}(\lambda) = \left\{1 + \frac{g_{Tm}(\lambda)\sigma_m(\lambda)}{M(\lambda)}\right\} 1/2$$

The above equations were incorporated into a computer program. The accuracy of the numerical procedure was examined relative to the following terms and expressions;

(i) Terms $V_r(\lambda)$, $u_r(\lambda)$, $M_r(\lambda)$, $Q_r(\lambda)$, $M(\lambda)$, and $Q(\lambda)$

(ii) Double integral in the joint acceptance

(iii) $\int_0^\infty (\ldots n)\, d\lambda$ and $\sum_r (\ldots n)$

ILLUSTRATIVE EXAMPLES

Symmetric Suspension Bridges Consisting of Three Suspended Spans with Hinged Stiffening Frames

Numerical calculations were made relative to six model designs, the essential properties of which are given in Table 1. The maximum bending moment occurs near x/L = 0.2 for the L1500 model, with the peak moment moving gradually toward the span center as the span lengths decrease. This means that the influence of the cable against the wind loading increases proportionally with the span length. The modification factor γ_2 for the various bridges is shown in Figure 1. In general, γ_2 does not vary, except for the L1500 model, and has an average value of about 1.35.

Symmetric Suspension Bridges Consisting of Three Suspended Spans with Continuous Stiffening Frames

The suspension bridges which have continuous stiffening frames, that were analyzed, are detailed in Table 2. The resulting modification factor γ_2 for these bridges is given in Figure 1-1. The characteristic feature of the continuous suspension bridge is that γ_2 increases around the point x/L = 0.2, where the bending moment changes its sign. It also appears that γ_2 increases gradually along the end of the side span.

It should be noted that the modification factor analyzed under the assumption of hinged suspension bridges is nearly equal to that of continuous bridges, except at the peak location.

Effects of Wind Characteristics on Gust Response

Table 3 shows the effect of the wind characteristics on the modification factor. In this table the power index p, the surface drag coefficient K and the cross-wind correlation factor k are chosen as variables. The functions K and k appear to be the governing factors.

FIELD OBSERVATION OF THE GUST RESPONSE AT THE KANMON BRIDGE

Observation System at the Kanmon Bridge

The instrumentation and data-recording system, designed to monitor and record wind speeds and direction as well as earthquakes, and to indicate their effects on the super- and sub-structures of the bridge, has been provided by Japan Highway Corporation. The location of instruments and elements are shown in Figure 2 and Table 4. The system was placed into operation last winter, just after the opening of the bridge.

Some Examples of the Observed Data

The original trace of the wind-induced vibration of the super-structure is given in Figure 3, with the wind record at that time tabulated in Table 5. Table 6 shows the results of a preliminary analysis. The natural frequencies obtained from the wind induced vibration record coincides with those obtained from field forced vibrations induced by a large scale excitor during tests conducted last September. However, the damping capacity could not be obtained from the power spectral density given in Figure 4. The damping capacity, as shown in Table 6, was derived from the forced vibration test. The observed data will be analyzed and compared with the theoretical values in the near future.

CONCLUSIONS

The authors have outlined the present status of a study on the gust response problems of long-span suspension bridges. In order to enhance the wind resistant design technique, vigorous research activities are necessary relative to the wind characteristics and aerodynamic response of a structure.

The Honshu-Shikoku Bridge Authority is now conducting a field observation test by using a large scale section model of the beach of Tateyama, located at the south apex of the Boso Peninsula. These tests whould provide us with useful information about the gust response as well as the flutter of a long-span suspension bridge.

ACKNOWLEDGMENT

The authors are indebted to Mr. Y. Kono and Mr. K. Nomura for considerable help in doing numerical calculation.

REFERENCES

1. Davenport, A.G., Application of Statistical Concepts to Wind Loading of Structures, Paper No. 6480, ICE.

2. Davenport, A.G., Buffetting a Suspension Bridge by Storm Winds, ST3, ASCE, June 1962.

3. Hino, M., Relationships Between the Instantaneous Peak Values and the Evaluation Time, N. 117, Trans. of JSCE, May 1965.

Table-1 Hinged suspension bridge model

item	model / unit	L1500	L1300	L1000	L800	L650	L500
span	m	1500	1300	1000	800	650	500
chord distance	m	36	36	33	33	33	33
truss height	m	14	14	11	11	8	8
sag	m	150	130	100	73	59	45
lateral bend. rigidity ($\times 10^{-9}$)	$t \times m^2$	1.266	1.249	0.923	1.012	0.731	0.781
dead weight of truss	t/m	20.28	20,25	19.32	19.66	19.01	19.01
dead weight of cables	t/m	11.40	9.35	7.95	5.57	4.51	3.47

Table-2 Continuous suspension bridge model

item	model / unit	L1100	L890
center span	m	1100	890
side span	m	260	326
chord distance	m	32	34
sag	m	100	82
lateral bend. rigidity ($\times 10^{-9}$)	$t \times m^2$	1.637	2.174
dead weight of trusses	t/m	31.82	44.51
dead weight of cables	t/m	15.91	14.23

Table - 3 Effect of wind characteristics on gust response factor

p	K	k	$BM^{\nu 2}$					$DP^{\nu 2}$				
			0.1	0.2	0.3	0.4	0.5	0.1	0.2	0.3	0.4	0.5
0.1250	0.001	7	1.1811	1.1837	1.1750	1.1668	1.1633	1.1347	1.1333	1.1310	1.1289	1.1280
	0.002		1.2436	1.2497	1.2418	1.2343	1.2314	1.1927	1.1915	1.1893	1.1872	1.1863
	0.003		1.2866	1.2950	1.2879	1.2812	1.2790	1.2333	1.2323	1.2302	1.2281	1.2273
	0.004		1.3203	1.3304	1.3239	1.3179	1.3163	1.2652	1.2643	1.2623	1.2603	1.2594
	0.005		1.3483	1.3599	1.3538	1.3485	1.3474	1.2918	1.2910	1.2890	1.2870	1.2862
0.1429	0.003	7	1.2850	1.2913	1.2813	1.2719	1.2680	1.2235	1.2219	1.2192	1.2166	1.2155
0.1667			1.2781	1.2809	1.2669	1.2540	1.2485	1.2054	1.2031	1.1994	1.1960	1.1946
0.1250	0.003	10	1.2533	1.2608	1.2544	1.2483	1.2463	1.2057	1.2047	1.2029	1.2010	1.2003
		15	1.2179	1.2243	1.2186	1.2134	1.2117	1.1763	1.1754	1.1738	1.1722	1.1766

Table - 4 Instruments at Kanmon Bridge

Observation item	Measuring point	Maximum measuring range	Instruments	Number of instruments	Number of elements		Rate of sampling (freq./sec)
					per M.P.	Total	
Acceleration	Ground	±500 gal	Submerged accelerometer	3	3	9	100
	Abutment	±500	Electro-magnetic accelerometer	4	1	4	50
	Pier	±500		8	1	8	
	Tower	±500		4	1	4	
	Stiffening frame	±200	Servo-accelerometer	6	1	6	25
Displacement	Stiffening frame	Horizontal ±2 m Vertical ±2 m	XY-Analyser	1	3	3	25
		Longitudinal ±25 cm	Differential transducer	1	1	1	25
Wind speed	Stiffening frame	Horizontal 60 m/sec Vertical ±10 m/sec	Supersonic anemometer	1	3	3	25
Wind direction		Horizontal 60 m/sec 540°	Propellar type anemomer	3	2	6	25
Wind speed	Top of Shimonoseki tower	Horizontal 60 m/sec		1	2	2	25
Wind direction		540°					

Table - 5 Wind record at Kanmon Bridge

Wind speed (m/sec)	M.P.	Order of observation			
		1	2	3	4
Mean	A	8.59	8.95	9.36	9.02
	B	9.80	9.99	10.58	10.23
	C	8.88	9.49	9.65	9.99
Maximum	A	10.52	10.75	11.45	11.97
	B	11.93	12.24	12.79	13.63
	C	11.22	11.39	11.38	14.88
Minimum	A	6.21	6.09	7.26	4.25
	B	6.44	5.88	8.39	4.11
	C	6.74	6.97	7.85	5.13
Standard deviation	A	0.85	1.22	1.48	1.97
	B	0.89	1.36	1.66	2.26
	C	1.06	1.42	1.59	2.41

Note M.P. - A the center of the center span

M.P. - B 40 m apart from M.P. - A to Shimonoseki

M.P. - C the quarter point of Shimonoseki side

Table - 6 Natural frequencies and damping capacity of Kanmon Bridge

Mode of vibration	Symmetry	Order	Natural frequency (C/S)			Logarithmic decrement
			Theoretical	Observed (1)	Observed (2)	
Vertical bending	Symmetric	1	0.200	0.212	0.213	0.0313
		2	0.270	0.298	0.296	0.0180
		3	0.429	-	0.450	-
		4	0.528	0.570	0.579	0.0090
		5	0.914	0.918	0.919	0.0087
	Antisymmetric	1	0.152	0.180	0.178	0.0501
		2	0.375	-	0.414	-
		3	0.705	0.740	0.739	0.0125
Torsional	Symmetric	1	0.384	0.387	0.388	0.0129
		2	0.766	0.717	0.721	0.0126
	Antisymmetric	1	0.492	0.472	0.468	0.0162

(Note) Theoretical natural frequencies were calculated by Bleich's method.
Observed (1): field experiment with excitors
Observed (2): wind induced vibration

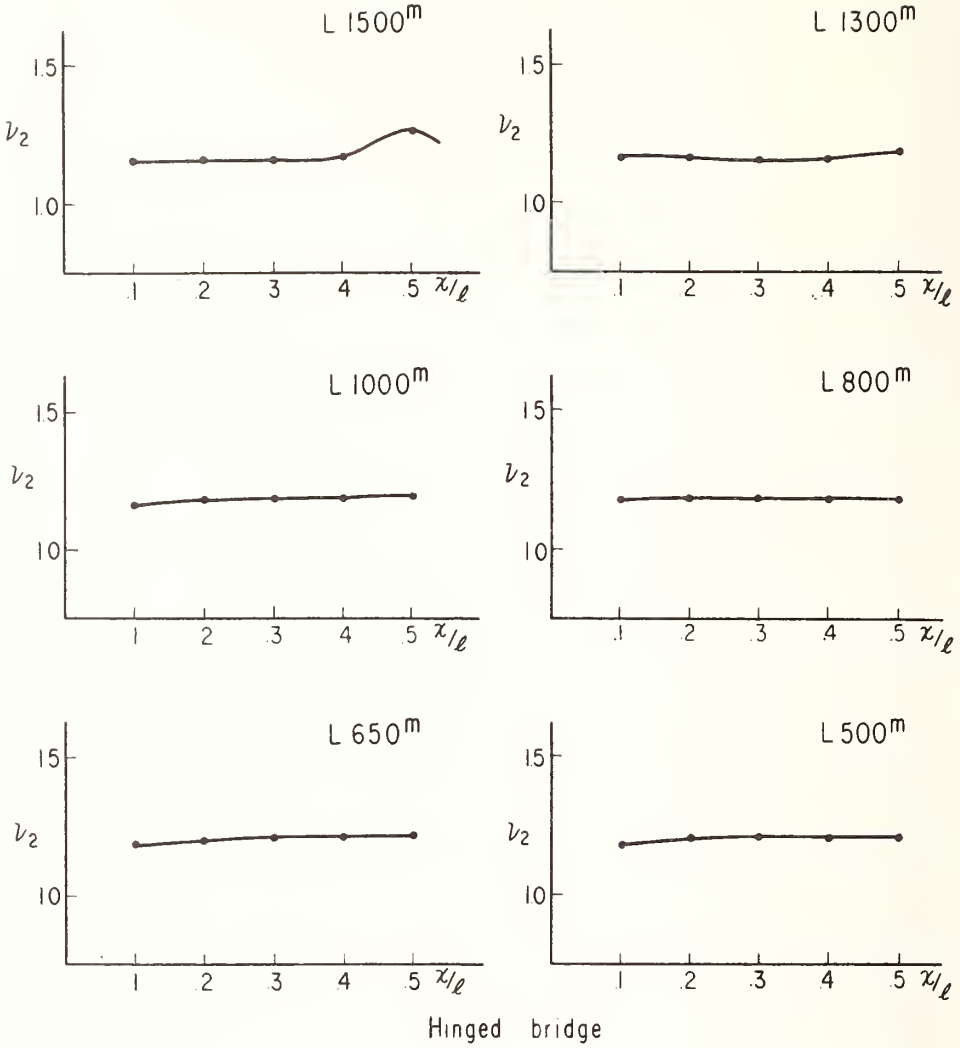

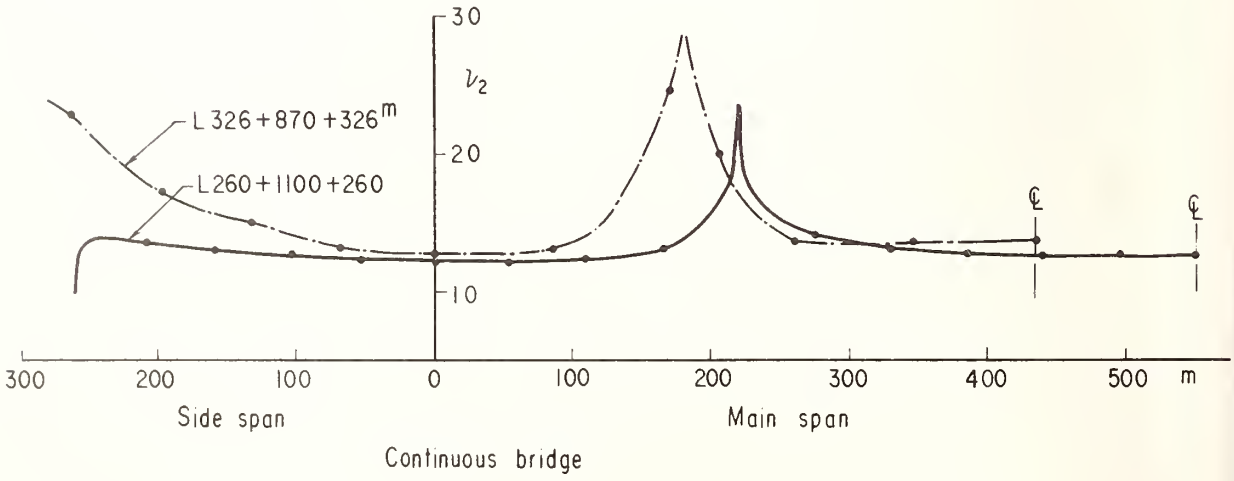

Fig. 1.1 Gust response factor (ν_2)

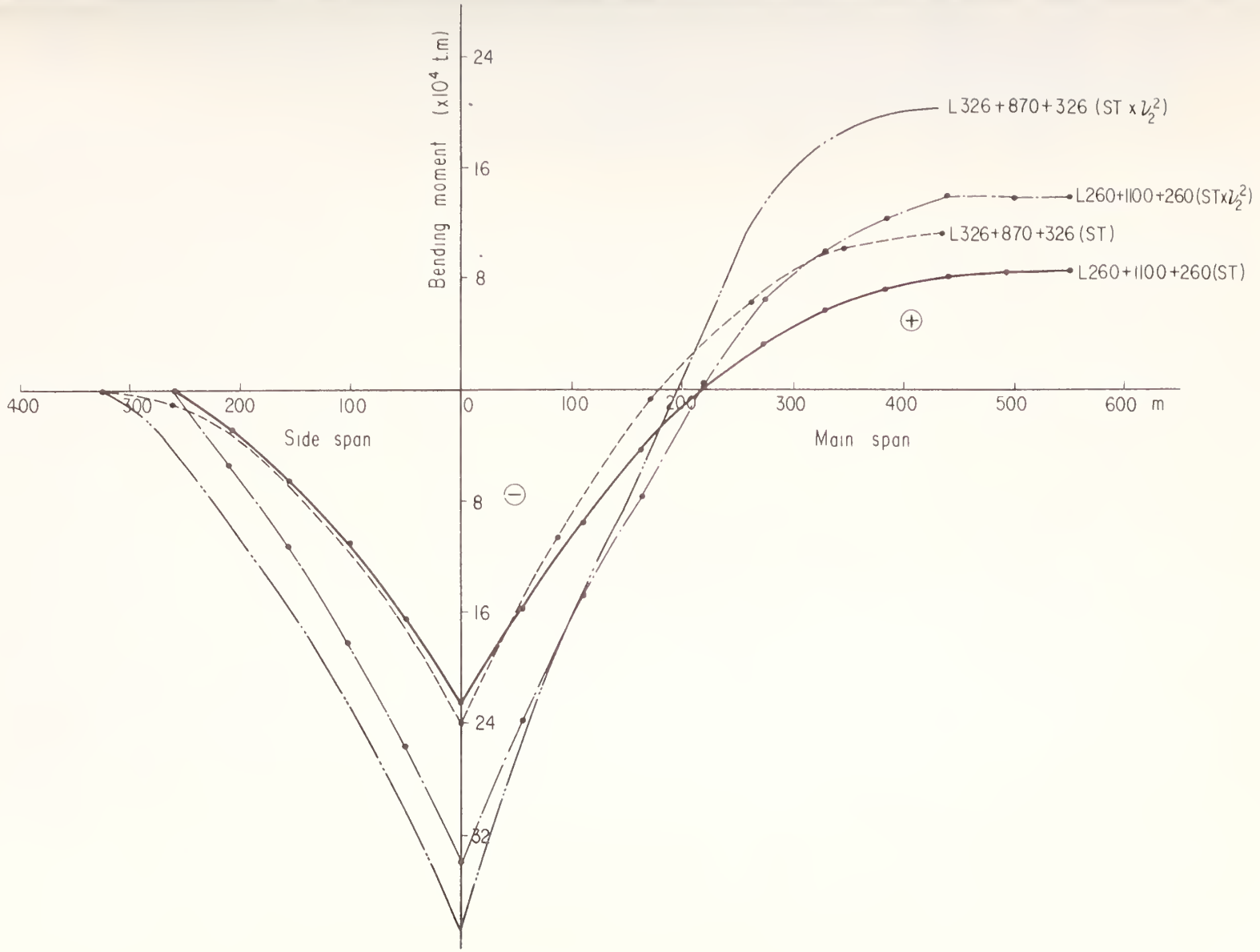

Fig. 1.2 Bending moment

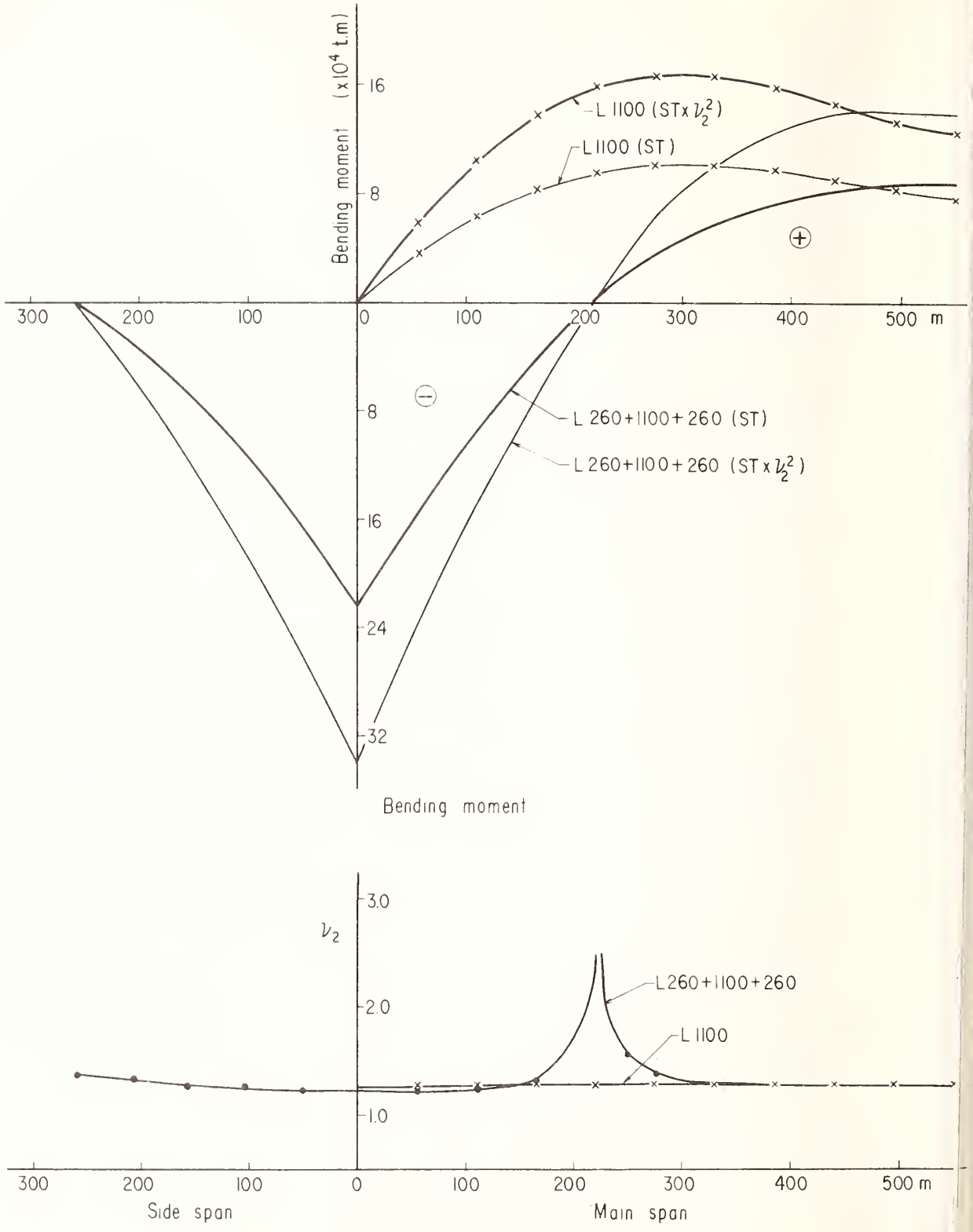

Fig. 1.3 Gust response factor (ν_2)

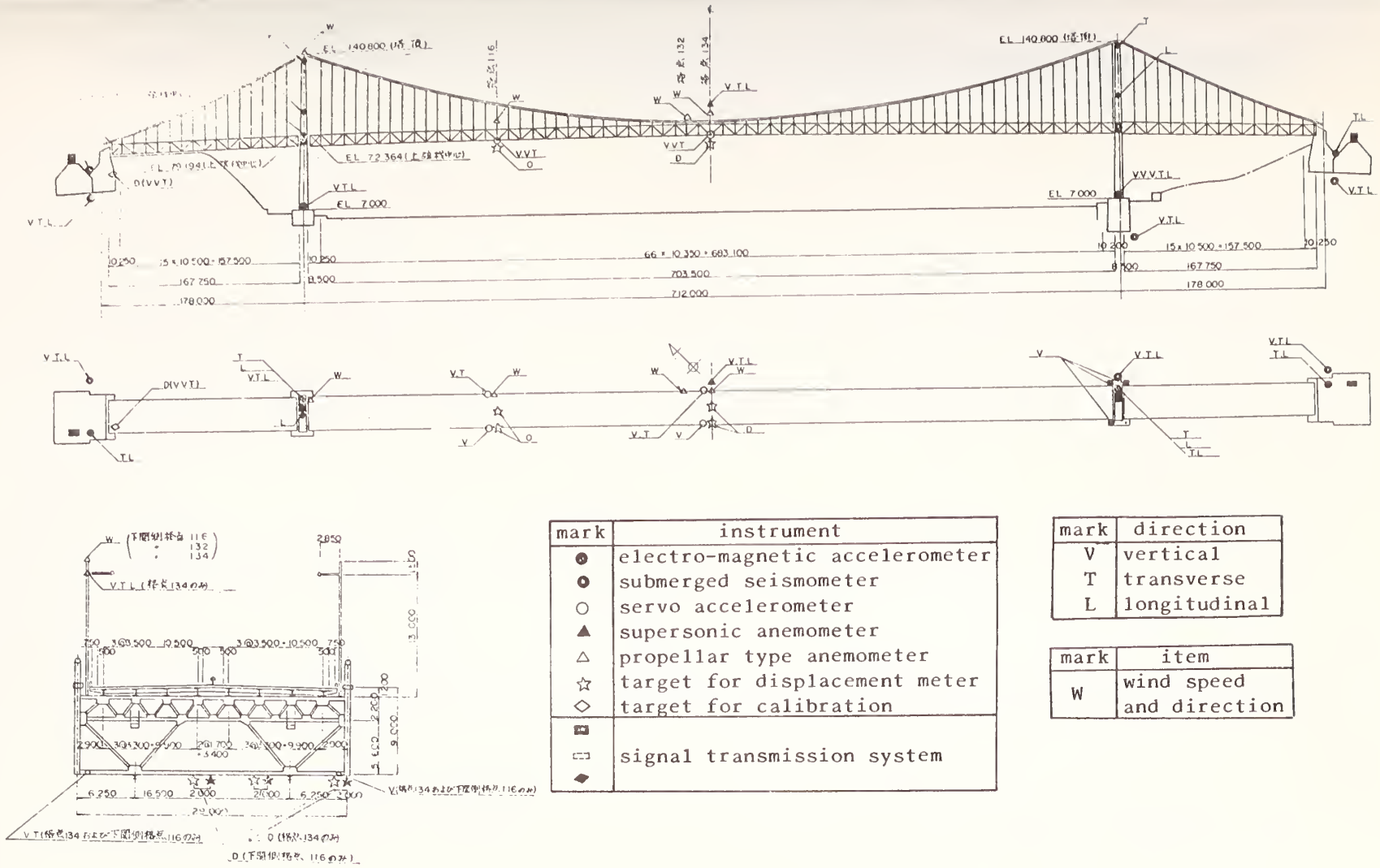

Fig. - 2 Long term observation system of the Kanmon Bridge

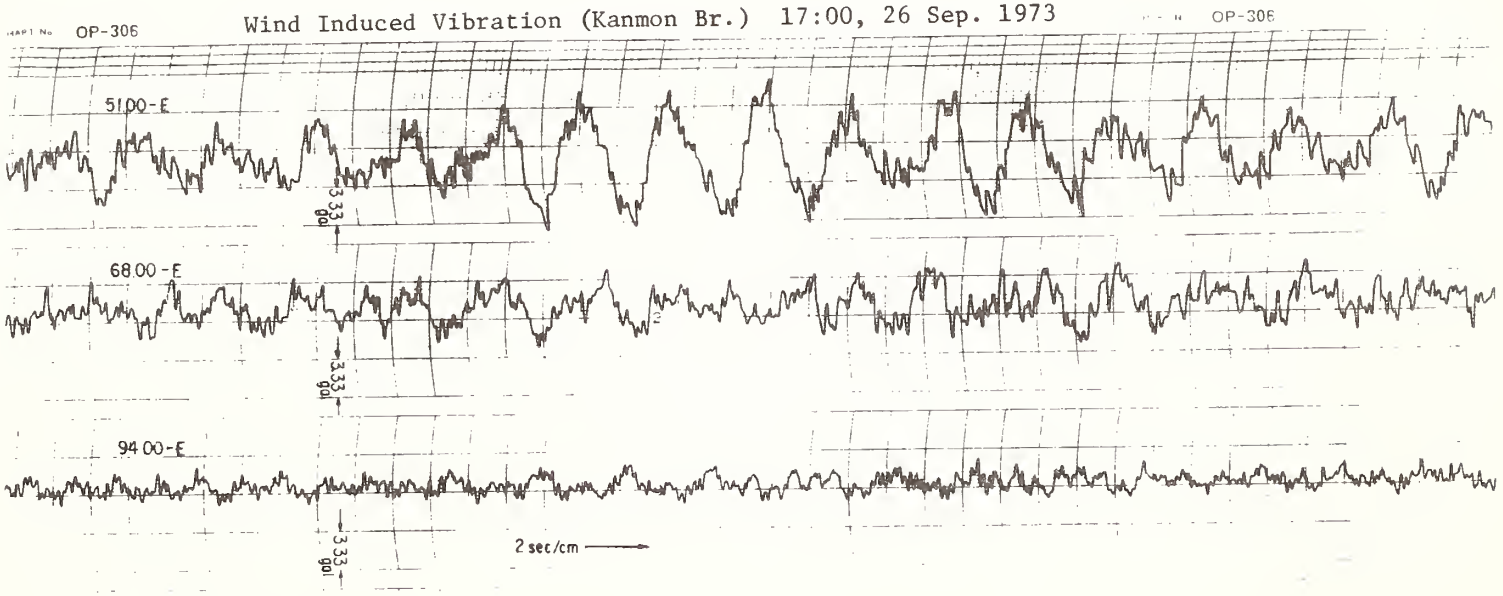
CHART No. OP-306
Wind Induced Vibration (Kanmon Br.) 17:00, 26 Sep. 1973
OP-306
5100-E
3.33 gal
6800-E
3.33 gal
9400-E
3.33 gal
2 sec/cm

(continued)

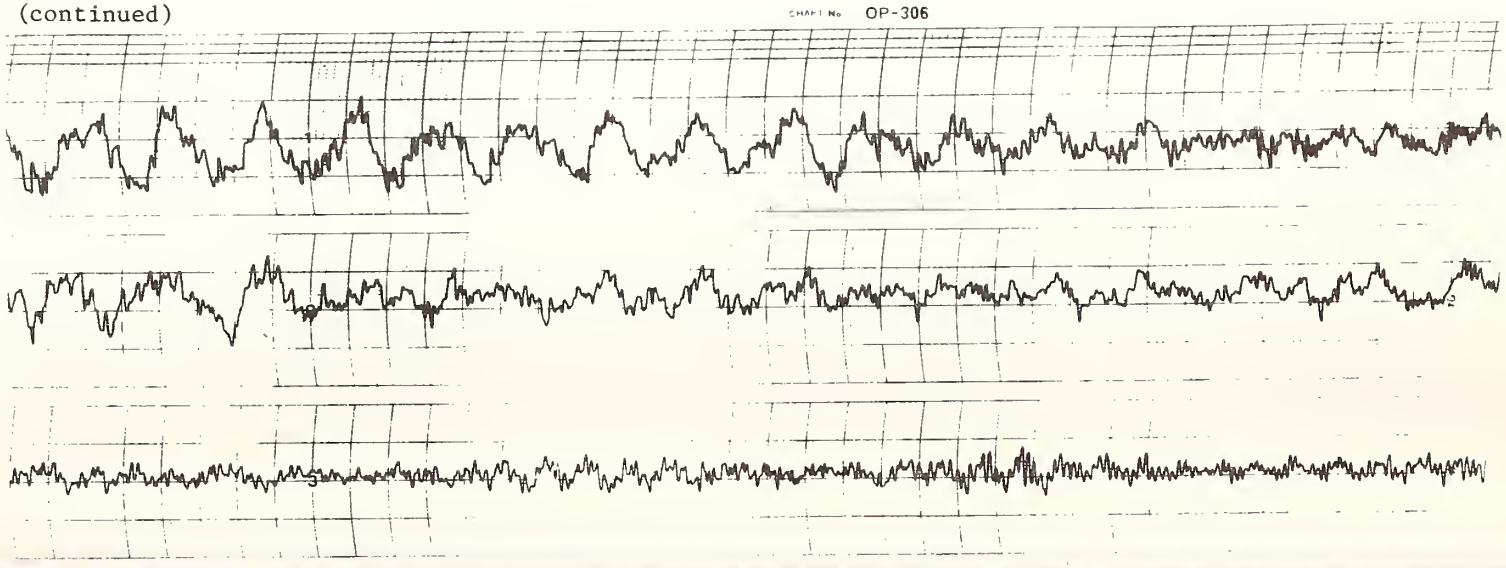
CHART No. OP-306

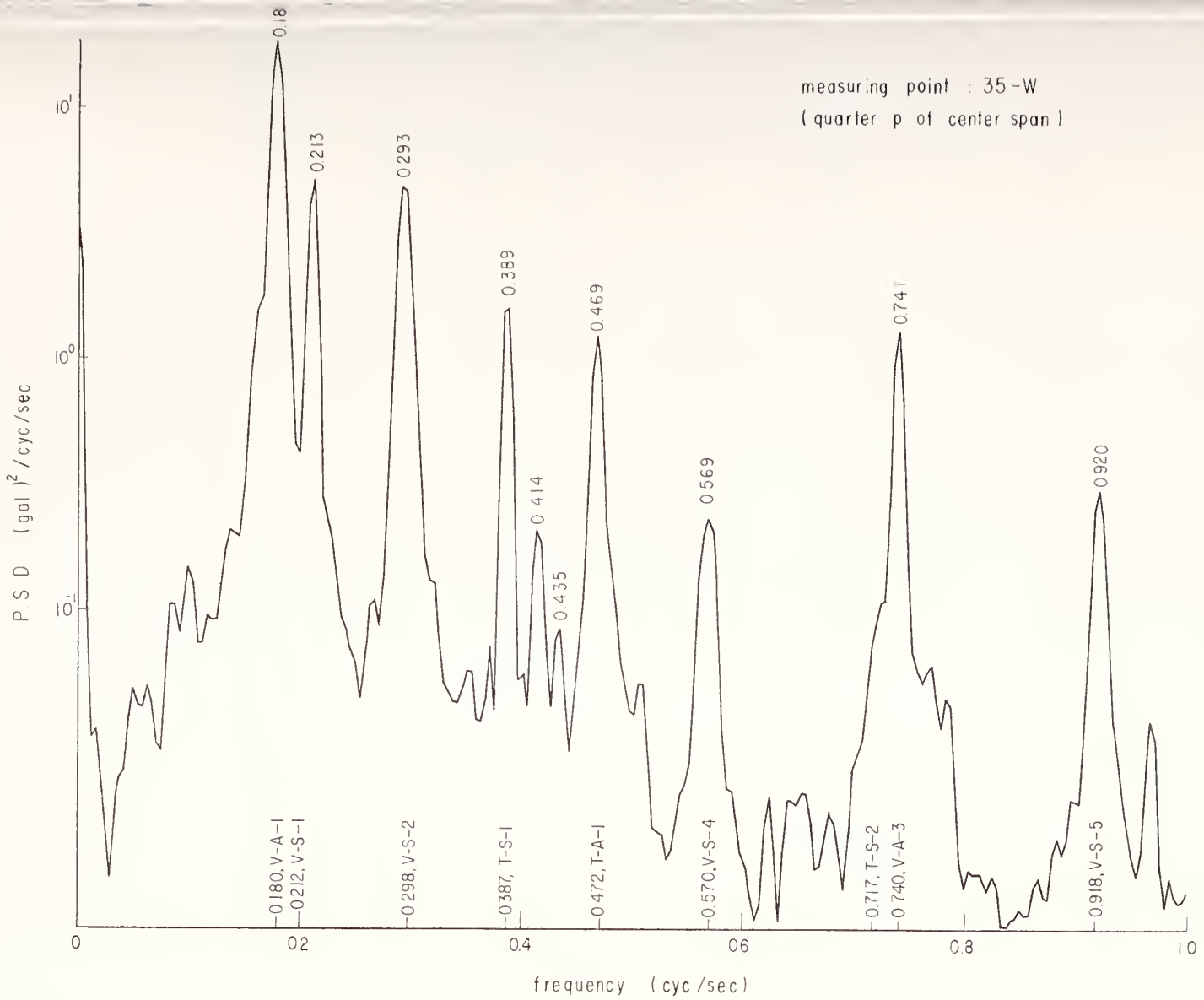

Fig. 4.1 Power spectral density

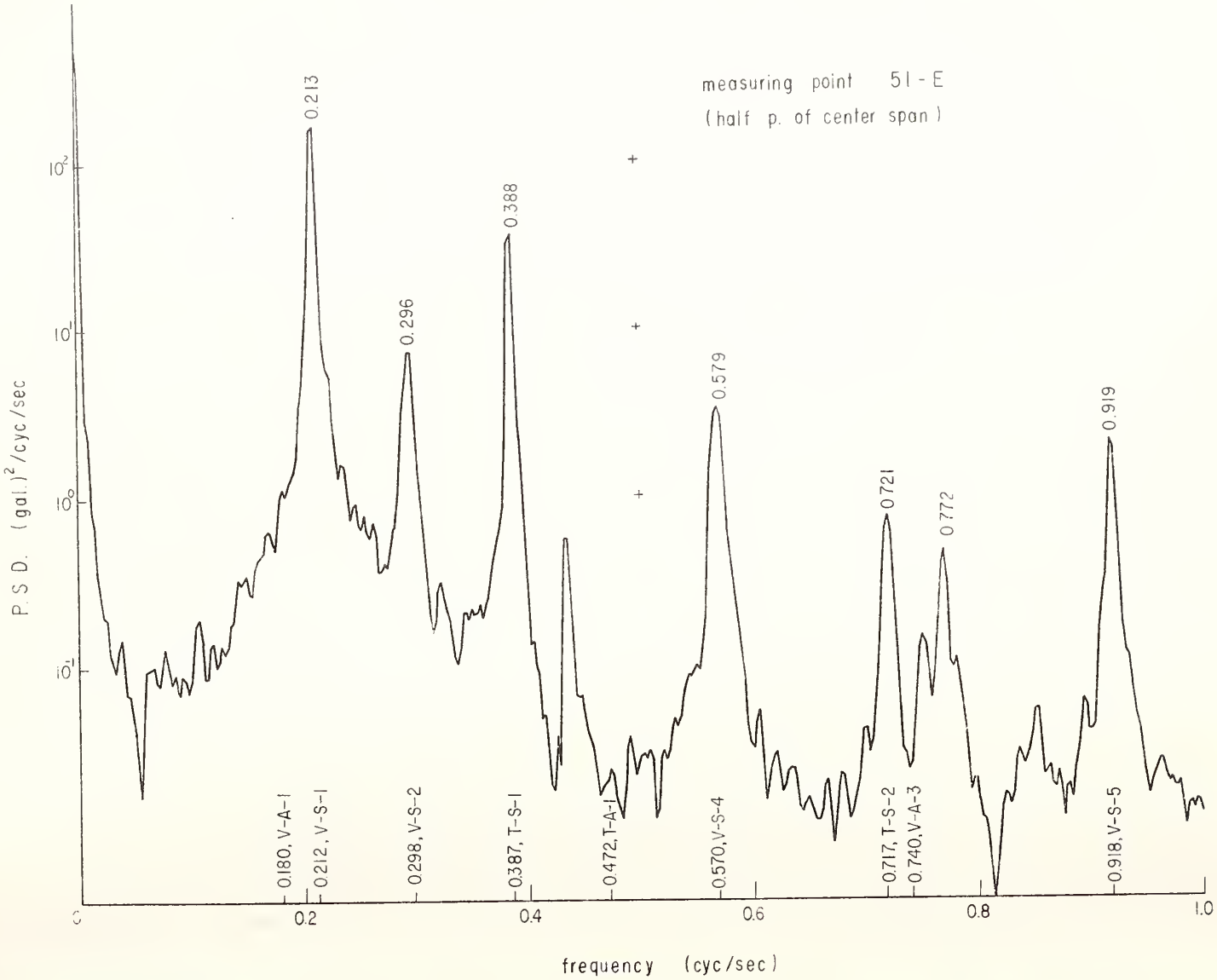

Fig. 4.2 Power spectral density

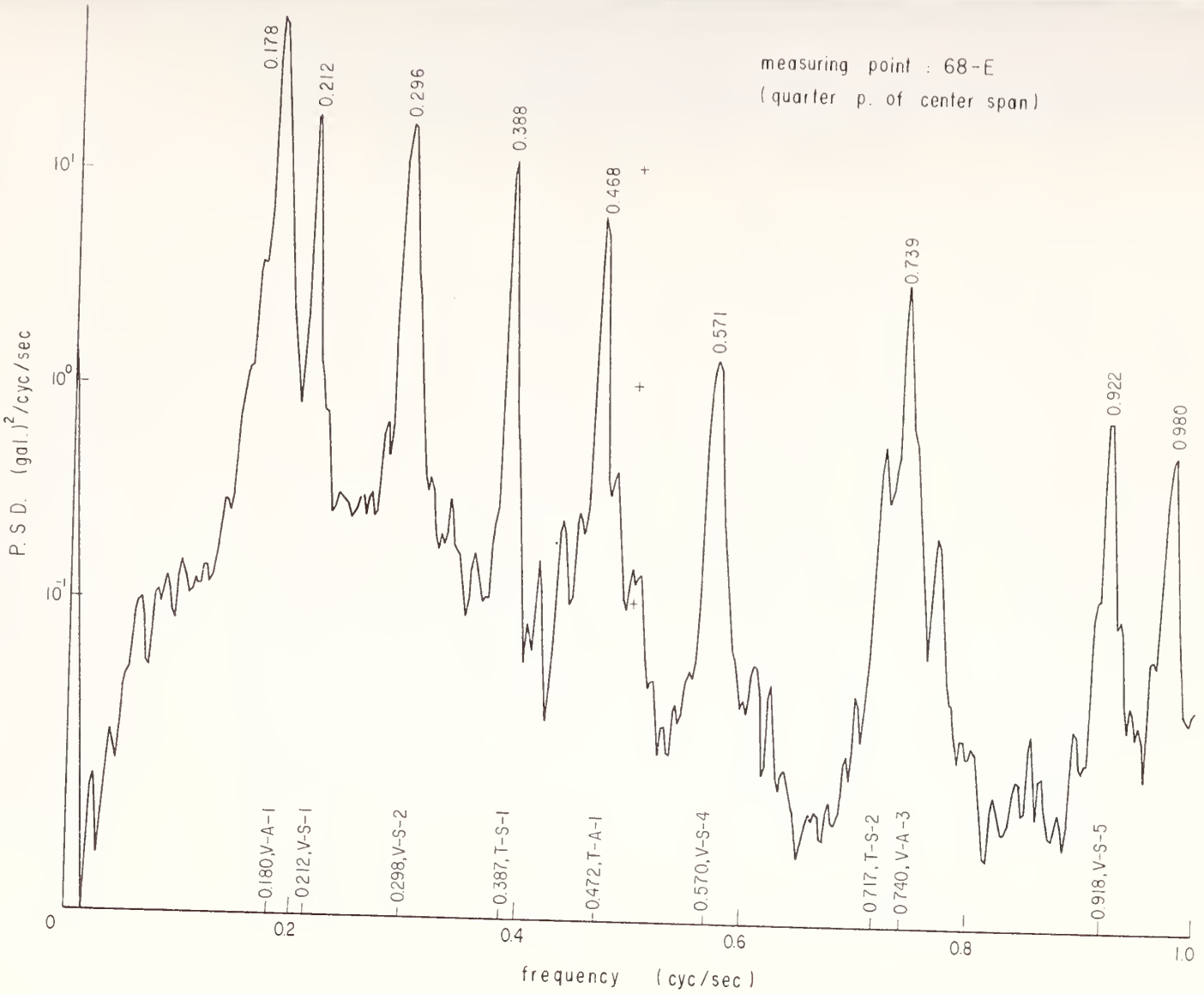

Fig. 4.3 Power spectral density

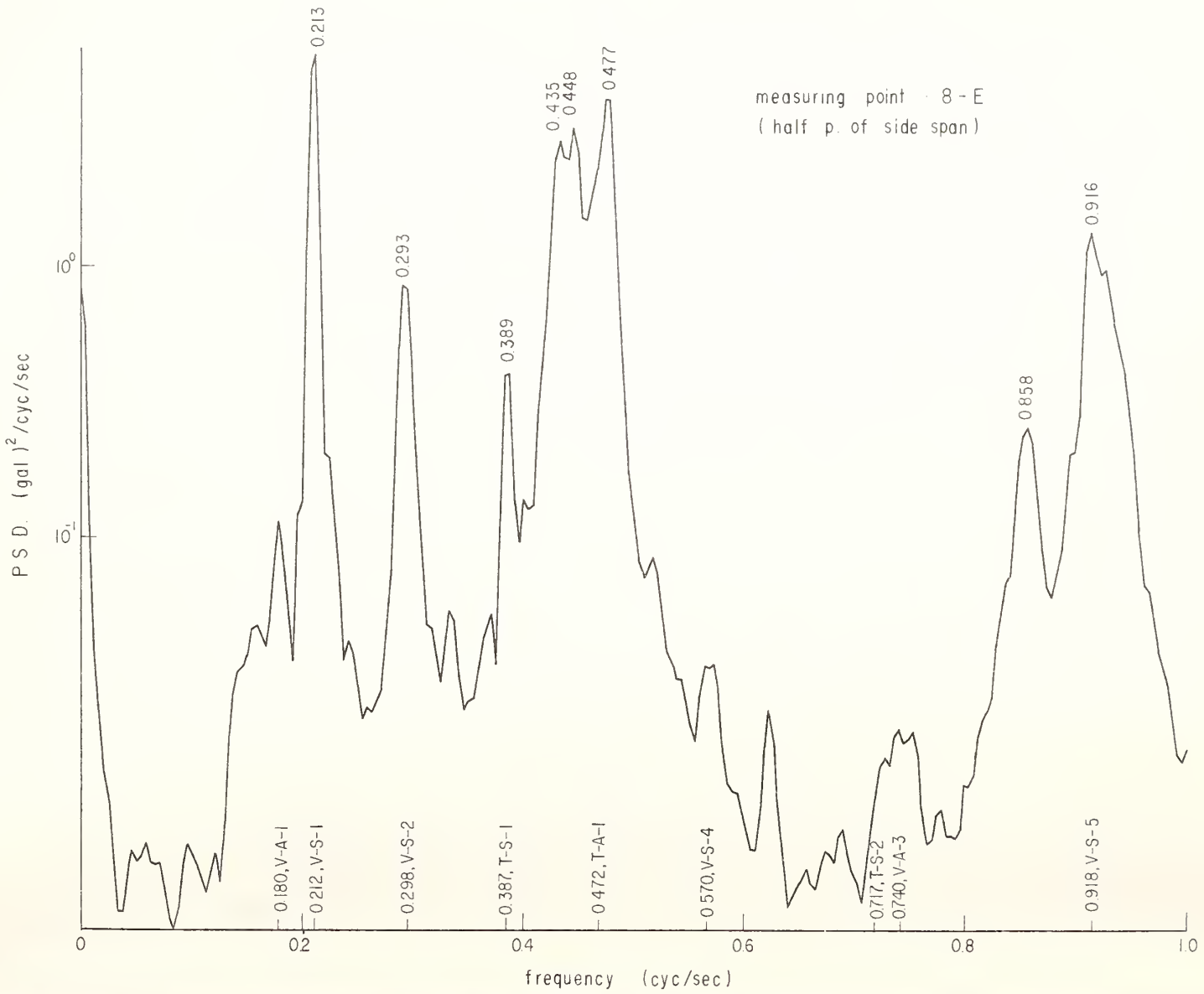

Fig. 4.4 Power spectral density

EXTREME WINDS IN HURRICANES AND POSSIBILITY OF MODIFYING THEM

by

R. Cecil Gentry

National Hurricane Research Laboratory
Weather Modification Program Office
Environmental Research Laboratories
National Oceanic and Atmospheric Administration
Miami, Florida

A hurricane (or similar storm called by other names) is the most destructive of nature's phenomena. This is partly because of the extreme winds associated with the storms (ranging up to 320 kilometers per hour), but also because the winds may continue blowing for several hours, and they are accompanied by rising ocean water, strong along-shore currents, and torrential rains.

Discussions will be presented of the frequency of hurricanes of various intensities, the rate at which the wind speeds decrease after the storm crosses the coast and moves inland, the effect of the winds on the storm surge, and the variation of the wind speed with height.

For several years, members of the United States Government have been experimenting to reduce the maximum intensity of the winds of hurricanes. Summaries will be presented of the progress and future prospects for this work.

Key Words: Cloud seeding; frequency distribution; hurricanes; typhoon; wind; wind intensities.

INTRODUCTION

Hurricanes are the most destructive of natural phenomena. While severe tornadoes may have stronger winds, those in hurricanes last longer and affect much larger areas. In addition, the storm surge, the associated strong coastal currents, and rain-induced floods, all combine with the winds to make the mature tropical cyclone the most dangerous weapon in nature's arsenal.

Because of the great intensity of hurricanes and similar tropical cyclones that go by different names in other parts of the world, the extreme winds experienced at many locations are those that occur in hurricanes. This paper will discuss the maximum winds in hurricanes, gusts associated with these winds, frequency of extreme winds, rates at which the maximum winds decrease as the storm moves inland, variation of wind speed with height, and possibility of moderating the hurricane by seeding the storm.

MAXIMUM WIND SPEEDS IN HURRICANES

It is rare that the maximum wind in a severe hurricane is measured. Rarely is an anemometer installed in the area of maximum hurricane winds, and most of them fail before the winds reach their peak values in the more severe storms. As a result most of our knowledge of the extreme winds is based either on interpretation of wind force from the damage or from knowledge of the pressure gradients in the storms which have a reasonably close relationship to the wind speeds since the two quantities are related physically.

A small but very severe hurricane with minimum pressure at sea level of 26.85 inches (909 mb) crossed the Florida Keys in 1935. Maximum winds were estimated at about 200 mph from the types of damage. Hurricane Camille struck the Mississippi coast in August 1969. The minimum central pressure was 905 mb, or less, shortly before the storm reached the coast. A reconnaissance aircraft measured 140 knots while still several miles from the maximum winds while flying at 3 km elevation before the storm reached land. Again the maximum winds were not measured at a land station, but were estimated at about 200 mph. Hurricane Janet (1955) crossed Swan Island in the Western Caribbean and the winds were estimated at 200 mph. It later struck Chetumal in Mexico where the minimum sea level pressure was 27.00 inches (914 mb). The winds were measured at 152 knots (175 mph) before the anemometer collapsed.

U.S. Air Force Reconnaissance aircraft have measured flight level (3 km) winds at 170 knots (197 mph) in at least three different storms in the Pacific: Typhoon Opal, December 1964, Typhoon Kit, June 1966, and Typhoon Nancy, 1961. The reconnaissance aircraft have also measured minimum sea level pressures of 877 mb in Typhoon Ida, 1958, and Typhoon Nora, 1973. In the Atlantic, the maximum winds measured by the Research Flight Facility were 157 knots (181 mph) in Hurricane Inez, 1966. Comparing the minimum pressure readings recorded in the Atlantic and Pacific would suggest that the extreme maximum winds in the Pacific from typhoons have probably exceeded those in hurricanes in the United States, but the writer has no knowledge of measured values at land stations in the Pacific exceeding the maximum values quoted above.

GUSTS IN HURRICANE WINDS

For certain types of structures the damage caused by winds is more a function of the gusts than of the sustained wind. If our knowledge of the maximum sustained wind (variously defined as the mean for an hour, mean for five minutes, fastest minute or fastest mile) is inadequate, our knowledge of the maximum gusts is even less. Many weather stations are not equipped to measure the short period gusts, and usually estimate the gusts by observing the wind speed dial over a five to ten second period.

The Royal Observatory in Hong Kong has used their recorded data including those measured by a Dines Instrument to derive ratios of winds for various periods to the mean wind for an hour. The data in Table 1 was copied from a report by Faber and Bell (1963).

Hebert and Neumann (1973) have used data reported by weather stations in the United States to also study the gust ratios. They concluded that the ratio varied not only with the period of the wind, but with the speed of the wind. At lower wind speeds they found the ratio of the gust to the sustained wind to be in general agreement with the Hong Kong data, but at the higher wind speeds it was of the order of 1.2. Their data are summarized in Figure 1. The regression line presents an empirical relationship between the steady wind and peak gust based on the available data. The major weakness in their study other than not having a lot of cases is that the term gust and sustained wind are not rigorously defined. Hebert examined the weather reports received from stations experiencing tropical cyclones during the years 1963-1970. In most cases the sustained wind would be either the fastest minute or the fastest mile. The gust in a few cases may have been measured with some special instrument, but in most cases would have been estimated by the observer after examining a recording of the anemometer output or after observing the wind speed dial readings for a few seconds.

EXTREME WIND FREQUENCIES IN HURRICANES

The frequency of extreme winds such as those described in the earlier paragraphs is, of course, very low. The data in Figure 2* give an idea how often winds of certain broad categories may occur in the United States. The number in the "A", "B" and "C" belts tell how many years during the period 1901-1965 a storm of the respective categories affected the various sectors of the United States Coastline. Hurricanes with a minimum central pressure of 29.00 inches (982 mb) include the storms whose maximum winds usually exceed 85 mph (38 mps) and whose maximum storm surge usually exceed 6 feet (1.8 m) in height. Hurricanes with a minimum central pressure less than 28.25 inches (957 mb) include the very intense hurricanes in which the maximum height of the storm surge will be 10 to 15 feet (3 to 4.7 m) or more above mean sea level in the sectors illustrated, and in which the maximum wind velocities will exceed 120 mph (54 mps).

The general subject of recurrence of extreme winds has been studied by Thom (1960). Figure 3 is reproduced from his report and shows the annual extreme-mile 30 feet (9.1 m) above ground, 50-year mean recurrence interval. His report includes similar charts for varying mean recurrence intervals. In his data the extreme winds along the Gulf of Mexico and Atlantic Coasts are in most cases from hurricanes.

REDUCTION IN HURRICANE WIND SPEEDS AS STORM MOVES INLAND

The hurricane wind speeds start decreasing soon after the storm crosses the coastline. The phenomena has been studied extensively by Malkin (1959) and by Goldman and Ushijima (1974). Figure 4 is copied from the later report and it includes the summary gust factors developed by Malkin. The Goldman and Ushijima report includes graphs similar to Figure 4 for two other storms. There is, as should be expected, some variation from storm to storm, and from one locale to another. The heavy broken arrow in Figure 4 shows the track of Hurricane Camille, 1969. The numbers written on the horizontal lines show the percent of peak gusts at landfall at the respective locations. The "Malkin's Factors" listed at the left end of each line are from Malkin's study.

Goldman and Ushijima summarize the results by writing, "The decrease in maximum hurricane winds after landfall has been shown to be both appreciable and variable. When compared with the earlier work, the maximums in the peak gusts of the three significant storms are in strong agreement with the general function of Malkin. However, the change in the two-dimensional distributions of peak gusts inland reveals that a more complicated function than Malkin's is necessary ...." The Goldman and Ushijima study showed considerable variation in gust factors between storms, so more studies are needed.

* Prepared by Gentry (1966) and adapted from an earlier chart prepared by U.S. Weather Bureau (1957).

VARIATION OF HURRICANE WIND SPEEDS WITH HEIGHT

The wind speeds in hurricanes vary with height. Within a millimeter of the ground the wind is blowing very slowly--even in a hurricane. The speeds increase with height up to some unknown but variable level which is believed to be between 300 and 1500 feet (90-460 m). Above that level the winds in the belt of maximum winds for the storm decrease very slowly up to six kilometers where the sustained winds are normally only 10 percent less than at low levels according to a study by Hawkins (1962).

Very little well documented data are available showing how the winds in hurricanes vary from 10 meters up to 100 meters. Various assumptions have been used by engineers and it is well known that the variation is a function of the roughness of the terrain.

POSSIBILITY OF MODIFYING HURRICANES

During the past ten years the average annual damage caused by hurricanes in the United States has been about $450,000,000 per year not including the damage from Hurricane Agnes, 1972, which was largely from rain-induced floods. Because of this and because research over the last decade has suggested means by which hurricanes might be modified, there is extensive research and experiments to modify hurricanes.

The principal damages from hurricanes can be attributed to three causes: (1) destructive force of the wind, (2) the storm surge, and (3) floods caused by hurricane rains. Results from the modification experiments conducted thus far and the supporting research suggest that the maximum winds in hurricanes may be reduced 10 to 15 percent if the hurricane clouds radially outward from the maximum winds are seeded with freezing nuclei. Since the force of the winds varies with the square of the wind speed, this could mean a reduction of 20 to 30 percent in the force of the wind and in damages caused by the winds. The storm surge is the result of complex interactions of a number of forces including the wind. More research is needed in this area, but there are reasons to believe that a reduction of maximum winds will also often result in a reduction of the storm surge. The rain-inducted floods will probably be little affected by the experiments.

Table 2 summarizes the results of previous experiments to modify hurricanes.

The only multiple seedings of the clouds near the eyewall made so far were in Hurricane Debbie. Gentry (1970) has reported the results.

The storm was seeded 18 August 1969 five times during a period of 8 hours. Before the first seeding the maximum winds were 98 knots (Figure 5). After the third seeding the maximum winds were considerably reduced, and by about 5 hours after the last seeding the maximum winds were down to 68 knots, which is a reduction of about 31 percent.

The crews rested on 19 August, and by 20 August Debbie had regained intensity. At the beginning of operations on 20 August, the maximum winds were 99 knots, but the storm structure had changed considerably. The inner maximum was about 10 nautical miles from the center and the outer maximum was approximately 20 nautical miles (Figure 6). The hypothesis requires that seeding be radially outward from the maximum winds. In this case it would mean starting the seeding runs at about 12 nautical miles and proceeding outward for about 20 more nautical miles. If the hypothesis is correct, this should result in a reduction in the maximum winds in the inner maximum, but an increase in the outer maximum. This is precisely what happened. The inner maximum decreased radically during the day and the outer maximum increased slightly. The fifth and last seeding started at about 20 nautical mile radius and proceeded outward; that is, it was radially outward from the outer wind maximum. The winds in the outer maximum then decreased and by about 6 hours after the fifth seeding the maximum winds were 85 knots, which is a reduction of 15 percent for the day.

The changes in the storm following the seedings on 18 and 20 August are very encouraging and are highly suggestive that the storm was modified. The natural variability of

hurricanes is such, however, that we cannot be sure that the changes observed were caused by the seeding.

Figure 7 shows the frequency distribution of 12-hour changes in maximum wind speeds in hurricanes (see Sheets, 1970). The changes are expressed in percent. See the horizontal axis. The data have been stratified according to the original intensity of the storm. Notice that even a reduction of 15 percent is a very rare event for any of the categories.

We have examined the weather maps for 18 and 20 August and have sought other explanations for the reduction in the maximum winds. On 18 August there was a trough in the upper troposphere moving eastward at more northernly latitudes which probably did affect Debbie and may have caused part of its weakening. This would suggest, therefore, that the 30 percent reduction should not be attributed entirely to the affects of the seeding.

If one considers the full sequence of events for the Hurricane Debbie case, however, one cannot help but be impressed by the results. On 18 August the storm was seeded five times, and the maximum winds were reduced about 30 percent. On 19 August there was no seeding and the storm reintensified. On 20 August the storm was seeded 4 times in such a fashion as to cause reduced winds at the inner maximum and it essentially disappeared. The fifth seeding was in such a fashion as to cause reduced winds in the outer maximum and a net reduction of 15 percent resulted. In view of the probabilities expressed in the frequency diagram, it is clear that such a sequence of natural events would be very rare.

The data from the experiments, and especially when backed up by calculations with the theoretical models, are highly suggestive that we do have an excellent chance of achieving beneficial modification of hurricanes to the extent of reducing the maximum winds by 10 to 15 percent. Since the force of the wind varies with the square of the wind speed, a reduction of 10 to 15 percent of maximum wind speed would mean a reduction of 20 to 30 percent in the maximum force exerted by the hurricane. If damages can be reduced by this much, it means savings of about $100 million per year for the United States alone.

REFERENCES

1. Faber, S.E. and G.J. Bell, 1963: Typhoons in Hong Kong and Building Design, The Engineering Society of Hong Kong, 29 pp.

2. Gentry, R. Cecil, 1966: Nature and Scope of Hurricane Damage. Hurricane Symposium, October 10-11, 1966, American Society for Oceanographers, Houston, Texas, pp. 229-253.

3. Gentry, R. Cecil, 1970: Hurricane Debbie Modification Experiments. Science, 168, pp. 473-475.

4. Goldman, Joseph L. and Toshimitsu Ushijima, 1974: Decrease in Hurricane Winds after Landfall. Journal of the Structural Division, Proceedings of the American Society of Civil Engineers, 100, No. ST1, January 1974, pp. 129-141.

5. Hawkins, H.F., 1962: Vertical Wind Profiles in Hurricanes. National Hurricane Research Project Report No. 55, U.S. Weather Bureau, Washington, D.C., 16 pp.

6. Hebert, Paul and Charles Neumann, 1973: A Comparison of Gusts and Sustained Winds in Hurricanes. Unpublished Manuscript of National Hurricane Center, Miami, Florida, 3 pp.

7. Malkin, William, 1959: Filling and Intensity Changes in Hurricanes Over Land. National Hurricane Research Project Report No. 34, U.S. Weather Bureau, Washington, D.C., 18 pp.

8. Sheets, Robert C., 1970: Application of Bayesian Statistics for Stormfury Results. Project STORMFURY Annual Report, 1969, Appendix H. U.S. Department of the Navy and U.S. Department of Commerce. pp. H 1-16.

9. Thom, H.C.S., 1960: Distributions of Exteme Winds in the United States. Journal of the Structural Division, Proceedings of the American Society of Civil Engineers, 86, No. ST4, April 1960, pp. 11-24.

10. U.S. Weather Bureau, 1957: Survey of Meteorological Factors Pertinent to Reduction of Loss of Life and Property in Hurricane Situations. National Hurricane Research Report No. 5. U.S. Weather Bureau, p. 21.

TABLE 1

RATIO OF WINDS OF VARIOUS PERIODS TO HOURLY MEAN WIND
(Data from Royal Observatory in Hong Kong)

Period of Wind	600 sec	300 sec	60 sec	30 sec	10 sec	5 sec	3 sec	Dines Gust
Ratio to Hourly Mean	1.05	1.09	1.28	1.42	1.64	1.72	1.81	2.05

TABLE 2

RESULTS OF EXPERIMENTS IN SEEDING HURRICANE CLOUDS
NEAR THE EYEWALL

Name	Date	Number of Seedings	Approximate Maximum Wind Speed Change (Percent)
Hurricane Esther	16 September 1961	1	-10
Hurricane Esther	17 September 1961	1	0*
Hurricane Beulah	23 August 1963	1	0*
Hurricane Beulah	24 August 1963	1	-14
Hurricane Debbie	18 August 1969	5	-30
Hurricane Debbie	20 August 1969	5	-15

*Seeding material dropped outside "seedable" clouds.

(In addition, a hurricane was seeded 13 October 1947 and Hurricane Ginger was seeded 26 and 28 September 1971. The clouds seeded in these storms were far removed from the central core of the storm and had only weak or no vertical currents. Their seeding, therefore, should not have caused much change in the storm's intensity or structure.)

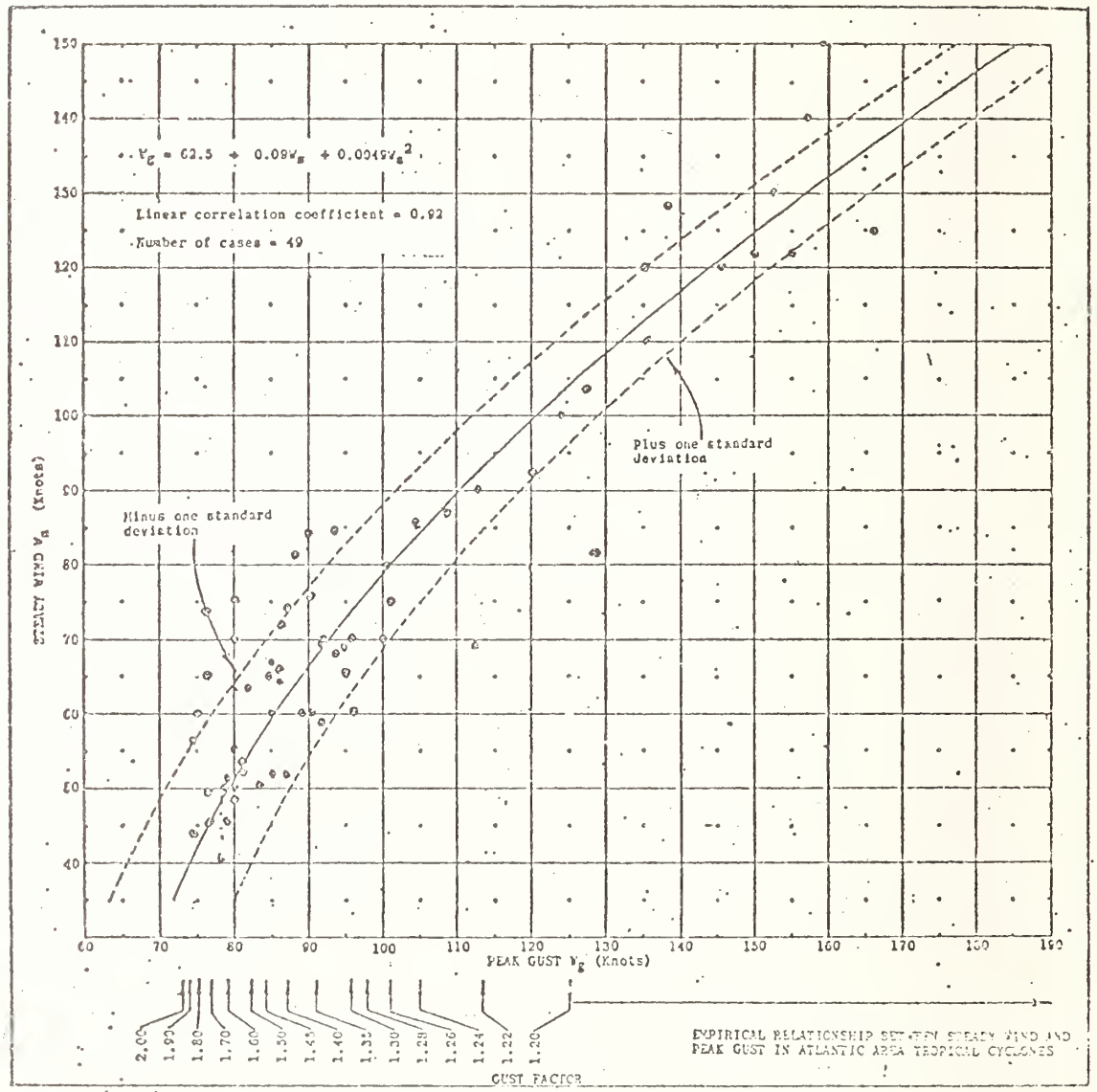

Figure 1. Empirical Relationships Between Steady Wind and Peak GUST in Atlantic Area Tropical Cyclones. Dots are data points. Solid line is regression line drawn to fit the data. (Prepared by Hebert and Neumann, 1973.)

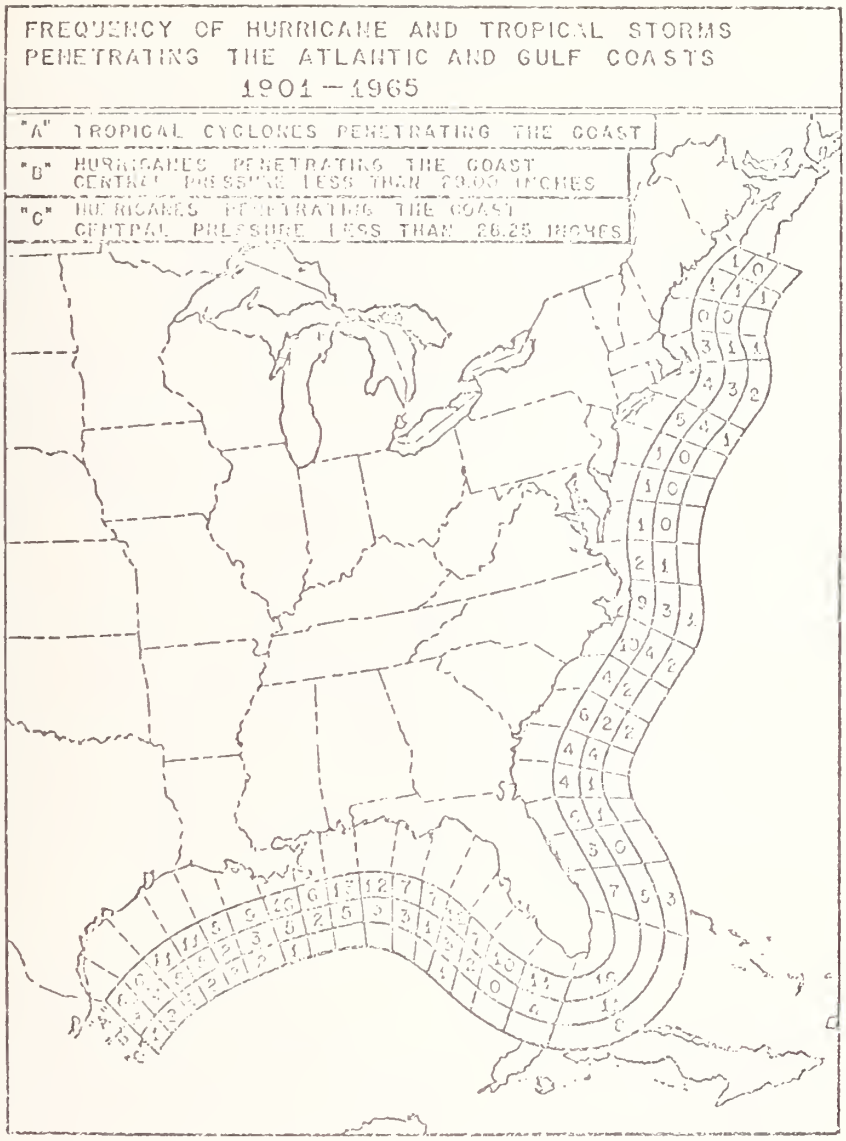

Figure 2. Frequency of hurricanes and tropical storms penetrating the United States coasts along the Atlantic and the Gulf of Mexico. (Gentry, 1966)

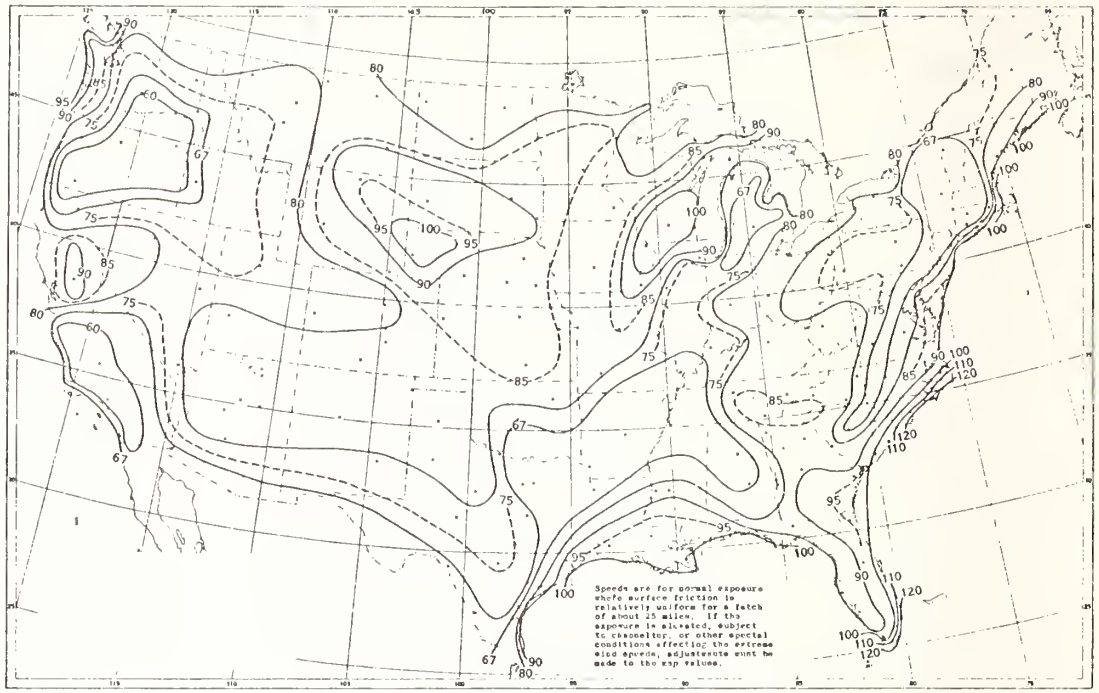

Figure 3. Isotach 0.02 Quantiles, in Miles Per Hour. Annual Extreme-Mile 30 Ft. Above Ground, 50-Yr. Mean Recurrence Interval. (Thom, 1960)

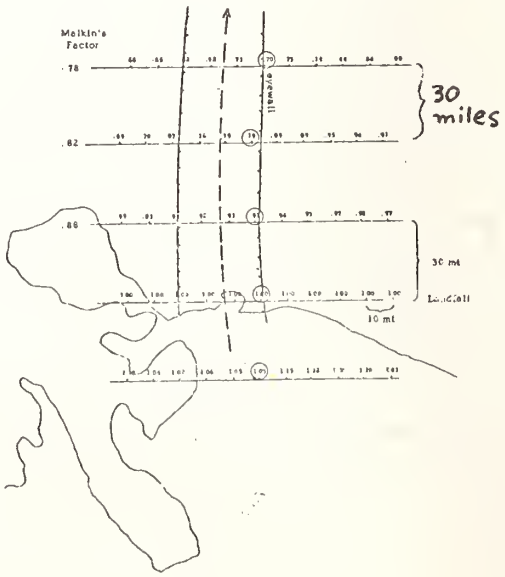

Figure 4. Percent of Peak Gusts at Landfall for Camille at 30-mile Intervals after Landfall (10-mile (16.1 km) increments from maximum are computed at each inland line. Circled values are maximum at each time.) (Goldman and Ushijima, 1974)

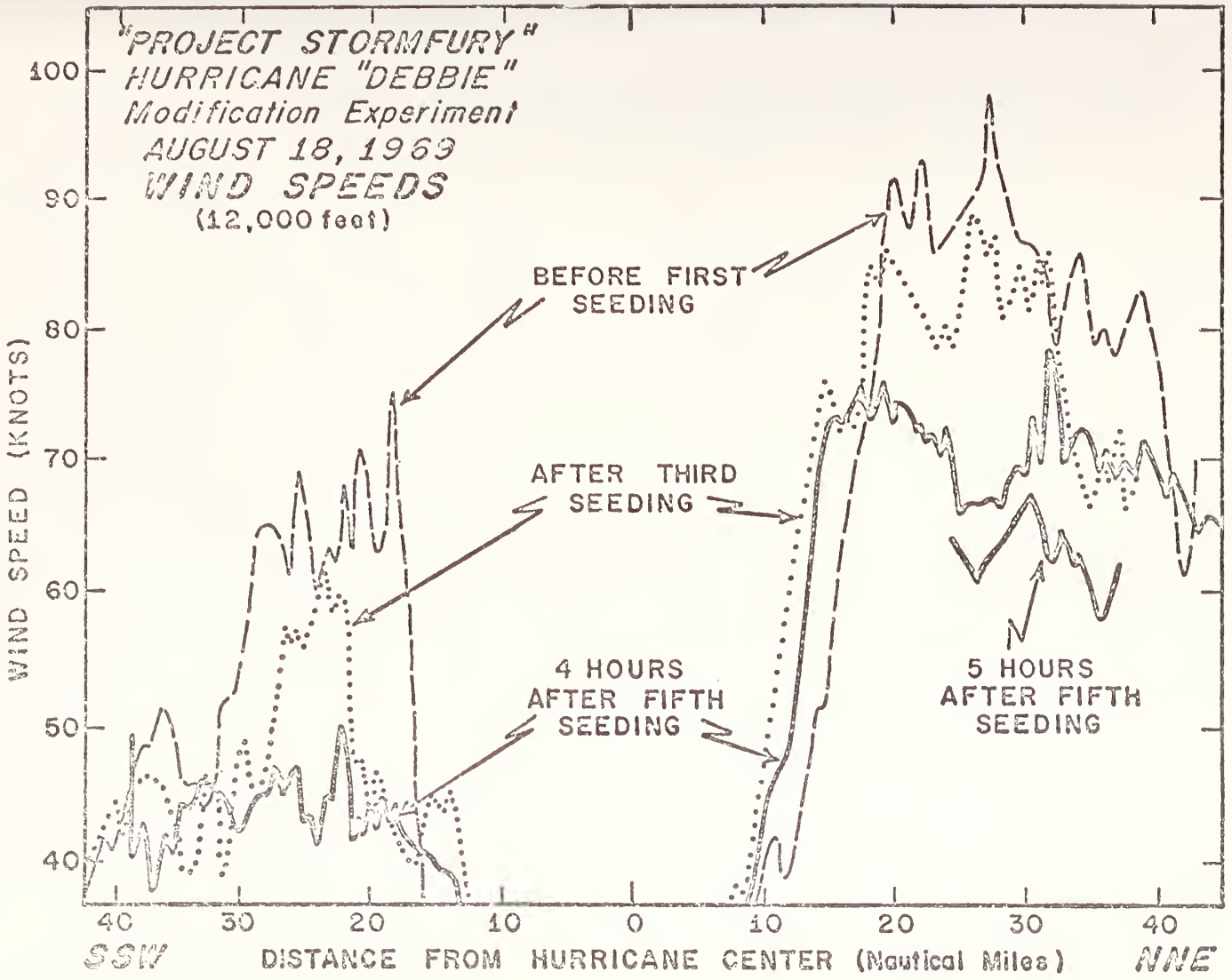

Figure 5. Wind Speed Changes in Hurricane Debbie, August 18, 1969. (Gentry, 1970)

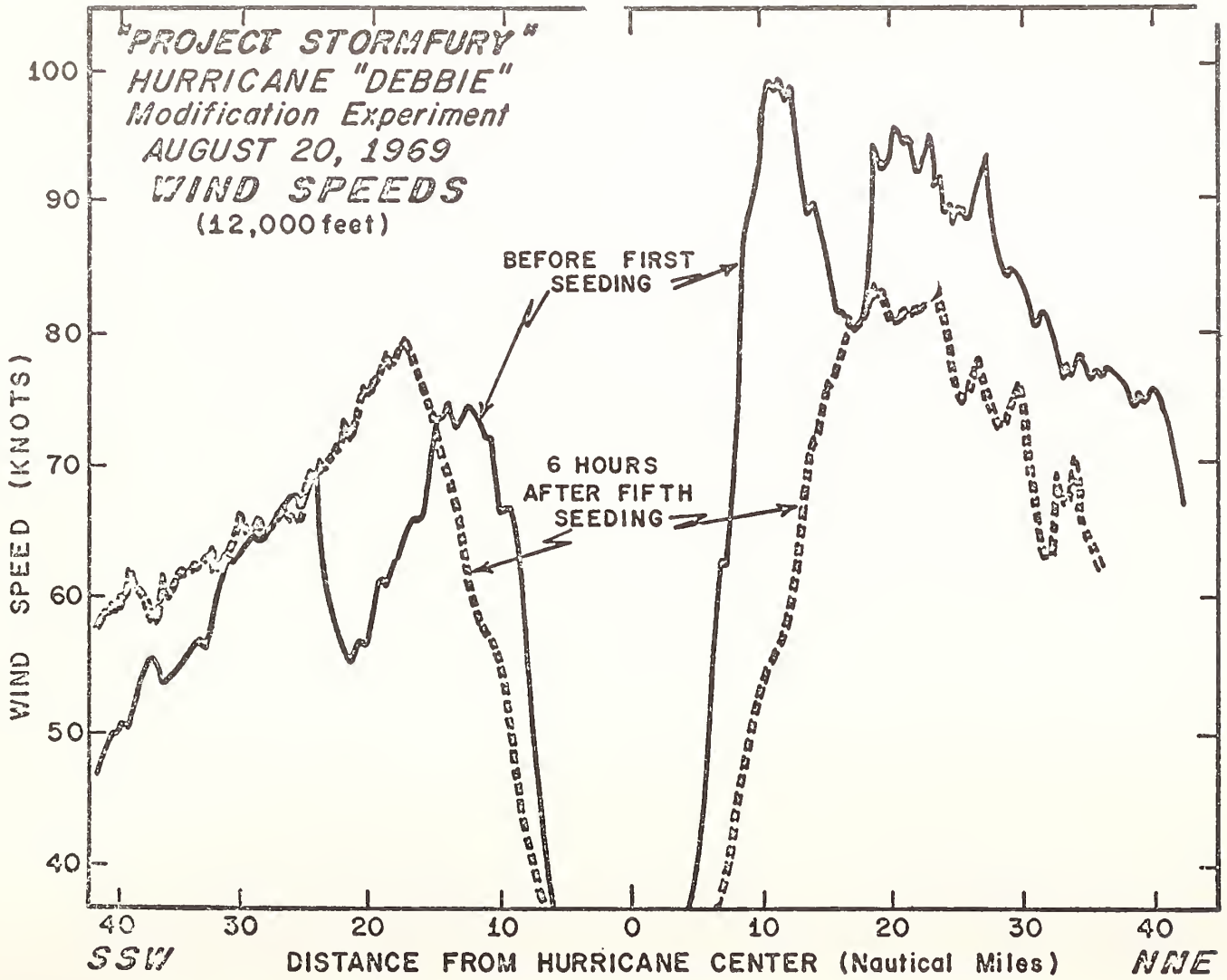

Figure 6. Wind Speed Changes in Hurricane Debbie, August 20, 1969. (Gentry, 1970)

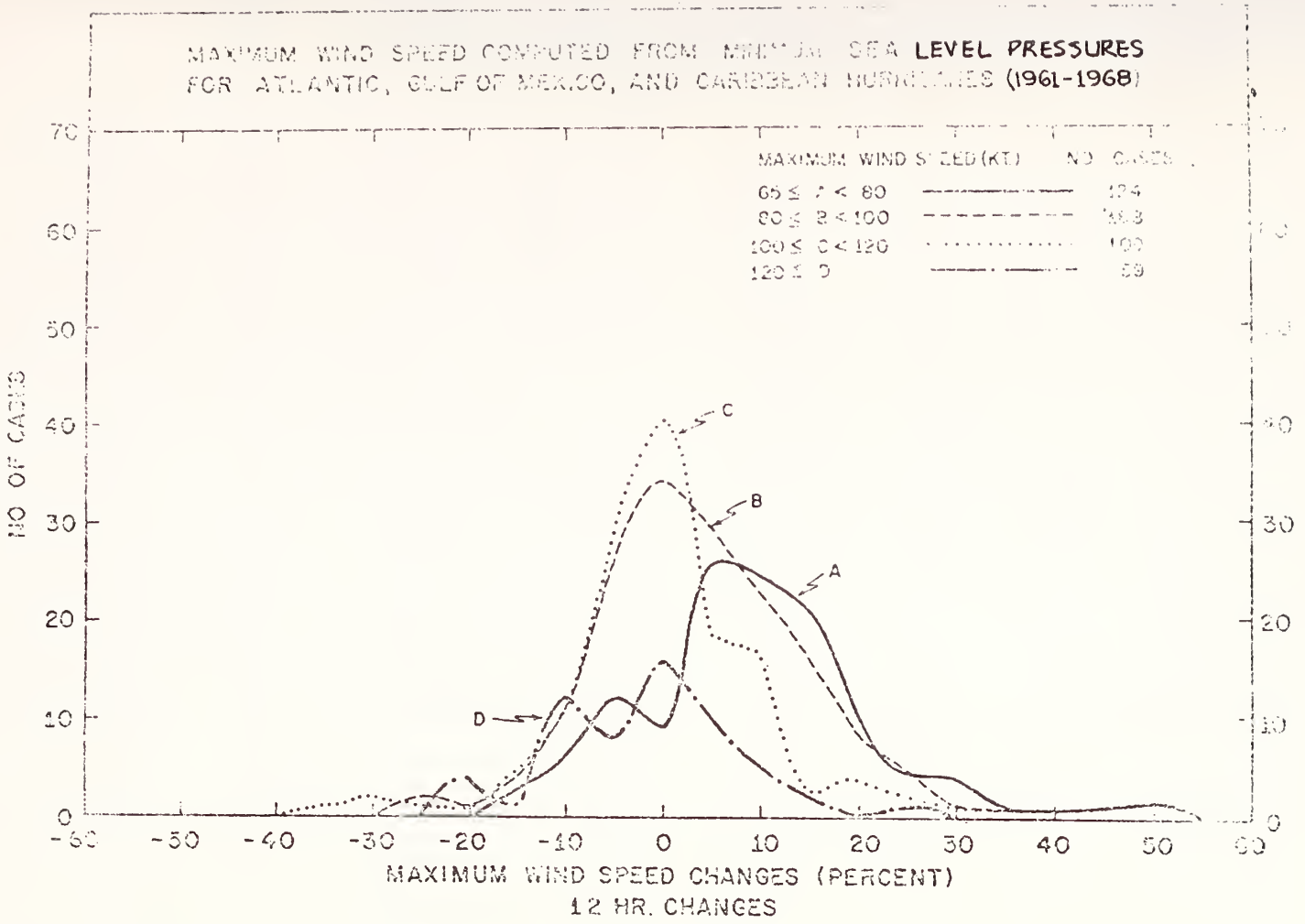

Figure 7. Frequency diagram for Wind Speed Changes. (Sheets, 1970)

EXTREME WINDS IN THE UNITED STATES

by

Arnold R. Hull
and
Patrick E. Hughes

Environmental Data Service
National Oceanic and Atmospheric Administration
U.S. Department of Commerce

The highest winds reported in the United States have been associated with tornadoes. Fujita (1971) has developed a tornado windspeed/damage classification system which permits extreme wind estimations without follow-up surveys. Fujita classifications of tornadoes for the 1965, 1971, and 1972 seasons, as well as extreme wind values associated with thunderstorms and extratropical cyclones during 1973 are reviewed as they relate to ANSI building code requirements for design loads. Next, a new observational tool, an acoustic, doppler-shift "sonar" capable of profiling low-level wind regimes at the actual building site, is briefly described. Finally, the proposed NOAA Severe Environmental Storms and Mesoscale Experiment (SESAME) is examined. SESAME is an observational/research effort to identify the processes and controlling parameters of extreme-wind generating severe weather systems such as squall lines, thunderstorms, and possibly tornadoes, and to aid in the development of conceptual and numerical models of these phenomena.

Key Words: Building code; damage classification; extreme wind; tornado; wind loads.

TORNADOES AND EXTREME WINDS

The highest winds and the greatest wind-related structural damage that occur in the United States are associated with tornadoes. Since anemometers are seldom located in the immediate area of a tornado and could not survive the highest winds if they were, windspeeds are estimated from structural damage and by other subjective methods. Engineering estimates reveal, for example, that winds up to 350 mph lasting a few seconds are likely to produce the most tornado damage in the Midwest (Fujita, 1971). Based on estimated windspeeds and photographs of actual tornado damage, Fujita developed the following windspeed/damage relationships, designed to permit extreme wind estimations without special damage surveys.

F0 40-72 mph, LIGHT DAMAGE

Some damage to chimneys and TV antennae; breaks twigs off trees; pushes over shallow rooted trees.

F1 73-112 mph, MODERATE DAMAGE

Peels surface off roofs; windows broken; light trailer houses pushed or overturned; some trees uprooted or snapped; moving automobiles pushed off the road. 73 mph is the beginning of hurricane wind speed.

F2 113-157 mph, CONSIDERABLE DAMAGE

Roofs torn off frame houses leaving strong upright walls; weak buildings in rural areas demolished; trailer houses destroyed; large trees snapped or uprooted; railroad boxcars pushed over; light object missiles generated; cars blown off highway.

F3 158-206 mph, SEVERE DAMAGE

Roofs and some walls torn off frame houses; some rural buildings completely demolished; trains overturned; steel-framed hangar-warehouse type structures torn; cars lifted off the ground; most trees in a forest uprooted, snapped, or leveled.

F4 207-260 mph, DEVESTATING DAMAGE

Whole frame houses leveled, leaving piles of debris; steel structures badly damaged; trees debarked by small flying debris; cars and trains thrown some distances or rolled considerable distances; large missiles generated.

F5 261-318 mph, INCREDIBLE DAMAGE

Whole frame houses tossed off foundations; steel-reinforced concrete structures badly damaged; automobile-sized missiles generated; incredible phenomena can occur.

F6 319 mph to sonic speed, INCONCEIVABLE DAMAGE

Should a tornado with the maximum windspeed in excess of F6 occur, the extent and types of damage may not be conceived. A number of missiles such as ice boxes, water heaters, storage tanks, automobiles, etc. will create serious secondary damage on structures.

1973 TORNADO SEASON

Last year 1109 tornadoes occurred throughout the United States on 208 days, shattering the old records of 929 tornadoes (1967) and 194 annual tornado days (1972). Tornadoes were reported in 46 States, skipping only Alaska, Rhode Island, Utah, and Washington.

The tornado season began on January 18 and ended on New Year's Eve. During the interval, 87 people were killed, 2481 injured, and property losses exceeded $500 million. Texas led the Nation in tornado fatalities (14), while Georgia recorded the most property damage, with estimates exceeding $150 million. Most of the Georgia losses were the result of a single storm (March 31), which moved east-northeastward through north-central Georgia causing extremely heavy and almost continuous damage along a 75-mile path. A State survey team estimated total damage at more than $113 million--the largest loss for any natural disaster in the State's history.

More recently, during the afternoon and evening of April 3, 1974, an outbreak of tornadoes killed more than 350 people in the United States and Canada in eight hours--three times as many people as had been killed by tornadoes in the entire previous three-year period. The area hardest hit extended from northern Alabama and Georgia, across Tennessee and Kentucky into Indiana and western Ohio. In Xenia, Ohio a swath of almost complete devastation was cut through the center of town.

EXTREME WINDS AND ANSI DESIGN LOADS

As you know, new distributions of extreme wind in the United States were incorporated into the revised American National Standards Building Code Requirements for Minimum Design Loads in Buildings and Other Structures, published in 1972. Based on the work of Thom (1968) of NOAA's Environmental Data Service, the new distributions increased the average period of data records used from 15 to 21 years, and the accuracy of the values by about 15%.

Although the ANSI Code does not consider tornadoes in its extreme wind distributions, many engineers must consider tornado winds in the design of such vulnerable structures as hospitals and nuclear powerplants. Indeed, at this moment, Texas Tech University in Lubbock is conducting a four-day short course on "Engineering for Extreme Winds and Tornadoes." The course includes "a balanced risk approach to structural design which may be used to provide occupant protection and economic tornado resistant designs...."

In a recent, related paper, "Residential Buildings Engineered to Resist Tornadoes," Sherman (1973) adopts two maximum loading conditions to design and render a typical ranch-style, wood-frame house tornado-resistant. For the maximum loading conditions recommended, the increase in construction costs amounts to only 19%.

Given the current engineering needs and interest, the advent of the Fujita classification system seems particularly timely. Since 1971, experimental Fujita estimates of tornado intensities have been made for practially all tornadoes reported. Estimates are also available for 1965 tornadoes from Tecson (1972). The table below is reproduced from Fujita and Pearson (1973) and shows the percentages of tornadoes reported by Fujita categories.

F Scale	1965	1971	1972
0	33%	20%	23%
1	44	42	46
2	17	26	24
3	5	8	6
4	1	2.5	0.8
5	0.1	0.2	0.0
Total	893	888	740

As you can see by comparing the Fujita classifications presented earlier and the ANSI 100-year recurrence values for basic windspeed (Figure 1), all tornadoes in categories F3 and above exceed the ANSI standard values and, except in a few hurricane-prone coastal areas of the Gulf and Atlantic States, so do the tornadoes in category F2. These categories total approximately 23%, 37%, and 31% of all the tornadoes reported in 1965, 1971 and 1972, respectively. In numbers, this works out to approximately 205, 329, and 229 tornadoes for these years. I might add parenthetically that the minimum design values on the 100-year recurrence chart is centered over southern Arkansas, in the heart of tornado alley.

Leaving tornadoes aside for the moment, and considering only extreme winds associated with thunderstorms and extratropical cyclones during 1973, 74 reported values exceeded the 100-year recurrence values. This in no way casts doubt on the validity of the standard values, but it does reflect the fact that the ANSI mean recurrence charts are based on only 21 years of climatological record. It would appear desirable to update these calculations when say 25 years, then 30 years of data become available. In each instance, the increased data sample should increase the accuracy of the standard extreme values.

ONSITE WIND MEASUREMENT

A promising new remote wind-measuring instrument, an acoustic echo sounder potentially capable of profiling low-level wind structures at actual building sites--as well as those associated with tornadoes--is now being tested by NOAA Environmental Research Laboratories (ERL) scientists. Developed by the ERL Wave Propagation Laboratory under an agreement with the Federal Aviation Administration (FAA), the sounder operates like sonar; a sound pulse is transmitted into the atmosphere and scattered by variations in the acoustic refractive index caused by temperature and wind fluctuations. Specifically, wind fluctuations produce doppler frequency shifts from which both vertical and horizontal wind components may be determined.

Work to date indicates that it is possible to determine wind profiles to altitudes of 1 km with the sounder (Beran, et al., 1973). In addition, the simplicity and relatively low cost of acoustic sounders as compared to radar or lidar makes it probable that such sounders will play an increasingly important role in boundary layer wind studies.

MODELING EXTREME-WIND GENERATING SYSTEMS

The atmospheric mechanisms which determine the type, severity, and variability of local weather events which generate extreme winds are mesoscale systems. Until recently, however, most atmospheric studies have concentrated on micro- and macroscale phenomena. Interest in the mesoscale has quickened in the past few years due largely to the development of doppler radar and acoustic sounders, which appear capable of defining the three-dimensional motion field of convection storms. This, in turn, has quickened interest in the three-dimensional numerical simulation of severe storms.

The proposed NOAA Severe Environmental Storms and Mesoscale Experiment (SESAME) is an observational/research effort designed to identify the processes and controlling parameters of extreme-wind-generating systems such as squall lines, thunderstorms, and possibly tornadoes, and to aid in the development of conceptual and numerical models of these phenomena. Satellite, acoustic echo sounder, radar (doppler, continuous-wave, and pulsed), radiosonde, and surface and aircraft observations--coordinated in a time and space framework pertinent to the phenomena studied--will be fed into computers to develop and test mesoscale numerical models.

A preliminary shakedown period is scheduled for the Fall of 1976 to provide for initial calibration and evaluation of the data system, and to allow a short period for minor alterations prior to the first three-month observational program, planned for the Spring of 1977. A second observational period is planned for the Spring of 1979. The 21-month gap will allow time for analysis of the 1977 observational data and permit revisions of any inadequate data acquisition procedures.

ACKNOWLEDGMENT

The authors would like to thank Allen Pearson, Director of the National Severe Storms Forecast Center, and Frank Quinlan and Vincent Cinquemani of the National Climatic Center for their considerable contributions to this article.

REFERENCES

1. Fujita, T.T., "A Proposed Characterization of Tornadoes and Hurricanes by Area and Intensity," SMRP Paper 91, University of Chicago, 42 pp., 1971.

2. Sherman, Z. (Dept. of Aerospace Engr., Pennsylvania State University, University Park), "Residential Buildings Engineered to Resist Tornadoes," American Society of Civil Engineers, N.Y. Structural Div., Journal, 99(4):704-714, April 1973. Refs. DAS

3. Tecson, J.J., "Characterization of 1975 Tornadoes by Their Area and Intensity," SMRP Paper 94, University of Chicago, 22 pp., 1972.

4. Fujita, T.T. and A.D. Pearson, "Results of FPP Classification of 1971 and 1972 Tornadoes, Eighth Conference on Severe Local Storms, AMS Conference Proceedings, Denver, Colorado, pp. 142-145, October 1973.

5. Beran, D.W., B.C. Willmarth, F.C. Carsey, and F.F. Hall, Jr., "An Acoustic Doppler Wind Measuring System," J. Acoust. Soc. Am., Vol. 55, No. 2, pp. 334-338, February 1974.

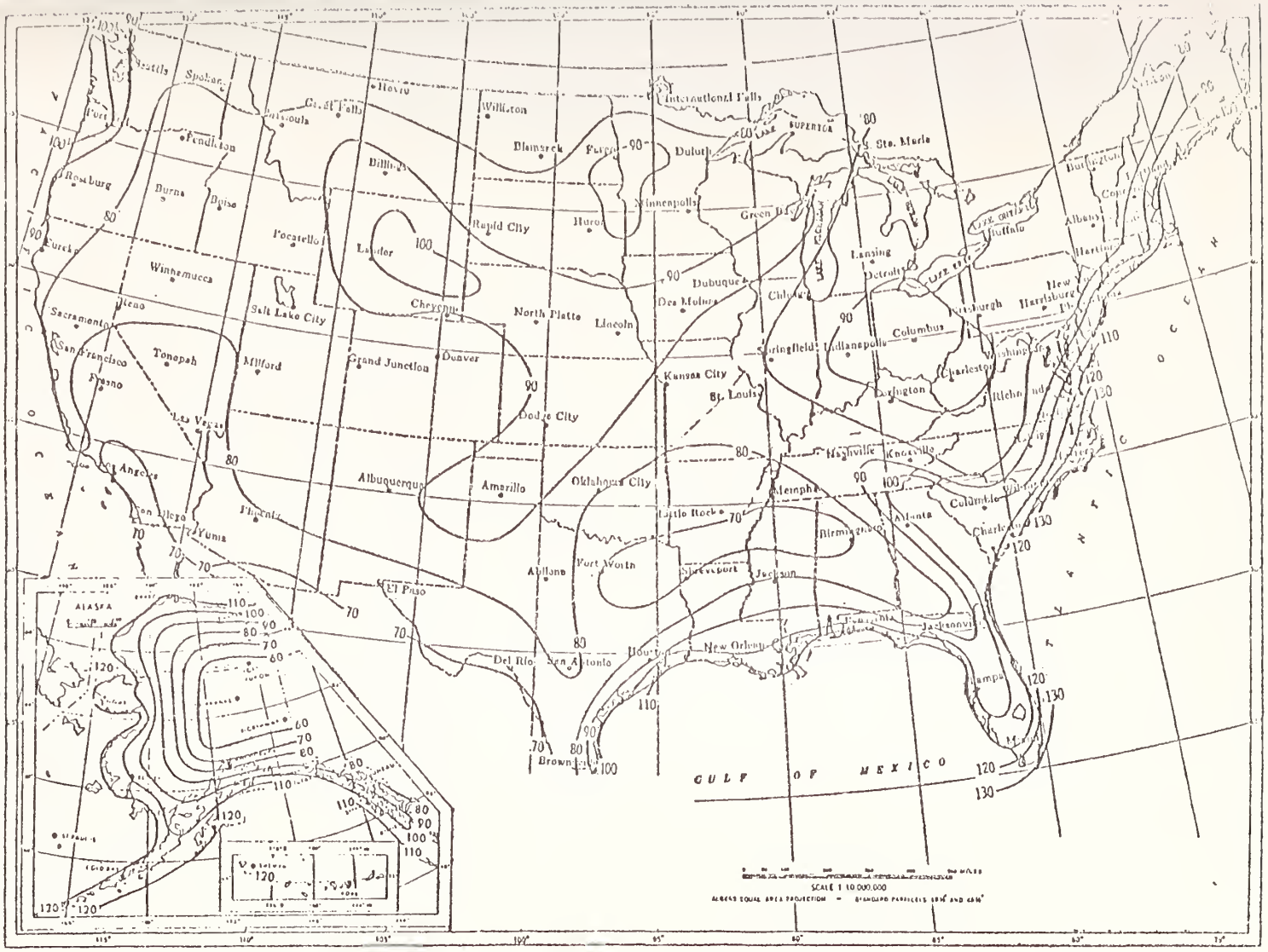

FIG. 1 - BASIC WIND SPEED IN MILES PER HOUR. ANNUAL EXTREME-MILE
30 FT ABOVE GROUND, 100-YR. MEAN RECURRENCE INTERVAL.

WIND TUNNEL EXPERIMENTS FOR STUDYING A LOCAL WIND

by

Ken Suda
Director, Meteorological Research Institute (MRI)

Seiji Soma
Physical Meteorology Laboratory, MRI

Kiyohide Takeuchi
Applied Meteorology Laboratory, MRI

In general, the study of the effects of local winds on structures is primarily based on data obtained from wind tunnel experiments. As an example of such studies, an investigation of air flow around Nakatojima Island relative to the wind resistant design of a long suspension bridge has been conducted and will be presented.

However, it is not reasonable to conduct such a study entirely related to wind tunnel experiments, as the similitude rule has not been established. Therefore, field observations have been made in parallel with the wind tunnel experiments and the data obtained by both sources are then compared. Thus, the results obtained from the wind tunnel experiment are more reliable.

Key Words: Bridge; gust; metorological data; topographical model; wind load; wind profile; wind tunnel.

INTRODUCTION

In studying the effects of local winds, the collection and analysis of field data is, needless to say, the most desirable. In practice, however, the acquisition of field data is laborious and requires a vast amount of time and expense, therefore, wind tunnel tests are conducted despite various difficulties notably the principle of similitude.

Because of these difficulties, wind tunnel tests were conducted in conjunction with field observations, and then comparisons of the data obtained from both sources was made. As will be noted, the field data does not always agree with the wind tunnel test data.

In collecting the data a reference point should be fixed so there is similarity between the tunnel and the natural winds and they are optimum. Therefore, the location of the reference points and the physical elements to be observed are usually determined during the planning of wind tunnel experiments. The number of the observation points, the elements to be observed, and the time required are generally greater than would be allowed because of budget restrictions. Also, the principles of similitude, which are most reliable in the area of effective Reynolds number, must be employed.

Based on these conditions, the effects of local winds on structures have been studied by using a wind tunnel. An example of the type of wind tunnel test study that can be conducted will be presented in relation to an investigation of the wind regime around the Nakatojima Island and the wind-resistant design of a long suspension bridge. Numerous other studies have been made in our laboratory, as detailed in Table 1.

INVESTIGATION OF THE WIND REGIME AT THE BRIDGE BUILDING SITE NEAR NAKATOJIMA ISLAND

In designing a suspension bridge for wind loading, the upward attack angle of the wind against the bridge is an important matter, and must be carefully considered. The wind effects, due to the land topography, were initially evaluated during a preliminary survey prior to the building of the Second Giant Bridge of Kurushima, which connects Honshu and Shikoku. The primary area where wind conditions are important is Nakatojima, a little island located four kilometers to the north of Imabari in the Shikoku District. In the construction of the bridge, the bridge axis is planned to pass north of and parallel with the ridge line of the island. Therefore, a considerably steep up-draft air flow can be expected during a northerly wind. Although the air current may not necessarily affect the entire span of the bridge, its vertical inclination can be exceedingly large and the region in which the air current appears from the different wind directions is not known. In case of a southerly wind, the bridge axis will be located on the leeward side of Nakatojima. Although the level of the bridge girder is a few meters higher than the island top, a violent turbulence is expected to dominate the leeward side air current. Therefore, the study included both the northerly and southerly wind directions.

The primary investigation was directed toward the wind tunnel experiments, however, in order to compare these results with those in the field, actual observations of the wind direction and speed were made at two points on Nakatojima Island during a three-month period. Location of the observation sites and the level of the instruments are given in Figure 1. Stations are distributed in such a way that the difference in wind speeds at two points in the island and the existence of separation phenomenon expected in the leeward side of the island can be examined.

TOPOGRAPHIC CONDITIONS

Nakatojima Island is located to the north of Imabari, approximately in the middle of Kurushima Straits. It is a small island, spanning a distance of 390 m. east to west and 180 m. north to south with a height of 63 m. above sea level. On its northern and souther shores, the slopes have an inclination of 40°. With this background, it can be easily understood that the peculiar topography of the island may provide strong air currents on

the island in addition to the fact that there is no nearby island which may affect the air current.

METHOD OF INVESTIGATION

(i) Wind Tunnel Experiment

For the wind tunnel experiment, three topographic models with reduced scales of 1/500, 1/1,000, and 1/1,500 were prepared. The first model which was used in the experiments, in conjunction with the Gottingen-type wind tunnel (1.5 m. in diameter), distributions of the wind angle and wind speed around Nakatojima, were measured in detail.

In order to study the behavior of the air current across the island, in case of stable stratification of the atmosphere, a second model was prepared.

The last model was used to study the topographic effect of a wider area, including Nakatojima and other adjacent islands, relative to the air flow.

(ii) Field Observation

In conducting the field tests, aerovanes were placed at two points on the island, one at the top of the island (Point A) and the other on the northern slope (Point B) in order to obtain data on the wind direction and speed. The levels of the aerovanes are 76.0 m. and 29.5 m., respectively. Point B, which is located at about half of the height of the island and susceptible to topographic effects, was chosen as an observation point to check similitude.

WIND TUNNEL EXPERIMENT

(i) Measurement and Analysis of the Vertical Inclination Angle

The vertical inclination angle of the air current over the northern slope of Nakatojima Island was the principle object of the present investigation. In the wind tunnel experiment, the vertical inclination was generally determined from the measurement of the U and W components of the wind, making use of the X-proble of the hot-wire anemometer. However, in order to improve the precision of measurement, a continuous record of the vertical inclination was made. This requires a modification to the electric circuit of the instrument, the details of which are not given herein. The tunnel wind speed that was used in the experiment was 7.0 m./s. for both the vertical inclination and wind speed distribution. Results of the measurement for each wind direction will be given as follows:

Case of Northerly Wind

In this case, the wind blows perpendicular to the bridge axis. As seen from the distribution curve of the vertical inclination given in Figure 2-A, there is a very strong up-draft current which has a maximum of 25° relative to the northern slope. This maximum inclination naturally corresponds to the top of the island. The up-draft of the wind is maintained for a considerable distance, even when the point of measurement is over the waters off the western edge of the island, as shown in Figure 2-A.

Case of Southerly Wind

Figure 2-B shows the result of the measurement for the case of the current blowing perpendicularly to the bridge with a southerly wind direction. In this case, the bridge girder seems to be in the wake of the island and thus, the vertical inclination changes so strongly that its upward or downward sense cannot be determined from the distribution curve.

(ii) The Measurement and Analysis of Wind Speed Distribution

The experiments were performed with the same topographic model, as described previously, with the same measuring line and points as stated above.

Case of Northerly Wind

The wind distribution along the bridge axis, as induced by the northerly wind, is shown in Figure 3-A. As seen by the distribution curve at that level where the bridge girder is located (second curve from the top in Figure 3-A), there is a tendency for the wind to decrease in the middle of the island and increase on both ends, relative to the tunnel wind speed. This tendency is especially prominent in the western part of the island.

Case of Southerly Wind

In this case, the distribution curve of the wind speed shows unusual characteristics (see Figure 3-B). Namely, on the leeward side at the middle of the island, the wind is exceedingly weak, being 1/7 or less of the wind tunnel speed. The distance where the wind speed decreases substantially is 200 to 250 m., after conversion to actual scale. On the eastern and western ends, the wind speeds conversely increase as the distance increases.

The decrease of the wind speed due to the southerly wind can be understood if we consider that the measuring line along the bridge axis is in the wake of the island. However, since the decrease of the wind speed was drastic, the level of the boundary surface between the general air current and the reverse air current due to separation was measured. The results of these measurements are shown in Figure 4. Although the level of the boundary surface changes strongly and is difficult to determine precisely, a general trend can be established. As seen in Figure 4, the level of the boundary is highest over the northern slope of the island and its height is nearly the same as that of the bridge girder.

In principle, this boundary surface represents the discontinuity between the general and reverse currents and is theoretically the surface on which the wind speed is reduced to zero. Accordingly, it is clear that the rapid decrease of the wind speed, as seen in the distribution curves given in Figure 3-B, is due to the coincidence in height of the bridge girder and the boundary surface.

(iii) Experiments in the Stratified Wind Tunnel

In order to visually obtain a pattern of the air flow passing over Nakatojima Island, and to establish the effect of the stratified atmosphere on the pattern, experiments were made with a model built to a scale of 1/1,000, and tested in the stratified wind tunnel.

The first investigation was conducted using a stable air flow pattern. Plate 2 shows the pattern when the wind speed is 0.4 m./s. and the vertical density gradient is 0.006 gr./cm.^{4}. A stagnant vortex, almost round, was found in the windward side of the island.

Note that the wind passing over the top of the island tends to descend on the leeward side. In such a case the boundary surface also decreases on the leeward side. Separation does not completely disappear and the reverse flow still exists.

The Froude number, which represents the stability in the atmosphere, is approximately 1.79 for the present experiments, which can be found in the real atmosphere. Accordingly, the flow pattern obtained in the experiments can exist in the atmosphere when the wind is light and the stratification is stable.

The next experiments that were conducted were under the condition that the wind speed was 1.5 m./s., the stratification was neutral, and a grid was installed in order to make the air flow turbulent. This pattern is shown in Plate 3. The streamline, in contrast with Plate 2, still ascended after passing over the top of the island.

(iv) Experiments with a Regional Topographic Model and Their Analysis

Experiments on a regional topographic model, built to a scale of 1/1,500, were made so as to include not only Nakatojima Island but adjacent islands. These islands can make the flow pattern much more complicated and should be considered in the bridge design.

Measurements of the vertical inclination of the air flow in the northerly direction shows that the wind blows up on the side of Nakatojima Island and Umajima Island (see Figure 5). A horizontal air flow can only be found at the central part of the straits.

The wind speed distribution has no marked characteristics, when the wind comes from the north, but the southerly winds show characteristics of a strait wind: i.e., the flow coverages and the speed increases all over the strait. Its increase rate is high at the coast of both islands and low at the central part of the strait (see Figure 6).

ANALYSIS OF FIELD METEOROLOGICAL DATA

In order to evaluate the reliability of the wind tunnel experiments, meteorological data was obtained from Nakatojima Island and then analyzed. The aerovane at the top of the island (Point A) was installed on the pole 15 m. above the ground, thus the wind speed can be considered to be general air flow. The wind at the north slope of the island (Point B) is compared with that obtained at Point A.

The results are depicted in Figure 7, where the wind is represented as a vector and the figure in the parentheses shows the frequency. Only the following wind directions were studied, because these have the main influence on the bridge:

Southerly Wind: SW, SSW, S, SSE, SE
Northerly Wind: NW, NNW, N, NNE, NE

The winds were divided into three groups: weak (0.5-5.0 m./s.), moderate (5.1-10.0 m./s.), and strong (higher than 10.1 m./s.), because separation depends upon the wind speed.

Case of Southerly Wind

When the general wind (namely, the wind at Point A) is southerly, the local wind at Point B has almost an opposite direction (see Figure 7-A), with separation taking place on the north slope of the island. Separation does exist even during a light wind. The wind speed at Point B is low, but increases almost proportionally with an increase of the general flow.

Case of Northerly Wind

When the general flow is northerly, the local wind at Point B has a rather large fluctuation of the direction, but has almost the same direction (see Figure 7-B).

FLOW IN THE WIND TUNNEL AND NATURAL WIND

In order to evaluate the results obtained from the wind tunnel, meteorological observations were made at two points on Nakatojima Island. Relationships between the air flow in the wind tunnel and the natural wind was then studied. The following will describe these relationships:

(i) Separation

During a southerly wind, separation was found over the north slope for both cases.

(ii) Ratio of Wind Speeds

The ratio of the wind speeds, between the two points, is shown in Table 2. In the northerly wind, the wind speed in the wind tunnel is a little lower than that observed at the actual sites. These values, however, seem to be in good agreement, considering the complicated characteristics of the winds.

In the northerly wind, when the flow pattern is much more complicated, the ratios show that the flow seems to agree fairly well between the model experiments and field observation.

In Table 2, the ratio of wind speeds as observed at Points C and D (see Figure 1) that were obtained a few years ago are presented. These values were obtained at a tower (110 m. high above the ground) which was used to support electric power lines, and at another tower (51 m.) used as a signal station for tidal current.

(iii) Similarity of Turbulence

In the present experiment, a grid was placed in the wind tunnel as a turbulence generator (see Plate 4). The grid consists of 40 mm. of square mesh, constructed of 10 mm. square bars. The turbulence thus generated should be similar to that developed by a natural wind. The similarity has not been completely studied, however, the grid seems to generate effective patterns which are similar for both cases (for example, separation and stagnant vortex).

(iv) Effective Reynolds Number

A complete solution has not been obtained of the similitude between the model in the wind tunnel experiment and the field observation. However, when the effective Reynolds number has the same value for both cases, the similarity seems to hold with a high degree of accuracy, at least under the condition that the strong wind passes over the isolated island such as Nakatojima. Here the effective Reynolds number is defined as the number using the turbulent diffusivity, K, in place of the kinematic viscosity, p. The effective Reynolds number R_E is expressed as follows:

$$R_E = \frac{LU}{K} \tag{1}$$

where U and L are the wind speed and the length, respectively.

However, from the theory of turbulence, $K = \ell u'$, where ℓ is the representative length of the "eddies," and u' is the RMS of the fluctuation of the turbulence. Accordingly, the following equation is obtained:

$$R_E = \frac{LU}{\ell u'} \tag{2}$$

The term U/u' is the reciprocal of the intensity of the turbulence and L/ℓ is the ratio of the representative length of the topography to that of the eddies. Consequently, an adjustment of the effective Reynolds number can mean an adjustment to both of these two terms. Both terms can be measured during the field observation, and they can be adjustable in the wind tunnel. From existing data obtained in the field, R_E can be estimated as 10 to 100. In the present experiments R_E in the wind tunnel is about 300. It means that the grid size is smaller, considering that the model is made on the scale of 1/500. Investigation of the effect of the difference of R_E has not been made.

CONCLUSION

Difficulties in the wind tunnel experiments are due to the fact that the similitude rule has not been established. However, because it is difficult to conduct intensive observations at the site and to analyze the long-term data, a combination of the wind tunnel experiments and rather simple field observations seems appropriate. In this manner the wind conditions at Nakatojima Island were examined and described herein.

Table 1. Examples of Studies Made By Wind Tunnel Experiment

Theme of Study	Point of Reference	Observation Point and Elements observed
Clear Air Turbulence on the leeward side of Mt. Fuji	Distinction of wind regimes whether it is mountain wave type or separation type	Tracking of non-buoyant balloon flown from summit by a tracking radar
Turbulent flow around an airport	Distinction of turbulent wind systems on the leeward side slope of a hill	Double theodolite observation of balloons over the runway and accelerometric observation of aircraft vibration
Strong winds around a high building	Comparison between general wind speed in urban area and the wind speed near the building	Surface wind observation at the roof-top of a building and around it
Determination of the anemometer level for Mt. Fuji Weather Station	Vertical inclination of air flow	Observation of vertical inclination by emitting smoke from the summit
Strait wind at the Kammon Straits	Vertical distribution of wind speed at a cape facing to the Straits	Observation of vertical distribution of wind on the power transmission tower
Strait wind at Mekari Straits	Comparison of winds at three points on the coast of Strait and on the sea	Wind observation by aerovane and observation of strait wind by non-buoyant balloon flown from three points on the sea
Wind regime around Nakatojima Island	Ratio of wind speeds at the top and on the slope of the island and the separation	Observation of wind direction and speed at the top and on the slope of the island.

Table 2. Ratio of the wind speeds

Wind direction		NW	NNW	N	NNE	NE	SSW	SW	S	SSE	SE
U_B/U_A	wind tunnel experiment	0.79	0.64	0.54	0.54	0.51	0.13	0.20	0.18	-	0.23
	field observation	0.92	0.73	0.73	0.62	0.67	0.30	0.18	0.12	-	-
U_D/U_C	wind tunnel experiment	0.91	1.00	1.08	0.96	0.94	0.96	-	0.94	-	0.46
	field observation	0.92	0.98	0.99	0.86	0.90	0.81	-	0.92	-	0.79

Plate 1. Nakatojima Is. viewed from the eastern sea. Northern and southern slopes are very steep.

Plate 2. Pattern of air flow in case of highly stable stratification and weak wind (experiment in the stratification wind tunnel). Air flows down after crossing the ridge of island.

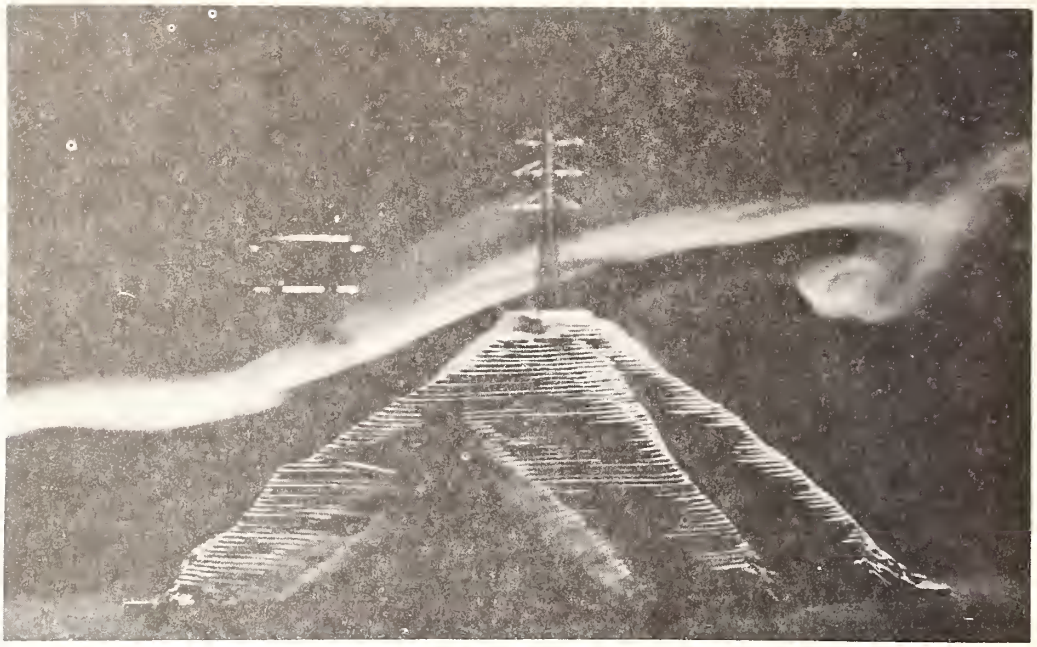

Plate 3. Pattern of air flow in case of neutral stratification and strong wind. Air continues to flow up after crossing the ridge of island.

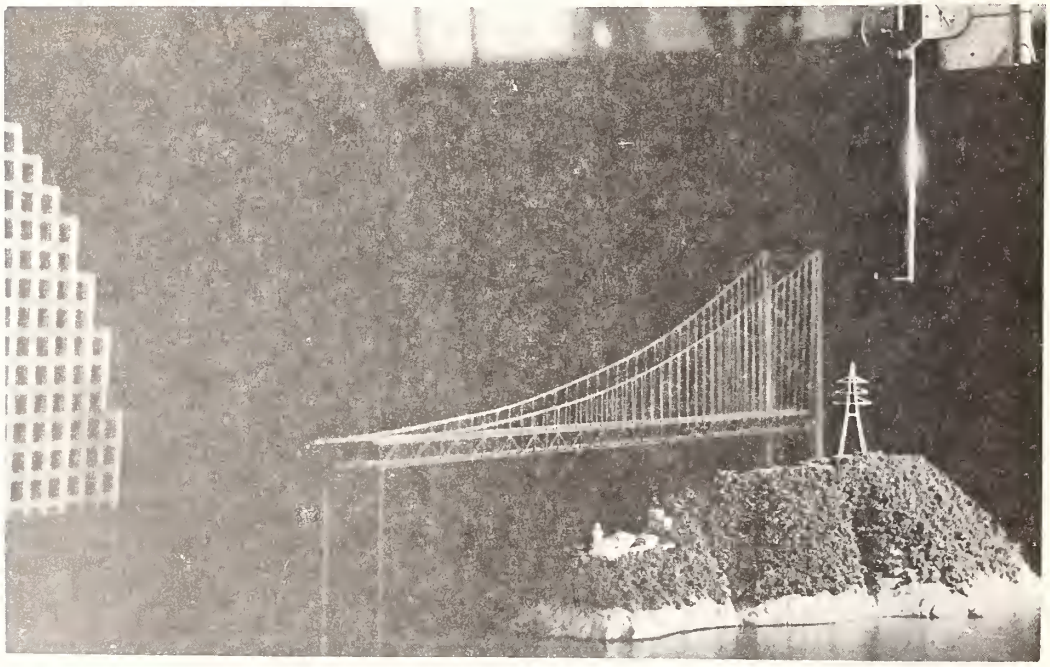

Plate 4. Models of Nakatojima Island and the Second Giant Bridge of Kurushima in the wind tunnel (scale: 1/500) and grid of turbulence generator on the left.

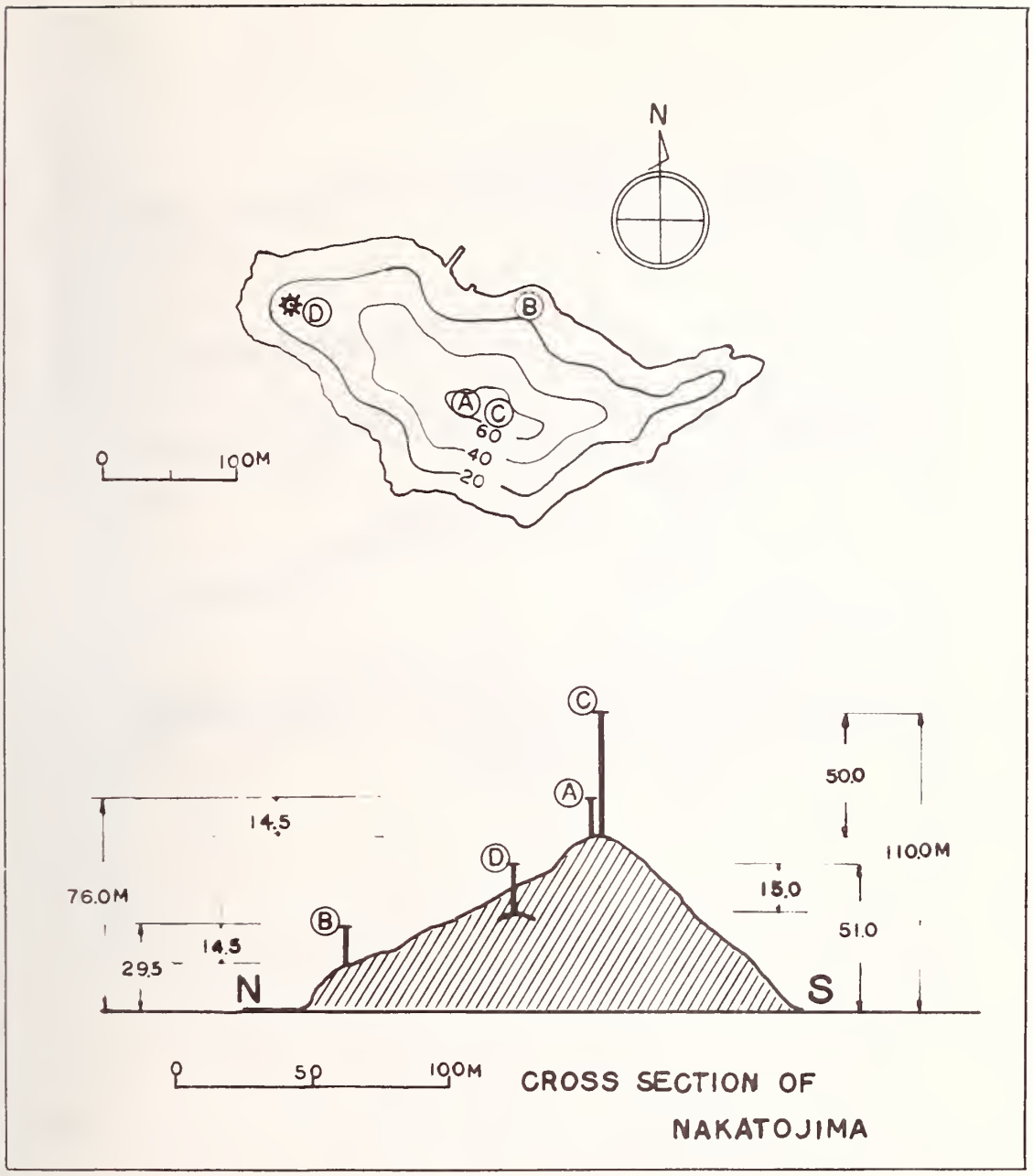

Fig. 1. Location and the level of observation of aerovane in Naktojima Is.

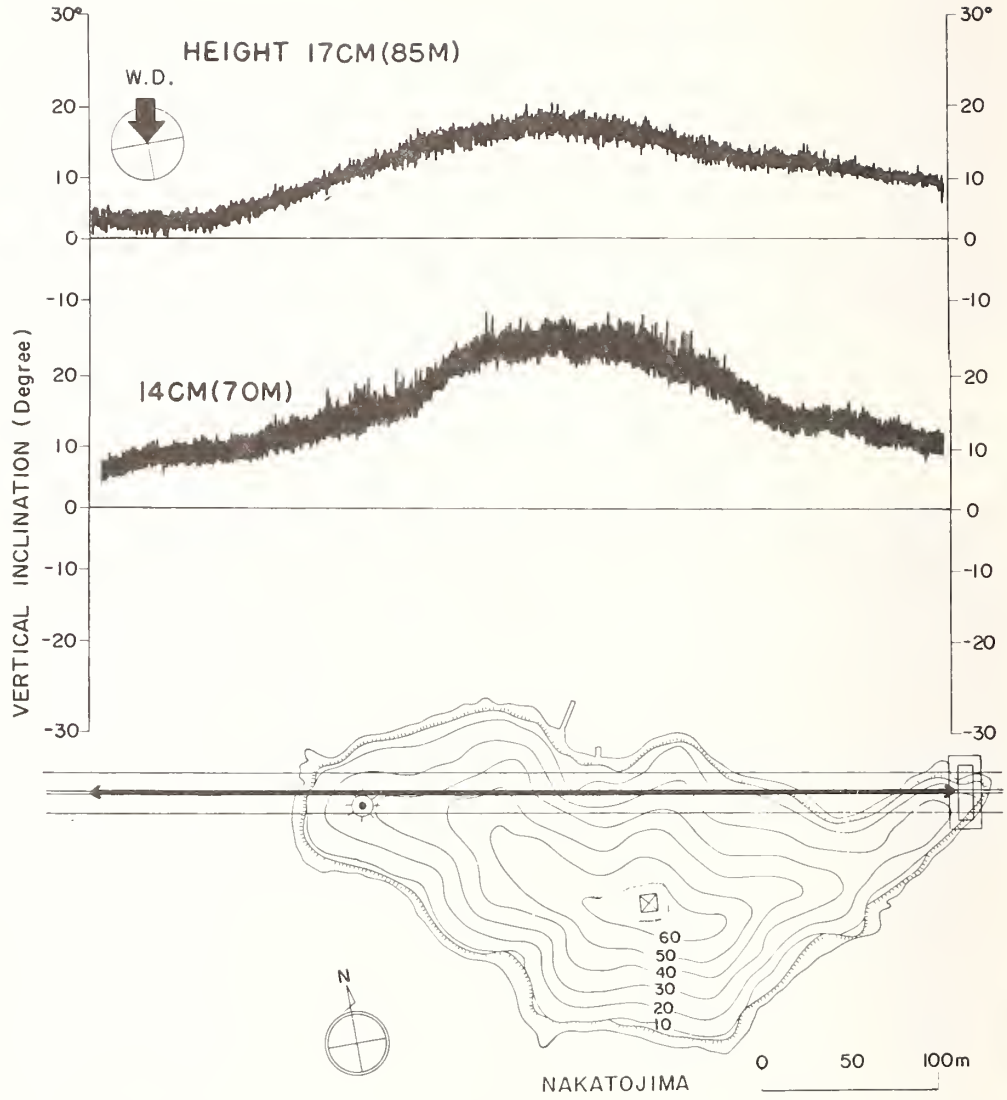

Fig. 2–A. Vertical inclination along the bridge axis on the northern side of Nakatojima obtained by wind-tunnel experiment. Wind direction N–NNE.

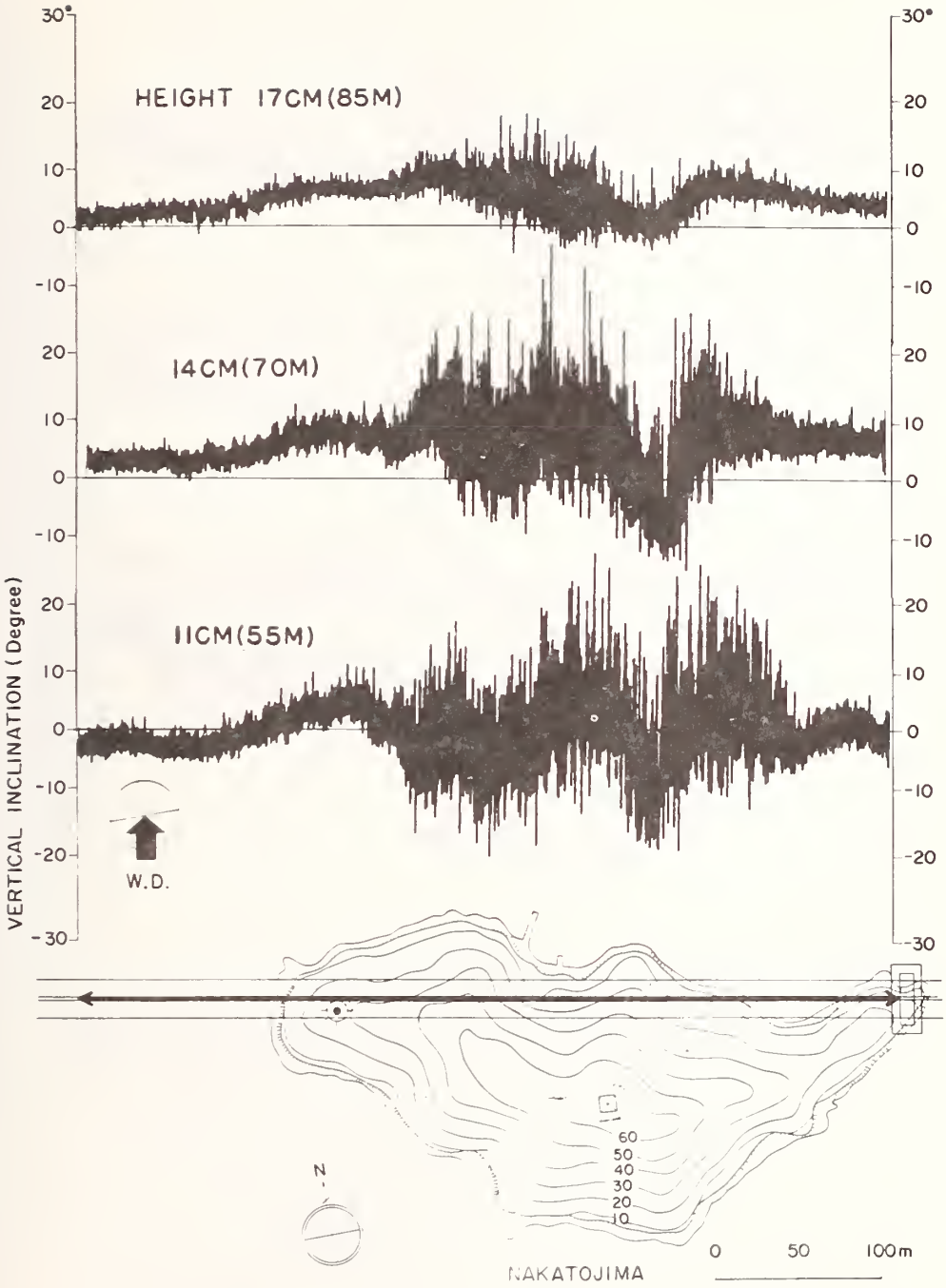

Fig. 2–B. Vertical inclination along the bridge axis on the northern side of Nakatojima obtained by wind-tunnel experiment.
Wind direction SSW–S.

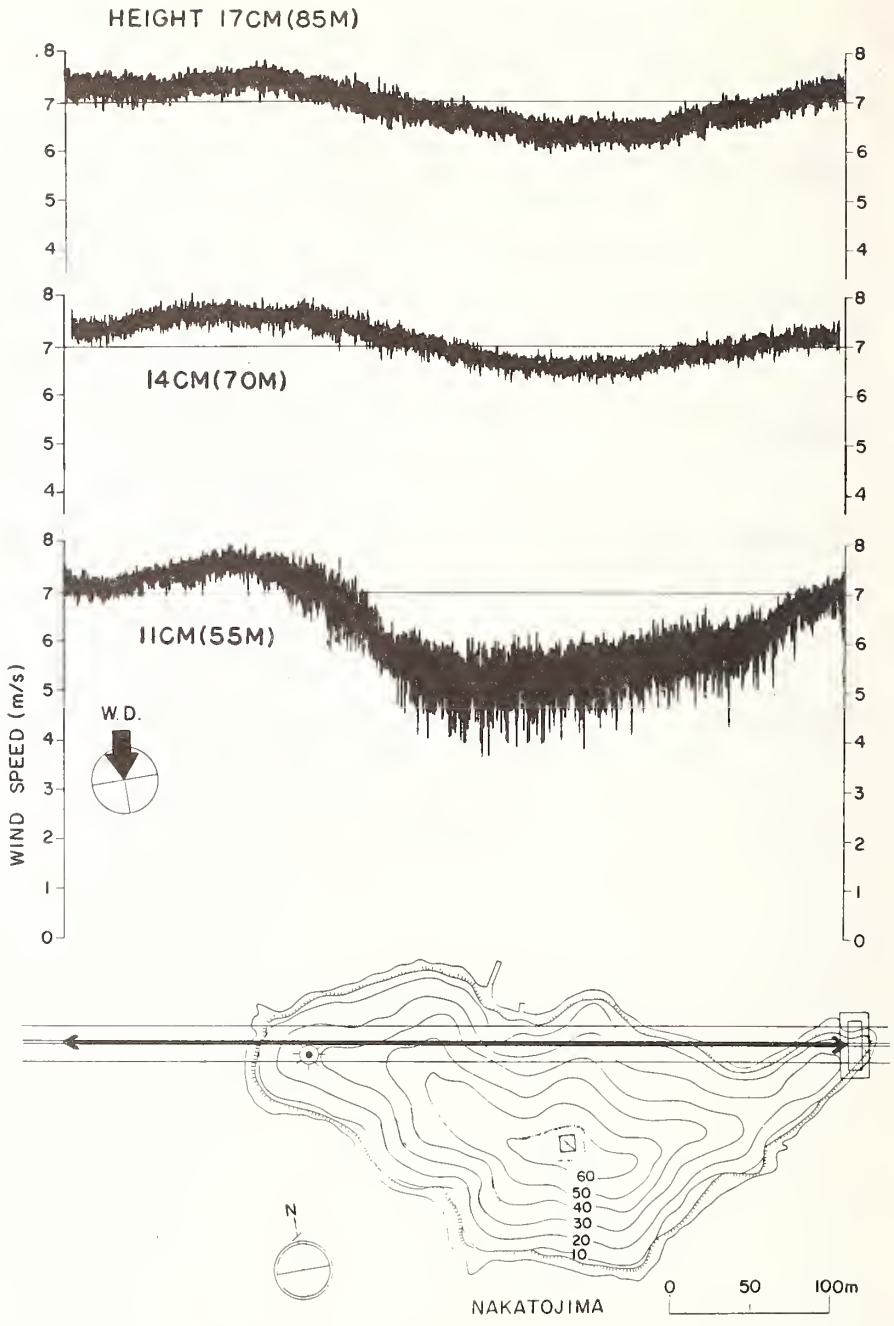

Fig. 3–A. Distribution of wind speed along the bridge axis on the northern side of Nakatojima obtained by wind-tunnel experiment.
Wind direction N–NNE.

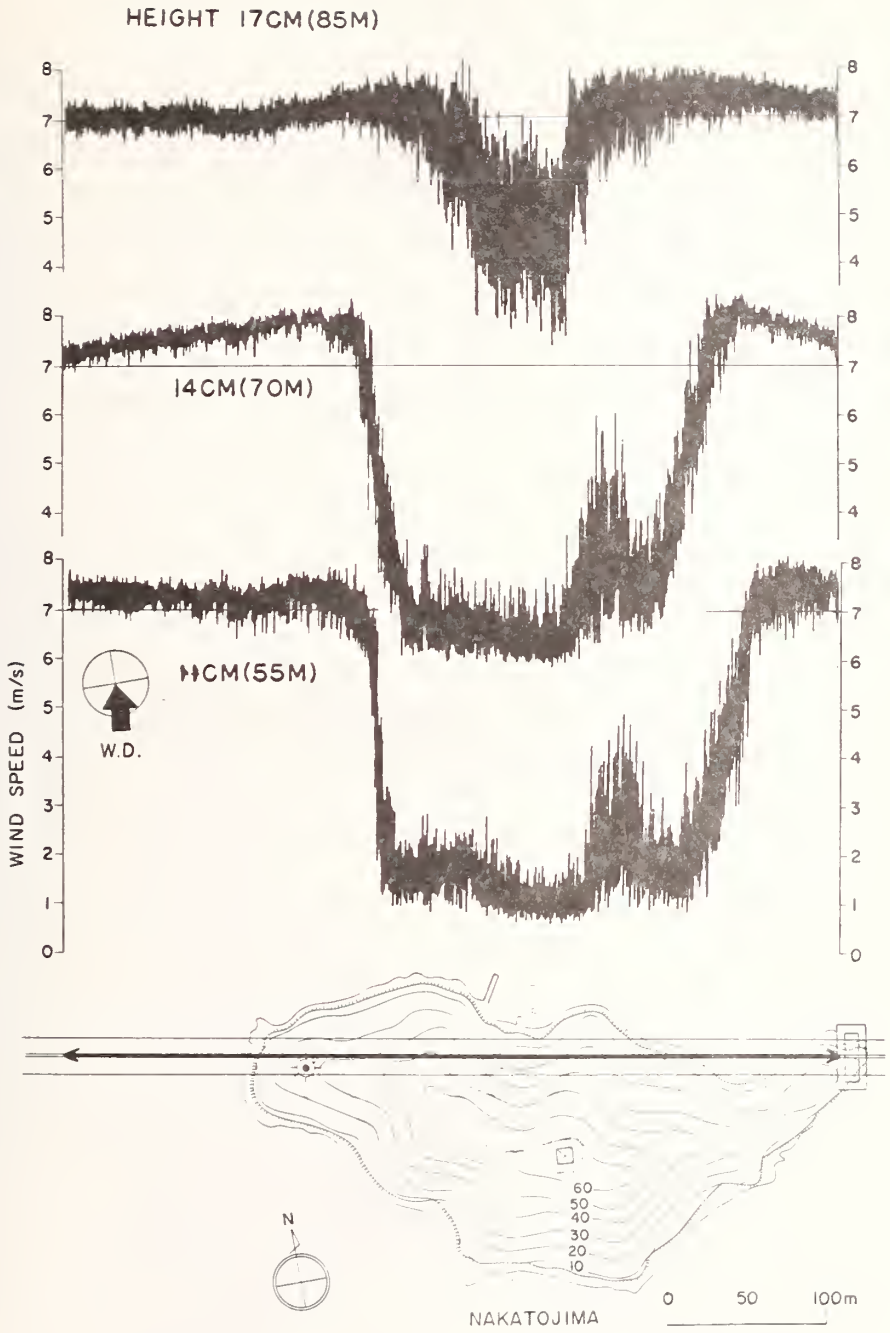

Fig. 3–B. Distribution of wind speed along the bridge axis on the northern side of Nakatojima obtained by wind-tunnel experiment.
Wind direction SSW–S.

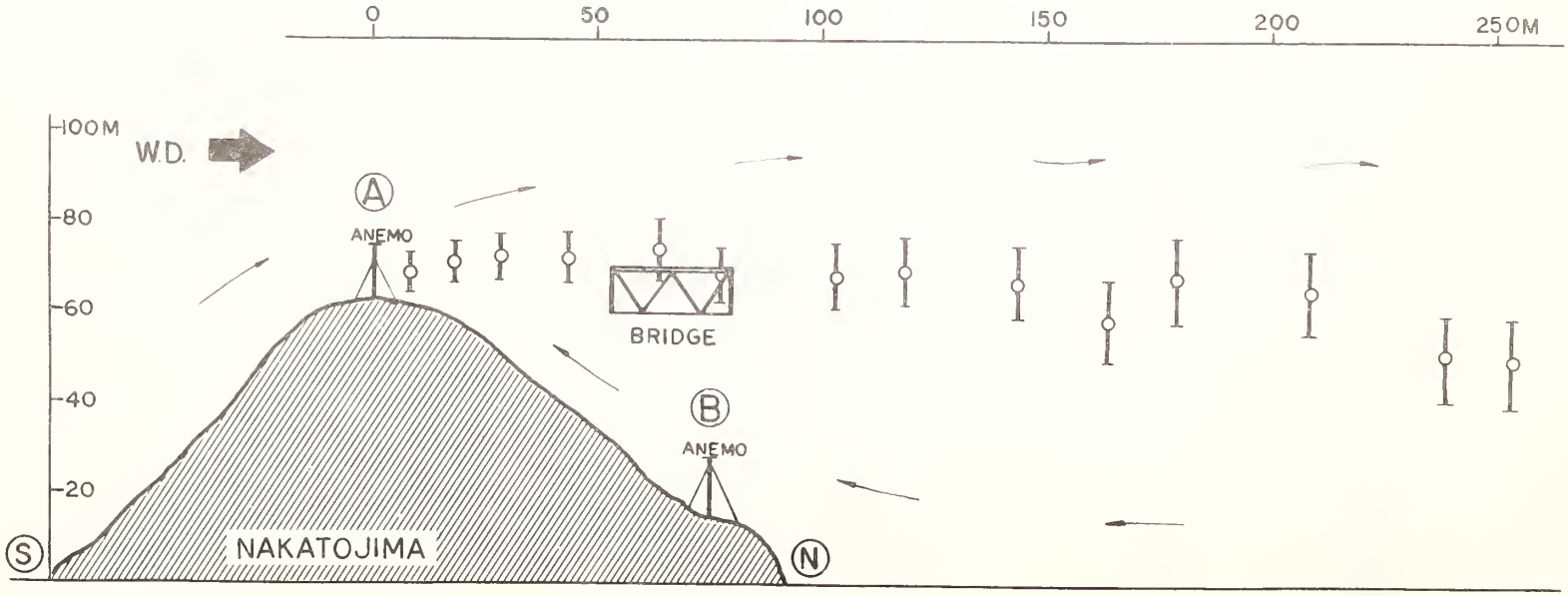

Fig. 4. Height of discontinuity in wind direction on the northern side of Nakatojima obtained by wind-tunnel experiment.
Wind direction SSW–S.

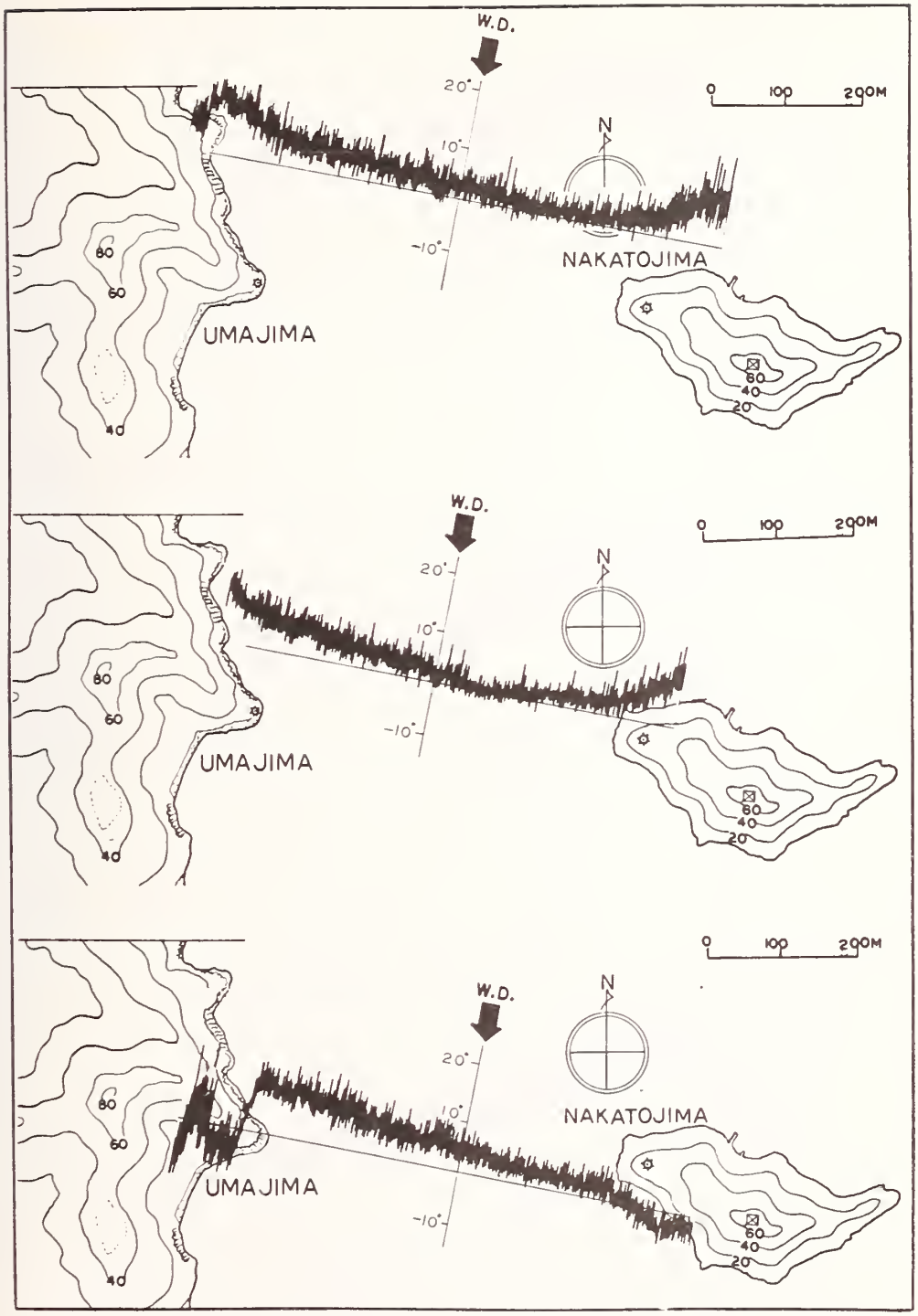

Fig. 5. Vertical inclination of the wind obtained with a regional topographic model including both Nakatojima and Umajima Islands.

Scale 1/1,500, Wind direction N–NNE

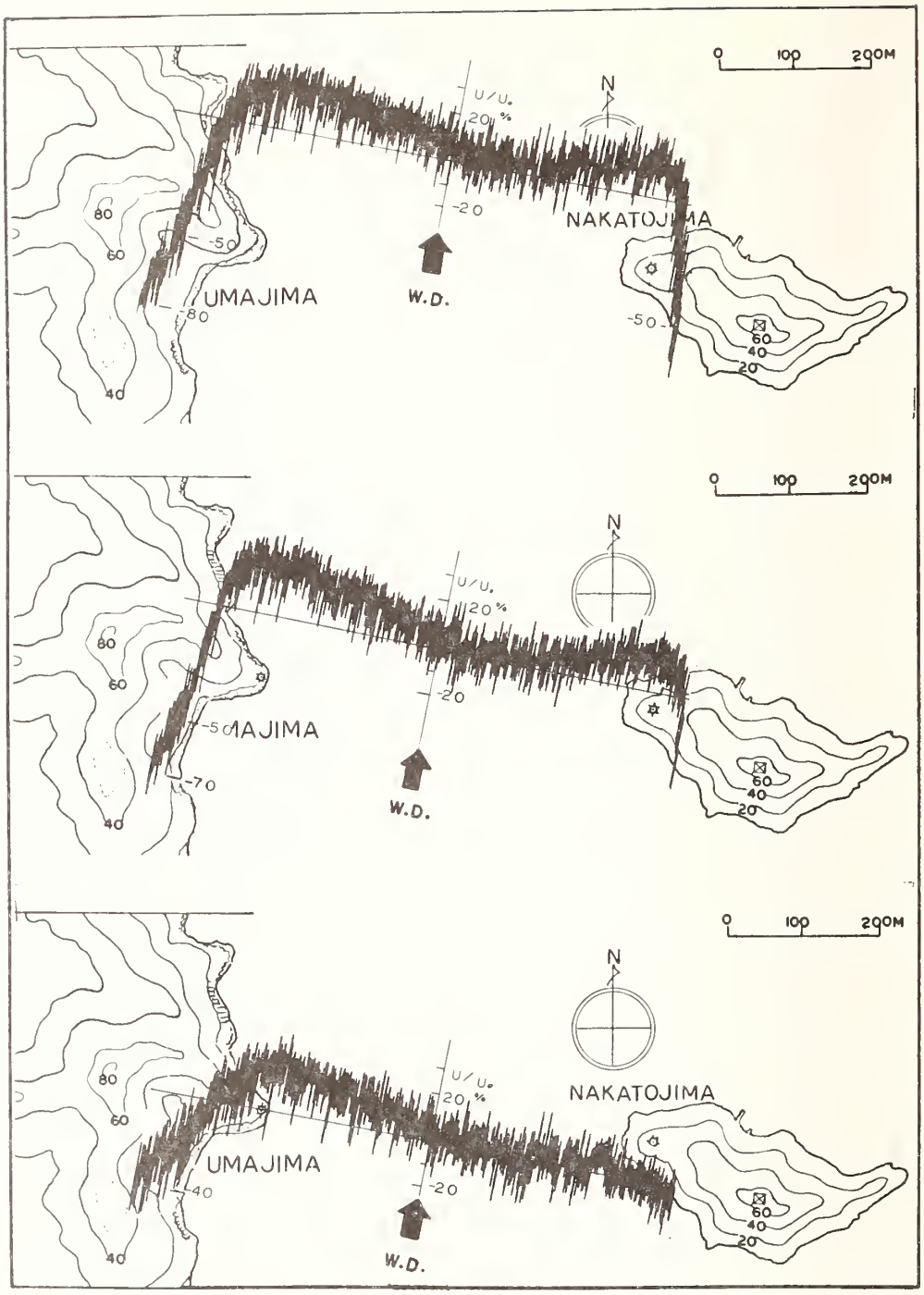

Fig. 6. Wind speed distribution with a regional topographic model

Scale 1/1,500, Wind direction SSW–S

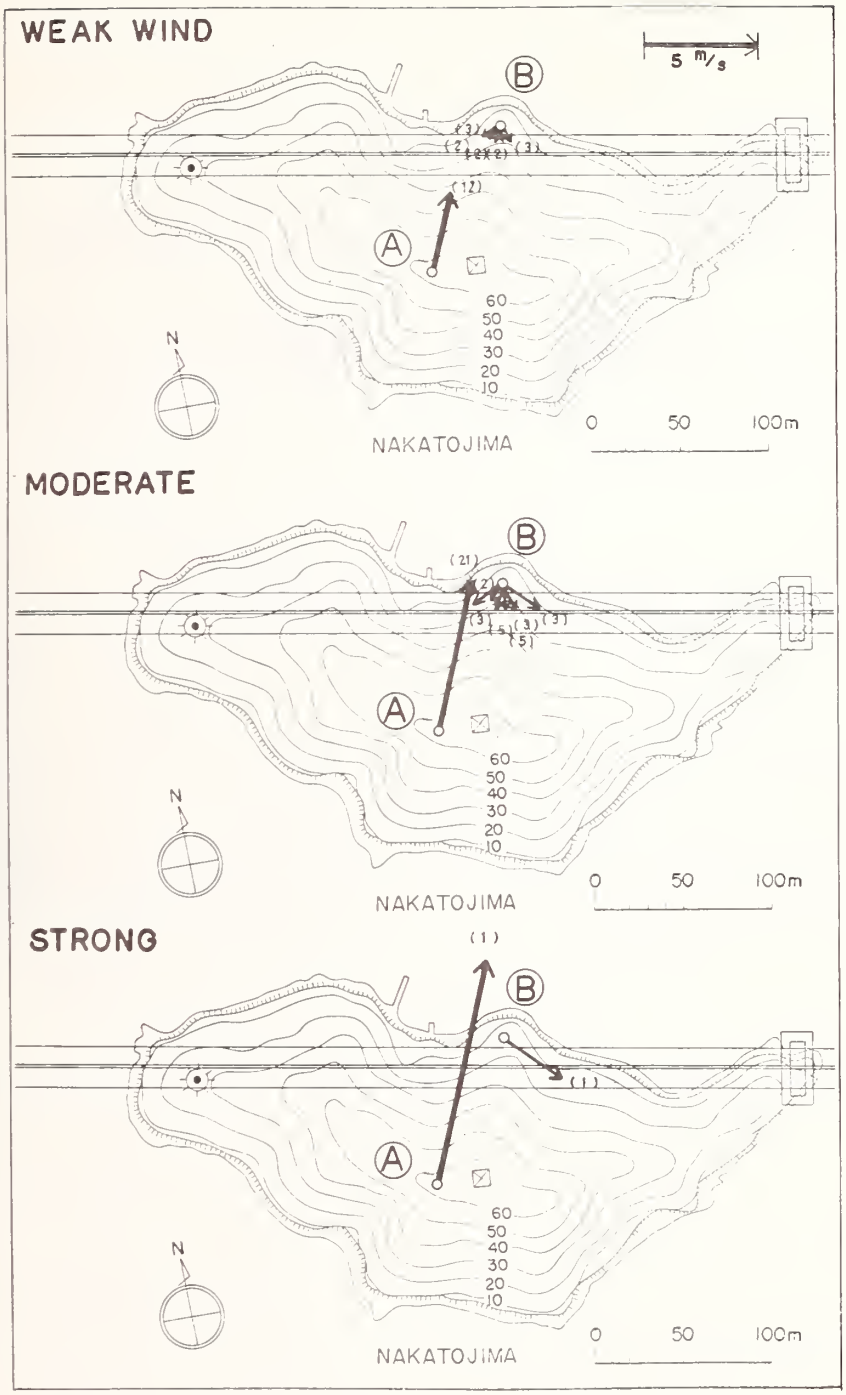

Fig. 7–A. Relationship between the wind at Points A and B in Nakatojima Island. Wind direction at Point A SSW

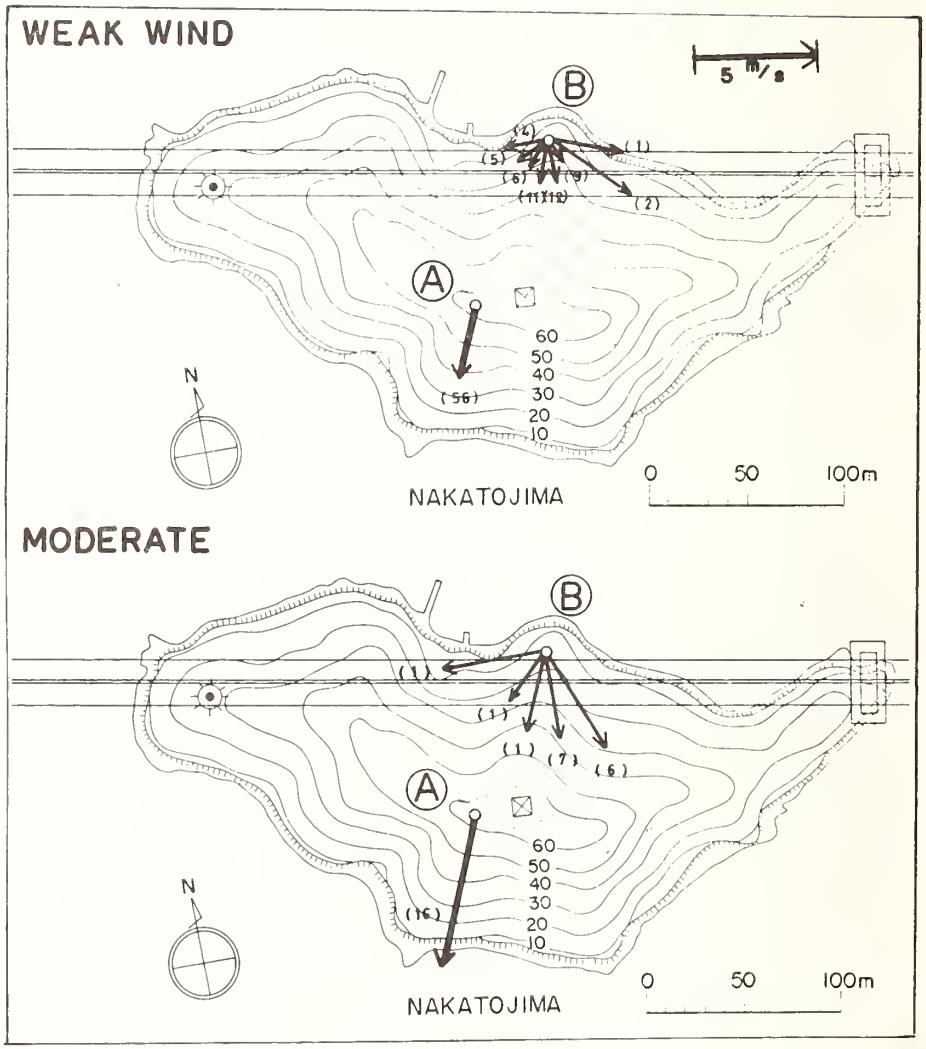

Fig.7–B. Same as in Fig.7–A but wind direction at Point A NNE

A STUDY OF WIND PRESSURES ON A SINGLE-FAMILY DWELLING IN MODEL AND FULL SCALE

by

R. D. Marshall

Structures Section
Center for Building Technology, IAT
National Bureau of Standards
Washington, D.C. 20234

Wind pressures measured on a single-family dwelling are compared with results obtained from a 1:50 scale model placed in a turbulent boundary layer. It is shown that the fluctuating components of surface pressures far exceed the mean or steady pressures and are well correlated over sizeable roof areas. The consistently low fluctuating pressure coefficients obtained from the wind tunnel model are attributed to improper simulation of the lower portion of the atmospheric boundary layer. Comparisons between actual loads and specified design loads suggest that certain current provisions are marginal for tributary areas and excessive for localized areas such as ridges, eaves and corners. A procedure for expressing loads on both localized and extended roof areas in terms of mean pressure coefficients and a peak factor is described.

Key Words: Aerodynamics; boundary layers; buildings; codes and standards; wind loads; wind tunnels.

1.0 INTRODUCTION

Research over the past ten years into the effects of wind on buildings and other structures is significantly influencing design philosophy and practice as is evidenced by recent major revisions of building codes and standards, both here in the United States and abroad. Perhaps the most significant improvement has been the recognition of wind loading as a stochastic process and the formulation of design criteria based upon acceptable levels of risk. Other improvements include provisions for various classes or categories of terrain roughness and the wind-tunnel simulation of the atmospheric boundary layer when measuring pressure coefficients and dynamic response factors.

In spite of these important advances, considerable work remains to be done. This is particularly true of those code provisions covering the design of low-rise buildings which have not benefited from this research in the same proportion as tall structures. It is interesting to note that pressure coefficients in current use are based in large part on wind tunnel studies carried out in uniform flows of low turbulence, using instrumentation capable of measuring only mean pressures. It is obvious, therefore, that a major effort must be made in the wind-tunnel modeling of low-rise structures. Prior to this, however, the validity of modeling techniques must be established by comparing test results with representative measurements obtained from full-scale buildings. The investigation described in the following sections is an attempt to provide a preliminary comparison between model and full-scale test results for a single-family dwelling.

2.0 THE TEST SITE

The site selected for this study is located at Malmstrom Air Force Base, Montana, directly to the east of the city of Great Falls. The region is noted for its "chinook" winds which regularly blow out of the southwest during the winter months. The terrain surrounding the test site is markedly flat and free of significant obstructions. Although the mean hourly speeds for the area are quite high (14-17 mph), extreme winds seldom exceed 70 mph.

The building investigated is a single-family dwelling, one of four quite similar units located in an area having a clear wind exposure extending from the west clockwise around to the south. A cluster of two-story housing units is located approximately 300 feet southwest of the test site and extends in that direction for approximately 1800 feet (see Figure 1). The test building and adjacent structures are shown in Figure 2. The test building has basic plan dimensions of 22 x 75 feet with a 16 x 19 feet wing (Figure 3). The roof pitch is 11.5 degrees and the eaves overhang is 2.5 feet.

3.0 FULL-SCALE TEST PROCEDURE

Surface pressures were measured at nine points on the roof (P1-P9) and at one point under the eaves (P10). In addition, the internal pressure was measured in the garage area (P12). An additional pressure tap (P11) was installed under the eaves in the wind-tunnel model. To avoid penetrating the roof membrane with pressure taps and at the same time accurately measure pressures over the roof surface, the pressure transducers were mounted under low-profile housings having a height of 1.4 inches and a diameter of 2 feet. All transducers were referenced to a vane-mounted pitot static tube located 9.5 feet above the ridge line, i.e., 20 feet above ground level.

Wind speed and direction were obtained with a propeller-vane anemometer located 21.5 feet above ground level. A standard National Weather Service three-cup anemometer was used to trigger the data acquisition system when wind speeds exceeded a preset level. Positions of the pressure transducers, pitot static probe, and anemometers are shown in Figure 3.

A fourteen-channel analog tape recorder was used to acquire data. In addition to the eleven pressure signals, wind speed, and wind direction, a time code was recorded to identify the data runs or records. Normal operating procedure was to set the system threshold at 40 mph and record for fifteen minutes. The system would then enter a one-hour hold period before checking the wind speed against the preset value. While this procedure resulted in a number of redundant records, it did provide data corresponding to peak winds in winter storms passing through the region. These storms generally had a duration of from one to three days. Barometric pressure, temperature, and other weather data were obtained from hourly observations made by the 3rd Weather Wing, USAF.

4.0 WIND TUNNEL TEST PROCEDURE

In order to increase the value of the full-scale test results, aid in their interpretation and explore the feasibility of modeling the natural wind at an unconventional scale, a series of wind tunnel tests were conducted during the course of the study using a model scale of 1:50.

The tunnel used for these tests is one of several operated by Colorado State University and has a 6 ft. square by 40-ft. long working section. To simulate the natural wind, a thick shear layer was established by use of a row of spires and a sawtooth fence installed at the working section entrance. In addition, all adjacent and upwind structures were modeled in the tunnel. This approach has been described by Melbourne (1) and Standen (2) and when compared with results obtained using surface roughness elements alone, it substantially increased the growth rate of the boundary layer and increased the scale of turbulence at the position of the model, 33.7 feet downstream from the spires. Spire details and position of the model are shown in Figure 4.

Pressures were measured with the same transducers and recording system used for the full-scale study. The orifice-tube combinations exhibited a satisfactory frequency response out to 100 Hz. All pressure measurements were referenced to a pitot static tube located four feet above the tunnel floor, directly over the building model. Wind speed records and static and dynamic pressures were obtained by means of a hot-wire anemometer and pitot tube located in the same relative positions as the instruments in the full-scale study. In addition, mean velocity profiles were obtained at the position of the model for each of the four wind directions studied.

5.0 DATA REDUCTION AND ANALYSIS

Analog tapes containing full-scale and wind tunnel data were processed using the data system described in Ref. 3. The usual procedure was to plot the full-scale wind speed and direction records on a stripchart recorder and to then select those records exhibiting a satisfactory degree of stationarity for detailed analysis. Analog to digital conversion was accomplished at a rate of sixteen samples per second with a total of 12,000 samples per record or a digital record length of 750 seconds. By using a reduced playback speed, it was possible to digitize the wind tunnel data at the same effective rate and account for the 50:1 change in time scale. Thus the time and frequency scales were assumed to be identical in the subsequent data analysis. With the exception of the hot-wire records, all records were obtained from transducers exhibiting linear characteristics.

A series of computer programs have been developed at the NBS for the analysis of random data. These include PROGRAM 2 which formats sequential channel samples into sequential samples for a given channel; CORREL which performs low-pass filtering and contains options for computing the mean, rms, auto- and cross-correlation, spectral density and coherence functions; PDF which computes probability densities and tabulates peak values and associated zero-crossing rates; and SUMP which generates a new data series based on the area integration of surface pressures. In addition, subroutines exist for linearizing hot-wire records and correcting fixed-direction propeller anemometer records for departures from the cosine law.

In the study reported herein, no attempt was made to remove trends from the data series prior to analysis, the records being visually screened before conversion. However, even with this screening, there were certain records processed which indicated significant trends as reflected by their segmental means and auto-correlation functions. Most steps in the analysis were preceded by low-pass filtering, each four successive samples being averaged and resulting in a record size of 3,000 samples. Auto-correlations were calculated for 200 lags, followed by a 0.02 Hz fixed-bandwidth spectral analysis.

6.0 MEASUREMENT RESULTS AND DISCUSSION

Field measurements at the Montana test site were obtained over a five-month period during 1971-72, yielding approximately fifteen hours of recordings under strong wind conditions. Four different wind directions were selected for subsequent wind tunnel simulation on the basis of differing obstructions over the wind fetch. Due to demands placed on test equipment, only a preliminary analysis of the field data was available at the time the wind tunnel studies were conducted. This proved to be unfortunate in that a better simulation of the natural wind could have been achieved with slight additional effort.

In the following sections, run numbers with three digits designate full-scale data and wind azimuth angles (β) are measured clockwise from north.

6.1 Simulation of the Atmospheric Boundary Layer

Because of the model scale used in this study and the physical size of the wind tunnel facility, a simulation of only the lower 100 feet of the atmospheric boundary layer was attempted. Restrictions placed on the use of the field test site did not allow the installation of a meteorological tower of sufficient height to establish

characteristics of the atmospheric boundary layer over this range. Field measurements of wind speed were thus limited to one point, 21.5 feet above ground level. As will be discussed later, this necessitated corrections to the mean reference speeds and pressures during the data analysis.

Typical mean velocity profiles measured at the position occupied by the model (33.7 feet downstream) are shown in Figure 5 as a power law representation. In plotting these profiles, it was assumed that the actual scale of the shear flow was 1:50 and that the thickness of the atmospheric boundary layer was 900 feet. The first profile corresponds to the case of only the spires and sawtooth fence installed and exhibits a satisfactory velocity distribution only up to a full-scale height of approximately thirty feet. The second profile corresponds to an azimuth angle of β = 341 degrees, the direction having the least number of structures upwind. Although the profile agrees well with the power law up to approximately ninety feet, there is a substantial departure above this height. Only for azimuth angles of 186, 211, and 256 degrees did the mean velocity profiles correspond to the power law above 100 feet. The departure of the profile for β = 211 degrees from the power law for $Z/Z_G < 0.025$ is due to the neighboring house directly upwind.

While the exponents obtained from the plots in Figure 5 are in good agreement with recommended values for terrain typical of the test site, there is nothing to suggest that the scale ratio is in fact 1:50. The profiles for β = 211, 256, and 341 degrees are plotted as a log law in Figure 6. The corresponding roughness heights (Z_o), were found to be 0.12, 0.23, and 0.007 inches (0.30, 0.58, and 0.02 cm). Helliwell (4) determined a value of 8 cm. for open country at Heathrow and Cardington. This would suggest a scale ratio of from 1:15 to 1:400 for the atmospheric boundary layer simulation. Only the very lowest portion of the profile for β = 341 degrees corresponds to the log law and it is suggested that the scale ratios associated with the peaks of the turbulence spectra are more meaningful.

Spectral density functions for β = 256 degrees (Run Nos. 311 and 22) and Z = 21.5 feet are plotted on Monin coordinates in Figure 7. The wavelengths associated with spectral peaks are approximately 10.8 and 870 feet for model and full-scale, respectively, indicating a scale ratio of 1:80 for this wind direction. It is seen that the slopes of the spectra below and above the peaks agree reasonably well with those of the von Karman spectral density function, +1.0 and -2/3, respectively. The scale ratios obtained in this manner for β = 211 and 341 degrees were found to be 1:90 and 1:60, respectively.

Flow properties for four groups of directions are listed in Table I. Unfortunately, turbulence measurements were obtained only at Z = 21.5 feet, these being limited to the longitudinal component. With the exception β = 211 degrees, the turbulence intensities measured in the tunnel are approximately fifty percent of the corresponding full-scale values. Run No. 24 for β = 211 degrees was obtained with the spires and upwind models removed from the tunnel, the boundary layer thickness for this case being approximately sixteen inches. Also included in Table I are the maximum speeds observed in the full-scale data over a time interval of 750 seconds, the average frequency of occurrence of peak values (commonly referred to as the zero crossing rate), and the mean velocity at Z = 10 meters. Full-scale values of $\bar{U}_{10}$ are based upon the ratio $\bar{U}_{10}/\bar{U}_R$ which was measured in the wind tunnel.

The use of spires and roughness elements in tunnels with short working sections results in mean velocity profiles that are quite acceptable when compared with either the log law or power law representations. However, it is obvious that the turbulence characteristics are not always in satisfactory agreement with full-scale values.

While the shapes of the spectral density functions agree fairly well with the full-scale functions, both the scale and intensity of turbulence are low. This suggests that the surface roughness elements must be modeled at a distorted scale and that a minimum roughness must be maintained in the tunnel when modeling relatively smooth prototype surface conditions.

6.1 Pressure Measurements

It was anticipated, and later confirmed by the wind tunnel tests, that corrections would have to be applied to the full-scale dynamic and static reference pressures due to the close proximity of the anemometer and pressure probe to the test building. The procedure was to determine a static pressure correction coefficient

$$C_{sp} = \frac{\bar{P}_R - \bar{P}_{10}}{1/2\ \rho\ \bar{U}_R^2}$$

in the tunnel and to then apply this correction as an offset to all full-scale pressure records. The dynamic pressure correction coefficient

$$C_{dp} = \frac{1/2\ \rho\ \bar{U}_{10}^2}{1/2\ \rho\ \bar{U}_R^2}$$

was applied in a similar manner. Both corrections were direction-dependent and values of C_{sp} and C_{dp} ranged from -0.10 to -0.21 and from 1.02 to 1.39, respectively.

The results of pressure measurements are summarized in Tables II - V and are compared graphically in Figures 8 and 9. The mean pressure coefficient, C_p, and the fluctuating pressure coefficient, C_{pf}, correspond to the usual definitions and are referenced to the free-stream dynamic pressure at Z = 10 meters. The peak factor, g, is defined as the number of standard deviations included in the maximum peak departure from the mean, i.e.,

$$g = \frac{|p_{max\ or\ min} - \bar{p}|}{p_{rms}}$$

The zero crossing rates (Table V) are as previously defined.

The mean pressure coefficients, C_p, plotted in Figure 8 indicate considerable disagreement between model and full-scale measurements. Equipment used to measure and record the field data was somewhat prone to zero drift with the extreme range of temperatures experienced at the test site (80°F to -20°F). The field test equipment has since been modified to provide transducer zero readings and recorder calibrations prior to each data run. Corrections for this drift could not be accurately determined and any resulting errors are directly reflected by Figure 8. With the exception of Run No. 310, the addition of a fixed value for a given full-scale run would improve the agreement between the two sets of coefficients.

Changes in equipment sensitivity due to temperature variations were found to be small and, therefore, greater confidence can be put in the measurements of pressure fluctuations. Fluctuating pressure coefficients, C_{pf}, plotted in Figure 9 indicate a fairly good correlation between model and full-scale, the former averaging approximately one-half of the latter. This discrepancy is believed to be due primarily to the low turbulence intensities observed in the model studies, although scale effects cannot be completely ruled out. There is no obvious explanation for the good agreement between Run Nos. 207 and 21, and the poor agreement between Run Nos. 311 and 22. It may be that the pressure fluctuations are quite sensitive to wind direction and that directions were not properly matched in the model studies. It is expected that a new series of tunnel tests in which the turbulence characteristics are more accurately simulated will bring the results into much better agreement.

Spectral densities for tap positions P3 and P10 (Run Nos. 311 and 22) are compared in Figures 10 and 11, respectively. The shapes of the spectra compare quite favorably and suggest a slope of -4/3 over the higher frequency range. As indicated previously, the wind data were normalized on the assumption that the scale ratio was

1:50. Although the peaks are not well defined, they suggest a scale ratio in line with that obtained by comparing the velocity spectra.

Spectral densities for the full-scale pressure fluctuations above the spectral peak usually exceeded those obtained from the wind tunnel model (see Figure 11). This is quite likely due to the fact that the analog filters used in the full-scale studies had a cutoff frequency of 10 Hz, resulting in aliasing errors in the spectral analysis. The wind tunnel pressure signals, on the other hand, were subjected to pronounced attenuation above 100 Hz which would appear as a 2 Hz cutoff in the analysis. Thus the aliasing errors can be expected to be considerably smaller for the wind tunnel data.

Another indication of similarity between model and full-scale pressure fluctuations is the coherence function. The coherence function, or more properly $(\text{coherence})^{1/2}$, is the normalized modulus of the cross-spectrum and is a measure of the correlation between fluctuations at two points over the frequency range for a given separation distance. This function for P1-P6 and Run Nos. 310 and 23 is plotted in Figure 12.

The peak factors, which are listed in Table IV, are fairly consistent and suggest an average value of 4.6. It has been shown, both theoretically and experimentally (5, 6), that the peak factor increases with length of record and a value of $g = 4.3$ has been suggested for calculating design loads on cladding elements for those situations where resonant response is insignificant. The peak factors in Table IV are based upon single records of 750 seconds and represent a worst-case excursion from the mean, i.e. negative excursions for pressure taps 1-9 and positive excursions for taps 10-12. It should be pointed out that the peak factors will vary from record to record for a given wind speed and direction and that several records would be required to establish their mean and variance.

Fluctuating pressure coefficients and peak factors determined from the area-integration of pressure records are presented in Table VI. The procedure was to construct a new pressure time series by multiplying the samples of each record to be summed by a weighting factor. The weighting factor was proportional to the area attributed to each pressure tap which implies that all pressure fluctuations over that area are perfectly correlated. The resulting record was then analyzed in the usual manner. As expected, the fluctuating pressure coefficients show a decrease in increasing area, but there is no indication of a similar reduction in the peak factor. Although the transducer separations used in this study do not permit a detailed assessment of the correlation of peak pressures acting over extended roof areas, some indication of the area reduction of peak pressures can be derived from Table VI. Comparing the product of the fluctuating pressure coefficient and peak factor for transducer combinations 1, 2, 3 for Run No. 332 with the product of the averaged fluctuating pressure coefficients and peak factors for the individual transducers (Tables III and IV), the corresponding reductions in peak pressure fluctuations are approximately 27 and 40 percent, respectively. A similar comparison for the combination 1, 2, 3, 6, 7, 10, 12 (Run No. 310) indicates a reduction of 42 percent. In averaging the pressure records, it was assumed that the pressure fluctuations under the eaves overhang were perfectly correlated and equal to the fluctuations measured by transducer No. 10. An increase of 42 percent was obtained from the combination 1, 2, 3, 10 for Run No. 310. It should be noted that the records for transducer Nos. 10 and 12 were inverted so that positive fluctuations acted in the same sense as negative fluctuations on the roof.

7.0 COMPARISON WITH RECOMMENDED DESIGN LOADS

In addition to providing a check on wind tunnel test results, the full-scale data reported herein allow some direct comparisons with current recommended design wind loads. American National Standard Building Code Requirements for Minimum Design Loads in Buildings and Other Structures, A58.1-1972, states a procedure for calculating wind loads on roofs

and considers both tributary (parts and portions) and total roof areas (7). The basic wind speeds used in this document are the fastest-mile speeds for a 50-year mean recurrence interval and flat, open country (Exposure C) at a height of 30 feet above ground.

Because they are defined differently, the pressure coefficients measured in full-scale and those specified in the A58.1 Standard cannot be compared directly. However, the pressure can be compared for a given wind speed and category of exposure. Assuming flat, open country and a basic wind speed of 90 mph, the corresponding effective velocity pressures for heights less than thirty feet are as follows:

q_f = 20 psf (A58.1 - Table 5 - Ordinary Buildings and Structures)

q_p = 31 psf (A58.1 - Table 6 - Parts and Portions)

For buildings with a ratio of wall height to least width of less than 2.4, the A58.1 Standard specifies a general external pressure coefficient of -0.7 for roofs. For gabled roofs with the wind direction perpendicular to the ridge and the height-width ratio and roof slope being considered here, a pressure coefficient of -1.0 is specified for the windward slope. The Standard also allows for local peak pressures which are assumed to act at ninty-degree corners and on strips running along the ridge and eaves. The width of these strips is taken as ten percent of the least width of the building normal to the ridge. The specified pressure coefficients are -2.4 for ridges and eaves and -3.9 for ninety-degree corners.

No specific provision is made for pressures on the underside of eaves, but this can be taken as the pressure acting on the windward wall for which a coefficient of 0.8 is specified. Internal pressures are based on the fastest-mile speed at thirty feet above ground for the appropriate terrain category and an internal pressure coefficient, C_{pi}, which is related to the distribution of wall openings and the ratio of open to solid wall area. The design pressures for the assumed wind speed and exposure are as follows:

(a) Leeward Slope, Total Area = (-0.7)(20) = - 14 psf

(b) Windward Slope, Total Area = (-1.0)(20) = - 20 psf

(c) Leeward Slope, Tributary Area = (-0.7)(31) = - 21.7 psf

(d) Windward Slope, Tributary Area = (-1.0)(31) = - 31 psf

(e) Ridges and Eaves = (-2.4)(31) = - 74 psf

(f) Ninety-Degree Corners = (-3.9)(31) = -121 psf

(g) Underside of Eaves = (0.8)(31) = 25 psf

(h) Internal Pressure = (0.3)(21) = 6.3 psf

At Z = 10 meters, the corresponding mean speed averaged over 750 seconds (the record length used in this study) is approximately 75 mph (see Ref. 8). For standard atmospheric conditions, the effective velocity pressure is 14 psf. Using the full-scale pressure coefficients listed in Tables II, III, and IV, the mean and peak pressures were calculated for ten transducer locations and four wind directions. The results are presented in Figure 13 along with the design pressures specified by the A58.1 Standard (Case f excepted.)

It is seen from Figure 13 that the negative design pressures for the total leeward and windward roof areas (Lines a and b) exceed the observed mean pressures for all transducer locations. However, the observed peak pressures dominate and exceed the design pressures for tributary areas (Lines c and d) at several locations. This may or may not be significant, depending on the degree to which pressure fluctuations are correlated over the roof area. The design pressures for ridges and eaves (Line e) substantially exceed the observed peak pressures and the design pressure for ninety-degree corners is approximately 2.5 times

the maximum observed negative pressure. The positive design pressure for the underside of the eaves (Line g) is exceeded by the observed peak pressure for two wind directions and the internal design pressure (Line h) is less than the measured peak internal pressure for all four wind directions.

As discussed previously, the fluctuating pressure coefficients determined from the area-integration of pressure records decrease with increasing area while the peak factors remain about the same. Although reductions from twenty to forty percent in the peak pressures (peak departures from the mean) are indicated for roof areas of up to fifty square feet, the data presented in Figure 13 suggest that the provisions of the A58.1 Standard for tributary roof areas are marginal.

The provisions for ridges and eaves and for ninety-degree corners, on the other hand, appear to be overly conservative. The maximum negative pressure, based on the measured coefficients, was -50 psf for transducer No. 1 at 256° while the design pressures are -74 psf for ridges and eaves and -121 psf for ninety-degree corners. It is recognized that extreme negative pressures are associated with vortices generated along the edges of the roof and that these vortices are extremely sensitive to wind direction and roof geometry. However, the wind tunnel studies described previously did not reveal any critical wind directions not covered by the full-scale data. If the effective velocity pressure of 20 psf (q_f) is used in place of 31 psf (q_p), the resulting design pressures are -48 psf for ridges and eaves and -78 psf for ninety-degree corners.

As with the negative pressures acting over the roof area, the peak pressures under the eaves (Transducer No. 10) and in the garage area (Transducer No. 12) far exceed the corresponding mean pressures averaged over the record length of 750 seconds. Again referring to Table VI and Figure 13, the average maximum pressure (peak plus mean) acting upward on the eaves is 3 - 3 + 35 = 35 psf for Run No. 310 and combination 1, 2, 3, 10. The corresponding design uplift pressure is 74 + 25 = 99 psf. For combination 1, 2, 3, 6, 7, 10, the average maximum pressure acting over a roof area of 258 square feet is 3 + 13 = 16 psf as compared with 2117 + 6.3 = 27 psf (tributary area plus internal pressure) as specified by the A58.1 Standard.

The maximum internal pressure (based on measured coefficients) in the garage area was approximately five times the corresponding design pressure. The ratio of effective open area to solid area is difficult to determine since all doors and windows were closed during the recording intervals reported herein. One door and one window of approximately nineteen and fifteen square feet, respectively, are located on the southeast wall, one window of fifteen square feet on the southwest wall, and an overhead garage door of 55 square feet is situated on the northwest wall. Because of the extremely cold winters in Montana, great care is usually taken to provide doors and windows with adequate seals or weatherstripping. It is probable, therefore, that infiltration rates for this garage area would compare with those for living quarters in regions having a mild climate.

8.0 A PROCEDURE FOR THE CALCULATION OF DESIGN PRESSURES

The 1970 edition of the National Building Code of Canada (NBC) (9) provides for risk of occurrence, terrain roughness, height above ground and building geometry in calculating design wind pressures

$$p = q\, C_e\, C_g\, C_p \qquad (1)$$

In this expression, q is a reference mean velocity pressure for a given mean recurrence interval, C_e is an exposure factor which varies with surface roughness and height above ground, C_g is a gust effect factor to provide for the dynamic response characteristics of the structure and surface pressure fluctuations caused by turbulence and localized flow phenomena, and C_p is the conventional mean pressure coefficient determined from wind tunnel tests. For the design of cladding, it is assumed that dynamic response can be neglected and a factor of 2.5 is used for C_g.

The form of Equation (1) is particularly convenient in that it allows a complex process to be treated as a combination of independent elements and provides for the separate treatment of mean and fluctuating components of pressure. The peak design pressure at any point on a roof area can be expressed as

$$p = C_g\bar{p} = \bar{p} \pm gp_{rms}$$

Or in terms of dimensionless pressure coefficients based upon a suitable reference pressure, such as the free-stream dynamic pressure at Z = 10 meters,

$$C_g = 1 + g\frac{C_{pf}}{|C_p|} \tag{2}$$

While Equation (2) is a practical means of expressing C_g, full-scale and wind tunnel measurements (Figures 14 and 15) suggest an empirical relationship between C_{pf} and C_p. If the envelope of full-scale C_{pf} values is expressed as

$$C_{pf} = 0.3(1 + |C_p|)$$

and it is assumed that g = 5.0, Equation (2) becomes

$$C_g = 1 + 1.5\frac{(1 + |C_p|)}{|C_p|} \tag{3}$$

As indicated earlier, the peak factor g does not appear to change with surface area. Therefore, it may be possible to determine a gust factor, C_g^a, for extended roof areas simply by reducing C_{pf} by means of a factor, R_p, roughly analogous to the size reduction factor used in calculating dynamic response. The gust effect factor would then be defined by

$$C_g^a = 1 + 1.5\frac{(1 + |C_p|)\ R_p}{|C_p^a|} \tag{4}$$

where C_p^a is the corresponding mean pressure coefficient for the extended roof area.

9.0 CONCLUSIONS

The use of spires at the entrance of a wind-tunnel working section substantially increases the growth rate of rough wall boundary layers, thereby placing the study of building aerodynamics within the capability of many conventional tunnels. However, the use of spires and scaled upwind roughness elements does not alone ensure the establishment of flows with proper turbulence characteristics. A minimum degree of surface roughness is required to establish suitable scales and intensities of turbulence. With some modification of the roughness elements, it is believed that close simulation of the lowest 100 feet of the atmospheric boundary layer can be achieved at a scale ratio of 1:50.

The agreement between model and full-scale spectra for both velocity and pressure fluctuations is encouraging. Measurements of coherence suggest that the spatial extent of surface pressure fluctuations can be modeled to an acceptable degree.

It is believed that the consistently low values of C_{pf} determined from the model result primarily from improper simulation of the turbulence. However, scale effects cannot be ruled out at this time. Peak factors were found to agree quite closely with previous measurements, the overall average for model end full-scale results being 4.6. Based on the preliminary results reported herein, it appears that a gust effect factor can be expressed in terms of a peak factor, mean pressure coefficients and a size reduction factor.

Wind pressures based on measured coefficients and an assumed wind speed suggest that certain provisions of the current A58.1 Standard deserve additional study. For the buildin

investigated, design pressures for tributary areas and interiors appear to be marginal while those for localized areas such as ridges, eaves, and corners appear to be excessive.

10.0 ACKNOWLEDGMENTS

Acknowledgment is made to the Tri-Services Committee, Department of Defense, for financial support of the field studies reported herein. The writer wishes to express his thanks to Lt. Col. C.Y. Holland, Jr., USAF, for his assistance at the field test site and to Col. R.A. Nelson and family whose home was instrumented during the course of the study. Special thanks are extended to Dr. H.I. Laursen who developed much of the computer software used in the data analysis.

11.0 BIBLIOGRAPHY

1. Melbourne, W.H., "Comparison of Pressure Measurements Made on a Large Isolated Building in Full and Model Scale." Proceedings, Third International Conference on Wind Effects on Buildings and Structures, Tokyo, 1971, pp. 253-262.

2. Standen, N.M., "A Spire Array for Generating Thick Tubulent Shear Layers for Natural Wind Simulation in Wind Tunnels." National Aeronautical Establishment Report LTR-LA-94, Ottawa, May 1972.

3. Marshall, R.D. and Hsi, G., "Techniques for Measuring Wind Loads on Full-Scale Buildings." Proceedings, Research Seminar on Wind Loads on Structures, University of Hawaii, October, 1970, pp. 133-148.

4. Helliwell, N.C., "Wind Over London." Proceedings, Third International Conference on Wind Effects on Buildings and Structures, Tokyo, 1971, pp. 23-32.

5. Dalgliesh, W.A., "Statistical Treatment of Peak Gusts on Cladding." Proceedings of the Structural Division, ASCE, September, 1971, pp. 2173-2187.

6. Davenport, A.G., "Note on the Distribution of the Largest Value of a Random Function with Application to Gust Loading." Paper No. 6739, Proceedings, Institution of Civil Engineers, Vol. 28, June, 1964, pp. 187-196.

7. American National Standard Building Code Requirements for Minimum Design Loads in Buildings and Other Structures, A58.1-1972. Issued by American National Standards Institute, New York, New York.

8. Deacon, E.L., "Wind Gust Speed; Averaging Time Relationships." Australian Met. Mag. No. 51, 1965.

9. National Building Code of Canada 1970. Issued by the Assoc. Comm. on the NBC, National Research Council, Ottawa, Canada.

NOTATION

The following symbols are used in this paper:

C_{dp} = Dynamic pressure correction coefficient

C_e = Exposure factor

C_g = Gust effect factor

C_p = Mean pressure coefficient

C_{pf} = Rms pressure coefficient

C_{sp} = Static pressure correction coefficient

I = Intensity of turbulence, in percent

U_{10} = Mean velocity at standard ten-meter height, in feet per second

U_R = Reference mean velocity at 21.5 feet

Z = Height above ground, in feet

Z_G = Gradient height

Z_o = Surface roughness height, in inches

g = Peak factor

p = Mean pressure, in pounds per square foot

p_{rms} = Rms pressure

p_R = Reference dynamic pressure at 21.5 feet

p_{10} = Reference dynamic pressure at ten meters

q = Reference dynamic pressure for open country

R_p = Size reduction factor

β = Wind direction measured clockwise from north, in degrees

ρ = Mass density of air, in slugs per cubic foot

LIST OF TABLES

TABLE I Flow Properties

TABLE II Mean Pressure Coefficients (C_p)

TABLE III Fluctuating Pressure Coefficients (C_{pf})

TABLE IV Peak Factors (g)

TABLE V Zero Crossing Rates

TABLE VI Area-Averaged Coefficients

LIST OF FIGURES

FIGURE 1 Aerial View of the Test Site

FIGURE 2 Test Site Layout

FIGURE 3 Plan and Elevation of the Test Building

FIGURE 4 Wind Tunnel Layout

FIGURE 5 Mean Velocity Profiles - Power Law Representation

FIGURE 6 Mean Velocity Profiles - Log Law Representation

FIGURE 7 Velocity Spectra (Runs Nos. 311 and 22)

FIGURE 8 Mean Pressure Coefficients

FIGURE 9 Fluctuating Pressure Coefficients

FIGURE 10 Pressure Spectra (P3, Run Nos. 311 and 22)

FIGURE 11 Pressure Spectra (P10, Run Nos. 311 and 22)

FIGURE 12 Coherence (P1-P6, Run Nos. 310 and 23)

FIGURE 13 Comparison of Measured and Specified Design Pressures

FIGURE 14 C_p vs. C_{pf} - Full Scale

FIGURE 15 C_p vs. C_{pf} - Wind Tunnel

TABLE I

FLOW PROPERTIES

Run* Number	Direction (degrees)	$\bar{U}_R$ (m/s)	$\sqrt{u^2}$ (m/s)	I (percent)	Maximum Peak (m/s)	Zero Crossing Rate (Hz)	$\bar{U}_{10}$ (m/s)
207	186	11.37	3.38	30	19.93	.267	12.07
21	186	11.89	2.54	21	-	-	12.62
310	217	7.77	2.93	38	18.41	.158	9.14
23	211	13.17	4.08	31	-	-	15.51
24	211	18.71	1.10	6	-	-	18.78
311	256	8.38	2.62	31	16.25	.169	8.47
22	256	14.69	2.59	18	-	-	15.06
322	309	9.91	2.35	24	15.64	.166	10.36
11	341	13.78	1.43	10	-	-	14.14
101	347	9.24	2.50	27	14.81	.211	9.45

*Run numbers with 3 digits denote full scale data.

TABLE II

MEAN PRESSURE COEFFICIENTS

C_p

Run Number	Direction (degrees)	Pressure Tap Number											
		1	2	3	4	5	6	7	8	9	10	11	12
207	186	-.38	-.43	-.59	-.45	-.64	-.44	-.29	-.32	-.56	-.08	-	-.20
21	186	-.49	-.59	-.76	-.68	-.62	-.22	-.24	-.06	-.14	.45	-.21	-
310	217	.26	.23	-.18	-.18	-.38	-.05	-.05	-.41	-	.22	-	.24
23	211	-.09	-.11	-.14	-.13	-.18	-.05	-.03	-.04	-.04	.08	.07	-
24	211	-1.00	-.60	-.53	-.55	-.63	-.22	-.12	-.16	-.02	.67	-.19	-
311	256	-.12	.12	-.36	-.45	-.61	-.84	-.21	-.70	-	.46	-	.35
22	256	.10	-.11	-.36	-.55	-.59	-.41	.10	-.54	-.18	.30	.37	-
322	309	-.52	-.05	-.22	-.20	-.24	-.78	-.47	-.47	-	-.09	-	.15
11	341	-.32	-.14	-.15	-.23	-.12	-.50	-.14	-.37	-.10	-.12	.30	-

TABLE III

FLUCTUATING PRESSURE COEFFICIENTS

C_{pf}

Run Number	Direction (degrees)	Pressure Tap Number											
		1	2	3	4	5	6	7	8	9	10	11	12
207	186	.24	.28	.32	.32	.31	.21	.19	.18	.21	.27	-	.19
21	186	.25	.28	.31	.33	.38	.08	.09	.10	.08	.26	.08	-
310	217	.38	.33	.28	.28	.32	.32	.25	.22	-	.29	-	.29
23	211	.14	.15	.15	.15	.17	.09	.07	.07	.04	.14	.11	-
24	211	.22	.10	.09	.09	.10	.09	.05	.07	.03	.16	.07	-
211	256	.70	.29	.32	.40	.43	.62	.31	.30	-	.44	-	.43
22	256	.12	.19	.18	.25	.20	.18	.09	.24	.05	.13	.16	-
322	309	.30	.15	.15	.17	.19	.34	.21	.18	-	.15	-	.18
11	341	.13	.05	.05	.07	.07	.19	.10	.11	.05	.04	.12	-
101	347	.31	.10	.24	.12	.09	.38	.25	.20	.10	.25	-	.49

TABLE IV

PEAK FACTORS

g

Run Number	Direction (degrees)	Pressure Tap Number											
		1	2	3	4	5	6	7	8	9	10	11	12
207	186	5.9	6.8	4.4	5.1	4.5	3.7	2.6	3.1	1.5	4.7	-	3.7
21	186	5.2	7.0	4.5	6.0	4.1	3.8	3.9	6.9	6.8	4.3	4.5	-
310	217	4.5	4.9	6.6	7.1	6.4	5.4	3.8	4.3	-	5.8	-	4.6
23	211	4.0	6.5	5.7	5.8	5.1	5.3	4.3	4.9	3.9	6.6	3.3	-
24	211	2.9	6.2	4.9	5.7	4.3	3.4	3.7	3.5	4.2	5.9	3.1	-
311	256	4.9	5.5	5.0	5.0	3.9	4.3	4.8	3.4	-	5.0	-	4.7
22	256	5.7	5.4	3.9	7.0	6.3	4.5	4.3	3.3	3.4	3.5	3.9	-
322	309	4.2	3.8	5.0	3.7	7.3	4.7	6.5	3.7	-	3.1	-	3.1
11	341	3.6	4.4	3.6	4.2	6.6	5.0	3.7	6.3	3.5	4.2	3.6	-
101	347	6.4	2.7	2.3	2.8	2.6	4.8	6.4	2.9	-	2.4	-	2.0

TABLE V

ZERO CROSSING RATES

(Crossings/Sec.)

Run Number	Direction (degrees)	Pressure Tap Number											
		1	2	3	4	5	6	7	8	9	10	11	12
207	186	.37	.34	.34	.35	.36	.36	.37	.39	.31	.37	-	.25
21	186	.39	.43	.31	.35	.33	.30	.36	.34	.15	.21	.26	-
310	217	.23	.26	.32	.31	.32	.29	.27	.31	-	.31	-	.11
23	211	.29	.33	.29	.32	.35	.29	.31	.34	.16	.21	.16	-
24	211	.47	.32	.30	.33	.28	.48	.45	.52	.17	.33	.31	-
311	256	.20	.28	.26	.21	.21	.24	.34	.20	-	.26	-	.17
22	256	.30	.33	.33	.36	.28	.24	.29	.20	.12	.19	.18	-
322	309	.40	.47	.45	.36	.37	.32	.41	.30	-	.31	-	.21
11	341	.34	.49	.32	.35	.35	.25	.27	.23	.11	.22	.25	-
101	347	.47	.46	.48	.34	.42	.33	.38	.47	.44	.26	-	.22

TABLE VI

AREA-AVERAGED COEFFICIENTS

Run Number	Direction (degrees)	Tap Combination	C_{pf}	g	Area (m^2)
310	217	1,2,3	.28	4.6	(.76) (4.27) = 3.25
"	"	1,2,3,10	.40	6.2	(.76) (4.27) = 3.25
"	"	1,2,3,6,7,10,12	.21	4.3	(5.61) (4.27) = 23.97
322	309	1,2,3	.12	4.3	(.76) (4.27) = 3.25
"	"	1,6	.27	5.3	(.82) (5.61) = 4.65
"	"	4,5,10	.12	8.8	(.76) (3.05) = 2.32

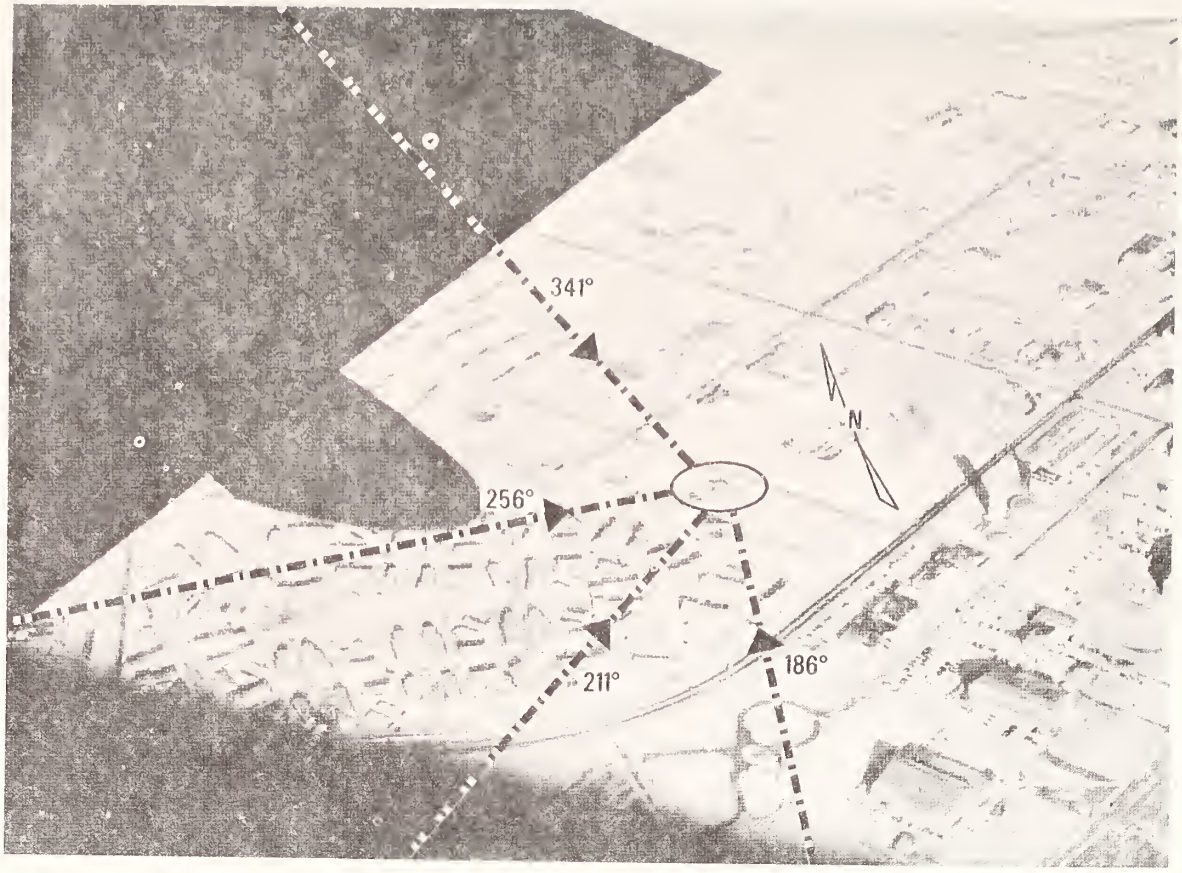

FIG. 1 AERIAL VIEW OF THE TEST SITE

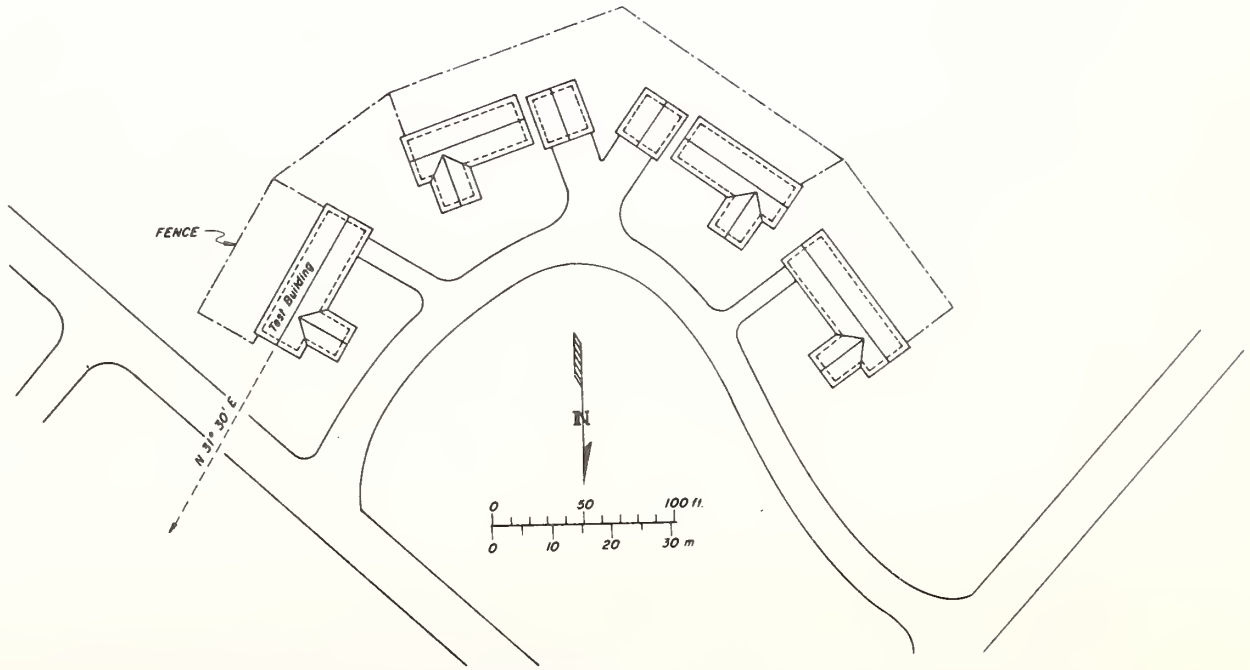

FIG. 2 TEST SITE LAYOUT

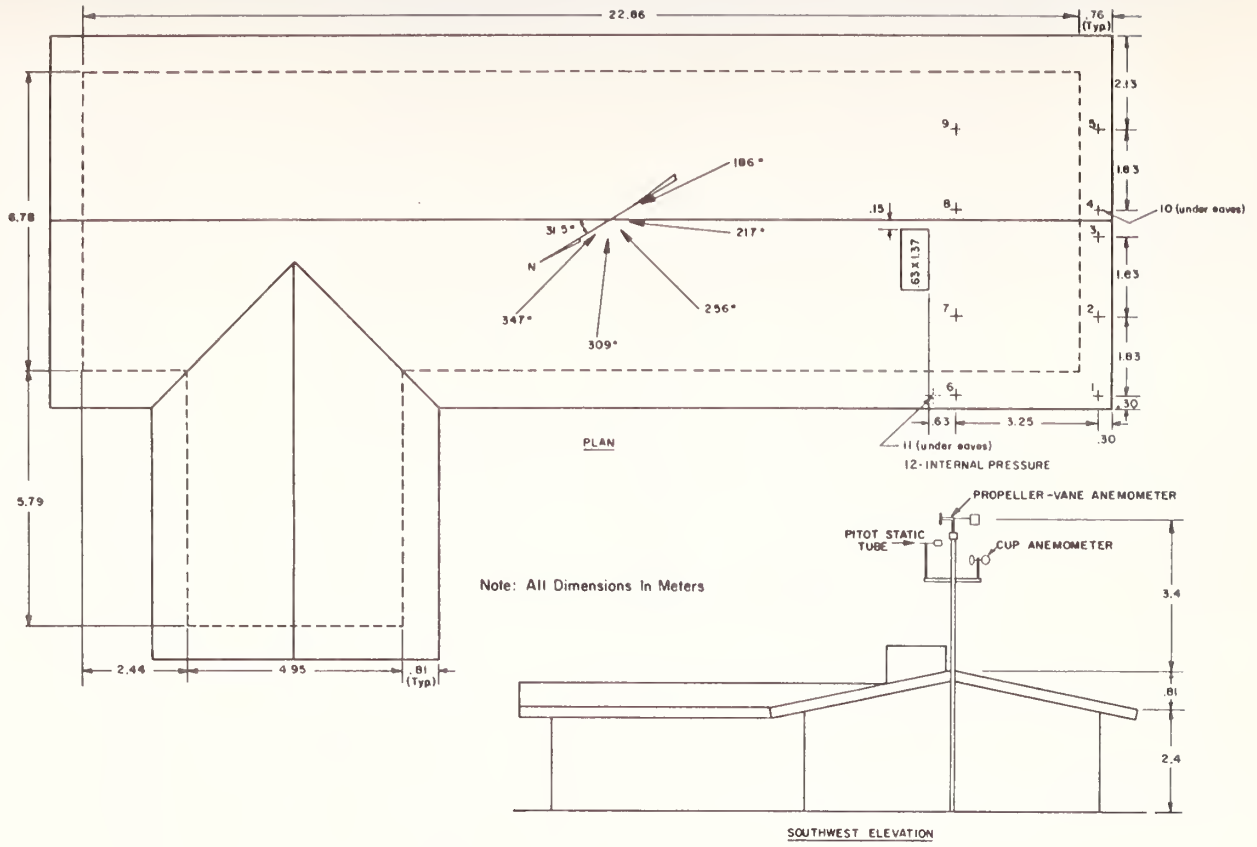

FIG. 3 PLAN AND ELEVATION OF THE TEST BUILDING

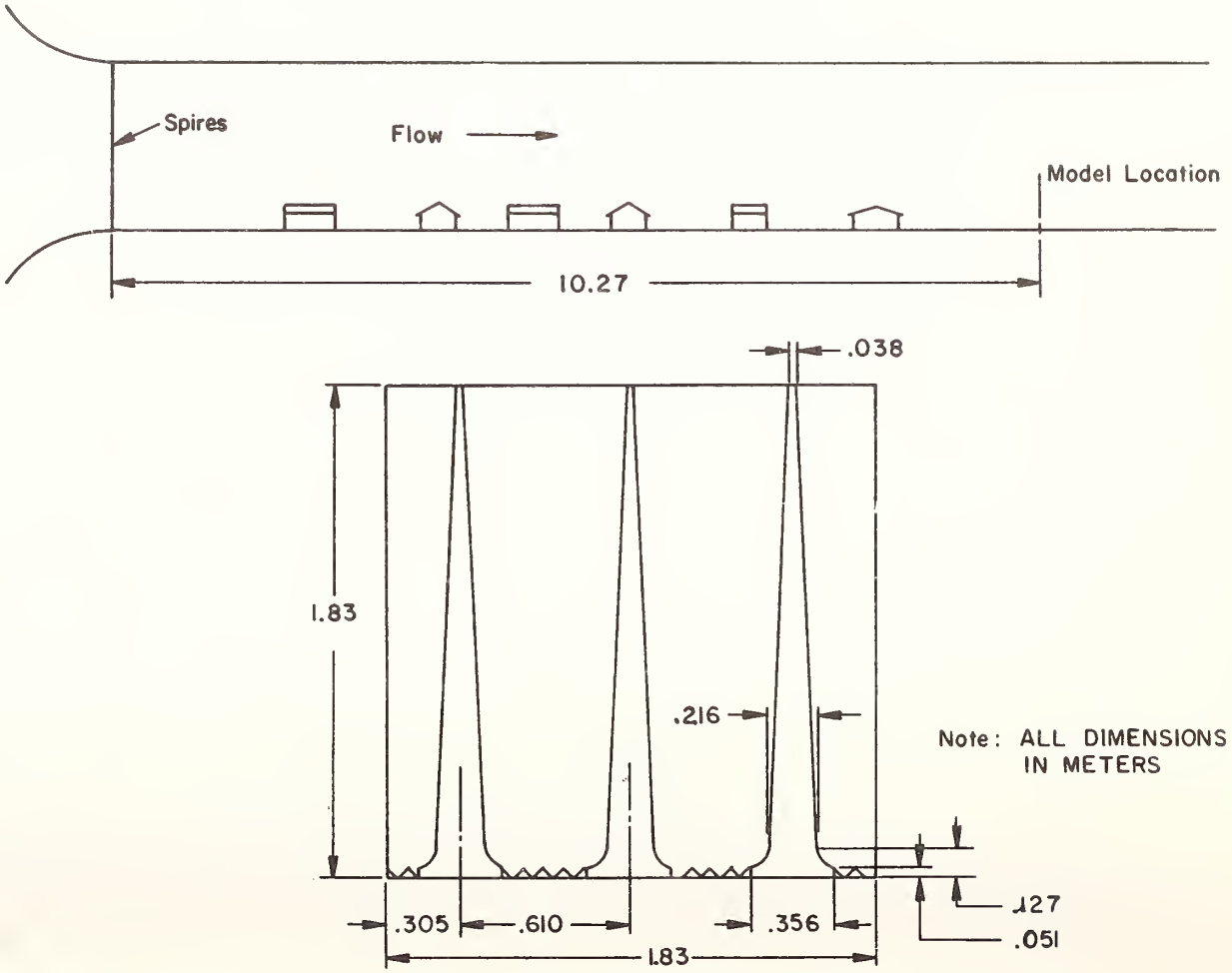

FIG. 4 WIND TUNNEL LAYOUT

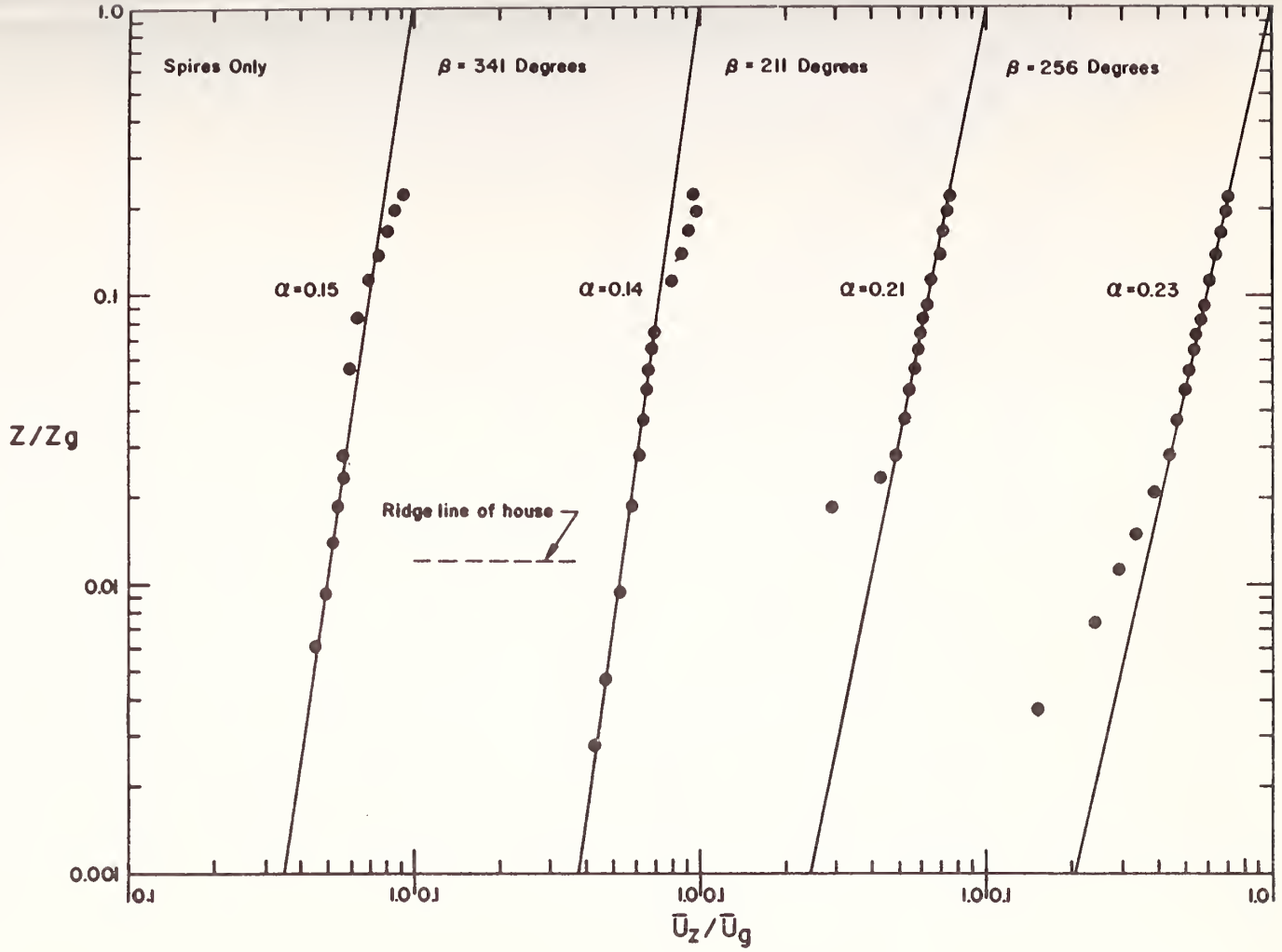

FIG. 5 MEAN VELOCITY PROFILES - POWER LAW REPRESENTATION

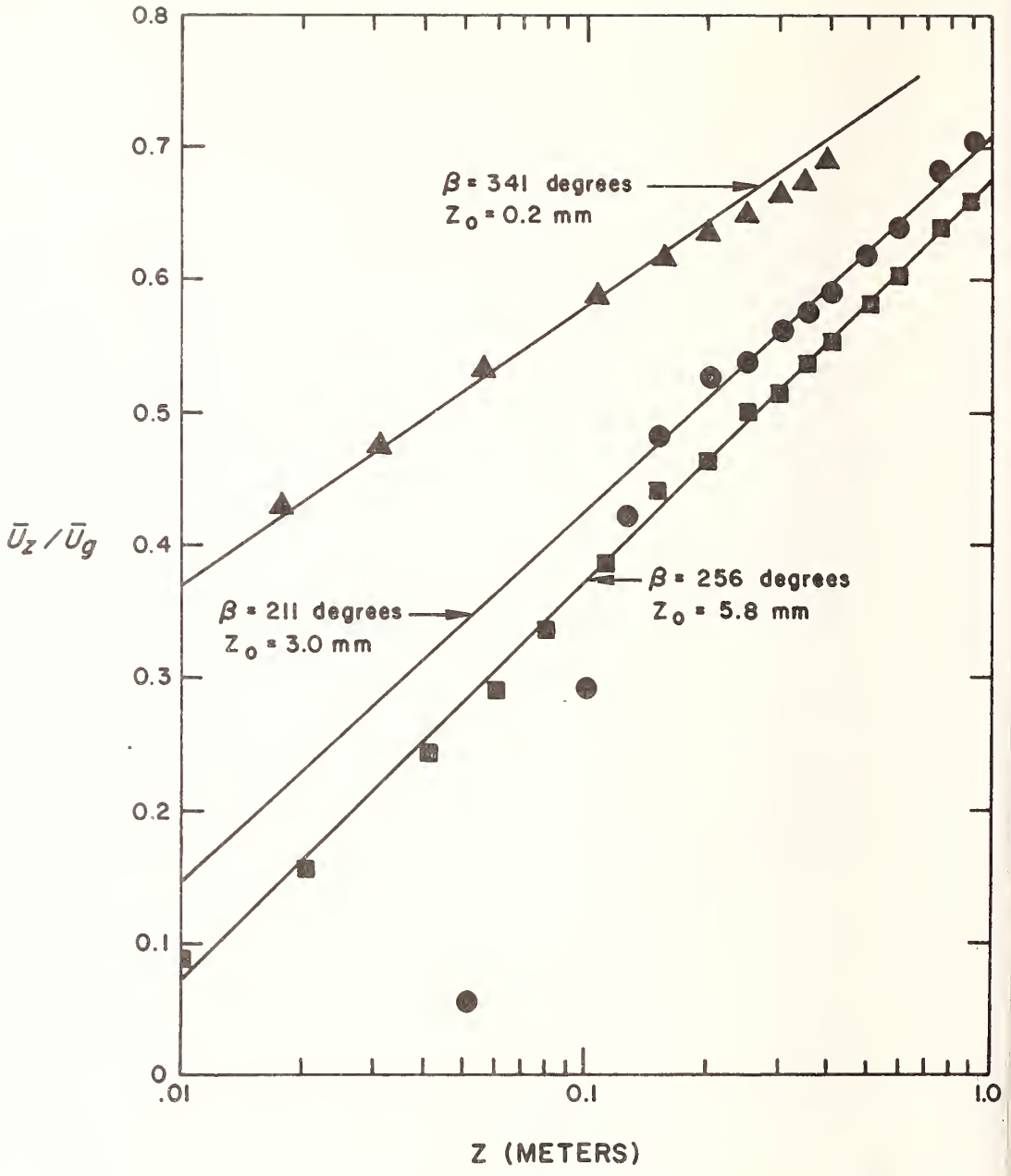

FIG. 6 MEAN VELOCITY PROFILES - LOG LAW REPRESENTATION

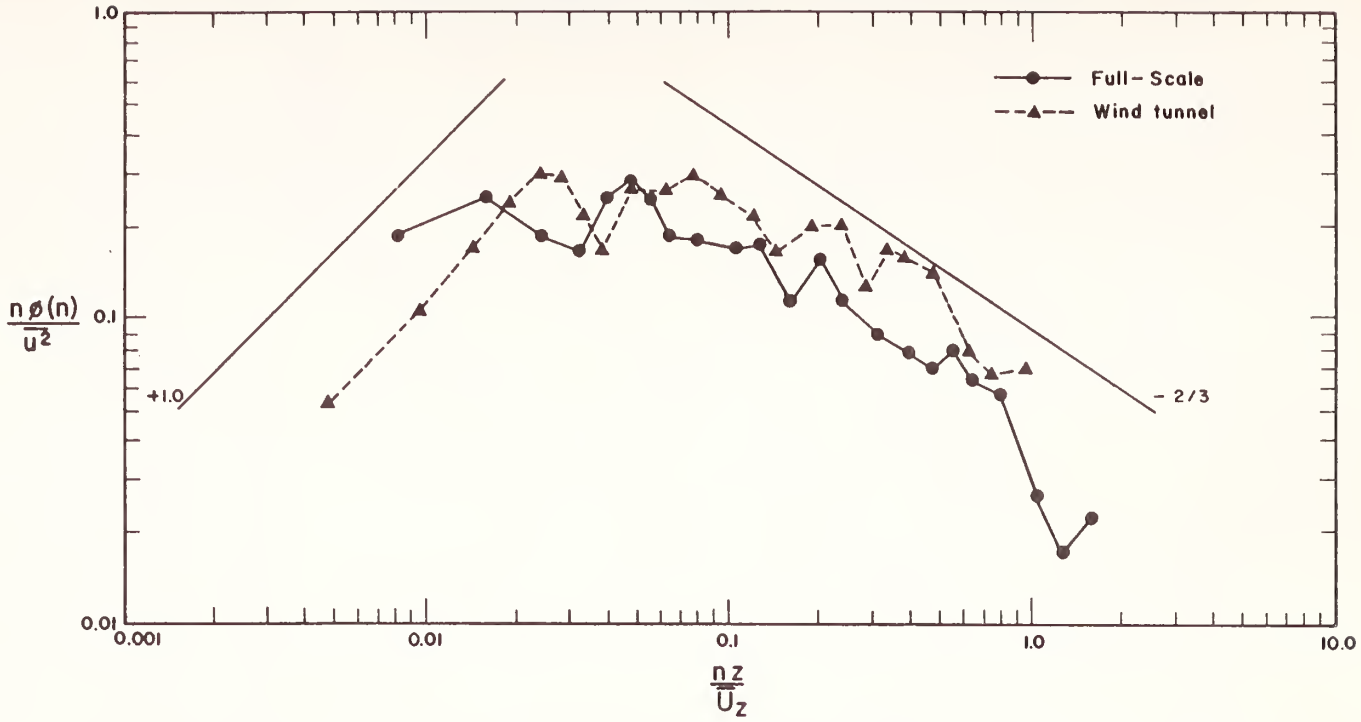

FIG. 7 VELOCITY SPECTRA (RUNS NOS. 311 & 22)

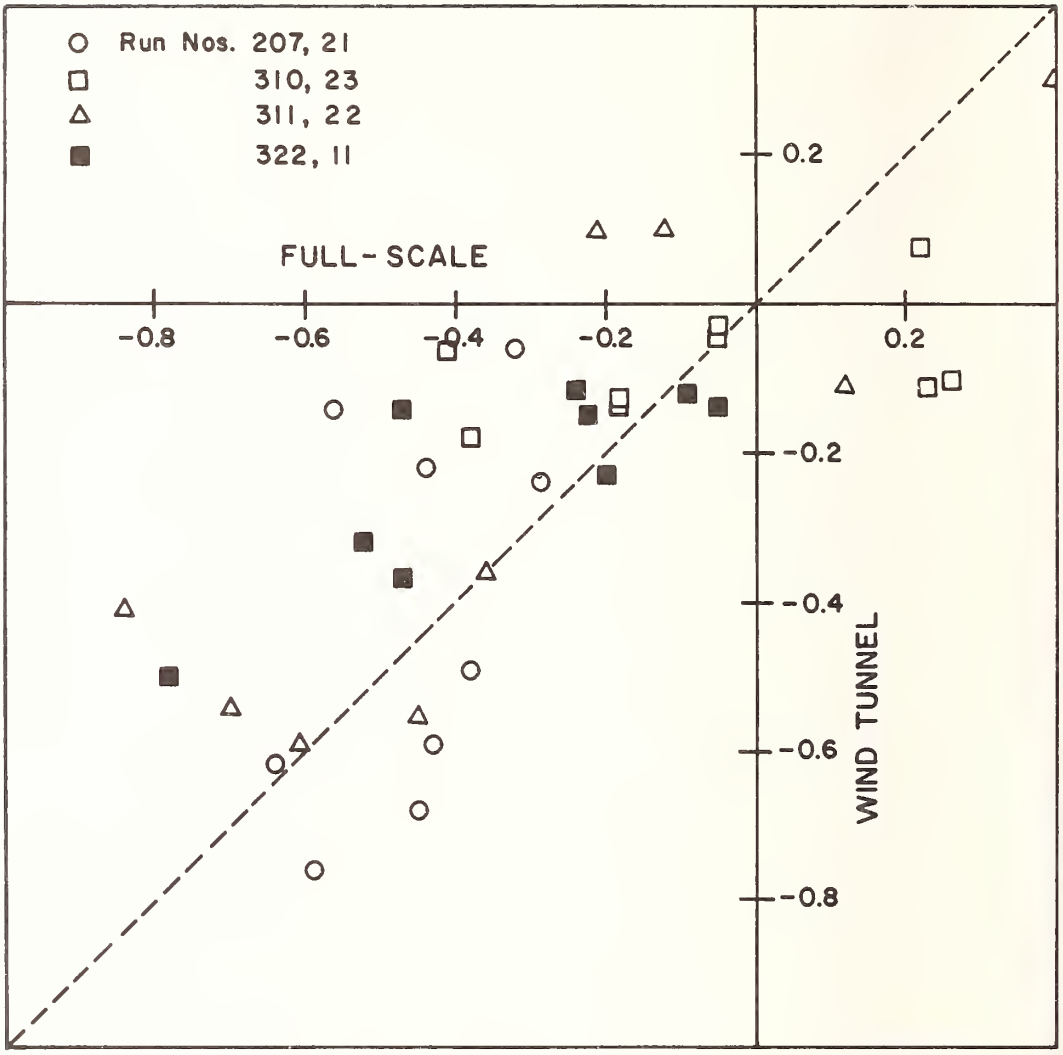

FIG. 8 MEAN PRESSURE COEFFICIENTS

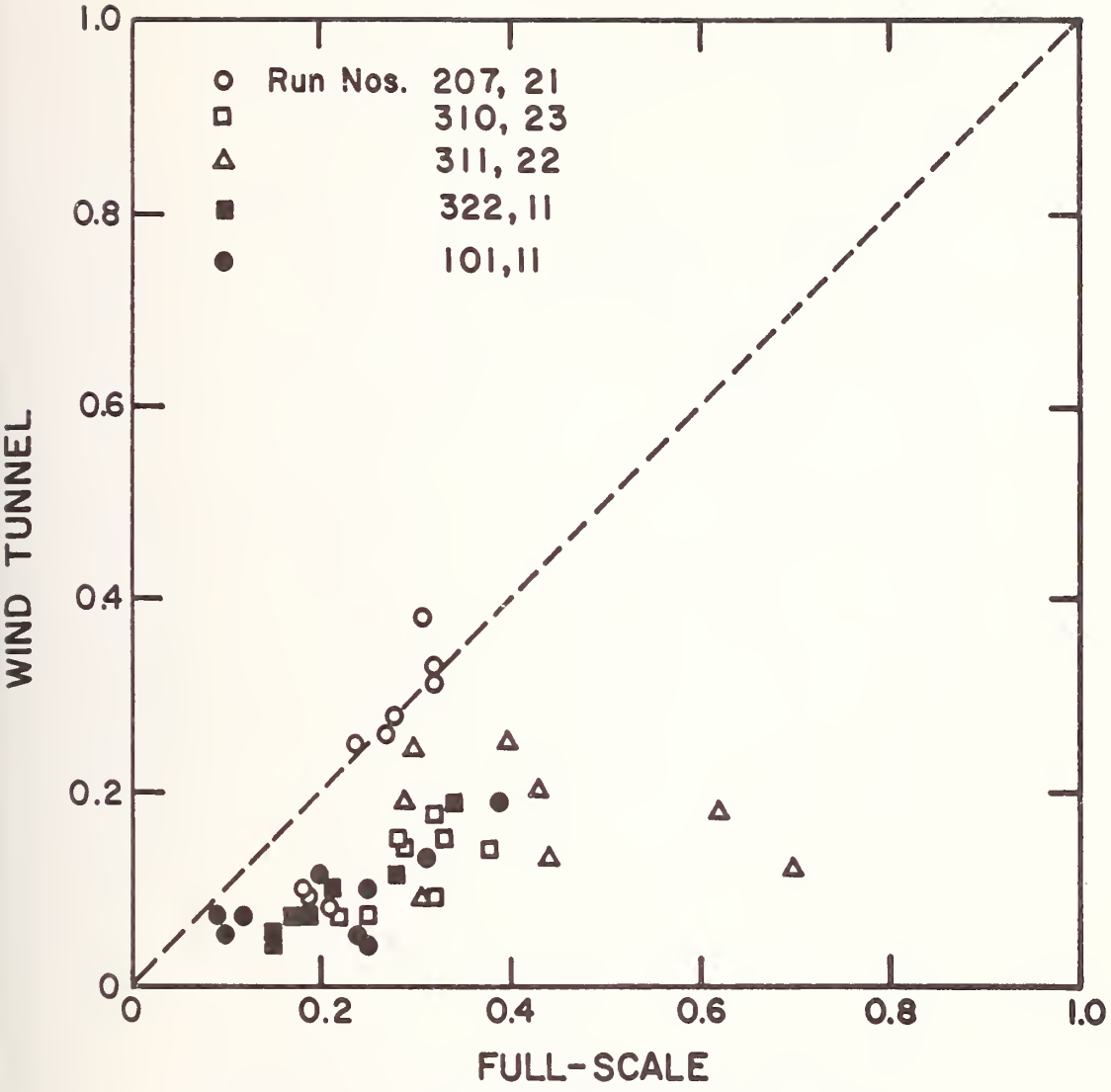

FIG. 9 FLUCTUATING PRESSURE COEFFICIENTS

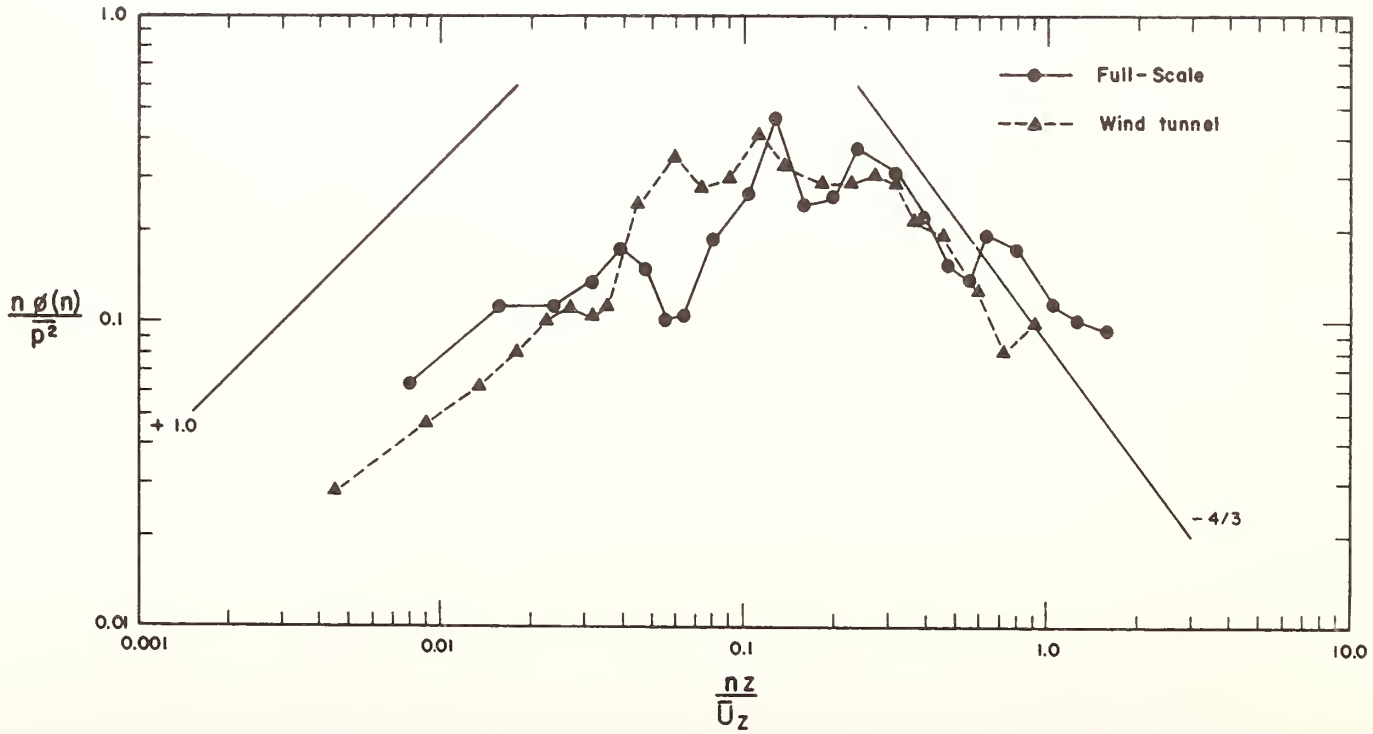

FIG. 10 PRESSURE SPECTRA (P3, RUN NOS. 311 & 22)

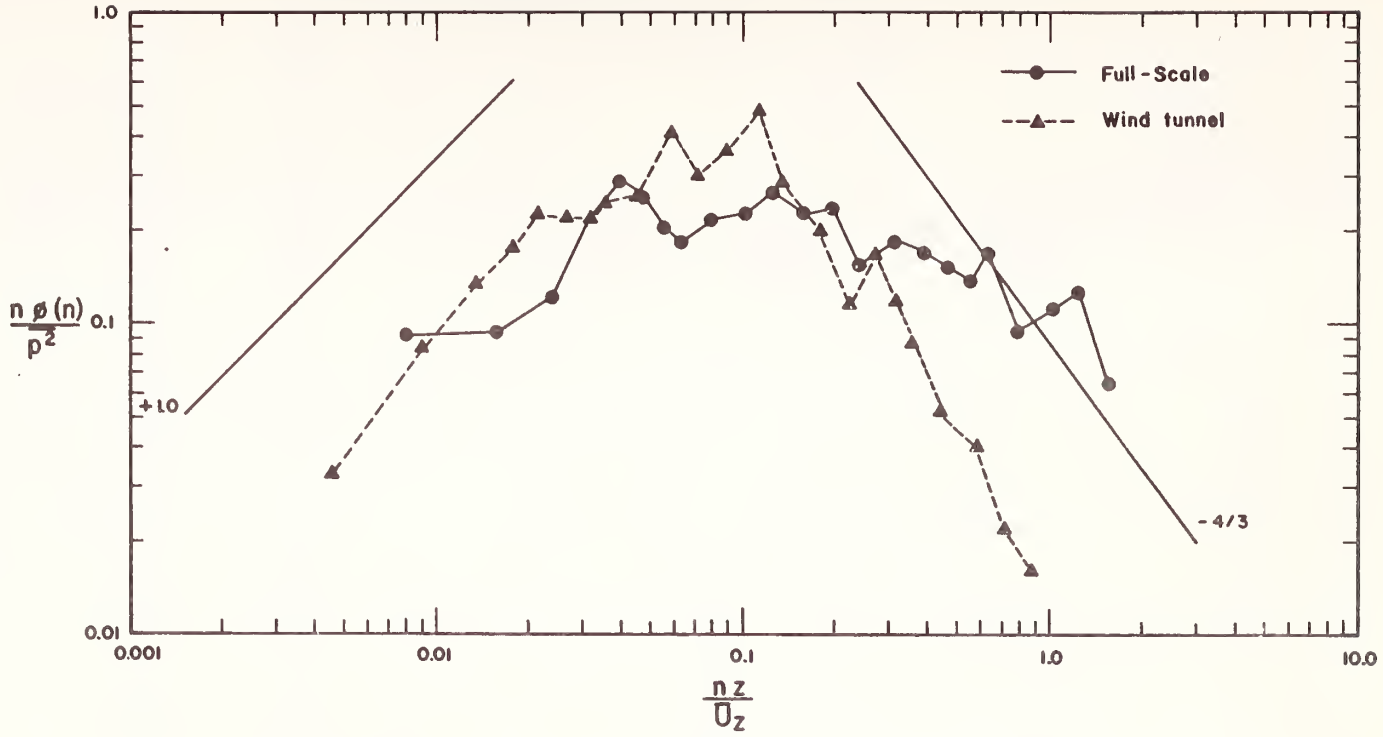

FIG. 11 PRESSURE SPECTRA (P10, RUN NOS. 311 & 22)

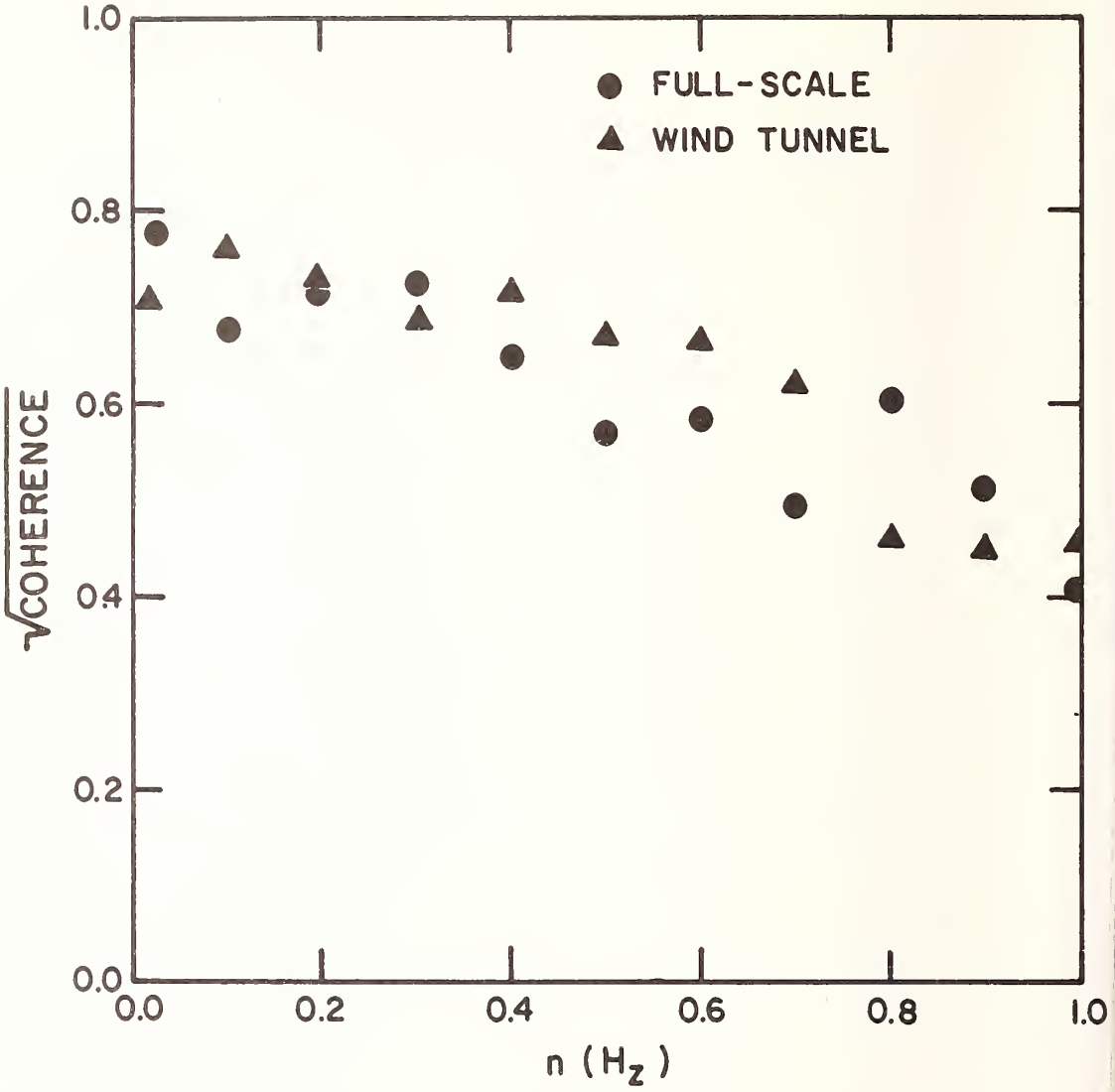

FIG. 12 COHERENCE (P1-P6, RUN NOS. 310 & 23)

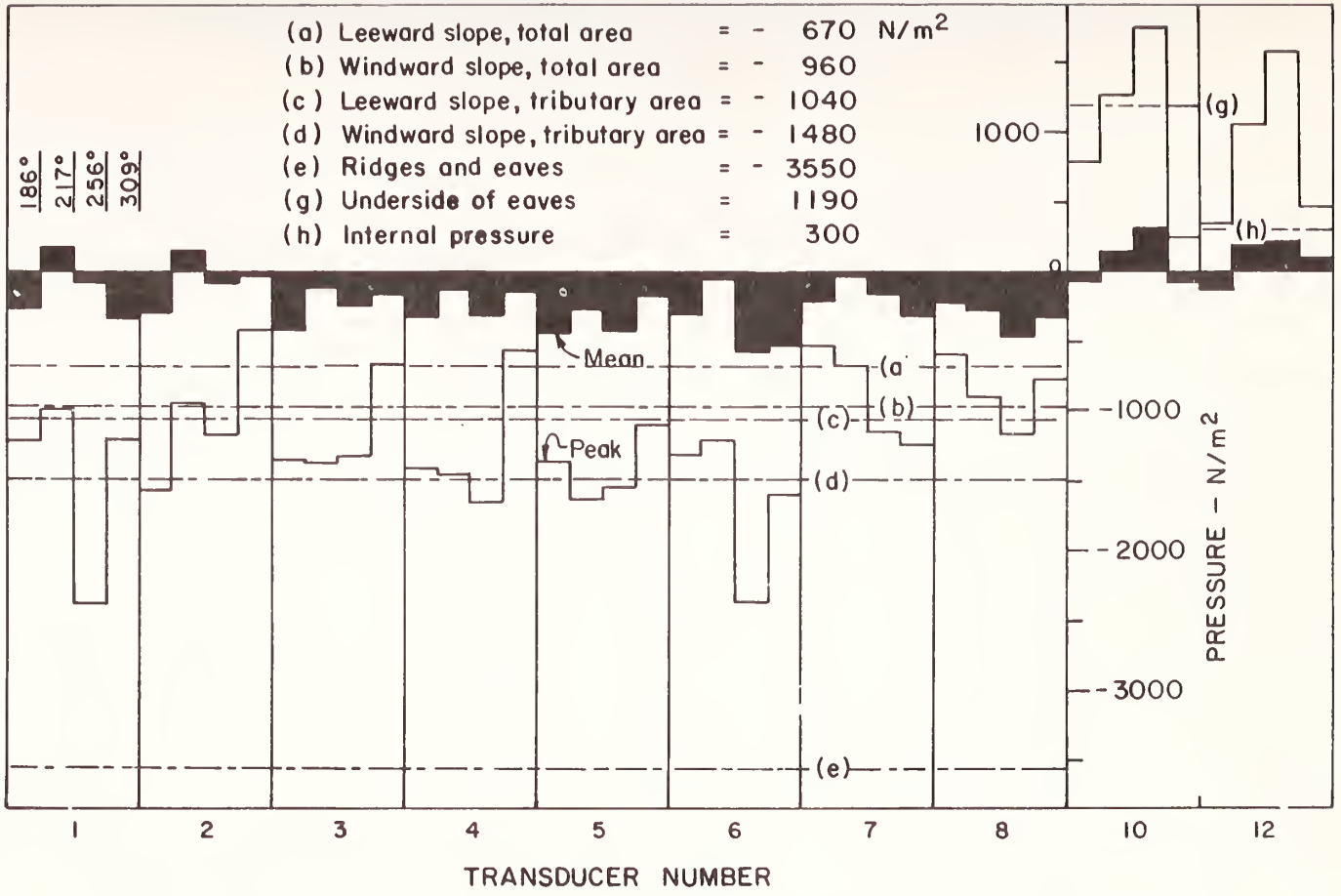

FIG. 13 COMPARISON OF MEASURED AND SPECIFIED DESIGN PRESSURES

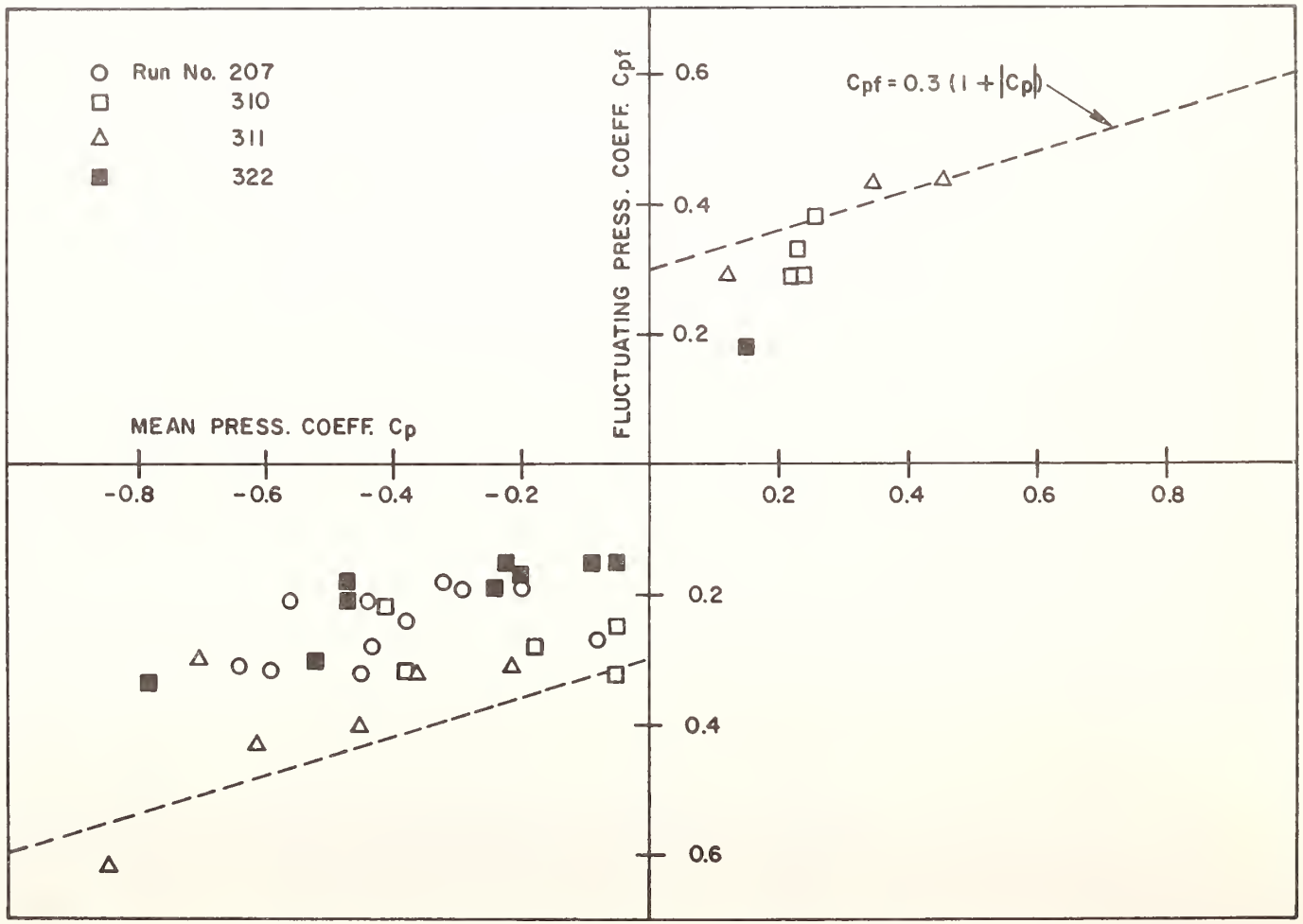

FIG. 14 C_p VS. C_{PF} - FULL SCALE

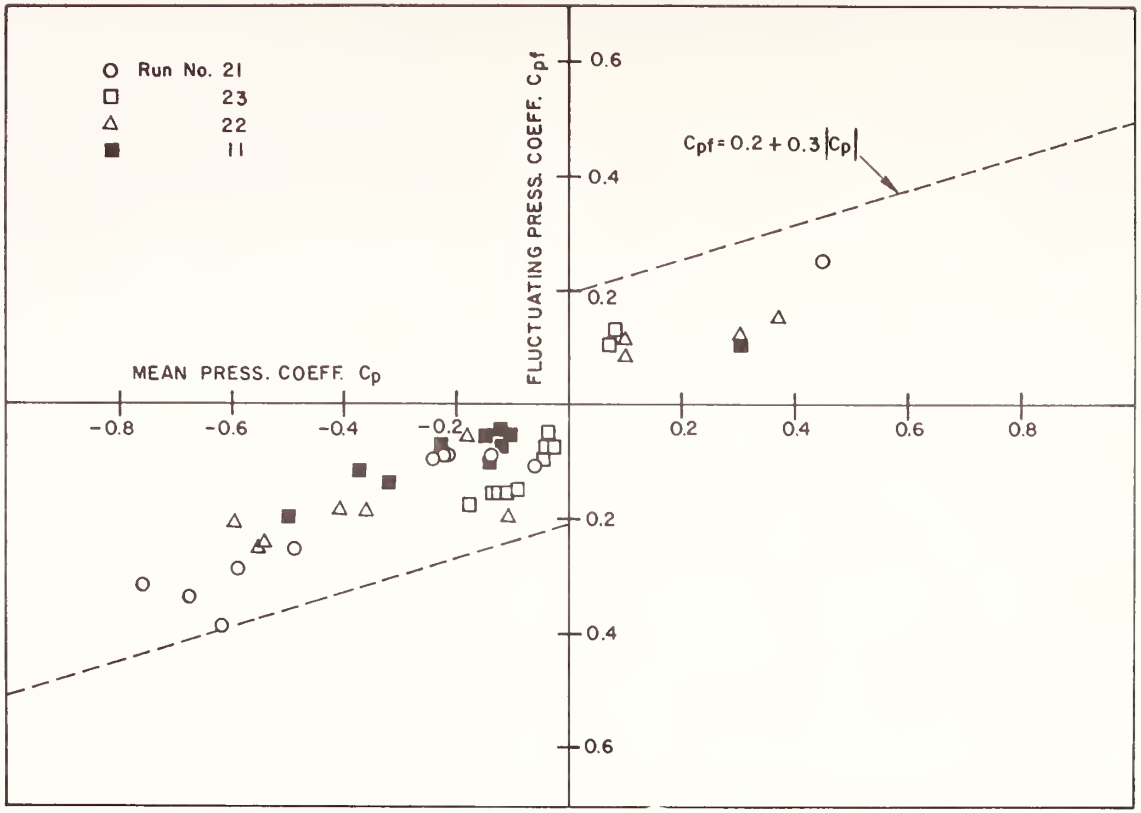

FIG. 15 C_P VS. C_{PF} - WIND TUNNEL

NONLINEAR CALCULATIONS OF GROUND RESPONSE IN EARTHQUAKES

by

William B. Joyner
Albert T.F. Chen
and
Patrick C. Doherty

U.S. Geological Survey
345 Middlefield Road
Menlo Park, California 94025

The response of soil to strong earthquake motion involves a high degree of nonlinearity. Because of the difficulties in solving the nonlinear problem, most calculations of ground response are currently made by a method--variously characterized as "equivalent linear", "quasi-linear", or "strain-compatible"--that assumes the true solution can be approximated by the response of a linear model whose properties are chosen to accord with the average strain that occurs in the model during excitation. The average strain level is determined by iterative calculation. To solve the nonlinear problem directly, we have developed algorithms by which the hysteretic behavior of an individual soil element can be efficiently modeled in a computer. The algorithms enable us to model any reasonable set of hysteresis loops of the Masing type that laboratory experiments may dictate. We are experimenting with various numerical techniques for integrating the basic nonlinear differential equations, including the method of characteristics as described by Streeter, Wylie, and Richart. A comparison was made between the equivalent linear and the nonlinear solution (using the method of characteristics) for a 200-meter section of firm alluvium excited at its base by the N21E component of the Taft accelerogram multiplied by four. This excitation produced peak strains of several tenths of a percent. The nonlinear solution showed substantially higher spectral levels of response at five percent damping for periods between 0.1 and 0.6 seconds.

Key Words: Elastic medium; engineering seismology; ground layer; numerical solution; shear wave.

INTRODUCTION

The problem we undertake to solve in this paper is basically a very simple one. We postulate a system of horizontal soil layers bounded above by the free surface and below by a semi-infinite elastic medium representing the bedrock. We further postulate a vertically incident shear wave in the underlying medium, and we ask the question, "How will the overlying layers respond and in particular, what will be the motion of a point on the free surface?"

This is a classical problem in engineering seismology. There is some disagreement concerning the range of applicability of the solution, but no one would deny the importance of solving this relatively simple problem correctly.

The problem was solved for the case of linear visco-elastic layers by Kanai (1952) some years ago. When we are dealing with input motion sufficiently intense to cause severe damage to structures, however, we cannot assume simple linear behavior. To do so would imply stresses many times greater than the strength of typical materials as measured in the laboratory.

To circumvent this difficulty, the method in common use currently is what we shall refer to as the "equivalent linear method" (Idriss and Seed, 1968; Schnabel, Seed, and Lysmer, 1972). It is based on the assumption that the response can be approximated by the response of a linear model whose properties are chosen in accord with the average strain that occurs in the model during excitation. The average strain level is determined by iterative calculation.

On an intuitive basis the equivalent linear assumption is reasonable with respect to the frequencies that are dominant in the strain history. It is less clear that the assumption is adequate with respect to higher frequencies, which may be important to the safety of small or rigid structures (Dobry, Whitman, and Roesset, 1971).

We undertook to obtain a solution without making any assumptions that bypass the underlying nonlinear character of the physical processes involved.

METHOD

The basic requirement for a solution to the problem is a constitutive relation--in simple terms we need a rule that will tell each soil element how to find its way around the stress-strain plane. For this purpose we have adopted a model (Figure 1) that was originally proposed by Iwan (1967). It is composed of simple linear springs and Coulomb friction elements arranged as shown. The friction elements remain locked until the stress on them exceeds the yield stress S_I. Then, they yield, and the stress across them during yielding is equal to the yield stress. Generally, the yield stress of the first element S_1 is set to zero. By choosing the spring constants K_I appropriately, we can model a very broad range of material behavior as dictated by laboratory experiments. The faithfulness of the modeling depends upon the number N of elements used. We have found it possible to use large numbers economically. For our typical problem N is 50; we have gone as high as 100 without unreasonable increases in computing time. There is one model of the kind diagrammed in Figure 1 for each soil layer in the system.

The type of hysteresis loops that such a model produces is shown in Figure 2, which illustrates the behavior of a single soil layer subject to cyclic loading of increasing amplitude. The loops of Figure 2 are plotted in terms of reduced stress and reduced strain--scaled in such a way that the maximum stress on the sample is one unit and the low strain modulus has a value of one. The spring constants of the model were chosen to give the behavior as a function of strain indicated by the experimental work of Hardin and Drnevich (1972a, 1972b).

To satisfy the boundary conditions at the base of the system of soil layers, we use a method described by Papastamatiou (1974). That method allows us to satisfy the boundary

conditions exactly for a vertically incident wave in the underlying elastic medium, given the density and shear velocity of the elastic medium. The approach is similar to that described by Lysmer and Kuhlemeyer (1969).

Given a constitutive relation and a boundary condition at the base of the system, we need only integrate the equations of motion step by step in time and space to obtain the motions at the surface. We have experimented with a number of methods of integration (Chen and Joyner, 1974). This experimentation is continuing and we are not yet prepared to discuss the relative merit of different methods, but we are satisfied that the method of characteristics, as described by Streeter, Wylie, and Richart (1973), gives accurate results and the example that follows was done with that method.

EXAMPLE

To demonstrate the method we chose the soil profile illustrated in Figure 3, representing a 200-meter section of firm alluvium. We evaluated the depth variation of maximum stress the low-strain modulus using the methods of Hardin and Drnevich (1972a, 1972b), with minor modifications. We assumed a density of 2.05 gm/cm^3 and converted shear modulus to shear velocity, which is plotted in Figure 3. A past consolidation vertical stress of 2.94 bars was assumed. As a result, the material was overconsolidated above a depth of 29 meters, causing kinks at that depth in the two curves on Figure 3. The underlying medium was assumed to have a shear velocity of 2.0 km/sec and a density of 2.6 gm/cm^3.

For imput we chose the N21E component of the Taft accelerogram, recorded during the 1952 Kern County, California, earthquake. We multiplied the amplitude by a factor of four so that the input motion, if incident on a free surface, would have a peak acceleration of 0.7 g and a peak velocity of 67 cm/sec. Figure 4 shows the input acceleration time history and compares the surface acceleration computed by the nonlinear method and the equivalent linear method. There are definite points of similarity, but it is clear that the equivalent linear approximation does not adequately represent the short-period components of motion present in the nonlinear solution.

Comparing the nonlinear solution with the input shows the effect of the postulated soil profile on ground motion. The peak acceleration is sharply reduced. The longer period components are amplified, however, and the overall effect may be a more damaging motion as will be illustrated subsequently.

Figure 5 shows the corresponding velocity time histories for the same example. Comparing the nonlinear and equivalent linear solutions, we see much better agreement, indicating that the equivalent linear approximation is adequate with respect to the longer period components that are dominant in the velocity time history. Comparing the nonlinear solution with the input shows clearly the amplifying effects of the soil profile for long-period motions.

To illustrate the consequences of these results for structures we have computed response spectra. Figure 6 shows the acceleration response at five percent damping for the three motions between zero and 1.2 seconds period. The line represents the input, hexagons the nonlinear solution, and crosses the equivalent linear solution. It is clear that the equivalent linear method significantly underestimates the intensity of motion for periods between 0.1 and 0.6 seconds. This period range corresponds to structures between one and about six stories. The importance is obvious.

Comparing the input response with the nonlinear response in Figure 6, one might be tempted to conclude that for short-period structures, the motions on alluvium would be less damaging than on bedrock. Considerable caution is indicated here. For one thing, different soil materials, dense sands, for example, might given more intense motions. Posible lengthening of structural periods due to deformation beyond the linear range reeds to be considered as well as the effects of duration not accounted for in the response spectrum. Consideration should also be given to the effects of ground deformation and ground failure.

Figure 7 compares the relative velocity response spectra at five percent damping for the range from zero to six seconds period. The results show that the equivalent linear approximation is adequate for the longer periods and that the soil site gives large amplification for longer periods.

During the running of the nonlinear solution, we monitored the peak strain for each depth interval. The maximum was 6×10^{-3} for the interval from 32 to 35 meters.

The comparative costs of the two methods is difficult to evaluate in the general case because it is possible to run the equivalent linear method using fewer layers, depending on the detail one wishes to represent in the soil profile. For the example presented here, however, using the same number of layers for both methods, the nonlinear solution required less than half as much computer time as the equivalent linear. So, we believe that, in general, it will be competitive, at least.

REFERENCES

1. Chen, A.T.F., and W.B. Joyner, 1974, Multi-linear Analysis for Ground Motion Studies of Layered Systems. Manuscript in process.

2. Dobry, Ricardo, R.B. Whitman, and J.M. Roesset, 1971, Soil Properties and the One-Dimensional Theory of Earthquake Amplification: School of Engineering, Massachusetts Institute of Technology, Cambridge, Massachusetts, Research Report R71-18, Soils Publication No. 275.

3. Hardin, B.O., and V.P. Drnevich, 1972a, Shear Modulus and Damping in Soils: Measurement and Parameter Effects: Proc. Am. Soc. Civil Eng., Journ. Soil Mech. and Found. Div., 98, 603-624.

4. Hardin, B.O., and V.P. Drnevich, 1972b, Shear Modulus and Damping in Soils: Design Equations and Curves: Proc. Am. Soc. Civil Eng., Journ. Soil Mech. and Found. Div., 98, 667-692.

5. Idriss, I.M., and H.B. Seed, 1968, Seismic Response of Horizontal Soil Layers: Proc. Am. Soc. Civil Eng., Journ. Soil Mech. and Found. Div., 94, 1103-1031.

6. Iwan, W.D., 1967, On a Class of Models for the Yielding Behavior of Continuous and Composite Systems: Jour. of Applied Mechanics, 34, 612-617.

7. Kanai, K., 1952, Relation Between the Nature of Surface Layer and the Amplitudes of Earthquake Motions: Bull. Earthq. Res. Inst., Tokyo Univ., 30, 31-37.

8. Lysmer, John, and R.L. Kuhlemeyer, 1969, Finite Dynamic Model for Infinite Media: Proc. Am. Soc. Civil Eng., Journ. of the Eng. Mechanics Div., 95, 859-877.

9. Papastamatiou, D.J., 1974, A Method for the Evaluation of Strong Ground Motion. Submitted for publication in Geotechnique.

10. Schnabel, P., H. Bolton Seed, and J. Lysmer, 1972, Modification of Seismograph Records for Effects of Local Soil Conditions: Bull. Seism. Soc. Am., 62, 1649-1664.

11. Streeter, V.L., E.B. Wylie, and F.E. Richart, 1973, Soil Motion Computations by Characterics Method, Meeting Preprint, 1952, Am. Soc. Civil Eng., National Structural Eng. Meeting, April 9-13, San Francisco, California.

LIST OF FIGURES

1. Model used for constitutive relationship. Model consists of simple elastic springs with spring constants K_I and Coulomb friction elements with yield stress S_I.

2. Hysteresis loops for the model shown in Figure 1. Stress and strain are scaled so that the maximum stress and the low-strain modulus are unity.

3. Dynamic properties for soil profile used in sample problem.

4. Acceleration time histories for sample problem.

5. Velocity time histories for sample problem.

6. Acceleration response at five percent damping for sample problem. The line represents the input, hexagons the nonlinear solution, and crosses the equivalent linear solution.

7. Relative velocity response at five percent damping for sample problem. The line represents the input, hexagons the nonlinear solution, and crosses the equivalent linear solution.

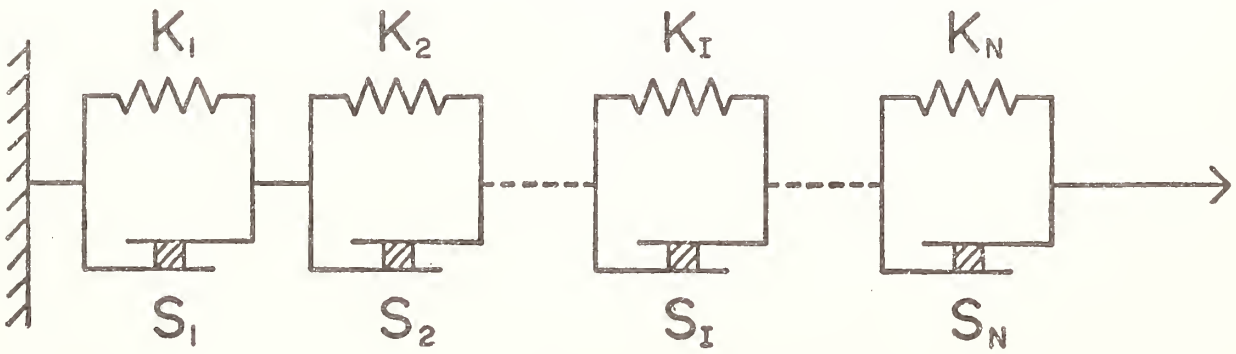

Figure 1

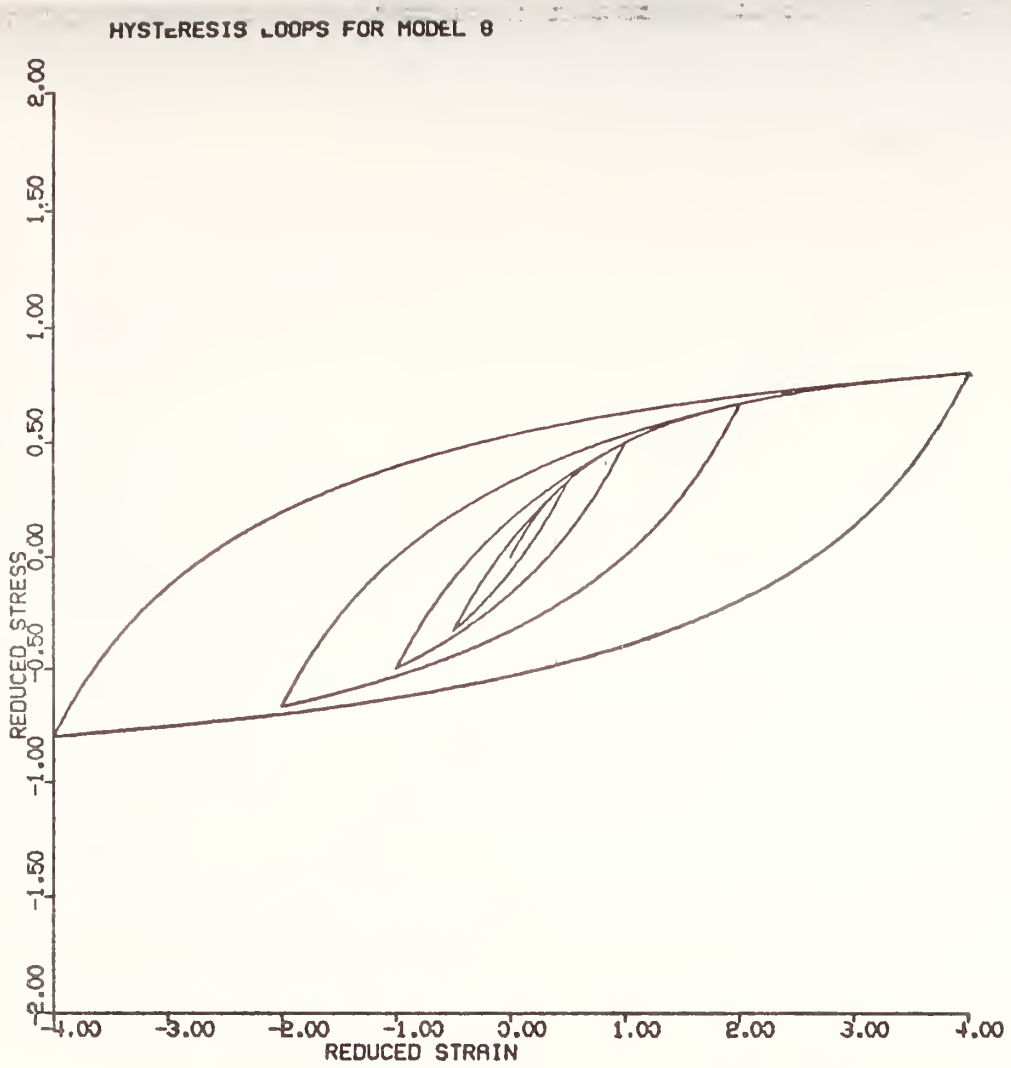
HYSTERESIS LOOPS FOR MODEL 8
REDUCED STRESS
2.00
1.50
1.00
0.50
0.00
-0.50
-1.00
-1.50
-2.00
-4.00
-3.00
-2.00
-1.00
0.00
1.00
2.00
3.00
4.00
REDUCED STRAIN

Figure 2

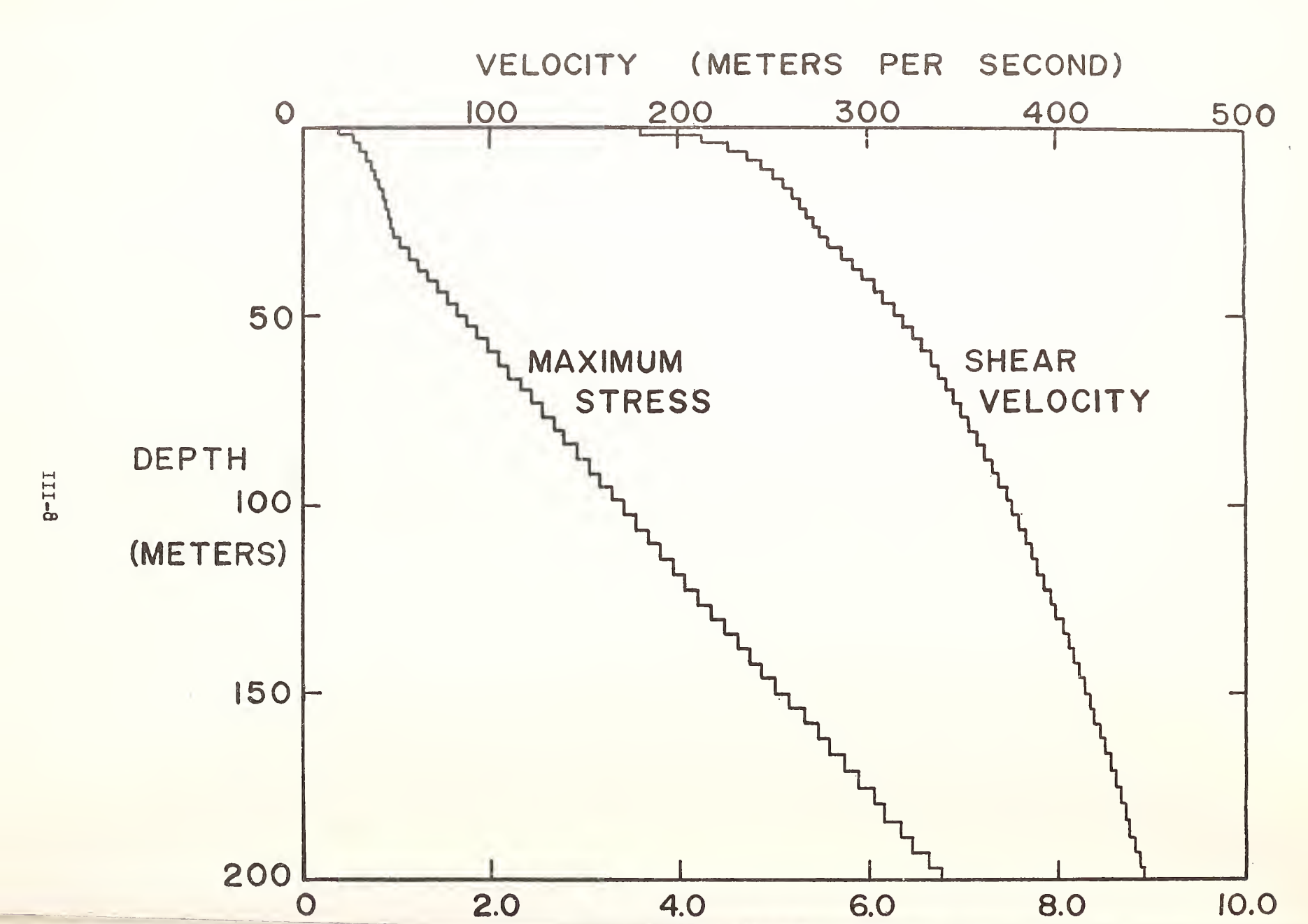
VELOCITY (METERS PER SECOND)
0
100
200
300
400
500
50
100
150
200
DEPTH
(METERS)
MAXIMUM
STRESS
SHEAR
VELOCITY
0
2.0
4.0
6.0
8.0
10.0

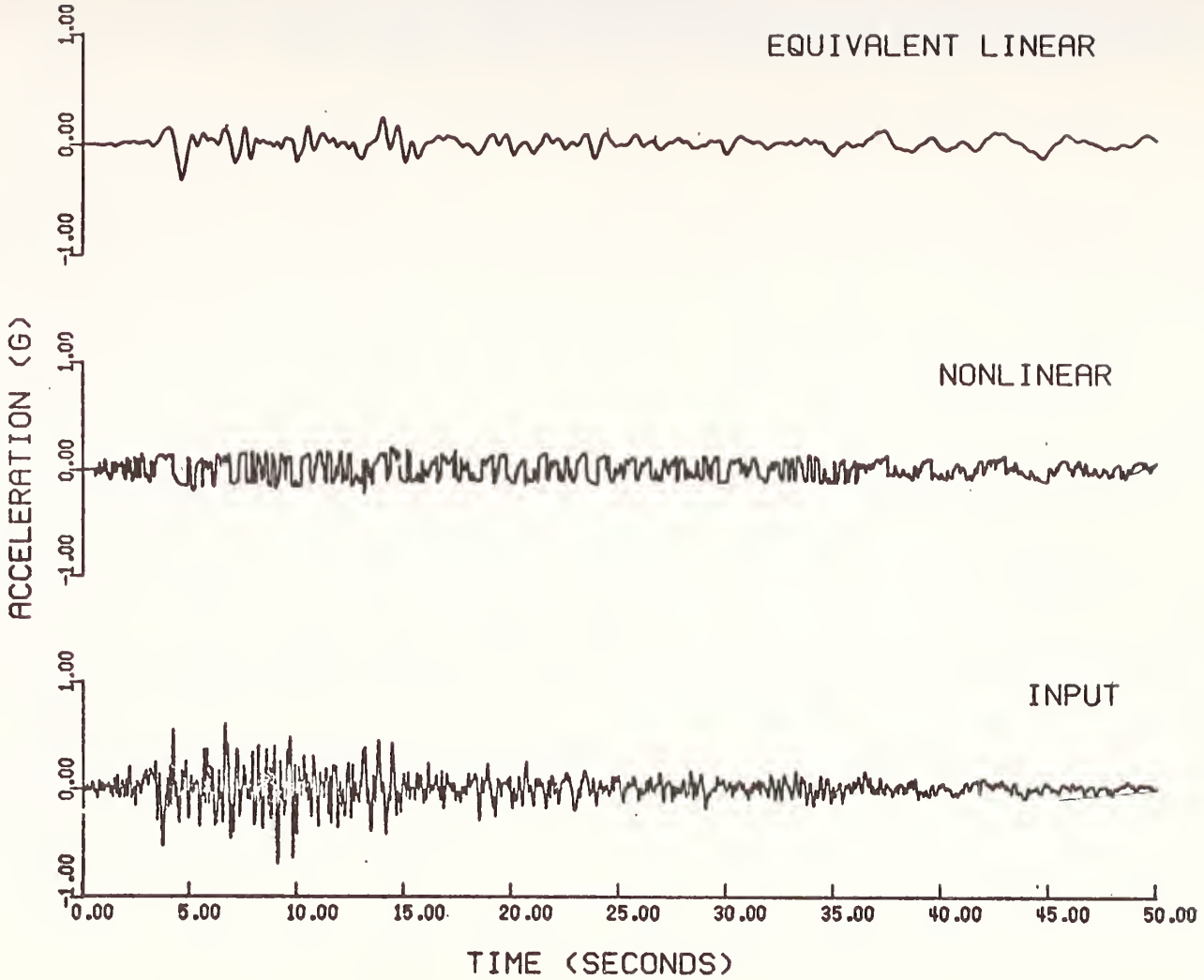
EQUIVALENT LINEAR
NONLINEAR
INPUT
ACCELERATION (G)
1.00
0.00
-1.00
0.00
5.00
10.00
15.00
20.00
25.00
30.00
35.00
40.00
45.00
50.00
TIME (SECONDS)

Figure 4

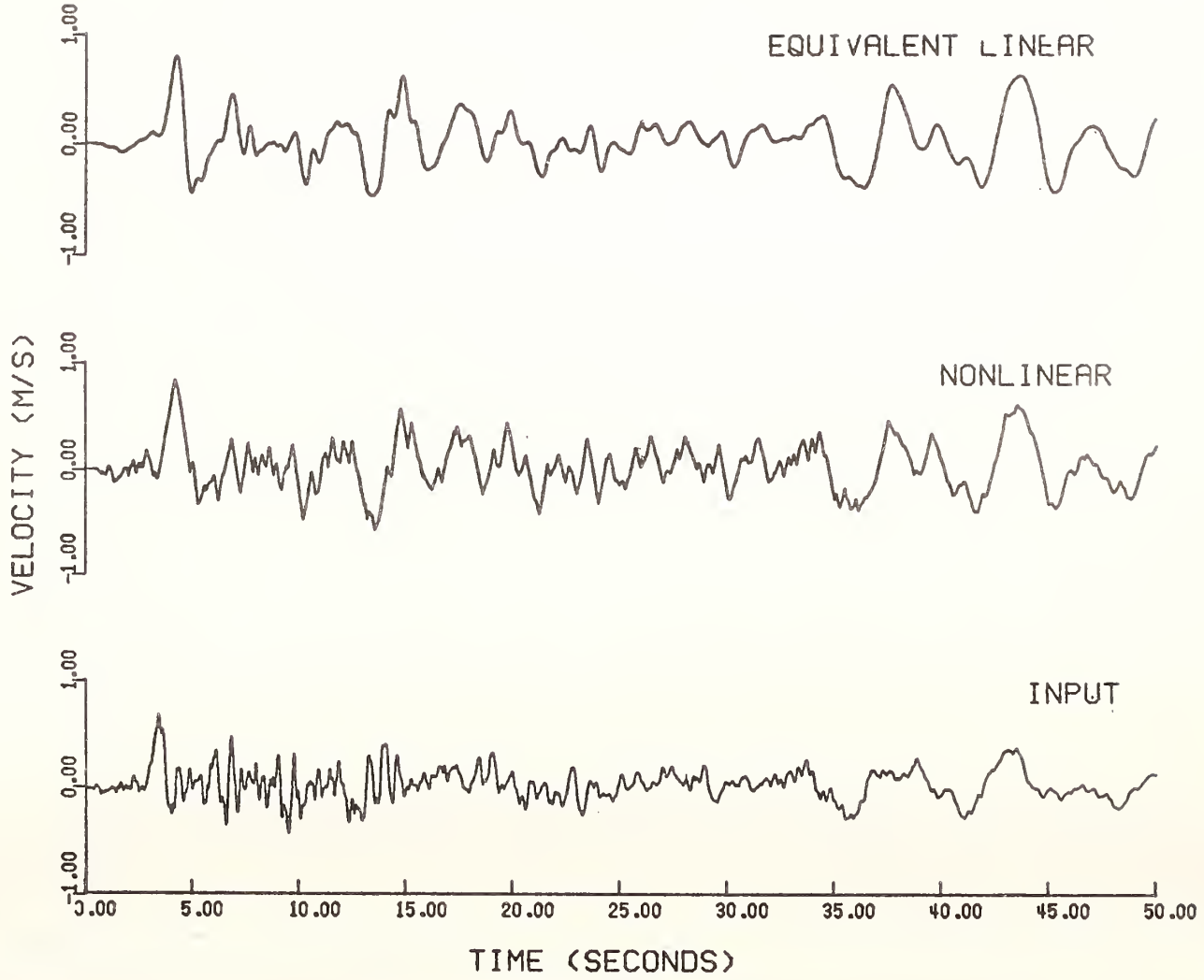
EQUIVALENT LINEAR
NONLINEAR
INPUT
VELOCITY (M/S)
1.00
0.00
-1.00
0.00
5.00
10.00
15.00
20.00
25.00
30.00
35.00
40.00
45.00
50.00
TIME (SECONDS)

Figure 5

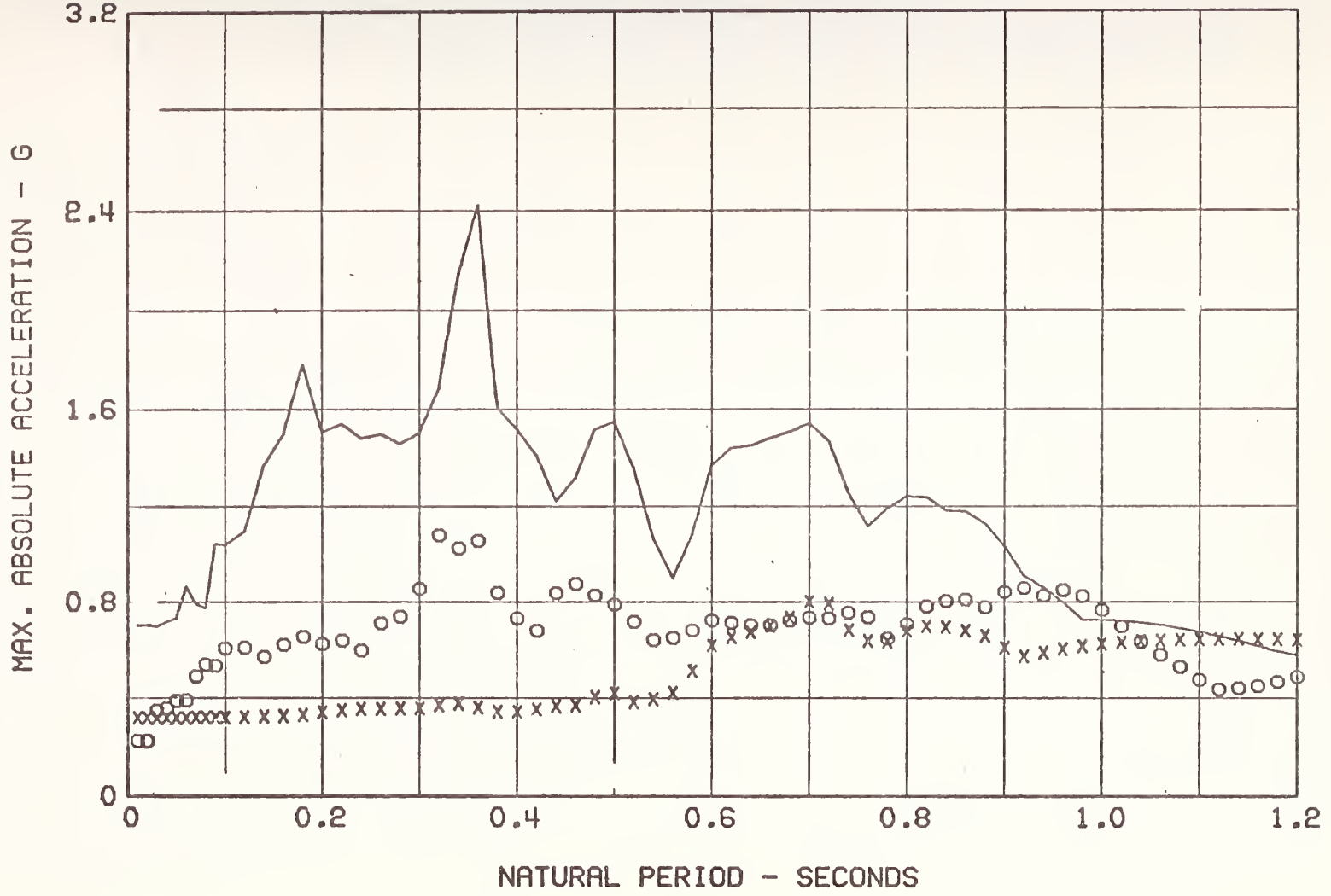
3.2
2.4
1.6
0.8
0
MAX. ABSOLUTE ACCELERATION - G
0
0.2
0.4
0.6
0.8
1.0
1.2
NATURAL PERIOD - SECONDS

Figure 6

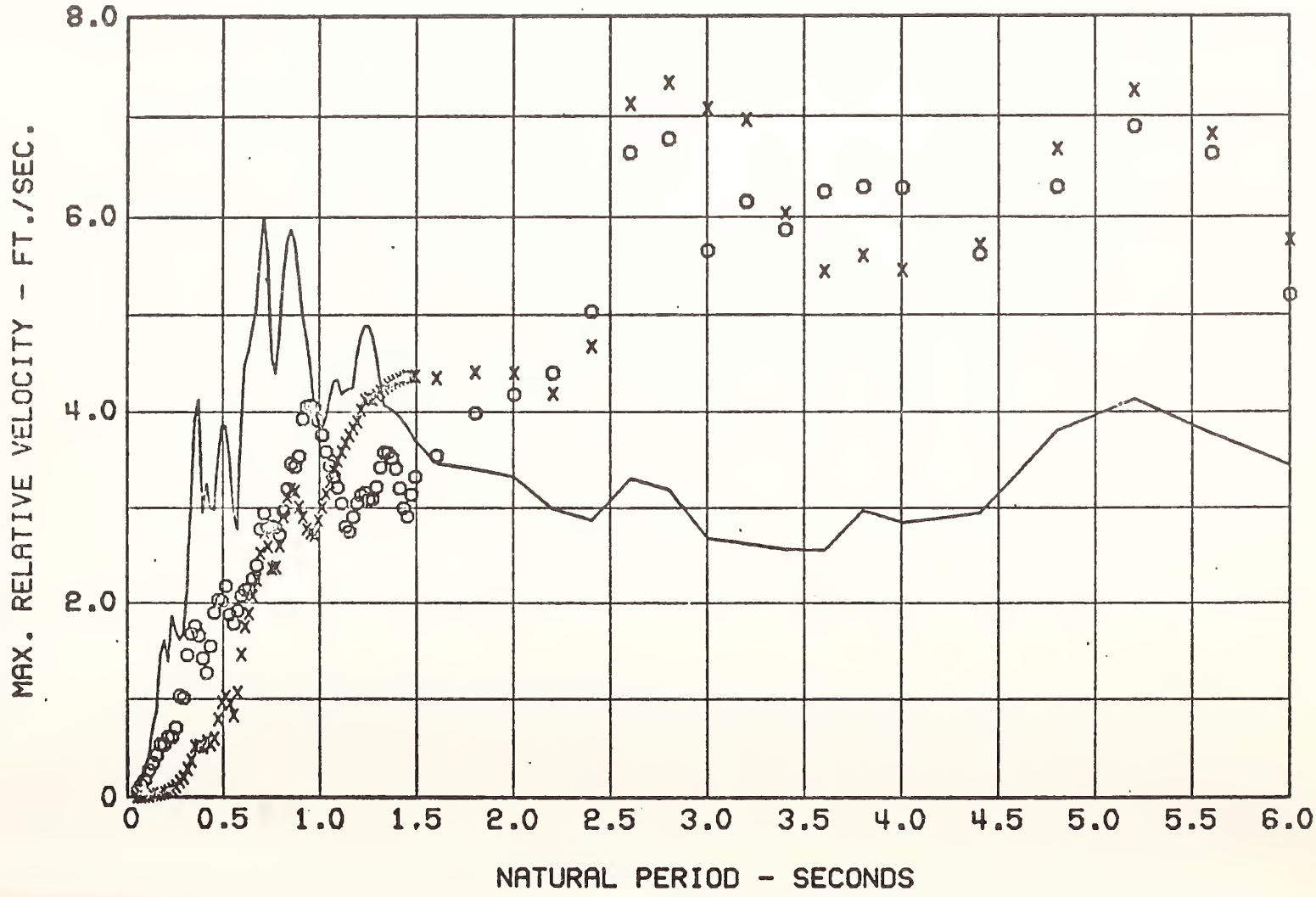
MAX. RELATIVE VELOCITY - FT./SEC.
8.0
6.0
4.0
2.0
0
0
0.5
1.0
1.5
2.0
2.5
3.0
3.5
4.0
4.5
5.0
5.5
6.0
NATURAL PERIOD - SECONDS

Figure 7

OBSERVATION AND ANALYSIS OF GROUND RESPONSE IN EARTHQUAKES

by

Satoshi Hayashi
Head, Structures Division
Port and Harbor Research Institute
Ministry of Transport

Hajime Tsuchida
Chief, Earthquake Resistant Structures Laboratory
Structures Division
Port and Harbor Research Institute
Ministry of Transport

In the field of port and harbor engineering, the ground response due to earthquakes is generally considered. However, there are many problems at present in idealization of the surface layer, input ground motions, and nonlinear behavior of the soil. In order to provide some design data in these areas, research has been conducted using six downhole seismometer arrays established in port areas in Japan. Typical observed acceleration time histories have been obtained and are shown and compared with those calculated by the multiple reflection theory. In order to investigate ground response relative to structures of large length, such as a tunnel, a two-dimensional seismometer array has been established. Examples of the considerations of the ground response required in practice are seen in microzonation in the earthquake proof design of a subaqueous tunnel.

Key Words: Earthquake; field data; ground response; seismic waves; seismometer; soil-structure interaction.

INTRODUCTION

In recent earthquake engineering practice, a concept has been introduced which considers the earthquake response of the ground; here the ground means surface layers overlaying the base rock. The amplification of ground motions through the surface layers was first observed and the theoretical analysis, so-called the multiple reflection theory, developed by Dr. Kanai (1). However, the introduction of this concept into design practice has taken several years. In the field of port and harbor engineering, the first step related to the amplification problem was to revise the procedure in determining the design seismic coefficient. The old design seismic coefficient was a function of only local seismicity. In the new procedure the design seismic coefficient is a function of subsoil condition underlaying the structure, as well as local seismicity and importance of the structure (2). Even in this revision, the subsoil condition was taken as only one of the factors, and only because of past experiences obtained during destructive earthquake events. It was noted that during these earthquakes, damage to the structures did depend on the subsoil conditions, however, a clear understanding of the amplification of the ground motions was not considered.

The soil structure interaction analysis, which has become one of the main topics in earthquake engineering research during the last decade, has provided insight to researchers and practicing engineers relative to the significance of ground motion response. Progress through the application of computer techniques has assisted in the introduction and the consideration of the earthquake response of surface layers to be used in practice. The International Conference on Microzonation, held in Seattle in 1972, clearly showed that many researchers and engineers intend to consider the earthquake response of surface layers in design practice. In the previous joint meetings of the U.S.-Japan Panel on Wind and Seismic Effects, UJNR, Dr. Joyner and Dr. Borchcherdt have presented reports on this topic (3) and (4).

In the present paper the authors will report on the practical problems involved in earthquake response calculations of the ground, observation of the ground response in port areas in Japan, analysis of observed records, and design examples in which the ground response in earthquakes is taken into consideration.

PRACTICAL PROBLEMS ON GROUND RESPONSE CONSIDERATION

From the viewpoint of the seismology, the ground response in earthquakes can be explained as follows: the seismic waves which enter the surface layer, travel from the epicenter to the base rock site in consideration and propagate upward into the surface layer, and during the propagation, the amplification and phase shift of the motion occurs. In principle, the process is quite clear, however, in practice, there are some problems. The first problem that confronts the engineers is the determination of the base rock. In many sites the rock formation is so deep that it is not possible to idealize the surface layer overlaying the base rock into a model to calculate the earthquake response.

The second problem involves the input base rock motions; in other words, the earthquake motions in the base rock. There are not many recorded records available of the base rock motion that can be used by engineers.

The third problem is the idealization of the surface layer. At present three well known major idealizations are used; they are 1) multiple reflection model, 2) finite element model, and 3) lumped mass model. There is, however, little information on the application of these idealizations for use by engineers. Also, all of the idealizations are faced with the problem of how to incorporate the non-linear behavior of the soil.

The solution to these problems have not been found. However, to apply the techniques, the engineer is forced to make reasonable assumptions within the present state of the art.

The following will present some of the answers relative to the problems concerning the earthquake proof design of port structures. When the base rock exists at considerable depth, and it is not practical to idealize the whole layer into a model to calculate the

earthquake response, a layer extending widely beneath the structure is considered as an assumed base rock instead of the real rock formation. The assumed base rock, however, must satisfy the following requirements: the shear wave velocity of the assumed base rock is significantly larger than that of a layer immediately overlaying it; the standard penetration value of practical base rock is equal to or greater than fifty.

The idealization of the surface layer depends on several conditions to calculate the earthquake response. The multiple reflection model is frequently used to estimate the ground amplification and to calculate the base rock motions, as obtained from the records at the ground surface. In soil structure interaction problems, the finite element model and the lumped mass model are applied more conveniently than the multiple reflection model. Non-linear behavior of soil is a very difficult problem to solve, therefore, the evaluation of the ground response in earthquakes, in connection with port structures, are treated assuming that the soil behaves linearly. However, it will be noted that in the calculation of the lateral resistance of piles, the non-linear behavior of soil has been taken into consideration (5). Also a quasi-non-linear approach is introduced into the amplification calculation, that is, the soil is considered as a linear material but the shear modulus is assumed as modified, depending on the calculated maximum strain of the layer. This approach essentially requires repetitive calculations.

The solution to the basic problem described herein depends largely on the findings from the analysis of strong-motion accelerograms and base rock accelerations, as calculated from the accelerograms obtained from the multiple reflection theory (6).

OBSERVATION OF GROUND RESPONSE IN EARTHQUAKES

Six downhole seismometer arrays have been established by the Port and Harbor Research Institute. The first array is located in the test field of the research institute in Yokosuka (7); the other four arrays are located in Tokyo, Funabashi, Nagoya, and Osaka Ports to provide information for coastal structure design, and the last array is in Kawasaki Port, to provide data for the earthquake proof design of a subaqueous tunnel. This tunnel will be constructed similarly to the procedure that was used for the BART tunnel crossing at San Francisco Bay. The arrays in the Tokyo Port and in the test field in Yokosuka have the lowest seismometers on rock formations.

The specification for the seismometers of the arrays, except those in Yokosuka, are as follows:

Type	Moving Coil Type
Component	Two/Three Components
Natural Frequency of Transducer	5 Hz
Natural Frequency of Galvanometer	110 Hz
Overall Sensitivity	About 1 mm/gal in max.

The signal corresponding to acceleration is recorded on an electro-magnetic oscillograph. A magnetic tape data recorder may be more sophisticated than the electro-magnetic oscillograph, however, the mechanism of the data recorder is very delicate and the oscillograph that was chosen has a higher reliability in recording operation. A disadvantage of the oscillograph is the time required to digitize the oscillograms. To overcome this disadvantage, an oscillogram digitizer has been directly connected to a small scale hydrid computer, which has been introduced into the authors' laboratory. With the digitizer, a trace of about seventy centimeters in length is digitized within a few minutes.

RECORDS AND ANALYSIS

As an example of the data that has been obtained, the records from the seismometer array in Kawasaki Port and the results of preliminary analysis will be described herein. As mentioned previously, the array has been established to obtain data for use in the earthquake proof design of the 1380 meter long Kawasaki Port subaqueous tunnel.

The array consists of four downhole seismometers, located at depths of 1, 15, 40, and 63 meters below the ground surface. The lowest seismometer rests in a sand layer, which has a standard penetration value exceeding fifty. This layer is considered as the assumed base rock in the earthquake response calculation. The subaqueous tunnel to be constructed will exist entirely above this layer. The boring log and the shear wave velocity are shown in Figure 1.

During the last year, eight earthquakes were recorded. Three of the records show relatively large amplitudes of the vertical distribution of maximum accelerations, as shown in Figure 2. It was observed that the maximum accelerations decrease with increase in the depth.

In Figure 3, reproductions of the acceleration time histories of the EW component recorded on April 6, 1973 are shown. The acceleration time histories at the boundaries between soil layers were calculated from the ground surface acceleration time history based on the multiple reflection theory. These results are shown in Figure 4, together with the recorded time history at 63 meters below the ground surface.

The results from the observation and the analysis, such as a frequency transfer function of the site, are reflected in the response calculation and the dynamic model test of the tunnel.

TWO DIMENSIONAL SEISMOMETER ARRAY

The seismometer arrays described previously are all vertically uni-directional. For many types of structures, such as a tunnel and a pipeline, relative ground movement along the structure is very important for their earthquake proof design. The Port and Harbor Research Institute has, therefore, established a two-dimensional seismometer array. This array is located at Tokyo International Airport along a straight line of 2500 meters, parallel with the C airport runway. Seven seismometers, each of which contains two horizontal transducers, were installed at an equal spacing of 500 meters along the 2500 meters. At one end of the line and at 500 meters inside from the other end the downhole seismometers were installed at about 50 and 67 meters below the ground surface. Therefore, the seismometer system can record a two-dimensional ground response in the vertical plane. The arrangement of the seismometers is illustrated in Figure 5.

Setting of the seismometers was completed in March of this year 1974.

EXAMPLES OF GROUND RESPONSE CONSIDERATION IN PRACTICE

Practical examples, in which the ground response to earthquakes should be considered, will now be explained. As described previously in this paper, in the earthquake proof design of the subaqueous tunnel in Kawasaki Port, the ground response was given in detail. The actual tunnel was modeled, together with the surface layer, using a lumped mass system in which the surface layer and the tunnel was connected by springs which represent the stiffness of the soil. The input earthquake accelerations that were used were obtained from the base rock accelerations calculated from the accelerograms at the ground surfaces given by the multiple reflection theory (8).

Another example was the microzonation in the coastal area along Tokyo Bay. At present, effort is being directed toward the examination of the seismicity of the coastal and port structures in the area, and the microzonation of the amplification of the earthquake

motion. In the zoning work, the amplification of the earthquake motions through the surface layer were calculated by the multiple reflection theory. Also, the quasi-non-linear approach was used (9)(10).

REFERENCES

1. K. Kanai: Relation Between the Nature of the Surface Layer and the Amplitude of Earthquake Motions, Bull. Earthquake Research Institute, Vol. 30, 1952, pp. 31-37.

2. The Japan Port and Harbor Association: Design Manual of Harbor Structures in Japan, 1967.

3. William B. Joyner and Richard E. Warrick: The Influence of Geology on Earthquake Ground Motion--Preliminary Results from a Downhole Seismometer Array on the San Francisco Bay Shore, Proceedings, Third Joint Meeting of U.S.-Japan Panel on Wind and Seismic Effects, UJNR, 1971.

4. Roger D. Borcherdt: A Preliminary Strategy for Zoning the San Francisco Bay Region on the Basis of Relative Ground Motion Prediction, Proceedings, Fifth Joint Meeting, U.S.-Japan Panel on Wind and Seismic Effects, UJNR, 1973.

5. Satoshi Hayashi, Hajime Tsuchida, and Takamasa Inatomi: Inelastic Response of Steel Pile Structure and Its Seismic Stability, Proceedings, Fourth Joint Meeting, U.S.-Japan Panel on Wind and Seismic Effects, UJNR, 1972.

6. Hajime Tsuchida and Tatsuo Uwabe: Characteristics of Base-Rock Motions Calculated from Strong-Motion Accelerograms at Ground Surface, Report, Port and Harbor Research Institute, Vol. 11, No. 4, 1972, pp. 191-270.

7. Hideo Arai and Moriyoshi Iwabuchi: Studies on the Vertical Distributions of the Earthquake Motions in the Superficial Soil Layers (1st Report) - Observation and Analysis of the Earthquake Motions in a Clay Layer, Report, Port and Harbor Research Institute, Vol. 12, No. 2, 1973, pp. 63-83.

8. Takuji Nakano and Kenji Mori: Earthquake Resistant Calculation and Dynamic Model Test on Trench Type Tunnel, Technical Note, Port and Harbor Research Institute, No. 172, 1973, 87 p.

9. Satoshi Hayashi, Hajime Tsuchida and Setuo Noda: Estimation of Aseismicity of Port Structures, Proceedings, Fifth Joint Meeting, U.S.-Japan Panel on Wind and Seismic Effects, UJNR, 1973.

10. Setuo Noda and Tatsuo Uwabe: Estimation of Maximum Ground Acceleration Around the Tokyo Bay Area During Great Earthquake, Technical Note, Port and Harbor Research Institute, No. 177, 1974.

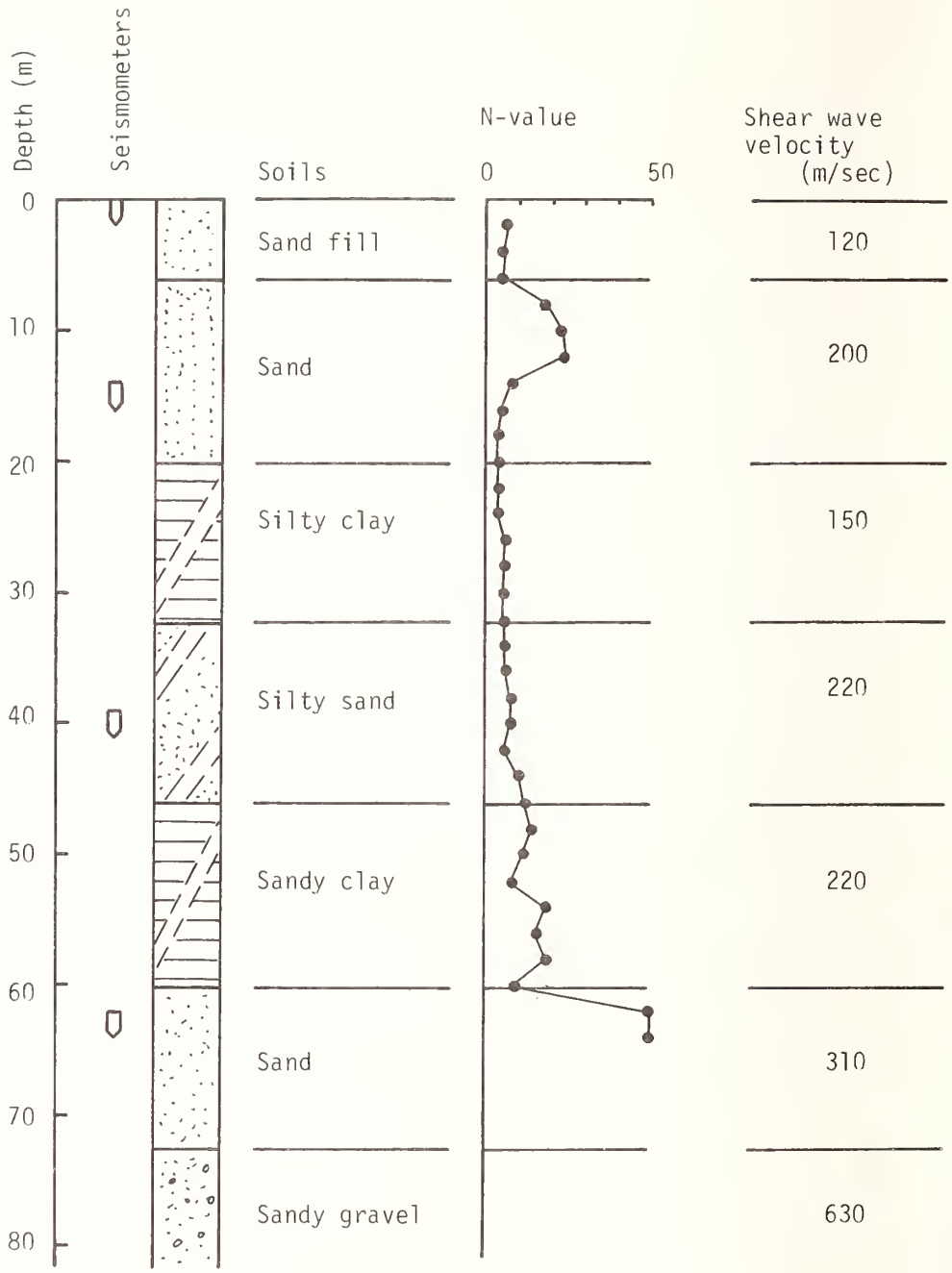

Fig. 1 Soil condition at seismometer array site (Kawasaki)

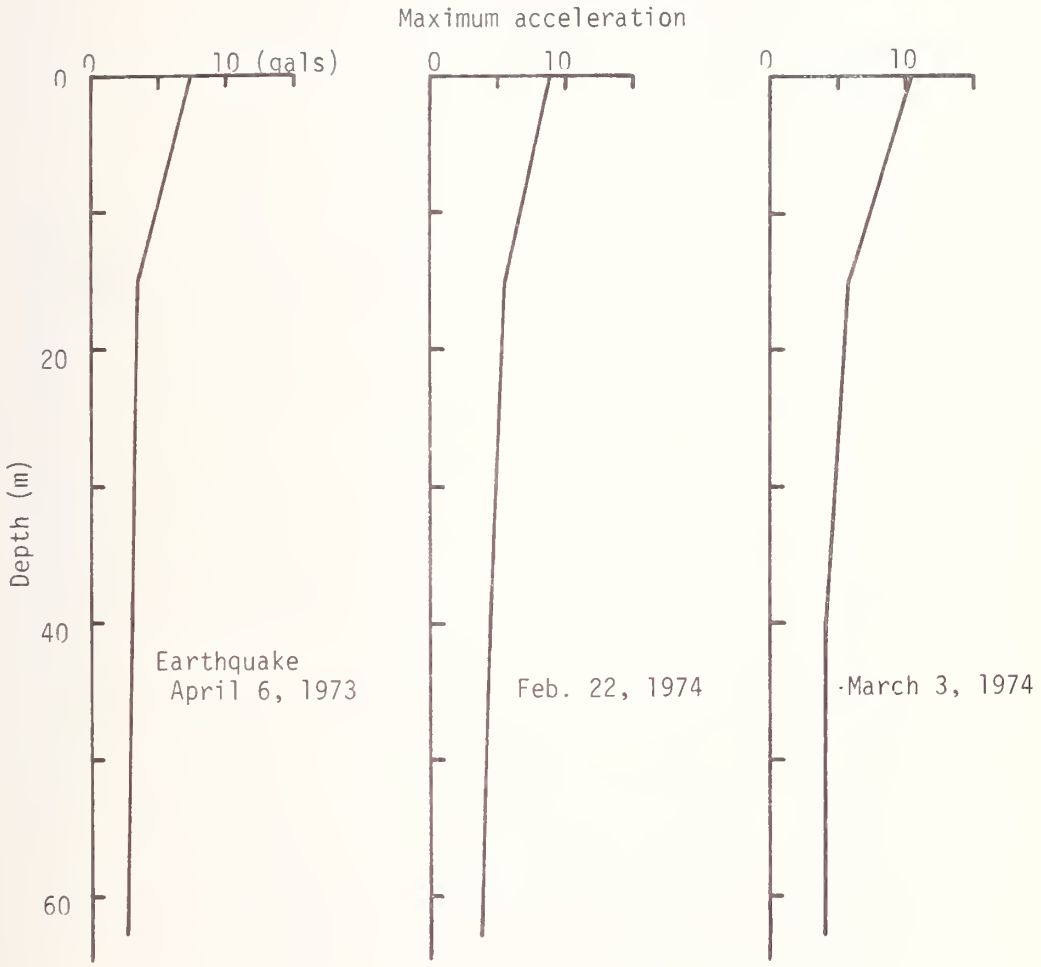

Fig. 2 Vertical distribution of maximum accelerations, EW component

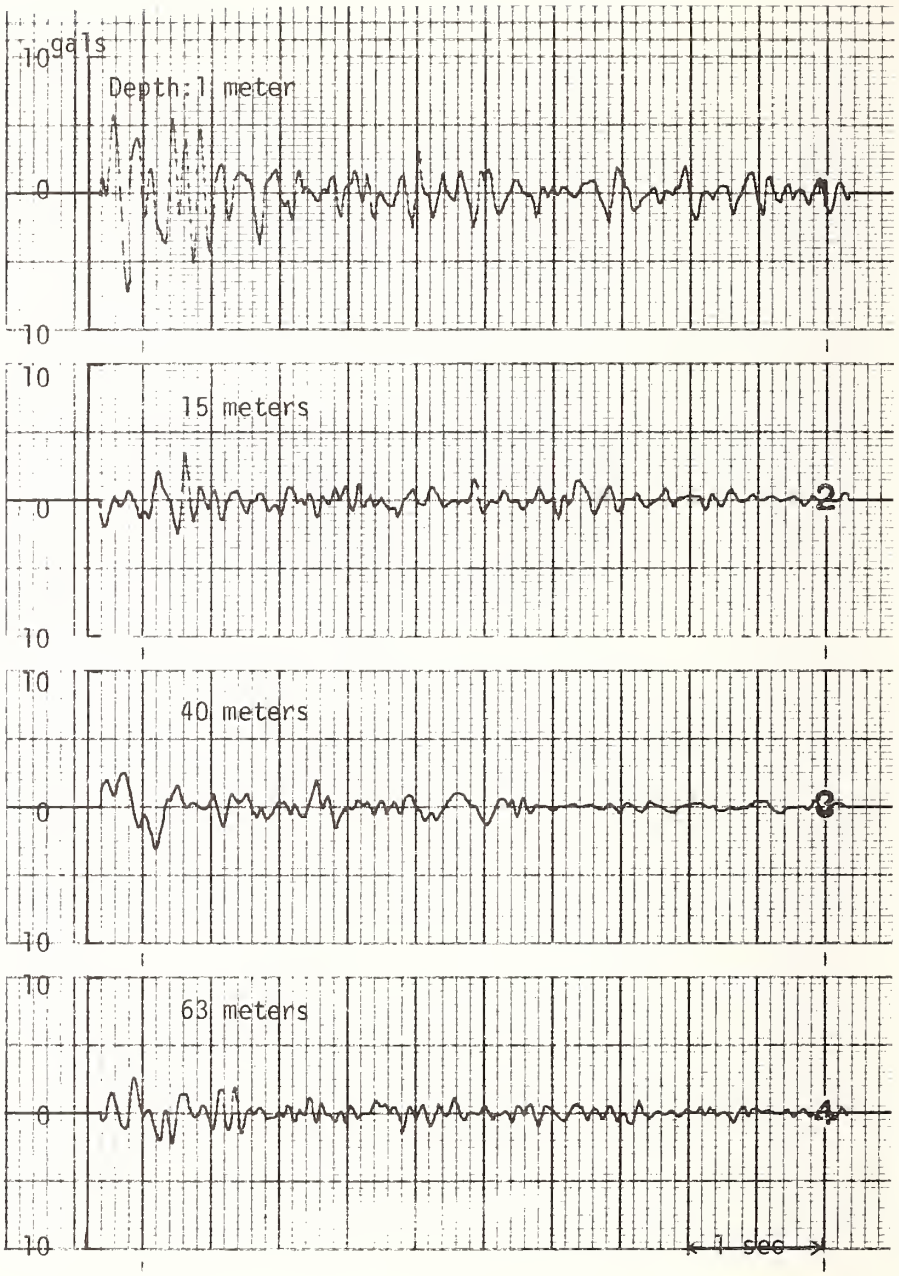

Fig. 3 Acceleration time histories
Earthquake of April 6, 1973, EW component

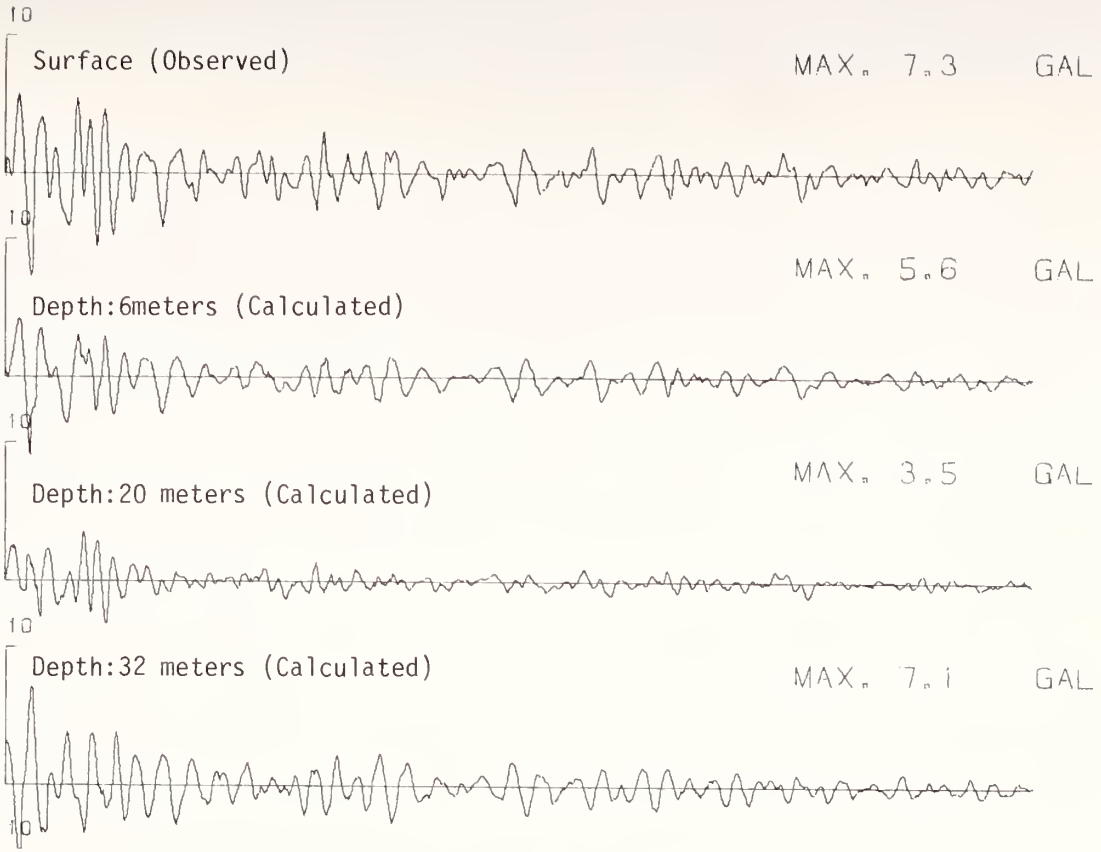

(to be continued)

Fig.4 Acceleration time histories, observed and calculated, April 6, 1973, EW component

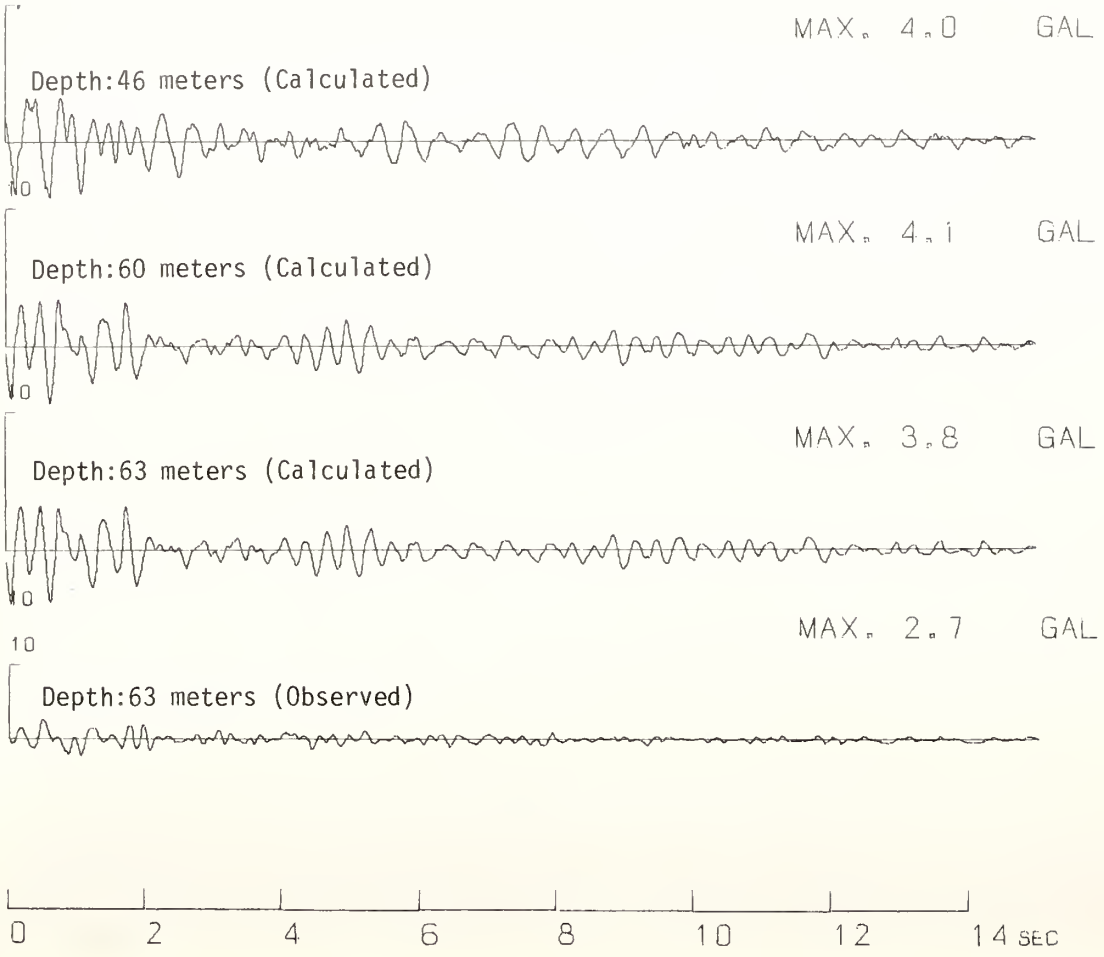

Fig. 4 Acceleration time histories (continued)

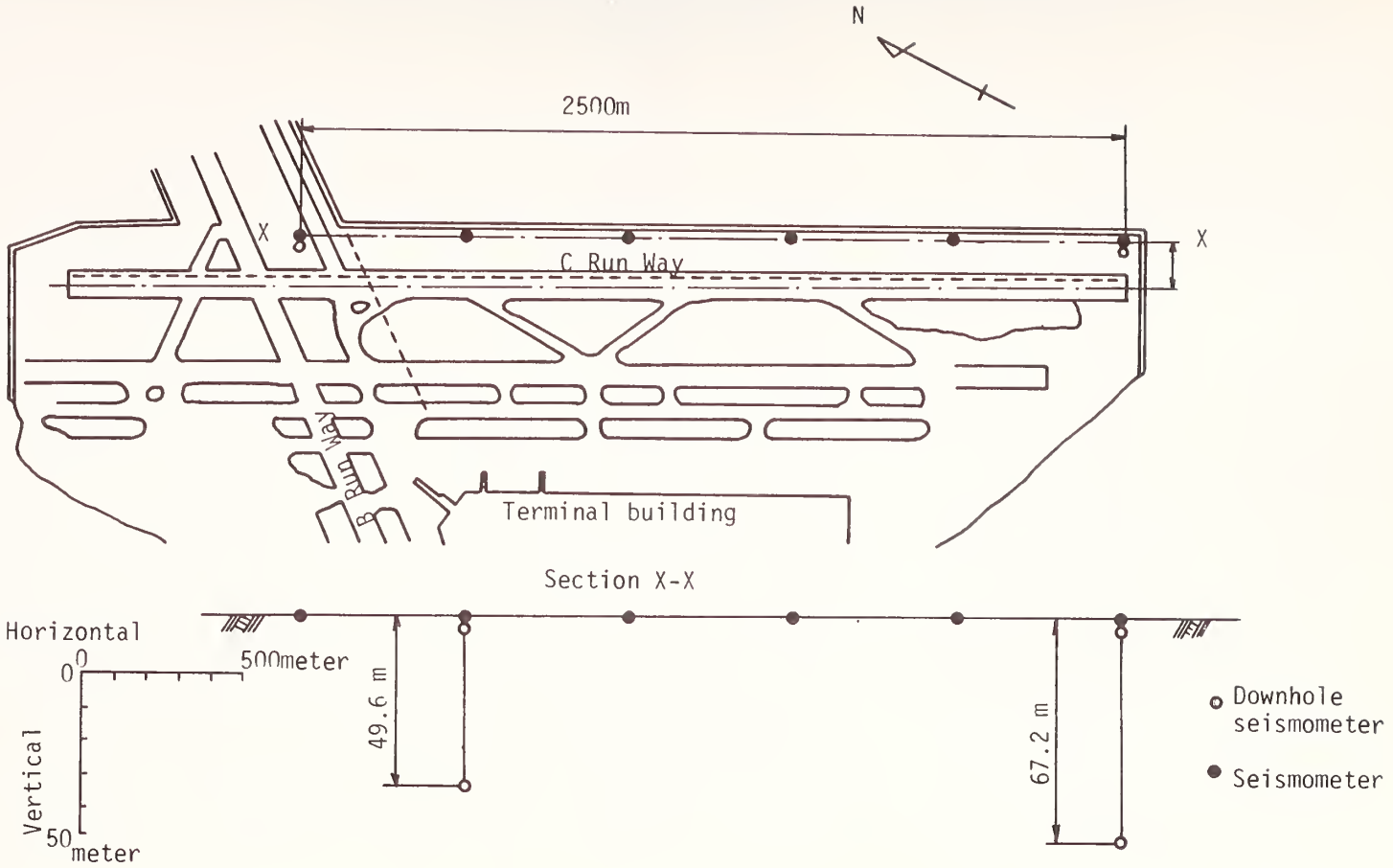

Fig. 5 Seismometer arrangement for two dimensional observation

RESEARCH STUDY ON LIQUEFACTION

by

W.F. Marcuson, III

U.S. Army Engineer Waterways Experiment Station
Vicksburg, Mississippi

A research program is being undertaken by the U.S. Army Corps of Engineers to evaluate the liquefaction phenomena relative to earthquake response of earth-filled dams. Present and future studies are summarized.

Key Words: Earthfill dams; earthquakes; ground shaking; liquefaction; soil density; stability.

INTRODUCTION

A major cause of damage of catastrophic failure associated with earthquakes is often attributed to liquefaction and/or slumping of cohesionless soils as a result of dynamic excitation. The importance of liquefaction was recently highlighted by the near failure of the Lower San Fernando Dam during the 9 February 1971, San Fernando Earthquake. Many other liquefaction failures have occurred and are documented in the literature (1, 2, 3, 4).

As a result of the near failure of the Lower San Fernando Dam, the Corps of Engineers (CE) initiated a research program on liquefaction phenomenon. A number of these investigations are being conducted at the U.S. Army Corps of Engineer Waterways Experiment Station (WES), Vicksberg, Mississippi. The objectives of these studies are (a) to evaluate the seismic stability of the CE hydraulic-fill dams, which fortunately are located in areas of low to moderate seismicity, (b) to evaluate the dynamic response of proposed Corps structures which are to be located in areas that are known to be seismically active and (c) to improve the Corps ability to determine in situ density and relative density or to develop an index which can be reliably related to liquefaction potential. This paper will discuss these activities.

CYCLIC TRIAXIAL COMPRESSION TESTS

Soil behavior under conditions of strong ground shaking is determined by cyclic triaxial compression tests. In such tests, the deviator stress is uniformly increased and decreased while maintaining a constant chamber pressure. The test equipment utilized by WES is shown in Figure 1. The pneumatic control unit consists of regulators and solenoid valves that are actuated by a cam-operated microswitch. The values provide alternating air pulses to a double acting air cylinder (loading) piston such that a cyclic load is transmitted from the air cylinder through the piston to the sample. Obviously, careful calibration was required, considering friction in the system and uplift pressures generated by the chamber pressure, to regulate the pulsating air pressures so that the desired loads are imposed on the specimens.

Electrical pressure transducers, a deformation transformer, and a load cell are used to measure pore pressure and chamber pressure, axial deformation, and axial load, respectively. Because of the rapid change in sample behavior at liquefaction, a high speed recorder is required to provide a continuous record of events during the tests. Figure 2 is a photograph of this equipment. The triaxial cell is on the right with a 2.8 inch diameter soil sample inside. The large rectangular unit in the center is the pneumatic control unit which houses the air pressure regulators and solenoid values. The unit on the left is a high speed recorder which provides a continuous record of the test data.

The majority of tests performed to date have been conducted on remolded samples of cohesionless material consolidated to isotropic or anisotropic conditions as required. A back pressure is applied to the specimen to ensure saturation. Saturation for these testing programs is defined in terms of Skempton's B-parameter. The B-parameter is equal to the ratio of the change in pore pressure to an induced change in chamber pressure. The value is checked in these tests by closing the drainage line and increasing the chamber pressure a desired amount, and observing the increase in pore water pressure. Typical B-values are 0.98 or greater for these testing programs. The specimens are subjected to a cyclic vertical load at a frequency of 2 Hz. Liquefaction consists of large deformation and a partial to total loss of strength. At the start of cyclic loading little deformation occurs, but as the cyclic loading progresses, the pore pressure increases thus reducing the effective stress. The CE presently defines initial liquefaction as the stage when the pore pressure first becomes equal to the chamber pressure giving an effective stress of zero. When this happens with a loose specimen, large deformations soon occur. This is shown in Figure 3, which is a plot of stress ratio $\sigma_{dc}/2\sigma_a$ versus cycles of loading for a cohesionless material at a density of 98 pcf or a relative density of approximately 60 percent. σ_{dc} is equal to the cyclic deviator stress and σ_a is equal to the ambient confining pressure. The curves are for initial liquefaction, ten and twenty percent peak-to-peak strain. Approximately three cycles of loading are required for the specimens to

undergo twenty percent strain after initial liquefaction has been reached. The response of a dense specimen is substantially different. Figure 4 is a plot of stress ratio versus number of cycles of loading for the same cohesionless material at a density of 109 pcf or a relative density of approximately ninety percent. At this density approximately fifty cycles of stress were required beyond initial liquefaction to reach ten percent peak-to-peak strain and twenty percent peak-to-peak strain was never reached.

WES has used the results of these tests along with dynamic finite element computer calculations to assess the stability of both operational structures and proposed structures (5, 6, 7, 8).

The CE is also currently funding cooperative research on laboratory testing in this area under the direction of Professor A. Casagrande at Harvard University. Dense sand specimens have been dynamically excited in a gyratory shear device. Specimens have been frozen immediately after liquefaction. Samples were then cut into many increments and soil properties of each increment are determined. Evaluation of these data is ongoing today and should be published within the year. Tentative results indicate that the behavior of dense sand specimens is governed by the migration of water within the specimen.

EVALUATION OF IN SITU DENSITY

The response of a cohesionless soil when subjected to dynamic loads is a function of its density or relative density. The accurate determination of the in situ density or relative density of a cohesionless material below the water table is a difficult and time consuming procedure. Work was conducted at WES in the 1950's which showed that undisturbed sand samples could be taken below the water table for density determinations (9). During this investigation, a procedure developed by WES (10) using a fixed piston sampler and drilling mud was employed to obtain undisturbed sand samples. Briefly this procedure is as follows: (a) As soon as the sample is removed from the drillhole, a packer is placed in the bottom of the sample tube and the sample is allowed to drain while remaining in a vertical position. (b) After drainage, a packer is also placed in the top of the tube and the sample is placed in a rack in a horizontal position and fixed against rotation. A rubber hammer is then used to tap the specimen 25 times from left to right and 25 times from right to left. (c) The sample is transported to a laboratory in this condition. (d) Once in the laboratory, the samples orientation is never changed (i.e., no rotation of the sample whatsoever). It is cut into three-inch increments for density determination. Presently WES is X-raying the sample and cutting the samples into increments as indicated in the radiograph for density determination. Figure 5 is a plot of height from bottom of sample tube versus correction for location of increment in tube for various relative densities and summarizes the results found during this earlier investigation. This plot shows that no correction is necessary near the center of the tube and the extreme density corrections are in the order of 2 pcf.

WES is presently checking the previously developed method of undisturbed sampling of sands to determine its adequacy for determining the in situ density of cohesionless materials below the water table. Indirect methods of in situ density determinations are also being evaluated. Penetration and sampling tests are being conducted inside a 4 ft. diameter by 6 ft. high stacked ring assembly. Figure 6 is a photograph showing a sand sample inside the stacked ring device. The rings are approximately one inch thick and have a tongue and grooved neoprene gasket between each ring. The purpose of this device is to minimize sidewall friction and thus give a more realistic stress gradient in the sample. The sand has a median size of approximately 0.2 mm and about five percent passing the No. 200 sieve. This material is placed inside the stacked rings using a raining technique developed at WES. Samples are placed at known densities in six inch lifts. Figure 7 is a schematic showing the entire stacked ring assembly and the sand sample. WES pressure cells are placed at three locations in the specimen. Each location has a series of six cells, three vertical and three horizontal. The assembly is located in a pit in the floor of the laboratory building. A rock filter exists below the sand sample and water is introduced at this elevation to submerge the sample. A water bag is placed on top of the sand sample and a loading device with three hydraulic rams is used to apply pressure

to the water bag thus ensuring a uniform stress distribution on the top of the sample. There is a five inch diameter hole in the center of the loading device and water bag and three three-inch diameter holes located thirteen inches out from the center on 120 degree radials. Figure 8 is a photograph of the bag before it is placed on the top of the sand specimen.

A vertical pressure is applied to the top of the specimen and consolidation is allowed to occur. Undisturbed fixed piston samples are taken in the center hole. Standard penetration tests (SPT) are conducted in each of the three radial holes. Figure 9 shows the overburden device assembled and the drill rig in its operational position. Tentative results of this work indicate that an accurate determination of density can be made using the fixed piston samples and add confidence to our earlier findings. Use of absolute instead of relative densities is desirable for seismic analysis of a specific project, but relative densities are needed to compare analyses and experiences at different sites.

Attempts have been made to correlate SPT "N" values (number of blows required to drive a splitspoon the last twelve inches of an eighteen-inch drive) to relative density. The analysis of these data is inconclusive at this time.

FUTURE INVESTIGATIONS

Most of the liquefaction analysis that have been made in the U.S. have been based on work done by Professor Seed and his coworkers at the University of California. This work has placed great emphasis on the liquefaction which occurred during the Niigata earthquake of 1964 (10). Professors Casagrade, Harvard University; Peck, University of Illinois; and Seed have all emphasized the need for direct determination of density at sites where liquefaction has occurred. It is believed that this is especially important at the Niigata site. Professor Casagrande also believes that the geologic age of the various sand deposits could be an important parameter which has not been studied to date. The CE feels that a program of undisturbed sampling at the Niigata site would greatly enhance existing knowledge on liquefaction phenomenon and recommends that such studies be made if feasible. WES would be pleased to offer technical assistance in this matter if desired.

WES has recently purchased a sophisticated closed loop loading apparatus. This equipment along with other apparatus that are currently being developed at WES should give the CE the capability of cyclicly testing up to fifteen-inch diameter specimens. This equipment also has the capability of using a random input (actual earthquake time history) to excite the specimen. The CE plans to utilize this equipment to gain insight into parameters such as the geometry effects, the effects of frequency, the effects of wave shape and form, and the assumptions currently used in going from the actual field earthquake to equivalent laboratory conditions.

The CE is extremely interested in developing a mathematical model which would predict liquefaction. Theoretical work is proposed in the near future to develop such a model. WES is currently funding research at the University of Michigan utilizing the method of characteristics to see if this approach can be used to predict liquefaction (11). The objective of this investigation is to see if the method of characteristics can accurately predict the response of the Lopez Dam during the 1971 San Fernando Earthquake.

REFERENCES

1. Seed, H.B., "Landslides During Earthquakes Due to Liquefaction," Journal of Soil Mechanics and Foundations Division, American Society of Civil Engineers, Vol. 94, No. SM5, September 1968, pp. 1053-1122.

2. Coulter, H.W. and Migliaccio, R.R., "Effects of Earthquakes of 27 March 1964, at Valdez, Alaska," Geological Survey Professional Paper 542-C, U.S. Department of Interior, 1966.

3. Seed, H.B. and Idriss, I.M., "Analysis of Soil Liquefaction, Niigata Earthquake," Journal of Soil Mechanics and Foundations Division, American Society of Civil Engineers, Vol. 93, No. SM3, May, 1967, pp. 83-108.

4. Seed, H.B. and Whitman, R.V., "Design of Earthquake Retaining Structures for Dynamic Loads," Proceedings of the Speciality Conference on Lateral Stresses in the Ground and the Design of Earth Retaining Structures, Soil Mechanics and Foundations Division American Society of Civil Engineers, 1970, pp. 103-147.

5. Marcuson, W.F., III and Collins, S.A., "Cyclic Triaxial Compression Tests, Center Hill Dam, DeKalb County, Tennessee," MS-74-5, March 1974, U.S. Army Engineer Waterways Experiment Station, CE, Vicksburg, Mississippi.

6. Marcuson, W.F., III and Gilbert, P.A., "Earthquake Liquefaction Potential at Patoka Dam, Indiana," Miscellaneous Paper S-72-42, December 1972, U.S. Army Engineer Waterways Experiment Station, CE, Vicksburg, Mississippi.

7. Marcuson, W.F., III, "One-Dimensional Wave Propagation Analysis, Patoka Dam, Indiana, Miscellaneous Paper (in publication) U.S. Army Engineer Waterways Experiment Station, CE, Vicksburg, Mississippi.

8. Marcuson, W.F., III, "Liquefaction Analysis of the W.G. Huxtable Pumpting Plant Site, Mississippi River," Report (in publication) U.S. Army Engineer Waterways Experiment Station, CE, Vicksburg, Mississippi.

9. Rotary Cone Penetrometer Investigations, Potomology Investigations, Report 18-1, June 1962, U.S. Army Engineer Waterways Experiment Station, CE, Vicksburg, Mississippi.

10. Undisturbed Sand Sampling Below the Water Table, Bulletin 35, June 1950, U.S. Army Engineer Waterways Experiment Station, C.E. Vicksburg, Mississippi.

11. Seed, H.B. and Idriss, I.M., "Simplified Procedure for Evaluating Soil Liquefaction Potential," Journal of Soil Mechanics and Foundation Division, American Society of Civil Engineers, Vol. 97, No. SM9, September 1971, pp. 1249-1273.

12. Streeter, V.L., Wylie, E.G., and Richart, F.E., Jr., "Soil Motion Computations by Characteristics Method," Journal of the Geotechnical Division, American Society of Civil Engineers, Vol. 100, No. GT3, March 1974, pp. 247-263.

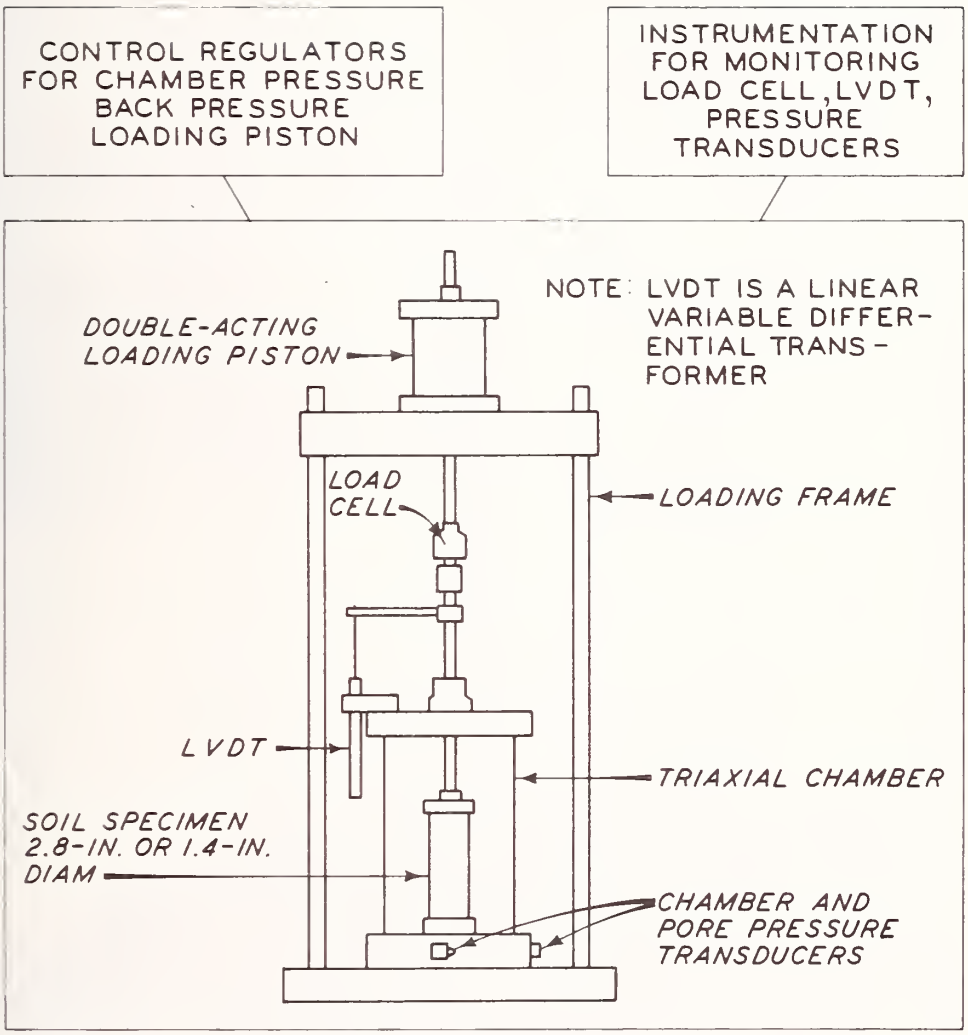

Fig. 1. Cyclic triaxial test equipment

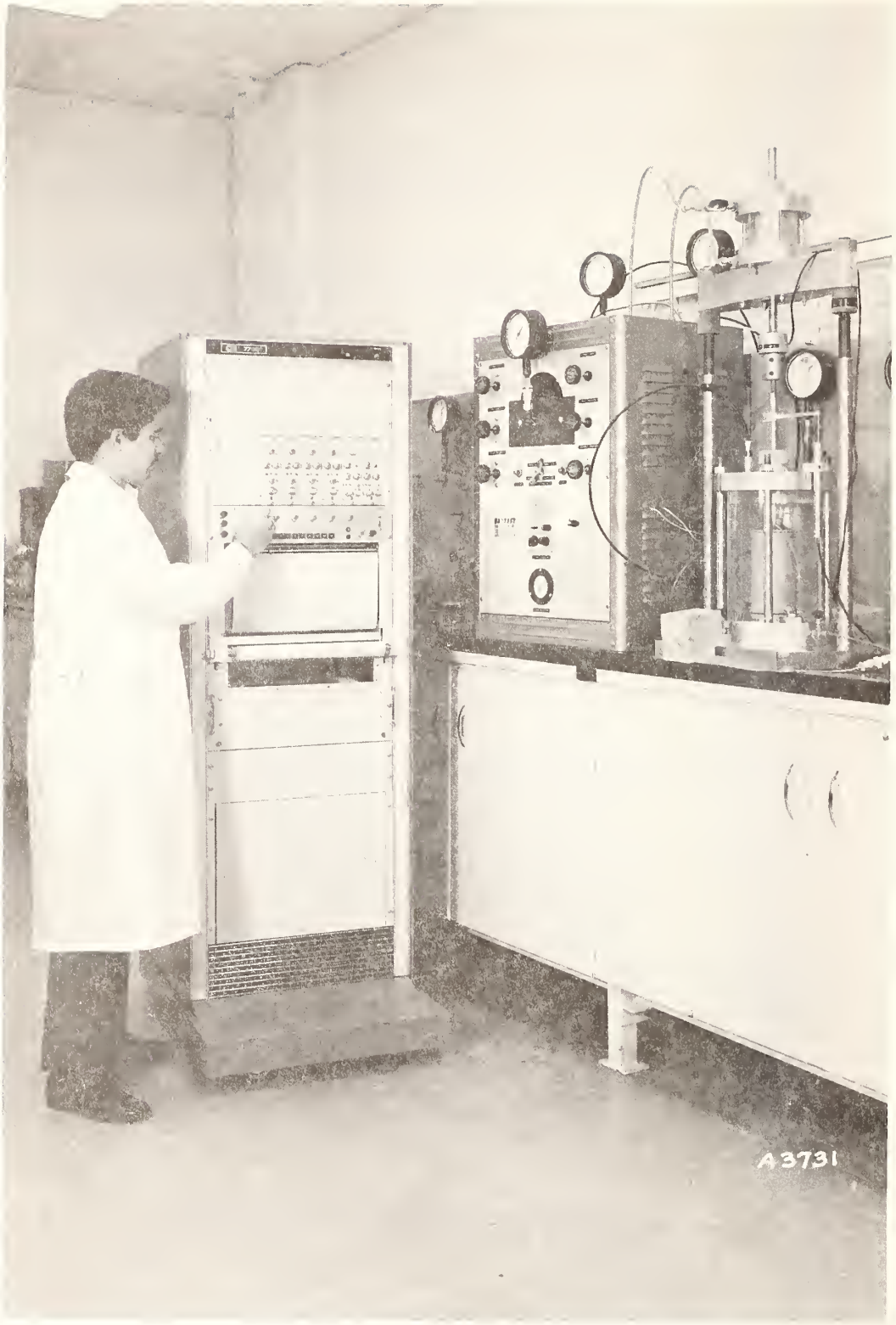

Fig. 2. Cyclic Triaxial Test Equipment

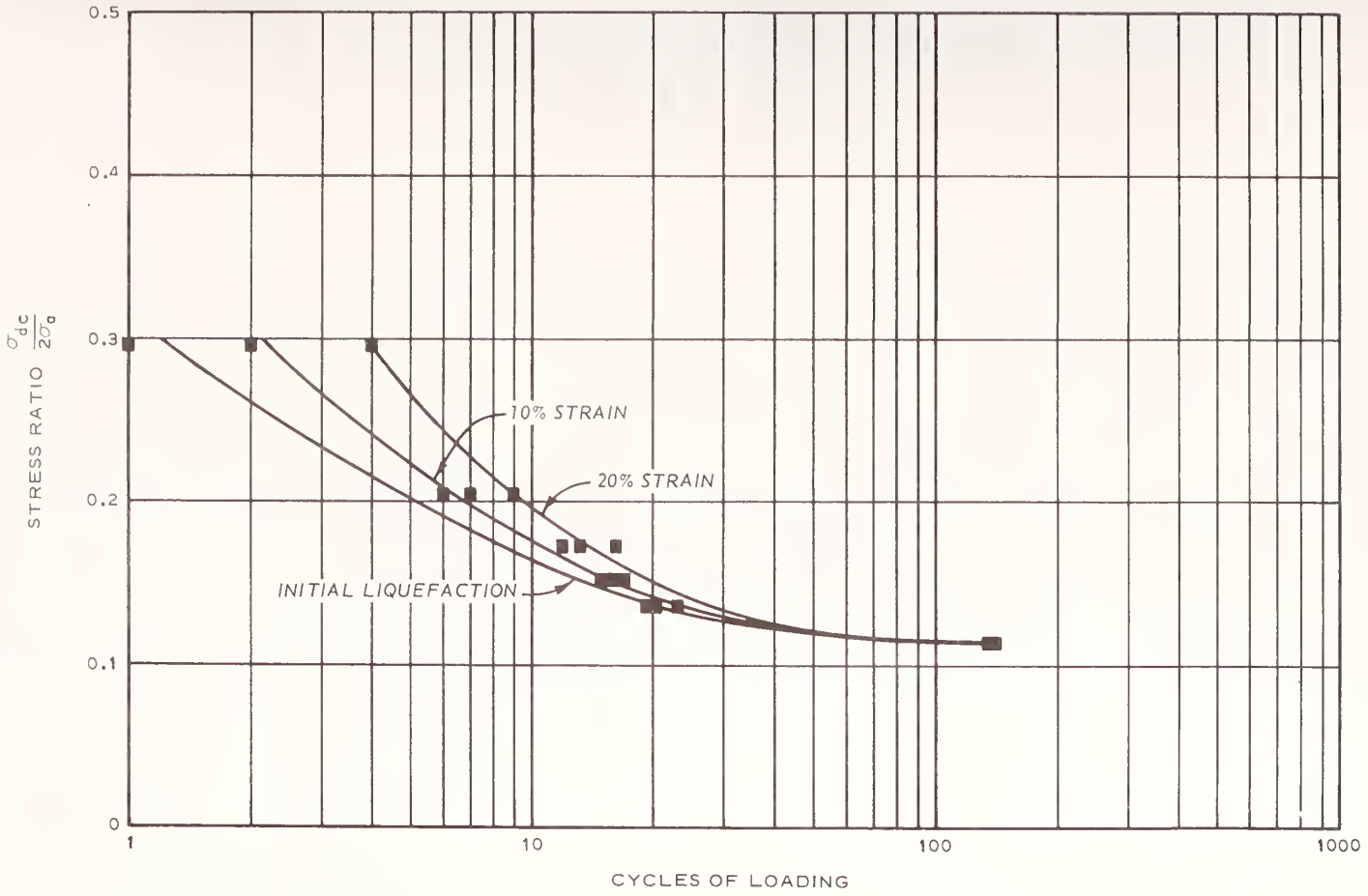

Fig. 3. Cyclic triaxial tests of materials at in situ density (98 pcf)

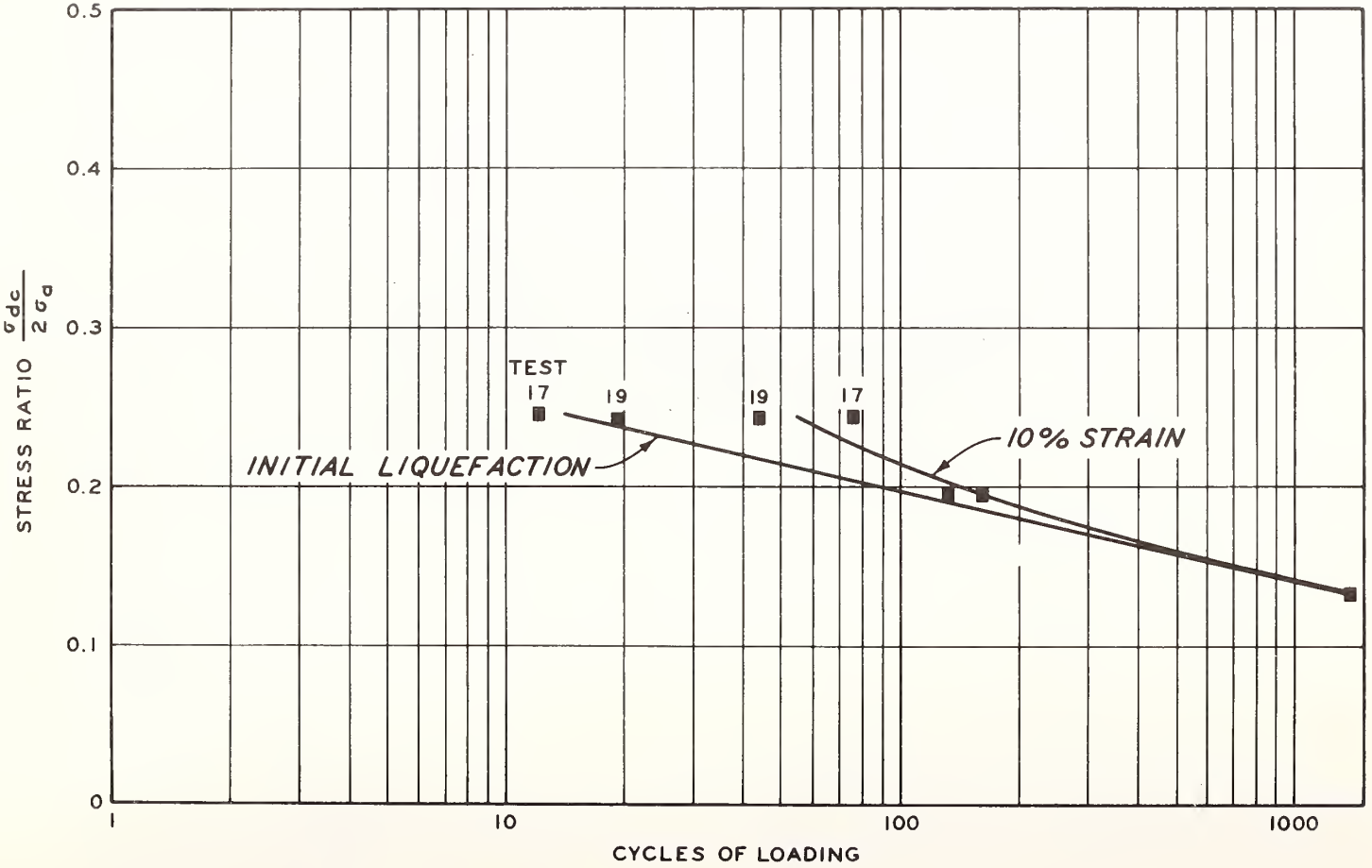

Fig. 4. Cyclic triaxial tests of material at 109 pcf

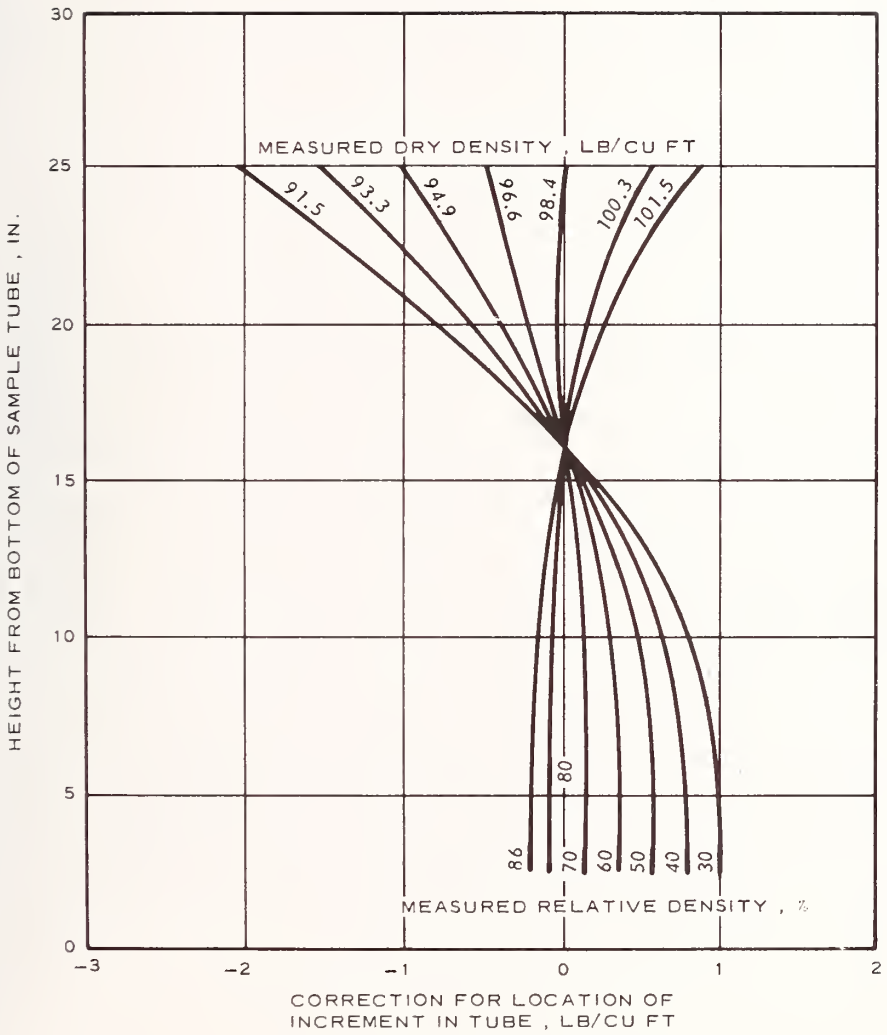

Fig. 5. Density correction for location in sample tube, combined plot

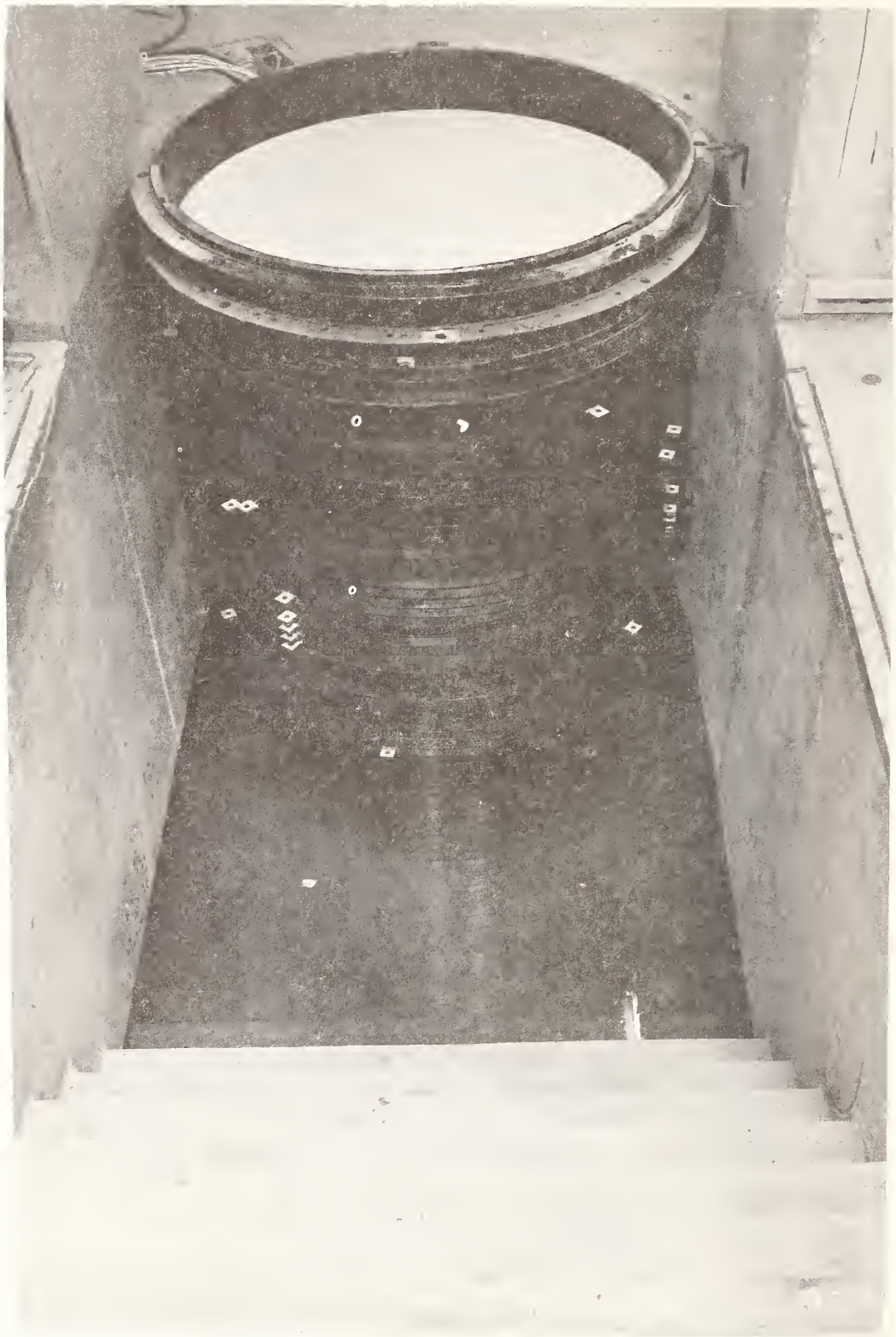

Fig. 6. Sand Sample in Stack Ring Assembly

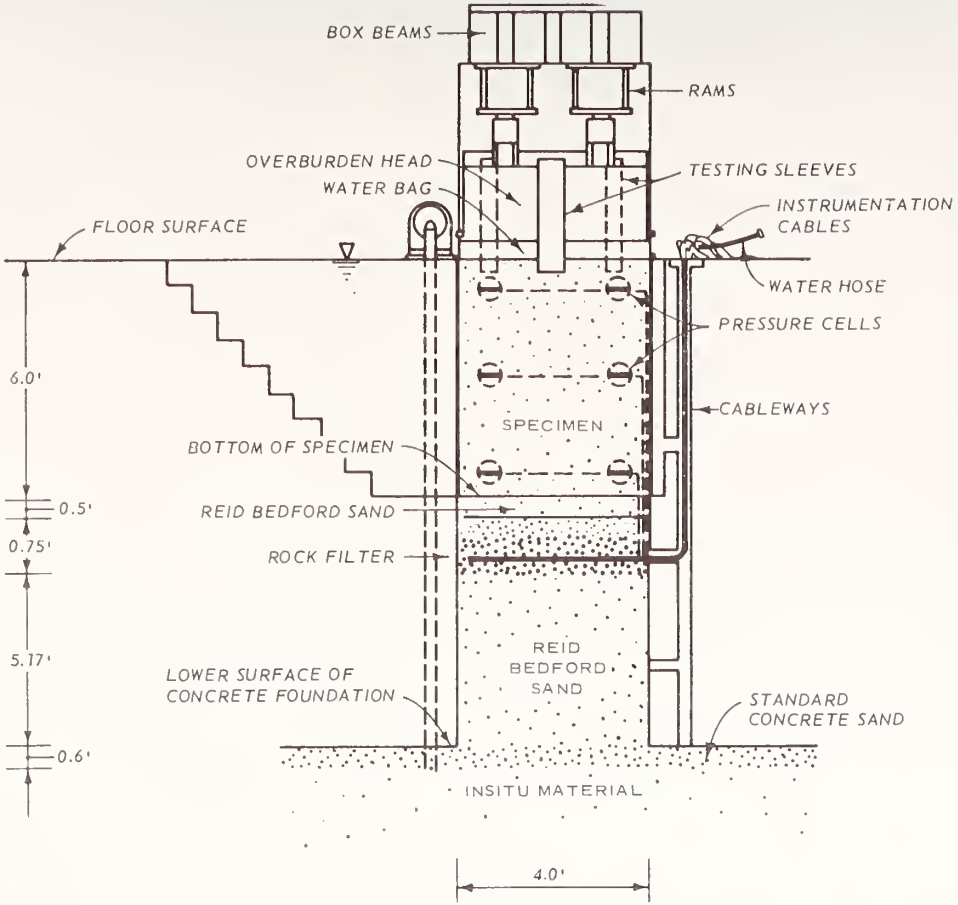

Fig. 7. Test device cross section with sample in place

Fig. 8. Water Balloon Prior to Assembly on Sample

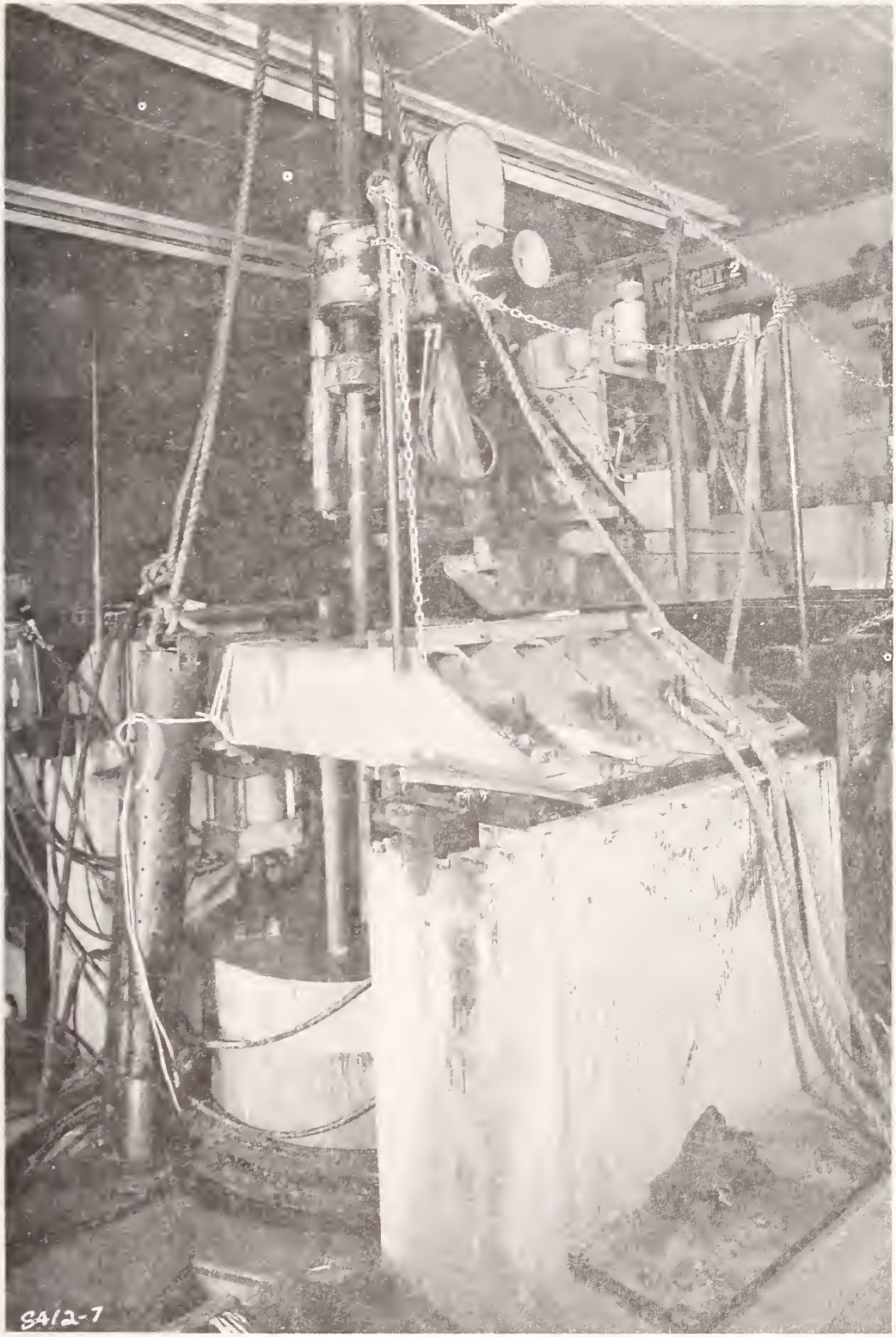

Fig. 9. Overburden Assembly and Drill Rig in Operational Position

ESTIMATION OF LIQUEFACTION POTENTIAL BY MEANS OF EXPLOSION TEST

by

K. Yamamura
Director
Kita-Shuto National Construction Office
Ministry of Construction, Japan

Y. Koga
Research Engineer
Soil Dynamics Section
P.W.R.I.

Ministry of Construction, Japan

A series of field vibration experiments were performed in order to estimate the liquefaction potential of sandy soil during earthquakes. Bore hole explosions were used as a vibration source. A significant relation was found between the ground stiffness and the pore-water pressure as caused by the explosion. A proposed method has been developed for estimation of the liquefaction potential.

Key Words: Earthquake; explosion test; ground strength; ground vibration; liquefaction; pore-water pressure.

PREFACE

Since the Niigata and Alaska Earthquakes in 1964, and the disastrous effects due to liquefaction of a sandy ground or a sandy embankment, there has been increased interest and concern in the liquefaction phenomena. Extensive research and study has, therefore, been conducted in various countries relative to this problem.

Based on the results of these studies, several simple methods have been proposed in order to estimate the liquefaction potential (1, 2, 3, 4). These methods use the N-value, as obtained from conducting standard penetration tests, the relative density and the grain-size distribution, etc. Other methods (5, 6) use a combination of the results obtained from dynamic shear tests and the analytical results of the ground vibration to estimate liquefaction potential. In addition to these methods, a technique which can estimate the liquefaction possibility of the soil in the in-situ position, that is at the field site, is most desirable. This is because generally the in-situ soil has the following characteristics;

(1) There may exist a certain cementation strength among the grains in an undisturbed state, even in a sandy soil, depending upon the age and the development of the deposit (for instance, old alluvial deposits or reclaimed land).

(2) The soil may not be uniform, but may have laminations which can include silt or gravel layers, or a surface soil may be present.

One of the most logical methods that can be employed to investigate the ground behavior under vibration is to apply an artificial vibration source at the actual test site. The inducement of an artificial vibration can be achieved by a bore hole explosion and by driving piles.

Explosion Method (7, 8, 9): Florin has proposed a criterion for the estimation of liquefaction potential, by examining the magnitude of the average settlement of the ground surface within the radius of 5 m from the explosion point, by blasting 5 kg of ammonite explosive at the depth of 8 m to 10 m and the ratio of settlement by three successive explosions at one place. By this method, if the average magnitude of the settlement of the ground surface within 5 m radius is below 8 m to 10 cm, there is no need to provide any measures against liquefaction of the soil.

Pile Driving Method (10): This method estimates liquefaction by reading the acceleration meters and the pore pressure gauges installed in the ground to measure the vibration of the ground caused by the driving of a steel tube pile or a sand compaction pile.

The following will describe an outline of the liquefaction estimation experiment, using the explosion technique, undertaken by the Public Works Research Institute.

PLAN OF EXPERIMENT

(1) Site of Experiment

The site where this experiment was performed was at the high water channel of the Agano River, in Niigata Prefecture. The embankment of this river had suffered cracks, slidings, and settlements at numerous places during the Niigata Earthquake, and was known to have a oil which could easily liquefy. Also, in selecting the site, it was remote from the inhabited area, thus eliminating any human complaints due to the tests.

(2) Soil Condition

The soil condition can be classified into three major zones, as shown in Figure 1 (a) to (c). A-zone has a layer of 0.5 - 1.0 m thick humus on the surface and a sand layer

underneath of approximately uniform fine and coarse sand partially intermixed with fine-grain gravels. The ground water level is approximately at the ground surface. The ground stiffness N-values are 3-8 at a depth of 5.5 to 6.0 m. Further down the N-values suddenly increase to a value of above twenty. The B-zone has a cross layer of fine and coarse sand mingled with gravel. The ground water level is located approximately at the depth of 0.7 to 1.3 m from the ground surface. The N-value to the depth of about 0.5 to 7.5 m is three to eight. Further down, the N-value shows a sudden increase to a value of thirty. The C-zone is covered with a layer 1.0 m of surface soil with an underneath cross layer of fine-coarse sand. The N-value, down to the depth of about 3.0 m, is three to six. At further depths, the value is ten to twenty. The ground water level is in the vicinity of 2.0 to 2.3 m from the ground surface. The grain size distribution of the sand in each zone is shown in Figure 2. Such a distribution curve is indicative of the type of sand which is prone to cause liquefaction.

(3) Test Method

Dynamite which was charged into a bore hole of 4-8 m deep was used for the explosion. No sand was filled in the explosive charged hole. Strain gauge type accelerometers, pore pressure gauges of the strain gauge type, and differential transformers were respectively installed. These units were placed in both the bore hole, surrounding ground, and in the shallow ground surface. The changes or fluctuations caused by the explosion were then recorded by a data-recorder (magnetic tape type) and an eletromagnetic oscillograph. All of the bore holes, which were made for monitoring, were filled with sand. The magnitude of the settlement of the wooden piles, installed in the ground surface, were measured before and after each explosion by use of a level. For some of the experiments, Swedish weight-sounding tests were performed before and after an explosion, in the vicinity of the explosion hole, to investigate the strength variation of the ground.

(4) Test Condition

Table 1 shows the test conditions of the experiments that were performed.

RESULTS OF EXPERIMENT

(1) Measured Records

Examples of the recorded acceleration data and the pore water pressure data are shown in Figure 3 (a) and (b). The initial shock part of the acceleration data, caused by the explosions, is from the body wave. The relatively long frequency appearing thereafter is thought to be either the reflected wave from the ground surface and the lower stratum, or by the surface wave. Even with the pore water pressure after it had shown an initial short cycle vibratory characteristic (Ud), it changed into a somewhat longer cycle vibration leaving a partial residual substance. This, however, rapidly dissipated generally in two to five minutes, and then remained constant. This is probably because the ground structure has been disturbed by the seismic motion as caused by the explosion, and there has occurred a phenomenon of a partial liquefaction causing an excess pore water pressure in the ground.

(2) Ground Acceleration

Figure 4 shows a diagram of the maximum value of the surface ground acceleration against the distance from the explosion hole to illustrate the ground acceleration characteristic. As shown by this diagram, the vertical acceleration is larger than the horizontal acceleration at the ground surface, with a greater scattering with respect to the vertical acceleration.

(3) Pore Water Pressure

Figure 5(a) represents the arrangement of the pore water pressure gauges and accelerometers installed for the test to measure the pore water pressure. Figure 5 (b)-(e)

illustrate the distribution of the shock pore water pressure Ud against the 1.0 kg dynamite explosion and the residual pore water pressure Ur. In these examples, there has occurred in the vicinity of these explosion holes an excess pore water pressure of 10% to 70% of the overburden pressure, and it is believed that a small scale liquefaction has taken place in the ground. To further indicate whether a liquefaction has actually taken place, such items as a sand blow, water spout, and ground settlement should be observed. However, neither a sand blow or a water spout did occur although ground settlement was noted, as will be detailed later. Figure 6 illustrates the relationship of Ud and Ur to the ground stiffness from all tests including those presented in Figure 5 (b)-(e). Ud and Ur have been non-dimensionalized by dividing them by the effective overburden pressure σ_v'.

According to this Figure 6, in C-zone where the ground is stiff, Ur is smaller than Ud, and by contrast in the B-zone where the ground is soft, the reverse trend occurs. As will be shown, there is a relationship between ground stiffness and liquefaction potential.

(4) Ground Surface Settlement

Examples of the measured ground surface settlement caused by the explosion are shown in Figures 7(a) and 7(b). The test data presented corresponds to the same tests presented in Figures 5(b) and (d). Assume now that the soil stratum above the explosive depth charge of GL-6m has a relation with the ground settlement rate. This can be illustrated by the relationship between the mean N-value of the soil stratum and the settlement rate at one meter from the explosion point, as shown in Figure 8(a). Further, consider the pore water pressure at a measuring point 6 m from the explosion hole and at the depth of 6 m, as shown in Figure 8(b). This figure shows the relationship between Ur, at this point, and the previously mentioned settlement rate. It appears from these plots that as the ground settlement rate increases, the ground becomes softer and Ur increases and vice-versa. Also by measuring the ground settlement rate in this manner, a greater potential of occurrence of Ur in the ground may be estimated.

(5) Variation of Ground Strength

In order to investigate the ground strength variation by explosion, a set of Swedish weight-sounding tests were conducted surrounding the explosion hole before and after the explosion, an example of which is shown in Figure 9(b)-(e). This experiment was carried out before and after the experiment No. 1-5. The position of these tests are shown in Figure 9(a). The following trends are noted from Figure 9. In the case where the ground strength is estimated in terms of an average number of half-turns per m (Nsw), the pre-explosion ground strength tends to increase with ground depth. However, after the explosion, its distribution range is apt to expand. This is particularly true in the vicinity of the explosion point, where its strength drastically decreases. At the central point, at a distance of 5 m from all the explosion holes, the strength throughout the entire stratum has substantially increased. This may be due to the ground compaction, as a result of the explosion vibration.

SIMPLE ANALYSIS OF TEST RESULTS

At present, the liquefaction phenomenon of sandy soil at the time of an earthquake is said to be caused by the repeated shear stress under the force of the earthquake and the dilatancy mechanism of sand rather than the ground acceleration or its inertia force. Therefore, even the seismic motion produced by explosion differs from that caused by an earthquake. A simple analysis was, therefore, tried, which would consider partial liquefaction to take place as caused by the dynamic shear stress.

The ground vibration by an in-bore hole explosion cannot be analyzed very simply because of the existance of bore holes surrounding the ground surface, as well as the non-uniformity of the ground strata and beddings. However, a simple approximation may be made by considering the ground vibration caused by an explosion as that due to a spherical wave (P wave) emitted from one point in an infinite elastic body.

Using the symbols given in Figure 10, the equation of motion in the radial direction r may be expressed (11) by the Equation (1).

$$-\frac{\partial \sigma_r}{\partial r} - \frac{2}{r}(\sigma_r - \sigma_t) = p\frac{\partial^2 u}{\partial t^2} \tag{1}$$

where: σ_r and σ_t represent the normal stresses in the radial and tangential directions, respectively. Taking the compression stress as a positive, the following expressions can be given by employing the modulus of elasticity E of the ground containing water, and Poisson's ratio ν:

$$\left.\begin{aligned} \sigma_r &= -\frac{E}{(1+\nu)(1-2\nu)}\left\{(1-\nu)\frac{\partial u}{\partial r} + 2\nu\frac{u}{r}\right\} \\ \sigma_t &= -\frac{E}{(1+\nu)(1-2\nu)}\left(\frac{u}{r} + \nu\frac{\partial u}{\partial r}\right) \end{aligned}\right\} \tag{2}$$

From Equations (2), the dynamic shear stress τ_d and mean principal stress σ_m are determined as:

$$\left.\begin{aligned} \tau_d &= \frac{\sigma_r - \sigma_t}{2} = \frac{E}{2(1+\nu)}\left(\frac{\partial u}{\partial r} - \frac{u}{r}\right) \\ \sigma_m &= \frac{\sigma_r + 2\sigma_t}{3} = \frac{E}{3(1-2\nu)}\left(\frac{\partial u}{\partial r} + \frac{\partial u}{r}\right) \end{aligned}\right\} \tag{3}$$

In order to satisfy Equation (1), the following equations are assumed:

$$u = \frac{\partial \phi}{\partial r} \qquad \phi = \frac{1}{r} f(r - Ct) \tag{4}$$

Substituting Equations (4) into Equations (3) gives:

$$\left.\begin{aligned} \tau_d &= \frac{E}{2(1+\nu)}\left(\frac{3}{r^3} f - \frac{3}{r^2} f' + \frac{1}{r} f''\right) \\ \sigma_m &= \frac{E}{3(1-2\nu)} \cdot \frac{1}{r} f'' \end{aligned}\right\} \tag{5}$$

The ratio of Equations (5) are:

$$\frac{\tau_d}{\sigma_m} = \frac{3(1-2\nu)}{2(1+\nu)} \cdot \left(\frac{3}{r^2}\frac{f}{f''} - \frac{3}{r} \cdot \frac{f'}{f''} + 1\right) \tag{6}$$

It is now desirable to evaluate the stress ratio at the time the P wave arrives at each point. Employing the following expression from the continuity conditions of displacement and velocity gives:

$$f = 0 \qquad f' = 0 \tag{7}$$

Then from Equation (6), the stress ratio at the time of P wave's arrival, namely, at the time when the initial shock wave motion is propagated, is;

$$\frac{\tau_d}{\sigma_m} = \frac{3(1-2\nu)}{2(1+\nu)} \tag{6'}$$

Assuming the ground is in a saturated state, the shock pore pressure Ud, produced by the arrival of this P wave, is considered to create an undrained condition because of the rapid occurrence of the phenomenon. Because of this, shock pore pressure is equal to the mean principal stress σ_m, or;

$$Ud = \sigma_m \tag{8}$$

Also, Poisson's ratio ν in an undrained condition of the saturated soil may be given by the following expression (12),

$$\nu = \frac{1}{2}(1 - nGCw) \tag{9}$$

where n = Porosity; G = Modulus of rigidity of the ground; Cw = Coefficient of compressibility of water and $\nu = 1/2$.

Substituting Equations (8) and (9) into (6') gives;

$$\tau_d = nGCw \cdot Ud \tag{10}$$

This equation states that the shock pore water pressure Ud, created immediately after explosion, is proportional to the dynamic shear stress which affects the soil.

Figure 11 summarizes the results of a dynamic triaxial compression test under a saturated undrained condition performed on sand similar to the sand at the test site. This diagram illustrates the effect of residual pore water pressure in the test specimens of different densities subjected to different dynamic shear stresses. These results indicate that at smaller densities, the residual water pressure increases. Thus, the greater the initial dynamic pore water pressure at the time of explosion, the softer the ground becomes and the greater will be the residual pore water pressure. Figure 6 shows this same trend. Figure 6 represents an approximate comparison of the classified ground for each test zone. This shows that as the density varies in the depth direction, the liquefaction potential may also differ. For the density at various stages of depth, a classification by use of the actually measured or estimated N-values was considered, since no sufficient sampling of the undisturbed test specimens was performed. For this reason, on Figure 6 there are listed the estimated N-values at each measuring point, and a tentative classification made by $N \gtrless 10$. According to this diagram, it may be said the differences between Ud and Ur are more evident than by the mere division according to zone. Therefore, the relation between Ud and Ur is closely related to the ground density and from the relationship of both values, it may be possible to estimate the ground density or possibly the liquefaction potential.

CONCLUSION

(1) A reasonable method for estimations of ground liquefaction potential by means of bore hole explosion has been obtained.

(2) As an estimated index for liquefaction potential, a relationship between the shock water pressure, residual water pressure caused by the explosion, and the ground settlement rate has been developed.

(3) Despite the above developments, the following problems remain to be solved:

(a) Determine the applicability of the technique for other soil conditions (creation process, soil property, density, etc.).

(b) Determine the applicability for deeper soil.

(c) Improve the accuracy of measuring ground acceleration and pore water pressure.

(d) Improve the accuracy of the measurement of soil densities.

(e) Examine further the characteristics of residual pore pressure as obtained by a laboratory dynamic shear test.

(f) Review of the analytical methods of ground vibration by explosion.

REFERENCES

1. Tsuchida, H.: Forecast and Measures of Sandy Ground (in Japanese), Technical Note of Port and Harbour Research Institute, 1970.

2. Ohsaki, Y.: Effects of Sand Compaction on Liquefaction during the Tokachioki Earthquake, Soils and Foundations, Vol. 10, No. 2, 1970.

3. Gibbs, H.J.: Earth Structure and Foundations Subjected to Seismic Loading, Preprints of 2nd Joint Meeting of U.S.-Japan Panel on Wind and Seismic Effects, 1970.

4. Japan Road Association: Aseismic Design Manual of Road Bridge (in Japanese), 1972.

5. Seed, H.B., Idriss, I.M.: Simplified Procedure for Evaluating Soil Liquefaction Potential, Proc. of ASCE, Vol. 97, No. SM9, 1971.

6. Iwasaki, T.: Study on Aseismic Design of Foundation of Structure and Ground (in Japanese), Technical Note of Public Works Research Institute, No. 764, 1972.

7. Florin, V.A., Ivanov, P.L.: Liquefaction of Saturated Sandy Soils, Proc. of 5th Int. Conf. on S.M. and F.E., Vol. 2, 1961.

8. Kummeneje, O., Eide, O.: Investigation of Loose Sand Deposits by Blasting, Proc. 5th Int. Conf. on S.M. and F.E., Vol. 2, 1961.

9. Prakash, S., Gupta, M.K.: Blast Tests at Tenughat Dam Site, Jour. of Southeast Asian Soc. Soil Eng., Vol. 1, 1970.

10. Fukuoka, M., Ishihara, K.: Measurement of Pore Pressure During Field Vibration (in Japanese), Preprints of 27th Annual Meeting, Japan Soc. Civ. Eng., 1972.

11. Timoshenko, S.P., Goodier, J.N.: Theory of Elasticity, 3rd ed., McGraw-Hill.

12. Ishihara, K.: Approximate Forms of Wave Equations for Water-Saturated Porous Materials and Related Dynamic Modulus, Soils and Foundations, Vol. 10, No. 4, 1970.

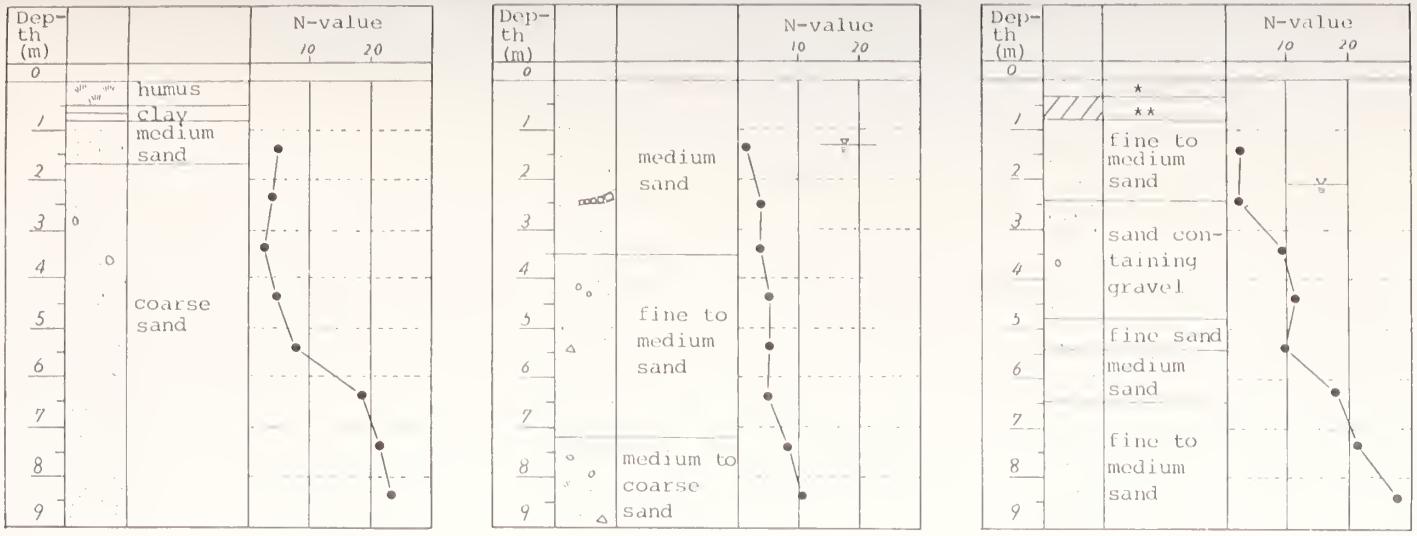

Fig. 1 Soil profile of test sites

* surface soil
** silty sand

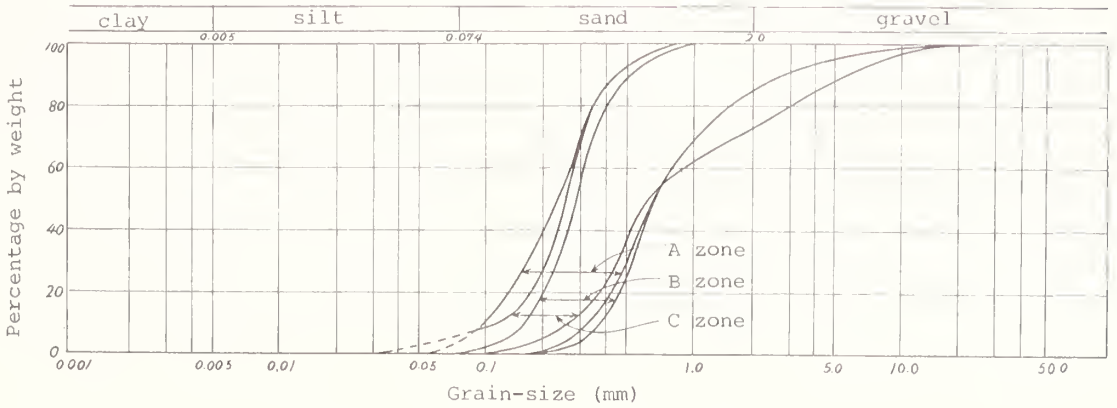

Fig. 2 Grain-size distribution curve

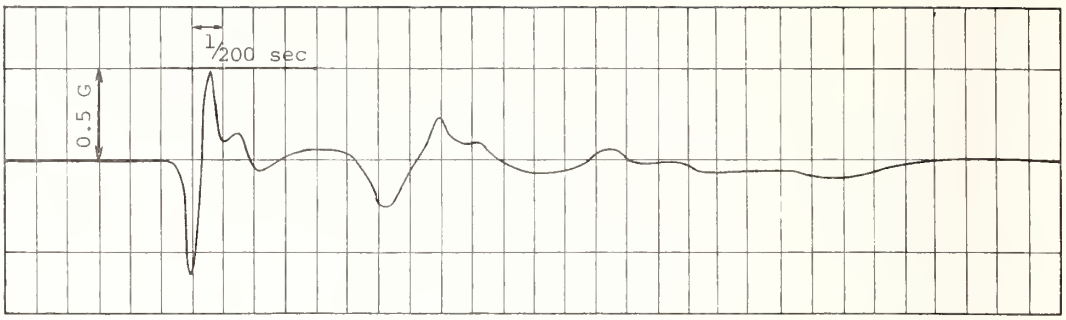

(a)

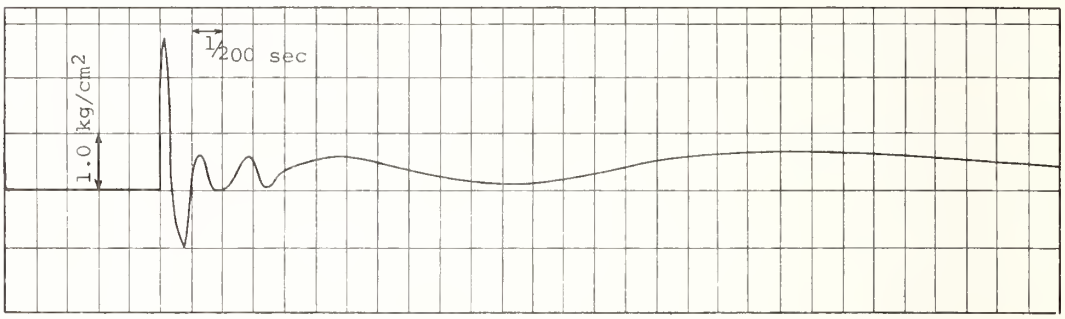

(b)

Fig. 3 Typical records (a) Acceleration (b) Pore water pressure

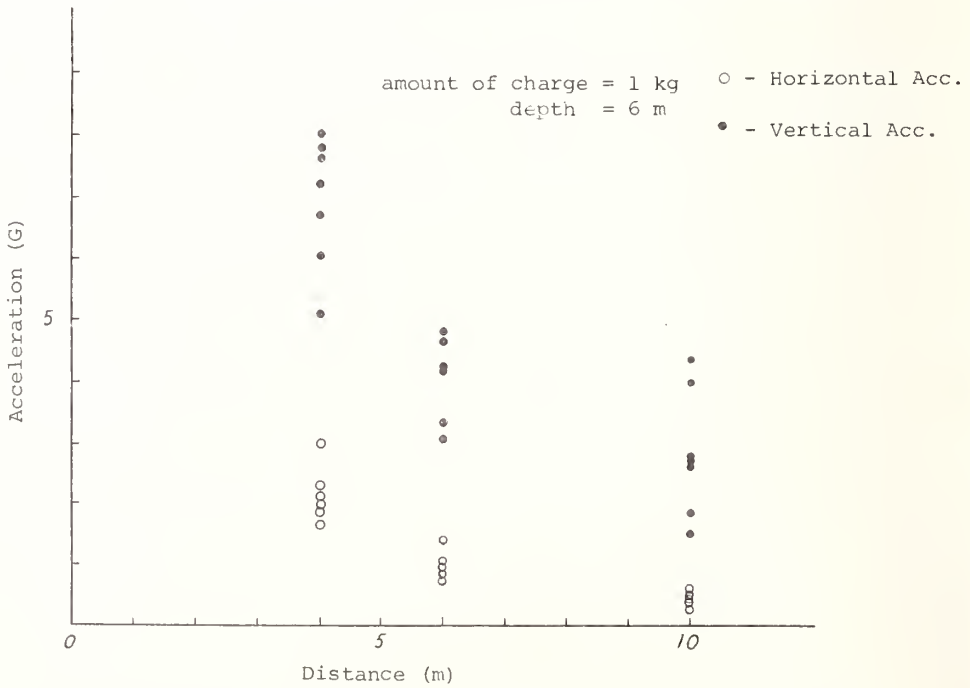

Fig. 4 Accelerations as functions of distances from explosion point

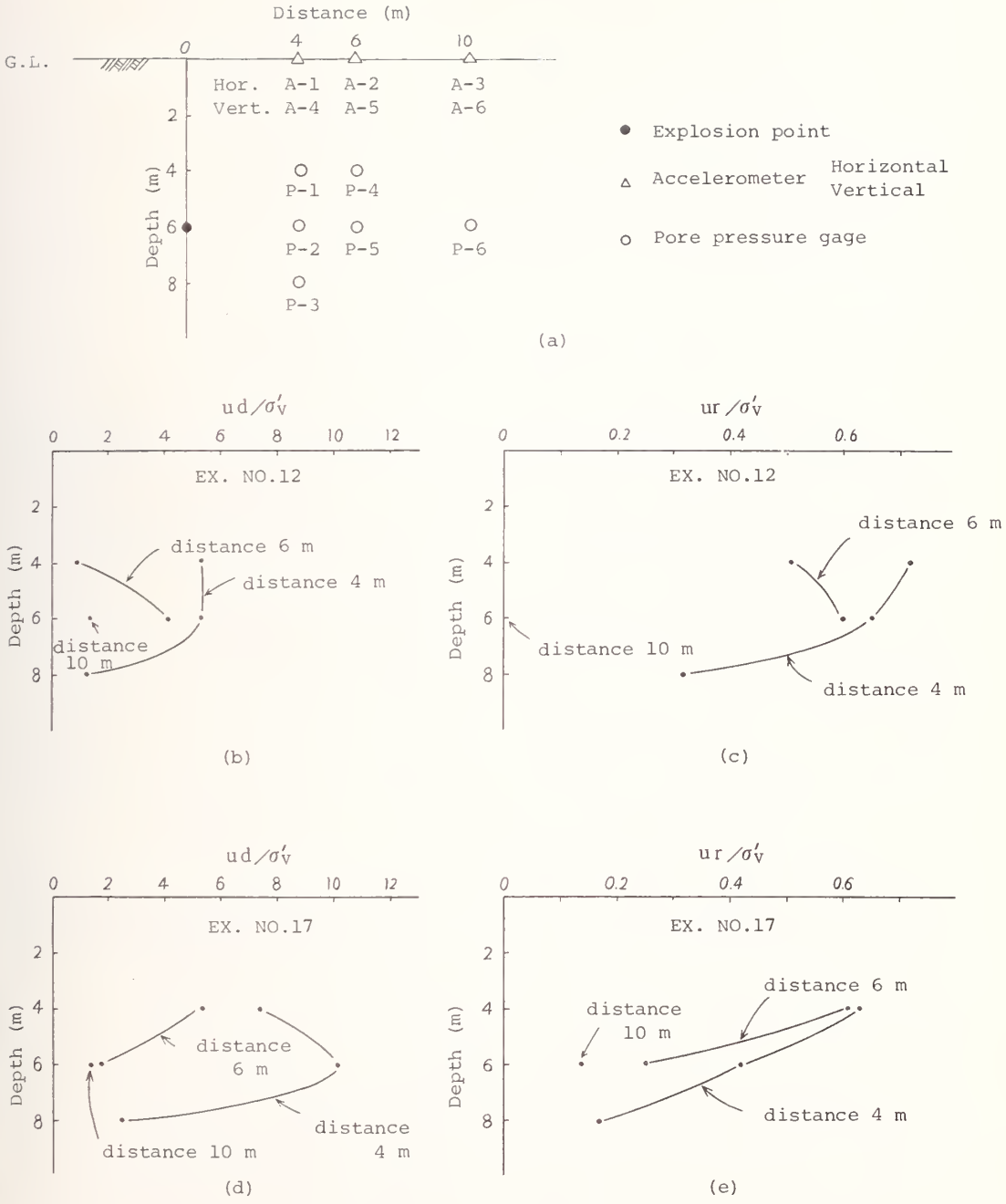

Fig. 5 (a) Cross-section showing the location of the explosion point and instruments
(b,c,d,e) Increase of pore pressure with depth

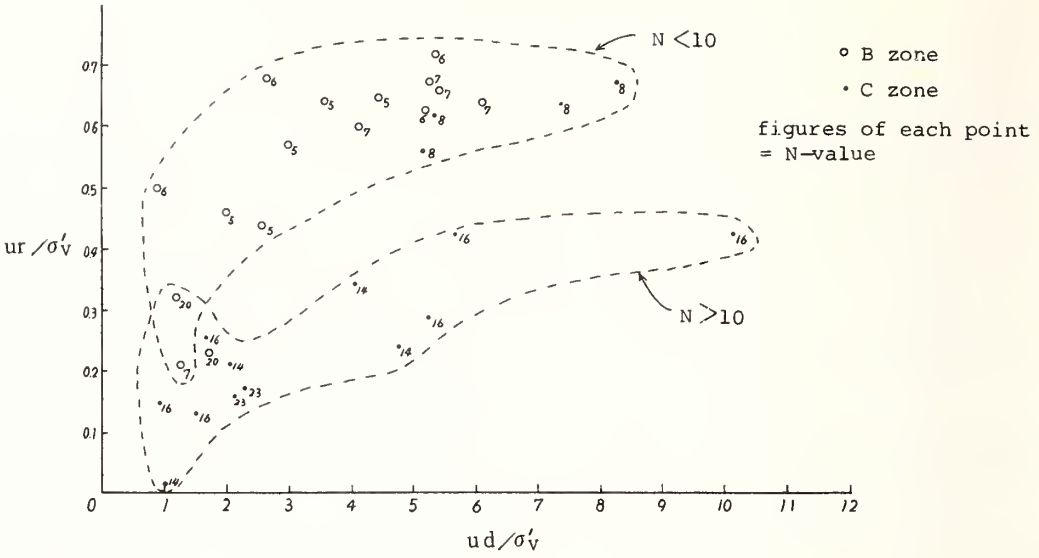

Fig. 6 Relation between dynamic pressure U_d and residual pressur U_r

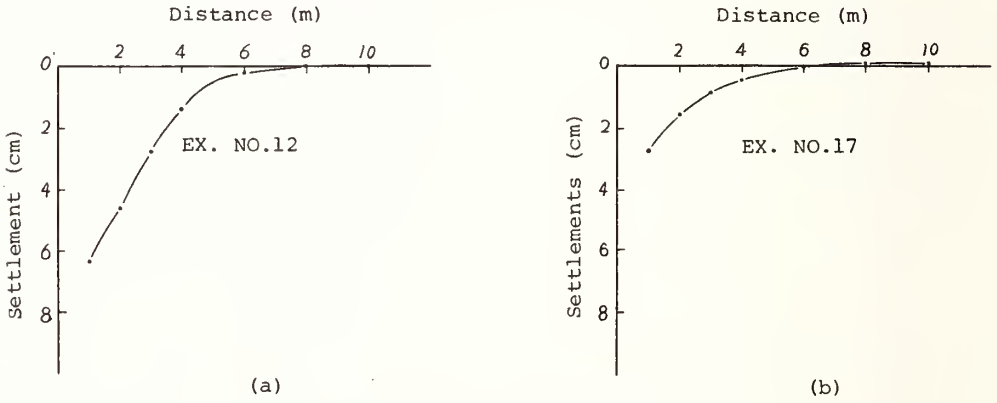

Fig. 7 Settlements of the ground surface

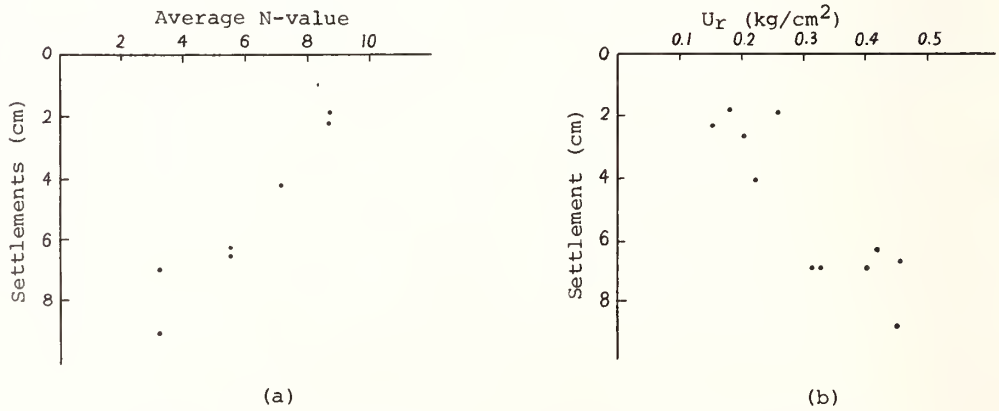

Fig. 8 Relation between settlement and (a) average N-value and (b) residual pressure

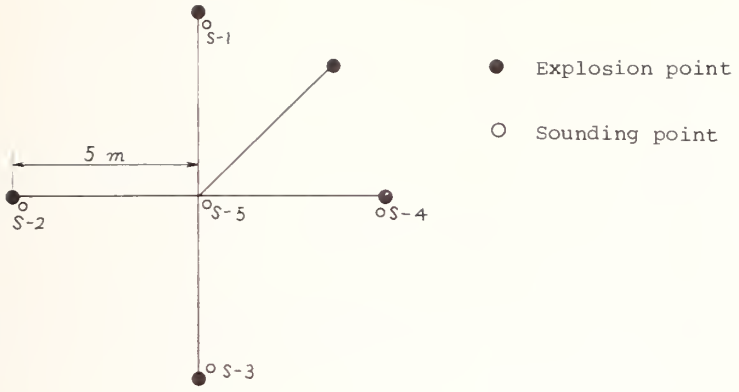

(a)

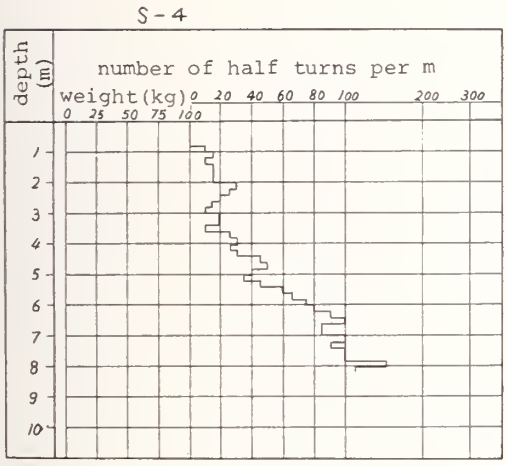

(b) before explosion

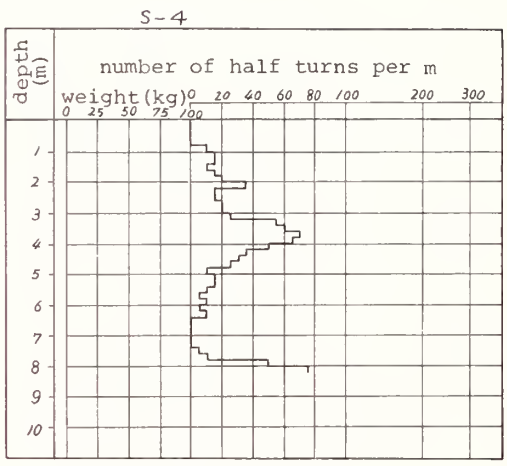

(c) after explosion

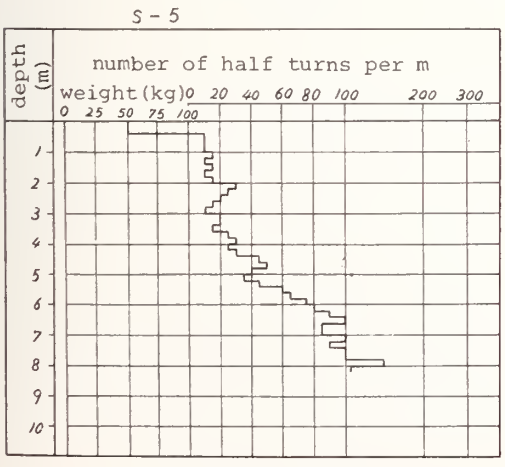

(d) before explosion

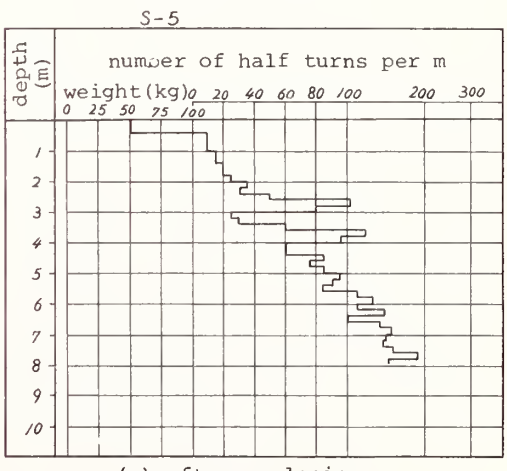

(e) after explosion

Fig. 9 (a) Location of the explosion point and the sounding point
(b,c,d,e) Penetration resistance with depth

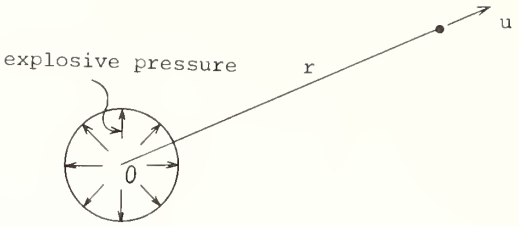

Fig. 10

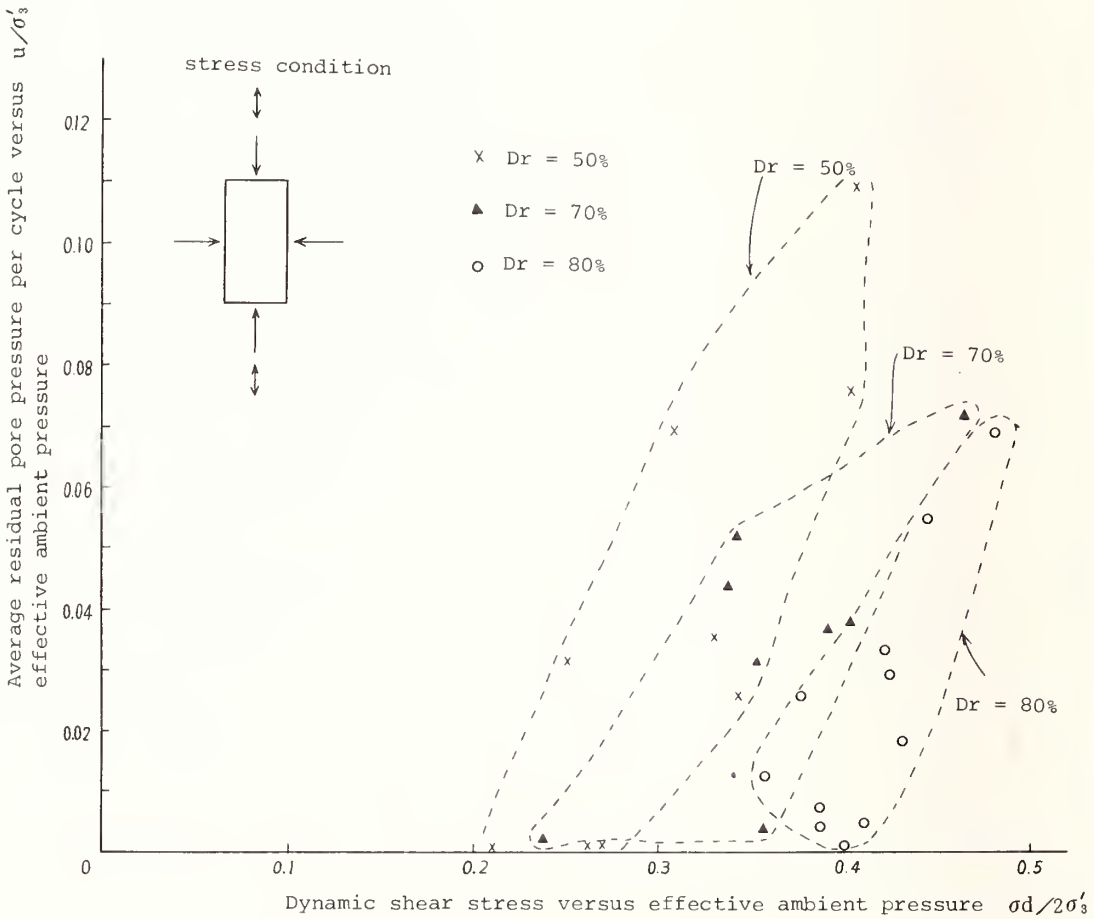

Fig. 11 Relation between dynamic shear stress and residual pore pressure by dynamic triaxial tests on fine sand

Table 1 Condition of experiments

EX. NO.	Test site	Amount of charge	Depth of explosion	Measured quantity
1	A	0.2 kg	4 m	Acceleration on ground surface
2		0.5	4	Pore water pressure
3		0.5	6	
4		1.0	6	
5		1.0	8	
6		1.0 x 2 (1 sec interval)	6	Acceleration on ground surface and under ground Pore pressure Settlement of ground
7		0.9	6	
8	B	0.2	6	Acceleration on ground surface
9		0.2	6	
10		0.2	6	Acceleration on ground surface and under ground
11		0.2	6	
12		1.0	6	Acceleration on ground surface Pore water pressure Settlement of ground surface
13		1.0	6	
14		1.0	6	Acceleration on ground surface Pore water pressure Settlement of ground surface
15		1.0	6	
16	C	1.0	6	Acceleration on ground surface Pore water pressure Settlement of ground surface
17		1.0	6	
18		1.0	6	Acceleration on ground surface Pore water pressure Settlement of ground surface
19		1.0	6	

LANDSLIDE INCIDENCE AND MECHANISMS DURING EARTHQUAKES

by

George E. Ericksen

U.S. Geological Survey
Reston, Virginia 22092

Strong earthquakes affecting mountainous terrain are generally accompanied by hundreds or even thousands of large potentially destructive landslides of certain types; earthquakes affecting areas of low relief cause fewer and generally different types of landslides, which, however, may be equally destructive to works of man. On steep slopes, among the many types of landslides that may occur, falls, slides, and avalanches of rock and soil are most frequent during earthquakes. These landslides take place where slides are commonly part of normal mass-wasting processes that affect hillslopes; the earthquake causes the reactivation of old slides as well as the formation of new slides. Surface movement on faults may also cause landslides by the formation of scarps that change slope stability although landslides of this type are relatively rare. In terrain of low relief, failures by rotational slump, translatory sliding, and lateral spreading are frequent causes of destruction in towns and cities that have been constructed on unstable, generally water-saturated soil or unconsolidated sediment.

Landslides, with the exception of those classified as falls, result from failure of earth materials under shear stress. Earthquake accelerations trigger landslides by causing a transitory increase in shear stress in earth materials at the site of the slide, and by causing a decrease in the shear strength of certain materials, such as water-saturated soil. Most slide failure takes place along one or more planes of weakness, except for flows or landspreading, wherein a given mass fails by loss of coherence. Among the most spectacular or earthquake-triggered landslides are large high-speed debris avalanches that move over a cushion of entrapped compressed air.

Key Words: Avalanches; earthquakes; falls; flows; land slides; mechanisms; slides.

INTRODUCTION

Landslides, which may be widespread and frequent during large earthquakes, are among the most destructive of earthquake-related phenomena. They have been major causes of destruction during large earthquakes ($M > 7.5$) in western North and South America during the past two decades. Among the most destructive were the translatory slides affecting seacoast towns and cities during the 1960 earthquake in southern Chile and the 1964 Alaska earthquake, both $M = 8.5$, and the Huascaran rockfall avalanche that obliterated the Andean city of Yungay during the 1970 Peru earthquake ($M = 7.7$). In addition, each of these earthquakes triggered thousands of other landslides that caused extensive damage to works of man.

Landslides are part of the mass wasting of hillsides and thus are part of weathering processes that over time result in leveling of terrain. Most landslides are the final result of the evolution of stress conditions which develop an unstable slope that only requires a triggering mechanism to produce a landslide. Earthquake vibration is one triggering mechanism that is unique in causing great numbers of slides to occur in seconds or minutes, slides that under normal conditions of weathering might occur over periods of hundreds or even thousands of years. The earthquake may cause renewed movement of old landslides as well as the formation of new slides, which may or may not fail under normal stress conditions. Some earthquake-triggered landslides are clearly larger than they would have been had they been triggered by some other mechanism. Causes of landslides other than earthquakes are: lubrication or saturation of the slide mass by water, overloading by manmade structures, and changes in slope stability because of stream undercutting, surface faulting, and manmade cuts.

The effect of earthquake-triggered landslides on terrain stability is variable. In some places, a given slide area is more stable after the earthquake, as, for example, where rockfalls and soilfalls on over-steepened slopes result in a more gentle stable slope; in others, the area is less stable, as, for example, in terrain where fissuring and incipient sliding caused by the earthquake result in increased water infiltration that causes a former stable terrain to become unstable. Examples of changes in slope stability such as these are generally readily recognizable in the field, but many times the stability of a given slope after an earthquake depends on more subtle geologic features that may be difficult to recognize.

CLASSIFICATION OF LANDSLIDES

The landslide classification used in this report follows that of Varnes (1958, p. 21), wherein landslides are characterized by type of movement and type of material (Figure 1). Landslides are considered to involve downward and outward movement of slope-forming materials consisting of bedrock, soil (includes all natural unconsolidated material on bedrock), and manmade fill. Movement may consist of falls, slides, and flows as well as combinations of these. In this report, translatory slides are considered to be landslides, even though their movement is essentially horizontal and failure in some (landspreading) may be due to incipient flow of liquefied materials or to plastic deformation.

The various types of landslides and their size and frequency are determined largely by the slope angle at the slide area and by the physical character and structure of the slide material. Falls of rock and soil break away from oversteepened or undercut slopes, and movement is largely by free fall of material through the air. Slides take place by gliding along one or more planes or zones of failure, which may be curving and concave upward (slump), inclined planar (block glide, soil slip, debris slide), or horizontal (translatory slide). Rotational and translatory slides (Figures 2 and 3) generally occur in poorly drained unconsolidated sediments and weak bedrock on gentle slopes or in horizontal terrain at the margins of topographic depressions. Debris slides (Figure 4) are most prevalent in cohesionless soil and weathered bedrock on steep slopes. Flows, which take place on slopes ranging from steep to nearly horizontal, result from loss of shear strength of a material so that it behaves as a viscous fluid (Figure 5). Flows generally form in water-saturated fine-grained sediments, which become liquefied because of external

forces such as earthquake vibration, but also occur in dry fine-grained sediments such as sand and silt. Complex landslides (Figure 1) involve a combination of the above types of movement and materials. In the strictest sense, nearly all landslides are complex althouc generally one type of material predominates in the slide mass, and one type of movement dominates in certain parts of a landslide or at a particular time during its movement.

Figure 2 shows the form and nomenclature of the component parts of a rotational slide or slump. This terminology may be applied to landslides of all types although most landslides are not as complex as the rotational slide, and consequently only part of the terms are applicable to these slides. The slide components may be defined as follows (Varnes, 1958, p. 1):

Main Scarp: Scarp or surface of rupture at the head of the slide, which continues beneath the slide and is the principal plane of failure, the surface of rupture.

Minor Scarp: Scarp in the slide formed by differential rotational movement between blocks within the slide mass; a plane of failure that may extend downward to the surface of rupture.

Head: Uppermost part of the slide mass.

Top: Uppermost part of the slide mass at the main scarp.

Foot: Line of intersection of the lower part of the surface of rupture and the original ground surface; may be either covered, as shown in Figure 2, or marked by an upthrust ridge.

Toe: Outermost limit of the slide material.

Flank: The side of the slide.

Crown: Relatively undisturbed material above the main scarp.

Transverse Cracks: Tensional fissures within the slide mass.

Longitudinal Fault Zone: Plane or zone of shear parallel to slide movement, caused by differential movement within component blocks of the slide.

LANDSLIDES DURING EARTHQUAKES

Mechanisms

Landslides take place in a given rock or soil mass when the internal shear stress exceeds the shear strength of the mass as a whole, or of planes or zones within or at its margins. Shear stress within an earth mass on ground that is not level is due to gravity and to seepage force.[1] Shear strength, the property that allows material to remain in equilibrium on surfaces that are not level, is a function of degree of cementation or induration of bedrock and of friction or electrostatic bonding between grains as well as cementation of soil.

Most types of rock have shear strengths so great that their only mode of failure is by rupture along structural planes of weakness such as faults, fractures, joints, and bedding planes. The shear strength of soil, on the other hand, is low. In the uncemented cohesionless soils (those lacking or having only sparse clay minerals), the shear strength

---

[1]Seepage force results from flow of water through a soil, and is equivalent to loss of head because of transformation of seepage force to effective stress by frictional drag. In an isotropic soil, seepage force acts on the direction of flow (Lambe and Whitman, 1969, p. 261-262).

is chiefly a function of friction between component grains and rock fragments, whereas in clay-bearing cohesive soils it is a function of bonding between grains that results from adsorbed ions. Cohesive soils are characteristically plastic because of the presence of clay minerals of colloidal size, and such soils tend to deform plastically when shear stress exceeds shear strength. Cohesionless soils, in contrast, are not plastic and fail either by rupture or flow.

Earthquake accelerations cause transitory increases of shear stress in materials on hillsides and significant decreases in shear strength in some materials such as water-saturated soil. Most earthquake-triggered landslides are due to the temporary increase in shear stress within a soil or rock mass that is already in a near-critical stress condition. Alternatively, cyclic loading due to the accelerations may cause a gradual increase in pore pressure in undrained cohesionless soil to a point of complete loss of shear strength and bearing capacity, and the soil liquefies (Lambe and Whitman, 1969, p. 444-445). This is referred to as a quick condition, and soil in this state will flow freely. A quick condition develops most readily in fine sand and silt; it does not develop in cohesive soils.

Many landslides fail by rupture along distinct geologic structures, such as beds and bedding planes in stratified rocks, and unconformities, faults, fractures, and joints in rocks and soils of all types, whereas others fail along planes or zones that do not mark any apparent structural discontinuity. Of these latter types of landslides, the planes of rupture of some are at interfaces in rock and soil that mark subtle changes in moisture content, leaching, and alteration, whereas the position of rupture in others is due to a combination of factors--slope angle, physical character of the slide mass, and intensity of earthquake shaking. Rotational slides are among those that typically lack a controlling structure at the plane of rupture (except for those that have been reactivated) and involve blocks that rotate about an axis parallel to the hillside. Rotation is due to moment imparted by gravity, whereby the block tends to move downward because of its weight and outward toward a free face. A curving surface of rupture is a resultant of these combined movements. Degree of saturation and flow of water at the slide site, including seepage force, may influence position and curvature of the surface of rupture. Earthquakes may trigger rotary slides when the transitory shear stress due to seismic loading acts in a direction that increases the moment about the axis of rotation.

Translatory slides, in contrast to rotary slides, occur in materials having horizontal planes of weakness that control failure or that deform plastically or by liquefaction. Movement at the head of some translatory slides is rotational, so that one or more slump blocks form; the heads of other translatory slides are marked by graben over a downdropped wedge, as shown in Figure 3. Most known translatory block glides during earthquakes have taken place along bluffs with extensive horizontal or near-horizontal surfaces in back and in front of them (Idriss and Seed, 1966, p. 2). The slide blocks involve material in and behind the bluff, which slides forward over the land surface in front of the bluff. Lateral movement is due to the thrust of slump blocks and downdropped wedges of material at the head of the slide and within the slide, as well as failure by landspreading and flow. Translatory slide blocks such as those at Anchorage, Alaska, triggered by the 1964 earthquake, probably move outward along a layer of sensitive clay or water-saturated fine-grained sediment that had been liquefied by cyclic loading during the earthquake (Hansen, 1965, p. A65).

Dry flows (Figure 1) may form during an earthquake either as a direct result of the transitory increase in shear stress, by destruction of coherence because of cyclic loading, or by transformation of a fall or slide to high-speed flow or avalance, many of which have air layer lubrication. Unconsolidated silt and sand, which have little shear strength, are the materials most subject to flow because of increased stress. Cyclic loading of fairly coherent fine-grained porous materials such as loess or dry mudflows, which are commonly stable in vertical cliffs, may destroy their coherence by causing collapse of the skeletal framework, so that a flow will form on any slope having an inclination greater than the angle of repose of the newly formed noncoherent material. Falls of these same materials may be pulverized upon impact and develop into flows. High-speed avalances may move on cushions of entrapped compressed air or contain entrapped air that keeps particles in suspension.

Falls. - Rockfalls and soilfalls (Figure 1) are frequent and widespread during earthquakes affecting mountainous terrain, particularly glaciated terrain. Most falls are small, ranging from a few $m.^3$ to a few hundreds $m.^3$, but large falls containing millions of $m.^3$ of material have occurred. Falls generally consist of masses of rock or soil that break away from a steep slope or cliff along a plane of weakness such as a bedding plane, fault, or joint. On steep hillsides the fall may change to a debris slide (Figure 4), or if large enough, an avalance (Figure 6). Also, rock fragments from a fall, as well as isolated boulders dislodged during the earthquake, tumble and bounce down steep hillsides, killing people and animals in their paths, and crashing through buildings. During the 1970 Peru earthquake, such rockfalls caused thousands of injuries and deaths to people and livestock, and destruction of farm buildings in the high Andes of northern Peru, an area where steep hillsides have been extensively farmed since pre-Columbian times. In contrast, the great number of rockfalls during the Alaska earthquake of 1964 caused comparatively little damage because they occurred chiefly in unpopulated areas.

During the Alaska earthquake of 1964 and the Peru earthquake of 1970 several high speed avalanches were generated by rockfalls. These falls were large, probably having volumes of more than a million $m.^3$ of material, and vertical drops of at least several hundred meters. The Huascaran debris avalanche (Figure 6), the most destructive landslide of historic time, originated by fall of a slab of granodiorite and ice from the near-vertical west face of the north peak of Nevados Huascaran. This slab was estimated to contain more than 25 million $m.^3$ of material, being approximately 800 m. wide and 1,000 m. long (Ericksen and others, 1970, p. 7-8). The average vertical fall of the slab, taken as the vertical drop at its center, was about 600 m.

Slides. - On the basis of mechanics of movement, two types of slides can be recognized one in which the slide mass is relatively little deformed and the other in which it is greatly deformed (Varnes, 1958, p. 23-24). Slumps and block glides (Figures 2 and 3) are typical of the undeformed slides, and debris slides and failure by lateral spreading are examples of deformed slides. In this report, slides are divided into three types on the basis of inclination and form of the plane of rupture as follows: 1) rotational, 2) inclined planar, and 3) translatory. Inclined planar slides are by far the most frequent of these types, and together with rockfalls and soilfalls make up most of the slides that are triggered by earthquakes. Comparatively few rotational and translatory slides occur during any given earthquake, but because they tend to occur in unstable material in areas of low relief, which also may be sites of towns and cities in mountainous areas and bordering coastal regions, they may be major causes of destruction.

Slumps and translatory slides tend to occur in terrain of gentle relief underlain by unstable bedrock or unconsolidated sediments. They tend to be large, commonly involving tens to hundreds of thousands or even millions of $m.^3$ of material. They may break and move either as essentially a single unit (Figures 3 and 7), as several segments (Figure 2), as many segments (lateral spreading)(Figure 3), or deform by incipient flow (landspreading). As also shown in these figures, a flow, slide, or upthrust ridge may form at the toe of the slide. Earthquake-triggered slides of these types commonly occur in areas where scars of earlier slides can be seen.

Slumps and translatory slides triggered during earthquakes in the Western Hemisphere during the past two decades caused extensive damage to cities, notably to coastal cities during the 1960 Chile earthquake, the 1964 Alaska earthquake, and the 1970 Peru earthquake. They also caused damage to transportation routes (Chile and Alaska earthquakes), and dammed streams to form temporary lakes that had to be drained (Chile and Peru earthquakes). A subaqueous slump on a delta at Kenai Lake, Alaska, caused destructive waves to form in the lake. The sequence of conditions at the site of the slide is shown in Figure 9. As can be seen in the figure, the slump caused a wave to wash over the area back of the main scarp. This wave and another that swept over the opposite lakeshore, a distance of about 100 m., each attained a maximum height of 10 meters above normal lake level (McCulloch, 1966, p. A8).

Inclined planar slides that are most frequent during earthquakes are debris slides on steep hillsides in unconsolidated regolith and in weathered rock. Such slides originate as failure of a thin slab of surface material along a flat to gently curved surface. On steep slopes, the moving material generally becomes a debris slide that moves downward away from the source area. Depending upon the type of material involved, movement becomes less and less on more gentle slopes, to a point where the slide remains essentially in place, being marked only by fracturing and small soil slips.

Debris slides, which may occur by the thousands during earthquakes, along with falls are among the most numerous but smallest of earthquake-triggered landslides. Most involve not more than a few tens to a few thousands of $m.^3$ of material, but they may be so numerous on some hillsides that it is almost impossible to distinguish individual slides. As in the case of rockfalls and debris falls, debris slides cause damage to farms and isolated small communities. An unusual type of damage by debris slides, which occurred during the 1970 Peru earthquake, was destruction of fields and trails in steeply inclined areas by sliding of thin soil to expose underlying fresh bedrock. Not only were farmlands destroyed but the construction of new trails across the newly-exposed bedrock was prohibitively expensive; in some areas, farm buildings and lands that were not otherwise damaged had to be abandoned.

Comparatively rare debris slides are those caused by surface faulting. Figure 10 shows the development of the scarp of a reverse fault that moved during the 1964 Alaska earthquake, and caused many slides to break away from the hillside on the upthrown block of the fault.

Flows. - Although flows of one type or another (Figure 1) are triggered by earthquakes, most are small and cause relatively little damage. The major exceptions are debris avalanches, which are potentially among the most destructive of all landslides. As has been noted, flows occur in both dry and wet or water-saturated material. The most notable earthquake-triggered dry flows were the loess flows during the 1920 earthquake of Kansu Province, China, where loess banks failed, and a fluid mass of dry powder filled valleys and buried villages (Close and McCormick, 1922). Flows of wet material range from the relatively viscous earth flow that moves only short distances (Figure 5) to debris and midflows, which are highly fluid masses that may travel for tens of kilometers.

Debris avalanches, which start as either wet or dry material, may become debris flows if they move into a channel having a flowing stream, as happened to an avalanche near Caraz (Figure 11) during the 1970 Peru earthquake and to the Huascaran avalanche as it flowed into the Santa River (Figure 6). Most earthquake-generated flows originate by liquefaction of water-saturated material under cyclic loading (see p. III-57). Liquefaction of bogs and swamps result in earth flows and mudflows during earthquakes. At least two major mudflows and many small earth flows originated in this way during the 1970 Peru earthquake.

Some submarine slides may be due to liquefaction of fine-grained material, as occurred at the port of Valdez during the 1964 Alaska earthquake, causing total destruction of the dock facilities (Figure 12). This slide, described by Coulter and Migliaccio (1966), involved about 75 million $m.^3$ of water-saturated silt and sand. Failure was sudden, taking place shortly after the earthquake tremors were first felt. The slide caused formation of destructive water waves as much as 10 m. high.

Subaqueous flows caused by liquefaction of water-saturated sediments are probably much more common than generally recognized. Undoubtedly, such flows occurred at other localities during the 1964 Alaska earthquake, and they probably took place along the south Chile coast during the 1960 earthquake. Large submarine flows did not occur during the 1970 Peru earthquake, but small submarine flows probably did occur in areas affected by landspreading, notably along the bayshore of the coastal city of Chimbote.

Avalanches are moving masses of earth materials that attain sufficient speed to move by flow rather than shear. They occur frequently during earthquakes, generally originating as falls or slides on slopes steep enough and with sufficient vertical drop for the moving mass to attain a velocity necessary to transform it into a flow. Thus, avalanches may be either dry or wet and consist of rock, soil, ice, or snow, or a combination thereof.

In areas of glaciers or regions of heavy winter snows, earthquake-triggered ice and snow avalanches may be numerous and widespread. Although such avalanches are potential earthquake hazards, they generally do not cause damage because most are confined to uninhabited ice and snowfields, or flow into sparsely inhabited valleys below. Such was the case of dozens to hundreds of snow and ice avalanches during the earthquakes in Alaska (1964) and Peru (1970), where large areas are covered with glaciers and snowfields.

Large high-speed avalanches are among the most awe-inspiring and potentially most destructive of all types of landslides. They are generally triggered by huge falls or slides of rock, on the order of millions of $m.^3$ minimum, on steep to vertical slopes where vertical drops are on the order of hundreds of meters. They may attain speeds of several hundred km/hr., and move for several kilometers outward over gently undulating to near-horizontal terrain at the base of steep mountain slopes. At high speed the avalanche tends to entrap air which is compressed into a cushion on which the avalanche overrides irregularities in terrain or even ridges without causing significant modification of their form. Observers have reported such avalanches as being accompanied by strong turbulent blasts of air (Plafker and others, 1971, p. 557).

The largest and most destructive avalanche of historical times was the Huascaran, a rockfall avalanche that occurred during the 1970 Peru earthquake (Ericksen and others, 1970; Plafker and others, 1971). This avalanche probably involved more than 50 million $m.^3$ of rock and ice; during its trajectory over a horizontal distance of 14.5 km and a vertical descent of about 3,000 m., it attained maximum velocities of more than 400 km/hr. The avalanche obliterated the Andean city of Yungay and nearby small settlements and farms over an area of about 22 sq. km, causing the death of more than 18,000 people.

REFERENCES

1. Baker, R.F., and Chieruzzi, Robert, 1959, Landslide Occurrence and Analysis: National Research Council, Highway Research Board, Bull. 216, 43 p.

2. Close, V., and McCormick, E., 1922, Where the Mountains Walked: Nat. Geog. Mag., V. 41, p. 445-464.

3. Coulter, H.W., and Migliaccio, R.R., 1966, Effects of the Earthquake of March 27, 1964, at Valdez, Alaska: U.S. Geol. Survey, Prof. Paper 542-C, 36 p.

4. Davis, S.N., and Karzulovic, K., Juan, 1963, Landslides at Lago Rinihue, Chile: Seismol. Soc. America, Bull., V. 53, No. 6, 1403-1414.

5. Eckel, E.B., 1970, The Alaska Earthquake, March 27, 1964: Lessons and Conclusions: U.S. Geol. Survey, Prof. Paper 546, 57 p.

6. Ericksen, G.E., Plafker, George, and Fernandez Concha, Jaime, 1970, Preliminary Report on the Geologic Events Associated with the May 31, 1970, Peru Earthquake: U.S. Geol. Survey, Circ. 639, 25 p.

7. Hansen, W.R., 1965, Effects of the Earthquake of March 27, 1964, at Anchorage, Alaska: U.S. Geol. Survey, Prof. Paper 542-A, 68 p.

8. Idriss, I.M., and Seed, H.B., 1966, The Response of Earth Banks During Earthquakes: Berkeley, California, University of California, Soil Mechanics and Bituminous Materials Research Lab., 22 p., Appendices.

9. Karol, R.H., 1960, Soils and Soil Engineering: Englewood Cliffs, N.J., Prentice-Hall, 194 p.

10. Komarnitskii, N.I., 1968, Zones and Planes of Weakness in Rocks and Slope Stability: New York, Consultants Bureau, 108 p. (English Translation of Vliyaniye zon i poverkhnostey oslableniya v porodakh na ustoychivost' otkosov: Moscow, Izd. "Nauka," 1966.).

11. Lambe, T.W., and Whitman, R.V., 1969, Soil Mechanics: New York, John Wiley and Sons, 553 p.

12. McCulloch, D.S., 1966, Slide-induced Waves, Seiching, and Ground Fracturing Caused by the Earthquake of March 27, 1964, at Kenai Lake, Alaska: U.S. Geol. Survey, Prof. Paper 543-A, 41 p.

13. McLerran, J.H., 1957, Glossary of Pedologic (Soils) and Landform Terminology for Soil Engineers: Natl. Research Council, Highway Research Board, Spec. Rept. 25, 32 p.

14. Plafker, George, 1967, Surface Faults on Montague Island Associated with the 1964 Alaska Earthquake: U.S. Geol. Survey Prof. Paper 543-G, 42 p.

15. Plafker, George, Ericksen, G.E., and Fernandez Concha, Jaime, 1971, Geological Aspects of the May 31, 1970, Peru Earthquake: Seismol. Soc. America, Bull., Vol. 61, No. 3, p. 543-578.

16. Ruiz F., Carlos, and Saint-Amand, Pierre, eds., 1961, Observations Concerning the Chilean Earthquakes of May 1960: Internat. Geol. Cong., 21st, Copenhagen, 1960, Rept. pt. 26, p. 116-133.

17. Varnes, D.J., 1958, Landslide Types and Processes, Chap. 3 of Eckel, E.B., ed., Landslides and Engineering Practice: Natl. Research Council, Highway Research Board, Spec. Rept. 29, p. 20-47.

TYPE OF MOVEMENT		TYPE OF MATERIAL			
		BEDROCK	SOIL		
FALL		Rockfall	Soilfall		
SLIDE	Rotational	Slump	Slump		
	Planar (Inclined)	Block glide; rock debris slide	Soil slip; debris slide		
	(Translatory)	Block glide	Lateral spreading; landspreading		
FLOW		Rockfall and rock-slide avalanches		Clastic	Fine grained
			Dry	Debris avalanche	Sand run, silt flow; loess flow
					Earth flow
			Wet	Debris flow	Sand or silt flow; mud flow
COMPLEX		(Combinations of materials or types of movement; classified according to nature of originating process or terminal moving mass)			

Figure 1. - Classification of landslides. Modified from Varnes (1958, Fig. 5).

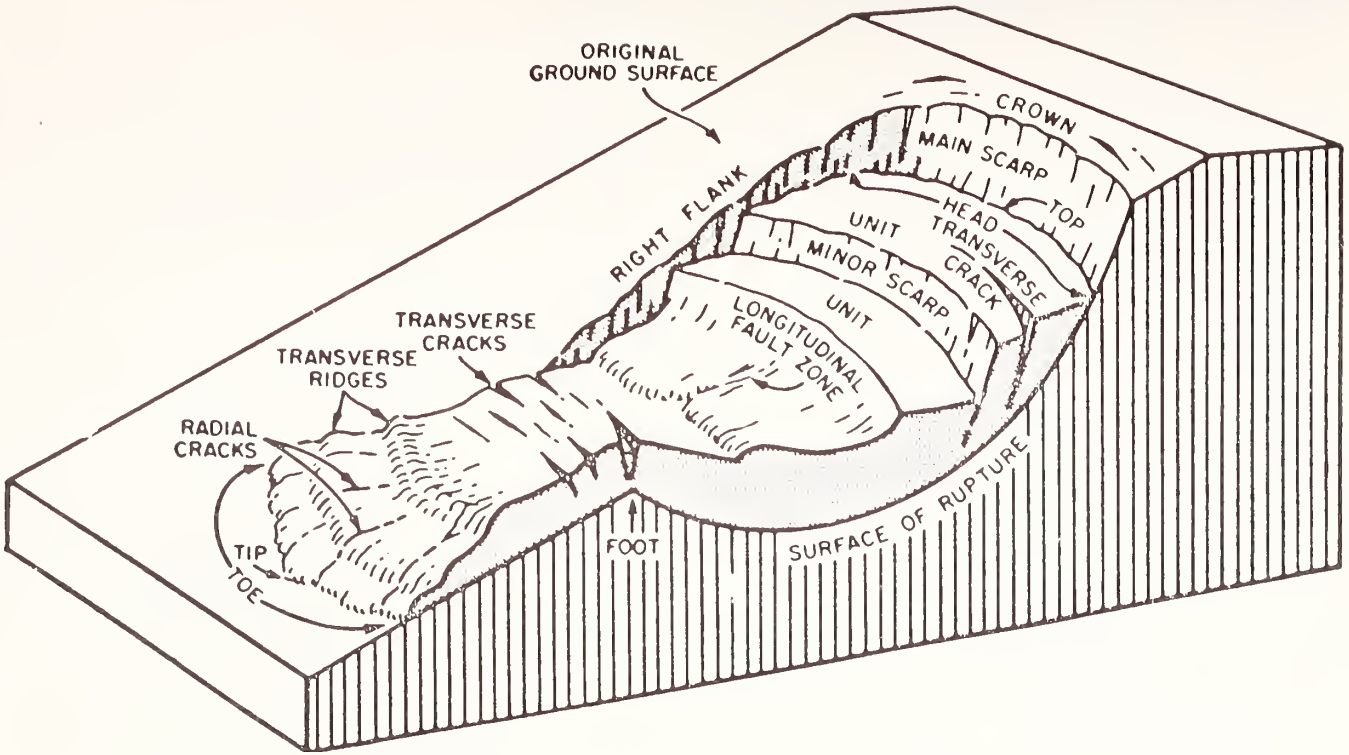

Figure 2. - Rotational slide showing terminology of component parts. From Varnes (1958, pl. 1).

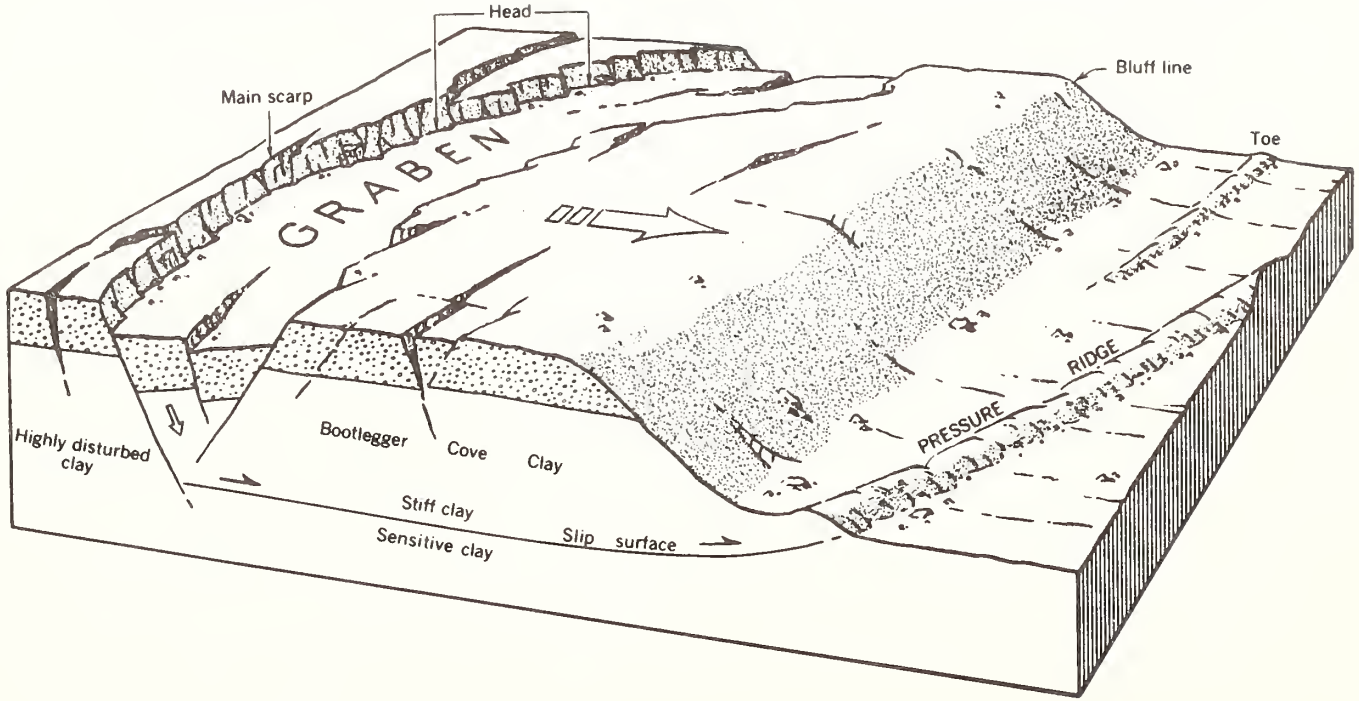

Figure 3. - Block diagram of a translatory slide of the type that occurred at Anchorage, Alaska, during the 1964 earthquake. From Hansen (1965, fig. 24).

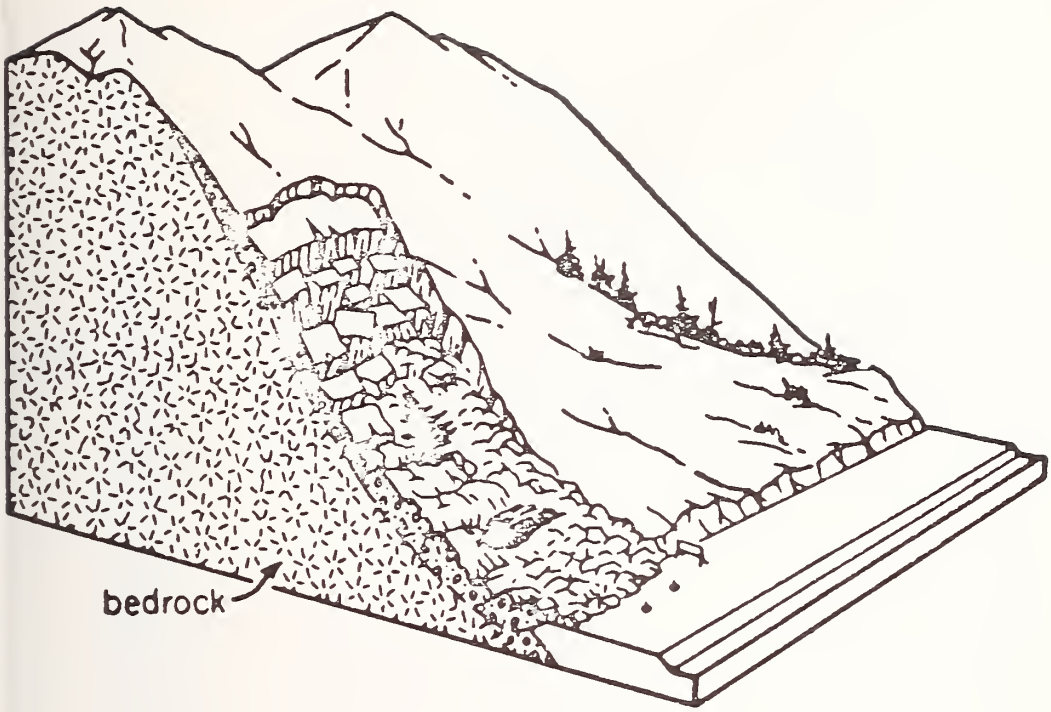

Figure 4. - Block diagram of a debris slide in which failure took place along the contact between soil and bedrock. From Varnes (1958, pl. 1).

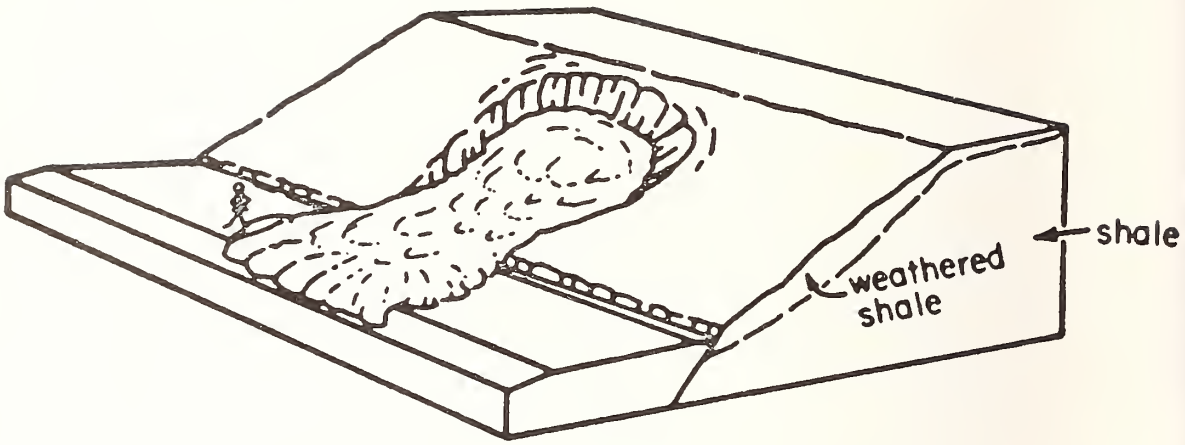

Figure 5. - Block diagram of an earthflow in weathered shale. From Varnes (1958, pl. 1).

Figure 6. - Oblique aerial view of the Santa Valley and snow-covered Cordillera Blanca showing the Huascaran rockfall avalanche that devestated the Yungay-Ranrahirca area during the 1970 Peru earthquake. Photograph by Servicio Aerofotografico Nacional del Perú, June 13, 1970.

Figure 7. - Rotational slide at Re , Peru; arrows mark main scarp that has a maximum height of 5m, and upthrust ridge that dammed Rio Santa.

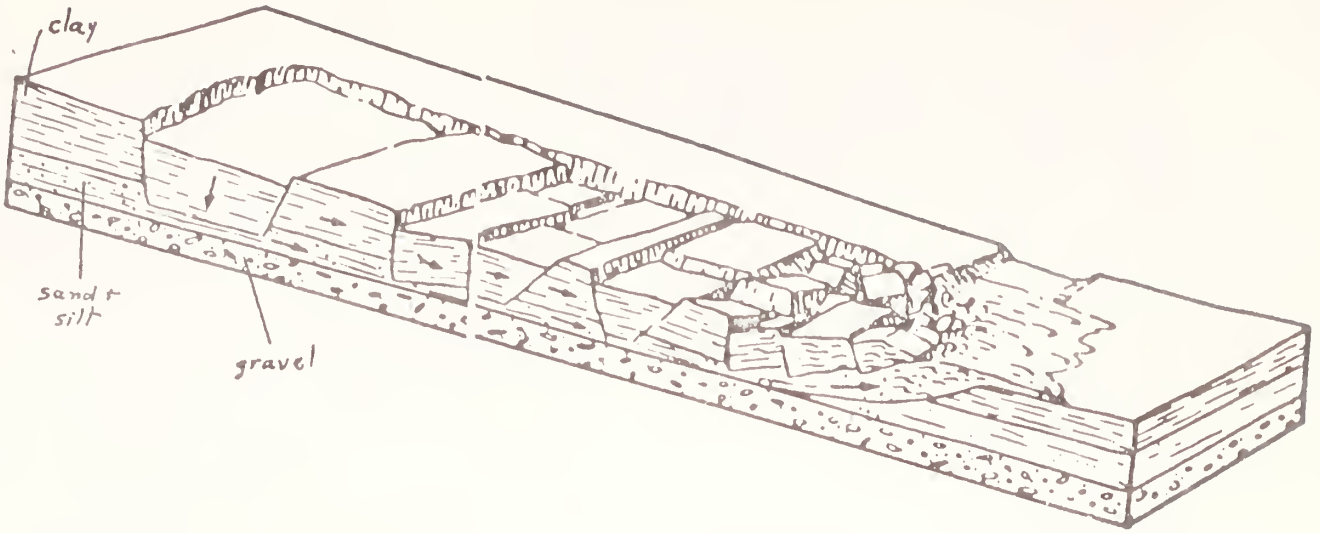

Figure 8. - Lateral spreading in a sequence of clay and underlying water-saturated silt and sand which rests on firm gravel. From Varnes (1958, pl. 1).

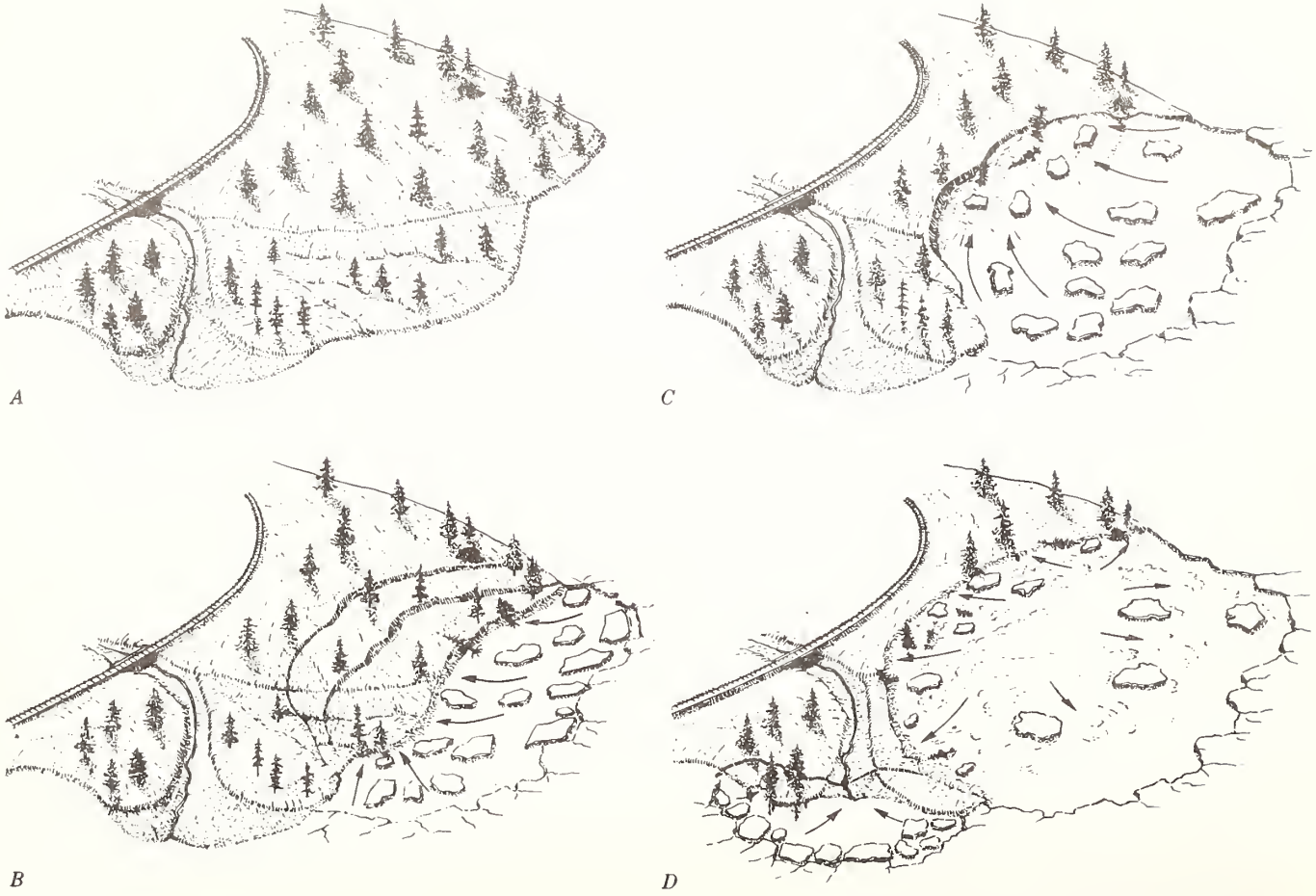

Figure 9. - Sequential sketches of backfill wave that developed by slumping at the margin of the Lakeview delta, Kenai Lake, Alaska, during the 1964 earthquake. A, Preslide delta. B, Start of slumping and water inflow. C, Inflowing water forms a welt of high water near scarp. D, Water flows outward from high water welt, causing flooding of area back of scarp; a second slump forms at mouth of creek. From McCulloch, 1966, fig. 9.

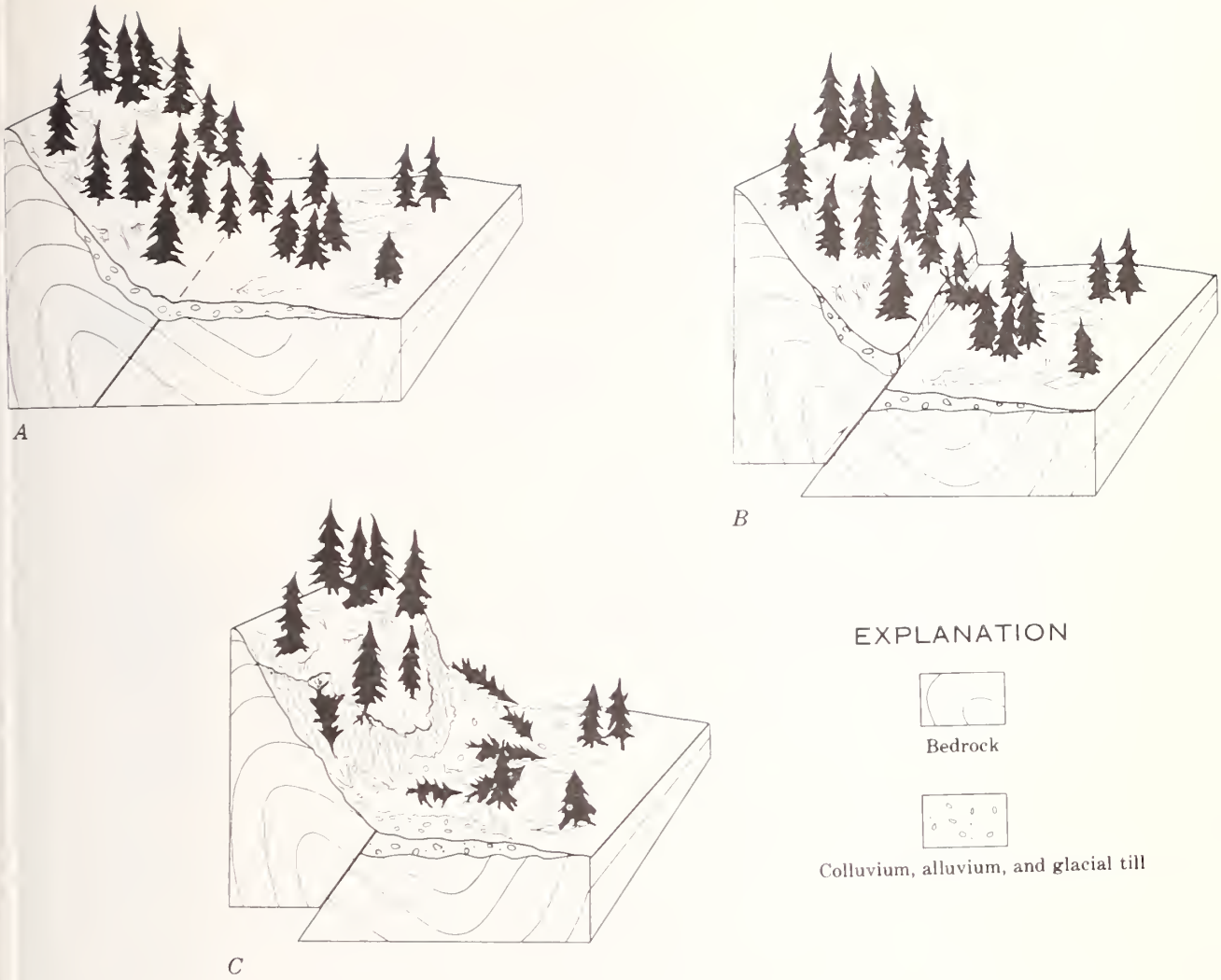

Figure 10. - Diagrams illustrating fault movement and landslide development along the Patton Bay fault, a reverse fault on which displacement took place during the 1964 Alaska earthquake. From Plafker (1967, fig. 17)

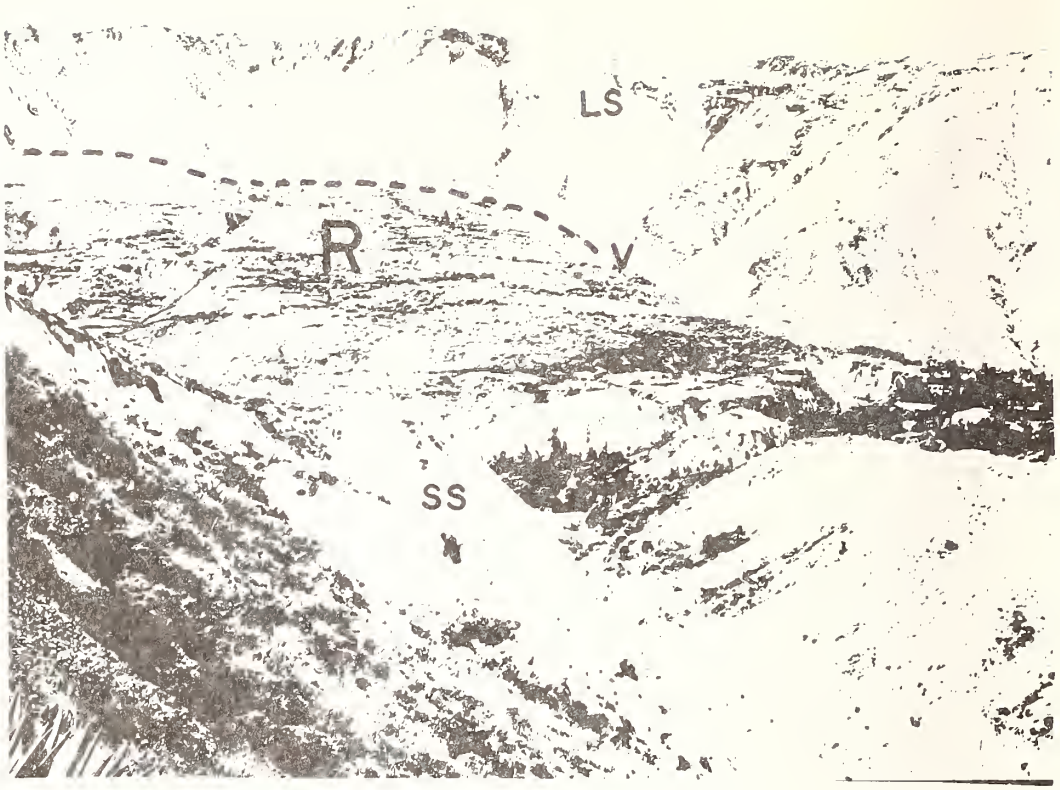

Figure 11. Huge ancient rotational landslide (R) in the Callejon de Huaylas, east side of Santa River, 2-3 m north of Caráz. This slide, which is 5 km long and averages 1 km wide, dammed the Santa River to form a lake in which was deposited a thick segment of silts and sands (SS) now exposed in river banks. Head of slide, outlined by dashed line, shows no evidence of movement during 1970 earthquake. Also shown is large landslide (LS), triggered by the 1970 earthquake, which developed into a fluid debris flow in small tributary valley (V); debris slide (light-colored scars) also were triggered by the 1970 earthquake.

Figure 12. - Submarine slide that destroyed dock facilities at Valdez, Alaska, during 1964 earthquake; water saturated silty and sandy delta deposits liquefied under cyclic loading due to earthquake accelerations. From Coulter and Migliaccio (1966, fig. 4).

STRESS CONDITION EFFECTS ON DYNAMIC PROPERTIES OF SOILS

by

Eiichi Kuribayashi
Chief, Earthquake Engineering Research Section
Public Works Research Institute
Ministry of Construction

Toshio Iwasaki
Chief, Earthquake Engineering Section
Building Research Institute
Ministry of Construction

In the engineering field, the evaluation of the dynamic characteristics of soils and foundation subgrades has been required in the course of studying vibrational problems and especially problems associated with earthquake engineering. The dynamic characteristics of soils have, therefore, been obtained by laboratory tests, using a resonant column method. These tests were conducted to evaluate the shear modulus and the damping characteristics in dry and saturated specimens of various soils in Japan.

The hollow cylindrical samples tested were 25 cm. in height, 10 cm. outside diameter, and 6 cm. inside diameter. This arrangement permitted a more uniform deformation of the sample cross-section. The specimens were fixed at the bottom, and at the top of the specimens oscillators were fastened to a rigid mass, which supply a torsional vibrational force to the system. A confining pressure, which was applied equally to the outside and inside of the test sample, was supplied by air pressure. An axial load was also applied, and was independent of the confining pressure in order to produce an anisotropic stress condition.

After the sample was prepared and all proper alignments and forces imposed, the frequency of the torsional excitation was introduced and then varied until the oscillator specimen system resonated. The resonant frequency varied from 40 cps to 100 cps, depending upon the dimensions and density of the sample and the applied stress condition and the shearing strain amplitude. The strain amplitude varied from 5×10^{-6} to 5×10^{-4} for these tests. The shear moduli were calculated from the resonant frequencies and the other parameters, as given above. The damping characteristics were obtained by using the amplitude-time decay response curves of the free vibrations.

In the triaxial state of stress, the mean principal stress, p, is defined by $(\sigma_a + 2\sigma_r)/3$ and the deviator stress, q, is given by $\sigma_a - \sigma_r$ are the axial and radial stresses, respectively. The test results indicate the following trends for the dynamic properties of soils;

(1) Under constant values of the other parameters, the shear moduli vary with 1/2 power of p and decreases with an increase in the void ratio and shearing strain amplitude. Furthermore, the damping capacity decreases with an increase in p and also increases with an increase of strain amplitude. However, the damping capacity remains constant irrespective of the change in the void ratio, when the other parameters remain constant.

(2) When the value of p is kept constant, the shear moduli are nearly constant irrespective of the value of q until the stress ratio, q/p, reaches a value of about 1.0. However, beyond this value of q/p, the shear moduli begin to decrease with an increase in q/p. This phenomenon is due to the anisotropic stress condition and the corresponding anisotropy in the inner structure of specimens.

Key Words: Damping; damping coefficients; shear modulus; soil; tests; torsional excitation.

INTRODUCTION

In the civil engineering field, the evaluation of the deformational characteristics of soils and foundation subgrades has been required for vibrational problems, especially for those problems associated with the earthquake response of structures. In order to obtain such information, relative to dynamics of soils, elastic wave measurements at field locations or laboratory tests using simple shear apparatus of triaxial apparatus have been conducted. However, the shearing strain amplitudes in the soil structures and subgrade during strong earthquake motions have produced magnitudes of values 10^{-3} to 10^{-4} of strain. It is, however, difficult to evaluate the deformational characteristics of soils at these magnitudes using ordinary methods.

Therefore, in order to obtain the shear modulus and damping characteristics of soils subjected to such magnitudes of shear strain, a special resonant column test has been designed and used to test dry and saturated specimens of various soils. This paper presents the required instrumentation and initial use of the resonant column test apparatus.

APPARATUS

The general apparatus and procedure used to evaluate the moduli of soil specimens in the laboratory by means of a vibrational method was conceived by Iida (1). However, the detailed equipment which can control the stress conditions and the magnitudes of the shearing strain was developed by Hardin et al (2). The principal of the apparatus, shown in the following figures, is the same as Hardin's apparatus. The schematic diagram and photograph of the apparatus is shown in Figures 1 and 2. Figure 3 shows the general stress condition on the test sample. The hollow cylindrical specimens that were tested were 25 cm in height and had a 10 cm outside diameter and 6 cm inside diameter. This arrangement permitted a more uniform deformation of the cross-section. The specimens were fixed at the bottom, and at the top of the specimens oscillators were fastened to a rigid mass, which supply a torsional vibrational force to the system. The confining pressure, which was applied equally to the outside and inside of the samples, was supplied by aid pressure. The axial load was introduced independent of the confining pressure in order to produce the anisotropic stress condition similar to the K_o --stress condition in the horizontal ground.

The quantities that were measured during a steady state vibration test were the resonant frequency of the oscillator-specimen system, the vibration amplitude at the top of the specimen, the length and volume change of the specimen, the confining pressure, and the axial load. Also, the amplitude time decay curves were recorded by shutting off the driving power. From all of these data, the shearing strain amplitudes, the shear moduli, and the logarithmic decrements were calculated for the various soils tested, as will be described in the following sections.

PRINCIPLE OF TESTING

Shear Strain Amplitude

The shear strain in a sample is denoted by γ, and is equal to;

$$\gamma = \frac{\partial u}{\partial x} = \frac{\partial (r, \theta)}{\partial x} \qquad \text{(rad.)} \tag{1}$$

where $u(x, t)$ is the displacement, $\theta(x, t)$ is the angular displacement in radians, x is the axial coordinate, and r is the radial coordinate as shown in Figure 4. The configuration of the specimen and the large mass at the top, produce linear deformations and accordingly a uniform shear strain condition over the entire length of the specimen. Furthermore, the shear strain in a horizontal section can be expressed in terms of the radius equal to a value of 4 cm. Accordingly, the shearing strain in the specimen is represented as,

$$\gamma = \frac{4}{\ell} \theta \qquad \text{(rad.)} \tag{2}$$

where ℓ is the length of specimen (cm).

Shear Modulus

The shear-strain curves of the sand specimens, loaded axially, yield the relationships shown in Figure 5 and where the hysteretic curve has sharp points. In the case of hysteretic damping, such as occurs in sands, the linear approximation can be used to model its dissipative behavior and to simplify the dynamic problems. The material constants of sands will be defined as;

G = Equivalent shear modulus

η = Hysteretic damping coefficient = $\Delta W/2\pi W$

W = Strain energy (shown in Figure 5)

ΔW = Damping energy (shown in Figure 5)

For an equivalent linear isotropic material having the same values of G and η, as given above, a more useful notation is in the form of a complex modulus, as shown in Figure 6. In this form τ and γ are the shear stress and strain in complex notation, and G and G' are the complex coefficients. Then, stress-strain relation is expressed as

$$\tau = (G + iG')\gamma \tag{3}$$

The hysteretic loop of such a linear material, excited by steady vibrational force, is such as shown in Figure 7 and has no sharp points. Defining the strain energy W and damping energy ΔW, as given in Figure 7, then the hysteretic damping coefficient η can be related to the complex modulus G and G' as

$$\eta = G'/2G \tag{4}$$

However, the wave propagation equation for the shear case is;

$$\rho\frac{\partial u}{\partial t^2} = \frac{\partial \tau}{\partial x} \tag{5}$$

where ρ is the density and u is the displacement orthogonal to the propagation direction. Then, substituting Equations (1), (3), and (4) into Equation (5) gives the wave equation for linear isotropic material used in the resonant column tests, and is;

$$\frac{\partial^2 \theta}{\partial t^2} = G(1 + i\,2\eta)\frac{\partial^2 \theta}{\partial x^2} \tag{6}$$

The analytical solution of this equation for the model shown in Figure 4 is not as simple as the one given by Hardin (3) and Hardin and Music (2). Under steady state vibration, the shear modulus G is a function of the density and the dimensions of the samples, the apparatus constants, and the resonant frequency. Thus, in order to obtain a value of G, an interative procedure using an electronic computer was required.

Damping Coefficients

By setting the system into a steady-state forced vibration and then shutting off the driving power, the logarithmic decrements, Δt was obtained. From the logarithmic decrements, the hysteretic damping coefficient η, which does not depend upon sample's dimensions and boundary conditions, was obtained. For the free vibration of the model, shown in Figure 4, we can assume a solution of the form;

$$\theta = A(x)e^{i(\omega_n - \Delta t)} \tag{7}$$

where A(x) is the mode of deformation, ω_n is the natural circular frequency of the system and λ is the attenuation factor with respect to time. Substituting Equation (7) into Equation (6) gives;

$$\lambda = \frac{\omega_n}{2}\left[-1 + \sqrt{1 + (2\eta)^2}\,\right] \approx \omega_n\eta \tag{8}$$

Then, relating the logarithmic decrement to the hysteretic damping coefficient as

$$\Delta t = \lambda \frac{2\pi}{\omega_n} \approx 2\pi\eta \tag{9}$$

Now using Equation (9), the hysteretic damping coefficient η can be obtained by measuring the logarithmic decrement. Furthermore, it is worthwhile to note that the logarithmic decrement depends only on the damping characteristics of the sample and does not depend upon sample's dimensions nor boundary conditions providing the hysteretic damping coefficient η of sample material does not vary with the frequency of the forced vibration.

TESTING METHODS

Two kinds of sands, Toyoura-sand and Senkenyama sand, whose physical properties are shown in Table 1 were tested.

Table 1
Physical Properties of Sands

	G_s	D_{10}	D_{60}	U_c	$e_{max.}$	$e_{min.}$
Toyoura-sand	2.641	0.12 mm	0.145 mm	1.21	0.953	0.686
Sengenyama-sand	2.695	0.16	0.38	2.37	0.961	0.484

Toyoura-sand has a uniform gradation with round particles and is used as the standard sand for testing in Japan. Sengenyama-sand from Sengenyama near Tokyo is considered well graded. The resonant column tests were conducted on samples having various void ratios. For the Toyoura-sand, air-dried and saturated samples were prepared and subjected to stress ratios (σ_3/σ_1) equal to 0.5 and 1.0. The Sengenyama-sand, in which only air-dried specimens were tested, the stress ratio (σ_3/σ_1) was set equal to 1.0.

After applying the confining pressure and the axial load to the sample, the stress condition that will be designated as (σ_3) and (σ_1) was kept constant and the vibratory shear strain amplitude was then increased above 5×10^{-6} to about 2×10^{-4}. Both the shear modulus and logarithmic decrement was measured at various values of shear strain amplitude. Then, another stress condition was imposed and the above mentioned procedures were repeated. Figure 8 describes the test results obtained from one of the Toyoura-sand samples. The term p is the principal stress denoted by $1/3(\sigma_a + 2\sigma_r)$ and e is the void ratio, which slightly changes value during consolidation. In one sample, it would be impossible to control all the values of the shear strain amplitude, stress condition, and void ratio. It is, therefore, necessary to convert the measured values of G into the values of the predetermined magnitudes of p, γ, and e. However, Hardin et al showed that the experimental G equation for Ottawa-sand, for a strain $\gamma = 10^{-4}$, is equal to;

$$G = 697 \frac{(2.17 - e)^2}{1 + e} p^{0.5} \tag{10}$$

where G is the shear modulus (kg/cm^2), p is the mean principal stress (kg/cm^2), and e is the void ratio. The exact values of G for strain $\gamma = 10^{-5}$ and 10^{-4} were first obtained. Then G was computed using Equation (10), where the mean void ratio value of the tested sample was used (e = 0.81). The change of the G values using this procedure varied by only a few percent. The values of G and p were then plotted on a full-log graph, as shown in Figure 9, then the values of G for p = 0.5, 1, 2, 3, 4, and 6 kg/cm^2 were obtained.

DYNAMIC CHARACTERISTICS OF SANDS

Effects of Shear Strain Amplitude on Shear Modulus

Figures 10 through 13 show the effects the shear strain amplitude has on the shear modulus. The ratios of G to $\{G\}\gamma = 10^{-6}$, i.e., (shear modulus at $\gamma = 10^{-6}$) and shear

strain amplitude, are plotted on a semi-log graph. It was found that $G/(G)_{\gamma} = 10^{-6}$ v_s. γ curves were not affected by changes in void ratio, principal stress ratio, and types of sands. However, when the mean principal stress is of a greater magnitude, the $G/(G)_{\gamma} = 10^{-6}$ ratio decreases with an increase in γ. It was also found that in these tests, the variation of the shear modulus with shear strain amplitude is smaller than the values given in a chart made by Seed and Idriss (5), even when p is as low as 0.5 kg/cm^2.

Effects of the Mean Principal Stress on the Shear Modulus

In all of the tests, the shear modulus varied with the 1/2 power of the mean principal stress, designated as p, as shown in Figures 9, 14, 15, and 16.

Effects of the Stress Ratio on Shear Modulus

Figures 17 and 18 show the effects of the stress ratio on the shear modulus when the mean principal stress is a constant for air-dried Toyoura-sand. It can be seen that the stress ratio has little effect on the shear modulus under a constant value of p within a certain range of stress ratio, i.e. $\sigma_3/\sigma_1 = 0.5, 1.0$. This is the same trend as noted by Hardin and Block (4). To examine the effects when the range of the stress ratio was greater, one test was conducted where the stress ratio was increased to failure under a constant value of p = (3 kg/cm^2). The results are shown in Figure 19, where the stress ratio is denoted by

$$q/p = \frac{\sigma_a - \sigma_r}{1/3\ (\sigma_a + 2\ \sigma_r)} \tag{11}$$

This figure shows that shear moduli are nearly constant, irrespective of the variation of stress ratio, q/p, until q/p reaches a value of 1.0, i.e. $(\sigma_3/\sigma_1) = 0.4$. However, beyond this value of stress ratio, the shear modulus begins to decrease with an increase in the stress ratio. This phenomenon is due to the anisotropic inner structure of the specimen which is caused by the anisotropic stress condition.

Effects of the Void Ratio on the Shear Modulus

All the data that was obtained is summarized in Figure 20, where the shear moduli and void ratios are plotted on a semi-log plot for the values of p = 1 and 6 kg/cm^2 for $\gamma = 10^{-4}$. As noted in Figure 20, it was found that all the data obtained agreed with Equation (10) for $\gamma = 10^{-4}$, in the range of $\sigma_3/\sigma_1 = 0.5$ to 1.0.

Logarithmic Decrements

As stated previously, the damping characteristics of the material tested can be represented by the logarithmic decrements of the system when the mechanism of damping in soils is one of hysteretic dissipation of energy. Figure 21 shows a typical vibration-decay curve, and by plotting each of the amplitudes against number of cycles on a semi-log plot, as given in Figure 22, the logarithmic decrements were obtained. In Figures 23 and 24, the logarithmic decrements are shown for the Sengenyama and Toyoura sands, respectively. In each case, it was found that the logarithmic decrements increased with an increase in the shear strain amplitude and with a decrease in the confining pressure. It was also noted that the values were independent of the void ratios. It has been shown by Hardin (3) that the log decrement experimental equation takes the form;

$$\Delta t = 2\pi \frac{1}{10} \gamma^{0.2}\ p^{-0.5} \tag{12}$$

for the range of $\gamma = 10^{-6}$ to 10^{-4}, and p = 0.244 to 1.46 kg/cm^2. Using Equation (12), the log decrement $\Delta t = 0.1$, for values of $\gamma = 10^{-4}$ and p = 1 kg/cm^2. Now examination of Figure 23 for the Sengenyama-sand $\Delta t = 0.17$ and in Figure 24 for Toyoura-sand, $\Delta t = 0.11$, thus it may be stated that the experimental values will take the form of Equation (12).

CONCLUSIONS

(1) The resonant column apparatus that has been developed provides a most effective technique in evaluating the shear modulus and damping characteristics of soils.

(2) The test results on samples of Toyoura-sand and Sengenyama-sand indicate that Equation (10) fits the experimental results for $\gamma = 10^{-4}$ and in the range of stress ratio $\sigma_3/\sigma_1 = 0.5 - 1.0$. However, when the stress ratio (σ_3/σ_1) is smaller than 0.5, the shear modulus decreases with a decreasing value of stress ratio (σ_3/σ_1).

(3) The logarithmic decrements obtained were in the range of $\Delta t = 0.1 - 0.2$ for $\gamma = 10^{-4}$ and $p - 1$ kg/cm^2.

ACKNOWLEDGMENTS

This research was encouraged and supported by Dr. Tadayoshi Okubo, Head of Structure and Bridge Division, P.W.R.I. The tests were conducted by Dr. Fumio Tatsuoka and Mr. Shyunichi Horiuchi, Earthquake Engineering Research Section, P.W.R.I. The authors gratefully acknowledge their help and cooperation.

REFERENCES

1. Iida, K. (1938), "The Velocity of Elastic Waves in Sand," Bull. Earthquake Res. Inst., 16. E.R.I., Tokyo University.

2. Hardin, B.O., and Music, J. (1965), "Apparatus for Vibration During the Triaxial Test," ASTM, STP, No. 392.

3. Hardin, B.O. (1965), "The Nature of Damping in Sands," J. of S.M.F.D., Proc. ASCE, Vol. 91, No. SM1, January.

4. Hardin and Block (1966), "Sand Stiffness Under Various Triaxial Stresses," ASCE, Vol. 92, No. SM2.

5. Seed, H.B. and Idriss, I.M. (1970), "Soil Moduli and Damping Factors for Dynamic Response Analyses." Report No. EERC 70-10, December, College of Engineering, University of California, Berkeley.

6. Iwasaki, T., Tasuoka, F., and Horiuchi, S. (1974), "A Measurement Method of Dynamic Deformational Characteristics Sand Samples," Proc. of the 1st Annual Meeting of Kanto Branch of JSCE, May. (in Japanese).

7. Iwasaki, T., Tatusoka, F. and Horiuchi, S. (1974), "Dynamic Deformational Characteristics of Soils with Resonant Column Apparatus," Proc. of 9th Annual Meeting of JSSF, June (in Japanese).

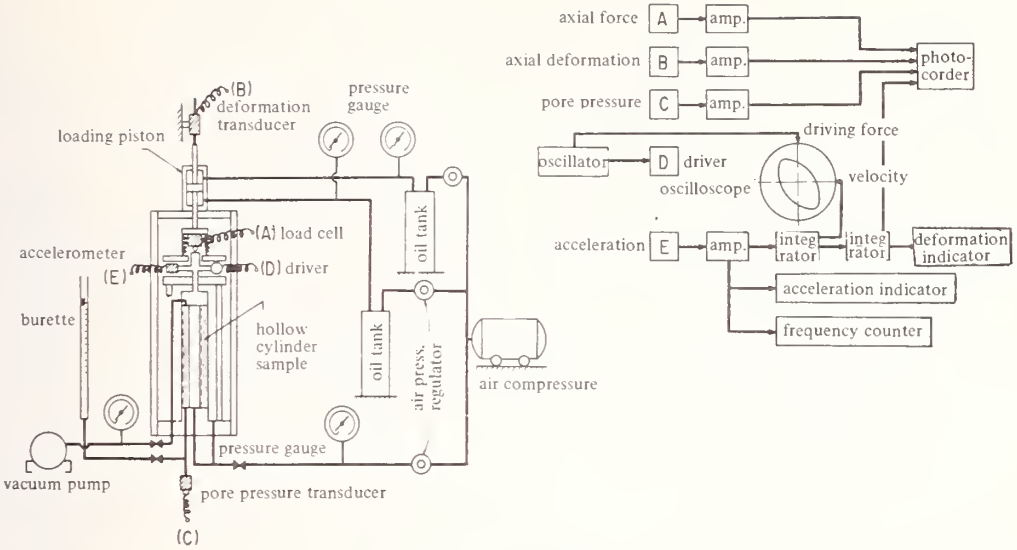

Fig. 1 Schematic diagram of the apparatus

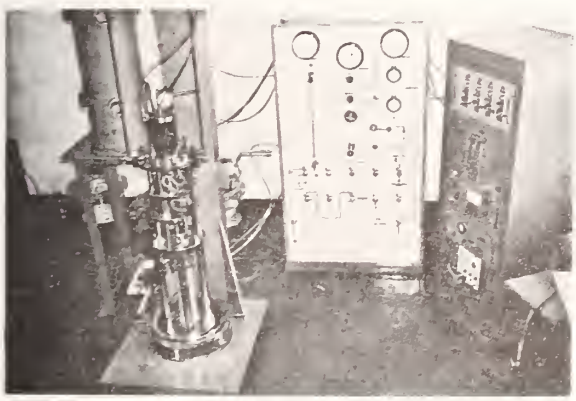

Fig. 2 Photograph of the apparatus

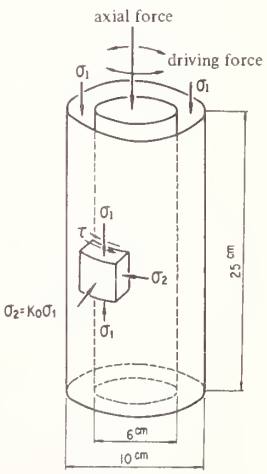

Fig. 3 Stress condition of sample

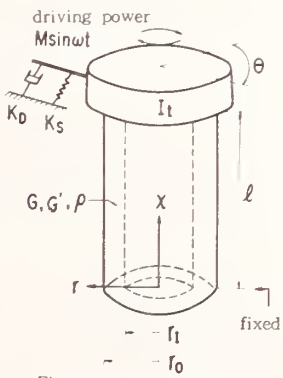

Fig. 4 model for the specimen-apparatus system

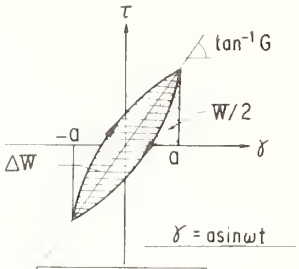

$$\eta = \frac{1}{2\pi}\frac{\Delta W}{W}$$

Fig. 5 Stress-strain curve of sands

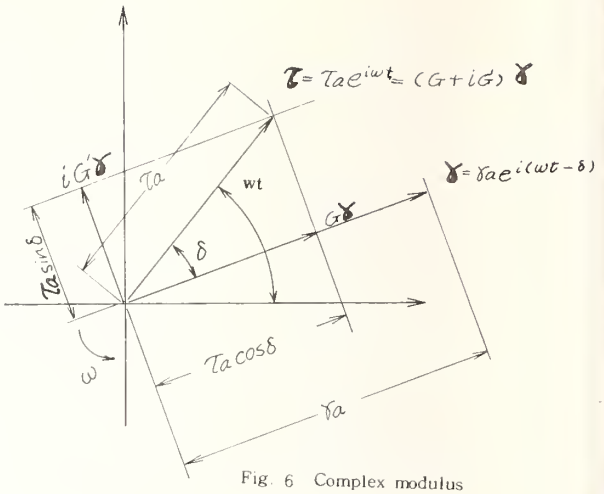

Fig. 6 Complex modulus

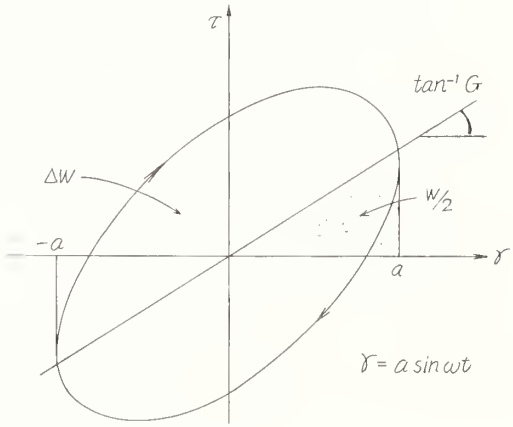

$$\eta = \frac{1}{2\pi}\frac{\Delta W}{W} = \frac{G'}{2G}$$

Fig. 7 Stress-strain curve of Voigt materials

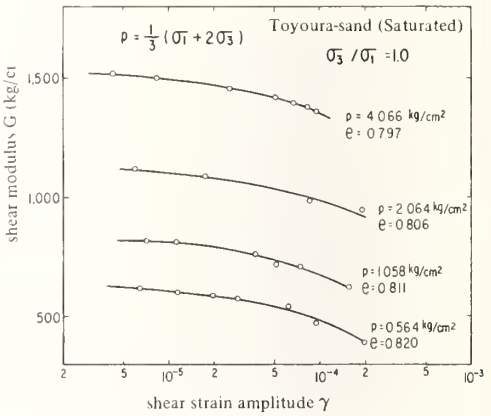

Fig. 8 Shear modulus versus shear strain amplitude

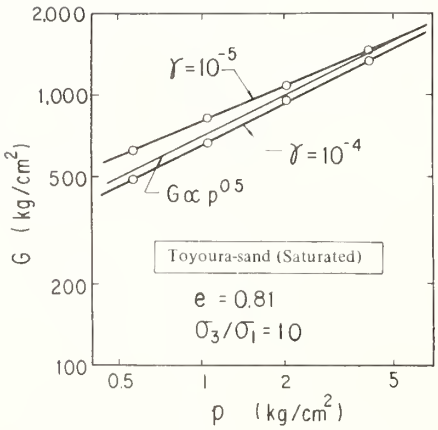

Fig. 9 Shear modulus and mean principal stress

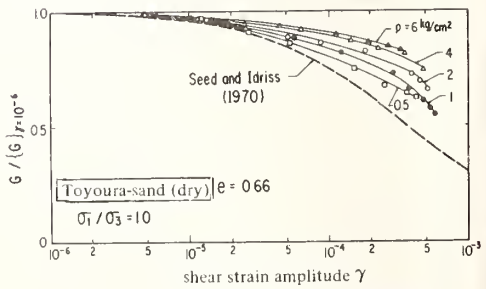

Fig. 10 Shear modulus versus shear strain amplitude

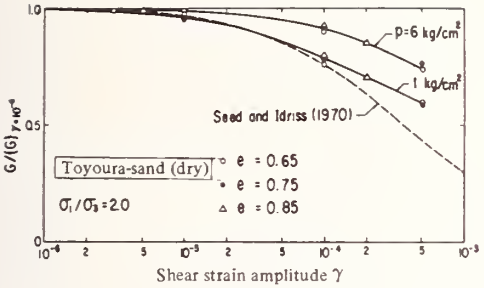

Fig. 11. Shear modulus versus shear strain amplitude

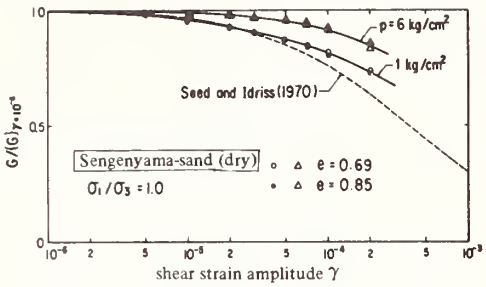

Fig. 12 Shear modulus versus shear strain amplitude

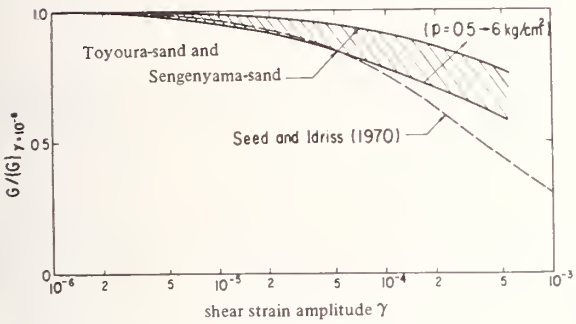

Fig. 13 Shear modulus versus shear strain amplitude

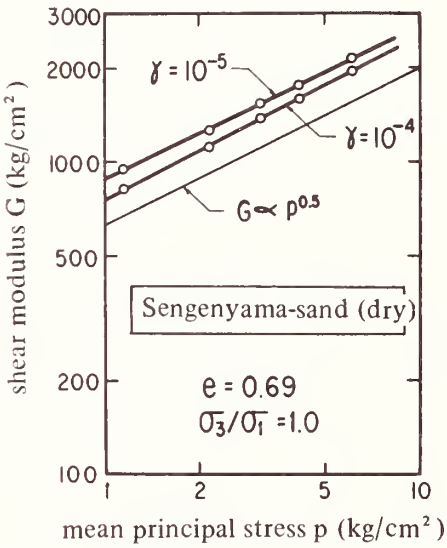

Fig. 14 Shear modulus versus confining pressure

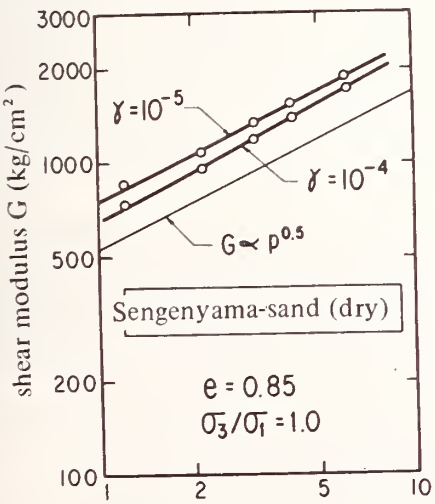

Fig. 15 Shear modulus versus confining pressure

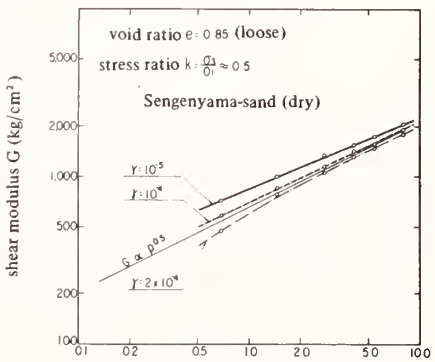

Fig. 16 Shear modulus versus mean principal stress

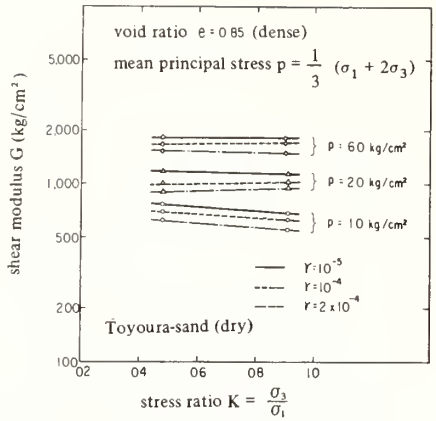

Fig. 17 Shear modulus versus stress ratio

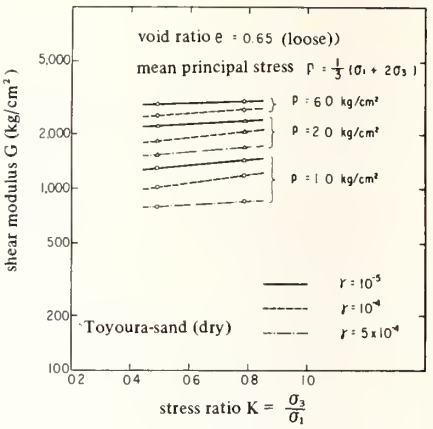

Fig. 18 Shear modulus versus stress ratio

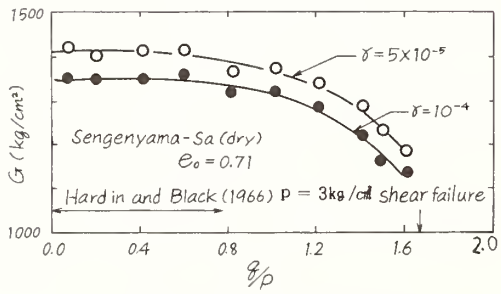

Fig. 19 Shear modulus versus stress ratio in case of p=constant = 3kg/cm²

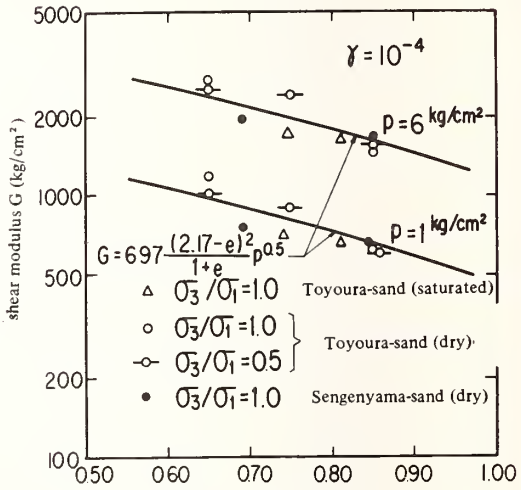

Fig. 20 Shear modulus versus void ratio

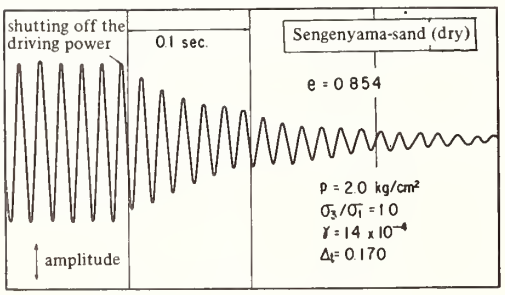

Fig. 21 Amplitude-time decay curves

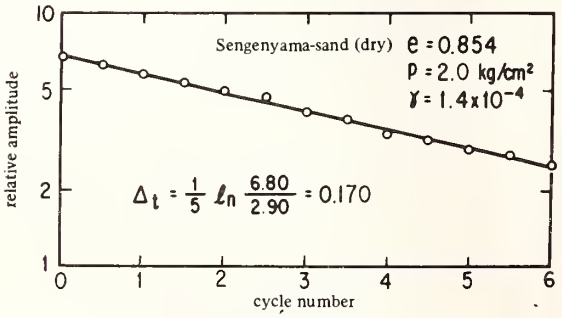

Fig. 22 Amplitude versus cycle number

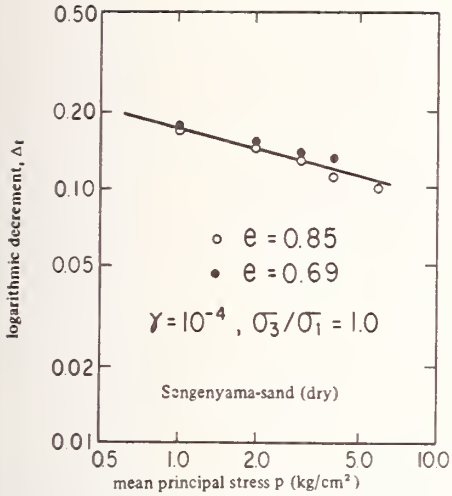

Fig. 23 (a) logarithmic decrement versus mean principal stress

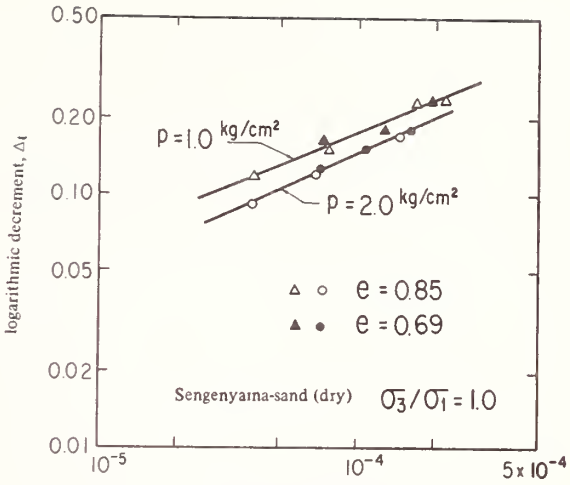

Fig. 23 (b) Logarithmic decrement versus shear starin amplitude

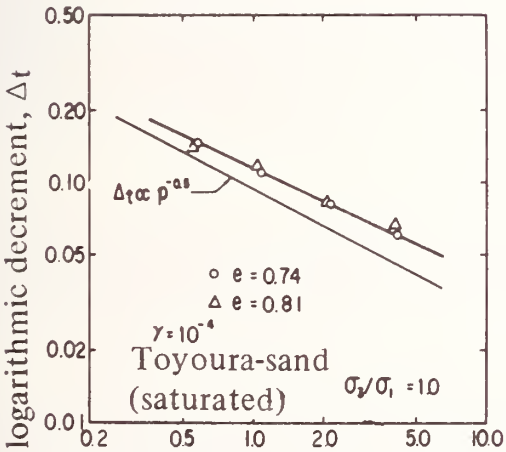

Fig. 24 (a)
Logarithmic decrement
versus mean principal stress

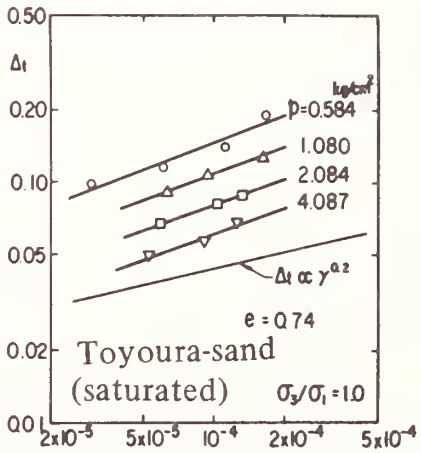

Fig. 24 (b)
Logarithmic decrement
versus shear strain amplitude

PREDICTION OF MAXIMUM EARTHQUAKE INTENSITIES FOR THE SAN FRANCISCO BAY REGION

by

Roger D. Borcherdt
and
James F. Gibbs

Office of Earthquake Studies
U.S. Geological Survey

The intensity data for the California earthquake of April 18, 1906, are strongly dependent on distance from the zone of surface faulting and the geological character of the ground. Considering only those sites (approximately one square city block in size) for which there is good evidence for the degree of ascribed intensity, the empirical relation derived between 1906 intensities and distance for 761 sites underlain by rocks of the Franciscan Formation is

$$\text{Intensity} = 2.30 - 1.90 \log (\text{Distance}).$$

For sites on other geologic units intensity increments, derived with respect to this empirical relation, correlate strongly with the Average Horizontal Spectral Amplifications (AHSA) determined from 99 three-component recordings of ground motion generated by nuclear explosions in Nevada. The resulting empirical relation is

$$\text{Intensity Increment} = 0.27 + 2.70 \log (\text{AHSA}).$$

Resulting average intensity increments for various geologic units are -0.29 for granite, 0.19 for Franciscan Formation, 0.64 for other pre-Tertiary, Tertiary bedrock, 0.82 for Santa Clara Formation, 1.34 for Older Bay sediments, 2.43 for Younger Bay mud. These empirical relations have been used to delineate areas in the San Francisco Bay region of potentially high intensity from future earthquakes on either the San Andreas fault or the Hayward fault.

Key Words: Earthquake; empirical relation; Franciscan Formation; geological character; ground shaking; intensity.

INTRODUCTION

The amounts of damage resulting from the great California earthquake of April 18, 1906, varied greatly for different areas in the San Francisco Bay region. In some areas the damage was WEAK with "occasional fall of chimneys and damage to plaster, partitions, plumbing, and the like," in other nearby areas the damage was VIOLENT with "... fairly general collapse of brick and frame structures when not unusually strong..." (Wood, 1908). These large variations were due in part to the geological character of the ground and to the distance from the zone of surface faulting (compare the intensity map for the city of San Francisco (Figure 1) with the geologic map (Figure 2)).

Comparative ground motion measurements made for 99 sites in the San Francisco Bay region (Gibbs and Borcherdt, 1974) show that a strong correlation exists between amplitude levels of observed ground shaking and the type of geologic unit. The purposes of this paper are:

1) To quantify the relationship between distance and the observed 1906 earthquake intensities for a particular bedrock unit, and

2) To show the existence of a relationship between intensity and the measured ground motion amplifications.

These relationships permit a quantitative estimate of the dependence of the observed 1906 intensities on the geological character of the ground. Such estimates are useful for delineating areas of potentially high intensity from future earthquakes on either the San Andreas fault or the Hayward fault.

INTENSITY VS. DISTANCE

The 1906 earthquake intensities ascribed sites on the same geologic unit generally decrease with increasing distance from the zone of surface faulting (Lawson, 1908). To quantify this apparent relationship, the 1906 intensity data for the San Francisco Bay region were reconsidered on a site-by-site basis. The intensity data from only those sites (approximately one square city block in size) for which there was good evidence for the degree of ascribed intensity were considered. For each site underlain by rocks of the Franciscan Formation, the distance to the zone of surface faulting was measured and plotted as a function of the ascribed 1906 earthquake intensity (Figure 3). The resulting empirical relation,

$$\text{Intensity} = 2.30 + 1.90 \log (\text{Distance}),$$

determined by the method of least squares, suggests that the ascribed intensity values for sites on the Franciscan Formation generally decrease as the logarithm of increasing distance. The empirical relation shows that the intensity values decrease very rapidly with distance, with sites 3 km from the fault having observed intensities more than two intensity units smaller than those at the fault.

The sites with the highest ascribed intensities ("A", 1906 San Francisco scale) are located within 0.7 km of the center of the zone of surface rupture. For most of these sites, the unit of intensity was assigned on the basis of evidence for some form of ground failure most of which was associated with surface faulting. The degree of intensity assigned to most of the other sites at greater distances from the fault was based on damage resulting from ground shaking or ground shaking induced ground failures. To quantify the dependence of the intensities due only to shaking on distance, another empirical relation was determined with the intensity data near the fault omitted. The resulting empirical relation is essentially the same as the one determined from the complete data set. (Intensities predicted by either relation differ by less than 0.02.) This similarity suggests that the dependence of intensity on distance is not influenced by the intensity data near the fault due to surface faulting. For explicitness only the relation determined from the complete data set will be referred to hereafter.

INTENSITY VS. MEASURED LOW-STRAIN AMPLIFICATIONS

Recordings of three components of ground motion generated by distant nuclear explosions have been made at 99 sites in the San Francisco Bay region (Figure 2)(Borcherdt, 1970; Gibbs and Borcherdt, 1974). Spectral amplification curves computed from these recordings show that low-strain ground motions of certain frequencies are amplified considerably by thick sections of unconsolidated alluvial deposits. Averages of the spectral amplification curves over the frequency band for which there is a good signal to noise ratio correlate strongly with the type of geologic deposit.

To compare the low-strain amplifications with the observed 1906 intensity data, intensity increments were defined for each of the recording sites as the difference between the observed intensity at the site and that predicted by the empirical relation for sites at the same distance on the Franciscan Formation. These intensity increments are plotted as a function of the corresponding Average Horizontal Spectral Amplification (AHSA) values (Figure 4). (The AHSA values plotted have been normalized by the average AHSA value determined for sites on the Franciscan Formation.) Empirical relations were determined using the method of least squares from the complete data set (".") and from only the data (" ") for sites in the city of San Francisco for which there was "unequivocal evidence" for the degree of ascribed 1906 intensity. The two empirical relations are similar with intensity increments predicted by either relation differing by less than two-tenths. The empirical relation ($\delta I = 0.27 + 2.70 \log (AHSA)$) based on only the good intensity data in the city of San Francisco is preferred.

The correlation coefficient of 0.95 computed for the preferred empirical relation ($\delta I = .27 + 2.70 \log (AHSA)$) shows that a strong correlation exists between the computed intensity increments and the amplifications observed at low-strain levels. The physical meaning of this empirical correlation is complex and does not necessarily mean that amplifications observed at low-strain levels can be extrapolated directly to high-strain levels. However, there are two possible reasons for this correlation:

1) For levels of ground shaking that did <u>not</u> cause ground failure, the higher amplifications indicate those sites that experienced the higher levels of ground shaking, and

2) For levels of ground shaking that <u>did</u> induce ground failure, the higher amplifications indicate those sites that were most susceptible to ground failure.

In either case, the sites of higher amplification would have experienced greater amounts of damage and be assigned higher degrees of intensity.

PREDICTION OF MAXIMUM EARTHQUAKE INTENSITIES

Fault studies (Wesson et al., 1974) indicate a high potential for large (magnitude, 7.6-8.3) earthquakes on both the San Andreas fault and the Hayward fault in the San Francisco Bay region. Historically, large earthquakes have occurred along both faults. Due to a lack of cultural development at the times of the earthquakes, the intensity data for an earthquake on the Hayward fault is very scanty and there are several presently developed areas with no 1906 intensity data. However, the empirical relation between the 1906 intensity increments and the AHSA values measured from the nuclear data provide a means for assigning intensities to these areas.

Using the empirical relation between intensity increments and the AHSA values, intensity increments were predicted for each of the 99 sites at which amplification values have been measured from the nuclear explosions. The predicted intensity increments were grouped according to the type of underlying geologic unit (see Borcherdt, 1970, for a description of the units). The means and standard deviations for the various samples are tabulated (Table 1). The mean increments for the various units range from -0.29 for granite to 2.43 for Younger Bay mud. These mean intensity increments provide a quantitative estimate of the dependence of the 1906 earthquake intensities on the geological character of the ground.

Utilizing the computed average intensity increments for the various geologic units, the empirical relation between intensity and distance, and a geologic map (compiled by K.R. Lajoie, personal communitcation), Borcherdt and Gibbs (1974) predicted absolute intensities on a regional basis for the San Francisco Bay region. The resulting predicted intensity map (Borcherdt and Gibbs, 1974) shows the maximum intensity predicted for a site that might result from an earthquake in the San Francisco Bay region on either the San Andreas fault or the Hayward fault. Such a map is useful for delineating general earthquake problem areas in the San Francisco Bay region and for evaluating the earthquake hazard in areas not developed at the time of the 1906 earthquake. In addition, the map is useful for evaluating the hazard due to another large earthquake on the Hayward fault. The map shows that earthquake hazards are not uniformly distributed throughout the San Francisco Bay region.

REFERENCES CITED

1. Borcherdt, R.D. (1970). Effects of Local Geology on Ground Motion Near San Francisco Bay, Bull. Seism. Soc. Am., 60, 29-61.

2. Borcherdt, R.D., and J.F. Gibbs (1974). Maximum Predicted Earthquake Intensity Map for the San Francisco Bay Region, in press.

3. Gibbs, J.F., and R.D. Borcherdt (1974). Effects of Local Geology on Ground Motion Near San Francisco Bay--A Continuation, in press.

4. Lawson, A.D. (Chairman)(1908). The California Earthquake of April 18, 1906, Report of the State Earthquake Commission, Carnegie Institute of Washington, Publ. 87, Washington, D.C.

5. Wesson, R.L., C.M. Wentworth, R.D. Brown, Jr., E.J. Helley, and K.R. Lajoie. A Preliminary Analysis of Seismic Zonation in the San Francisco Bay Region--Chap. I Faults and Future Earthquakes, U.S. Geological Survey Circular, in press.

6. Wood, H.O. (1908). Distribution of Apparent Intensity in San Francisco in The California Earthquake of April 18, 1906, Report of the State Earthquake Investigation Commission, Carnegie Institute of Washington, Publ. 87, Washington, D.C.

TABLE 1

STATISTICS FOR SAMPLES OF LOW-STRAIN AMPLIFICATIONS AND INTENSITY INCREMENTS WITH RESPECT TO FRANCISCAN FORMATION FOR VARIOUS GEOLOGIC UNITS

Geologic Unit	Average Horizontal Spectral Amplification		Intensity Increment (1906 San Francisco Scale)	
	Mean	Standard Deviation	Mean	Standard Deviation
Granite	0.63	0.11	-0.29	0.21
Franciscan Formation	1.00	0.38	0.19	0.47
Pre-Tertiary, Tertiary Bedrock*	1.42	0.45	0.64	0.34
Santa Clara Formation	1.70	0.64	0.82	0.48
Older Bay Sediments	2.76	1.16	1.34	0.58
Younger Bay Mud	7.06	3.78	2.43	0.58

ILLUSTRATIONS

Figure 1. Map showing distribution of apparent 1906 intensities for the city of San Francisco, California (after Wood, 1908).

Figure 2. Map showing distribution of geologic units for the city of San Francisco, California (compiled by K.R. Lajoie from data of Schlocker and others).

Figure 3. Observed 1906 intensities for sites (one square city block in size) underlain by rocks of the Franciscan Formation versus perpendicular distance from the zone of surface rupture during the 1906 earthquake. For sites with "unequivocal evidence" in the city of San Francisco (Map No. 19, Lawson, 1908), the number of observed intensity values is shown below the corresponding distance interval. For sites intersected by an "examined route" south of the city of San Francisco (Maps No. 21 and 22, Lawson, 1908), the number of observed intensities is shown above the correponding distance interval. The observed 1906 intensities are expressed in terms of the 1906 San Francisco intensity scale with the letters A-E corresponding respectively to the numbers 4-0 (see Appendix 1 for detailed description of intensity scale).

Figure 4 Increments in 1906 intensities versus average spectral amplification computed at corresponding sites from recordings of nuclear explosions. Both the intensity increment values and the average spectral amplification values were computed with respect to the corresponding average value determined for sites underlain by rocks of the Franciscan formation.

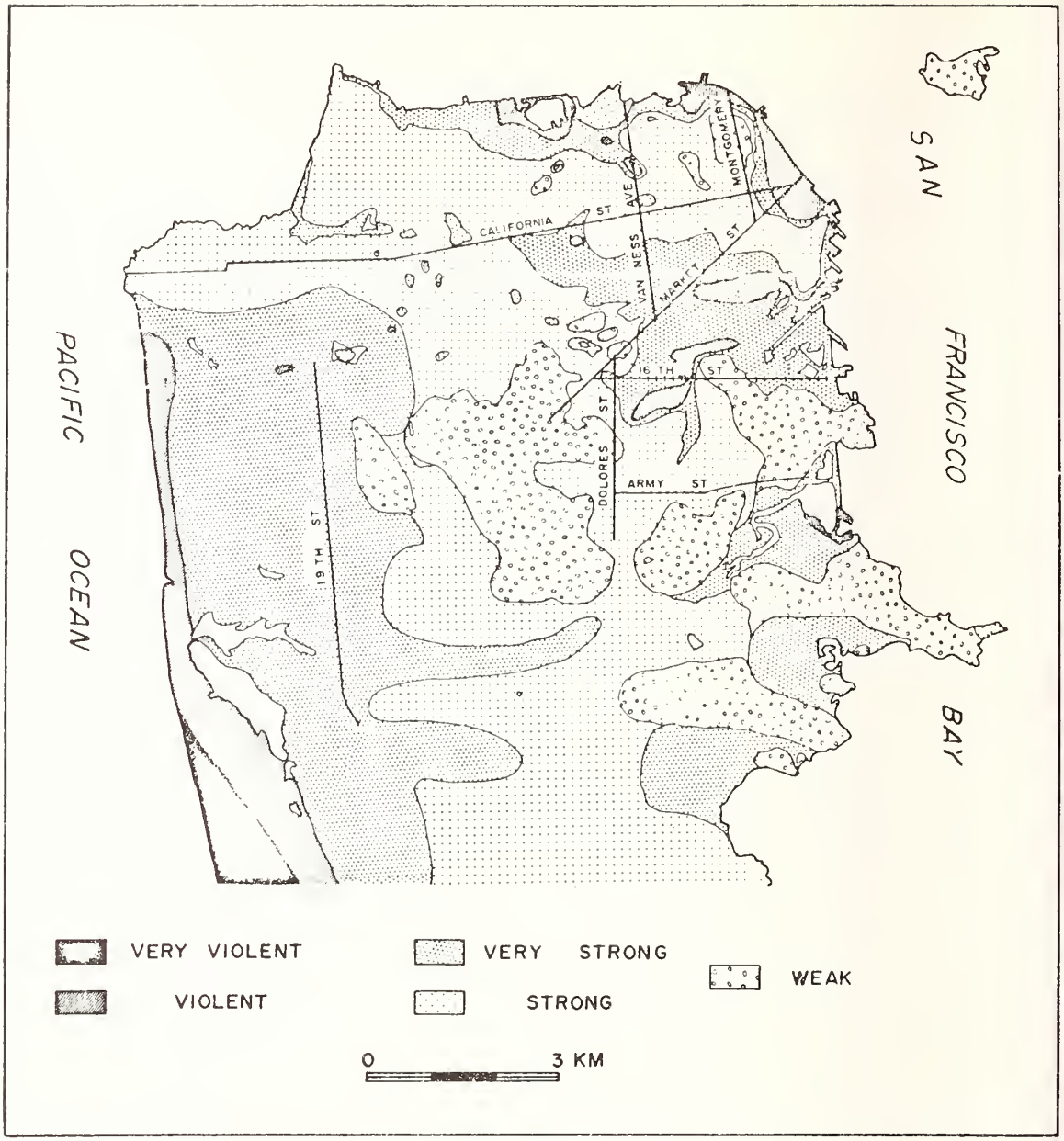
SAN FRANCISCO BAY
PACIFIC OCEAN
CALIFORNIA ST
VAN NESS AVE
MONTGOMERY ST
MARKET ST
16 TH ST
DOLORES ST
ARMY ST
19TH ST
VERY VIOLENT
VIOLENT
VERY STRONG
STRONG
WEAK
0
3 KM

Figure 1

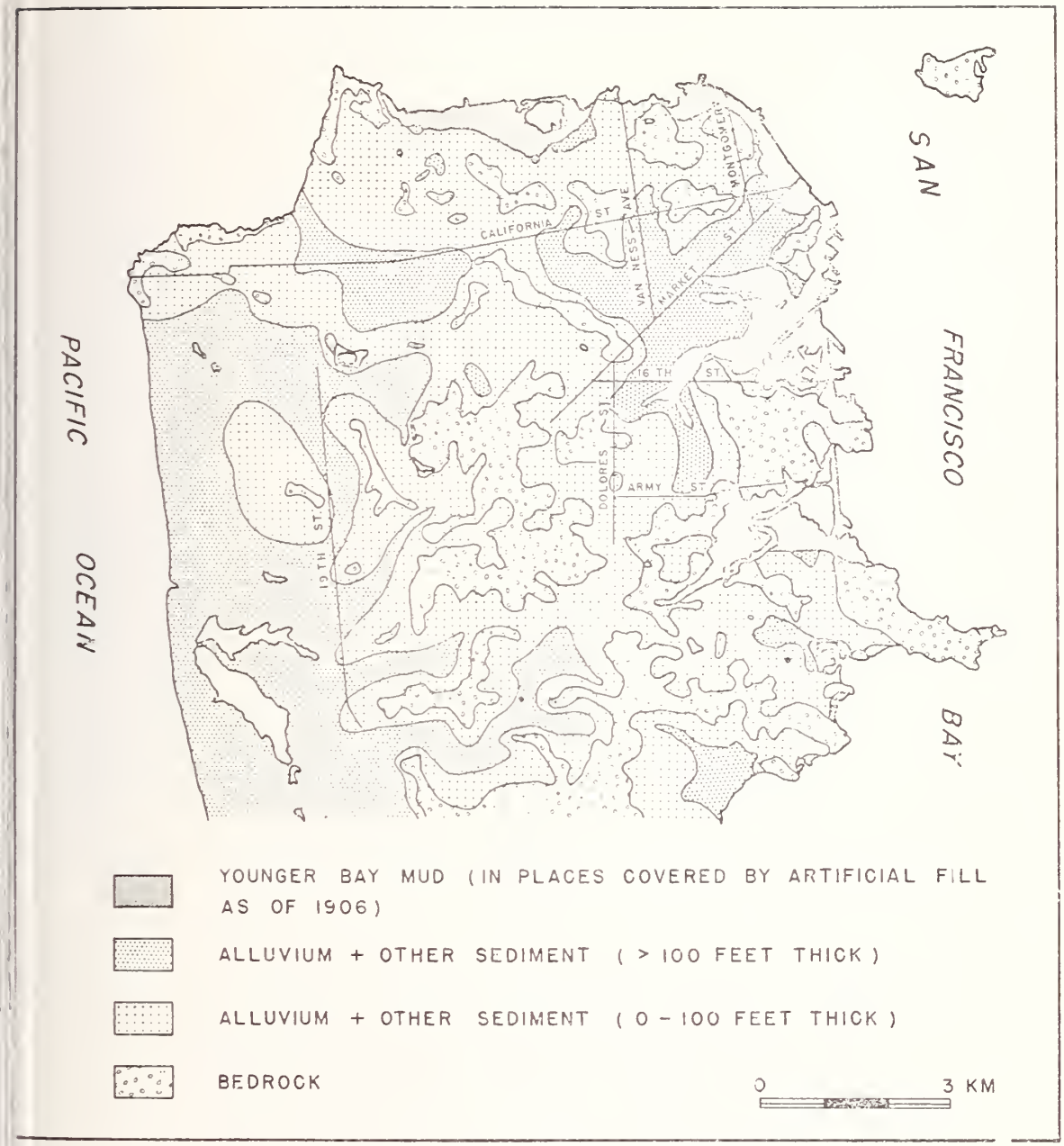
SAN
FRANCISCO
BAY
PACIFIC
OCEAN
CALIFORNIA ST
VAN NESS AVE
MARKET ST
16 TH ST
ARMY ST
DOLORES ST
19TH ST
YOUNGER BAY MUD (IN PLACES COVERED BY ARTIFICIAL FILL AS OF 1906)
ALLUVIUM + OTHER SEDIMENT (> 100 FEET THICK)
ALLUVIUM + OTHER SEDIMENT (0 - 100 FEET THICK)
BEDROCK
0
3 KM

Figure 2

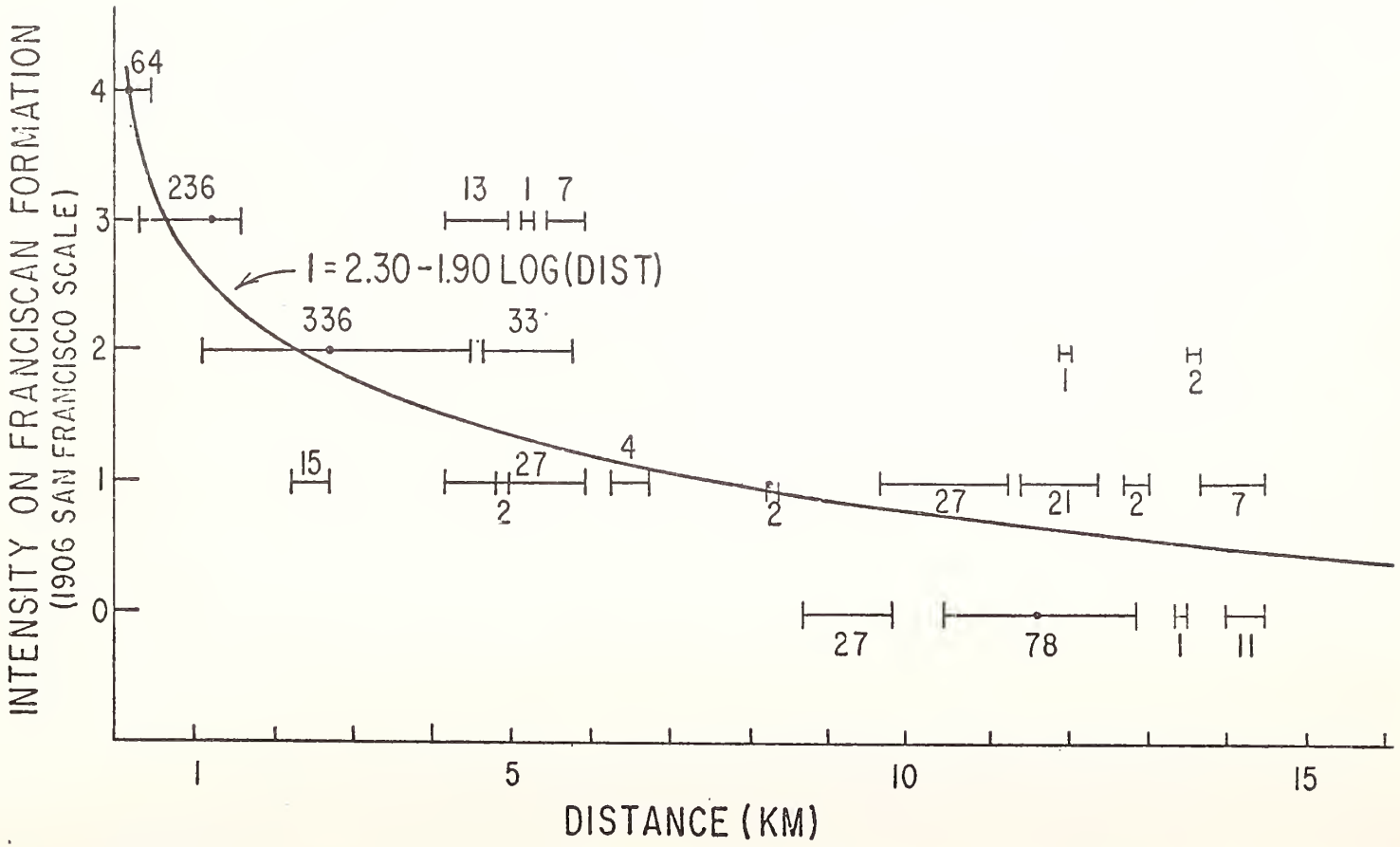
INTENSITY ON FRANCISCAN FORMATION
(1906 SAN FRANCISCO SCALE)
I = 2.30 - 1.90 LOG(DIST)
DISTANCE (KM)
0
1
2
3
4
1
5
10
15
64
236
13
1
7
336
33
15
27
2
4
2
27
21
2
7
27
78
1
11

Figure 3

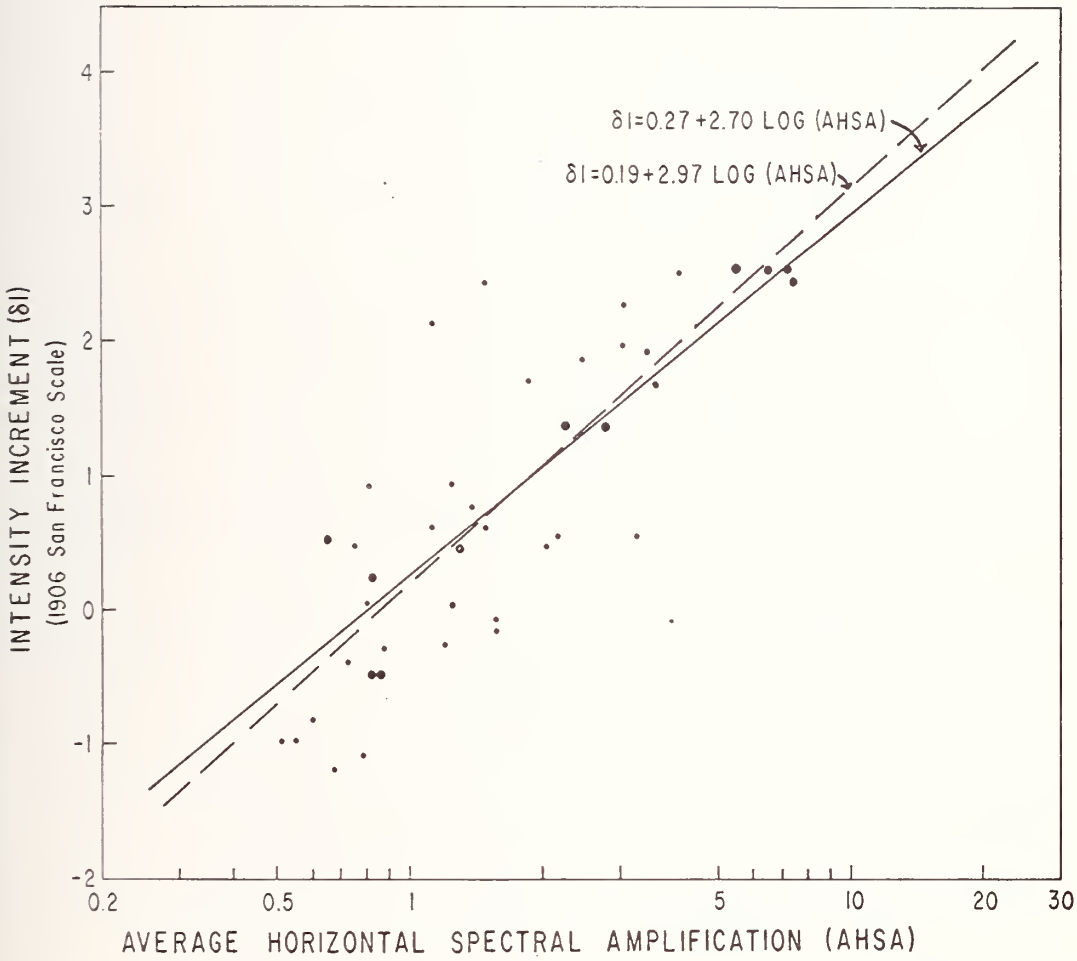
δI=0.27+2.70 LOG (AHSA)
δI=0.19+2.97 LOG (AHSA)
INTENSITY INCREMENT (δI)
(1906 San Francisco Scale)
AVERAGE HORIZONTAL SPECTRAL AMPLIFICATION (AHSA)
4
3
2
1
0
-1
-2
0.2
0.5
1
5
10
20
30

Figure 4

APPENDIX 1
SAN FRANCISCO APPARENT INTENSITY SCALE

The following grades of apparent intensity were ascribed by H.O. Wood (1908, pp. 224-225) in the city of San Francisco to describe damage which resulted from the California earthquake of April 18, 1906.

Grade A. Very Violent - Comprises the rending and shearing of rock masses, earth, turf, and all structures along the line of faulting; the fall of rock from mountain sides; numerous landslips of great magnitude; consistent, deep, and extended fissuring in natural earth; some structures totally destroyed.

Grade B. Violent - Comprises fairly general collapse of brick and frame buildings when not unusually strong; serious cracking of brick work and masonry in excellent structures; the formation of fissures, step faults, sharp compression anticlines, and broad, wave-like folds in paved and asphalt-coated streets, accompanied by the ragged fissuring of asphalt; the destruction of foundation walls and underpinning structures by the undulation of the ground; the breaking of sewers and water-mains; the lateral displacement of streets; and the compression, distension, and lateral waving or displacement of well-ballasted streetcar tracks.

Grade C. Very Strong - Comprises brick work and masonry badly cracked, with occasiona collapse; some brick and masonry gables thrown down; frame buildings lurched or listed on fair or weak underpinning structures, with occasional falling from underpinning or collapse; general destruction of chimneys and of masonry, brick or cement veneers; considerable cracking or crushing of foundation walls.

Grade D. Strong - Comprises general but not universal fall of chimneys; cracks in masonry and brick work; cracks in foundation walls, retaining walls, and curbing; a few isolated cases of lurching or listing of frame buildings built upon weak underpinning structures.

Grade E. Weak - Comprises occasional fall of chimneys and damage to plaster, partitions, plumbing, and the like.

A STATISTICAL APPROACH TO LOADING AND FAILURE OF STRUCTURES

by

Ronald G. Merritt

U.S. Army Construction Engineering Research Laboratory

A fundamental problem of structural engineering is the examination and selection of loading criteria. It is imperative that any solution to the problem center around a rationale that relates information available on loading to selected criteria. Such available information is generally in the form of data. It is the purpose of this brief paper to abstract the problem and outline preliminary work on a rationale for addressing the problem.

The paper begins by defining the general nature of the problem. Solution to the problem is related to consideration of available information in the form of data. The next three sections of the paper discuss the initial stages of a rationale for consistent examination and selection of loading criteria. The first of the sections examines available information on structural load and the second examines available information on instances of structural failure. Classes of statistical methods are discussed in the third section. This section also includes discussion of a proposed method for assessing the overall information content of the available data. Finally, several illustrative examples of application of statistical methods to load and failure data are presented and the paper concludes with a discussion of future extension to this preliminary work.

Key Words: Failure; probability theory; random process; safety; statistical analysis; structural engineering.

GENERAL NATURE OF THE PROBLEM

Examination and selection of loading criteria involves the consideration of a statement S with quantifiers that relate variables useful in description of the load. This may be written generally as

$$(1) \qquad S{:}C = C(\bar{t}, \bar{r}, \bar{a})$$

for

S = Loading criteria statement

C = Load function

$\bar{t}$ = Time vector

$\bar{r}$ = Space vector

$\bar{a}$ = Parameter vector

The statement S has a quantifier the load function C which is expressible in terms of time space and a finite set of parameters. The expression is general enough to allow for several components of time, space, and parameters, as denoted by the vector notation. The problem may now be stated in terms of examination of the validity of S.

Validity of S is usually established through some subjective and objective evaluation of available information related to S. In order to be consistent in this evaluation of information, a rationale for carrying out this evaluation must be set forth. The preliminary outline of the rationale proposed in this paper centers upon a means of assessing available information related to S by use of statistical techniques, correlating this information and obtaining quantitative factors upon which the validity or invalidity of S may be established. In a real sense this rationale, in part, already exists in that statistical interpretation of collected data is commonplace in examination of load data. The discussion to follow extends this rationale. However, it is important to note here that "all" available information is to be examined in evaluating the validity or invalidity of S. This includes consideration of load information for one. But in addition, since the invalidity of S tacitly implies possibility of structural failure because of load, one must also consider structural failure information. It is the general nature of these sets of information that provides the basis for this preliminary work on development of the rationale.

LOAD INFORMATION

Load information is obtained in a quantity termed a datum. Such datum may be in a raw form or in a summary form. The raw form consists of the most basic unit and results from direct quantization of the phenomenon under observation. The summary form results from a transformation of raw data.

Upon collection of data on loading, e.g., wind loading, it became apparent that some way of classifying individual pieces of datum would need to be developed. Once classified, then groups of datum within any one designated category could be examined for consistency and their relationship to the proposed loading criteria. The discussion to follow defines the datum classification system and the example in Section VI illustrates application of a statistical technique to a piece of datum within the system.

The requirements on a load data classification system are very basic. First, a single piece of datum must be recognized as such in the system and second, a piece of datum must be classifiable within the system. In order to facilitate this a "generalized random process", L, is defined whose "sample functions" consist of pieces of datum described by a

set of parameters related to the load phenomenon (1).* This is most easily expressed as

$$L(\bar{t}, \bar{r}, \bar{a}) = \{l(\bar{t}, \bar{r}, \bar{a}) : \bar{t} \varepsilon T, \bar{r} \varepsilon R, \bar{a} \varepsilon A\}$$

where

$L(\bar{t}, \bar{r}, \bar{a})$ = Generalized random process

$l(\bar{t}, \bar{r}, \bar{a})$ = A piece of datum

$\bar{t}$ = Time related description of the datum

T = Time indexing set

$\bar{r}$ = Space related description of the datum

R = Space indexing set

$\bar{a}$ = Parameter related description of the datum

A = Parameter indexing set.

It is assumed that every piece of datum related to a load phenomenon belongs to $L(\bar{t}, \bar{r}, \bar{a})$ and that each piece of datum is uniquely defined through an ordered triple of vectors $(\bar{t}, \bar{r}, \bar{a})$.

The advantages of such a means of classifying data by evaluation of $\bar{t}$, $\bar{r}$, and $\bar{a}$ are readily apparent. First, in evaluation of $\bar{t}$, $\bar{r}$, and $\bar{a}$ datum sets are established within $L(\bar{t}, \bar{r}, \bar{a})$ that relate similar information about the load phenomenon under investigation. Second, correlation of information through evaluation of $\bar{t}$, $\bar{r}$, and $\bar{a}$ allows one to assess the overall information content of the available data. Third, ready evaluation of data within a given datum set is possible and links amongst datum sets provide a key to links amongst data within different datum sets. Finally, this approach lends itself well to either the synthesis approach or the analytical approach to criteria selection. In the synthesis approach, all data is structured into a description of the load phenomenon and criteria are selected from this description. In the analytical approach, the datum is checked against the proposed criteria for consistency and selection of criteria is based upon this check. In either case, the pertinent datum is easily identified.

A total of twenty-two parameters that must be evaluated for each piece of datum were selected. The twenty-two parameters may be divided into five groups. Brief mention of these five groups will suffice for the present discussion. The first group consisting of two parameters uniquely identifies the piece of datum. The second group consisting of five parameters identifies the datum by defining the overall load phenomenon properties, e.g. static, deterministic, stationarity, its source, its spatial extent. The third group consisting of eight parameters describes the piece of datum in terms of the time history information available. The fourth group consisting of five parameters describes the datum in terms of the spectral information available. Finally, the fifth group of parameters consisting of two parameters gives a brief narrative description of the piece of datum along with a source reference.

This general scheme of datum referencing permits a consistent examination of structural load data. Extensions to this general scheme will be discussed in the last section of this paper.

---

*Numbers in parentheses denote references.

STRUCTURAL FAILURE INFORMATION

The consideration of data on instances of structural failure in the preliminary stages of development has provided for some most interesting ideas on structuring of data from diverse and complex phenomenon. In the case of structural load data, the content of individual pieces of datum was described in terms of a set of parameters and the raw or summary form data lay within each of the random process sample functions. Data analysis was assumed to take place on a "level below" the datum structures, $L(\bar{t}, \bar{r}, \bar{a})$. For the case of structural failure, the nature of the available data and information desired from the data requires that the description of the datum, i.e., instance of structural failure, be complete enough for data analysis. That is, the analogous structural failure "generalized random process" should contain the available information concerning the structural failure. This approach to structural failure datum is the product of several considerations. First, quantitative structural failure data is difficult to obtain since few instances of structural failure are instrumented. Second, unless the failure is controlled in some manner, quantitative data tends to be meaningless because of the complex load-response path that usually describes the failure. Third, any one case of structural failure is but one of many possible structural failures and it may or may not share properties in common with other cases of structural failure. Fourth, detailed quantitative data from instrumentation of a structural failure would present a prohibitively high collection and reduction cost to information ratio. Finally, detailed reduction of quantitative data obtained during or after structural failure would tend to de-emphasize the overall characteristics of the structural failure. Structural failure data was considered in the following way.

It was hypothesized that structural failure may be considered a "generalized random process" (1). Thus, it can be represented by an expression

$$S(\bar{t}, \bar{r}, \bar{a}) = \{s(\bar{t}, \bar{r}, \bar{a});\ \bar{t}\varepsilon T,\ \bar{r}\varepsilon R,\ \bar{a}\varepsilon A\}$$

$S(\bar{t}, \bar{r}, \bar{a})$ = Structural failure generalized random process

$s(\bar{t}, \bar{r}, \bar{a})$ = Structural failure sample function

$\bar{t}$ = Time vector

T = Time indexing set

$\bar{r}$ = Spatial vector

R = Spatial indexing set

$\bar{a}$ = Parameter vector

A = Parameter indexing set.

All instances of structural failure belong to $S(\bar{t}, \bar{r}, \bar{a})$ and every failure is in $S(\bar{t}, \bar{r}, \bar{a})$ either explicitly through collected data and parameter evaluation or implicitly in cases where the structural failure is unrecorded but the indexing sets are broad enough for description. The problem of structural failure data structuring now becomes a matter of defining T, R, and A and evaluating $\bar{t}$, $\bar{r}$, and $\bar{a}$ from collected data on structural failure.

Ultimately, forty-five parameters were considered adequate to define the structural failure random process, i.e., forty-five parameters were considered sufficient to describe any instance of structural failure. Obviously, only the overall gross characteristics of an instance of structural failure were considered appropriate for description and most pertinent to the overall rationale.

The forty-five parameters fall into nine major categories. For the sake of brevity, these nine major categories will be listed with a few comments regarding the parameters within each category.

1. Identification - This category includes information on the source and information content of the structural failure data available.

2. Structure Characteristic Information - This category includes all information related to the structure that experienced the failure. The dates of construction and failure are recorded along with general structural, material, and functional characteristics of the structure. The geometrical dimensions of the structure along with those of the failed portion of the structure are also recorded.

3. General Failure Description - This category describes the cause of the failure, the extent of the failure both in qualitative and quantitative terms, the nature of the failure in terms of progressive or nonprogressive characteristics, horizontal or vertical characteristics, the total time of the failure, and the stages of failure.

4. Global Failure Description - For failures in which a major portion of the overall structure has failed, the failure takes on a global nature. This is subsequently described by three parameters naming elements of the structures that failed, modes of failure, and material composing the failed elements of the structure.

5. Local Failure Description - A failure of a structure may include a small portion of the overall structure in which case the failure takes on a local nature. The same three parameters as for the global failure description provide for the local failure description.

6. Global Load Description - Loading on a structure that is over a large portion of the structure may be termed a global load. It is described in terms of four parameters including identification, general dimensions, a general statement, and estimated value if this is available or able to be deduced.

7. Local Load Description - Loading on a structure that is over a small portion of the structure may be termed a local load. The same four parameters as in the case of global load description describe the local load.

8. Load-Failure Relationship - In most instances of structural failure, there exist a general spatial relationship between load and failure. This relationship may be expressed in terms of local load-local failure, global load-local failure, local load-global failure, global load-global failure. This parameter provides insight into the nature of the extent of the loading and the corresponding failure.

9. General Statement - This final parameter group consisting of one parameter is a general statement about the failure and its cause.

Here again it is well to remind the reader that structural failure does not relate well to phenomenological description because of its complexity. The categories of parameters and the parameters themselves provide for an overall view of the structural failure process. Given data on structural failure, the parameters of $S(\underline{t}, \underline{r}, \underline{a})$ can be evaluated and $S(\underline{t}, \underline{r}, \underline{a})$ better defined. The statistical techniques to be discussed in the next section are applied directly to the parameters of $S(\underline{t}, \underline{r}, \underline{a})$.

Extensions of this scheme for structuring failure data will be discussed in the last section of this paper.

BASIC CONSIDERATIONS FOR STATISTICAL ANALYSIS

The nature of the problem under consideration and breadth of the field of statistics make it possible to consider only a few topics in relating statistical methods to the datum within the framework of the load and failure generalized random processes discussed above.

One of the first considerations in applying statistical methods to data of the processes above is an examination of the way in which data is measured. There exist four acceptable statistical data measures by which the measure of data is defined (2)(3). Listed in order from least to most powerful they are as follows: nominal, ordinal, interval, and ratio. A brief description of each is in order. The nominal measure applied to data implies the data may be categorized according to a set of mutually exclusive conditions. The ordinal data measure applied to data implies there exists an order relationship amongst pieces of the datum. The interval data measure applied to data implies a relationship of the form

$$x - y > 0 \ , \ x - y = 0 \ , \text{ or } x - y < 0$$

exists between any two pieces of datum. The data is in some way commensurable. Finally, the ratio data measure applied to data implies numerical relationships for the datum are available and for $y \neq 0$, x/y is a meaningful expression between any two pieces of datum. The data is numerically commensurable.

Although there are a number of ways of dividing statistical methods into categories for purposes of this discussion perhaps the categories distribution and distribution free will suffice. Distribution related statistical methods, in general, correlate with instances in which finite parameter distribution functions may be utilized in the statistical analysis of the data. Distribution free related statistical methods, in general, correlate with instances in which lesser restrictions are imposed upon conditions that must be satisfied for application of the method to a given set of data. These statistical methods may be further subdivided into methods concerned with point estimates of parameters, confidence regions for parameters, or significance tests for parameters.

In the illustrative examples to follow, distribution free statistical methods are applied to both load data and failure data. In general, distribution related methods apply well to load data because of its tendency to be describable in terms of the ratio data measure and distribution free related statistical methods apply well to structural failure data because of its tendency to be describable in terms of data measures less powerful than the ratio measure.

In work to date emphasis has been placed on consideration of structural failure data. It has become important to consider categorical distribution free statistical techniques for use on parameters of the structural failure random process. Categorical techniques are most applicable because structural failure data is for the most part of a categorical nature. Distribution free techniques are most applicable because of the difficulty in determining the distributions and their related parameters because of lack of large amounts of data.

It is found useful when considering the structural failure generalized random process to construct a statistical method-process parameter matrix whereby statistical methods applicable to given process parameters are correlated one to another. Table 1 below provides a segment of this matrix.

The construction of the matrix in Table 1 leads naturally to an assessment of the overall information content of a set of data based upon an evaluation of factors useful in defining the overall characteristics of a statistical method (4). Table 2 lists factors useful in evaluating the effectiveness of a statistical method along with proposed weights for these factors. The overall information content of a set of data is determined by associating a set of statistical techniques with the data and proceeding to tabulate weight values for the various factors. A relative measure of information content amongst sets of data is obtained.

There exist several major weaknesses in the approach. First, not all statistical methods may be accurately evaluated in terms of these factors. Second, it presumes that one has selected an optimal set of statistical methods to operate on a given set of statistical data. Third, it presumes that data information content is related to abstract measures on the statistical method independent of the data. Finally, it assumes the

weighting factors are accurate and constant over the ranges of statistical methods. Even though these weaknesses exist, a matrix relating statistical method versus weighting factor provides a crude measure of the relative information content of a set of data to which the statistical method may be applied.

ILLUSTRATIVE EXAMPLES

The examples in this section of the paper are illustrative in the sense that (a) they are not based upon all the data that is available and (b) they present a rather new approach in the reduction of civil engineering data. The first point is a result of the preliminary nature of this work and ability to reduce only a portion of the data available. The second point refers to the use of distribution free statistical techniques on categorical data. In general, measurement distribution oriented statistical techniques are used on numerical data resulting from a well controlled experiment. The results of the statistical analysis are then presented in some concise form. Categorical distribution free statistical techniques require data to be categorized and are often times related to a statistical hypothesis test which may or may not be related to a parameter describing the data, e.g., trend or randomness of data may be under investigation.

It is also well to point out that the conclusions drawn from the illustrative example may seem trivial, however, each example conclusion presents only a minute piece of information extending that which is already known about the case under investigation. That is to say, the effectiveness in use of techniques in this way comes by way of construction of an overall view of the case by means of statistics. This implies application of many statistical techniques in many different ways to the data available. Fortunately, once a data base has been constructed and the statistical techniques selected, this becomes a rather simple and automatic procedure.

Example 1. The first illustrative example concerns correlation of external wind pressure coefficient with structure configuration. Wind tunnel data given in Table 3 (5) relates the external wind pressure coefficient on four sides of a structure (from wind blowing at two different angles of incidence to a reference face of the structure, Figure 1) to the relative dimensions of the structure. A measure of the structure configuration is taken as the "relative volume" of the structure defined by

$$V = hbL/(\max\{h, b, L\})^3.$$

Utilizing a variation of Spearman's Rho test for a measure of correlation between V and the external pressure coefficient, the results of the rank correlation coefficient computation are shown in Table 4.

A few observations that may be made on the basis of this single analysis are as follows:

(1) Positive correlation, i.e., large V associated with large Cpe, on walls denoted A, B $\alpha = 0°$ and A', B', C' $\alpha = 45°$ and negative correlation, i.e., large V associated with small Cpe, on walls denoted C, D $\alpha = 0°$ and D' $\alpha = 45°$,

(2) A lower degree of correlation between V and Cpe when Cpe is negative,

(3) In the case of wall C, C', there is a change in sign of correlation coefficient with change in angle of incidence of wind,

(4) The correlation between V and Cpe is in no instance very strong.

Example 2. From some data available on failure of structures (6), the cause of failure of structures has been placed into one of sixteen categories, as presented in Table 5. Table 5 also presents the empirical distribution of causes for some 88 cases of failure. In order to establish a distribution function for cause, attempts are

made to fit a uniform distribution curve and an arbitrary distribution curve to the data of Table 5. The chi-square goodness of fit test is utilized in both instances.

A formal statement of the problem for the case of uniform distribution fitting is as follows:

$$H_o : F(x) = F^1(x) \qquad \text{All } x$$

$$H_1 : F(x) \neq F^1(x) \qquad \text{At least one } x$$

where

$F^1(x)$ is a uniform distribution over all values of x.

Utilizing the chi-square goodness of fit test, H_o is rejected at all meaningful levels of significance. This is not surprising from an examination of the data. In the case of an empirical distribution fit to the data of Table 5 again, a formal statement of the case is as follows:

$$H_o : F(x) = F^1(x) \qquad \text{All } x$$

$$H_1 : F(x) \neq F^1(x) \qquad \text{At least one } x$$

where

$F^1(x)$ is an arbitrary distribution function over all values of x given in Table 6. $F^1(x)$ is similar to the distribution function for the normal distribution.

Utilizing the statistic

$$T = \sum_{j=1}^{8} \frac{(O_j - E_j)^2}{E_j}$$

and after combining expected frequencies, causes, and observations consistent with the statistical method and computing T on the basis of data in Table 6, one finds

$$T = 5.6.$$

The arbitrary empirical distribution fits the data well and H_o is accepted at the 100l level. It should be noted that combining of failure of structure causes and observations implies a transformation of the original data. Care must be exercised in interpreting the empirical distribution curve fit to the data.

Example 3. The final illustrative example examines the relationship between load and failure in terms of the qualitative terms local and global. A 2 x 2 continuing table made up of 86 pieces of datum is shown in Table 7 with a key for identification of the variables and their values. The hypothesis for McNemar test for significance of change applied to the contingency table in Table 7 may be stated as follows:

$$H_o : P(X_i = 0) = P(Y_i = 0) \qquad \text{All } i$$

$$H_1 : P(X_i = 0) \neq P(Y_i = 0) \qquad \text{All } i$$

or

$$H_o : P(X_i = 1) = P(Y_i = 1) \qquad \text{All } i$$

$$H_1 : P(X_i = 1) \neq P(Y_i = 1) \qquad \text{All } i$$

In a physical sense in the first set of hypotheses, H_o states that the probability of a local load is equal to the probability of a local failure and H_1 the negation of this for all observations of load and failure. In the second set of hypotheses H_o states that the probability of a global load is equal to the probability of a global failure and H_1 the negation of this for all observations of load and failure. Application of the McNemar test statistic rejects both hypotheses H_o at the .001 level. It should be noted that in the McNemar test for significance, an inner consistency in the data must be assumed. This is difficult to verify for the data available.

The use of contingency tables for categorical data is an important key to a consistent approach to examination of load and failure data.

CONCLUSION

The above represents a very preliminary basis for a statistical examination of the load and failure of structures and a rational approach to examining available information related to loading criteria. The next stage in the development will consider construction of a data base of available data along with establishing a broader group of statistical techniques. This should lead to the consideration of mathematical pattern language in the correlation of collected data and in the utilization of appropriate statistical techniques on the collected data. In addition, it is anticipated that more advanced mathematical techniques, e.g., in the area of combinatorial methods will be used for investigating general relationships amongst the diverse pieces of datum.

The ideas expressed above form a basis for a rationale for the examination and selection of load criteria. The rationale is based upon a consistent and thorough statistical analysis of available load data and failure data. Given the statement S representative of a statement of load criteria, the validity of S is deduced from the consistent and thorough statistical analysis of all available data. Work to date described above is a first step in the rationale development.

ACKNOWLEDGMENT

The author would like to express his appreciation to Dr. W.E. Fisher of the Structural Mechanics Branch at CERL and CERL for their support during this study.

REFERENCES

1. Merritt, R.G., "A Statistical Approach to Loading and Failure of Structures," CERL Technical Report to be published.

2. Conover, W.J., Practical Nonparametric Statistics, John Wiley and Sons, Inc., 1971.

3. Stevens, S.S., "On the Theory of Scales of Measurements," Science, 103, pp. 677-680.

4. Walsh, J.E., Handbook of Nonparametric Statistics, Vol. I, D. VanNostrand Company, Inc., 1962.

5. "Wind Forces on Structures," Final Report, Task Committee on Wind Forces Committee on Loads and Stresses, ASCE Paper No. 3269, Transactions of ASCE, Vol. 126, Part II, 1961, pp. 1124-1198.

6. McKaig, T.H., Building Failures, Case Studies on Construction and Design, McGraw-Hill, 1962.

TABLE 1

STATISTICAL METHOD - FAILURE PROCESS PARAMETER MATRIX

FP \ SM	1	2	3	4	5
6	X	X	X		
7	X	X		X	
8	X	X		X	
9					

Key:

Failure Parameter (FP)	Statistical Method (SM)
6 Descriptive Name	1 Binominal Test
7 Construction Date	2 Chi-Square Test for Goodness of Fit
8 Failure Date	3 Wald-Wofowitz Runs Test
9 Structural Characteristics	4 Quantile Test

TABLE 2

FACTORS FOR EVALUATING THE EFFECTIVENESS OF A STATISTICAL METHOD WITH WEIGHTS

Statistical Data Measure	(10)
Nominal	2
Ordinal	4
Interval	6
Ratio	10
Sample Size	10
Data Transformation and Restrictions on Data Parameters	2
Level of Computational Effort	2
Extent of Use of Symmetry	2
Sensitivity of Procedure to Assumptions	4
Precision Level	(10)
Exact	10
Theoretical Approximate	7
Judgment Empirical	4
Efficiency of Method	10
Consistency of Method	10
Sensitivity of Procedure to Assumptions and Difficulty in Verifying Assumptions	10
Population Properties and Importance Amongst Other Data Groups	5

TABLE 3

STRUCTURAL CONFIGURATION AND EXTERNAL PRESSURE COEFFICIENT Cpe
AT ANGLES OF INCIDENCE OF 0° AND 45°

		α = 0°				α = 45°			
h:b:L	V	A	B	C	D	A'	B'	C'	D'
1:1:1	1.00000	.9	-.5	-.6	-.6	.5	-.5	.5	-.5
2.5:2.5	0.20000	.9	-.5	-.7	-.7	.6	-.5	.4	-.5
2. :2.5	0.20000	.9	-.5	-.7	-.7	.6	-.5	.4	-.4
2.5:2.5	0.20000	.9	-.5	-.8	-.8	.6	-.5	.4	-.4
1:4:4	0.25000	.9	-.3	-.4	-.4	.5	-.4	.5	-.4
1:8:16	0.03125	.8	-.5	-.5	-.5	.5	-.5	.4	-.3
2.5:1:1 p	0.16000	.9	-.6	-.7	-.7	.5	-.5	.5	-.5
2:1:2	0.50000	.9	-.5	-.8	-.8	.6	-.5	.4	-.4
1:2.4:12	0.10667	.9	-.5	-.6	-.6	.5	-.6	.4	-.4
1:1:5	0.04000	.9	-.5	-.6	-.6	.5	-.8	.4	-.5

TABLE 4

RANK CORRELATION COEFFICIENT OF STRUCTURAL CONFIGURATION
AND EXTERNAL PRESSURE COEFFICIENT

Variables	Correlation Coefficient
V-A	.41
V-B	.32
V-C	-.25
V-D	-.25
V-A'	.36
V-B'	.61
V-C'	.42
V-D'	-.20

TABLE 5

FAILURE OF STRUCTURES CAUSE WITH EMPIRICAL DISTRIBUTION

Failure of Structure Cause	1	2	3	4	5	6	7	8	9	10	11	12	13	14	15	16
Observations	1	21	0	2	7	1	5	15	0	7	15	0	5	2	7	0

Key: Failure of Structure Cause

1 Unknown

2 Structural

3 Material

4 Functional

5 Workmanship

6 Structural and Material

7 Structural and Functional

8 Structural and Workmanship

9 Material and Functional

10 Material and Workmanship

11 Functional and Workmanship

12 Structural, Material and Workmanship

13 Structural, Functional and Workmanship

14 Material, Functional and Workmanship

15 Structural, Material and Workmanship

16 Structural, Material, Functional and Workmanship

TABLE 6

EMPIRICAL DISTRIBUTION FUNCTION WITH DENSITY FUNCTION AND EXPECTED FREQUENCY OF OCCURRENCE FOR N = 88 CASES

x	$F^1(x)$	$f^1(x)$	$E_j = f^1(x)N$		Failure of Structure Cause	Observations, O_j	
1	0.0005	0.0005	.004		3	0	
2	0.0010	0.0005	.004		9	0	
3	0.0100	0.0090	.792	7.040	1	1	8
4	0.0300	0.0200	1.760		4	2	
5	0.0800	0.0500	4.400		7	5	
6	0.1800	0.1000	8.800		5	7	
7	0.3200	0.1400	12.320		10	7	
8	0.5000	0.1800	15.840		8	15	
9	0.6800	0.1800	15.850		2	21	
10	0.8200	0.1400	12.320		11	15	
11	0.9200	0.1000	8.800		15	7	
12	0.9700	0.0500	4.400		13	5	
13	0.9900	0.0200	1.760		14	2	
14	0.9990	0.0090	.792	7.040	6	1	8
15	0.9995	0.0005	.044		12	0	
16	1.0000	0.0005	.044		16	0	

TABLE 7

2 x 2 CONTINGENCY TABLE FOR LOAD-FAILURE RELATIONSHIP

	Y = 0	Y = 1
X = 0	4	33
X = 1	4	45

Key: Load and Failure Type

Local Load X = 0 Global Load X = 1

Local Failure Y = 0 Global Failure Y = 1

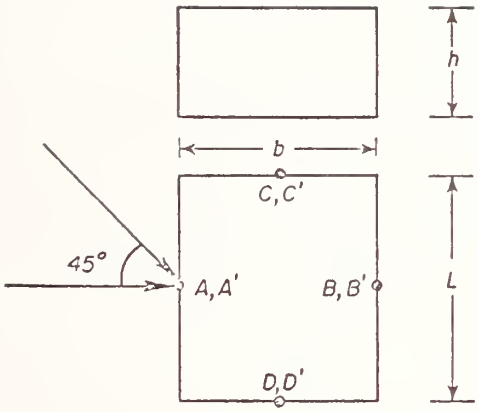

FIGURE 1 STRUCTURAL CONFIGURATION FOR WIND PRESSURE COEFFICIENTS

SYNTHETIC EXPERIMENTAL RESEARCH ON THE DUCTILITY OF SHORT REINFORCED CONCRETE COLUMNS UNDER LARGE DEFLECTION

by

Kiyoshi Nakano
Head of the Third Division
Building Research Institute
Ministry of Construction, Japan

Masaya Hirosawa
Chief Researcher of the Third Division
Building Research Institute
Ministry of Construction, Japan

In general, short reinforced concrete columns will fail in a brittle manner. In order to create and establish better ductility in such columns, a synthetic research experimental program has been conducted. This program consisted of the testing of 125 short column specimens, subjected to multi-cycles of flexure-shear loadings. The result from these tests indicate the following:

1) The ductility of structural members is influenced by shear, bond, and buckling of the compression bars.

2) To prevent buckling of compression reinforcement, under small curvature, the spacing of the web reinforcement must be controlled.

3) In order to prevent a shear failure of structural members within reasonable ductility, an effective set of restrictions on the combination of axial force, tensile reinforcement ratio, and shear span ratio are required.

4) The bond failures which were observed in the test members, where deformed bars were used as axial reinforcement, consisted of bond-splitting of the cover concrete. The conventional method, which uses bond strength as an index to verify bond failure, is not effective for the bond-splitting failure mode. It is, therefore, necessary to restrict the tensile reinforcement ratio in order to prevent this type of bond failure.

Key Words: Column; ductility; earthquake; reinforced concrete; shear tests; structural engineering; web reinforcement.

INTRODUCTION

In a country such as Japan, where severe earthquakes occur often, the structural safety of buildings is governed largely by earthquake design criteria.

Due to the results obtained from many strong motion earthquakes and relative to response analyses and earthquake damage observations, it has become gradually clear that the actual influence of earthquakes on structures is more severe than the simulated earthquake load which is designated in many countries as a design seismic force coefficient. In fact, during the 1968 Tokachi-Oki earthquake, several buildings, which had yield shear coefficients greater than 0.5, were destroyed.

In general, it is not practical to construct all buildings strong enough so they can resist severe shocks as controlled by their load-carrying capacities. However, it is possible to construct ductile buildings with appropriate load-carrying capacity and rigidity, which can survive severe shock.

Reinforced concrete buildings constructed in Japan are designed with a seismic shear coefficient of 0.2 or greater, however, the resulting ductility factors required to resist severe earthquake shocks does not seem excessively large. Therefore, a synthetic experimental research project was initiated to determine how to make reinforced concrete short columns ductile.

This research was sponsored by the Ministry of Construction and a committee was thus organized to execute this project. This committee consists of members selected from various research organizations belonging to government, universities, and private firms.

In this report, the failure modes and the factors which affect the ductility are disdussed based on results of tests of 125 specimens.

OUTLINE OF EXPERIMENT

Objective and Master Plan of Experiment

The objective of this synthetic experimental research was to obtain quantitative design criteria to insure that reinforced concrete columns are ductile.

The mean unit axial compressive stresses in the first story columns of reinforced concrete buildings in Japan due to permanent load is about 40 kg/cm^2. Assuming a value of 0.4 as the yield shear coefficient, the mean unit shearing stresses during a severe shock are generally less than 20 kg/cm^2. The quantity of web reinforcement required to meet the above stress conditions will not cause construction difficulties during fabrication of the columns.

However, as columns are the most important of the various structural members, it is preferable to keep them ductile even under the maximum shear force expected during severe earthquake shocks. The maximum shear force corresponds to the shear force that is present when the column yields at both ends.

Therefore, the combinations of the ratio of tensile reinforcement and shear span ratio were first selected so that their maximum shear capacities did not become excessively large under constant axial load, which corresponded to a value of 40 kg/cm^2. Next, the reinforcing details such as quantity, spacing shape of web reinforcement, and axial bar arrangement were examined experimentally in order to induce a ductile condition.

The standard shear span ratio that was adopted was intentially small and thus contradicts the characteristics relative to a ductile condition.

Outline of Test Series and Specimens

A. Variable Factors

Based on the past experimental and research results, the committee selected ten variables as those factors which effect ductility. These factors are shown in Table 1 and are listed as F1 to F10. The values and characteristics of some of the variables shown in Table 1 were determined from previous investigations which were conducted on various existing reinforced concrete buildings.

The selection of the standard size of cross-section, web reinforcement ratio, loading hysteresis and loading apparatus was then determined, as will now be described

1) Scale Effect

Reliable data relative to the scale effects on concrete columns is scarce. Also, due to limitation in budget and facilities, it is often impractical to conduct full-scale tests. Therefore, the size of the main test cross-section that was selected was 25 square cm. Also, a series of 50 square cm sections was tested to investigate the scale effect.

2) Web Reinforcement Ratio

The method to be used for calculating a reasonable web reinforcement ratio, in order to obtain ductile columns, has to date not been established. Therefore, it was tentatively decided to use Arakawa's minimum equation to set the standard web reinforcement ratio. This experimental equation determines the minimum required shear strength of reinforced concrete members when not subjected to an axial force. This equation is used as a basis for the regulations of A.I.J. code for shear reinforcement. That is, one of the standard values of the web reinforcement ratio was tentatively set as P_{w_1} which can be obtained by substituting the flexure capacity, cQ_{BU}, equal to the shear force, given in Arakawa's minimum formula. Half of the P_{w_1} value was also adopted as part of the standard.

3) Loading Excursion

Until a rational dynamic method has been established for estimating the seismic properties of structural members, it is difficult to evalute these properties from the results of special vibration tests. However, some standard static cyclic loading method must be adopted in the test program. Therefore, a multi-cycles alternate loading method, as shown in Figure 1, was adopted as a standard loading excursion. This loading pattern was selected for the following reasons:

a) The ductility factors determined from a response analyses of medium height buildings during severe shocks is approximately three or four providing their strength and rigidity is not excessively small.

b) The number of acceleration responses which correspond to approximately 80% of the maximum has been reported to be of the order of ten.

c) The structural characteristics of members under alternate cyclic loading at constant deflection is usually determined within ten cycles of the loading.

4) Loading System

In most past experiments, simple beam systems were used as the loading system for the structural members. However, this method is not acceptable for the investigation of the seismic behavior of reinforced concrete columns because of the following reasons:

a) When discussing shear and bond problems in members, a restrained beam type is better than simple beam type in simulating the real condition of columns in actual buildings during an earthquake.

b) Both ends of the column sections should be kept parallel and without inclination with respect to each other to simulate the actual conditions.

c) In discussing the characteristics and effects of large deformations, it is preferable that the influence of additional moment due to eccentric axial load be easily estimated.

d) It is preferable to impose many cycles of load reversals and that the developing cracks be easily observed and recorded.

A new loading apparatus, as shown in Figure 2, was developed and was used to test the series of columns. In order to discuss the influence of the loading systems, two test series were also conducted on continuous beams.

B. Typical Series and Specimen Details

On the basis of the previous discussions, it was decided that a typical series should consist of a total of fifteen specimens. Each series was subdivided into types, dependent on the variables to be investigated. For example, three specimens were a function of P_t, two specimens were dependent on σ_o, two specimens relative to M/QD, and two a function of P_w. A list of the specimens relative to a typical series is shown in Table 2.

In the other series, each common factor, for example, C^{σ_B} or size of section, etc., was systematically varied. Figure 3 shows an example of the details of the specimens.

To date, ten series, a total of 165 specimens, have been tested, as detailed in Table 3. The results on the first seven series of these tests will be discussed in this report. In Figures 4a to 4d, the frequency distributions of P_t, σ_o, M/QD, and P_w of the 125 specimens are shown with their failure modes and estimated grade of ductilities.

OUTLINE OF TEST RESULTS

Failure Mode of Tested Specimens

The following will describe the typical failure modes that were observed during the testing of these specimens:

1) Shear failure prior to or after flexure yielding (Notation of mode; S·SC, F·SC, S·DT, S·ST, F·ST). This mode can be divided into shear tension failure including diagonal shear tension failure and shear compression failure.

2) Bond split failure prior to or after flexure yielding (B·B, F·B).

3) Compression failure of concrete after flexure tensile yielding with or without compression steel buckling (F, F·C, $F \cdot C \cdot B_u$).

Classification of Ductilities

When discussing the deflection abilities of structural members, the critical angle of rotation of the members or the critical deflection is called the ductility and is used as an index.

In this report, the test results were classified by the ductilities, as defined in Table 4.

Relationship Between Failure Modes and Estimated Ductilities

The test results of 125 specimens were classified by their failure modes, estimated ductilities, and their interrelationships and frequencies, as shown in Figures 5a and 5b. As observed in these figures, the most ductile failure mode is type F·C followed by type SC.

Many specimens failed in the type ST mode and type B mode, which indicated poor ductilities. Accordingly, one of the most important subjects then is to determine how to prevent such brittle failures as revealed by failure mode types SC, ST, and B.

The resulting shear force-deflection relationships, cracking patterns, and deteriorations of the load-carrying capacity of typical specimens are shown in Figures 6, 7, and 8.

DISCUSSION ON TEST RESULTS

Steel Buckling

Buckling of the compressive reinforcement was observed during testing of 32 specimens and failed in type F·C mode. Ten of the specimens buckled with a ductility factor equal to 2∿4, and thus caused deterioration of the load-bearing capacity. The test results of these specimens indicate the following:

1) The length of steel which buckled, ℓ_k, was approximately 1∿2 times the spacing of the web reinforcement, S. In the case of spiral hoops and welded square hoops, ℓ_k was nearly equal to S.

2) The slenderness ratio, λ, was calculated for each specimen assuming $\ell_k = S$. The relationship between λ and the angle of rotation of the member at the buckling load R_{BU} was determined relative to those specimens which did not fail in bond or shear. These results indicate that when $\lambda \geqq 34$, the buckling load $R_{BU} \cong \frac{1}{100} \sim \frac{1}{50}$, however, when λ is less than 34, steel buckling did not commence until fairly large deformations occurred.

3) Thus, when $\lambda \geqq 34$, the web reinforcement spacing $S \leq 8\phi$, where ϕ is the diameter of the compression bar.

4) In conclusion then, the spacing of web reinforcement at a column end should be less than eight times the diameter of the axial bar reinforcement.

Discussion on Shear Failure Mode

During the testing of the specimens, 41 failed in shear prior to or after flexure yielding. Nineteen of the 41 specimens failed in shear compression, ten of the specimens failed due to diagonal shear tension and twelve failed in shear tension.

Consideration of the Use of Arakawa's Formula

As there are no quantitative equations which relate the ductility of members to the web reinforcement ratio, the failure mode considering Arakawa's formula was used. This equation was adopted as the basis for calculating the web reinforcement in the specimens.

The relationship between the observed ductility and the ratio of calculated shear strength, cQ_{ARA}, was studied in relationship to the calculated flexure strength, cQ_{BU}. The formulas that were used to calculate cQ_{ARA} and cQ_{BU} are given as Equations

(1) and (2). All of the test results, with the exception of 52 specimens which failed due to bond-splitting, are shown in Figure 9. As observed from this figure, the estimated ductility in which cQ_{ARA}/cQ_{BU} is greater than one are for cases A or B. When the ratios are less than one, the estimated ductility results are referenced to cases C or D. It should also be noted that as τ_{max} increases, the ductility tends to become poor.

$$cQ_{ARA} = \left\{ \frac{0.0754\ p_t^{0.23} k_u (c\sigma_B + 180)}{M/Q + 0.12} + 2.7\sqrt{p_w \cdot s\sigma_{wy}} \right\} x \frac{7}{8} bd \qquad (1)$$

where

$$k_u = 0.80(d = 21.5\ cm),\ 0.72(d = 43\ cm)$$

$$cQ_{BU} = \{ a_{t.s.y.g} + 0.5\ ND(1 - \frac{N}{bDc\sigma_B}) \}/A \qquad (2)$$

Diagonal Tension Failure

Initially, the diagonal tension cracking load, Q_{DTC}, was investigated. Thus, theoretical load value (cQ_{DTC}) was obtained by assuming the principal tensile stress equal to $1.8\sqrt{c\sigma_B}$. This stress was calculated at the center of the section, neglecting the appearance of other cracks, and the influence of the axial bars. This results in the following:

$$cQ_{DTC} = \frac{c\sigma_t}{1.5} bD \sqrt{1 + \sigma_0/c\sigma_t} \qquad (3)$$

The ratio of test variable (TQ_{DTC}), to the calculated values (cQ_{DTC}) for 23 specimens, in which diagonal tension cracks appeared, varied from 0.66 to 1.13 with an average value of 0.87.

Next, the critical web reinforcement, (P_{wDTC}), was calculated by assuming the web reinforcement carries the diagonal tension, which was initially carried by the concrete before the appearance of the crack. This results in the following:

$$P_{wDTC} = \frac{c\sigma_t}{\cos\theta \cdot s\sigma_{wy}} \qquad (4)$$

where

$$\theta = \frac{1}{2} \tan^{-1}(2\sqrt{c\sigma_t/\sigma_o + (c\sigma_t/\sigma_o)^2}) \qquad (4a)$$

The values of (P_w/P_{wDTC}) vs. (TQ_{max}/cQ_{DTC}) excluding those test specimens which failed due to bond-splitting have been plotted, as shown in Figure 10. The terms TQ_{max} and P_w represent the tested maximum shear strengths and the web reinforcement ratio, respectively.

It can be observed from this figure that the specimens, which have a value of TQ_{max} greater than 0.8 times (cQ_{DTC}) and (P_w) and less than (P_{wDTC}), show a diagonal tension failure mode.

Shear Tension Failure

The initial shear tension cracking load, (Q_{STC}), was first examined. The theoretical value (cQ_{STC}) was calculated by using the following formula, which was derived assuming the following:

when $A_1 = A/D < 0.75 + 0.283\ k_o$

$$cQ_{STC} = 0.589\ k_o \cdot c^{\sigma}t \cdot bD \tag{5a}$$

when $A_1 \geq 0.75 + 0.283\ k_o$

$$cQ_{STC} = \{0.78 - 1.04\ A_1 + \sqrt{(0.78 - 1.04\ A_1)^2 + 0.694\ k_o^2}\ \}c^{\sigma}t\ bD \tag{5b}$$

where $k_o = c^{\sigma}t + \sigma_o/c^{\sigma}t$

The ratios of (TQ_{STC}) to (cQ_{STC}) for 119 of the test specimens in which shear tension cracks appeared varied from 0.62 to 1.59 with an average value of 0.91.

The second critical web reinforcement ratio, $(P_{w_{ST}})$, which is required to have the specimens reach flexure strength after the appearance of a shear tension crack, was determined from the following:

$$P_{w_{ST}} = \frac{1.6\ jx_1 \cdot P_t \cdot s^{\sigma}y}{A_1^{1.25} \cdot s^{\sigma}wy} \tag{6}$$

where

$$jx_1 = \frac{d - xn}{D} \doteq d_1 - \frac{\sigma_o + P_t \cdot s^{\sigma}v \cdot A_1^{-0.75}}{0.85\ c^{\sigma}B} \tag{6a}$$

The values of $(P_w/P_{w_{ST}})$ vs. (TQ_{max}/cQ_{STC}), excluding those test values which failed due to bond-splitting, are plotted in Figure 11.

As shown in this figure, there are many specimens which have values of (TQ_{max}) greater than (cQ_{STC}). It is also observed that the specimens with a value of (TQ_{max}) greater than $0.8\ cQ_{STC}$ demonstrated a shear-tension failure mode when (P_w) was less than $(P_{w_{ST}})$.

Shear Compression Failure

Because shear compression failure is primarily caused by crushing of the concrete in the compression zone, it is reasonable to assume that there is a limiting degree of ductility that can be expected, even if the quantity of web reinforcement is increased. The determination of this limitation is difficult to evaluate and was not possible in this report. However, certain trends have been established as will now be described.

To achieve reasonable ductility, it is necessary to maintain the intensity of the axial stresses at the appropriate level. In general, the influence of the shear stress on ductility is not important. Therefore, the distance from the neutral axis to the extreme compressive fiber, X_n, can be determined by neglecting the compression reinforcement in the compression zone and assuming the ratio of tensile principal stress to concrete tensile strength, $(\sigma_1/c^{\sigma}t)$ is calculated assuming that all of shear force is carried only by the concrete in the compression zone at the critical section, thus,

$$X_{n_1} = \frac{X_n}{D} = \frac{N + a_t \cdot s^{\sigma}t}{0.85 \cdot c^{\sigma}B \cdot bD} \tag{7a}$$

$$\sigma_1 = -0.425\ c^{\sigma}B + \sqrt{(0.425\ c^{\sigma}B)^2 + \tau^2} \tag{7b}$$

where

$$\tau = \frac{TQ_{max}}{bX_n} \tag{7c}$$

The third critical web reinforcement ratio, (P_{wz}), was calculated by the so-called truss-analogy, which is used as one of the shear strength theories for beams.

$$P_{wz} = \frac{{}_{T}Q_{max}}{b \cdot j \cdot s\sigma_{wy}} \tag{7d}$$

where

$$j = 0.875\ d$$

The values of ($\sigma_1/c\sigma_t$) vs. X_n, excluding those 52 test specimens exhibiting bond-split failures, were then plotted as shown in Figure 12.

As observed in this figure, many of the specimens which satisfy the following limitation showed good ductility even though P_w may be less than or greater than P_{wz}.

$$\frac{\sigma_1}{c\sigma_t} + 6\frac{X_n}{D} \leq 3 \tag{8}$$

Using these results, the value corresponding to the left side of Equation (8) was calculated for each specimen. Relationship between the above value and (P_w/P_{wz}) are shown in Figure 13. Clearly shown on this figure are the zones of the shear-tension failure modes, the shear-compression failure modes, and the flexure-compression failure modes.

If a design control, as given by Equation (8), can be refined through more rigorous tests and study, it may be possible to provide a limitation on the effective web reinforcement ratio and a combination of P_t, σ_o, and M/QD within which the web reinforcement is not effective.

Bond-Splitting Failure

A distinguishing feature of the experimental results was the presence of bond-splitting failures of various test specimens. This type of failure mode occurred in 52 specimens and was observed in those specimens which had high tensile reinforcement ratios. The tensile reinforcement ratio (P_t) was 0.95% for 47 specimens and 46 specimens showed this type of failure mode.

For those specimens which failed in this mode, a small inclined crack first appeared at the position of the tensile bar close to the end of the so-called shear crack. As the number of cyclic loadings increased or as the horizontal deflection increased, similar cracks progressed in number near the center of the specimen. Spalling of the concrete cover then commenced and the shear capacity of the specimen decreased. Thus, this initial small inclined crack, called a bond-splitting crack, was considered to be the triggering mechanism for this type of failure mode.

The shear force and bond stress at a point on the tensile bar at a distance "d" of the member, where the shear force corresponds to this initial crack, (cQ_{BO}), may be obtained by setting the principal tensile stress equal to ($c\sigma_t$), as caused by the bending moment;

$$cQ_{BO} = \frac{-c\sigma_t \cdot B + \sqrt{c\sigma_t{}^2 \cdot B^2 + 4C^2(c\sigma_t{}^2 + c\sigma_t \cdot \sigma_o)}}{2C^2} \text{ (kg)} \tag{9}$$

where

$$C = \frac{1}{1.75\ n' \cdot b' \cdot d} + \frac{6.1(D \cdot dt - dt^2)}{Ie\ b \cdot D^3}$$

$$B = \frac{(M/Q - d) \cdot D}{2Ie}, \quad c\sigma_t = 1.8\sqrt{c\sigma_B}$$

b' = Minimum value as given by $(2\sqrt{2}\ dt - \phi_o)$ and $\dfrac{b - \sum\phi_o}{n'}$

n' = Number of tensile reinforcement bars

ϕ_o, $\sum\phi_o$ = Diameter of the tensile reinforcement and the summation, respectively

I, Ie = Moment of inertia with and without the effect of the bars, respectively

Comparison of the calculated to the test results, (TQ_{BO}), are shown in Figure 14. As shown in this figure, (TQ_{BO}) generally is greater than (cQ_{BO}) as (M/QD) and (P_t) decrease and as (σ_o) increases. However, the influence of the web reinforcement ratio cannot be perceived.

Next, the ratio of (cQ_{BU}/cQ_{BO}) vs. the ratio of (F_{max}/F_{al}) for all of the test results are plotted in Figure 15 in accordance to their failure mode and ductility. The terms, F_{max} and F_{al}, represent the maximum test results of the mean bond stress and the allowable bond stress in accordance with the A.I.J. (Architectural Institute of Japan) code. As shown in this figure, the value of $(cQ_{BU}/cQ_{BO}0$ has a greater influence on the bond-splitting failure mode than does F_{max}/F_{al}.

Figure 16 shows the relationship between the value of (P_w/P_{wZ}) and the estimated ductility of the specimens, which had failed due to bond-splitting.

As shown in this figure, their ductilities cannot be improved, even if the web reinforcement is increased. However, in those specimens where (σ_B) is greater than 270 kg/cm^2 and when (cQ_{BU}) is less than 1.4 times (cQ_{BO}) and (P_w) and is approximately equal to (P_{wZ}), good ductility can be observed. It is further presumed from their cracking patterns that the confinement of the concrete within the core of the spiral hoops is effective.

CONCLUSION

Multi-cycle flexure-shear tests were conducted on 125 short column specimens; the following items relative to their ductility were observed:

a) The factors which control ductility of a structural column include not only shear, but also bond and buckling of the compression bar.

b) To prevent compression reinforcement from buckling at small curvature, the spacing of the web reinforcement should be less than eight times the diameter of the axial reinforcement.

c) Examination of the bond stress is not an effective means for preventing members from developing a bond-split failure. However, it is effective in keeping the flexure capacity within 1.4 times the initial bond-splitting cracking load, as given by Equation (8). Increasing the number of rectangular-type hoops is not as effective in preventing bond-splitting failure as is using more spiral hoops.

d) When the flexure capacity is more than 0.8 times the diagonal tension cracking load, as given by Equation (3), an effective means in preventing members from developing a diagonal tension failure is to place more web reinforcement than is indicated by Equation (4).

e) When the flexure capacity is more than about 0.8 times the shear tension cracking load, calculated by Equation (5), it is effective to place more web reinforcement that is indicated by Equation (6).

f) There is a limiting combination of (P_t), (σ_o), and (M/QD) where the shear compression failure cannot be avoided, even with an increase in web reinforcement.

This limiting combination is not apparent, however, Equation (8) can be considered to be one such control. When a combination of (P_t), (σ_o), and (M/QD) of the specimens satisfy Equation (8) and when (P_w) is greater than (P_{wZ}), as shown in Equation (7d), good ductility should be achieved. However, there is a possibility that the value of (P_{wZ}) may decrease the ductity.

ACKNOWLEDGMENT

The authors wish to thank the following members of the Reinforced Concrete Structures Committee in B.R.I. for conducting this experimental research and to Mr. M. Ohkubo, Assistant, Tokyo Metropolitan University, Mr. K. Yamamoto, Research Member, and to Fujita Kogyo for helping in the preparations of this report.

Chairman: Y. Higashi, Tokyo Metropolitan University

Members: H. Aoyama, University of Tokyo; Y. Kanoh, Meiji University; M. Fukuhara, Tokyo Institute of Technology; S. Ohmori, Kajima Construction Company, Ltd; S. Yoshizaki, Taisei Construction Company, Ltd.; T. Takeda, Obayashi-gumi Construction Company, Ltd.; Y. Fukada, Shimizu Construction Company, Ltd.; O. Chiba, Toda Construction Company, Ltd.; K. Yamamoto, Fujita Kogyo; I. Yamaguchi, Takenaka Komuten; N. Yanagisawa, Secretary of the Committee

REFERENCES

1. M. Ozaki, M. Wakabayashi, and M. Hirosawa, "Experimental Study on Large Models of Reinforced Concrete Columns," Proceedings of the Fifth World Conference on Earthquake Engineering in Roma, 1973.

2. M. Hirosawa, "Synthetic Research on Preventing Reinforced Concrete Columns from Total Collapse (in Japanese)," Building Research Institute BRI Transactions of Main Research in 1972, 1972.

3. M. Hirosawa, "A List of Past Experimental Results of Reinforced Concrete Columns," Kenkyu Siryo No. 2, Building Research Institute, 1973.

4. The 1971 AIJ Standard for Structural Design of Reinforced Concrete Construction.

NOTATION

b, D	:	width and overall depth of specimen, respectively (cm)
d_t	:	distance from extreme tension fiber to centroid of tension reinforcement (cm)
d	:	distance from extreme compression fiber to centroid of tension reinforcement (cm
g	:	= d - dt (cm)
Pt	:	tensile reinforcement ratio
Pw	:	web reinforcement ratio
$s\sigma_y$	:	yield stress of tensile reinforcement (kg/cm^2)
$s\sigma_{wy}$	:	yield stress of web reinforcement (kg/cm^2)
$c\sigma_B$, $c\sigma_t$	:	compressive and tensile strength of concrete, respectively (kg/cm^2)
Q	:	shear force (kg)
N	:	constant axial force (kg)
σ_o	:	= N/bD (kg/cm^2)
M	:	bending moment at critical section (kg·cm)
A	:	= M/Q (cm)

ADDITIONAL REMARKS

The following analytical studies will be conducted by the committee and authors, the results of which will be presented in the near future;

1. Influence of scale effect, loading system and loading excursion on the ductility of structural members.
2. Quantification of the rational web reinforcement ratio to cause structural members to be ductile.
3. Pursuit of a structural device in preventing the members having split-bond failure.
4. Estimation of hysteresis damping of the test results.
5. A method for estimating the seismic properties of the members by using the results of certain static cyclic loading tests.

TABLE 1 LIST OF FACTORS COMMON TO SPECIMENS

	COMMON FACTORS	NOTE
F1	Section: b x D = 25 x 25 cm, d_t=d_c=3.5 cm	SE Series: b x D = 50 x 50 cm, d_t=d_c=7.0 cm
F2	Concrete: Normal concrete, F_c=210 kg/cm^2 (Design)	FC Series: F_c = 350 kg/cm^2 (Design)
F3	Shape of web reinforcement: Rectangular hoop with a standard hook at each end	PILOT Series: Welded rectangular hoops used in the half of specimens
F4	Web bar: SR24 Round bar	Specified yield point of 2400 kg/cm^2
F5	Axial bar: SD35 Deformed bar	Specified yield point of 3500 kg/cm^2
F6	Tensile reinforcement ratio: p_t=0.34% (3-D10), 0.61% (3-D13), 0.95% (3-D16)	PILOT Series: p_t= 0.41% (2-D13), 1.24% (2-D22) AF Series: p_t=1.38 (3-D19)
F7	Shear span ratio M/QD: M/QD = 1 and 2	PILOT and LS Series: M/QD = 1.5 and 3.0
F8	Axial stress: N/bD = 210/4 and 210/8 kg/cm^2	30 kg/cm^2 (PILOT S.), 0 and -210/10 kg/cm^2 (AF S.)
F9	Web reinforcement ratio: by Arakawa's min. Equation	PILOT Series: by A.I.J. Equation
F10	Loading method: Restrained beam type, reversal loading of multi cycles	WAKABAYASHI-type (PILOT S.), Inverse-Symmetrical-type (LM1, SE S.), B.R.I.-type (other series)

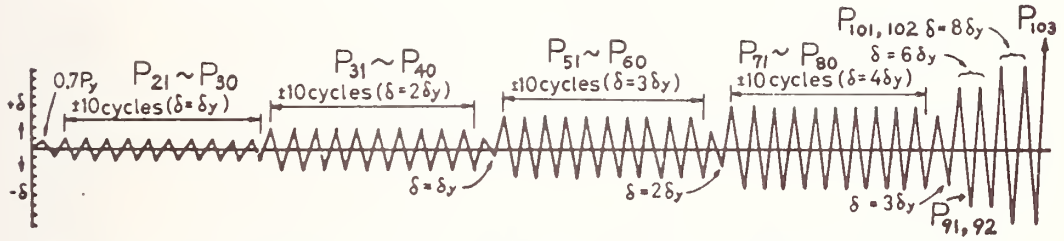

P_{mn}: Load at test equals shear force Q of specimen, (mn; loading number).

P_y: Load when tensile reinforcement yields at test, ($P_y = P_{21}$).

δ_y: Measured horizontal displacement at yielding.

FIG. 1 LOADING PROCEDURE USED IN ALL SPECIMENS

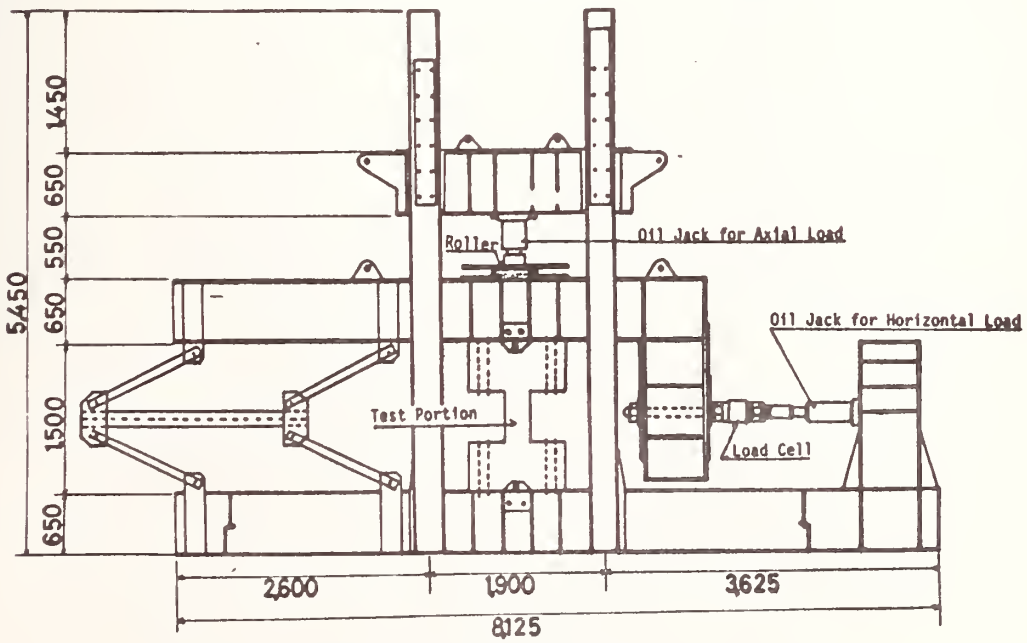

FIG. 2 B.R.I.-TYPE LOADING APPARATUS

TABLE 2 LIST OF SPECIMENS BELONG TO A TYPICAL SERIES

Mark	Tensile Reinforcement	Tensile Reinforcement Ratio	Shear Span Ratio	Web Reinforcement	Web Reinforcement Ratio	Axial Unit Stress
	Number-Size	$P_t = a_t/bD$ (%)	$\frac{M}{Q\,D}$	Number-Size-Spacing (mm)	$p_w = a_w/bs$ (%)	$\sigma_o = N/bD$ (kg/cm^2)
1B	3-D10	0.34	1	16- 9 - 33.3	1.53	210/4
2A	3-D10	0.34	2	15- 9 - 71.5	0.71	210/4
2B	3-D10	0.34	2	17- 6 - 62.5	0.36	210/4
3A	3-D10	0.34	1	10- 9 - 55.5	0.92	210/8
3B	3-D10	0.34	1	11- 6 - 50.0	0.45	210/8
4A	3-D10	0.34	2	10- 4 - 55.5	0.18	210/8
4B	3-D10	0.34	2	10- 4 - 111.1	0.09	210/8
5A	3-D13	0.61	1	12-13 - 45.5	2.33	210/8
5B	3-D13	0.61	1	12- 9 - 45.5	1.12	210/8
6A	3-D13	0.61	2	24- 6 - 43.5	0.51	210/8
6B	3-D13	0.61	2	28- 4 - 37.0	0.27	210/8
7A	3-D16	0.95	2	24- 4 - 43.5	2.44	210/4
7B	3-D16	0.95	2	25- 9 - 41.7	1.22	210/4
8A	3-D16	0.95	2	26- 9 - 40.0	1.27	210/8
8B	3-D16	0.95	2	28- 6 - 37.0	0.61	210/8

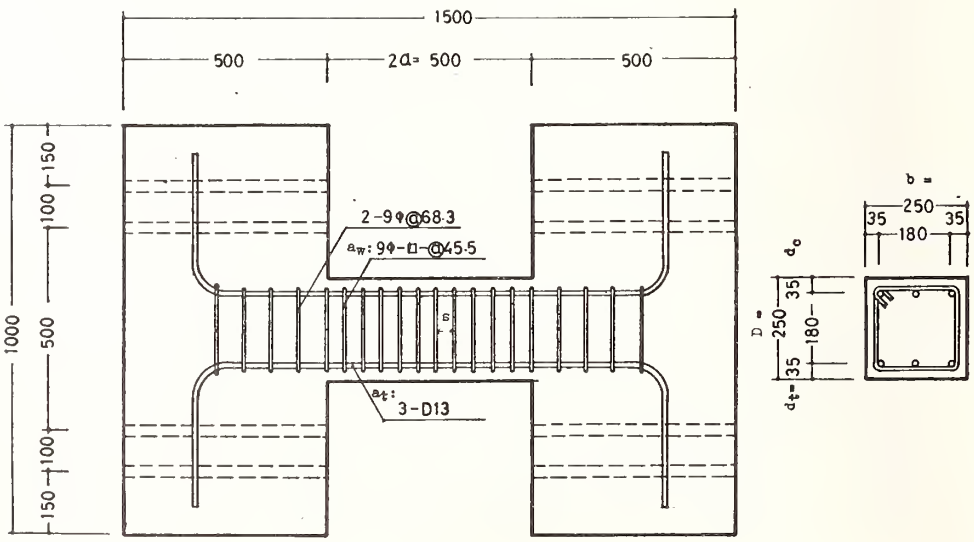

FIG. 3 AN EXAMPLE OF SPECIMEN DETAILS (in mm)

TABLE 3 LIST OF TEST SERIES

Name of Series	Section of Specimen (cm x cm)	Shear Span Ratio (M/QD)	Loading *1 System	Institution *2 in Charge	Year	Main Objective	Number of Specimens
Pilot	25 x 25	1.5, 3.0	W - Type	B.R.I.	1971	Welded Hoop	36
LM1	25 x 25	1.0, 2.0	R,B - Type	T.I. of Takenaka Komuten	1972	Loading System Scale Effect	15
LM2	25 x 25	1.0, 2.0	BRI - Type	Tokyo Institue of Technology	1972	Loading System	15
SE	50 x 50	1.0, 2.0	R,B - Type	Meiji Univ. and B.R.I.	1972	Scale Effect	15
FC	25 x 25	1.0, 2.0	BRI - Type	T.I. of Taisei Const. Co., Ltd.	1972	Concrete Strength	15
WS	25 x 25	1.0, 2.0	BRI - Type	T.I. of Obayashi-Gumi Co., Ltd.	1973	Welded Hoop of Deformed Bar	15
AF	25 x 25	1.0, 2.0	BRI - Type	T.I. of Fujita Kogyo	1973	Axial Force	15
CW	25 x 25	1.0, 2.0	BRI - Type	Tokyo Metropolitan Univ.	1973	Columns with Side Wall	10
WS2	25 x 25	1.0, 2.0	BRI - Type	T.I. of Kajima Const. Co., Ltd.	1973	Spiral Hoop	15
LS	25 x 25	1.5, 3.0	BRI - Type	T.D.C. of Toda Const. Co., Ltd.	1973	Shear Span Ratio	15

*1 W - Type : Loading System devised by Dr. Wakabayashi
R,B - Type : Restrained Beam Type
BRI - Type : Loading System newly developed in B.R.I.

*2 T.I. : Technical Institute
T.D.C. : Technical Development Center

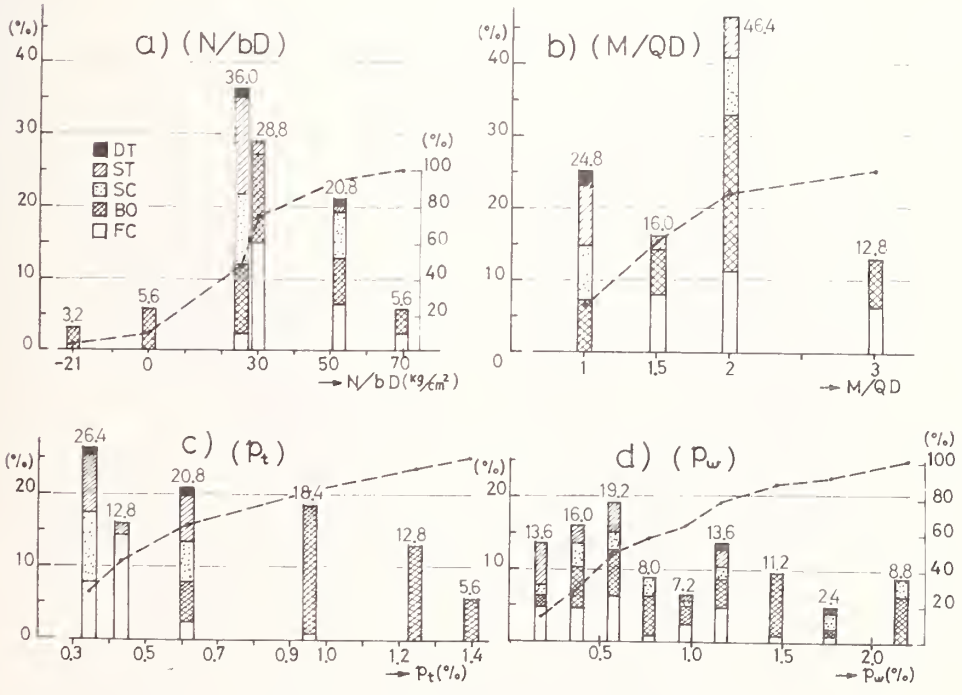

FIG. 4 FREQUENCY DISTRIBUTION OF σ_o, M/QD, P_t and P_w

TABLE 4 CLASSIFIED DUCTILITY

DUCTILITY	CHARACTERISTICS
A	Very ductile columns which failed by shear or by buckling of compression bars at horizontal large deflection. ($P_{21} \sim P_{91} \geq 0.8_{c}Q_{FU}$, $_{c}Q_{FU}$: Flexural strength obtained by A.I.J. formula)
B	Ductile columns, whose deterioration of shear capacity were small untill $\mu = 4$, ($\mu = \delta / \delta y$), but which failed by shear or by bond or by buckling of bar before $\mu = 6$. ($P_{21} \sim P_{71} \geq 0.75_{c}Q_{FU}$)
C	Columns yielded by flexure at first, but deteriorated remarkably due to shear or bond failure or buckling of bars before they reached to large deflection. ($P_{21} \sim P_{31} \geq 0.75_{c}Q_{FU}$)
D	Columns failed by shear or by bond before flexural yielding. (Others than A, B and C)

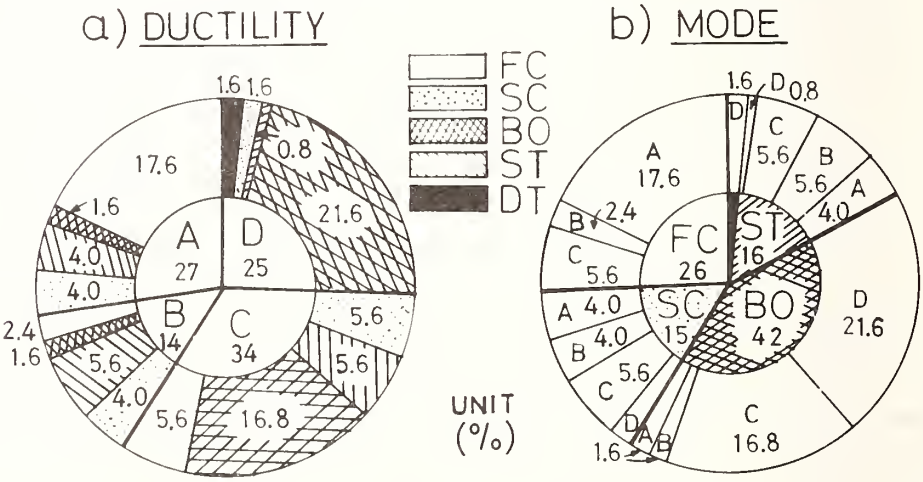

FIG. 5 CLASSIFICATION OF TEST RESULTS BY DUCTILITY AND FAILURE MODE

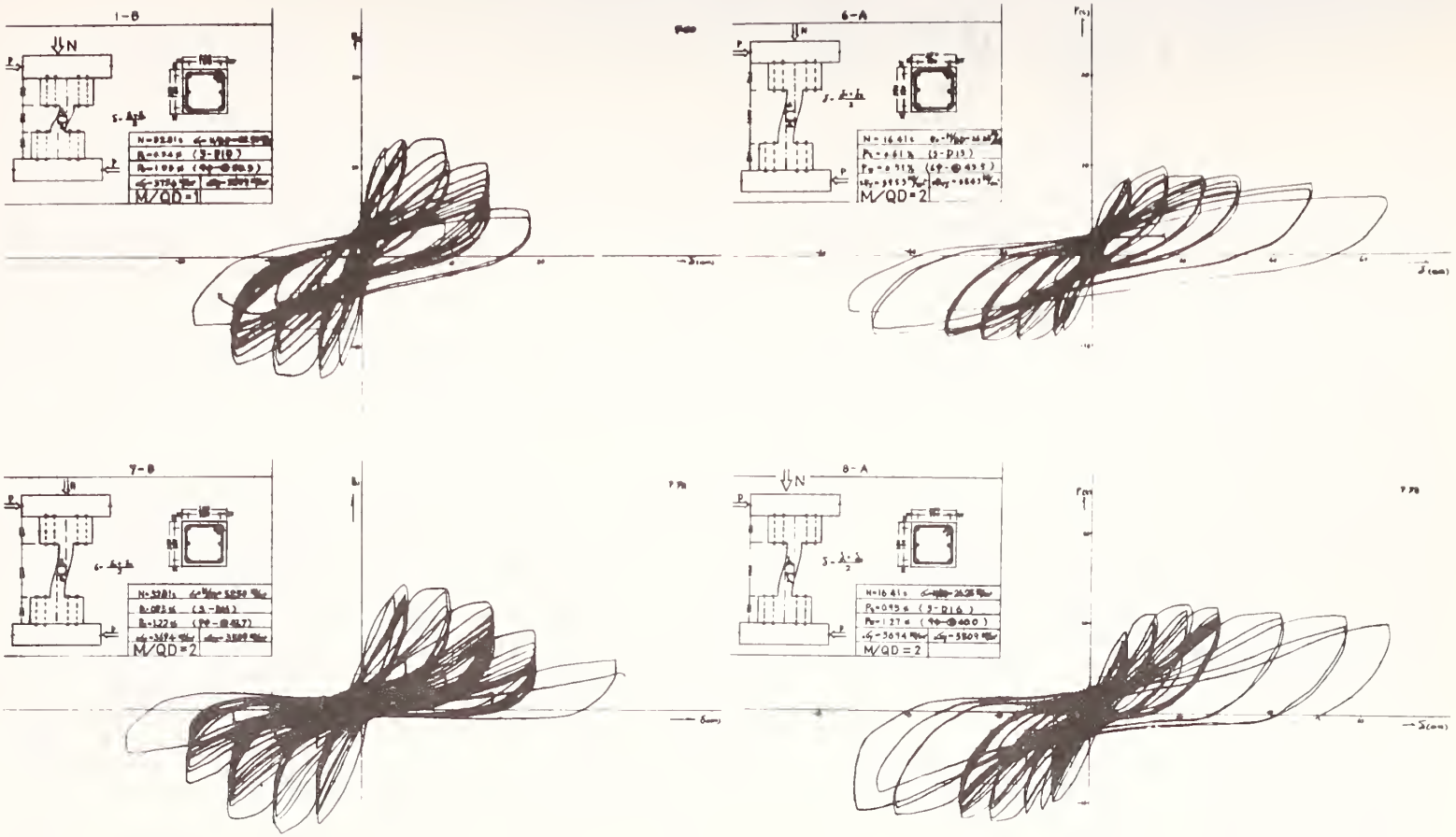

FIG. 6 LOAD-DEFLECTION CURVES OF TYPICAL SPECIMENS

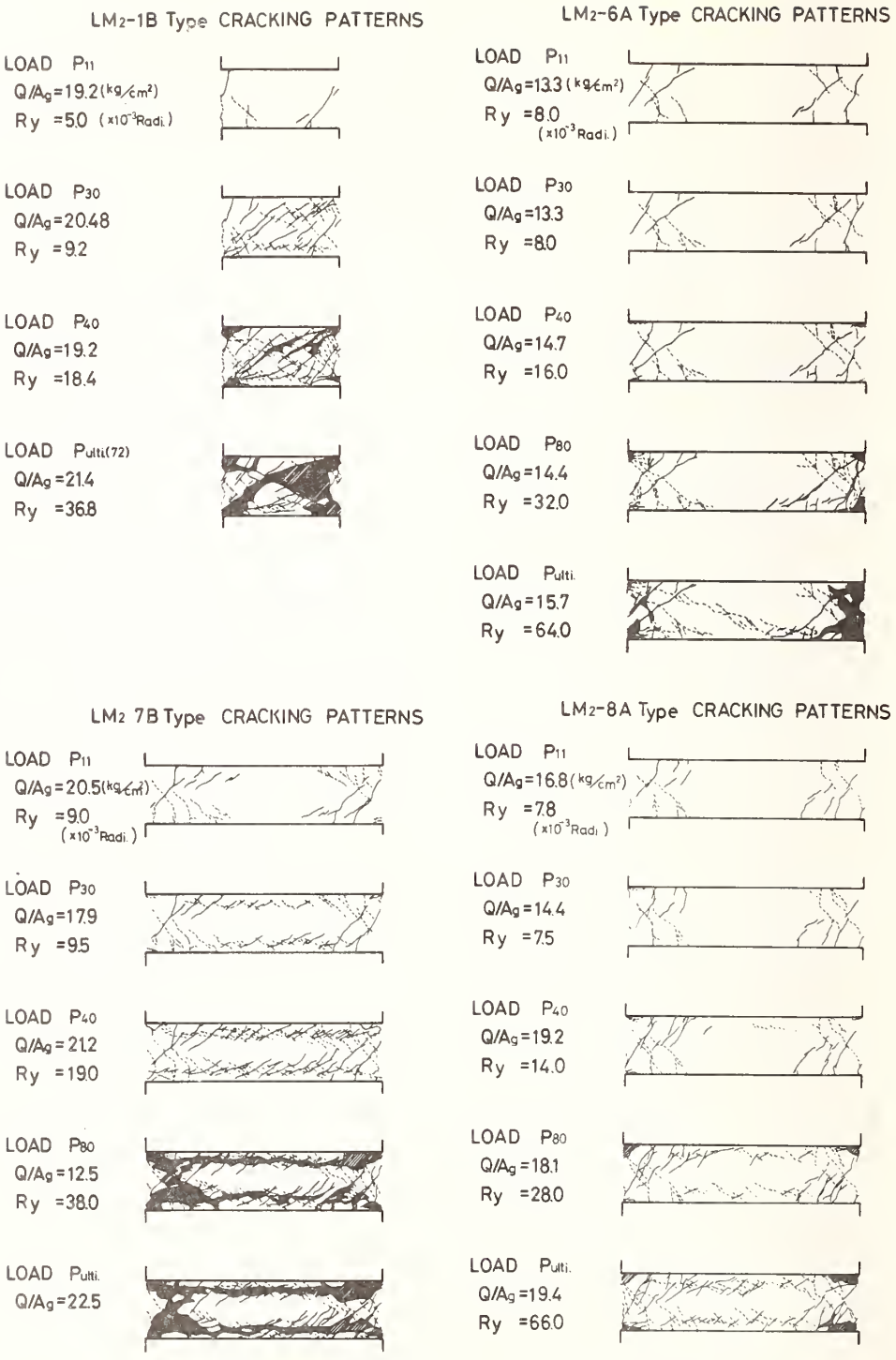

FIG. 7 CRACKING PATTERNS OF TYPICAL SPECIMENS

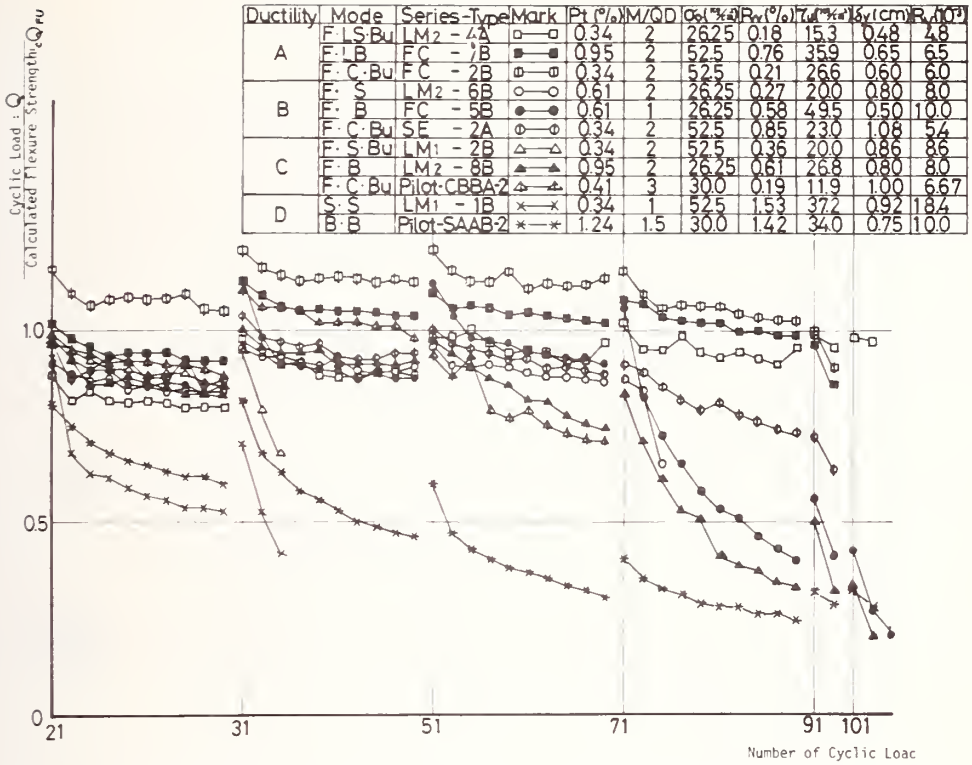

FIG. 8 DETERIORATION OF SHEAR CAPACITY BY CYCLIC LOADING ON TYPICAL SPECIMEN

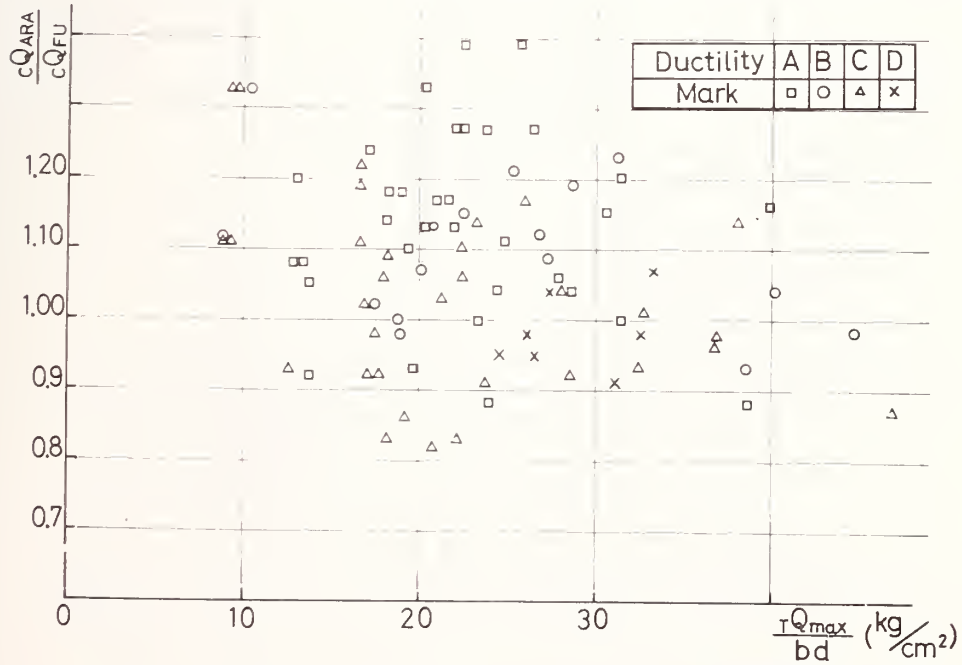

FIG. 9 DISCUSSION OF DUCTILITY BY ARAKAWA'S EQUATION

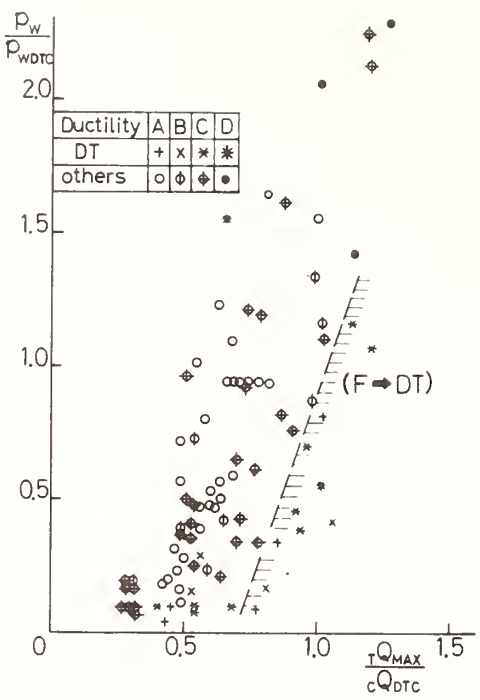

FIG. 10

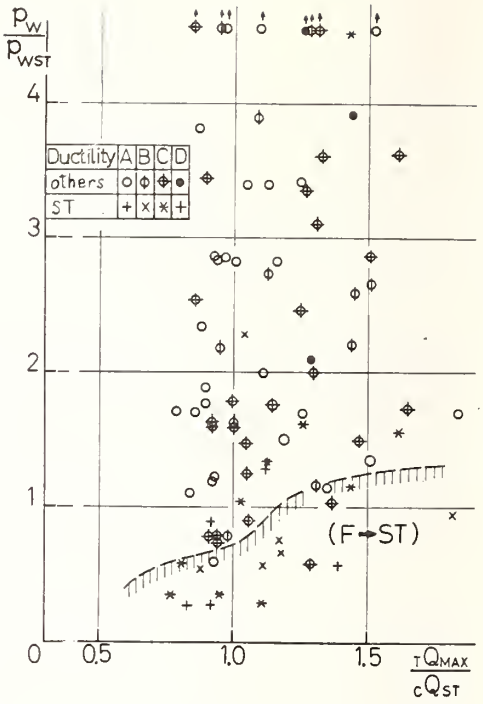

FIG. 11

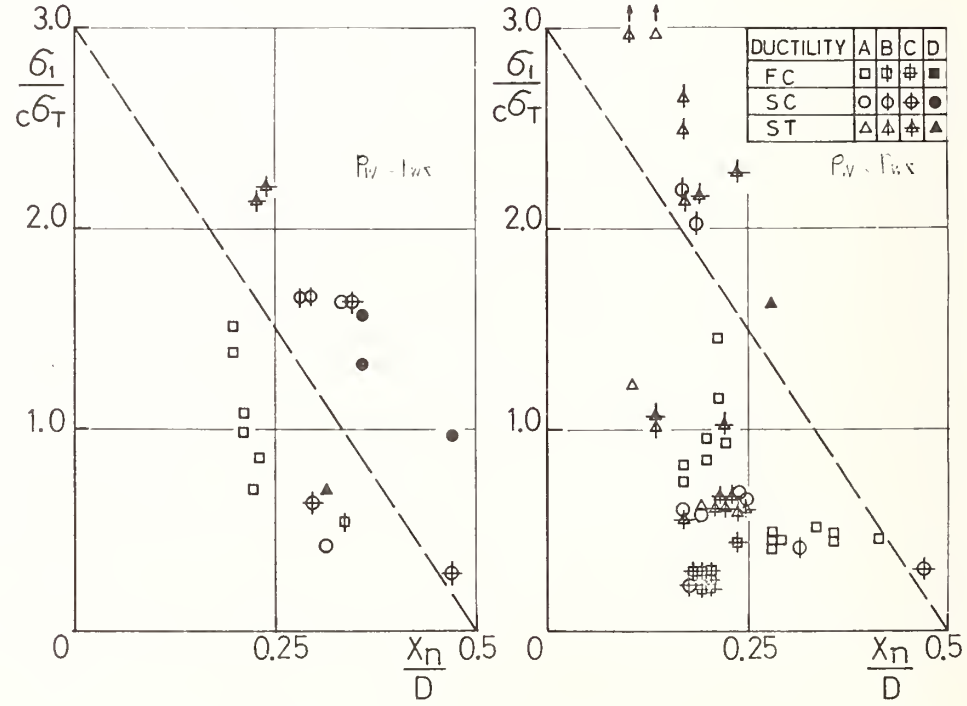

FIG. 12

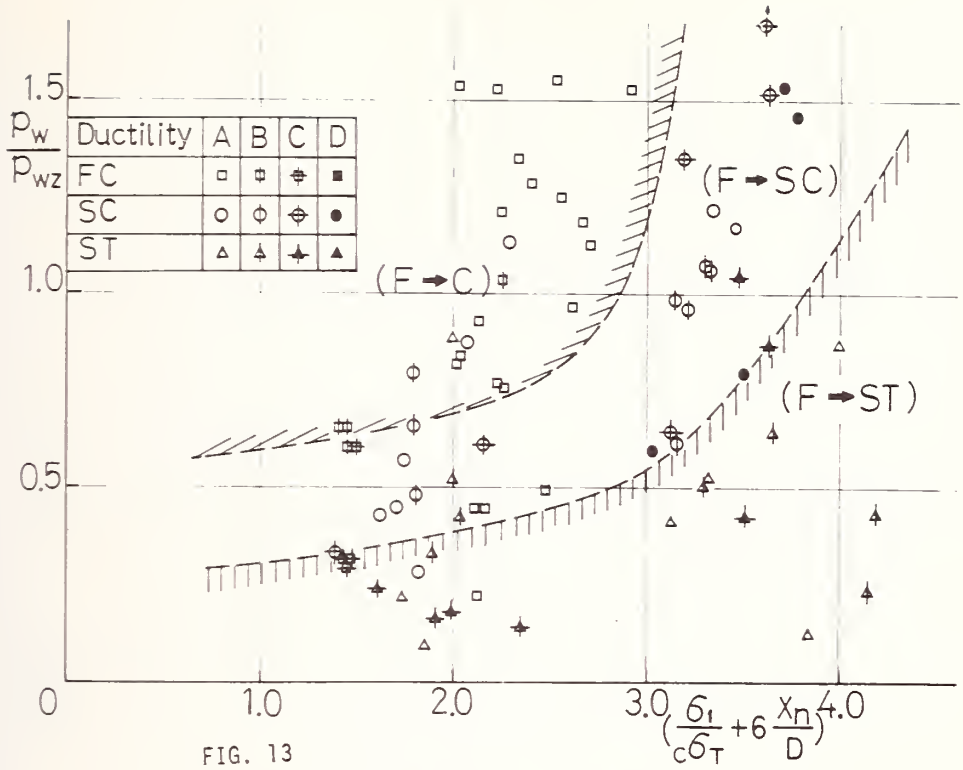
1.5
1.0
0.5
0
$\frac{p_w}{p_{wz}}$
Ductility | A | B | C | D
FC
SC
ST
(F→C)
(F→SC)
(F→ST)
1.0
2.0
3.0
4.0
$(\frac{\sigma_1}{c\sigma_T} + 6\frac{x_n}{D})$

FIG. 13

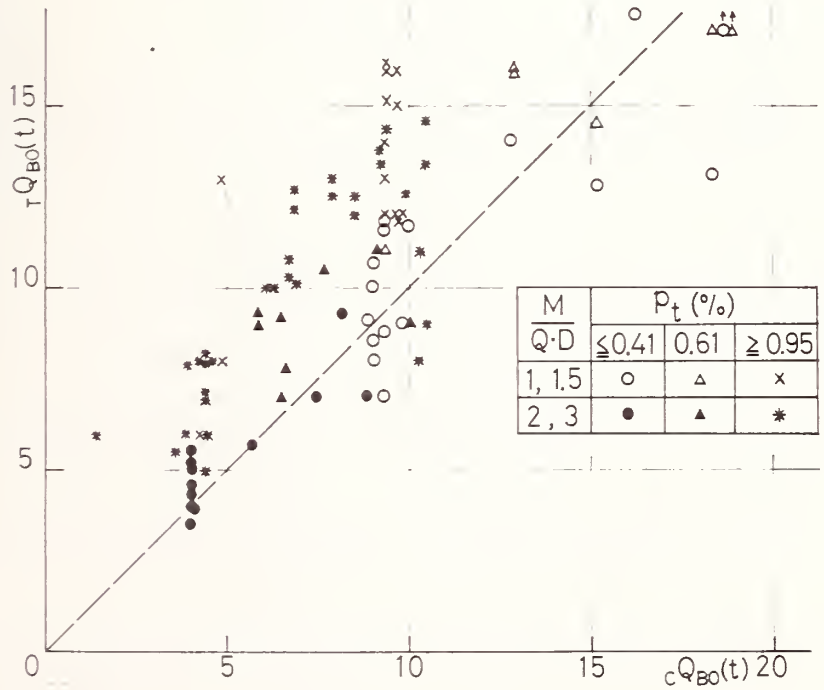
15
10
5
0
$_rQ_{BO}(t)$
$_cQ_{BO}(t)$
20
M / Q·D
p_t (%)
≦0.41
0.61
≧0.95
1, 1.5
2, 3

FIG. 14

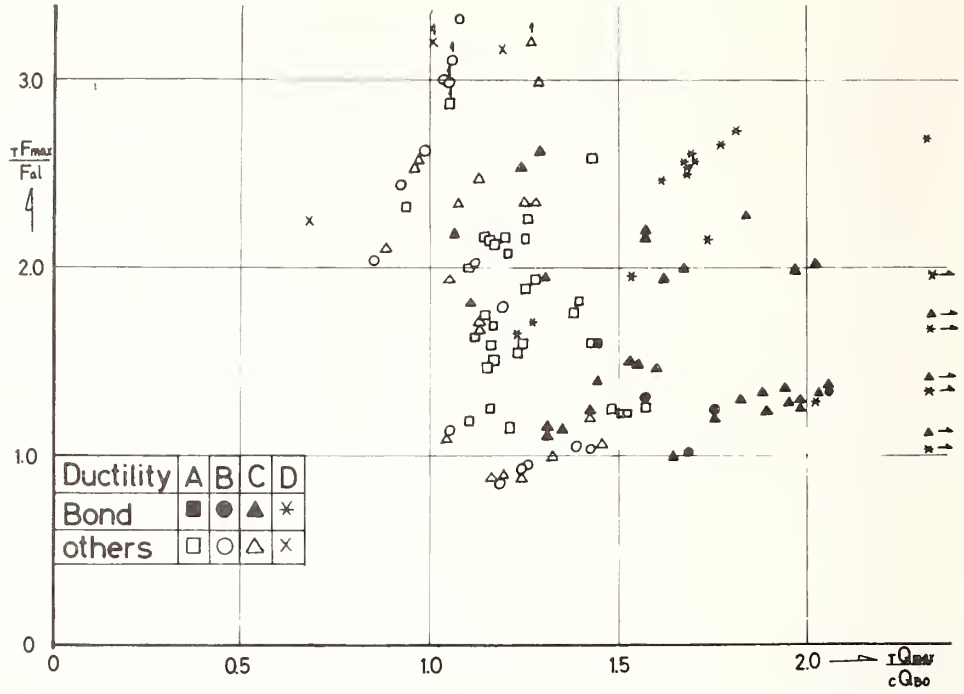
3.0
2.0
1.0
0
0.5
1.5
2.0
Ductility A B C D
Bond
others

FIG. 15

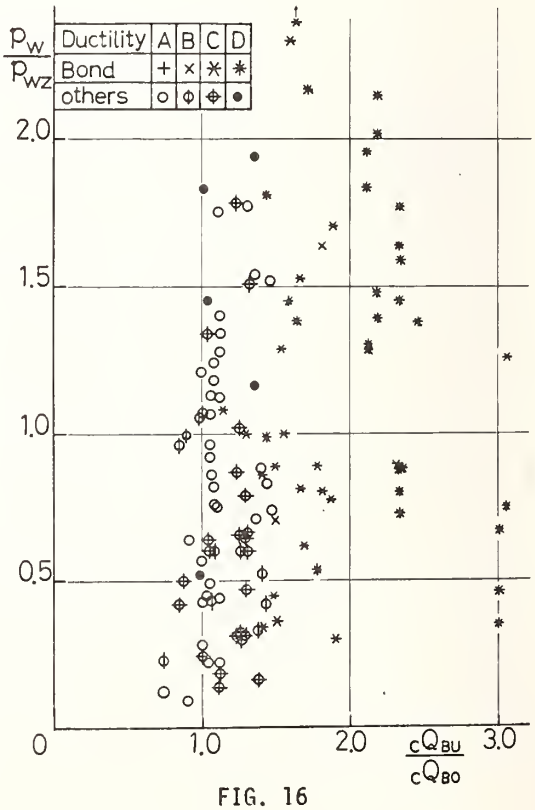
Ductility A B C D
Bond
others
2.0
1.5
1.0
0.5
0
1.0
2.0
3.0

FIG. 16

NONLINEAR ANALYSIS OF A GUYED TOWER

by

S.K. Takahashi
Research Structural Engineer

W.A. Shaw, Ph.D.
Head, Civil Engineering Department

Civil Engineering Laboratory
Naval Construction Battalion Center
Port Hueneme, California

The Civil Engineering Laboratory has performed an analysis of a tower at a Naval communication facility. The tower is about 600 feet high and is guyed at three levels. The upper guy level contains twelve wires; the middle and lower guy levels have three wires each. The guy wires had numerous large electrical insulators attached, each weighing 510 pounds.

A nonlinear finite element analysis of the guyed tower was conducted. Separate finite elements were used for portions of the tower and the guy wires were modeled with a truss element. Deflections, forces, and stresses in the tower and guy wires were determined from dead load and an equivalent static wind load corresponding to 90 miles per hour.

Eigenvalue solutions were obtained for the first five mode shapes and natural frequencies of one of the top guy wires; the guy wire had concentrated masses at five different locations and was initially prestressed.

Key Words: Finite element; guyed tower; structural analysis; structural engineering, vibration analysis, wind load.

OBJECTIVE

The objective of this paper is to present results of a structural analysis of a 600-foot tall radio tower which is guyed at three levels; the analysis was conducted using a three-dimensional nonlinear computer program. The tower was idealized as a vertical continuous beam supported at three elevations by guy wires. In the analysis, the tower and guys were subjected to gravity loads and equivalent wind loads corresponding to a horizontal wind speed of 90 miles per hour.

The free vibration analysis of one of the top guy wires with concentrated vertical loads (insulators) and initial tension in the wire was also performed.

BACKGROUND

The U.S. Navy has numerous tall guyed towers for radio communication located throughout the world. Many of these towers were designed and constructed over ten years ago. These towers are often subjected to high winds; the accompanying vibrations of the towers and guy wires have, at times, resulted in damage to non-structural elements such as beacon lights and copper straps which attach the electrical wires to the tower.

Concern has been expressed about the structural integrity of these towers from the standpoints of injuries to personnel, damage to equipment, and inability to carry out the assigned defense mission.

There have been several significant failures of tall towers in the United States during 1973. A 1600-foot television tower collapsed and killed two men near Tampa, Florida in June (1)*; the failure of this tower was attributed to loosening the wrong bolts during modification of the tower. In October, a 2000-foot television tower fell in Cedar Rapids, Iowa and killed five men (2); this failure may have been caused by deterioration of a guy wire at the 500-foot level. A third tower collapsed near Des Moines, Iowa in December; the failure of this 1882-foot television tower was caused by severe ice and wind loadings (3).

The U.S. Navy believed it desirable to re-analyze some of the towers in its communication system. The Civil Engineering Laboratory, Naval Construction Battalion Center, Port Hueneme, California has devoted some effort to this task. A nonlinear computer program has been used in the analyses. This paper discusses the analysis of one of these towers.

The analytical investigation was sponsored by the Naval Facilities Engineering Command.

DESCRIPTION OF TOWER

Two 600-foot guyed towers have been in operation at one of the Naval communication facilities for more than ten years. A photograph of one of these towers is shown in Figure 1. Some of the components of this tower are shown in Figure 2. This tower has three levels of guy wires; the two lower levels have three guy wires each and the top level has twelve guy wires. An elevation sketch of this tower is shown in Figure 3. Insulators are located in the guy wires as shown in this figure; each circle represents one insulator which weighs 510 pounds. Insulators are on each wire although they are shown only on one side in Figure 3. Figure 4 shows the numbering system of the guy wires.

The guy cables are pre-stretched, multiple strand, zinc-coated Bridge rope with wire strand cores. Table 1 provides information on the diameter, minimum breaking strength, and initial tension for the guy wires. (The last two columns in this table will be discussed later in this paper.) Figure 5 shows the location of attachment of the guy wires and defines terms used in this paper. The modulus of elasticity of the guy wires is 19,000 ksi and the allowable stress is 64 ksi.

*Numbers refer to references given at the end of the paper.

The main legs of the tower are extra strong round steel pipes. From the base up to node 3, 8-inch round pipe was used; 6-inch round pipe was placed between nodes 3 and 5; the top portion of the tower had 4-inch round pipe. The cross-sectional area and moment of inertia of these pipe sections are tabulated in Table 2. The main tower legs are spaced nine feet apart and are braced with horizontal angle sections and diagonal tension rods, as shown in Figure 6.

FORCES ON THE TOWER

Loads on a guyed tower result from dead load of the tower members and guy wires, initial tension in the guy wires, wind load, and ice load. The tower under consideration is located in an area where ice loads are not a problem.

Dead Load of Tower Members and Guy Wires

The total gravity weight of the angle irons, tensile rods, gusset plates, bolts, ladder, and platforms is approximately 100 lb./ft. of height. The total weight of the three legs and the other members is calculated as:

Section	Diameter of Pipe (in.)	Weight (lb/ft)	Weight of Three Legs (lb/ft)	Total Weight (lb/ft)
Top	5	20.78	62	162
Middle	6	28.57	86	186
Bottom	8	43.39	130	230

As shown in Figures 1 and 3, the guy wires carry numerous insulators that weigh 510 pounds each. To simplify the analysis, it was decided to represent the actual guy wire and the insulators by a guy wire equivalent weight and diameter so that the length of this guy wire is equal to the length of the actual guy wire (4). This equivalent guy wire procedure is useful where only cable end reactions, spring constants, and maximum cable tensions are of interest. A computer program based on Reference 4 has been used and the resulting equivalent properties of the guy wires are as follows:

Guy Level	Equivalent Diameter (in.)	Equivalent Weight (lb/ft)	Actual Metallic Area ($in.^2$)
Top	1.531	7.760	0.361
Middle	1.921	7.510	1.270
Bottom	1.879	7.710	1.080

Initial Tension in Guy Wires

The initial tension at ambient temperature for the top, middle, and lower levels of guy wires is 7.52 kips, 23.20 kips, and 31.04 kips, respectively.

Wind Load

The wind is assumed to be blowing perpendicular to one of the flat faces of the tower. For a typical 14-foot height of panel section, the wind surface area of the flat face of the angle irons and tension rods is approximately 0.445 sq. ft. per foot of height. The wind surface areas of the pipe legs are as follows:

Section	Outside Diameter (in.)	Surface Areas of Two Pipes (sq ft/ft)	Total Area Times Shape Factor* (sq ft/ft)
Top	5.563	0.927	2.425
Middle	6.625	1.104	2.695
Bottom	8.625	1.438	3.205

*Shape Factor for Flat Members = 2.28

Shape Factor for Cylindrical Members = 2/3 x 2.28 = 1.52

The uniformly distributed horizontal load, W, on the tower segments is obtained from the formula:

$$W = A \times q$$

where A is the projected area (including the shape factor) per unit height and q is the velocity wind pressure.

The velocity wind pressure is obtained from

$$q = 0.00256\ V^2 C_h$$

where V is the wind velocity of 90 mph and C_h is the correction coefficient for height or $(h/30)^{2/7}$.

Using the mid-height elevations of 540.2 ft., 376.6 ft., and 139.3 ft. for the sections with the 5-, 6-, and 8-inch diameter pipes, respectively, the height correction factors and resulting uniformly distributed horizontal load on the tower sections for a 90 mph wind are as follows:

Section	Height Correction Factor, C_h	Velocity Pressure q (ksi)	Uniform Horizontal Load, W (kips/ft)
Top	2.28	0.0473	0.115
Middle	2.06	0.0427	0.115
Bottom	1.55	0.0321	0.103

NONLINEAR ANALYSIS OF GUYED TOWER

The information in the previous section was used as input data to a computer program which idealizes a tower as a vertical continuous beam supported at the specified elevations by guy wires (5). The assumptions used in the program are the following:

1. Each tower segment is prismatic (i.e., the section properties defining resistance to bending about either principal axis and axial, shear, and torsional deformations are constant between tower nodes).
2. The cable profile is a parabola for all loading conditions.
3. Anchorage cable tensions and total cable weight are known.
4. Wind loads on the tower shaft are known and are uniform between tower nodes.

5. Concentrated forces can be applied at tower nodes only.

6. The guy wires are uniformly loaded by the wind.

7. The average wind velocity is the same for all guy wires.

8. The wind is blowing parallel to the ground.

9. Lift and drag coefficients for each guy wire are computed automatically using the formulas given in Reference 6.

The printed output of the computer program contains the following:

1. All input data.

2. Data checking parameters such as guy chord lengths, unstressed cable lengths, initial attach point cable tensions, etc.

3. Global translations and rotations of all tower nodes for each load case.

4. Global translations of all cable attach points.

5. Shear, moments, axial forces, and torques acting on the ends of each tower segment.

6. Attach point and anchor point cable tensions and global components of the cable resultant forces.

7. Tower base reactions.

The computer program required six iterations before the solution converged. A summary of the displacements at various locations of the tower is given in Table 3. The maximum displacement at the top of the tower was found to be 7.39 feet; this is more than twice the deflection at the middle level of the guy wires which indicates that the top portion of the tower is quite flexible compared to the bottom two portions of the tower.

A tabulation of shear, axial force, and bending moment in the tower is presented in Table 4. The base shear of 6.0 kips is well below the 15 kips shear to which the base of the tower was tested, however, the axial force of 433 kips at the base of the tower is slightly greater than the 400 kips axial test load. The maximum moment of 2,154-foot kips occurred just above the middle guy level. Figure 7 graphically shows the deflection, shear, axial force, and bending moment in the tower.

The axial compressive stresses in the main columns of the tower were computed from the axial loads and bending moments given in Table 4. These stresses in the leeward column are summarized in Table 5. The highest stress of 47.8 ksi occurs at the intersection of the 5- and 6-inch diameter pipe sections and is caused by the large deflection at the top of the tower. High stresses of approximately 40 ksi also occur at the connecting point of the middle level of guy wires.

Table 6 summarizes the final tensions at the anchor end and the attachment point to the column for all guy wires. Figure 4 shows the designation of the guy wire numbers. The allowable stress of 64 ksi was slightly exceeded at the attach point for guy wires 8, 9, 17, and 18. The design working load for the guy insulators was 78 kips; the maximum tension of 65.4 kips occurred in guy wires 4 and 6.

FREQUENCY ANALYSIS OF GUY WIRE

A general nonlinear finite element computer program called NONSAP (Reference 7) was used to determine the natural frequencies and mode shapes of one of the top level guy

wires. This wire is pinned at both ends. The computer model is represented by twelve truss elements and thirteen nodal joints. Concentrated loads of 510 pounds each were placed at joints 2, 4, and 6; a cluster of six 510-pound loads was placed at joint 8. Initially, the deformed shape of the wire was determined considering only the gravity weight of the wire and insulators. This deformed shape and initial tension in the guy wire was used in the computer program to determine the natural frequencies of the wire; the first five mode shapes and natural frequencies are shown in Figure 8. Except for the first mode shape, the cluster of six concentrated loads at Node 8 forces the cable to cross the initial position at this node for the remaining four mode shapes; it is as if two separate cables were oscillating independently.

SUMMARY

A 600-foot high guyed tower which was designed in 1960 was re-analyzed using a non-linear finite element computer program. The tower shaft was represented by a series of co-linear beam segments interconnected at tower nodes. The tower was analyzed for a wind velocity of 90 miles per hour imposed on one of the flat faces of the triangular guyed tower. The analysis showed that a maximum deflection of 7.39 feet occurred at the top of the tower. The base shear force of 6.0 kips was considerably below the proof load of 15 kips; the axial force of 433 kips at the base of the insulator, however, was in excess of the 400-kip proof load. The allowable guy wire stress of 64 ksi was exceeded by four of the twelve top guy wires by less than six percent and should not be of great concern.

A frequency analysis of one of the top guy wires shows that mode shapes 2 through 5 had a node at the location of the cluster of six insulators.

REFERENCES

1. Engineering News Record, "Collapse of a Guyed 1,600-ft TV Tower Kills Two Workers," June 14, 1973.

2. Engineering News Record, "2,000-ft. Tower Falls, Killing Five," October 11, 1973.

3. Engineering News Record, "Ice-laden, 1,882-ft-high TV Tower Collapses," December 13, 1973.

4. R.C. Morales, "Shear-Volume Method of Solving Tensions in Cables," ASCE, J. Structural Division Proceedings, 5718 ST1, January 1968.

5. F.E. Peterson, "Tower Analysis Program," Engineering Analysis Corporation, June 1973.

6. W.S. Diehl, "Engineering Aerodynamics", Revised Edition, New York, 1936, p. 280.

7. K.J. Bathe and F.E. Peterson, "Theoretical Basis for NONSAP, A Nonlinear Structural Analysis Program for Static or Dynamic Analysis of Nonlinear Structural Systems Modeled with Finite Elements," by Engineering Analysis Corporation for Civil Engineering Laboratory, October 1973.

Table 1. Guy Cable Characteristics

Guy Levels	Diameter of Cable (in.)	Minimum Breaking Strength (kips)	Initial Tension at Ambient Temp. (kips)	Equivalent Diameter (in.)	Equivalent Weight (lb/ft)
Top	7/8	70	7.52	1.531	7.763
Middle	1-5/8	246	23.20	1.921	7.507
Lower	1/1/2	208	31.04	1.879	7.712

Table 2. Properties of Round Steel Pipes (extra strong)

Section	Pipe Size (in.)	Area ($in.^2$)	Moment of Inertia ($in.^4$)
Top	5	6.112	35.650
Middle	6	8.405	49,020
Lower	8	12.76	74,420

Table 3. Summary of Tower Displacements

Tower Node No.	Displacement (ft)
6	7.39
5	3.37
4	3.04
3	1.20
2	0.95
1	0

Table 4. Forces and Moments in Tower

Segment No.	Segment End	Shear (kips)	Axial Force (kips)	Bending Moment (ft-kips)
5	Upper	2.1	160	-160
	Lower	17.4	182	1,807
4	Upper	17.4	182	1,807
	Lower	19.2	185	2,154
3	Upper	-19.0	279	1,922
	Lower	2.1	313	946
2	Upper	2.1	313	946
	Lower	6.7	323	1,219
1	Upper	-18.9	378	1,142
	Lower	6.0	433	0

Segment No.	Segment End	Axial Stress (ksi)	Bending Stress (ksi)	Total Stress (ksi)
5	Upper	8.78	- 0.3	8.5
5	Lower	9.9	37.9	47.8
4	Upper	7.2	27.6	34.8
4	Lower	7.3	32.9	40.2
3	Upper	11.1	29.3	40.4
3	Lower	12.4	14.4	26.8
2	Upper	8.2	9.5	17.7
2	Lower	8.4	12.3	20.7
1	Upper	9.9	11.5	21.4
1	Lower	11.3	0	11.3

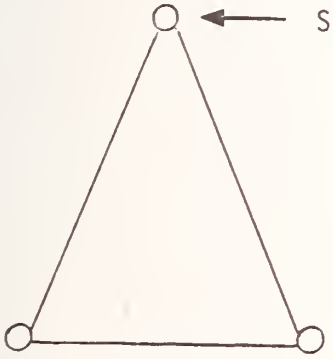

Table 6. Guy Wire Forces and Stresses

Guy Number	Attach Point to Column			Anchor Point		
	Tension Force (kips)	Stress (ksi)	Percent of Design Stress	Tension Force (kips)	Stress (ksi)	Percent of Design Stress
1	49.1	45.5	71.1	47.4	43.9	68.6
2	16.9	15.7	24.5	14.9	13.8	21.6
3	49.1	45.5	71.1	47.4	43.9	68.6
4	65.4	51.5	80.5	62.3	49.0	76.6
5	2.8	2.2	3.4	1.0	0.8	1.3
6	65.4	51.5	80.5	62.3	49.0	76.6
7	22.5	62.4	97.5	18.3	50.8	79.4
8	23.3	64.3	100.5	19.1	52.9	82.7
9	24.4	67.6	105.6	20.3	56.2	87.8
10	22.7	63.0	98.4	18.3	50.7	79.2
11	16.8	46.5	72.7	12.1	33.4	52.2
12	9.0	25.0	39.1	4.3	11.8	18.4
13	4.1	11.5	18.0	1.1	3.1	4.8
14	9.0	25.0	39.1	4.3	11.8	18.4
15	16.8	46.5	72.7	12.1	33.4	52.2
16	22.7	63.0	98.4	18.3	50.7	79.2
17	24.4	67.6	105.6	20.3	56.2	87.8
18	23.3	64.3	100.5	19.1	52.9	82.7

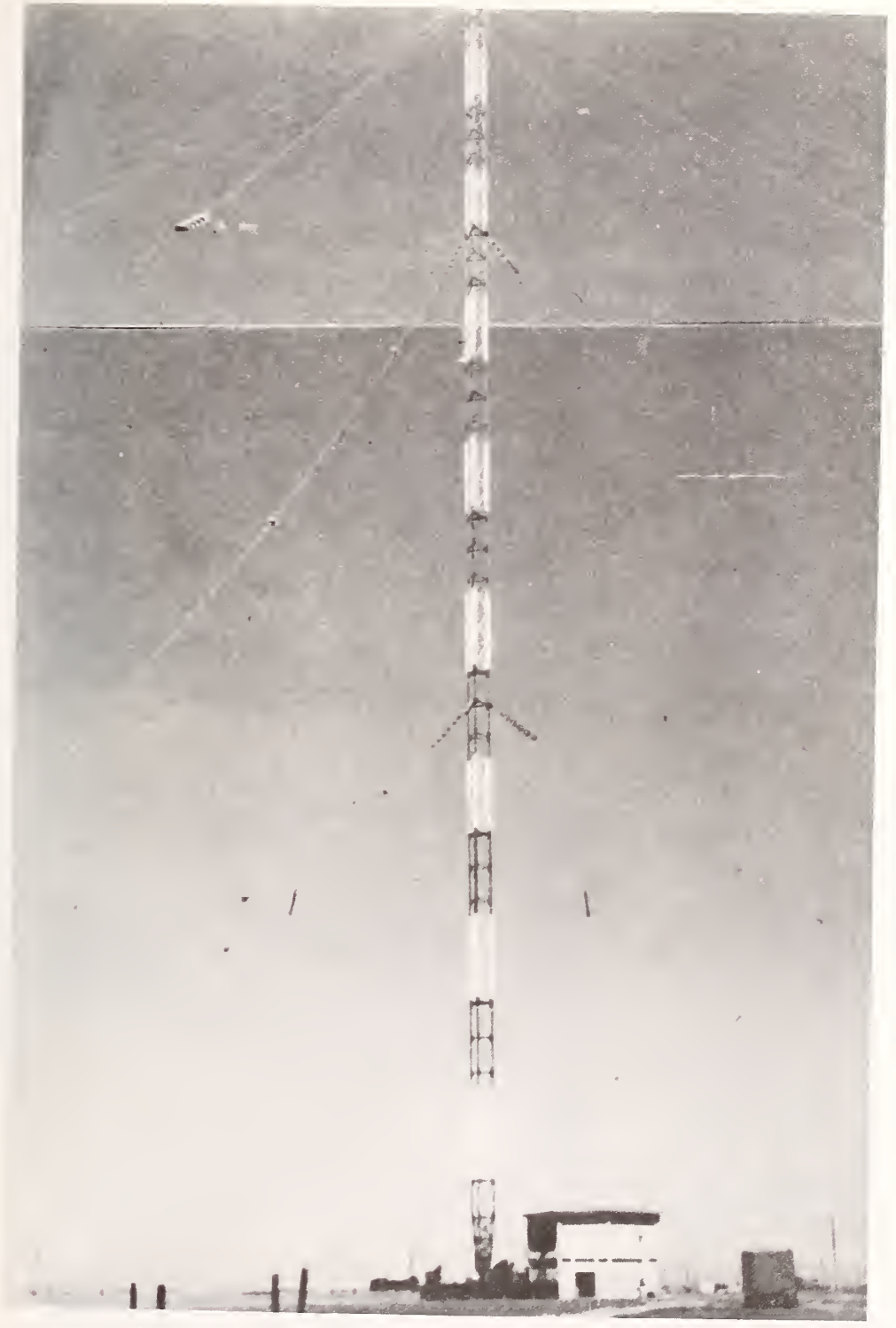

Figure 1. 600-ft high guyed tower at Dixon, CA.

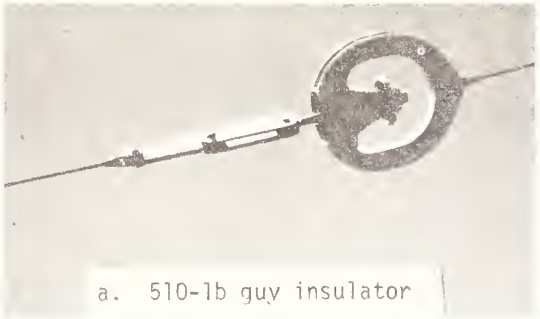

a. 510-lb guy insulator

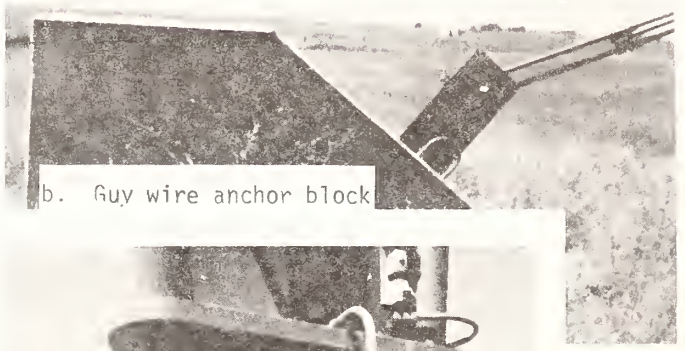

b. Guy wire anchor block

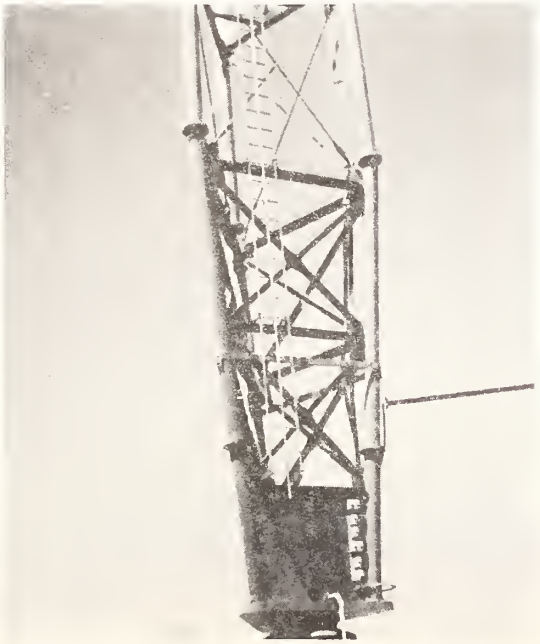

c. Bottom of tower structure

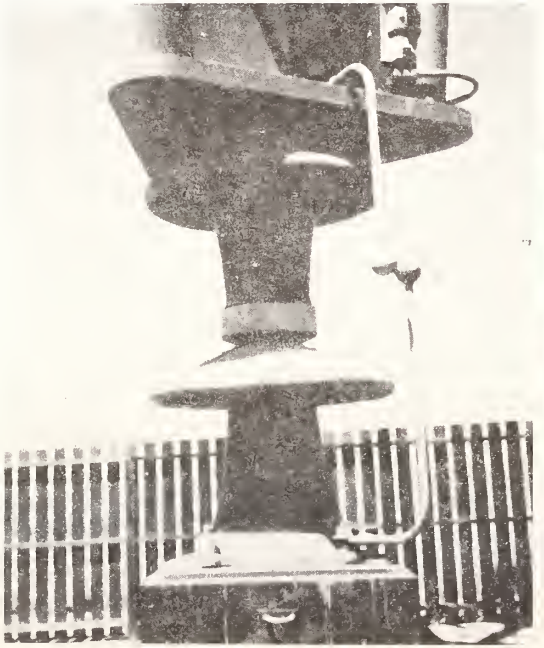

d. Insulator base.

Figure 2. Components of tower.

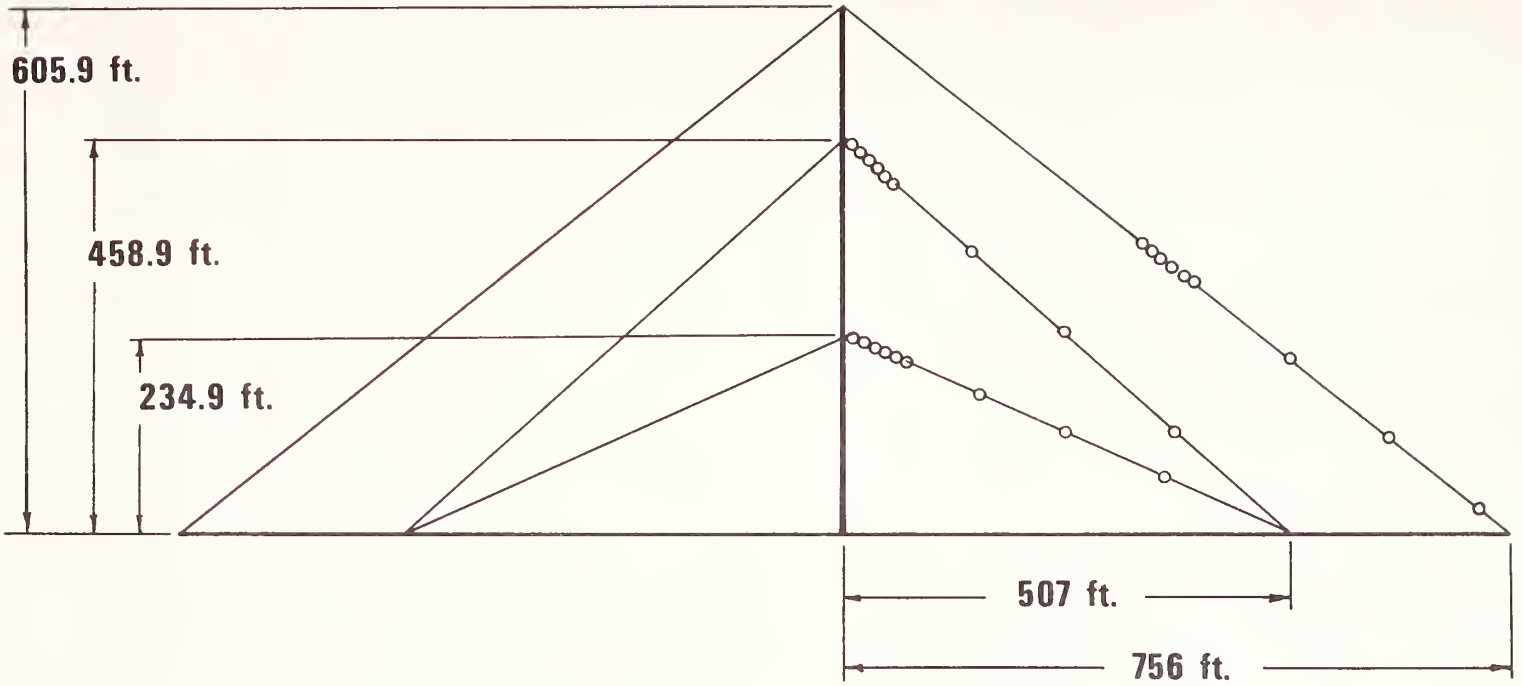

Figure 3. ELEVATION SKETCH OF GUYED TOWER

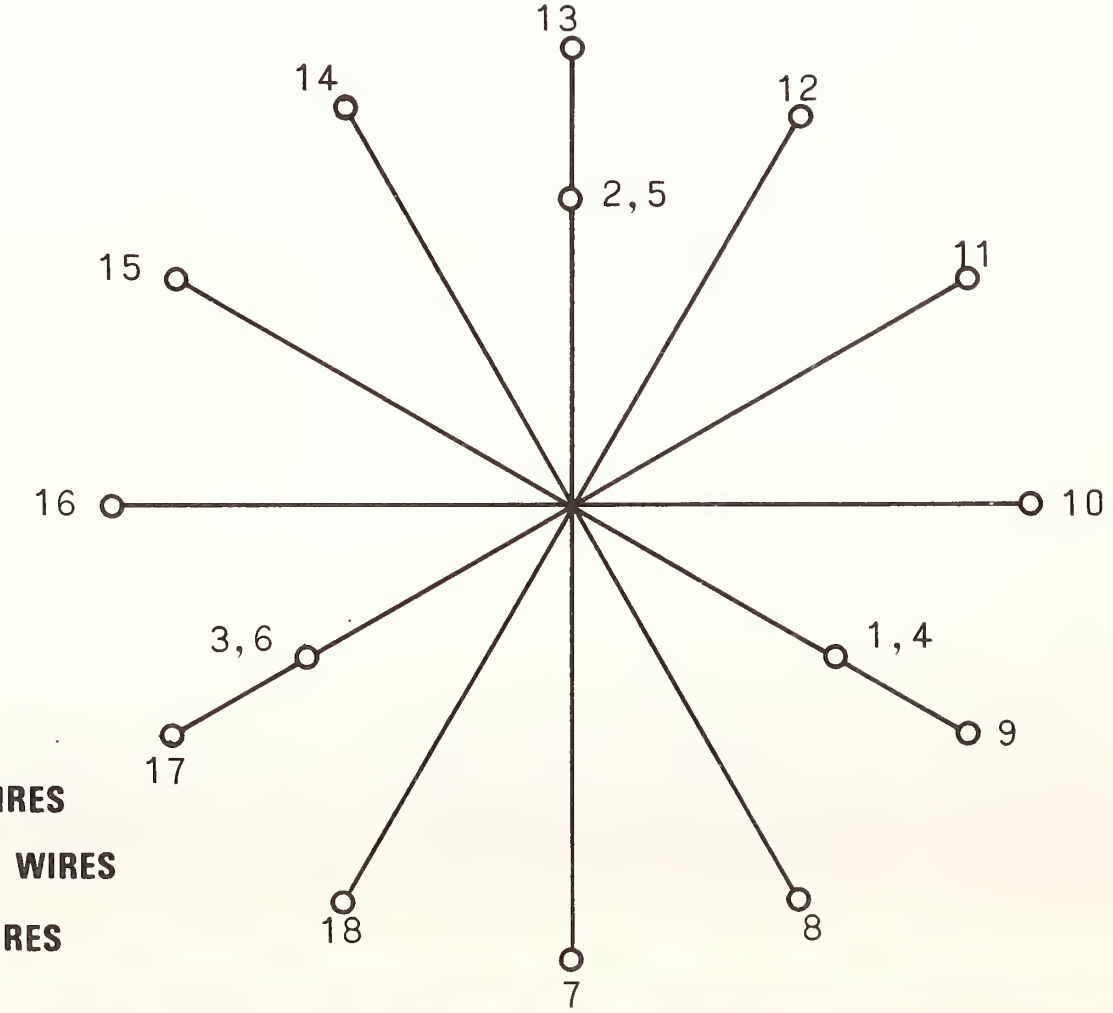

1 - 3 LOW LEVEL OF GUY WIRES

4 - 6 MIDDLE LEVEL OF GUY WIRES

7 - 18 TOP LEVEL OF GUY WIRES

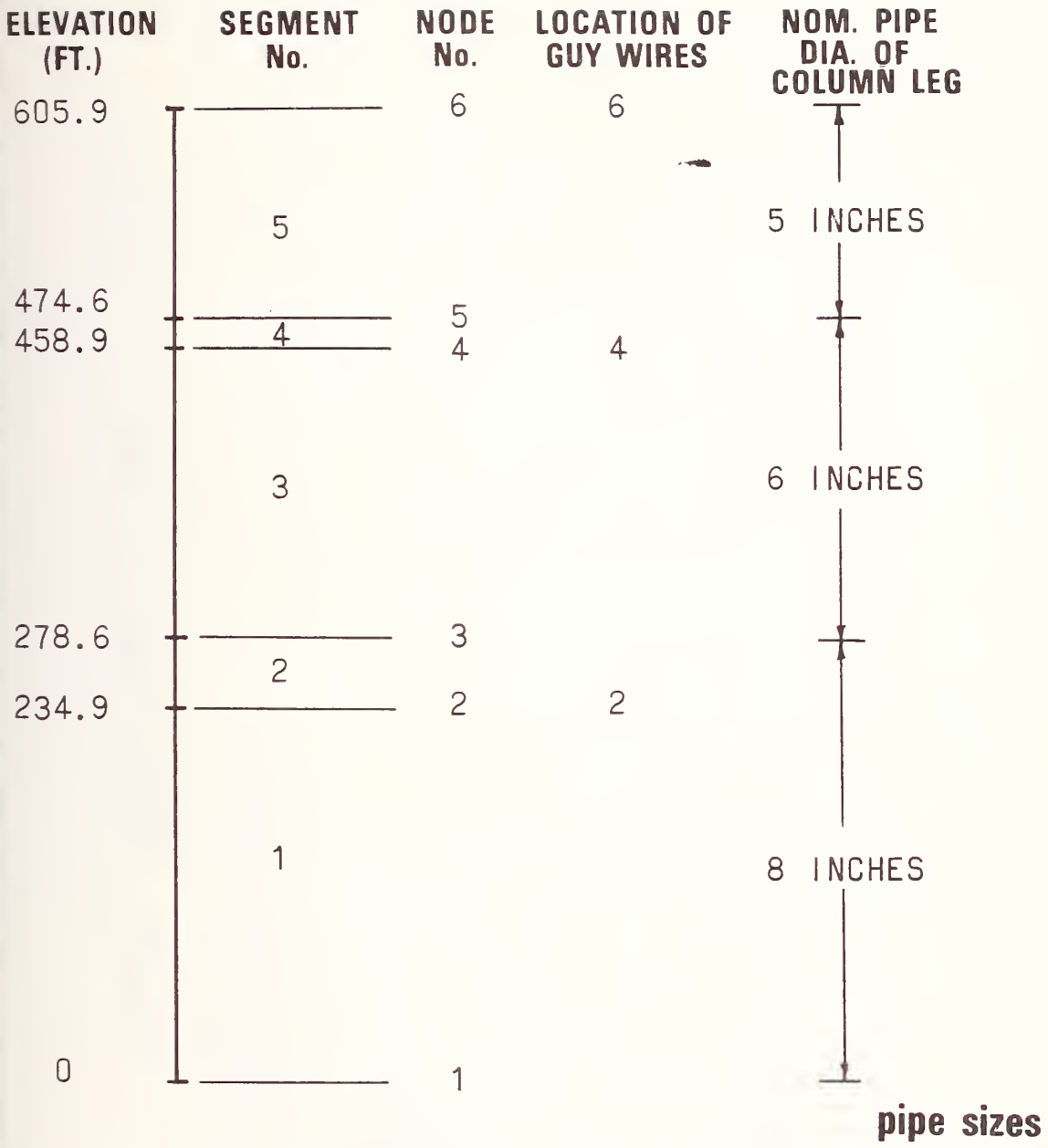

Figure 5. Definition of terms and location of guy wires and

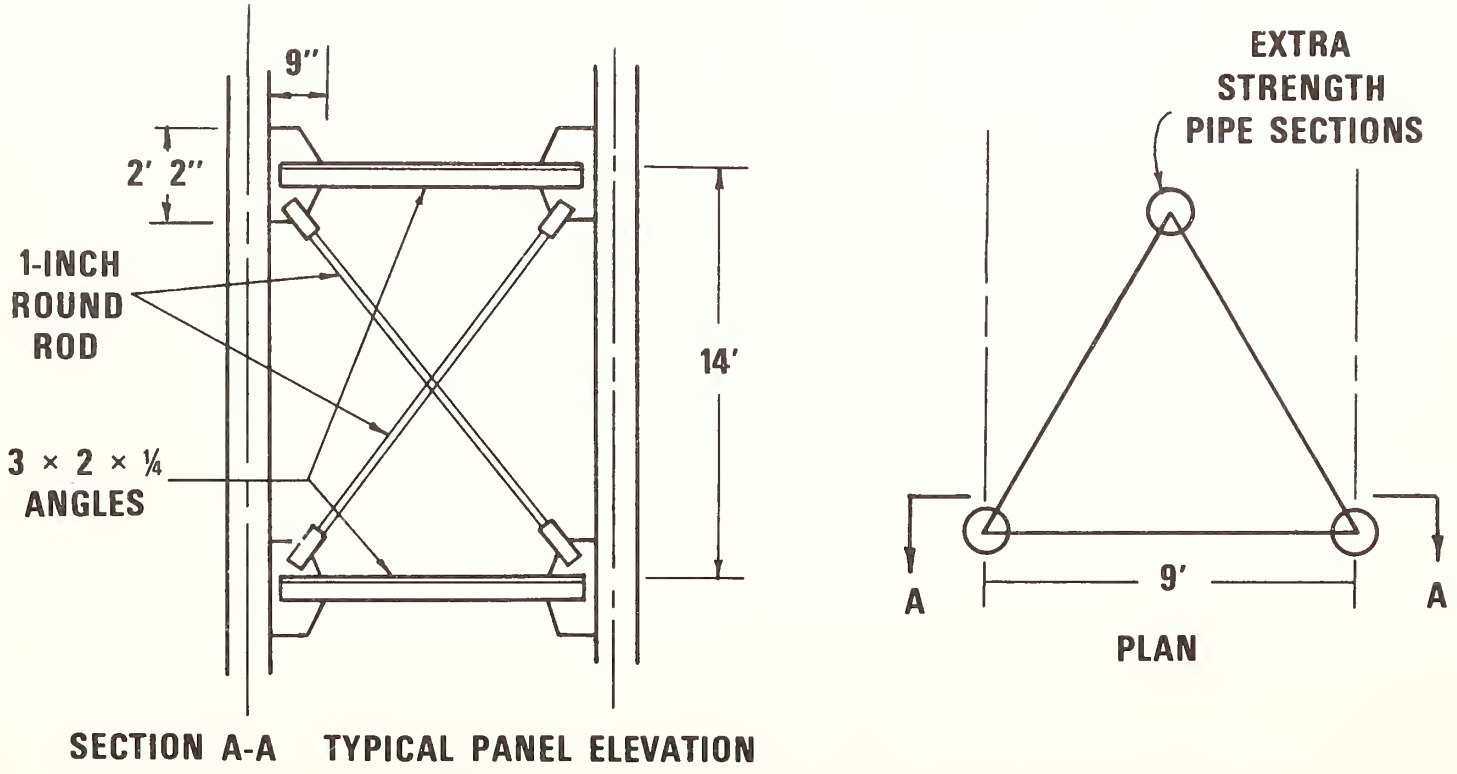

Figure 6. Sketch of main tower legs and bracings

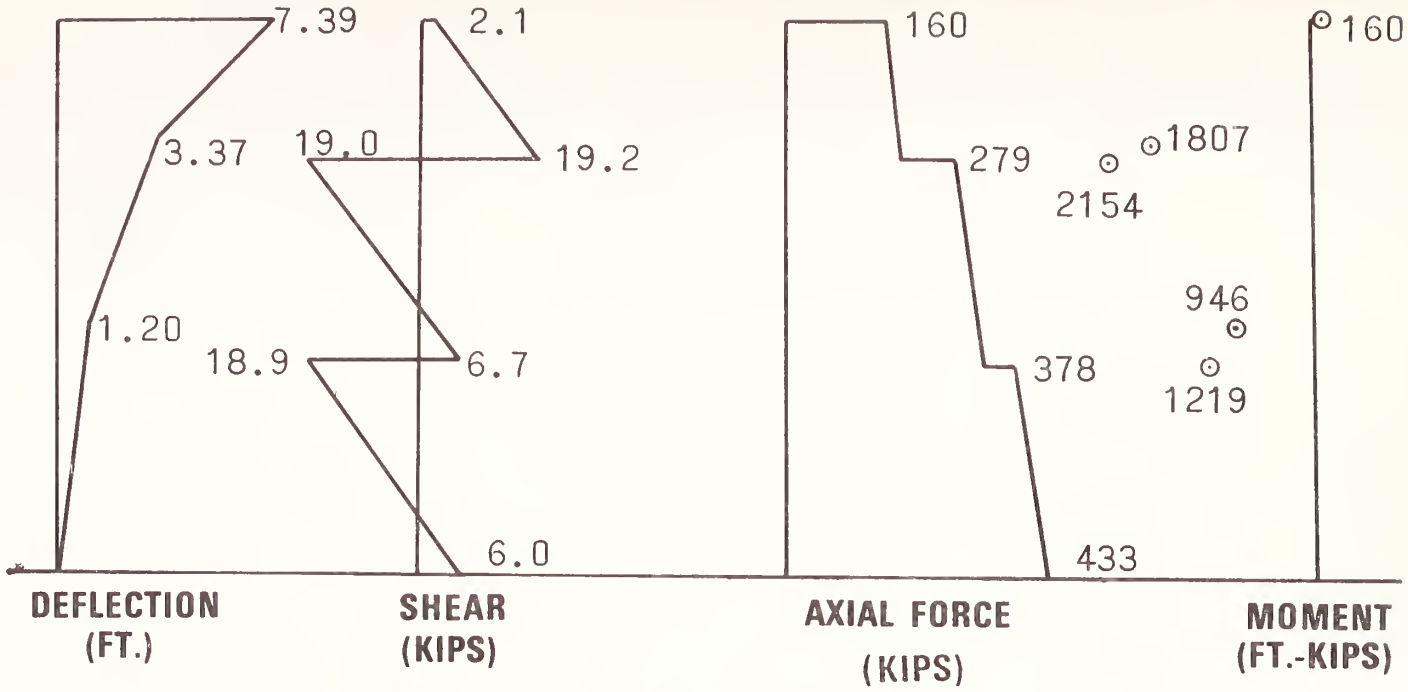

Figure 7. Diagrams of deflection, shear, axial force, and bending moment

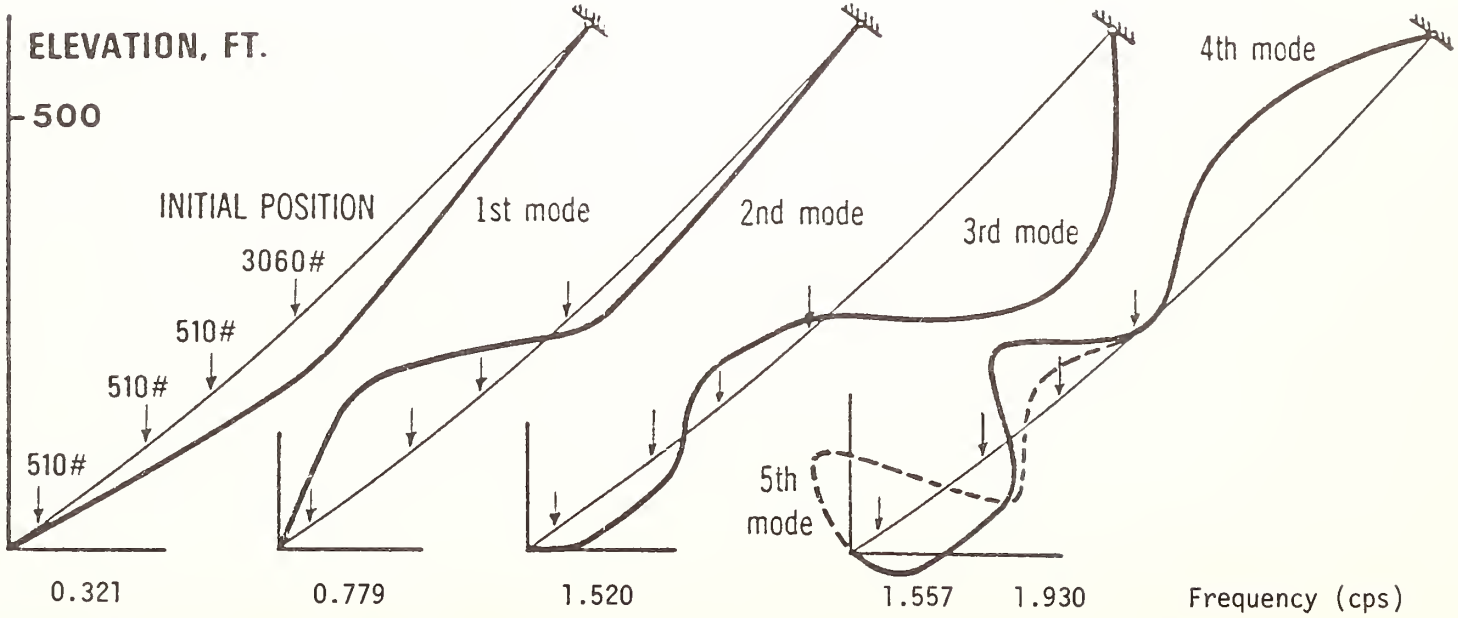

Figure 8 First five mode shapes and periods of guy wire with concentrated insulator loads and initial prestress

A STANDARD FOR THE STRUCTURAL INTEGRITY OF PREFABRICATED DWELLINGS

by

Kiyoshi Nakano
Head, Dr. Eng., Third Division
Building Research Institute
Ministry of Construction, Japan

Masaya Hirosawa
Chief Researcher, Third Division
Building Research Institute
Ministry of Construction, Japan

Tatsuo Murota
Research Associate, Third Division
Building Research Institute
Ministry of Construction, Japan

In 1973, the Ministry of Constuction of Japan presented a standard for the performance of prefabricated housing. The purpose of this standard was to provide consumers with an index for selecting their dwellings. The standards are related to fire, heat, sound, durability, and structural safety against earthquakes, winds, snow, etc.

The criteria for evaluating structural properties are outlined in this paper, as well as the history and present status of prefabricated dwellings in Japan. A typical prefabricated structural system is shown in the last section.

Key Words: Earthquake; housing; performance specification; prefabricated dwelling; standards; structural design.

A HISTORICAL SKETCH OF THE PREFABRICATION OF DWELLINGS IN JAPAN AND THE PRESENT STATUS OF THEIR CONSTRUCTION

In 1945, just after the Second World War, the number of houses required in Japan was 4,200 thousand units, which represented 20% of the total number of households at that time In order to efficiently solve the housing shortage, the Ministry of Construction recognized the necessity to industrialize dwelling construction. Therefore, the Building Research Institute initiated studies to develop a new system of dwelling construction that would reduce the construction cost, the time required for construction, and the labor force. The results of these studies were reflected in the construction of dwellings supervised under public management.

Since that period, restoration of buildings and structures have been required due to damage caused by the Isewan Typhoon in 1959, and a subsequent building boom due to an increase in business prosperity in 1960. This has led to a shortage of construction materials and skilled laborers. At this time, the Ministry of Construction had decided to accelerate the industrialization of dwelling construction, and since 1961, introduced mass-produced systems into the construction of publicly managed dwellings. In 1962, in response to this policy, private enterprise has established the Prefabricated Building Association.

At the end of 1962, 835 low-rise (one or two stories), mass-produced dwellings were constructed under public management and in 1965, the quantities of low-rise mass-produced dwellings accounted for one-third of all publicly managed dwellings constructed that year.

In the latter half of the 1960's, construction of prefabricated dwellings began to increase rapidly. This was because the demand for a greater number of dwellings had occurred with a corresponding increase in the standard of living. This demand, therefore, was characterized not by the shortage of the number of dwellings (the shortage in numbers was solved in 1963), but for an increase in a higher standard of house. Figure 1(a) shows the increase in the number of prefabricated dwellings, constructed each year, during 1966 through 1972. Figure 1(b) shows the percentage of the total number of dwellings constructed in the same period. According to these figures, the number of prefabricated dwellings constructed in 1972 exceeded 200 thousand, which was more than 10% of the total dwellings constructed.

The details of the prefabricated dwellings constructed in the same period is shown in Figure 2. The ratio of the low-rise dwellings to those of more than three stories was 78 to 22 in 1966; this ratio then became 61 to 39 in 1972. The increase in the construction of high-rise dwellings is due to the rising value of land, which is estimated to continue in the future.

Single- or two-story prefabricated dwellings are divided into three types, according to the material used in the main parts of the structures, i.e., wooden type, steel type, and concrete type. The low-rise prefabricated dwellings constructed in 1972 consisted of the follwoing percentages: 52.4% were of the steel type, 36.4% were of the wooden type, and 11.2% of the concrete type.

As many as 100 firms are presently producing these low-rise dwellings of more than 1,000 plan types, however, some of these have notable defects.

In 1973, the Ministry of Construction developed a performance standard for low-rise prefabricated dwellings in order to provide consumers with a criteria in selecting their dwellings. According to this regulation, the Minister of Construction stipulates the performances relative to fire, heat, sound, durability, and structural safety, and notifies the consumers of these performances with the exception of structural safety.

In the following section, an outline of the criteria, relative to how the structural performance was evaluated, will be described.

CRITERIA FOR THE EVALUATION OF THE STRUCTURAL PERFORMANCE OF PREFABRICATED DWELLINGS

The establishment of a criteria for prefabricated dwelling systems first requires one to satisfy the structural performances specified by the Building Code of Japan and the Specifications of the Architectural Institute of Japan. In addition to satisfying these basic requirements, the criteria must include the specifications peculiar to dwellings such as flexibility of partitions, rigidity of floors, etc. Also the evaluation of the aseismicity of reinforced-concrete dwellings, utilizing a new method based on the earthquake energy absorpotion capacity of the structure, has been adopted.

The criteria will be referenced to the following two areas:

1) Structural Design Philosophy

2) Detail of Structure

STRUCTURAL DESIGN PHILOSOPHY

The structural design philosophy relative to dead and live loads, earthquakes, winds, and snow must be clear and reasonable. Complex and/or unreasonable structural plans and elevations will not be governed by these design criteria. If the structural elements are arranged to resist horizontal loads, such as bracings and shear walls, they must be inspected into detail. If the structural system has wall panels which resist horizontal loads (this system will be called a "load-bearing wall panel system"), the maximum distance between two adjacent lines of walls positioned in the same direction shall be less than 7.5 m and at least one load-bearing wall panel, which has a minimum width of 80 cm, shall be placed at every corner of the exterior wall lines. If the housing structure is made of precast concrete panels, in addition to the above-mentioned regulations, the following requirements relative to seismic characteristics shall be verified by calculation or experiment.

a) In case of verification by calculation

The coefficient of the horizontal load-carrying capacity, S, shown in Equation (1) shall not be less than 0.5.

$$S = k_1 \cdot k_2 \cdot k_3 \cdot S_E \tag{1}$$

where

k_1 = Coefficient based on the arrangement of the wall panels in plan and elevation, (0.7 ∿ 1.0)

k_2 = Coefficient of the horizontal rigidity of the floor, (0.7 ∿ 1.0)

k_3 = Coefficient for the difficulty of construction, (0.8 ∿ 1.0)

S_E = The standard seismic strength coefficient, the smallest of the values obtained from S_{E_S} in Equation (2) or S_{EB} in Equation (3).

The shear strength coefficient, S_{E_S}, shall be calculated by using Equation (2),

$$S_{E_S} = k_{fc} \cdot k_{pw} \cdot k_{hj} \cdot k_{vj} \cdot S_w \tag{2}$$

where

k_{fc} = Coefficient associated with the wall panel strength of concrete, (0.2 ∿ 1.1)

k_{pw} = Coefficient of the shear reinforcement ratio of the wall panel, (0.9 ∿ 1.4)

k_{hj} = Coefficient corresponding to the shear strength of the horizontal joint, (0.6 ∿ 1.0)

k_{vj} = Coefficient corresponding to shear strength of the vertical joint, (0.6 ∿ 1.0)

S_w = Coefficient of the standard horizontal load-carrying capacity defined by 10 A_w/W

A_w = Total cross-sectional area of the shear walls in one direction per unit floor area of the first story, ($cm.^2/cm.^2$)

W = Total weight of the house per unit floor area at the first story ($kg./cm.^2$)

10 = Assumed value of the standard unit of strength of the shear wall, ($kg./cm.^2$)

The flexural strength coefficient, S_{EB}, shall be calculated by using Equation (3),

$$S_{EB} = a \cdot B \cdot k_{pt} \cdot k_d \cdot S_w \qquad (3)$$

where

a = Coefficient corresponding to the reinforcement effect of the walls perpendicular to the direction under examination, (1.0 ∿ 1.4)

B = Coefficient corresponding to the flexural strength of the collar beams (1.0 ∿ 1.5)

k_{pt} = Coefficient corresponding to the bending reinforcement and anchorage of the shear walls

k_d = Coefficient corresponding to the ductility, (1.0 or 1.5)

b) In case of verification by experiment

i) The test specimen shall be a full-scale two- or three-dimensional structure fixed rigidly to the basement.

ii) The loading shall be cyclic and shall be controlled by horizontal deflection. There will be four loading stages with three cycles of loading for every stage. The various stages will consist of 1, 2, 3, and 4 times the deflection that occurs due to the design horizontal load and the deflections which correspond to the rotation angles of 1/22, 1/100, and 1/50. After the cyclic loads, this specimen shall be loaded to collapse.

iii) The following requirement shall also be satisfied,

Critical Condition	Required Value of "S"
A. Condition when severe structural damage is observed	Not less than 0.4
B. Ultimate Condition	Not less than 0.6

The coefficient "S" may be calculated by using the following equation,

$$S = k_1 \cdot k_2 \cdot C_B \cdot \sqrt{2\mu - 1}$$

where k_1, k_2 are the variables as defined for Equation (1),

C_B ; P/W

P is as defined in the following table (see Figure 3)

Critical Condition	A	B
P	80% of P_A, which is the maximum load observed before the specimen reaches Condition A	80% of P_{max}

W is the total weight of the specimen, including live load

μ is $\overline{\delta}/\delta$

DETAILS OF STRUCTURE

A. Load-bearing Wall Panels

The height of load-bearing wall panels shall be less than three times the width. The structural performance of the wall panels shall be checked by the following experiments specified in the Japanese Industrial Standard JIS 1414.

i) In-plane Shearing Test

ii) Eccentric Loading Test

iii) Bending Test

iv) Impact Test

In the case of steel structures, the design shearing force of the load-bearing wall panels shall not exceed 2/3 of the maximum shearing force, as obtained from the above shear-test. In addition, the shearing test results shall satisfy the following:

i) The horizontal displacement at the top of the panel, when the design shearing force is applied, shall not exceed 1/150 of the panel height.

ii) When the horizontal displacement at the top of the panel becomes three times the displacement due to the design shearing force, the panel shall be able to resist a shearing force equal to 5/4 times the design shearing force.

iii) Failure or large local deformations shall not occur on the surface of the cladding at a minimum horizontal displacement of 1/150 of the panel height.

B. Other Wall Panels

The same type of tests, as described above, shall be performed for other wall panels. In the in-plane shearing test, failure or large local deformations shall not occur until the horizontal displacement at the top of the panel equals 1/100 of the panel height.

C. Floors and Beams

Floors and beams shall maintain sufficient safety against dead and live loads. Vertical deflection shall not exceed 10 mm. nor 1/300 of the span. Failure or large local deformations shall not occur on the surface of the floors when a locally concentrated load of 150 kg magnitude is applied at any point.

D. Roofs

The vertical displacement of roofs, due to snow loads, shall not exceed 1/200 of the span.

Steel or wooden roofs shall be safe against wind loads. Deflection of the eaves when subjected to a distributed load of 240 kg./m.^{2} shall not exceed 1/100 of the spray length and the eaves shall not fail under a distributed load of 360 kg./m.^{2}.

E. Horizontal Plane Structures

Horizontal plane structures such as roofs and floors shall be rigid enough to transmit shearing forces to columns or walls. It is, therefore, necessary to provide horizontal bracings or to rigidly connect the roof or floor panels.

F. Columns

The column slenderness ratio of steel structures shall not exceed 200. The buckling length of a column shall be taken as its total length. Columns which consist of vertical ribs of wall panels and are connected to each other by bolts, the slenderness ratio shall be estimated from the loading test, as specified in JIS A 3304. The bearing capacity shall also be confirmed by full-scale tests.

G. Foundations

Foundations shall transmit external forces safely to the ground and resist overturning and differential settlement of the dwellings.

AN EXAMPLE OF INDUSTRIALIZED HOUSING STRUCTURE
(A Medium-sized Concrete Panel System)

As described in the first section, mass-production of industrialized housing in Japan started in the 1960's. During this period, the industrialized house was primarily constructed of prefabricated reinforced concrete panels. They were called "mass-produced publicly managed dwelling type", because they were adopted as publicly managed houses. Classification of the current industrialized houses of reinforced concrete structures are shown in Table 1. The most prevalent system at present is a medium-sized concrete panel system listed as Type "A" in the table. This sytem was developed by improving on the above-mentioned "mass-produced publicly managed dwelling type", and is now one of the most typical industrialized houses in Japan. In this section an outline of this type of medium-sized concrete panel system will be described relative to the structure.

OUTLINE OF THE STRUCTURAL SYSTEM

Medium-sized concrete panel systems consist of precast wall panels and floor panels which are connected to each other by bolts. The wall panels are surrounded by framing ribs and are about 250 m in height, about 90 cm. in width, and 4 cm. in thickness. The floor panels are approximately 270 to 360 cm. in length and 90 cm. in width. Some of the systems have collar beams between the wall and floor panels.

An outline of this structural system and typical construction procedures are shown in Figure 4. Arrangement of the reinforcement in a typical wall panel and the details of the wall base are shown in Figures 5 and 6, respectively.

FUNDAMENTAL PRINCIPLES FOR THE STRUCTURAL DESIGN

The fundamental principle for the structural design of this system is to set up rigid boxes by properly arranging wall panels and floor panels. That is;

a) To arrange seismic wall panels uniformly and effectively.

b) To connect the wall panels tightly to the collar beams or to the floor panels.

c) To connect the floor panels to each other and thus increase the rigidity of the horizontal plane.

d) To construct a continuous footing and to integrate the whole structure effectively.

e) To arrange the connecting bolts at the connections between the structural members.

In addition to these controls, the following must be taken into account;

f) Prevent occurrence of harmful cracks in members and joints under permanent load.

g) Prevent excessive deflections and unpleasant vibration in the floor.

h) Provide ductility to the structure and non-structural members and thus insure development of large horizontal displacements.

i) Prevent rusting of joining metals and reinforcing bars in the precast panels.

DETAILS OF EARTHQUAKE RESISTANT DESIGN

The procedure of the eathquake resistant design is as follows;

a) Determine the minimum values of wall length that are necessary for each floor and evaluate the maximum allowable distance between these walled panels

b) Arrange the wall panels and floor panels uniformly using the values determined above for each direction and at each story.

c) Calculate the stresses in each member and joint and check the appropriateness of the above arrangement.

Usually design procedures are dependent on the controls given in specific design manuals. The design earthquake load that has been adopted is the value which corresponds to a coefficient of 0.2, as given in the Building Code of Japan. The structural behavior of shear wall panels can be determined by a simplified method, as shown in Figure 7. In this method the height of the inflection points of the walls are determined by tests. Therefore, the effect of the bolt connection at the vertical joints, between wall panels, is neglected (see Figure 8). At the wall base shown in Figure 9, the cross-sectional areas of the reinforcements, a_t, and the anchor bolts, B^{at}, are determined from the tensile forces due to bending. The shear resistance at the wall base is determined by tests.

ESTIMATED STRUCTURAL PERFORMANCE AND PROBLEMS TO BE STUDIED IN THE FUTURE

From investigations on the structural characteristics of existing houses and test results on structural members, the following structural performance criteria are estimated.

i) Compressive Strength of Concrete — Approximately 300 $kg/cm.^2$

ii) Shear Strength — Design Value ($k = 0.2$) $\tau_D = 3 \sim 4$ kg/cm^2

Maximum Value by Test, $\tau_u = 7 \sim 13$ kg/cm^2

$\tau_D/\tau_u = 2 \sim 3.3$

In the case of a two-story house of this system, the total weight per unit area is $1.0 \sim 1.5$ t/m^2, and with the minimum wall length per unit area equal to $15 \sim 20$ cm/m^2. The yield base shear coefficient is estimated as $0.4 \sim 0.8$.

The following additional problems need to be studied for this type of structural system;

a) Although the elastic rigidity of this kind of structure is high, the plastic rigidity is remarkably low due to the additional deformation of the many joints. Further studies are, therefore, required to clarify the effects of these joints on earthquake response.

b) The durability of thin panel concrete shells and of exposed steel bolts should be improved.

Table 1 Classification of Industrialized Housing Structures of Concrete

	Kind of Member	Used Concrete	Connection Method	Structural System
A	Medium-sized thin panel with surrounding ribs	Normal concrete	Bolt	Walled system
B	do	Light weight aggregate concrete	Bolt or continuous bolt	do
C	Large-sized panel	Normal concrete	Bolt or welding of plate	do
D	do	Light weight aggregate	Bolt or high tension friction bolt	do
E	do	Foamed concrete	Anchored reinforcement shear cotter	do
F	A.L.C. panel	Autoclaved foamed concrete	Welding of bar or mortar cotter	do

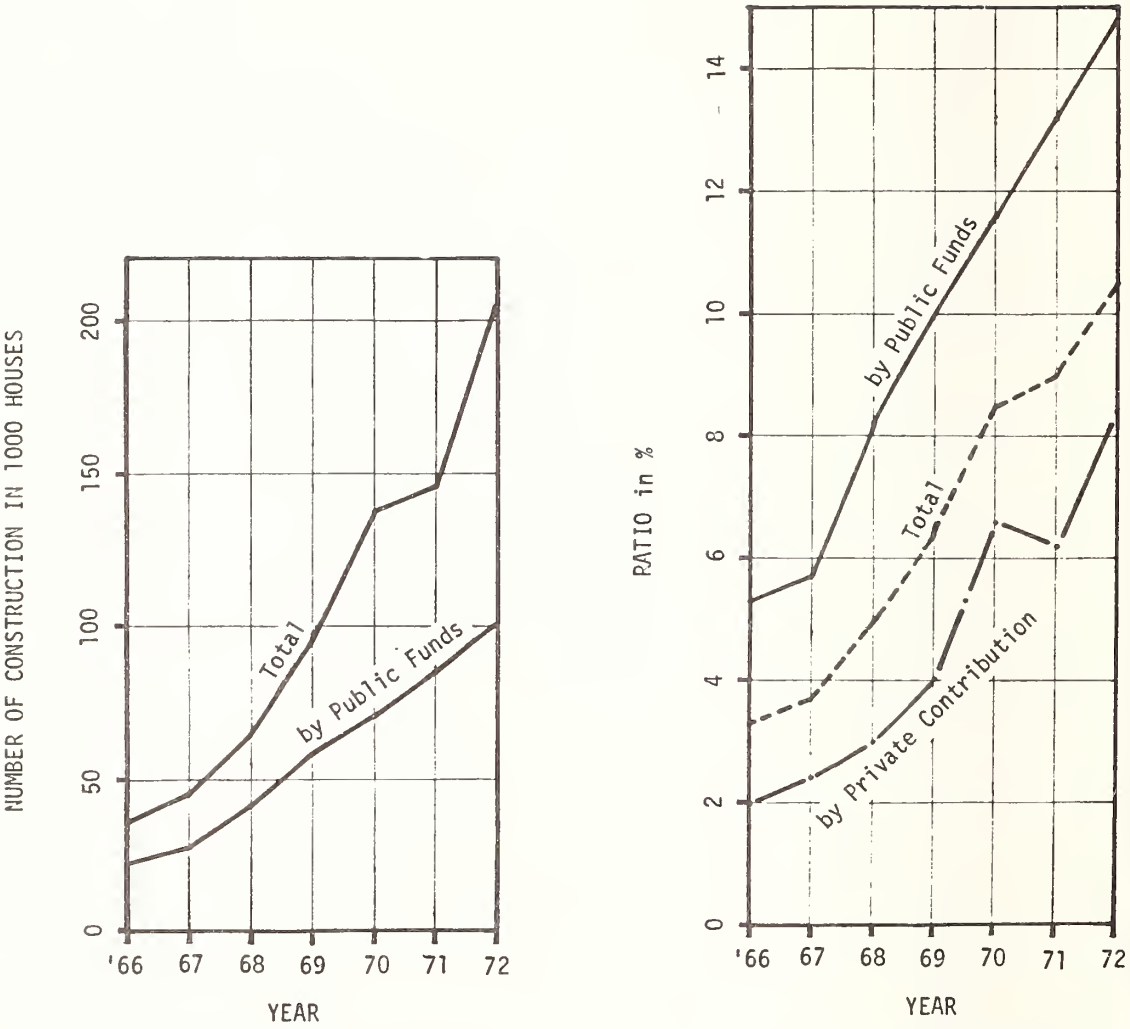

(a) NUMBER OF PREFABRICATED DWELLING CONSTRUCTION

(b) RATIO OF PREFABRICATER DWELLING CONSTRUCTION TO THE TOTAL DWELLING CONSTRUCTION

FIG. 1 YEARLY CHANGES OF PREFABRICATED DWELLING CONSTRUCTION IN JAPAN FROM 1966 TO 1972

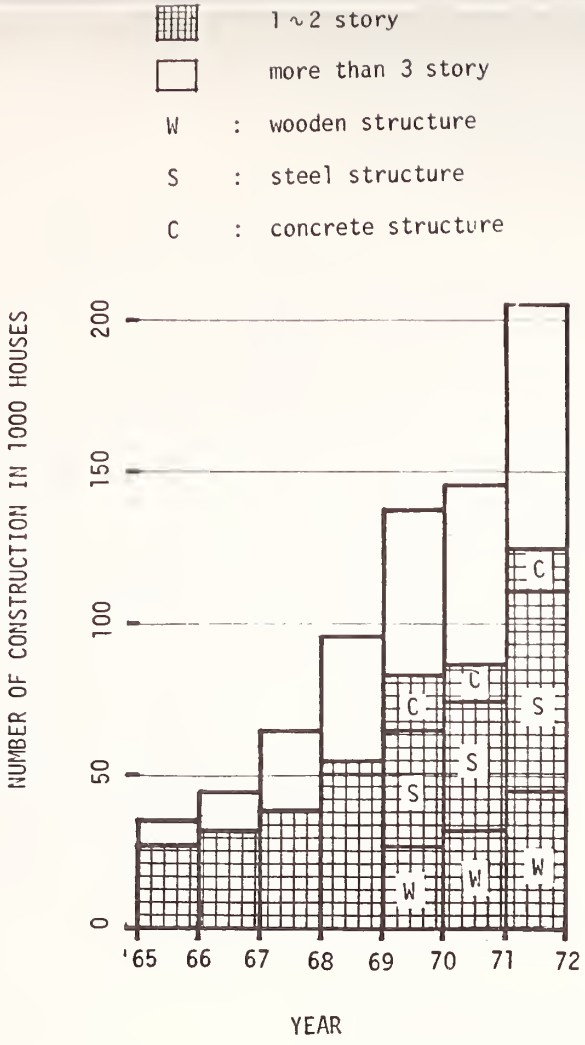

FIG. 2 YEARLY CHANGES OF THE CONSTITUTION OF PREFABRICATED DWELLING CONSTRUCTION

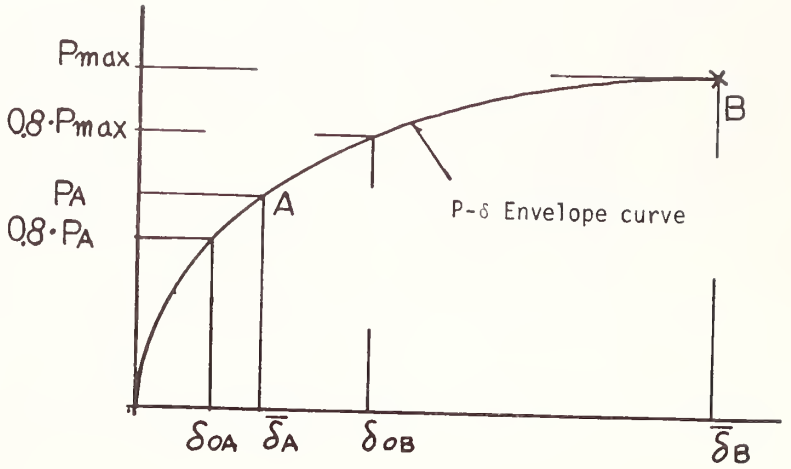

FIG. 3 CRITICAL LOADS AND DEFLECTIONS

FIG. 4 MEDIUM-SIZED PRECAST PANEL CONSTRUCTION WITH COLLER BEAMS

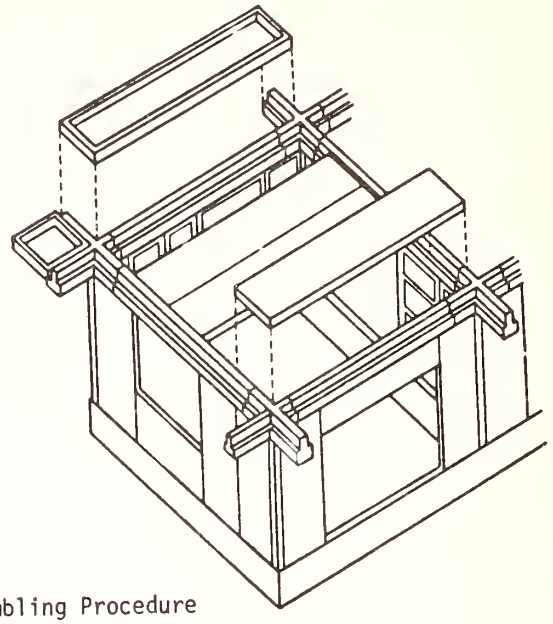

Assembling Procedure

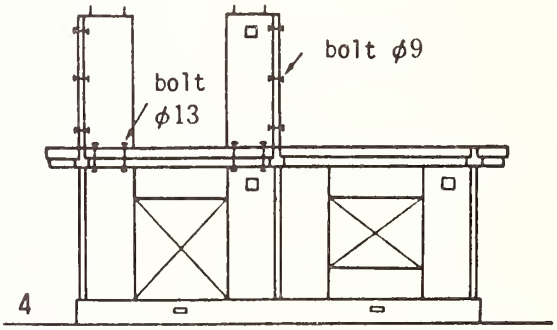

Construction of wall panels at the second floor

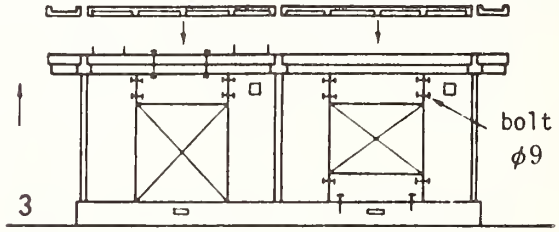

Construction of collor beams and floor slabs

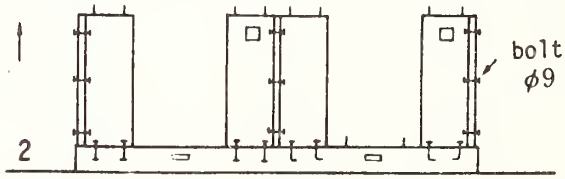

Construction of wall panels at the first floor

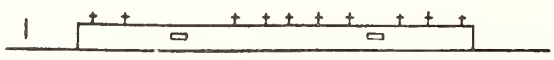

Construction of footing with anchor bolts

FIG. 5 DETAILS OF SEISMIC WALL PANELS

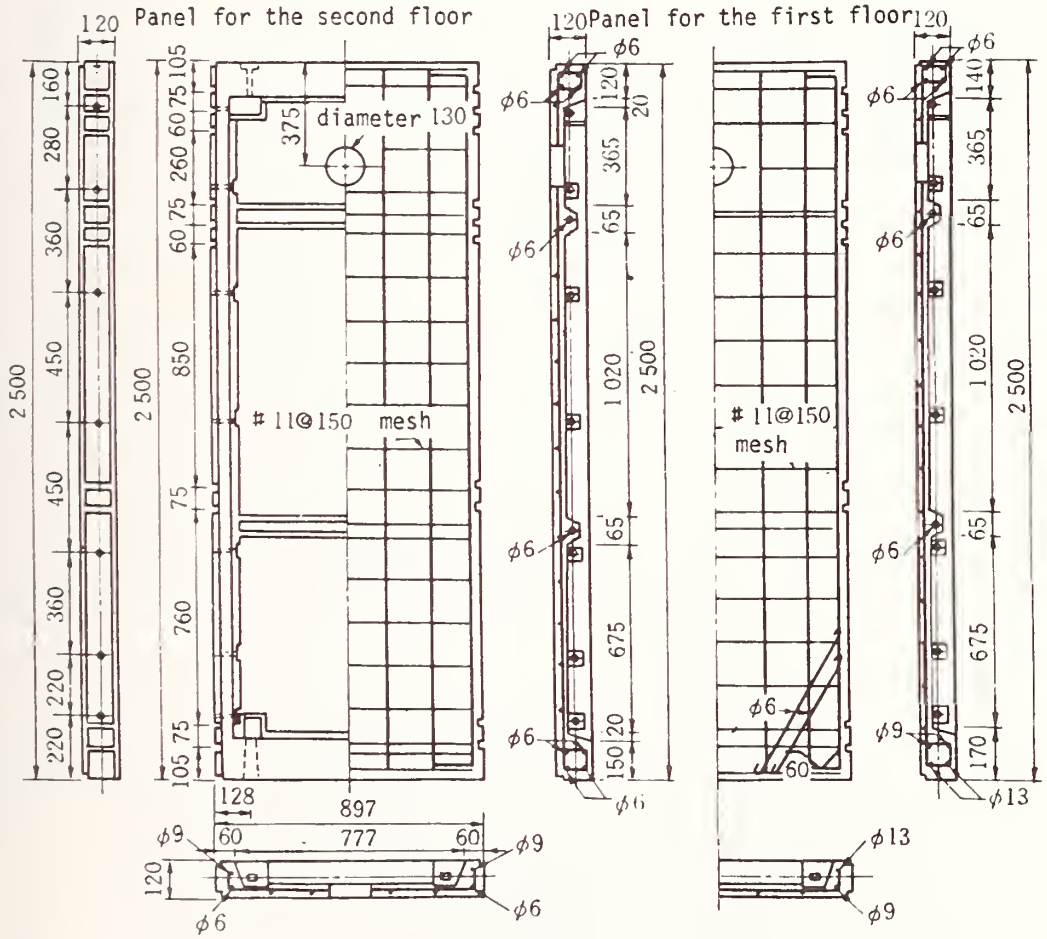

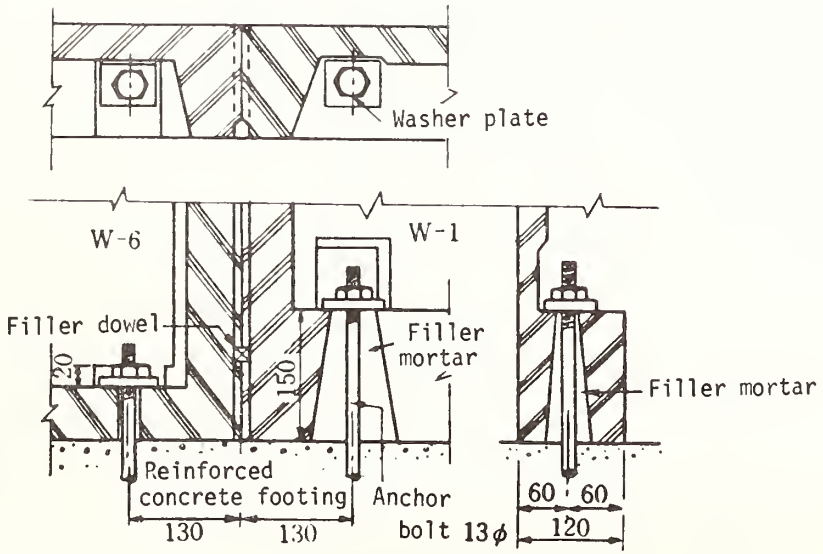

FIG. 6 DETAILS OF WALL PANEL BASE

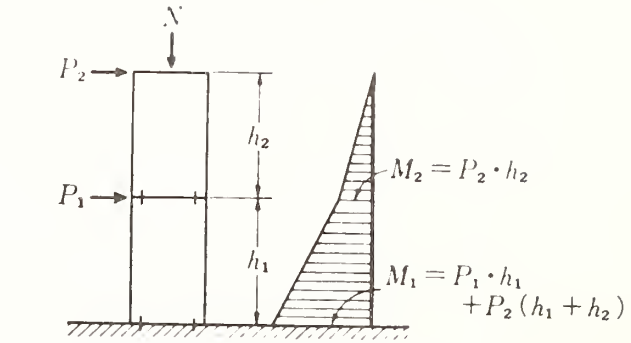

(a) In case without coller beams

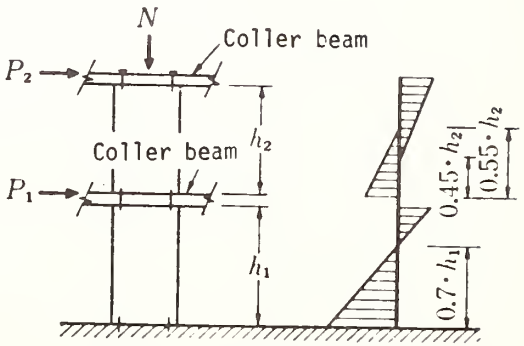

(b) In case with coller beams

FIG. 7 DESIGN BENDING MOMENT DISTRIBUTION OF SEISMIC WALL PANELS

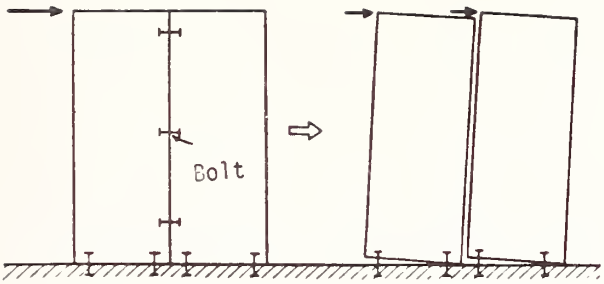

FIG. 8 NEGLECT OF CONNECTION BOLTS AT VERTICAL JOINT

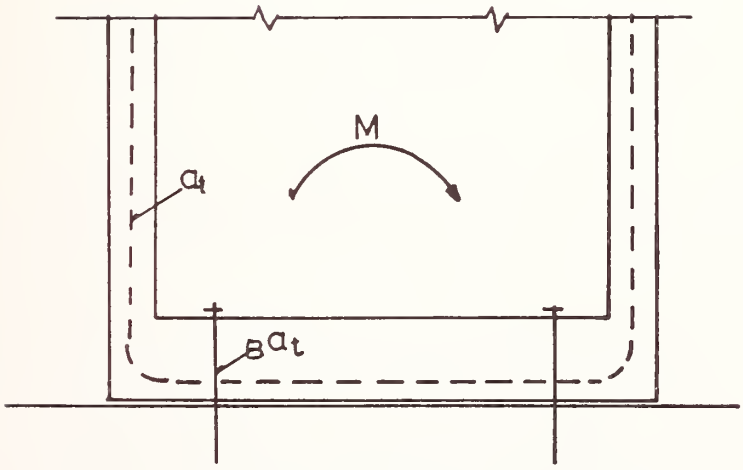

FIG. 9 RESISTING REINFORCEMENTS AGAINST MOMENT

AN ANALYTICAL MODEL FOR DETERMINING ENERGY DISSIPATION IN DYNAMICALLY LOADED STRUCTURES

by

John F. McNamara
Assistant Professor
Department of Civil Engineering

Sushil K. Sharma
Research Assistant
Department of Theoretical and Applied Mechanics

University of Illinois
and
Construction Engineering Research Laboratory
Champaign, Illinois

An analytical procedure is developed which predicts nonlinear cyclic structural response under large reversals of plastic strains. The structure is discretized by means of the finite element approximation, and the material behavior is simulated by a refined analytical model which describes the realistic hysteretic stress-strain curves of A36 steel under arbitrary cycles of load. In order to test the validity of this material model, some comparisons are made with experimental values of the inelastic response of a simply supported beam under cyclic bending. The model is subsequently used in the dynamic analysis of a portal frame subjected to a selected portion of the El Centro NS earthquake acceleration record. The improved cyclic response with the current approach is illustrated by comparing results with those obtained using a simple bilinear kinematic hardening material approximation. Comparisons are also made with values obtained using a commercially available nonlinear frame analysis computer program. Some final comments are made regarding the rate of solution convergence with integration time step size for two different temporal integration operators used in this analysis.

Key Words: Analytical model; dynamic analysis; dynamic loading; earthquake; energy dissipation; finite element; seismic response; structural engineering.

INTRODUCTION

The dynamic analysis of framed steel structures under earthquake loading would appear to be well in hand, and many studies and applicable computer programs are readily available (1, 2, 3). In terms of building configuration, structural elements, and applied loading, the programs are general in nature, but all assume that material behavior can be approximated in terms of moment-rotation joint relationships. A simple bilinear or Ramberg-Osgood (2, 4, 5) curve fit is usually adapted to model this material resistance function and appears adequate for most engineering applications. Currently accepted design criteria for steel structures with respect to lateral displacements, ductility ratios, and lateral forces have evolved from studies using the above computer programs. However, the complexity of the load-displacement hysteresis loops for frame type structures, where buckling, plastic straining, large displacements, and joint slip are active, can be judged from the survey given in (6) of computations and experiments on model structures.

A current study presents some results obtained during the course of a continuing research project on the magnitude and distribution of energy dissipation in dynamically loaded structures. A significant point of this research is that the behavior of the structure is found by means of a material model with properties derived from the exact hysteretic stress-strain behavior of A36 steel. Measurements of the cyclic behavior of A36 steel were carried out in (8), and the analytical model was developed and validated in (7) for uniaxial and multiaxial stress states. By means of this model, one can incorporate the results of advanced research in material behavior into engineering analysis. In all cases known to the writers, cyclic material behavior has been deduced from monotonic test curves while, in fact, highly accurate results on cyclic behavior are readily available (9, 10, 11). The development of this higher order material model supplements the current activity in the cyclic testing of structures through large strain reversals (12).

Since the material resistance is synthesized from knowledge of a pointwise stress-strain relation rather than a moment-rotation relation at a joint, the finite element method rather than a stiffness method is used to model the structure. The element used is a simple beam-column with the stiffness matrix obtained by numerical integration along the length and through the depth of a member element. A finite element plane stress analysis of a simply supported beam, cycled through three load reversals with large plastic strains, was used in (7) to check the material model under discussion. Further analysis of the same problem, using a beam-column element and idealized material properties, is given in (13). The purpose of the study in (13) was an assessment of the accuracy of numerical solution techniques with a particular reference to cyclic loading. The refined material model has been incorporated in a general purpose finite element computer program (14) capable of analyzing the nonlinear static and dynamic responses of engineering structures.

The objective of this research is to formulate an analytical procedure for determining overall structural energy dissipation properties on the basis of experimental cyclic material behavior. A projected use of the numerical results is an assessment of the effect of nonlinear material behavior on the damping properties of structures. The preliminary results given here are aimed at verifying the overall analytical model and the accuracy of the numerical solution procedures. For the case of a simple portal frame under earthquake excitation, it is shown that considerable differences in displacement values occur between the current results and those obtained using a bilinear kinmatic hardening stress-strain relation.

METHOD OF ANALYSIS

(i) Finite Element Formulation

The general equation of motion for a body, derived from the principle of virtual work, is written in terms of initial geometry as

$$(M)\{\ddot{q}_t\} = -\int_V (B)^T\{S\}\ dV + \{P_t\} \qquad (1)$$

where (M) is a consistent or diagonal mass matrix. $\{q\}$, $\{\ddot{q}\}$ are the generalized displacement and acceleration vectors. $\{P\}$ is a vector of equivalent nodal forces. $\{S\}$ is a vector of generalized stresses. The matrix (B) transforms generalized displacement increments at the nodes to generalized strain increments at any point in an element. It is defined by the equation

$$\{\Delta E\} = (B)\{\Delta q\} \tag{2}$$

and is a nonlinear function of displacement. The expressions used in forming (B) in the current study are given in the Appendix.

A modified, or corrected, linear incremental form (14) of Equation (1) is obtained as

$$(M)\{\Delta\ddot{q}_{t+\Delta t}\} = \int_V (\Delta B)^T \{S\}\, dV - \int_V (B)^T\{\Delta S\}\, dV + \{\Delta P_{t+\Delta t}\} + (-(M)\{\ddot{q}_t\} - \int_V (B)^T \{S\}\, dV + \{P_t\}) \tag{3}$$

The incremental stress vector $\{\Delta S\}$ can be expressed in terms of $\{\Delta q\}$ by using Equation (2) and the following linear incremental stress-strain relation

$$\{\Delta S\} = (D_{ep})\{\Delta E\} \tag{4}$$

The construction of the elastic-plastic stress-strain transformation matrix (D_{ep}) with reference to the new material model follows the approach outlined in (15). By substituting Equation (4) in Equation (3) and following procedures described in (15), Equation (3) can be written as

$$(M)\{\Delta\ddot{q}_{t+\Delta t}\} = -(K_t)\{\Delta q_{t+\Delta t}\} + \{\Delta P_{t+\Delta t}\} + \{I_t\} \tag{5}$$

where the tangential stiffness matrix (K_t) is formed by combining the first two integrals on the right hand side of Equation (3), and the "load correction term", $\{I_t\}$, is the contribution of the terms inside the parenthesis in Equation (3). $\{I_t\}$ is the total unbalanced force at time t.

(ii) Time Integration

The controversy over an optimum temporal integration operator has produced a large volume of studies in recent years. Direct methods (16) are available for estimating the accuracy of these operators when applied to linear systems (17), but it seems that only numerical experiments can provide a measure of their worth in the nonlinear case. In a recent analysis (18) of the performance of several popular operators, namely; the Houbolt (19), the Wilson (20), the Newmark Beta (21), and the central difference operator, it was noted that the accuracy and stability of solutions with these operators were very different between corresponding linear and nonlinear applications. The overall conclusion arrived at in (18) is that inaccuracies in nonlinear solutions accumulate very rapidly when integration operators are used with time increments larger than that of the stability limit given by the central difference operator.

In order to further investigate the result described above, both the central difference operator and the Newmark operator with $\beta = 1/4$ and $\gamma = 1/2$ were used in the current study. The latter operator is generally applied in earthquake engineering and is the basis of the solution method in (3). The incremental value of the displacement vector is given by the central difference operator as

$$\{\Delta q_t\} = \{\Delta q_{t-\Delta t}\} + \Delta t^2\{\ddot{q}_{t-\Delta t}\} \tag{6}$$

The solution cycle is formed by calculating the displacement increment from Equation (6) and using this value to compute the integral on the right hand side of Equation (1). The acceleration for the next step is found by solving Equation (1) for $\{\ddot{q}_t\}$. The operator is not self-starting and suitable initial values are outlined in (18).

Because of its implicit form, the Newmark operator is more conveniently combined with a linearized equation of motion such as given by Equation (5). The increment of acceleration is given by

$$\{\Delta\ddot{q}_{t+\Delta t}\} = \frac{1}{4\Delta t^2}(\{\Delta q_{t+\Delta t}\} - \Delta t\,\{\dot{q}_t\} - \frac{\Delta t^2}{2}\{\ddot{q}_t\}) \tag{7}$$

Substitution of Equation (7) into Equation (5) yields

$$(\frac{4(M)}{\Delta t^2} + (K_t))\,\{\Delta q_{t+\Delta t}\} = \{\Delta P_{t+\Delta t}\} + \{I_t\} + \frac{4(M)}{\Delta t^2}(\Delta t\{\dot{q}_t\} + \frac{\Delta t^2}{2}\{\ddot{q}_t\}) \tag{8}$$

In this approach $\{\Delta q_{t+\Delta t}\}$ is first calculated from Equation (8) and then substituted back into Equation (7) to find the acceleration increment. The velocity vector is given by

$$\{\Delta\dot{q}_{t+\Delta t}\} = \{\dot{q}_t\} + \frac{\Delta t}{2}(\{\ddot{q}_t\} + \{q_{t+\Delta t}\}) \tag{9}$$

Damping forces of the equivalent viscous type are not included at present since they would complicate the interpretation of the effect of material nonlinearity in the response.

(iii) Constitutive Relation and Refined Material Model

The new refined material model is an extension of the work of Martin (22) and Jhansale (23) and is described in detail in (7, 8). A mechanical analog of the basic series model with only three elements is shown in Figure 1. Each spring of the system has a linear stress-strain relationship. The springs in the parallel spring-slider elements are not deformed until the applied stress reaches the yield stress of the slider in that element. If the applied stress in an element reaches above the yield stress, then the difference is stored in the element as a residual stress. The tangent modulus E_i^* on a given segment of the curve is obtained from the relation

$$\frac{1}{E_i^*} = \frac{1}{E} + \sum \frac{1}{E_i} \tag{10}$$

where the summation is extended over all those spring-slider elements which have yielded. The stress-strain response with this model follows Massing's hypothesis where the closed hysteresis loops are the same form as the stablized initial branch OA of the stress-strain curve except for an enlargement by a factor of two (10). The hypothesis also implies that after a small hysteresis loop EFGH, the loading branch will follow the path EI instead of EJ. This is an example of the "memory" effect which is created by the distribution of residual stress in the elastic springs.

This basic model cannot, however, accurately trace the hysteretic stress-strain curve of A36 steel for two reasons. Firstly, A36 steel in its "stable" condition does not obey Massing's hypothesis. This is shown in Figure 2 where the cyclic stress-strain curve, increased by a factor of two, does not accurately describe the hysteresis loop shapes, and the upper hysteresis loop tips do not fall along the upper trace of the largest loop. Secondly, A36 steel cyclically hardens or softens before becoming stable. It was observed in (23) and (7) that even during the hardening and softening process each upper branch of stress-strain curve (except for the initial flat top branch) could be fitted to the double skeleton curve for the "stable" material by translating the loop along the elastic line. The loop is translated along the elastic line until the upper loop tip is approximately tangent to the double skeleton curve. An outer trace of a given loop is then described in terms of this skeleton curve and an appropriate stress offset, S_{os}, which defines the amount that the loop must be displaced along the elastic line. In Figure 3 the individual branches of hysteresis loops obtained from constant amplitude strain controlled tests have been fitted to the double skeleton curve. As shown in the figure, the stress offset, S_{os}, depends on the number of reversals and the total strain range. In this study S_{os} is approximated by a family of linear functions of the number of reversals and the total strain range.

The analytical material model also incorporates cycle-dependent mean stress as described in (7), but this feature is not activated in the present study. An added feature is that the initial response of the model is determined by a set of constants derived from the "flat-top" stress-strain curve obtained by testing a virgin specimen of A36 steel. The spring constants and slider stress values for subsequent reversals after the first loading are found separately from the skeleton curve obtained from constant amplitude strain controlled cyclic tests of steel specimens. The procedure, used to compute the spring constants and slider stress values, is described in detail in Appendix A of (7). Agreement between the refined material model and a complicated cyclic stress-strain history for a virgin steel is shown to be highly satisfactory by the results depicted in Figure 4.

NUMERICAL RESULTS

(i) Verification of Material Model in Structural Application

In order to test the validity of the material model in structural applications, the beam problem, described in Figure 5, was developed. Ten spring-slider elements were used in the material simulation, and the dimensions of the beam were chosen in order to obtain large plastic strains without introducing nonlinear geometric effects. The beam was loaded and reloaded through three cycles, as shown in Figure 5. In the earlier investigation of Plummer (7), the beam half-span was modeled by fifteen plane stress eight-node isoparametric finite elements (24). With a view to later, more general frame-type structural applications, the half-span was modeled with ten simple beam-column elements in the present study. The generalized strain-displacement relations on which the beam-column element is based are outlined in the Appendix.

The numerical and experimental results for the beam are compared in Figure 6. The geometric shapes of both curves are so clearly similar that it appears that a slight extension of the elastic range would allow perfect agreement. The dimensions of the beam span, cross-section, and concentrated loading also make it likely that shear deformations contribute in part to the difference in results. This is investigated in Figure 7 where the results of the plane stress analysis from (7) are compared with the current beam-column results. The continual redistribution of the two-dimensional stress state in the plane stress results means that, even for zero hardening, the load will continue to increase after the critical mid-section has become totally plastic. In a similar example, Felippa (25) found a 35 percent increase in load capacity beyond the limit load in simple bending at a displacement of approximately five times the elastic limit value. The effect in this case is to give the plane stress curve a greater slope on the initial branch which leads to high residual stresses in the spring elements before the first reversal. The residual stresses for the beam-column case are practically zero except for one element, and this means a flatter response will occur on the subsequent reversal. It is felt that this effect rather than shear displacement causes most of the difference in results in Figure 7 at the end of the second reversal.

These preliminary results indicate that further tuning of the analytical material model may be in order. Current suggestions in this respect are to drop the initial monotonic "flat-top" behavior and use the cyclic skeleton curve for calculating one set of spring and slider values for all cases. Omission of the "flat-top" first cycle may result in an overall improved response. It was suggested in Appendix A of (7) that fictitious residual stresses be built in at the end of the "flat-top" cycle, but this may overly complicate the parameters of the model. Another modification under study concerns the fact that in the current model, the effect of the increase in elastic range, described as a stress offset in Figure 3, is not added to the first slider, or first segment of the stress-strain curve. It was commented on earlier that the experimental values appear to indicate that an extended elastic range is necessary for improved agreement, and the relaxation of this restriction on the first slider may be helpful.

(ii) Response of a Portal Frame to Seismic Loading

The portal frame described in (26) was modeled with three finite elements per member and subjected to a selected four seconds (1.5 sec. - 5.5 sec.) of the El Centro NS earthquake acceleration record magnified by a factor of 1.5. The equations of motion must be adjusted to reflect this type of loading and Equation (8) is replaced by

$$\left(\frac{4(M)}{\Delta t^2} + (K_t)\right) \{\Delta u_{t+\Delta t}\} = \{\Delta P_{t+\Delta t}\} + \{I_t\} + \frac{4(M)}{\Delta t^2}\left(\Delta t \{\dot{u}_t\} + \frac{\Delta t^2}{2}\{\ddot{u}_t\} - \frac{\Delta t^2}{4}\{\ddot{Q}_t\}\right) \tag{11}$$

where $\{\Delta u_{t+\Delta t}\}$ is now the generalized displacement relative to base of the structure. The vector $\{\ddot{Q}_t\}$ is formed by the components of base acceleration input. The equilibrium correction term is also changed to

$$\{I_t\} = -(M)(\{\ddot{u}_t\} + \{\ddot{Q}_t\}) - \int_V (B)^T\{S\}\, dv + \{P_t\} \tag{12}$$

For the solution with the central difference operator, Equation (1) is solved as it is written for the absolute acceleration, and the relative structural acceleration is obtained from the relation

$$\{\ddot{u}_t\} = \{\ddot{q}_t\} - \{\ddot{Q}_t\} \tag{13}$$

Displacements relative to the base, for the purposes of calculating internal forces, are found in the usual manner as

$$\{\Delta u_t\} = \{\Delta u_{t-\Delta t}\} + \Delta t^2\{u_{t-\Delta t}\} \tag{14}$$

The stiffness matrix (K_t) is generated numerically using three Gaussian points along the length, and the cross-sections of the I-beams are modeled by three specially weighted integration points, one placed in each flange and one at the center. The number of points in all cases can be varied, and an option also exists which allows stresses to be computed at one or all Gaussian integration points. A diagonal mass matrix is formed in the program by collapsing all rows of the consistently formed matrix onto the diagonal. The diagonal mass matrix is used with Equation (1) and the central difference operator, and the consistent mass matrix is used in Equation (11) since there is no apparent computational advantage in using the diagonal form.

The dotted line in Figure 8 indicates the response of the frame with the new material model and the central difference operator. In the same figure, the solid line passing through the triangles represents the response with kinematic hardening idealized by a simple bilinear stress-strain curve given by $E = 30 \times 10^6$ psk, $\sigma_y = 36 \times 10^3$ psi, and $E_T/E = 0.1$. A comparison of these two curves indicate the influence of the added cyclic hardening effect in the refined material model over the idealized behavior. The results clearly demonstrate a cumulative effect as the divergence between the results increases with each reversal of the response. It is emphasized that the model structure is a simple portal frame loaded with only a fraction of a typical earthquake input, and greater differences can be expected in the analysis of more complex framed structures under an extended earthquake input.

The solid line passing through the circles in Figure 8 shows the values given by DRAIN-2D which is a standard stiffness-type program developed by Kanaan and Powell (3). The material response is based on a bilinear moment-rotation joint, or node, relationship, and the moment-axial force interaction diagram with shape code 2 (3) was adopted. Each frame member was divided into three equal elements, and the elastic constants and hardening modulus mentioned above were employed in the analysis. Inspection of Figure 8 shows that the results with DRAIN-2D agree in general with those found using bilinear kinematic hardening. The divergence of these curves at the final peak values in the response may be attributed to the different yield criteria and to the manner in which the structural stiffnesses are computed in the respective computer programs. The agreement between

DRAIN-2D and the results of the refined material model at the final peak displacement appears to be fortuitous since the displacement histories are considerbly different up to this point.

(iii) Selection of Time Increment for the Temporal Integration Operators

For linear problems, the choice of an implicit versus explicit integration operator, such as the Newmark over the central difference operator, is often governed by the fact that the latter is only conditionally stable with respect to time increment size. Also, accurate solutions with comparatively large time increments can be obtained from Newmark's operator with $\beta = 1/4$ since the amplitude of each mode is conserved (21). However, the results obtained in (18) for a geometrically nonlinear simple beam problem showed that all implicit methods suffered serious inaccuracies for time increments greater than that found to give stable results with the central difference operator, and that the Newmark method was the worst in this respect.

In the current study the portal frame, described in Figure 8, was subjected to a sinusoidal base excitation in order to find suitable integration time-steps for the central difference and the Newmark operator. The response was obtained with the refined material model as well as with DRAIN-2D which also uses the Newmark operator, and the results are shown in Figure 9. The limiting stable time increment size for the central difference operator was found to be 0.0025 seconds, and an apparently stable response was obtained with the Newmark operator for a time step of 0.00625. Figure 9 indicates clearly the problem of identifying between stable but not necessarily accurate solutions. In this case all results were in agreement up until a time of 0.45 seconds when both DRAIN-2D and the finite element solution with Newmark's method begin to diverge from the central difference solution. Therefore, it was decided to assess this phenomenon more accurately by running the problem described in Figure 8 with decreasing time increments until convergence was achieved for the response over the time of the earthquake input. The results obtained with DRAIN-2D for increments of 0.005 and 0.0025 are shown in Figure 10. No change occurred with a reduction in step size to .00124 and so convergence is assumed for Δt equal to .0025. The problem is now evident in that apparent convergence occurs over the first cycle or so with subsequent slow, but finally appreciable, divergence after approximately two seconds of the response. The recommendation is made to use the stable central difference time increment in that the seemingly apparent stability and delayed appearance of gross inaccuracies with implicit operators could lead one to believe that one had a convergent solution at larger time steps.

The results under discussion in this section, with the exception of the central difference case, were all obtained using the incremental form of the equations of motion with an elementary equilibrium, or load, correction term. It can be argued that an iterative solution at each step would improve the accuracy of the implicit solution schemes. This was attempted in (18), and for the problem studied, the iterated scheme made a difference only at those time increments which had already caused large errors, and no overall significant improvement was apparent. Further study in this respect is necessary, but the economic aspect of an explicit central difference versus an iterated implicit solution may be the deciding factor in favor of the former method. An added consideration is the simplicity of central differnce solution scheme and its considerable advantage with respect to computer storage demand over the other methods.

CONCLUSIONS

An analytical procedure has been described which incorporates constitutive relations based on a higher order material model. A comparison of analytical and experimental results for a virgin A36 steel coupon and for a simply supported beam has shown the capability of the refined model to accurately predict the cyclic hysteretic material behavior.

The responses of a portal frame subjected to the El Centro NS earthquake acceleration record have been compared for the refined material model, a bilinear kinematic hardening model, and the DRAIN-2D model. The significant differences in the computed results have

clearly demonstrated the effect of cyclic hardening on seismic structural response, and warrant a further study of this phenomenon with respect to energy dissipation and fatigue life of steel structures. The preliminary dynamic results suggest that for comparable accuracy, the time increments for implicit integration operators and for the central difference operator must be of the same order in the case of nonlinear problems with complex time-motion histories.

ACKNOWLEDGMENT

The writers express their thanks to Dr. F.B. Plummer, Esso Production Research Company, Houston, Texas, for his assistance in inserting his computer model of material behavior into their program.

REFERENCES

1. Rea, D., Bouwkamp, J.G., and Clough, R.W., "The Dynamic Behavior of Steel Frame and Truss Buildings," American Iron and Steel Institute, Bull. No. 9, April 1968.

2. Goel, S.C., "Response of Multistory Steel Frames to Earthquake Forces," American Iron and Steel Institute, Bull. No. 12, November 1968.

3. Kanaan, A.E., and Powell, G.H., "DRAIN-2D...Inelastic Dynamic Response of Plane Structures," NISEE/Computer Applications, University of California, Berkeley, California, 1973.

4. Ramberg, W., and Osgood, W.R., "Description of Stress-Strain Curves by Three Parameters," Technical Note 902, NACA, July 1943.

5. Jennings, P.C., "Periodic Response of a General Yielding Structure," Journal of the Engineering Mechanics Division, ASCE, Vol. 90, No. EM2, April 1964, pp. 131-166.

6. Wakabayashi, M., "Frames Under Strong Impulsive, Wind or Seismic Loading," Proceedings of the International Conference on Planning and Design of Tall Buildings, Lehigh University, Bethlehem, Pennsylvania, 21-26 August 1972.

7. Plummer, F.B., "A New Look at Structural Energy Dissipation," Technical Report M-82, Construction Engineering Research Laboratory, Champaign, Illinois, 1974.

8. Martin, John F., "Cyclic Mechanical Tests and an Appropriate Analytical Stress-Strain Model for A36 Steel," Technical Report M-86, Construction Engineering Research Laboratory, Champaign, Illinois, 1974.

9. Landgraf, R.W., Morrow, J., and Endo, T., "Determination of the Cyclic Stress-Strain Curve," Journal of Materials, Vol. 4, No. 1, March 1969, pp. 176-188.

10. Morrow, J., "Cyclic Plastic Strain Energy and Fatigue of Metals," Internal Friction, Damping, and Cyclic Plasticity, ASTM STP 378, American Society for Testing and Materials, 1965, pp. 45-87.

11. Iwan, W.D., "On a Class of Models for the Yielding Behavior of Continuous and Composite Systems," Journal of Applied Mechanics, Vol. 34, No. 3, September 1967, pp. 612-617.

12. Popov, E.P., and Benter, V.V., "Cyclic Loading of Steel Beams and Connections," Journal of the Structural Division, ASCE, Vol. 99, No. ST6, June 1973, pp. 1189-1204.

13. McNamara, J.F., "Numerical Solution Techniques for Highly Nonlinear Static Structural Behavior," Proceedings of the 1974 Army Numerical Analysis Conference, Philadelphia, Pennsylvania, 12-14 February 1974.

14. McNamara, J.F., and Marcal, P.V., "Incremental Stiffness Method for Finite Element Analysis of the Nonlinear Dynamic Problem," Int. Symposium on Numerical and Computer Methods in Structural Mechanics, Urbana, Illinois, September 1971.

15. Marcal, P.V., "Finite Element Analysis of Combined Problems of Nonlinear Material and Geometric Behavior," Division of Engineering, Brown University, Report N00014-007/2, June 1969.

16. Nickel, R.E., "Direct Integration Methods in Structural Dynamics," Journal of Engineering Mechanics Division, ASCE, V. 99, No. EM2, April 1973, pp. 303-317.

17. Goudreau, G.L., and Taylor, R.L., "Evaluation of Numerical Integration Methods in Elastodynamics," Computer Methods in Applied Mechanics and Engineering, Vol. 2, 1972, pp. 69-97.

18. McNamara, J.F., "Solution Schemes for Problems of Nonlinear Dynamics," to be published, Journal of Pressure Vessel Technology, ASME.

19. Houbolt, J.C., "A Recurrence Matrix Solution for the Dynamic Response of Elastic Aircraft," Journal of Aeronautical Sciences, Vol. 17, 1950, pp. 540-550.

20. Bathe, J.E., and Wilson, E.L., "Stability and Accuracy Analysis of Direct Integration Methods," International Journal of Earthquake Engineering and Structural Dynamics, Vol. 1, 1973, pp. 283-291.

21. Newmark, N.M., "A Method of Computation for Structural Dynamics," Journal of the Engineering Mechanics Division, ASCE, Vol. 85, No. EM3, July 1959, pp. 67-94.

22. Martin, J.F., Topper, T.H., and Sinclair, G.M., "Computer Based Simulation of Cyclic Stress-Strain Behavior with Applications to Fatigue," Materials Research and Standards, ASTM, Vol. 11, No. 2, February 1971, pp. 23-29.

23. Jhansale, H.R. and Topper, T.H., "An Engineering Analysis of the Inelastic Stress Response of a Structural Metal Under Variable Cyclic Strains," Cyclic Stress-Strain Behavior--Analysis, Experimentation and Failure, ASTM STP 519, 1973, pp. 246-270.

24. Zienhievicz, O.C., The Finite Element Method in Engineering Science, McGraw-Hill Publishing Company Limited, London, 1971.

25. Felippa, C.A., "Refined Finite Element Analysis of Linear and Nonlinear Two-Dimensional Structures," Ph.D. Thesis, University of California, Berkeley, California, 1966.

26. Toridis, T.G., and Khozeimch, K., "In elastic Response of Frames to Dynamic Loads," Journal of the Engineering Mechanics Division, ASCE, Vol. 97, No. EM3, June 1971, pp. 847-863.

APPENDIX

Beam-Column Finite Element

The axial and normal displacments U and V at a point (X, Y) of the beam are approximated by a linear and a cubic interpolation function of X, respectively.

$$U = a_0 + a_1 X \tag{A-1}$$

$$V = b_0 + b_1 X + b_2 X^2 + b_3 X^3 \tag{A-2}$$

where a_0, a_1, b_0,...., b_3 are generalized displacement coefficients.

It is convenient to separate the strain E at (X, Y) into its membrane and bending components E_m and E_b, where

$$E_m = \frac{dU}{dX} + \frac{1}{2}\left(\frac{dU}{dX}\right)^2 + \frac{1}{2}\left(\frac{dV}{dX}\right)^2$$

$$E_b = - Y \frac{d^2V}{dX^2} \tag{A-3}$$

From Equations (A-1) and (A-2)

$$dU/dX = a_1$$

$$dV/dX = b_1 + 2b_2 X + 3b_3 X^2 \tag{A-4}$$

An increment of strain is obtained from Equation (A-3) as

$$\Delta E_m = \Delta\frac{dU}{dX} + \frac{dU}{dX}\left(\Delta\frac{dU}{dX}\right) + \frac{dV}{dX}\left(\Delta\frac{dV}{dX}\right)$$

$$\Delta E_b = - Y\left(\Delta\frac{d^2V}{dX^2}\right) \tag{A-5}$$

Substituting Equation (A-4) into (A-5), ΔE_m and ΔE_b can be expressed in terms of increments of generalized displacements as

$$\begin{Bmatrix} \Delta E_m \\ \Delta E_b \end{Bmatrix} = \begin{bmatrix} 0 & 1 + \frac{dU}{dX} & 0 & \frac{dV}{dX} & 2X\frac{dV}{dX} & 3X^2\frac{dV}{dX} \\ 0 & 0 & 0 & 0 & - 2Y & - 6XY \end{bmatrix} \begin{Bmatrix} \Delta a_0 \\ \Delta a_1 \\ \Delta b_0 \\ \Delta b_1 \\ \Delta b_2 \\ \Delta b_3 \end{Bmatrix} \tag{A-6}$$

From Equation (A-6), matrix (B) which relates generalized incremental strains with generalized incremental displacements is readily identified as

$$(B) = \begin{bmatrix} 0 & 1 + \frac{dU}{dX} & 0 & \frac{dV}{dX} & 2X\frac{dV}{dX} & 3X^2\frac{dV}{dX} \\ 0 & 0 & 0 & 0 & - 2Y & - 6XY \end{bmatrix} \tag{A-7}$$

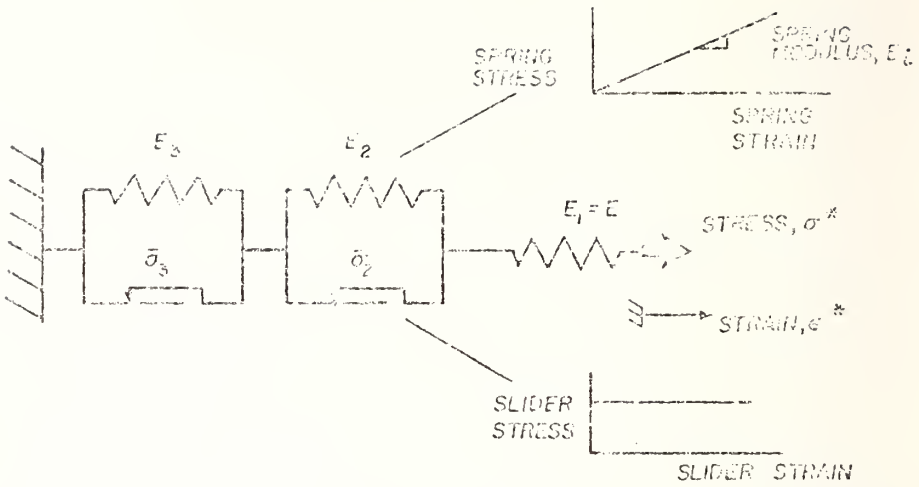

MECHANICAL ANALOG OF THE STRESS--STRAIN SIMULATION FOR A 36 STEEL

$$\frac{1}{E_i^*} = \frac{1}{E} + \Sigma \frac{1}{E_i}$$

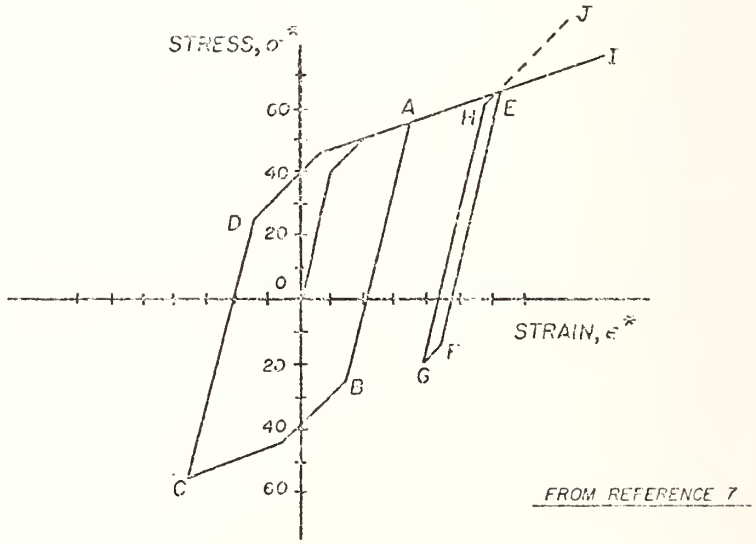

FROM REFERENCE 7

FIGURE 1. STRESS - STRAIN RESPONSE OF THE SERIES MODEL

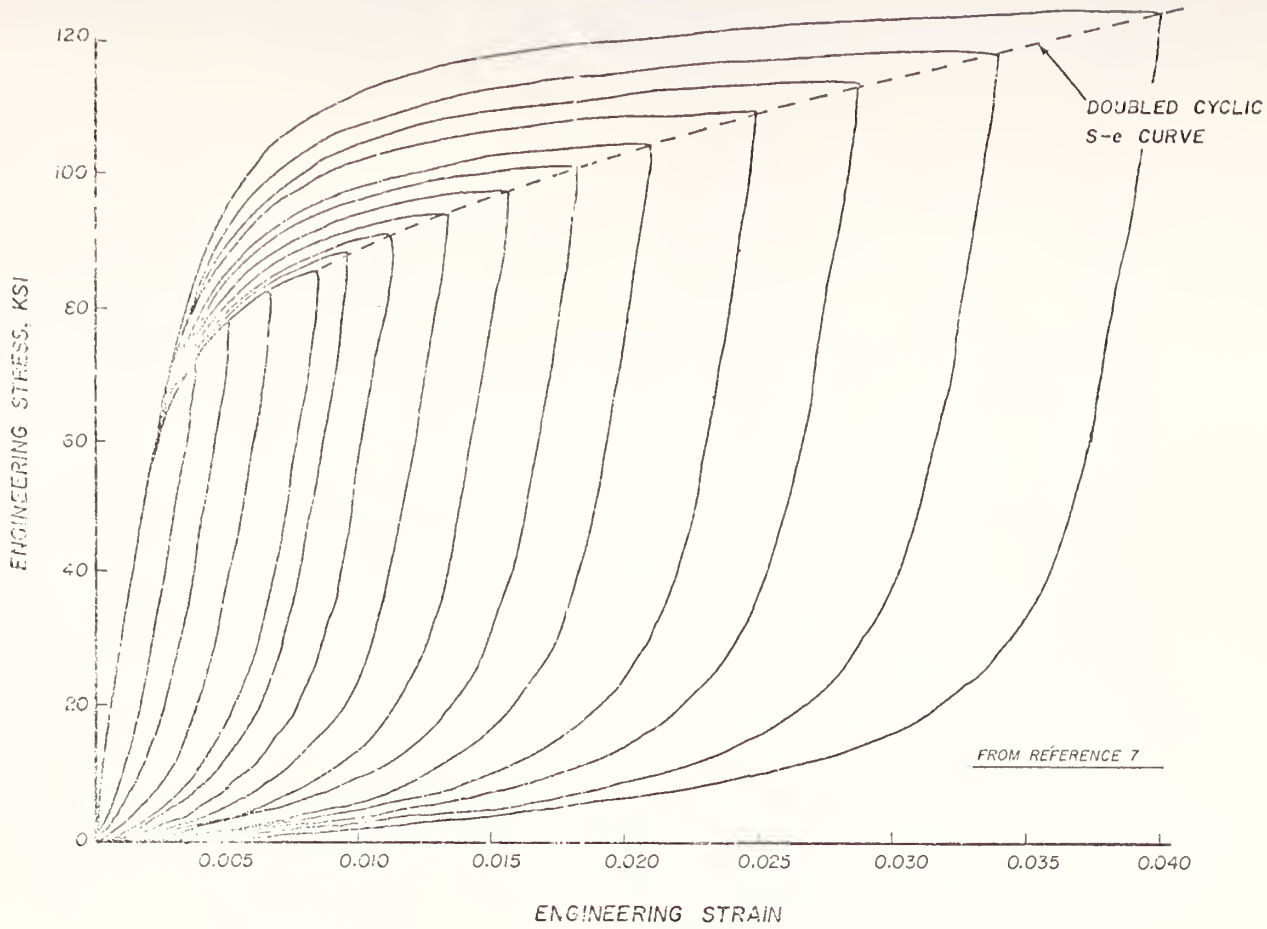

FIGURE 2. "STABLE" HYSTERESIS LOOPS FOR A36 STEEL WITH A COMMON ORIGIN

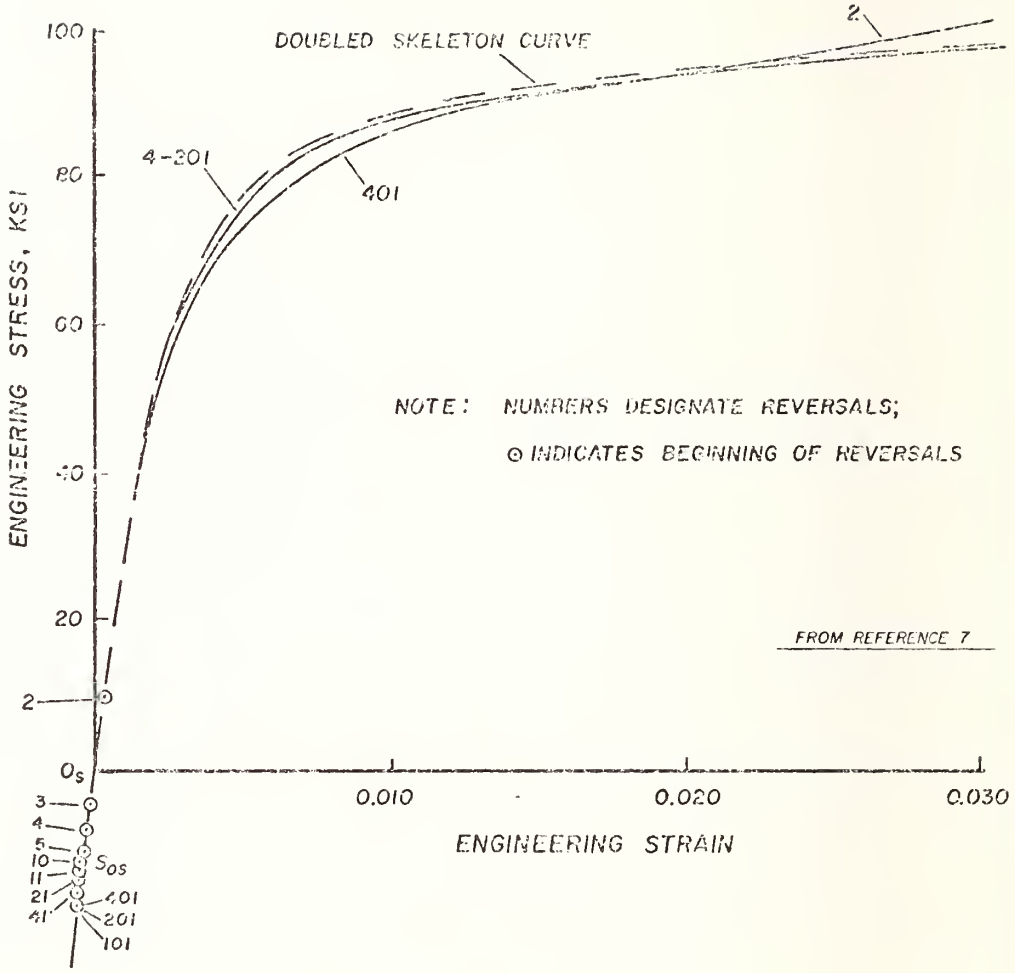

FIGURE 3. HYSTERESIS LOOP BRANCHES FITTED TO THE SKELETON CURVE

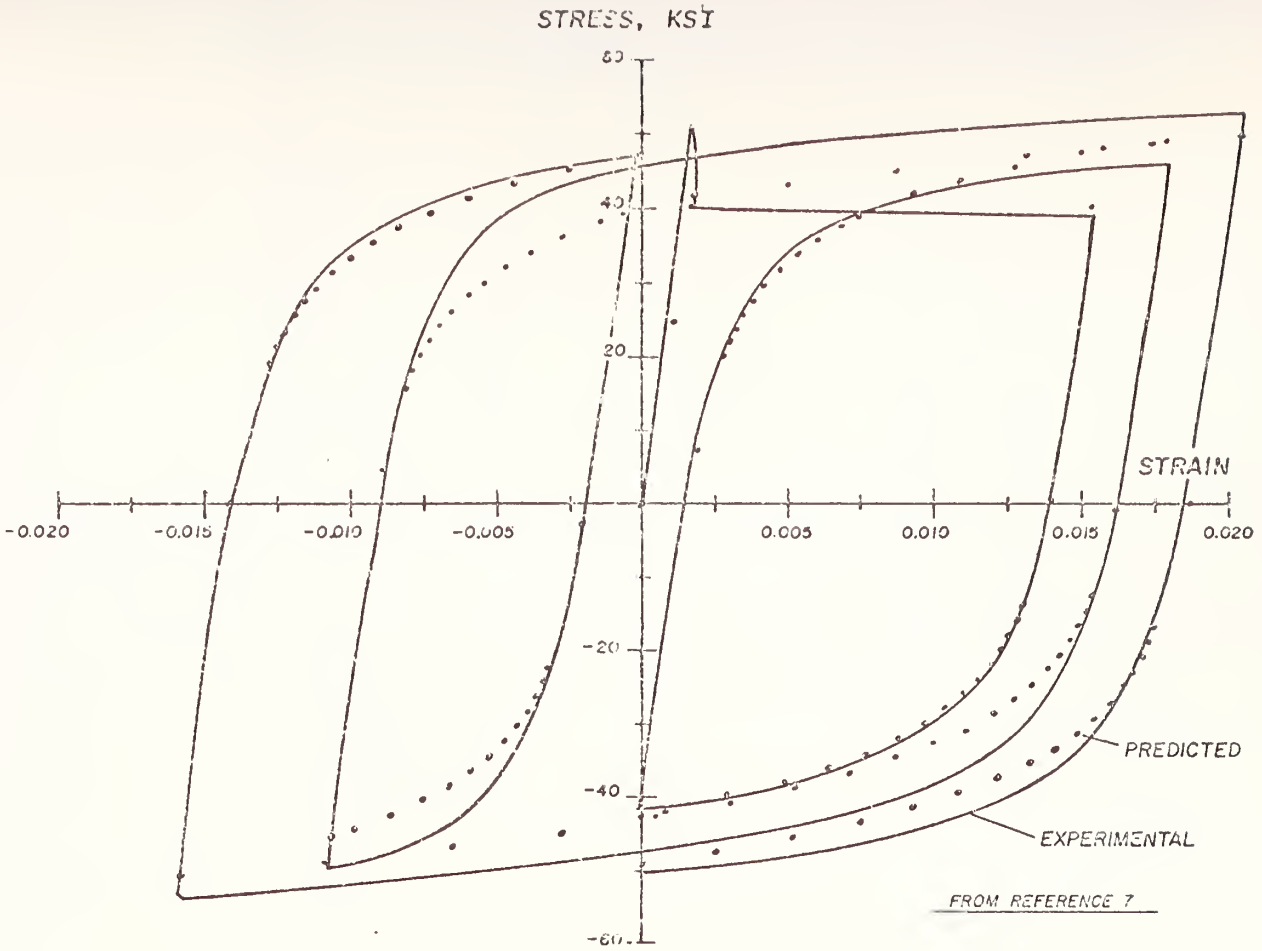

FIGURE 4. PREDICTED AND EXPERIMENTAL STRESS–STRAIN BEHAVIOR FOR VIRGIN A36 STEEL

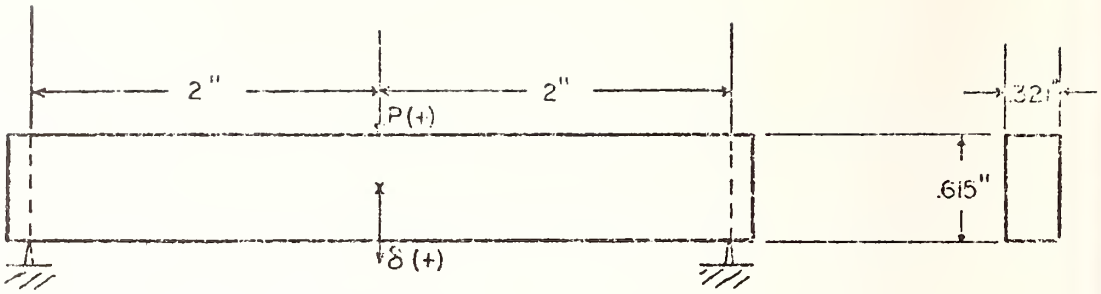

BEAM EXAMPLE

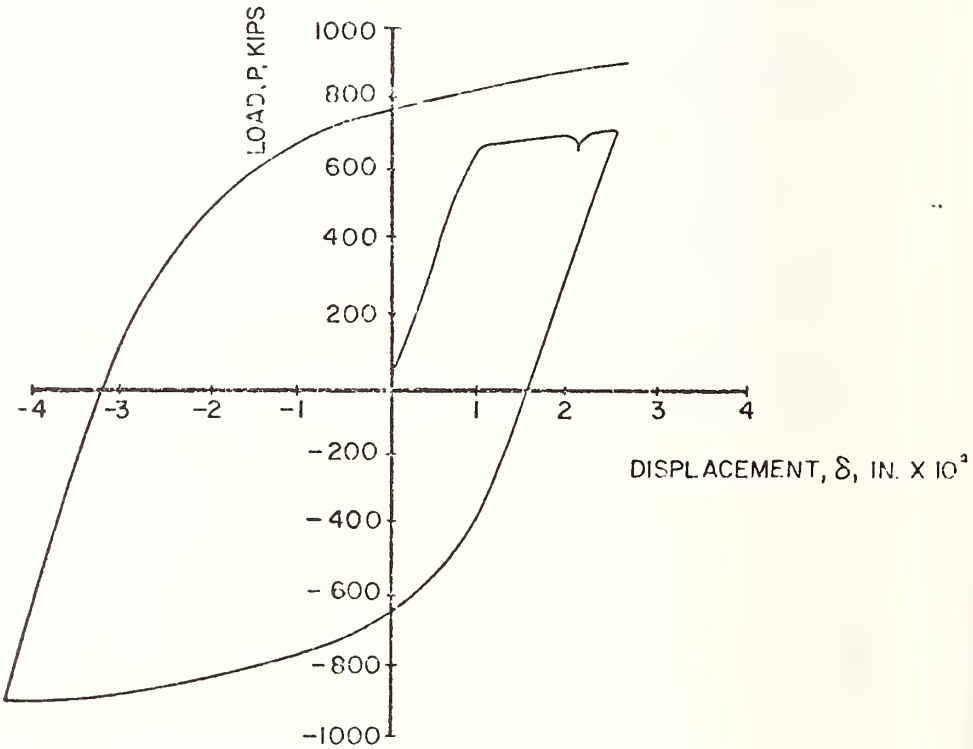

FIGURE 5. EXPERIMENTAL PROGRAM

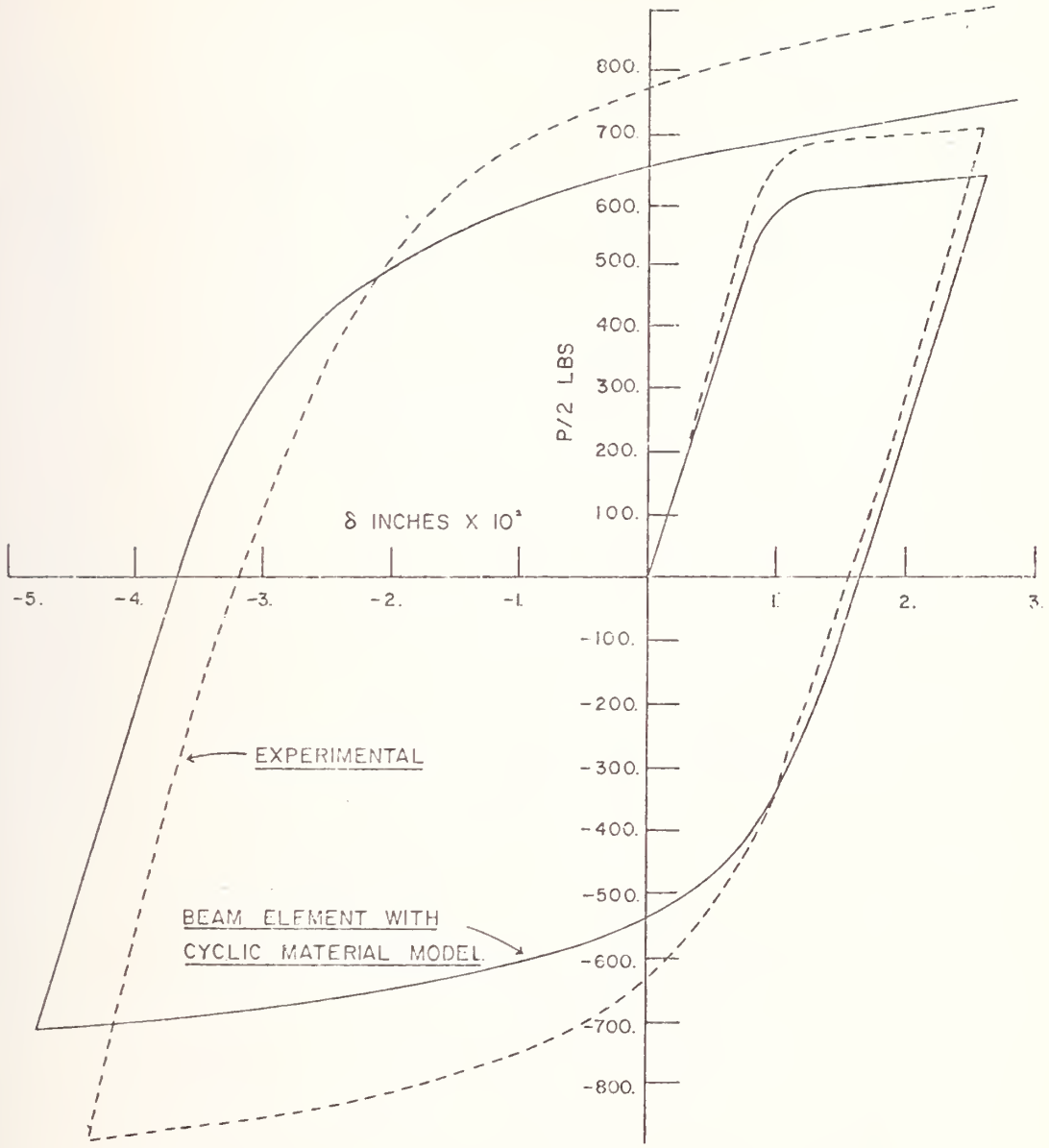

FIGURE 6. COMPARISON OF BEAM FINITE ELEMENT RESULTS WITH EXPERIMENTAL VALUES

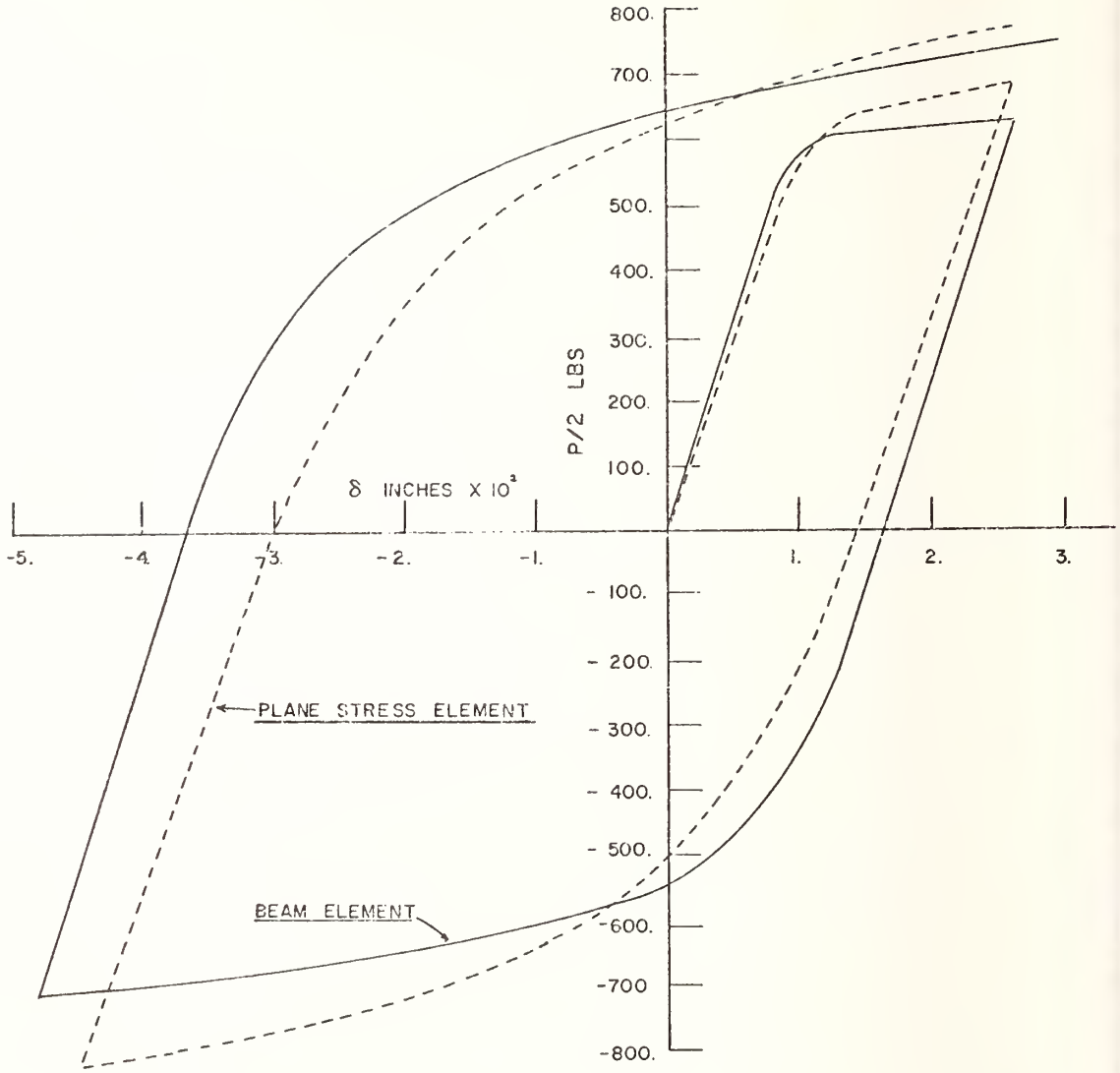

FIGURE 7. COMPARISON OF PLANE STRESS AND BEAM FINITE ELEMENT RESULTS FOR CYCLIC MATERIAL MODEL

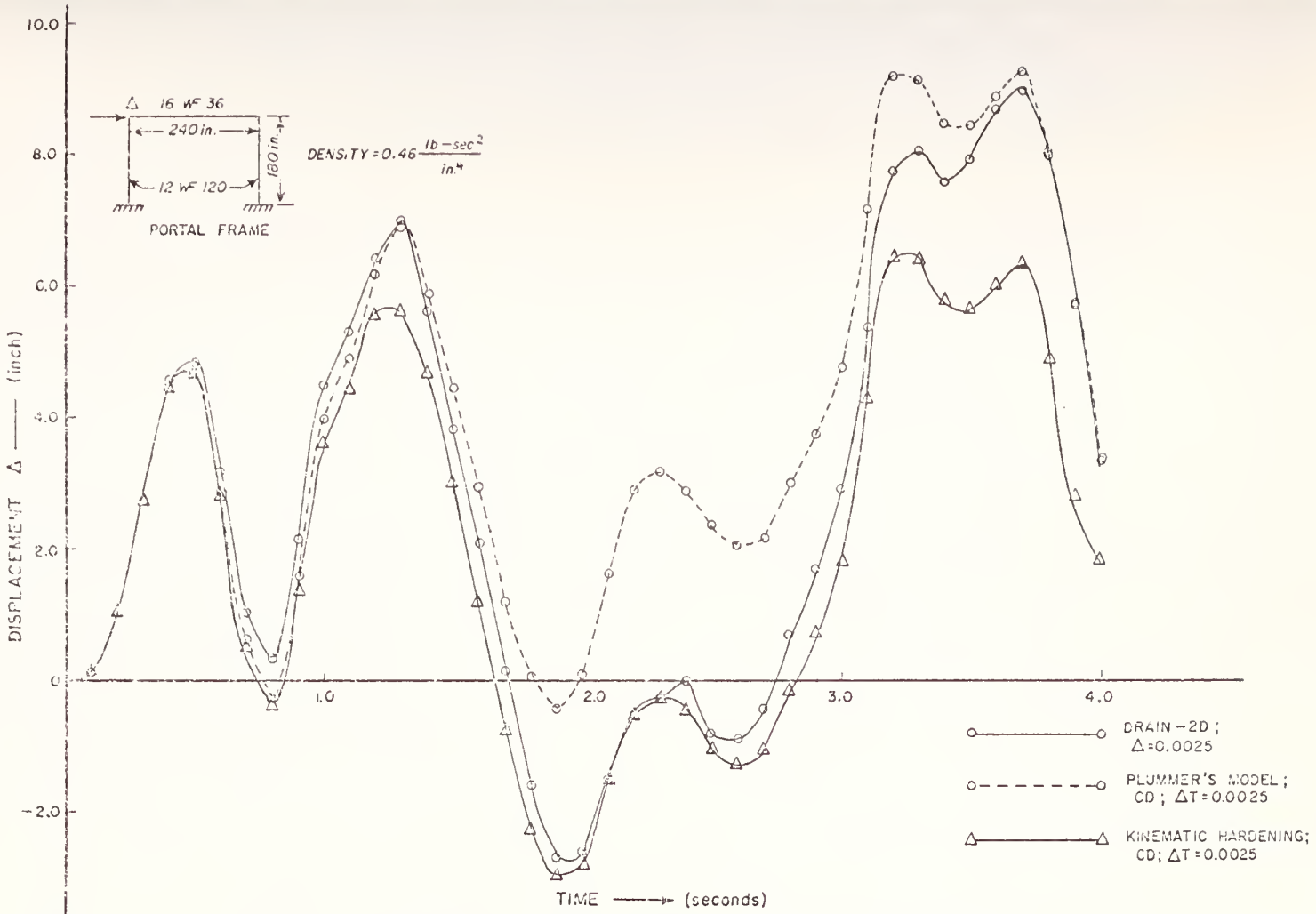

FIGURE 8. RESPONSE OF PORTAL FRAME TO EL CENTRO EARTHQUAKE

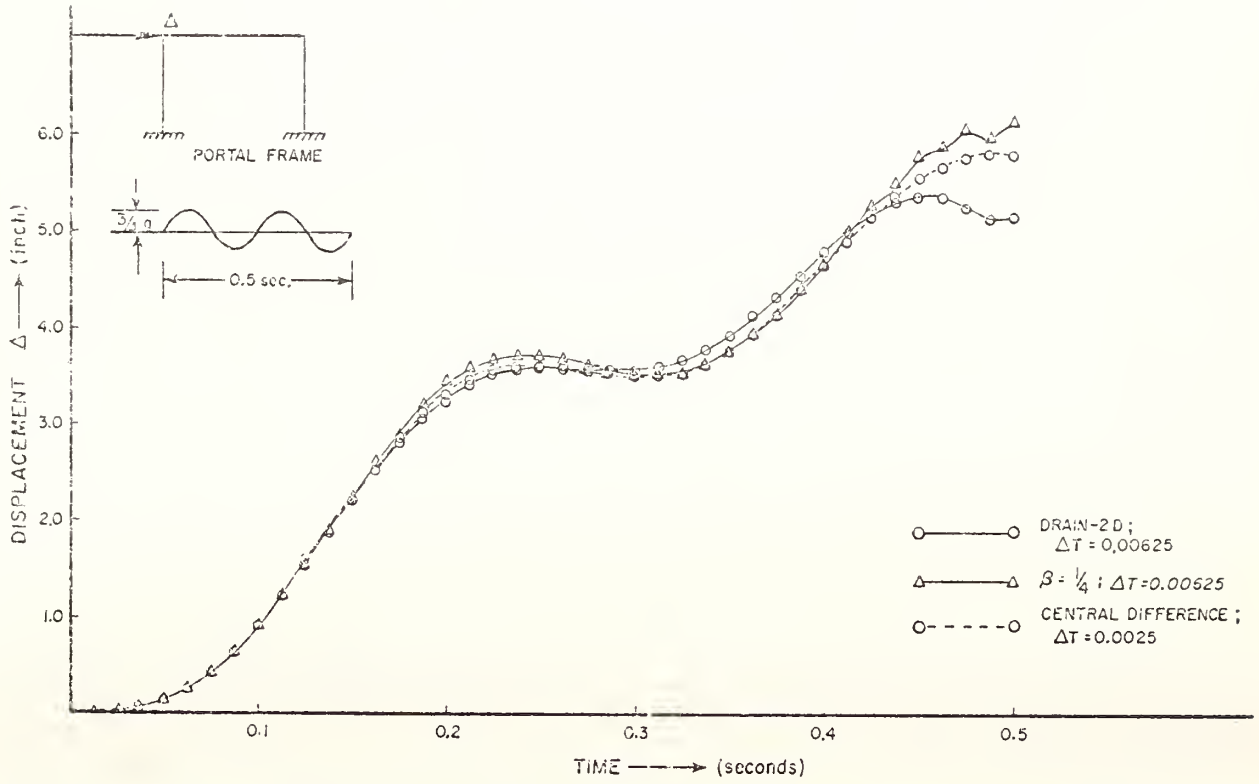

FIGURE 9. RESPONSE OF PORTAL FRAME TO SINUSOIDAL BASE MOTION

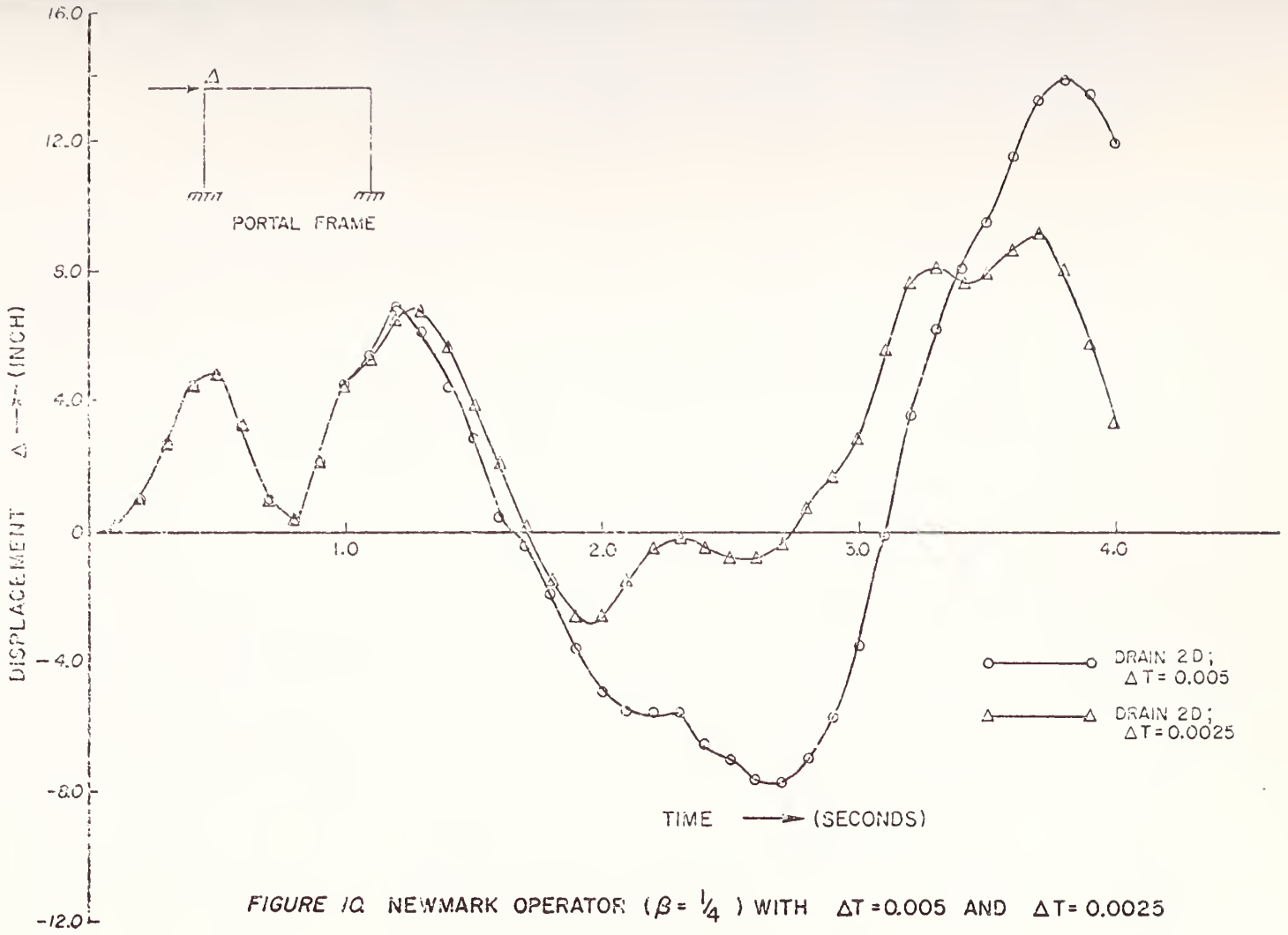

FIGURE 10. NEWMARK OPERATOR ($\beta = \frac{1}{4}$) WITH $\Delta T = 0.005$ AND $\Delta T = 0.0025$

DESIGN OF PILE FOUNDATIONS SUBJECTED TO LATERAL LOADS

by

Mitswru Nagao
Tadayoshi Okubo
Keiichi Komada
and
Asao Yamakawa

Public Works Research Institute
Ministry of Construction
Japan

This report presents a number of basic items relative to the design of pile foundations subjected to lateral loads, and deals with the present design status of highway bridges in Japan. Also presented are items to be further studied for the design standardization of pile foundations subjected to lateral loads. Such problems as the deformation mechanism of group-pile structures are examined.

This report presents the method by reinforcement of the pile-head.

Key Words: Design; earthquake; highway bridges; lateral loads; piles; pile head; structural engineering.

INTRODUCTION

Because Japan is subjected to frequent earthquakes, it is necessary to consider the effects of these earthquakes in designing structures. Such design specifications are stipulated under Paragraph 1-8-1, "Kinds of Load" in the Volume I of the "Common Rules" of Japan's Highway Bridge Specification (Technical Standards of Ministry of Construction), and also in Volume V of the specification given under the title "Specification for Earthquake Resistant Design."

The design of sub-structures of highway bridges is performed in compliance with the Specification's Volume IV, "Specifications for Sub-Structure Design." The provisions relating to the "Design of Pile Foundations" in this bridge specification were established in 1964 and have subsequently become rather obsolete. Amendment and revision to these specifications are now underway in order to incorporate the latest technology and field and laboratory data.

This report will present various ideas and methods outlined in several studies, which relate to the design of pile foundations subjected to lateral or seismic loads. Although these studies are still in progress, various parts are being incorporated into the provisions of the "Highway Bridge Specification." Consequently, the text of this report will indicate the new provisions of the Japan Highway Bridge Design Code.

The general contents of this report will be presented as follows.

In the section "Design of Piles," there will be introduced a conventional method and a rigorous method of design. The former method evaluates the pile's head reaction and displacement by balancing the three forces, while the latter considers the displacements. For most foundations, the simple conventional method is sufficient, however, this method may cause, in some cases, some serious errors. Therefore, in these instances, a suggestion for applying the rigorous method is given. In general, the use of these methods considers the piles to be long. In the case where the piles are short, the displacement method must be revised, a description of which will be given.

For the section "Calculation of the Lateral Coefficient of the Ground Reaction," there is introduced a method as deduced from the results of soil tests, the lateral coefficient of ground reaction which can be applied to the analysis of the stress and displacement of the pile, with the aid of the theory of beams on an elastic foundation.

This method was proposed on the basis of experiments performed on 150 lateral load tests and their correlation between the soil properties.

In the "Design of Pile Head" section, a design method for connecting the pile's head with footing is described. There is no practicable design method to rigidly connect the head to the footing. But the Public Works Research Institute of the Ministry of Construction, desiring a strong and rigid connection, issued a design standard. In order to test and verify the appropriateness of this standard, a series of nearly full-size scale load tests were conducted. A description is given of the basic concept of the design process of the connection of a pile to the footing and the results of the experiment.

The section entitled "Behavior of Pile Foundation with Free Length" describes the lateral resistance of a pile foundation having a free length and the results obtained from a vibration test.

There have been various vibration tests conducted on pile foundations, in which the footings are buried in the ground. From these vibration tests and through experience obtained during actual earthquakes, the earthquake resistance of such units have been verified. However, there have been minimal experiments undertaken with respect to pile foundations of free length since it is entirely a new type of foundation concept. This section will, therefore, present the results of an experiment on nearly full-sized scale foundation, as performed by the Public Works Research Institute.

Calculation Method of Pile Head Reaction and Displacement

There are two methods designated as the "Rigorous Method" and the "Conventional Method", which can be used to determine the reaction and displacement which may occur at the head section of each pile due to external forces (V_o, H_o, M_o), as shown in Figure 1. It will be assumed that the footing is a rigid body and the ground is elastic, both in the axial and the lateral directions of the pile. The calculation method presented is applicable only in the case where the piles are sufficiently long and are deemed to have an infinite length.

The applicable extent of this calculation method and the calculation method for short piles are presented in the following paragraphs.

(1) Rigorous Method

The following equations, when solved simultaneously, will give the deformations of the footing-pile unit, where the lateral displacement of the footing is δ_x, vertical displacement is δ_y, and the rotary angle is α.

$$\begin{aligned} A_{xx}\delta_x + A_{xy}\delta_y + A_{x\alpha}\alpha &= H_o \\ A_{yx}\delta_x + A_{yy}\delta_y + A_{y\alpha}\alpha &= V_o \\ A_{\alpha x}\delta_x + A_{\alpha y}\delta_y + A_{\alpha\alpha}\alpha &= M_o \end{aligned} \qquad (1)$$

where;

$$A_{xx} = \sum_i (K_1 \cos^2\theta_i + K_v \sin^2\theta_i)$$

$$A_{xy} = A_{yx} = \sum_i (K_v - K_1) \sin\theta_i \cos\theta_i$$

$$A_{x\alpha} = A_{\alpha x} = \sum_i \{(K_v - K_1)\, x_1 \sin\theta_i \cos\theta_i - K_2 \cos\theta_i\}$$

$$A_{yy} = \sum_i (K_x \cos^2\theta_i + K_1 \sin^2\theta_i)$$

$$A_{y\alpha} = A_{\alpha y} = \sum_i \{(K_v \cos^2\theta_i + K_1 \sin^2\theta_i)\, x_i + K_2 \sin\theta_i\}$$

$$A_{\alpha\alpha} = \sum_i \{(K_v \cos^2\theta_i + K_1 \sin^2\theta_i)\, x_i^2 + (K_2 + K_3)\, x_i \sin\theta_i + K_4$$

$$K_1 = \frac{12\, EI\, \beta^3}{(1 + \beta h)^3 + 2}$$

$$K_2 = K_3 = K_1 \frac{1 + \beta h}{2\beta}$$

$$K_4 = \frac{4\, EI\, \beta (1 + \beta h)^3 + 0.5}{1 + \beta h (1 + \beta h)^3 + 2}$$

$$\beta = \sqrt[4]{K_H D / 4\, EI}$$

D = Pile diameter (m)

EI = Pile's bending rigidity (kg/cm^3)

K_H = Lateral coefficient of the ground reaction for a pile (kg/cm^3)

K_v = Axial coefficient of the ground reaction of a pile (kg/cm)

When δ_x, δ_y, and α are evaluated from the Equation (1), the pile's axial force P_{N_i} working upon each pile head, lateral force P_{H_i}, and the pile head moment M_i can be calculated from the following equations;

$$P_{N_i} = K_v\{\delta_x \sin\theta_i + (\delta_y + \alpha x_i)\cos\theta_i\}$$

$$P_{H_i} = K_1\{\delta_x \cos\theta_i - (\delta_y + \alpha x_i)\sin\theta_i\} - K_2\alpha \qquad (2)$$

$$M_i = -K_3\{\delta_x \cos\theta_i - (\delta_y + \alpha x_i)\sin\theta_i\} + K_4\alpha$$

(2) Conventional Method

As an expedient design method, it is possible to perform an approximate analysis by assuming the following;

i) In the case of only vertical piles:

$$P_{N_i} = \frac{V_o}{n} + \frac{M_o + \lambda H_o}{\sum_i x_i^2} x_i$$

$$P_{H_i} = \frac{H_o}{n}$$

$$M_i = -\lambda P_{H_i} \qquad (3)$$

$$\delta_x = \frac{H_o}{nK_1}$$

$$\delta_y = \frac{V_o}{nK_v}$$

$$\alpha = \frac{M_o + \lambda H_o}{K_v \sum_i x_i^2}$$

where:

$$\lambda = \frac{1}{2}(h + 1/\beta)$$

ii) In the case of skew piles:

In reference to Figure 1, the following relationships are obtained;

$$V_i = \frac{V_o}{n} + \frac{M_o + \lambda H_o}{\sum x_i^2} x_i$$

$$H_i = V_i \tan\theta_i + \frac{\sec\theta_i}{\sum_i \sec\theta_i}(H_o - \sum_i V_i \tan\theta_i)$$

$$P_{N_i} = V_i \cos\theta_i + H_i \sin\theta_i$$

$$M_i = -\lambda P_{H_i} \qquad (4)$$

$$\delta_x = \frac{H_o}{\sum_i (K_1 \cos^2\theta_i + K_v \sin^2\theta_i)}$$

$$\delta_y = \frac{V_o}{nK_v}$$

$$\alpha = \frac{M_o + \lambda H_o}{K_v \sum_i x_i^2}$$

(3) Limiting Application of the Conventional Method

When the pile foundation is constructed with only vertical piles and has a symmetrical arrangement, both the rigorous and conventional methods agree for both the pile-head reaction and lateral displacement when $K_v = \infty$. In the case when $K_v = 0$, the behavior of each pile is the same as that which occurs in a single pile. An actual pile foundation exists between these two states, therefore, consider first a non-dimensional parameter as defined by the following expression, which relates the rigidity ratio in the vertical direction to the horizontal direction, and is expressed as;

$$\Phi = \frac{K_v \sum_i x_i^2}{K_v \sum_i x_i^2 \frac{nEI\beta}{1+\beta h}} \quad (0 \leq \Phi \leq 1) \qquad (5)$$

where, n = Number of piles.

Using this parameter Φ, the solution (defined as f) by the rigorous method for both the pile-head reaction and displacement can be simply expressed by the following;

$$f = f_{(K_v = 0)} + \Phi\{f_{(K_v = \infty)} - f_{(K_v = 0)}\}$$

where $f_{(K_v = 0)}$ is the solution when $K_v = 0$, and is the calculated value of a single pile. $f_{(K_v = \infty)}$ is the solution when $K_v = \infty$, and is the calculated value by the conventional method. Namely, the parameter Φ approaches 1 as the vertical direction rigidity of an entire pile foundation increases relative to the lateral direction rigidity. Consequently, the gap between the rigorous method and the conventional method narrows. From the results of a preliminary calculation of various types of foundations, it has been ascertained that if $\Phi > 0.95$, the gap between the two calculation methods is less than twenty percent.

In the case where skew piles are involved, it is difficult to obtain a simple parameter, as mentioned above, but in general when the vertical direction rigidity is small and the oblique angle is substantially great, the error arising from the conventional method will be large.

Design of Short Piles

In general, in the design of piles, the pile is considered as a beam on an elastic foundation. The pile's displacement y in the model is presented in Figure 2 and can be

expressed by the following fourth order differential equation,

$$EI \frac{d^4y}{dx^4} + K_H D_y = 0 \tag{6}$$

Solving this equation including the boundary condition, the pile head displacement rate at the time when the lateral force H_o effects the pile head can be expressed as;

$$\delta = \frac{1}{\alpha} \cdot \frac{2 \beta H_o}{K_H D} \tag{7}$$

where $2 \beta H_o / K_H D$ is the pile head displacement rate for the case when the pile length ℓ is infinite. The coefficient α is a correction coefficient for the pile because it has a limited length, while $\beta\ell$ alone is expressed by a function. The pile head displacement rate becomes $\delta = 4H_o / K_H D\ell$ because the coefficient α in the Equation (7) is $\alpha = \beta\ell/2$, when the pile is regarded as a rigid body.

Figure 3 represents the relation between α and $\beta\ell$, and it can be seen from this plot that if $\beta\ell > 3$, $\alpha \rightarrow 1$, which is close to the solution of an infinite log beam. If $\beta\ell < 1$, $\alpha = \beta\ell/2$, which is close to the solution of a rigid body.

The above description relates to only piles displaced under the influence of a lateral force. However, similar trends will occur for other loadings. It is, therefore, possible to make the following classification based on the design principle:

$\beta\ell \geqq 3$ ..... Elastic body, infinite length

$1 < \beta\ell < 3$ ..... Elastic body, limited length

$\beta\ell \leqq 1$ ..... Rigid body

A pile falls in-between the "rigid body" region and the "elastic limited length" region and is, therefore, a "short pile," and, therefore, the boundary conditions at the end-point of the pile must be taken into consideration.

Figure 4 shows the details of a lateral load test on a Φ2m, ℓ17m PC well, which was performed. In this case, with $\beta\ell = 2$, the pile belongs to the region of "short piles," and thus, its end-point is driven 5 m deep into the gravel soil.

Figure 5 represents the comparative values as derived by calculating the measured oblique angle distribution and three possible boundary conditions at the pile's end-point (free, hinged and fixed). As shown in this case, when the end-point is driven into the gravel layer, the calculated values and the measured values agree fairly well when the end-point is assumed as a hinge.

Figure 6 illustrates the influence of the support conditions, at the end-point of the pile, upon the flex distribution of the pile and the bending moment distribution.

LATERAL COEFFICIENT OF GROUND REACTION (K_H)

The most important factor to control the pile's lateral resistance is the lateral resistance of the ground itself. The load-deformation characteristics of the ground are generally nonlinear, and moreover, when a load is applied by or through such a flexible body as a pile, it is extremely difficult to determine a definite yield-point. This is because there is a breakdown which takes place at the upper section of the pile as the load is applied. Because of this, in designing, the ground is assumed to be elastic by taking into consideration the precise data of the ground survey, and the pile is deemed as a beam supported by this elastic body. Thus, the design load is determined from the

allowable displacement rate and the pile's permissible stress. In this case, as the ground is nonlinear, the standard ground surface displacement rate is determined and a virtual free spring constant rate is employed. From this comes the lateral coefficient of the ground reaction K_H. In order to determine the reliability of this term, a number of experiments have been undertaken.

First, in order to investigate the effect the loading plate size has upon the lateral coefficient of the ground reaction, test pits were made in sandy and loam soil. The plates were circular and had 30 cm., 60 cm., 90 cm. and 120 cm. diameters, respectively. The series of horizontal plate loading tests that were conducted are shown in Figure 7. This figure is expressed as a ratio of K_H to K_{30}, where K_{30} is the value when D = 30 cm. It was found that K_H decreased in an inverse proportion to the loading plane diameter raised to 3/4 power, regardless of the ground depth or pile buried depth, as given by;

$$\frac{K_H}{K_{30}} = \left(\frac{D}{30}\right)^{-3/4} \tag{8}$$

The virtual deformation coefficient was obtained from the plate loading tests by using the 30 cm loading plate and assuming the K_{30} value as the control. In order to examine the inter-relation in the various ground investigation methods, an experiment was conducted for E_{30} against the deformation coefficient E_p, as obtained by a boring hole circular loading test. The deformation coefficient E_c was obtained by either mono-axial or tri-axial tests by using a sample of the materials and the standard penetration test value N. The results are shown in Figures 8 and 9, resulting in an approximate experimental expression as shown below;

$$E_{30} = 4E_p = 4E_c = 28N \tag{9}$$

By adding a proportional constant which is experimentally determined from a pile loading test, a relationship between Equations (8) and (9) can be obtained, as given in the following expression; this proposed expression gives an estimate of the lateral coefficient K_H of the ground reaction for a pile.

$$K_H = \frac{E_{30}}{4.8D^{3/4}} = \frac{E_p}{1.2D^{3/4}} = \frac{E_c}{1.2D^{3/4}} = \frac{7N}{1.2D^{3/4}} \tag{10}$$

Figure 10 shows the comparison between the results obtained from a single pile loading test performed on loam soil and the expression (8). Figure 11 illustrates the relation between $7N/K_H$ and the pile's diameter (D) as based on the expression (10). The data that has been plotted was obtained by collecting the information on 150 horizontal loading pile tests throughout Japan. The value of K_H that was used was the ground surface displacement at 10 mm. For the standard penetration test value N, the mean value at a depth from the ground surface equal to $1/\beta$, where ($\beta = \sqrt{K_H D/4\ EI}$) was employed.

DESIGN OF PILE HEAD

Since the load applied to the superstructure or the substructure of a pile must be transferred without failure to the foundation structure, the connection between the pile body and the footing structure is extremely important. In the case of a pile foundation where the cross-section has a portion which will suddenly change, a smooth transfer of load is imperative.

At present, the substructure design of a highway bridge requires the connection between the piles and the footing be considered as a rigid unit by using either of the following two methods:

Method A: Piles which are buried in a footing at a certain depth, the combined structure shall resist the pile head confining moment using the buried portion of the pile. This method is applicable to steel pipe piles, PC, and RC piles. The details of the connection are shown in Figures 12(1) and 12(2).

Method B: The pile head confining moment shall be resisted mainly by reinforcing of the piles, even if the length of the buried pile into the footing is short. This method is applicable to any steel pipe pile, PC pile, RC pile, or cast in-place reinforced concrete pile. The methods shown in Figure 12(3) to 12(5) pertain to this method.

The design method is specified by each type of pile and by the connection method A or B. For example, the design of a steel pipe pile, which is connected by using Method B, is outlined as follows:

(1) The connection of the pile and the footing is designed as a rigid structure, and the pile's head should be designed to resist all punching, pull-out, and lateral forces and the moment.

(2) The length of pile head to be buried into the footing shall be 10 cm.

(3) The vertical bearing stress of the footing concrete shall be (refer to Figure 13):

$$\sigma_{cv} = \frac{P}{\frac{\pi}{4} D^2} \leq \sigma_{ca}$$

(4) The lateral bearing stress of the footing concrete shall be:

$$\sigma_{ch} = \frac{H}{D\ell} \leq \sigma_{ca}$$

(5) The pull-out shear stress of the footing concrete shall be:

$$\tau = \frac{P}{\pi (D + h_1) h_1} \leq \tau_a$$

(6) The coverplate and the cross reinforced plate shall be:

$$t_1 = t_2 = 22 \text{ mm} \qquad h_2 = 30 \text{ mm} ,$$

which are applicable to piles of not more than 1.0 m. in diameter, where:

t_1 = Thickness of the coverplate (cm)

t_2 = Thickness of the cross reinforced plate (cm)

h_2 = Height of the cross reinforced plate (cm)

(7) Hypothetical reinforced concrete cross section stress. A punching force P, the moment M, or the pull-out force P_t is assumed to act on a cross-section of the reinforced concrete and the stress of concrete and the reinforcement is then examined.

(8) Anchoring of reinforcement

i) The shearing stress at the welded section shall be;

$$\tau_s = \frac{\sigma_{sa} A_{st}}{1.4\ \lambda \ell_o} \leqq \tau_{sa}$$

where

σ_{sa} = Allowable tensile stress of the reinforcement (kg/cm^2)

A_{st} = Cross-section of the reinforcement ($cm.^2$)

λ = Leg length of the fillet weld (cm)

ℓ_o = Weld length (cm)

ii) The anchor length of the reinforcement shall be;

$$L_o = \frac{\tau_{sa} A_{st}}{\tau_{oa} \cdot u}$$

where

τ_{oa} = Allowable bond stress of concrete (kg/cm^2)

u = Hoop length of the reinforcement (cm)

(9) The lateral pull-out shearing stress at the end of the footing will be studied.

The results of model tests on steel pipe piles which are connected by Method B will now be given; the details of the test model are given in Figure 14.

The detail of the pile head connection is shown in Figure 15, which has a 10 cm. built-in and is reinforced with eight steel bars of 16 mm. diameter. On the pile's head there is provided a steel coverplate of 16 mm. thick and 16 mm. reinforcement ring. This ring is provided around the steel pipe pile to resist the circumferential tensile stress.

The maximum applied vertical load was 90 tons and the resulting stress distribution on the concrete footing and the pile head coverplate under this maximum load is shown in Figure 16. The comparison between these measured stresses and the calculated values are given in Figure 17. The calculated coverplate stress can be obtained by assuming the entire bearing stress acts on the coverplate or;

$$\sigma = \frac{99}{320} \sigma_c (D/t)^2$$

where:

σ_c = Bearing stress (kg/cm^2)

D = Pile diameter (cm)

t = Pile thickness (cm)

It should be noted that the transfer of the vertical load acting upon the pile actually is concentrated along the wall thickness, and, therefore, the actual measured value of stress on the coverplate is smaller than the calculated value.

The vertical load was then removed and a maximum lateral load of 70 tons was then applied. Figure 18 shows the comparison between the actual measured stresses and the

calculated values with respect to piles P_1 and P_4. These results indicate that there exists a definite gap in the behavior of P_1 on the punching side and P_4 on the pull-out side. It is known from the bearing stress distribution that the entire area of P_1 is compression, while on P_2 there occurs some rotation at the built-in section. This clearly means that the confinement on the part of P_4 is rather weak and the pile head is not perfectly fixed.

In general, the established pile head connecting method has a sufficient design strength, and the stress which occurs inside the footing is safe.

BEHAVIOR OF PILE FOUNDATION WITH FREE LENGTH

The multiple-pillar foundation of a rigid structure can be formed by groups of large diameter columns or pillars which penetrate and are embedded into a designated bearing strata with their head section rigidly held together by a top coverplate. This type of foundation excels when working in water and can be constructed very rapidly. Even in large-scale projects, such as those highway bridges which link the mainland and Shikoku Island, this type of foundation structure was used. For the purpose of examining the lateral resistance characteristics and behaviors of the pile groups with free lengths, a series of experimental large-size models have been undertaken. The results are given as follows.

As shown in Figure 19, two models having different top coverplate thicknesses were fabricated. Various types of tests were conducted using these models and included a lateral loading test, a free behavior test, and a forced vibration test (the top coverplate). The symbols A, B, and C indicate the location of the applied load and the loading direction.

Figure 20 illustrates the relation between the average lateral coefficient of the ground reaction (K_H) and the ground surface displacment, as obtained from the lateral loading test. Due to the group-pile effect, K_H declined more than in the case of a single pile, and it also fluctuated with the loading position. Figure 21 shows the fluctuation of K_H as a ratio of the central pile, which was set as the standard. The front line of the piles took 50% more of this ratio than that of other piles. Figure 22 represents the torsion-spring constant for the case of an eccentric loading (loading postion B). In this case, the pile's torsional resistance took 80% of the entire applied torque, while only 20% was absorbed by the lateral ground reaction. With the multiple-pillar type foundation having a lower rigidity, it becomes necessary to check its torsion rate.

Figure 23 shows the acceleration mode, free vibration at the tower-end postion (C). Table 1 and 2 present the results of the inherent vibration frequency and the damping constant obtained from the free vibration test and the forced vibration test.

The inherent period of the multiple-pillar foundation can be determined by replacing the foundation with a model of one degree of freedom. The total mass of the ground surface is taken as the mass which relates to the vibration. K_H is then determined as follows;

Top-cover axial free vibration (A) $\rightarrow K = 1.23\ kg/cm^3$

Tower axial free vibration (C) $\rightarrow K = 1.24\ kg/cm^3$

Forced vibration (top-cover position) $\rightarrow K = 1.08\ kg/cm^3$

These values are comparable to or slightly lower than K_H value obtained from the static load.

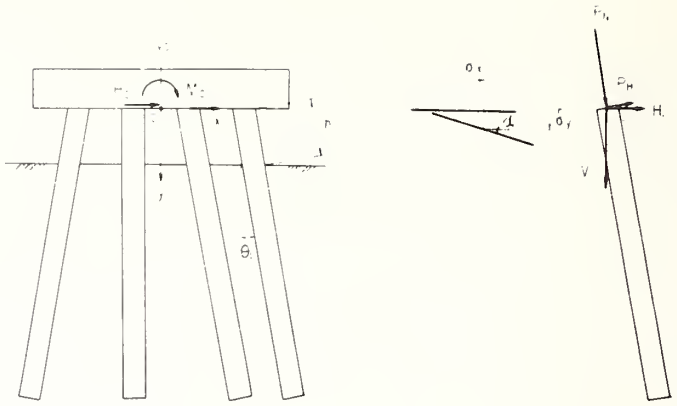

Fig 1 Calculation model of pile foundation

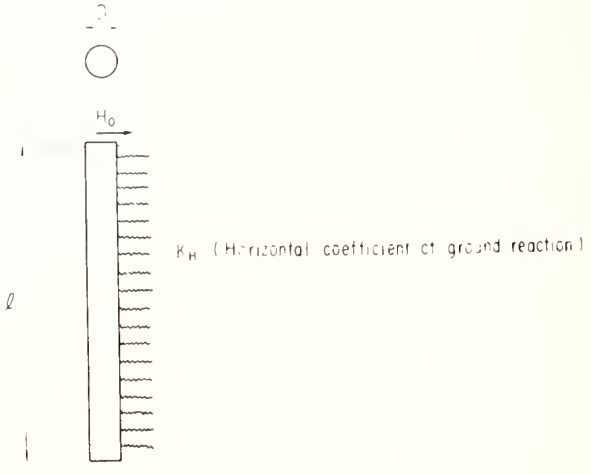

Fig. 2 Calculation model of single pile

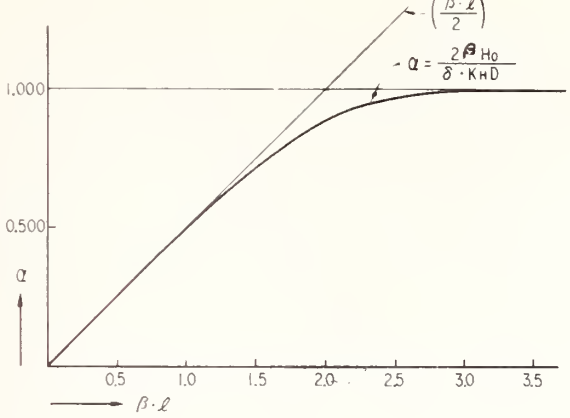

Fig 3 Relationship between α and $\beta\ell$

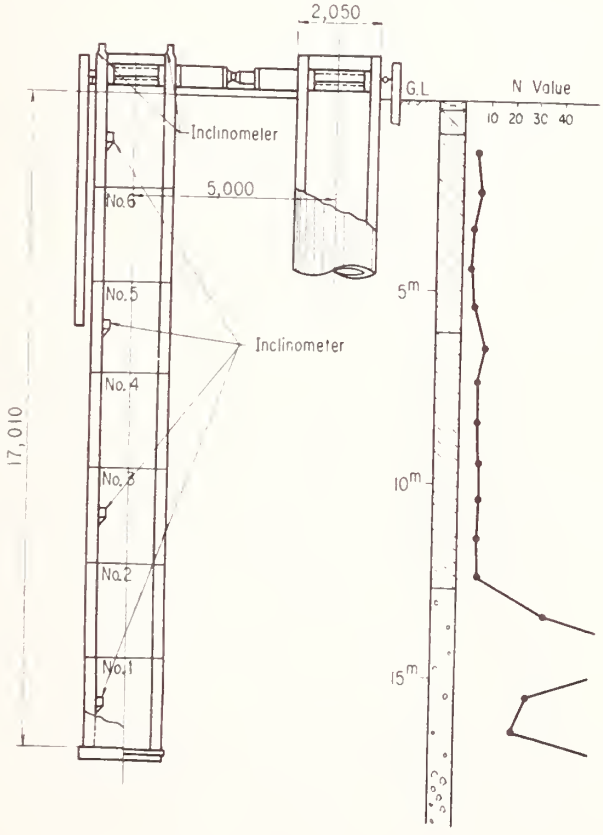

Fig 4 Horizontal loading test of PC pile with large diameter

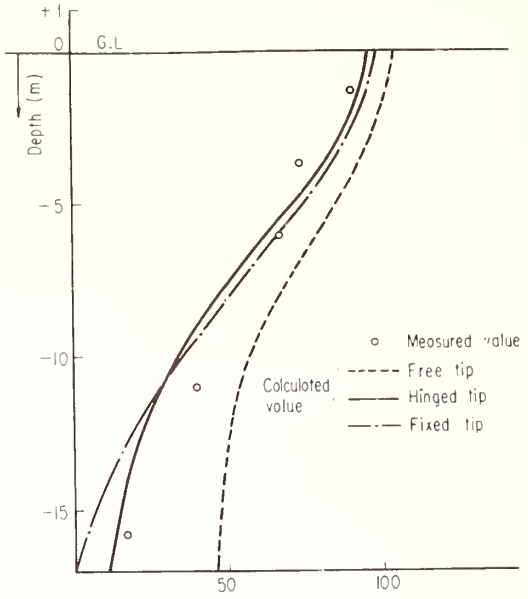

Fig 5 Distribution of angle of inclination (Comparison with calculated value)

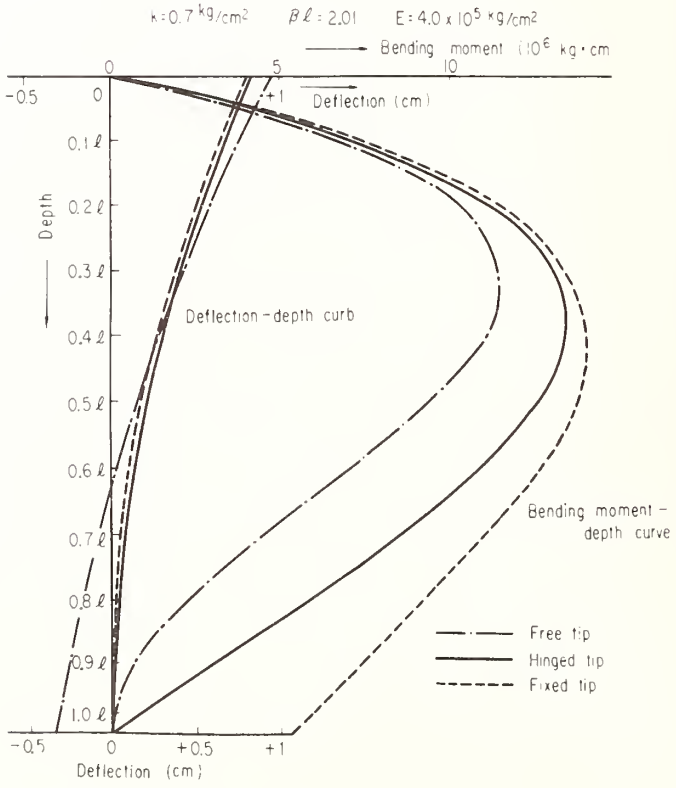

Fig 6 Difference due to supporting condition at pile tip

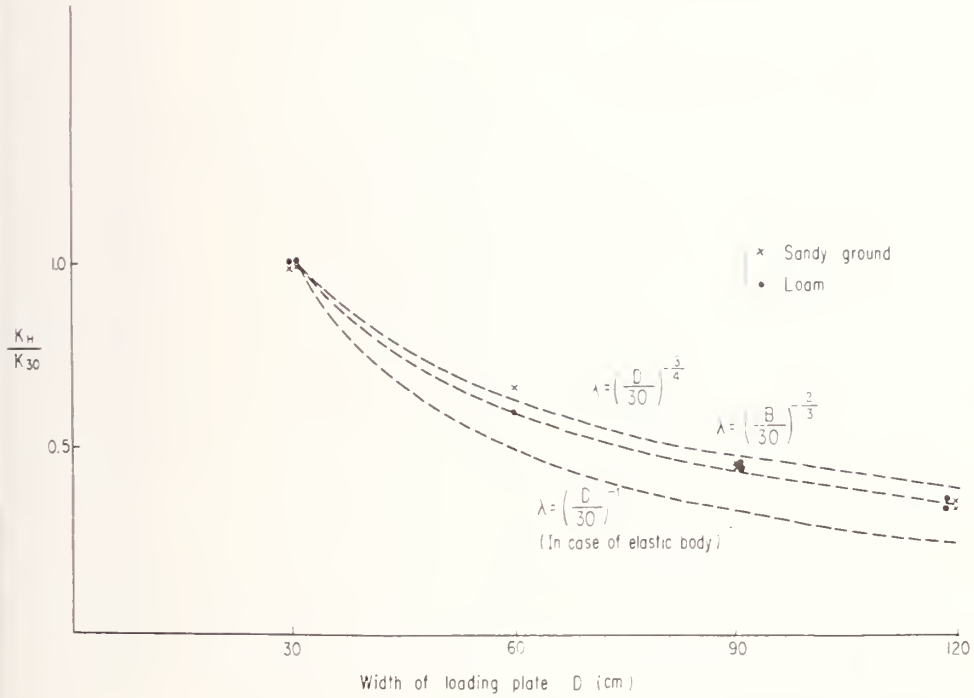

Fig. 7 Relationship between loading plate and coefficient of ground reaction

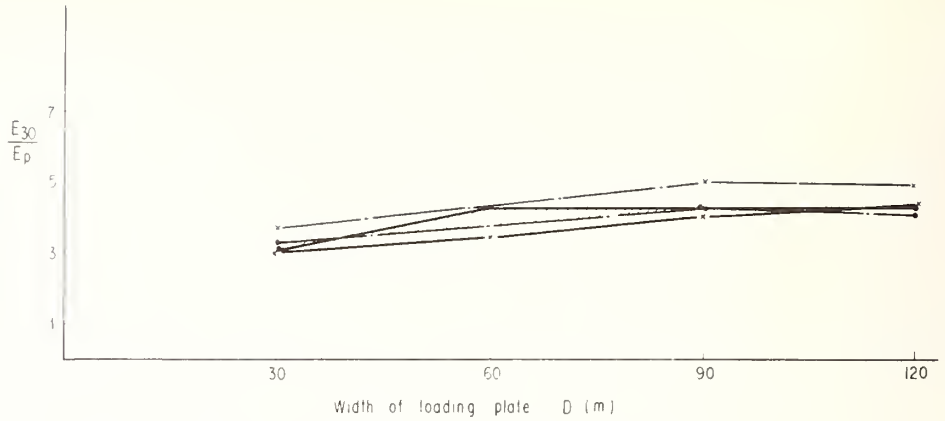

Fig. 8 Relationship between E_p and E_{30}

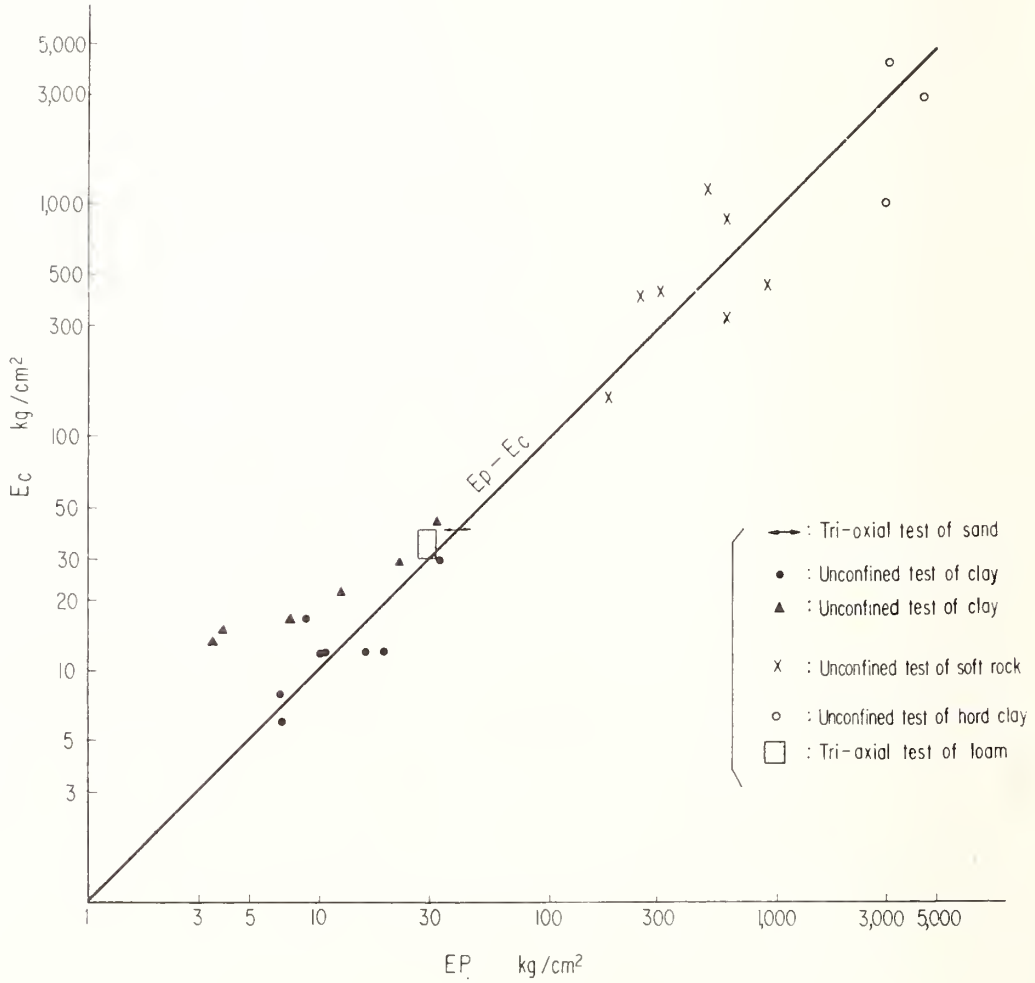

Fig. 9 Relationship between E_p and E_c

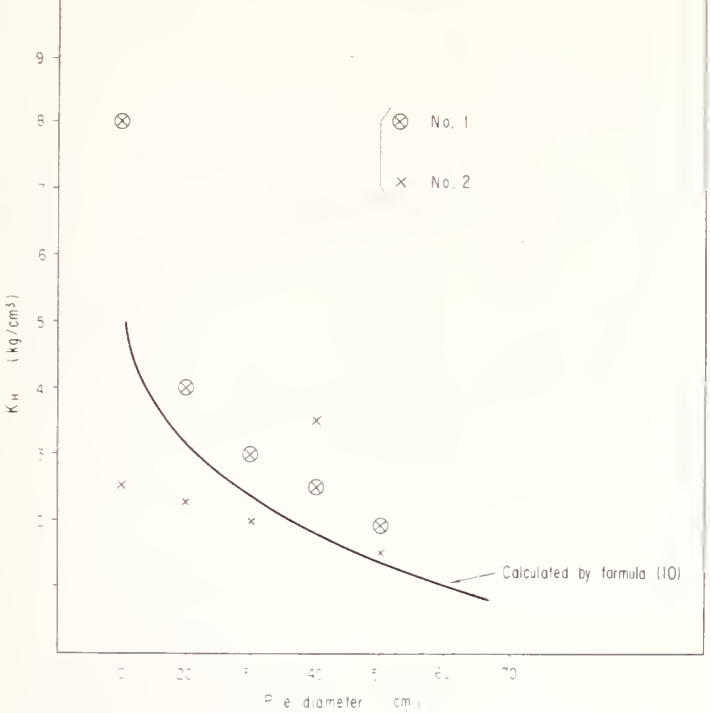

Fig 10 Relationship between pile diameter and K_H

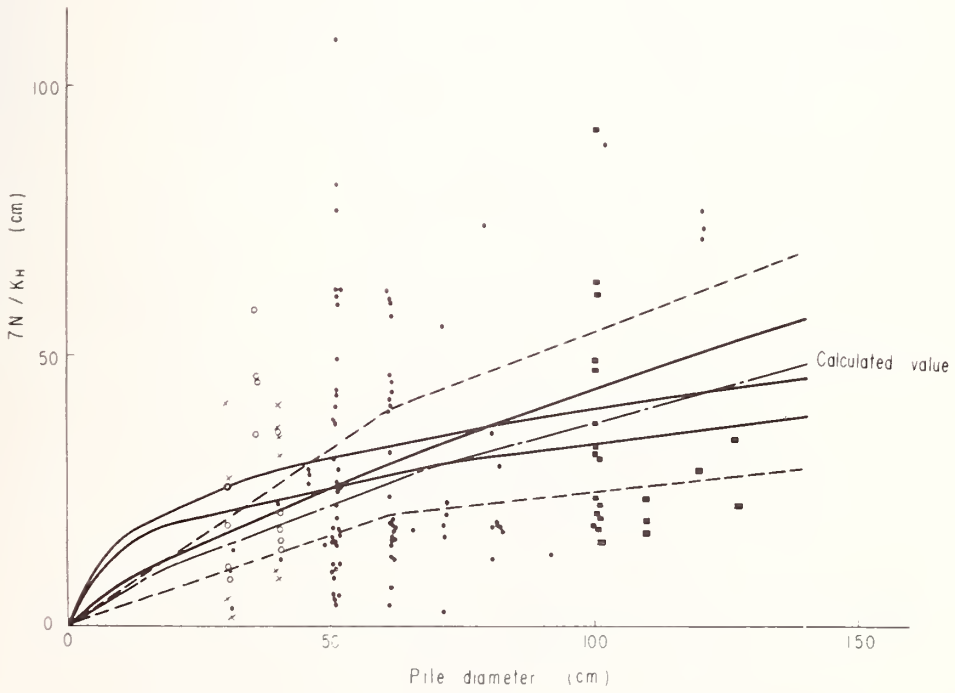

Fig. 11 Pile diameter and K_H

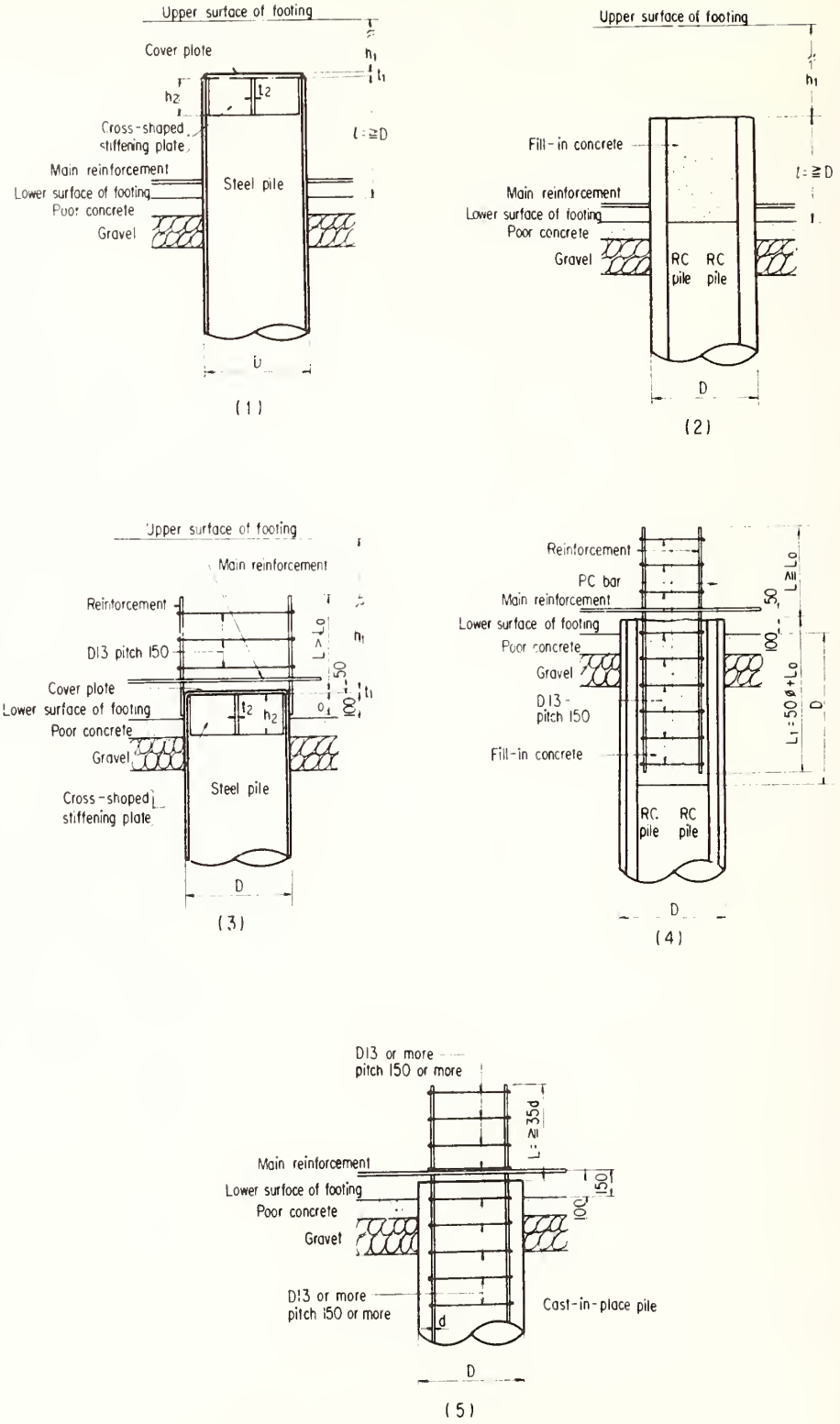

Fig. 12 Connection between pile and footing

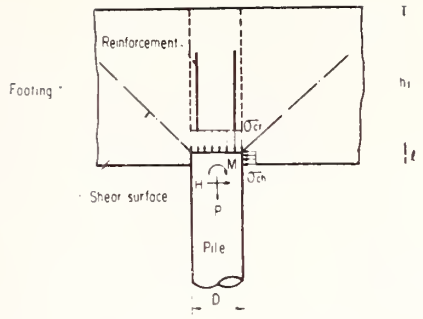

Fig 13 Design model to method B

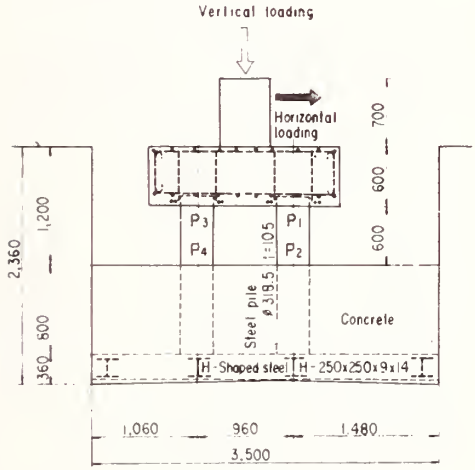

Fig 14 Shape and size of model

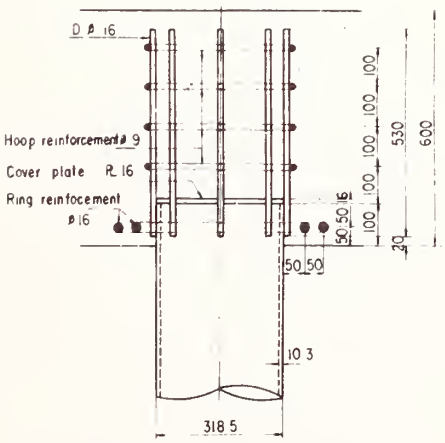

Fig 15 Detail of connection

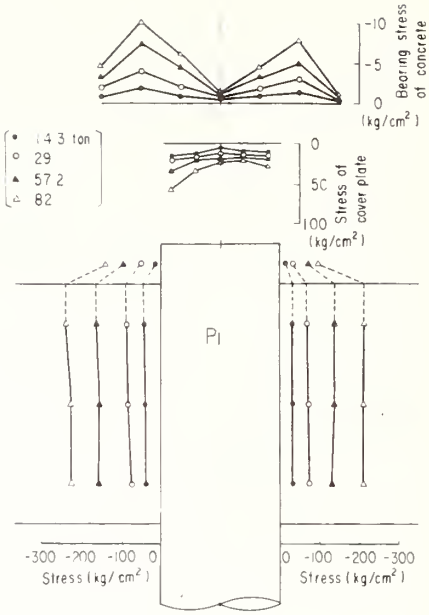

Fig 16 Distribution of stress

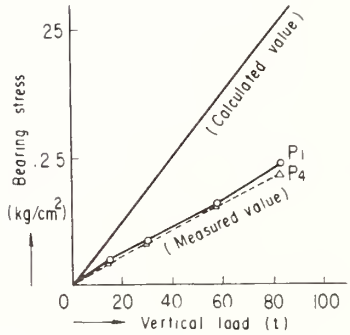

(a) Bearing stress of footing concrete

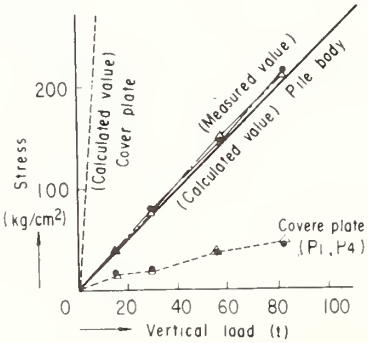

(b) Stress of pile body and cover plate

Fig 17 Comparison between measured value

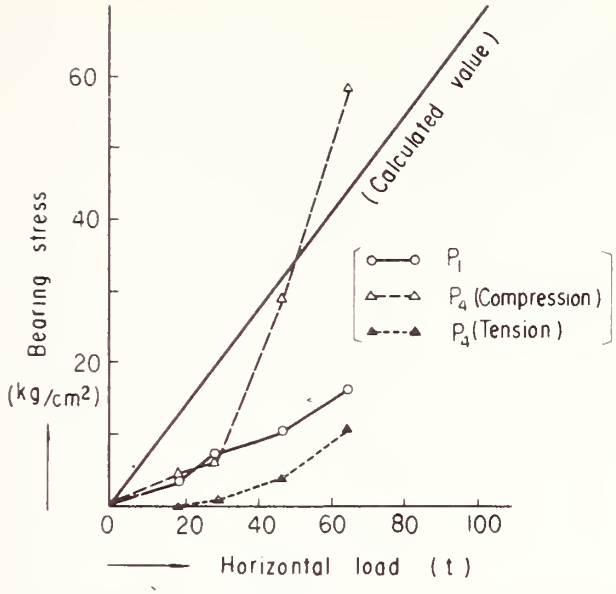

(a) Bearing stress of footing concrete

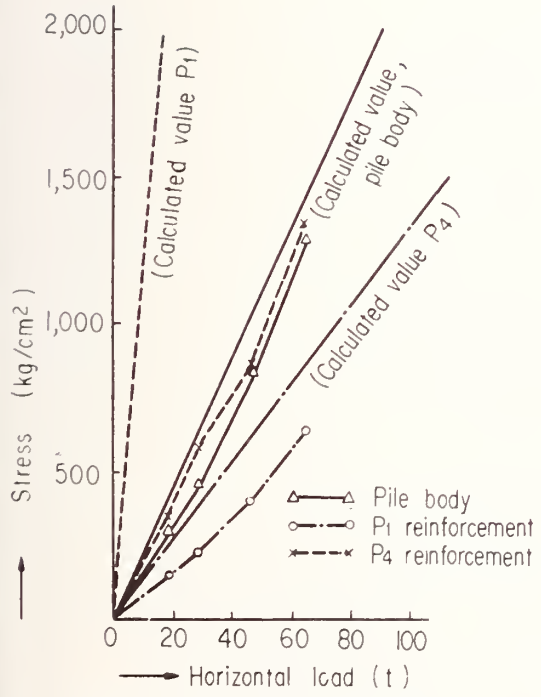

(b) Stress of stiffening reinforcement

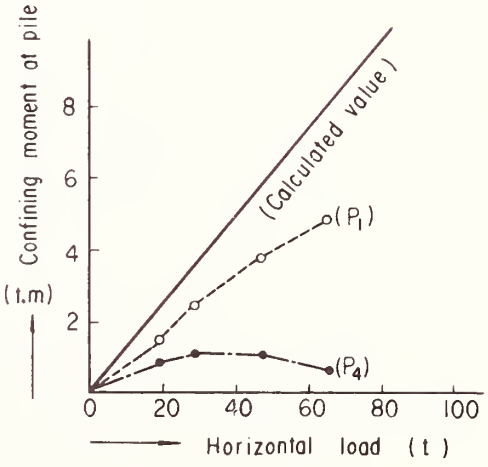

(c) Confining moment at pile

Fig 18 Comparison between calculated value and measured value

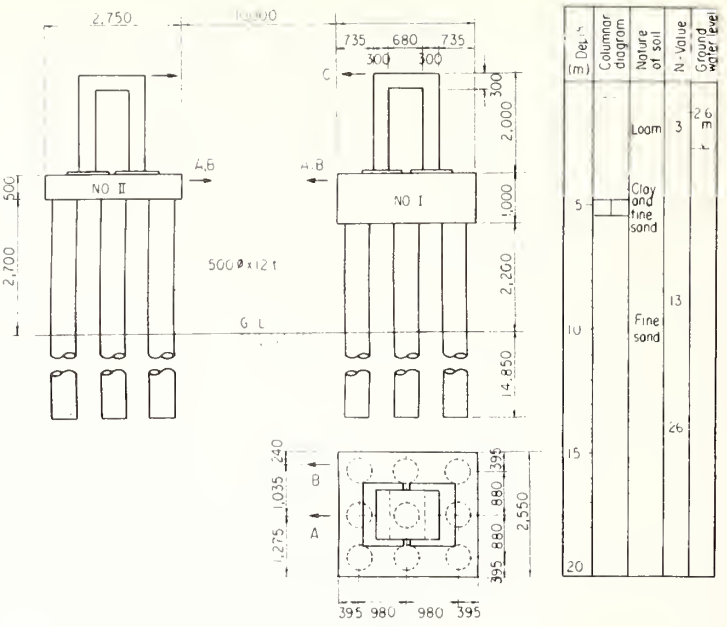

Fig 19 Structure and dimensions of models Ground condition

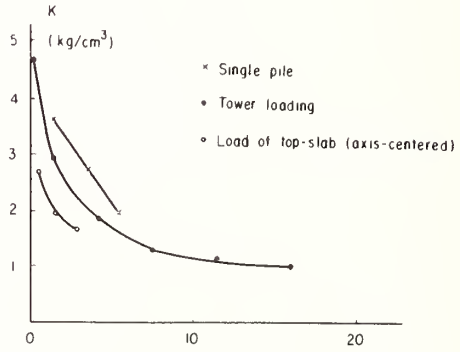

Fig 20 Displacement of pile at the ground surface vs. lateral ground reaction coefficient K (mean)

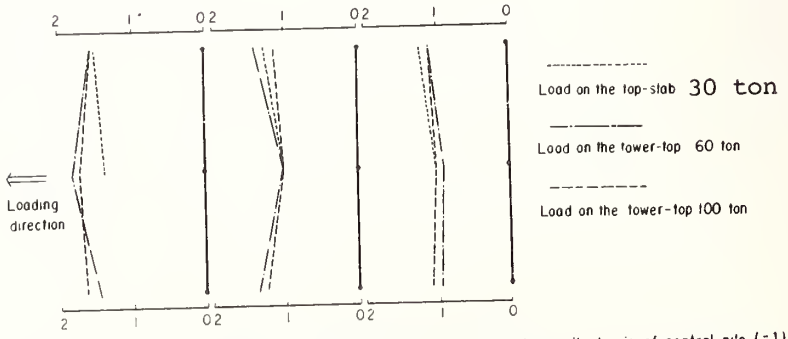

Fig 21 Lateral ground reaction coefficient ratio of each pile on the basis of central pile (=1)

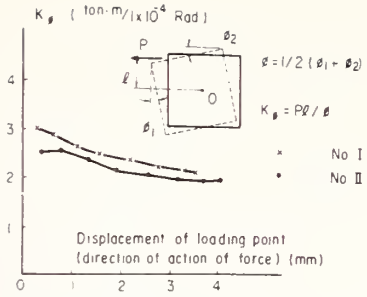

Fig.22 Eccentric horizontal load on the top-slab, displacement vs tarsional spring constant an the tap-end af the top-slab

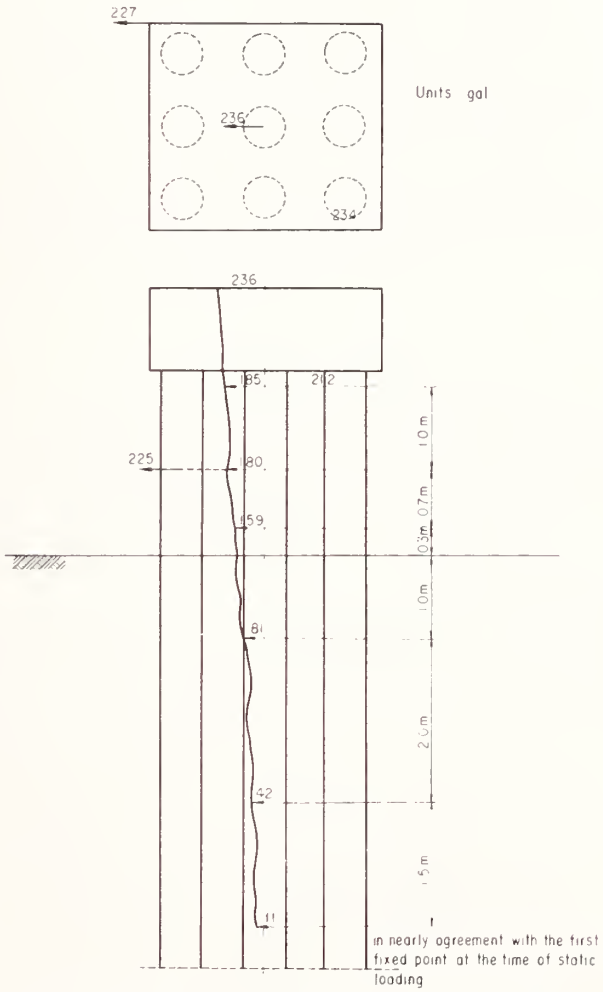

Fig 23 Acceleration made of natural vibration at the tower-top position

Table 1. Natural frequency f(c/s), damping factor h (natural vibration)

Set position of Accelerometer		Axis-centered natural vibration test at the top-slab		Eccentric natural vibration test at the top-slab		Axis-centered natural vibration test at the tower-top	
		f	h	f	h	f	h
No. I	Axial direction on the center of the top-slab	8.5	0.074	8.5	0.088	7.8	0.068
	Perpendicular-to-axis direction on the center of the top-slab	-	-	9.5	0.058	-	-
	Axial direction on the upper corner of the top-slab	8.5	0.071	8.0	0.058	7.8	0.062
	Perpendicular-to-axis direction on the upper corner of the top-slab	-	-	15.2	0.064	-	-
	Axial direction at 2m above the ground of the central pile	8.5	0.075	8.3	0.086	7.8	0.075
	Axial direction at 0.3m above the ground of the central pile	8.5	0.088	8.3	0.097	7.8	0.071
No. II	Axial direction on the center of the top-slab	9.5	0.128	10.0	0.153	8.3	0.058
	Perpendicular-to-axis direction on the center of the top-slab	-	-	18.0	0.077	-	-

Table 2 Resonance frequency

f'(C/S)

Damping factor h

Natural frequency f (C/S)

$f = f'\sqrt{1-2h^2}$

(No. I, central pile, from the measured strain, at the point 1.7m above the ground)

Vibrational power	f'(C/S)	h	f
0.3	7.3	0.073	7.85
0.3	7.85	0.078	7.9
0.6	7.85	0.078	7.9
0.6	7.85	0.080	7.9
1.8	7.65	0.087	7.7
1.8	7.50	0.066	7.55

COMPREHENSIVE SEISMIC DESIGN PROVISIONS FOR BUILDINGS

by

Charles G. Culver
Disaster Research Coordinator

Office of Federal Building Technology
Center for Building Technology
National Bureau of Standards
Washington, D.C.

A review of the development of earthquake design provisions for U.S. building codes is presented. Suggested revisions to the current provisions are noted. A cooperative project directed toward developing comprehensive seismic design provisions is described. The organizational structure for the project including a breakdown of the Task Committees required to develop the provisions and work statements for each Task Committee are included.

Key Words: Buildings; building codes; design; earthquakes; structural engineering.

INTRODUCTION

Annual property losses from earthquakes in the United States average approximately $14 million. Approximately eight lives are also lost annually. On a comparative basis, losses from flooding and extreme winds such as hurricanes and tornadoes are much greater (1). The sudden loss potential for earthquakes, however, is great. It is estimated, for example, that if the New Madrid earthquakes of 1811-1812 occurred today, losses would probably total well over 50 billion dollars and countless lives (2).

The population growth and increasing urbanization in the United States have resulted in a large number of structures built in seismically hazardous areas. Building codes and regulations setting minimum standards for construction methods and materials are one means for mitigating losses from earthquakes. The purpose of this paper is to examine activities in the United States directed toward the development of improved seismic design provision for buildings.

Following is a brief review of the history of U.S. earthquake codes, proposed changes these regulations and a comprehensive project directed toward updating these provisions will be considered.

HISTORY OF EARTHQUAKE CODES IN THE UNITED STATES

Although earthquakes have occurred in many portions of the United States, the most seismically active area is west of the Rocky Mountains. Most of the activity involved in developing seismic design requirements, therefore, has been concentrated in California. Following the 1906 San Francisco earthquake, the city was rebuilt under a code which provided 30 psf wind force to effect both wind and earthquake resistance. The Newtonian concept in which lateral earthquake forces are proportional to the mass of the structure was employed by structural engineers, but was not incorporated in the early building codes. The requirements in the 1927 edition of the Uniform Building Code were among the first earthquake provisions to be written into any widely used building code in this country. Following the Long Beach earthquake in March, 1933 and passage of the Field Act in California, public school buildings were required to be designed for lateral forces ranging from 2% to 10% g. The Riley Act of 1933 required all California buildings, except certain types of dwellings and farm buildings, to be designed for lateral forces.

Since the time of these early code requirements, earthquake provisions have continually evolved. A significant step in this process involved the formation in 1948 of a Joint Committee on Lateral Forces of the San Francisco Section, ASCE, and the Structural Engineers Association of Northern California. The lateral force provisions advocated by the committee were based on Biot's work on earthquake spectra (3). Following formation of the Seismology Committee of the Structural Engineers Association of California (SEAOC) in 1957, the first edition of a comprehensive set of requirements was published as "Recommended Lateral Force Requirements" in 1959 (4). These have been continually updated and the latest edition published in 1973.

Following the San Fernando Earthquake in 1971, revision of existing seismic code requirements received considerable attention. A dynamic type code utilizing in an explicit fashion the response spectra concept was proposed for the City of Los Angeles. New requirements were developed for hospitals and other critical facilities in California. Also various Federal agencies including the Veterans Administration and the Department of Health, Education, and Welfare developed new seismic design criteria.

Although many of the proposed new seismic provisions are similar, considerable differences exist in many cases. As a result, it became apparent that a need existed to update U.S. seismic design provisions. The next section describes a comprehensive project in this area undertaken by the National Bureau of Standards (NBS) and the National Science Foundation (NSF).

IMPROVED SEISMIC DESIGN PROVISIONS

The last major revision in seismic code provisions in the U.S. occurred in the 1960's. Since that time, there have been significant advances in knowledge of the response of building systems to seismic ground motion and correspondingly in analytical techniques and design procedures. One of the recommendations developed at a workshop on disaster mitigation sponsored by NBS and NSF in 1972 (5) indicated that model code provisions for seismic design should be prepared on a top priority basis to bring the minimum level of practice into line with the current state of knowledge. Similarly, the Joint SEAOC-ASCE Committee on Seismic Forces recommended strongly that existing seismic design requirements be revised (6).

As part of the Cooperative Federal Program in Building Practices for Disaster Mitigation, NBS and NSF initiated a project to develop comprehensive nationally applicable seismic design provisions. The overall project involved two phases, as outlined in the following discussion.

Phase I - Evaluation of Response Spectrum Approach

Many of the proposed revisions to seismic design provisions advocated a response spectrum approach and the Joint SEAOC-ASCE Committee felt that if dynamic design criteria were established, a spectrum approach should be used (6). Recognizing this, NBS initiated a project in May 1973 to evaluate such an approach. The scope of this effort was confined to a study of the practicality, additional costs, and related effects. Working with design professionals and researchers, a set of provisions for the design of the structural systems of regular buildings based on a response spectrum approach was developed by a five-man Engineering Panel from the Applied Technology Council (STC). ATC functions as the research arm of the Structural Engineers Association of California.

The Newmark-Hall response spectrum method was used in developing the provisions together with ground motion values for acceleration, velocity, and displacement representative of a given site in Southern California. Two sets of spectra were used. The first, the Damage Threshold Spectrum, was assumed representative of moderate earthquake motions at the site having a moderately low probability (about 50%) of being exceeded during the life of the structure (70 years). The design philosophy adopted was assumption of the acceptability of the prevention of significant structural damage during such an earthquake. For the second set of spectra, the Collapse Threshold Spectrum representative of major intensity earthquake motions at the site having a very low prability (about 10%) of being exceeded during the life of the structure (70years), it was assumed acceptable to prevent collapse of the structural system.

The design provisions were based on a linear elastic modal analysis using the two sets of spectra. Ductility modification factors were employed to account for the effects of inelastic action. Structural members were designed using available ultimate strength provisions for concrete and steel and factored allowable stress provisions for masonry and wood.

Following development of the design provisions, they were applied in the redesign of eleven existing California buildings. The buildings selected for this phase of the work are indicated in Table 1. Note that the selection includes a sampling of basic construction material, height of structure, and type of lateral force resisting system. The original design firms for the buildings were commissioned to do the redesign in accordance with the new provisions. Since the buildings were originally designed using varying code requirements in existence at the time, they were all first redesigned to the provisions of the 1973 Uniform Building Code (UBC) to provide a common baseline for comparison.

The cost involved in applying the new design provisions was evaluated. The difference in construction costs resulting from the new provisions as compared to the designs based on the 1973 UBC were determined. In addition, the extra engineering costs associated with the new provisions as compared to the engineering costs required to apply the equivalent static force provisions of the 1973 UBC were determined.

A final report including the design provisions and commentary, the results of the redesign study, analysis of the cost noted above, and recommended modifications to improve the design provisions are contained in a final report currently under review. It is anticipated that this report will be published by July 1974, following review by NBS, the SEAOC Seismology Committee, and structural engineers from California.

Phase II - Comprehensive Nationally Applicable Provisions

The study described under Phase I was of limited scope. First, it only considered seismic design provisions for structural systems. Second, the general problem of risk analysis and determination of seismic forces was restricted to one site in Southern California. Numerous other factors must be considered in establishing comprehensive provisions applicable to seismic design throughout the U.S. (6). To develop these provisions, NBS and NSF working with ATC initiated a second project in December 1973. The provisions will be based on the current state of the art incorporating the latest research results in earthquake engineering. The organizational phase of this project was recently completed and it is anticipated that initiation of the work to develop the provisions will begin in July 1974.

Since it is intended that the provisions will be national in scope and adaptable for implementation by existing model code groups and consensus standards organizations, broad based participation in the project was necessary. For this reason, two groups were established to participate in both organizing the work and serving in an advisory capacity throughout the course of the project--a Seismic Design Review Group (SDRG) and a Building Code Consultant Group (BCCG). These two groups together with ATC, NBS, and NSF determined the organizational committee structure and work statements for the committees to be charged with developing the provisions.

The SDRG is comprised of national authorities in earthquake engineering representing both the design profession (architects, engineers, geologists) and the research community. They will participate in the technical areas of the program. The BCCG consists of code enforcement officials from throughout the U.S. representing model codes and state and local regulatory groups. This group is charged with advising on the structuring of the format and content of the new provisions as related to implementation.

The organizational structure established by these groups to develop the new provisions is shown in Figure 1. A total of five task groups each with a number of committees has been formed. An objective and brief work statement for each group is given in Table 2. Detailed lists of topics to be considered by each committee and specific questions to be resolved have also been developed.

Referring to Figure 1, the numbers in parenthesis following each committee indicate the number of committee members. Approximately 90 individuals will be involved in the project. In selecting the committee members, broad based participation from the standpoint of technical disciplines (geology, seismology, engineering, architecture, etc.) and geography will be considered. Balanced participation by design professional and researchers will be provided.

Recognizing that the various areas considered by each committee are inter-related, provisions have been made for appropriate interactions in developing the various portions of the provisions. Similarly, the provisions developed by each committee will be reviewed by the two advisory groups, NBS, and the SEAOC Seismology Committee.

In carrying out the project,provisions have been made for maintaining liaison with the design professions, public officials, and other groups to inform them of the development of the provisions and solicit their comments.

A time period of eighteen months has been established for the work with an anticipated completion date of December 1975.

CONCLUSION

The activities described in this paper represent the first step in the development of improved building practices in the United States to mitigate losses due to earthquakes. After completing the design provisions, a continuing effort will be required to keep them updated incorporating new knowledge as it becomes available. In addition, a substantial educational effort should be initiated to present the provisions to design professionals, discuss their interpretation, and facilitate appropriate implementation.

REFERENCES

1. Sav, G. Thomas, "Losses Due to Natural Disaster," National Bureau of Standards Internal Report, Washington, D.C., 1974.

2. Wiggins, John H., "Toward a Coherent Natural Hazards Policy," Civil Engineering Magazine, April, 1974, pp. 74-76.

3. Rinne, John E., "Building Code Provisions for Aseismic Design," Proceedings, EERI Symposium, June 1952.

4. Recommended Lateral Force Requirements and Commentary, Seismology Committee, Structural Engineers Association of California, 171 Second Street, San Francisco, California, 1973.

5. Building Practices for Disaster Mitigation, Building Science Series 46, National Bureau of Standards, Washington, D.C., February, 1973.

6. Degenkolb, Henry J., Chmn., "Basic Design Criteria of the Recommended Lateral Force Requirements and Commentary," Journal of the Structural Division, ASCE, Vol. 98, No. ST9, Proc. Paper 9182, September, 1972, pp. 1913-1922.

7. Uniform Building Code Standards, 1973 Edition, International Conference of Building Officials, 5360 South Workman Mill Road, Whittier, California.

TABLE 1

TEST BUILDINGS FOR RESPONSE SPECTRUM PROVISIONS

1	5 Stories Ductile reinforced concrete frame
2	19 Stories Steel frame; moment resistant in one direction Braced in the other direction
3	10 Stories Reinforced concrete frame in one direction Shear wall in the other direction
4	14 Stories Shear wall
5	7 Stories Shear wall
6	2 Stories Steel frame with vertical bracing system
7	3 Stories Masonry shear wall with concrete-metal decking diaphragm
8	9 Stories Shear wall with vertical load-carrying concrete frame
9	1 Story Tilt-up, plywood diaphragm
10	2 Stories Moment resistant steel frame
11	1 Story Masonry plywood diaphragm

TABLE 2

COMMITTEE WORK STATEMENTS FOR DEVELOPMENT
OF COMPREHENSIVE SEISMIC DESIGN PROVISIONS

Task Group No. 1 - Definition of Seismic Input

Engineering Seismology Committee

Objective: To develop the concepts involved and to describe the procedures for selecting and describing the earthquake ground motions to be used in design, and for laying out the Design Maps.

Statement of Work: With due consideration of the regional geology and tectonic structure, distance from active or potentially active faults, historical records and geological evidence of the location and intensity of regional earthquakes, and the recurrence interval between major earthquakes, develop means of characterizing the earthquake ground motions that should be used for both dynamic and pseudo-static design.

Site and Foundation Effects Committee

Objective: To develop the concepts involved and to describe procedures for evaluating the factors that affect ground motions and stability at a site.

Statement of Work: Consideration should be given to all possible site and foundation factors that affect motion intensity, motion frequency distribution, and soil-structure interaction including:

Distance from seismic source

Travel path from source

Type of seismic source

Site geology both vertically and laterally

Other factors as listed in the attached Guidelines to Geologic/Seismic Reports

Risk Analysis Committee

Objective: To develop the concepts involved and to describe procedures for evaluating the seismic exposure and risk potential for a given site, area, or region.

Statement of Work: Evaluation of seismic risk should take into account the available seismological and geological information pertinent to the occurrence of earthquakes. The probability of earthquakes of various magnitudes occurring near a building site, and the probability of ground shaking of various intensities at the site should be considered. (A structure at a site where strong shaking is to be expected once in 500 years should not have the same seismic design criteria as a structure at a site where such ground shaking is expected once in 50 years). The evaluation of seismic risk should include consideration of special geological conditions such as proximity to a major active fault, extreme softness of foundation soil (fill, bay mud, etc.), potential landslides, or potential soil liquefaction.

A performance criteria adaptable for a building code should logically be based on the notion of acceptable probability of experiencing damage more severe than some specified degree of damage. Seismic Design Zoning Maps should, therefore, reflect not only the probability of ground shaking of various intensities, but should also reflect the acceptable probability of exceeding a specified level of damage. Level of damage should reflect life safety considerations, and for critical facilities should also reflect maintenance of function, and should be based on typical structures.

The analysis of seismic risk encompasses two separate aspects: the relative risk exposure for different seismic areas and the level of seismic risk to structures which will be considered acceptable. Considering all available information such as historical records, geologic information, and regional tectonics, develop procedures for estimating the probability of occurrence of different levels of earthquake motion at a site or area. In conjunction with Task Group No. 2 and utilizing available data, develop methods for evaluating the effects on structure design and construction of the different motion levels.

Task Group No. 2 - Structural Behavior

Structural Design and Details Committee

Objective: To develop detailed seismic design provisions with appropriate commentary, suitable for adoption by building codes in all areas of the United States, for the structural design and required details for earthquake resistant design in concrete, metals, timber, and masonry considering material properties, construction capabilities, and member stresses and ductilities.

Statement of Work: It is assumed that other task group committees will define the appropriate design ground motions, effects of soil-structure interaction, level of risk, importance considerations, and the structural analysis methods required to determine member and element forces and deformations for design purposes, including the effects of setbacks, sudden changes of stiffness or mass, torsion, and three-dimensional loadings.

Determine and define the appropriate material design stress or deformation levels required to achieve suitably uniform factors of safety and the required level of ductility achievable with various materials. Define the details of construction necessary to achieve the required ductility. National and regional material specifications may be used, but detailed supplements must be added to make the result suitable for use in seismic regions.

Typical requirements may be quantitative design requirements for collector bars, trim bars, degree of tying elements of a structure together, panel zones, P-Δ effects if large ductility factors are permitted, specific requirements related to anchoring parts of a building together (parapets, tilt-up walls), diaphragm action, and accompanying details, necessity for complete force path, etc. Criteria are also required for shear wall design, interaction of walls and frames, differences in performance of various framing methods,

basement wall pressures, necessity for or design methods for transferring ground motion to structure (pile bending), etc.

Structural Analysis Committee

Objective: To develop methods for determining the design forces and/or deformations in the members and joints of structures caused by the action of the specified earthquake input.

Statement of Work: Methods shall be developed to define values of earthquake response quantities included in the structural system which are suitable for use in design. Since the design earthquake may produce structural stresses or strains which are significantly greater than the elastic limit of the materials, the methods shall be capable of recognizing these conditions. Emphasis shall be placed upon approximate analysis procedures because the approximate nature of the design earthquake precludes any exact analysis, but different methods shall be specified for various classes of structures depending on the complexity of their dynamic response.

In order to expedite the work of other Task Committees, the Structural Analysis Committee should as first priority, decide on the general types of analyses and conditions under which they are appropriate. Those results should then be disseminated to the others. The Committee should then turn to developing details of the analytical procedures.

Soil-Structure Interaction Committee

Objective: To develop procedures for determining when soil-structure interaction effects are significant and design provisions to provide for same.

Statement of Work: Under certain conditions, there is significant interaction between a building and the soil on which it bears. In effect, the soil and the structure together constitute a system that responds to the free field seismic motion. Where the natural periods of the structure, when assumed to be on a rigid base, tend to coincide with one or more natural periods of the supporting soil, there may be greatly increased amplification of the building's response. The dynamic characteristics of of the building may be significantly affected by the compliance of the soil. In some cases, the building may affect the soil as, for example, the weight of the building or the rocking of the building may cause a decrease in ultimate soil bearing pressure when there is excess pore pressure in the material from liquefaction at lower levels.

Quality Assurance Committee - Structural

Objective: To prepare a state-of-the-art report and quality assurance provisions regarding:

1. Quality control of structural materials at the manufacturer and in the field.

2. Acceptable tolerances in fabrication (shop and field) and on-site construction.

3. Inspection--qualifications, duties, authority, and responsibility of inspectors and of design engineer.

Statement of Work: The effectiveness of a design is only as good as the materials used and quality of the actual construction. The Committee shall study present materials and procedures, develop preferred specifications and procedures, and present same in format compatible with those used in building codes.

Task Group No. 3 - Non-Structural Components

Architectural Systems Committee

Objective: To study the effects of earthquake-induced structural deformations on architectural systems and to develop appropriate design guidelines and provisions to minimize life-safety related damage to architectural systems.

Statement of Work: The Committee should consider in their deliberations seismic design requirements affecting architectural considerations including the following:

1. Size - Should there be limitations on undivided floor areas; should sub-buildings be considered; are volume restrictions applicable?

2. Shape - Should there be limitations on proportions of areas and volume; should sub-buildings be considered horizontally and vertically?

3. Dimension - Should there be any ultimate limitation on dimension; should there be conditions that would reduce such limitations?

4. Circulation - Should egress requirements be restated as to protection offered--distance, number of routes?

5. Materials - Should type of materials used restrict other limitations? Should chemical or physical properties restrict material selection?

6. Detailing - Should finish materials be connected to structure? Should strength of connections be controlled? Should provisions be made so that structure elements can move independently (within limits) of cladding, partitions, ceilings, and other non-structural elements? Should secondary attachment systems be required or is a single anchorage system adequate?

7. Equipment - Should moveable equipment be restricted; should equipment design be controlled?

8. Damage Control Systems - Should self-contained alarm and/or support and/or extinguisher systems be required?

9. Interrelations - Should options be given the designer and/or client through selection of systems affecting other

requirements? What about effects on adjacent buildings or people outside the building?

Mechanical-Electrical Systems and Equipment Committee

Objective: To evaluate problems involved with life-safety as related to mechanical and electrical systems and equipment, to determine which systems and equipment should be subject to seismic resistant design, and to develop design provisions consistent with design levels (or quality) specified for the building structure.

Statement of Work: The Committee should make a detailed review of damage data, existing provisions, if any, now listed for seismic-resistant design and develop seismic design guidelines and provisions for life-safety systems.

Present efforts should be limited to mechanical and electrical systems that are supportive to the building function, i.e., heating, ventilating and air conditioning systems, elevators, emergency power (for essential systems), light fixtures, etc., and operative systems for critical facilities.

Considerations should be given to structure-system (or equipment) interaction or coupling, equipment or system response to dynamic motions, interaction between equipment, and better detailing.

Quality Assurance Committee - Architectural, Mechanical, and Electrical

Objective: To develop the concepts involved and to describe procedures for ensuring effective quality assurance for Architectural-Mechanical and Electrical systems and/or equipment.

Statement of Work: The Committee should study present quality assurance procedures to determine whether or how they should be modified or expanded to ensure that design, fabrication, and construction or architectural-mechanical and electrical systems and/or equipment will function as contemplated by the design provisions developed by the other Task Group No. 3 Committees.

Task Group No. 4 - Liaison and Format

Liaison and Information Dissemination Committee

Objective: To assist the Task Committees in developing liaison with the design professions and public officials so as to inform them of the development of the design provisions and to solicit their comments.

Statement of Work: The Committee should work with the other Task Groups and Committees to ascertain their progress and to develop appropriate means of informing the design professions, public officials, and the public of the development of these design provisions and the potential future benefit from using them.

The Committee should consider the need for informing the many interested groups on a timely basis.

Design Provisions Format Committee

Objective: To edit design provisions prepared by other Task Groups and Committees into editorial format compatible with those used by building codes.

Statement of Work: The Committee shall work with the Building Code Consultants Group to develop a format outline and distribute same to the Task Groups and their Committees. The Committee should assist Committees as required and edit draft material before issuance to outside groups.

Task Group No. 5 - Existing Buildings

Inspection and Evaluation of Damage Committee

Objective: To develop procedures and criteria for assessing the structural safety of buildings subjected to earthquake ground motions.

Statement of Work: It is often difficult to quickly inspect and fully evaluate the structural safety of a building and its components after it has been subjected to significant seismic ground motion. It is necessary for the protection of the public safety that orderly and efficient procedures be developed for inspecting damaged structures and determining whether or not they are safe for human occupancy. There is also a need for developing procedures for evaluating the damage in detail to determine whether repair work is required.

Procedures and criteria shall be developed by which buildings can be inspected and damage evaluated so as to determine whether they are safe for immediate occupancy. Procedures and criteria shall also be formulated for assessing the extent of the damage and the amount of structural repair required.

Repair of Earthquake Damage Committee

Objective: To develop procedures for determining the extent, type, and adequacy of required repairs of earthquake-damaged buildings and components so as to ensure life safety.

Statement of Work: Procedures and criteria shall be developed for determining the extent, type, and adequacy of repairs required to ensure the structural stability of earthquake-damaged buildings and components. Repairs to both structural and nonstructural elements shall be considered where their failure or instability under normal or earthquake conditions could endanger life safety of occupants or passer-bys.

Evaluation of Existing Buildings Committee

Objective: To develop procedures and criteria for inspecting and evaluating existing buildings and structures for possible structural inadequacies that could endanger life safety in the event of an earthquake.

Statement of Work: A large proportion of existing buildings were built before adequate seismic design standards were developed and connections, ties, mortar, etc. have deteriorated. Many of these buildings have conditions that are potential safety hazards in the event of an earthquake. Such conditions may vary from minor appendages to parapet walls to the entire structure

Provisions shall be developed delineating procedures and criteria to be followed in evaluating such potential hazards and determining the extent of strengthening required.

Strengthening of Hazardous Buildings Committee

Objective: To develop minimum standards for strengthening of existing buildings, outline priorities for strengthening based on potential hazard and formulate procedures for evaluating the adequacy of proposed strengthening measures.

Statement of Work: Other committees in Task Group No. 5 have the responsibility for developing procedures and criteria for inspecting and evaluating earthquake damage, repair of such damage, and inspection and evaluation of existing structures for potential hazards. This Committee shall develop minimum standards for strengthening structures which have been determined to be either hazardous or inadequate for earthquake resistance. Procedures for establishing possible priorities for strengthening based on degree of potential hazard or life exposure shall be developed. Provisions for evaluating the adequacy of proposed strengthening measures shall also be formulated.

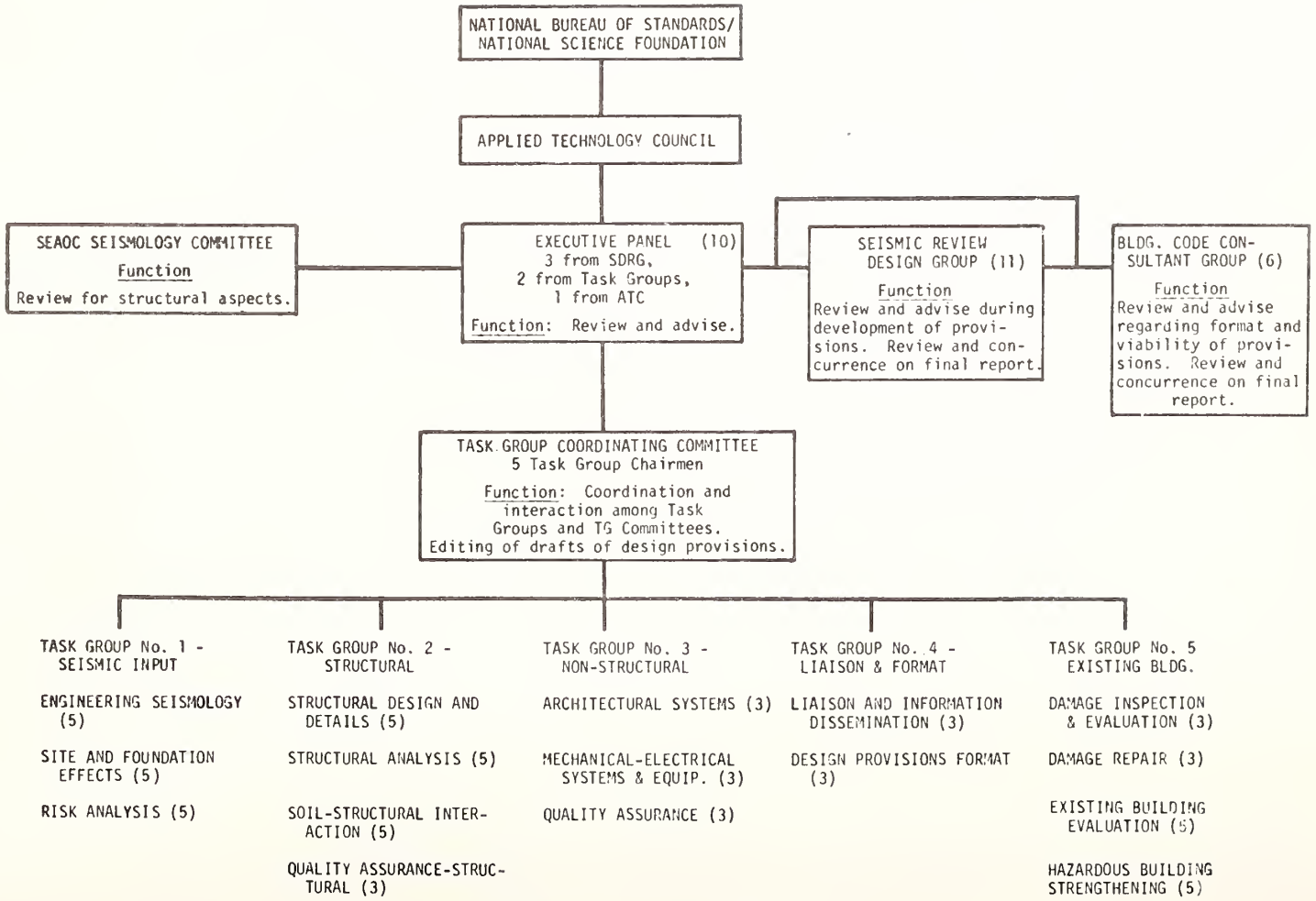

DEVELOPMENT OF COMPREHENSIVE SEISMIC DESIGN PROVISIONS
Fig. 1 - ORGANIZATION CHART

WIND LOADING AND MODERN BUILDING CODES

by

Emil Simiu
Structural Research Engineer

R. D. Marshall
Structural Research Engineer

Center for Building Technology
National Bureau of Standards
Washington, D.C.

The differences between the dynamic alongwind response, the gust factors, and the total alongwind response obtained using various current procedures may in certain cases be as high as 200%, 100%, and 60%, respectively. The purpose of this paper is to investigate the causes of such differences. To provide a framework for this investigation, the paper presents an overview of the questions involved in determining alongwind structural response, and a critical description of the basic features of procedures currently in use. A comparison is made between alongwind deflections of typical buildings selected as case studies, calculated by both new and traditional procedures, some of which are described in various building codes. The reasons for the differences between the respective results are pointed out. The procedures were evaluated on the basis of a recently developed method which utilizes a logarithmic variation of wind speed with height above ground, a height-dependent expression for the spectrum of the longitudinal wind speed fluctuations. The method also allows for realistic cross-correlations between pressures on the windward and leeward building faces.

Key Words: Building codes; buildings; deflections; dynamic response; gust factors; structural engineering; wind loads.

INTRODUCTION

Following an increasing recognition of the importance in tall building design of the dynamic effects due to the gustiness of wind, several procedures for computing alongwind response have been proposed in the last decade (6, 19, 24, 25). Two of these procedures are described in Ref. 1, herein referred to as the A58.1 Standard, and in Refs. 5, 11, herein referred to as the NBC. The purpose of these procedures is to calculate equivalent static loads whose effect upon the structure is the same as that of the gusty wind.

For a given structure in terrain of given exposure and in a given wind climate, it might be expected that roughly comparable equivalent static loads (and, therefore, comparable values of the calculated response to wind) will be obtained regardless of what method of computation is used. This, however, is not the case; as has been reported before (25), depending upon whether the procedure described in the A58.1 Standard or in the NBC is used, values of the response that may differ considerably from each other are obtained. Such differences may be as high as 50% or more. An investigation into causes of such discrepancies is thus believed to be in order.

Such an investigation is the intent of this paper. To provide a framework for the investigation, an overview of the question of alongwind structural response will be presented first. This will be followed by a comparative analysis of the various procedures presently in use. A comparison will also be presented between response obtained by these procedures and that obtained by assuming wind loads traditionally used in structural design and specified by various building codes. On the basis of these comparisons, an assessment will be made of the procedures analyzed.

ALONGWIND RESPONSE: AN OVERVIEW

As a framework for the evaluation of current procedures for computing alongwind response, an overview of the questions involved in determining such response is presented in the following. These questions include the relation between alongwind response and wind pressures, the relation between wind pressure and wind speeds, and the definition of wind speeds as functions of height above ground, roughness of terrain, climate and desired level of safety of the structure. A summary of relations defining the alongwind response in terms of mechanical and environmental parameters will also be presented.

Relation Between Alongwind Response and Fluctuating Wind Pressures

It is known from elementary calculus that a periodic function may be expressed as a sum of fluctuating harmonic components with discrete frequencies. Its mean square value can then be expressed as the sum of the square of the amplitudes of the harmonic components. Similarly, a stationary random function F(t) may be viewed as a superposition of fluctuations of frequencies n, with n covering the entire interval from zero to infinity, while its mean square value may be expressed as a sum of contributions associated with these fluctuations, i.e.;

$$\overline{F^2(t)} = \int_0^\infty S_F(n)\,dn \tag{1}$$

The quantity $S_F(n)$ is a measure of the magnitude of the fluctuating component of frequency n and is known as the spectral density function of F(t).

Consider a linearly elastic structure subjected to the action of a stationary random force $F_P(t)$ of known spectral density $S_{F_P}(n)$ and applied at a point P. The spectral density of the fluctuating deflection $a'(t)$ at some point M of the structure can be shown to be (16)

$$S_a(M, n) = H^*(M, P, n)H(M, P, n)S_{F_P}(n) \tag{2}$$

in which H(M, P, n) = mechanical admittance = response of the structure at point M due to action at point P of a unit complex harmonic force, and $H^*(M, P, n)$ = complex conjugate of H(M, P, n).

If the structure is acted upon by two stationary random forces $F_{P_1}(t)$ and $F_{P_2}(t)$ applied at points P_1, P_2, respectively, the spectral density of the response a'(M, t) can be shown to be (16)

$$S_a(M, n) = H^*(M, P_1, n)H(M, P_1, n)S_{F_{P_1}}(n) + H^*(M, P_2, n)H(M, P_2, n)S_{F_{P_2}}(n) + H^*(M, P_1, n)H(M, P_2, n)S_{F_{P_1}F_{P_2}}(n) + H^*(M, P_2, n)H(M, P_1, n)S_{F_{P_2}F_{P_1}}(n) \quad (3)$$

in which $S_{F_{P_1}F_{P_2}}(n)$ = cross-spectral density function of $F_{P_1}(t)$ and $F_{P_2}(t)$. If $F_{P_1}(t) \equiv F_{P_2}(t)$, then $S_{F_{P_1}F_{P_2}}(n) = S_{F_{P_1}}(n)$. Methods for computing $S_{F_{P_1}F_{P_2}}(n)$ are described in Refs. 4, 16. The imaginary part of the cross-spectral density function is known as the quadrature spectrum and has been found by measurement to be negligibly small for most wind engineering purposes (6, 8, 24, 26).

If the quadrature spectrum is negligible, it is convenient to express the cross-spectral density of two functions $F_{P_1}(t)$, $F_{P_2}(t)$ in the form

$$S_{F_{P_1}F_{P_2}}(n) = S^{1/2}_{F_{P_2}}(n)\, S^{1/2}_{F_{P_2}}(n)\, R_F(P_1, P_2, n) \quad (4)$$

in which $R_F(P_1, P_2, n)$ is the square root of the coherence function and can usually be determined only on the basis of experiment. $R_F(P_1, P_2, n)$ is a measure of the extent to which the functions $F_{P_1}(t)$, $F_{P_2}(t)$ are correlated. If these functions are perfectly correlated (e.g., if $F_{P_1}(t) \equiv F_{P_2}(t)$), then $R_F(P_1, P_2, n) \equiv 1$. Otherwise, $R_F(P_1, P_2, n) < 1$.

Equation (3) can easily be seen to reflect the obvious fact that the response due to two forces increases as their correlation increases. For example, assuming $S_{F_{P_1}}(n) \equiv S_{F_{P_2}}(n)$, $S_a(M, n)$ will be twice as large if $R_F(P_1, P_2, n) \equiv 1$ than if $R_F(P_1, P_2, n) \equiv 0$. Poorly correlated random forces may thus be thought of as forces which, in a sense, work at cross-purposes.

If a distributed stationary random loading is applied to an area A, Equation (3) may be generalized (16):

$$S_a(M, n) = \int_A \int_A H^*(M, P_1, n)H(M, P_2, n)S_p(P_1, P_2, n)dA_1dA_2 = \int_A \int_A H^*(M, P_1, n)H(M, P_2, n)S^{1/2}_p(P_1, n)S^{1/2}_p(P_2, n)R_p(P_1, P_2, n)dA_1dA_2 \quad (5)$$

in which P_1, P_2 = centers of elemental areas dA_1, dA_2; $S_p(P_1, n)$, $S_p(P_2, n)$, $S_p(P_1, P_2, n)$= spectral and cross-spectral densities of pressures at points P_1, P_2; $R_p(P_1, P_2, n)$ = cross-correlation coefficient = square root of coherence function. The mechanical admittance function incorporates the parameters describing the mechanical properties of the structure and may be expressed as:

$$H^*(M, P_1, n)H(M, P_2, n) = \sum_r \sum_s \frac{\mu_r(M)\mu_s(M)}{16\Pi^4 M\, M\, n_r^2 n_s^2} \frac{(1 - n^2/n_r^2)(1 - n^2/n_s^2) + 4\beta_r\beta_s(n/n_r)(n/n_s)}{[(1 - n^2/n_r^2)^2 + 4\beta_r^2 n^2/n_r^2][(1 - n^2/n_s^2)^2 + 4\beta_s^2 n^2/n_s^2]} \quad (6)$$

in which $\mu_r(M)$, M_r, n_r, β_r = modal shape, generalized mass, natural frequency and damping

ratio, respectively, in the r^{th} mode. For a building of height H

$$M_r = \int_o^H \mu_r^2(z)\ m(z)dz \tag{7}$$

where z = height above ground and m(z) = mass of structure per unit height. It follows from Equations (1), (6), and (7) that the mean square value of the fluctuating response of a linearly elastic structure can be obtained if, in addition to the geometry and the mechanical properties of the structure (mass distribution, modal shapes, natural frequencies, and damping ratios, including aerodynamic damping which can be determined as shown in Ref. 26), the spectral density function and the cross-correlation coefficient of the pressure fluctuations are known. As will be shown subsequently, these quantities can be determined using basic aerodynamic considerations and relevant information on the characteristics of the atmosphere boundary layer.

Aerodynamic Considerations: Relation Between Wind Pressures and Wind Speeds

The pressure acting at a point P of elevation z on the surface of a building immersed in a flow which has a steady mean velocity $\bar{v}(z)$ may be expressed as

$$\bar{p}(P) = 1/2\ \rho C_p(P)\ \bar{v}^2(z) \tag{8}$$

In this expression $\bar{v}(z)$ = undisturbed mean velocity of the flow, i.e., its velocity at a sufficiently large distance upwind from the building, and C_p is a dimensionless mean pressure coefficient. For blunt bodies in turbulent flow, $C_p(P)$ can usually be determined only by experiment.

For the windward and leeward sides of a rectangular tall building, the mean pressure coefficients specified by the A58.1 Standard are $C_w = 0.8$ and $C_\ell = -0.6$, respectively. Wind tunnel measurements reported by Baines (2) suggest that these values are, on the average, conservative. Also, measurements indicate that mean pressure coefficients for full-scale buildings are smaller than those obtained in wind tunnel tests, i.e., are slightly decreasing functions of Reynolds number (11).

An extension of Equation (8) to include the effects of velocity fluctuations takes the form

$$p(P) = \bar{p}(P) + p'(P) = 1/2\ \rho C_p(P)[\bar{v}(z) + v'(z)]^2 + \frac{\pi}{4}\rho C_M(P)B(z)v'(z,\ t) \tag{9}$$

in which p'(P) and v'(z) = pressure and velocity fluctuations, $C_M(P)$ = added mass coefficient and B(z) = width of structure. The last term in Equation (9) is known as the added mass term. The question of its relative importance in Equation (9) has been examined by Vickery and Kao (26). On the basis of wind tunnel pressure measurements (8), these writers showed that in determining pressures on buildings the added mass term may be neglected. The contribution to this term of its low frequency components is insignificant because the accelerations of these components are very small (26). To explain the experimental results of Refs. 8 and 26, according to which the contribution of the high frequency components is also negligible, it may be argued that, while for the small eddies, the accelerations are large, the corresponding added mass coefficients are very small. Indeed, while in the case of an infinite mass of fluid being accelerated with respect to a body $C_M \quad C_p$, in the case of a turbulent eddy the accelerated mass is of the order of the eddy size and, therefore, decreases as the frequency increases. Thus, neglecting the added mass term, it follows from Equations (8) and (9),

$$p'(P) = \rho C_p(P)\bar{v}(z)\ v'(z)[1 + 1/2\ v'(z)/\bar{v}(z)] \tag{10}$$

If $v'(z)/\bar{v}(z)$ is small (i.e., $\overline{v'^2(z)}^{1/2}/\bar{v}(z) < 0.1$) and the linear dimensions of the body are small compared with the length characteristic of the turbulence, the assumption that the non-linear term in Equation (10) may also be neglected is confirmed by indirect experimental evidence (3). In the atmosphere it may be assumed that $\overline{v'^2(z)}^{1/2}/\bar{v}(z) \simeq$

$2.54\ u_*/2.5\ u_*[1\ n(z - z_d)/z_o]$, in which u_*, z_d, z_o = frictional velocity, zero plane displacement, roughness length, respectively (13, 18, 19). Thus, for tall buildings this ratio is of the order of 0.05 to 0.3, depending upon building height and roughness of terrain. Also, except in the case of slender, line-like structures, the ratio of building dimension to scale of turbulence is not necessarily very small. Questions may thus arise as to whether the non-linear term may be neglected in the case of buildings with typical widths in atmospheric flow. Practical difficulties have prevented so far the carrying-out of simultaneous full-scale measurements of $p'(P)$, $\bar{v}(z)$, and $v'(z)$. However, wind tunnel measurements have been performed (7, 26) and appear to confirm the assumption that Equation (10) may be linearized. Also, the effect of the non-linear term was analyzed in Ref. 23, according to which the contribution of this term to the fluctuating alongwind response of a 300 m. tall structure appears to be of the order of 5% (i.e., a contribution to the total alongwind response of about 3%). It thus appears that the linearization of Equation (10) is acceptable and that

$$p'(P) = C_p\ \bar{v}(z)\ v'(z) \tag{11}$$

Research aimed at developing an improved model of the relation between alongwind fluctuating pressures and velocities is clearly desirable. It appears, however, that Equation (11) may represent a reasonably adequate engineering model for this relation. If Equation (11) is used, it follows

$$S_p(P_1, P_2, n) = C_p^2 \rho^2 \bar{v}(z_1)\bar{v}(z_2)\ S_v(P_1, P_2, n) \tag{12}$$

in which the cross-spectral density of the velocity fluctuations can be written as

$$S_v(P_1, P_2\ n) = S_v^{1/2}(P_1, n)\ S_v^{1/2}(P_2, n)\ R_v(P_1, P_2, n) \tag{13}$$

It follows from Equations (5), (12), and (13) that $R_p(P_1, P_2, n) \equiv R_v(P_1, P_2, n)$.

If Equation (11) is applied to express the pressures on the windward and leeward sides of the building:

$$p_w'(P) = C_w \bar{v}(z)\ v'(z) \tag{15}$$

$$p_\ell'(P) = C_\ell \bar{v}(z)\ v'(z) \tag{16}$$

As noted in Ref. 17, in reality the flow in the separation bubble is quite dissimilar from that in the oncoming flow. Measurements suggest that the fluctuating pressures on the leeward side are small compared to those on the windward side and, therefore, that Equation (16) may be slightly conservative.

Planetary Boundary Layer Flow: Mean Wind Speeds

The mean wind speeds used in design depend upon roughness of terrain, wind climate, and desired level of safety of the structure.

The roughness of terrain determines the shape of the mean velocity profile which can be shown to be given by the relation

$$\bar{v}(z) = 2.5\ u_*\ \ln \frac{z - z_d}{z_o} \tag{17}$$

in which $u_* = 0.4\ v(z_1)/\ell n[(z_1 - z_d)/z_o]$ and z_1 is some reference height. Equation (17) is the well-known logarithmic law (14, 15, 18) and values of z_o, z_d are given in Ref. 18. It the terrain is uniform over a sufficiently large fetch, Equation (18) is valid up to a height

$$z_p \simeq 100\ \bar{v}(z)/\ln[(z - z_d)/z_o] \tag{18}$$

in which $\bar{v}(z)$ is expressed in units of length per second (18). For example, if $z_o = 0.07$ m, $z_d \simeq 0$ (open terrain) and $z = 9.15$ m (30 ft.), $\bar{v}(z) = 35\ ms^{-1}$ ($\simeq$ 80 mph), then $z_p \simeq 720$ m.

For a given angle of latitude, the geostropic wind speed (the wind speed in the free atmosphere, flowing under barotropic conditions along straight isobars) is determined solely by the magnitude of the pressure gradient force. Near the ground, however, the wind speed also depends upon the roughness of the terrain. To any given geostrophic wind there will thus correspond mean velocity profiles denoted by $\bar{v}(z, z_o, z_d)$ which are related to each other as shown in Figure 1. For example, if over open terrain with $z_o = 0.08$ m, $z_d = 0$, the mean wind speed at $z_1 = 10$ m is $\bar{v}(z_1, z_o, z_d) = 20$ ms^{-1} (45 mph), over built-up terrain with $\tilde{z}_o = 0.78$ m, $\tilde{z}_d = 21$ m the corresponding mean wind at $z_2 = 43$ m can be found (Figure 1) to be $\bar{v}(z_2, \tilde{z}_o, \tilde{z}_d) = 15.8$ ms^{-1} (35.5 mph).

The description of the mean wind structure incorporated in Equation (17) and Figure 1, which will be referred to herein as the similarity model, is based upon recent results of atmospheric boundary layer studies for which a satisfactory theoretical, as well as experimental foundation, exists. In the A58.1 Standard and the NBC, an empirical power law model is employed. The power law exponents are assumed to be constant up to the gradient height and are specified for three standard terrain roughness conditions, classified as open, suburban, and urban. The power law model has shortcomings which may lead to results that are not consistent with actual measurements. An analysis of these shortcomings and comparisons between the similarity and the power law models can be found in Ref. 18.

In the Uniform Building Code (22), the United States is divided into seven wind intensity zones. In the A58.1 Standard and the NBC, the design wind speeds are based upon formal statistical analyses of wind records, i.e., they are defined in probabilistic terms on the basis of assumed probability distribution functions and of specified mean recurrence intervals.

Planetary Boundary Layer Flow: Longitudinal Wind Speed Fluctuations

It can be shown that the following expression is a correct representation of the spectrum of the longitudinal wind speed fluctuations in the higher frequency range and is consistent with the requirements that (1) the spectral density must approach a finite value as n 0, (2) the product $nS_v(P, n)$ reaches its maximum at some value of the frequency below the inertial subrange, and (3) the mean square value of the longitudinal wind speed fluctuations is $\overline{v'^2(P)} = 6.0\, u_*^2$:

$$nS_v(P, n)/u_*^2 = 200\, f/(1 + 50\, f)^{5/3} \qquad (19)$$

in which $f = n(z - z_d)/\bar{v}(z)$ is known as the similarity (or Monin) coordinate. In Equation (19) the peak similarity coordinate (the value of f for which $nS_v(n)$ is a maximum) is $f_{pk} = 0.033$. As noted, for example, in Refs. 15, 19, in reality f_{pk} varies rather erratically between sites and between atmosphere and laboratory, as well as with height above ground. Orders of magnitude of f_{pk} are suggested in Refs. 15 and 19. The effect upon structural response of the variation of f_{pk} can be verified as will be subsequently done in this paper by using alternative expressions for the spectra in which the peak similarity coordinate appears as a parameter. Such expressions can be found in Ref. 19 (Equations 5, 9, and 10).

In the A58.1 Standard and in the NBC, as well as in Vickery's procedure (25), an expression for the spectrum of the longitudinal wind speed fluctuations is assumed which is invariant with height (6) and thus violates the similarity requirements which prevail in the higher frequency range (14, 15, 19). From a structural engineering point of view, the drawback of this expression is that it over-estimates the spectral densities at frequencies equal, or nearly equal, to the natural frequencies of tall structures and that it thus results in over-estimates of the resonant part of their dynamic response (19).

It is convenient to express the cross-correlation coefficient $R_v(P_1, P_2, n)$ in the form

$$R_v(P_1, P_2, n) = R(y_1, z_1, y_2, z_2\, n) \qquad (20)$$

in which y_i, z_i are the coordinates of point P_i ($i = 1, 2$) in a plane perpendicular to the direction of the mean wind, $R(y_1, z_1, y_2, z_2, n)$ = acrosswind, and $N(P_1, P_2, n)$ = alongwind correlation coefficient.

The following expression for the acrosswind correlation coefficient has been proposed by Davenport (7):

$$R(y_1, z_1, y_2, z_2, n) = \exp\{-2n\sqrt{C_z^2(z_1 - z_2)^2 + C_y^2(y_1 - y_2)^2}/[\bar{v}(z_1) + \bar{v}(z_2)]\} \quad (21)$$

in which $C_z \simeq 10$, $C_y \simeq 16$ (25). By definition, if the points P_1, P_2 are in the same plane perpendicular to the mean wind direction, $N(P_1, P_2, n) \equiv 1$. Otherwise, $N(P_1, P_2, n) < 1$; its magnitude decreases as the alongwind separation between P_1, P_2 increases and as the frequency n increases. For the purposes of Equation (5), useful information regarding the magnitude of $N(P_1, P_2, n)$ is provided by results of measurements of cross-spectra of pressures on the windward and leeward sides of structures. Such measurements, carried out on a full-scale building, have been reported by Lam Put (9), who found that $N(P_{1_w}, P_{2_\ell}, n) < 0.2$ (the subscripts w, ℓ indicate that the points P_1, P_2 are on the windward and leeward sides, respectively; points P_{1_w}, P_ℓ and P_{2_w}, P_{2_ℓ} have coordinates y_1, z_1 and y_2, z_2, respectively). Form a comparison of the results of wind tunnel measurements reported by Kao (Figures 5.1, 5.19, 5.21 of Ref. 8), it also follws that, except for extremely low frequencies corresponding to eddies of negligible energy, $N(P_{1_w}, P_{2_\ell}, n)$ is nearly zero.

Alongwind Response

From Equations (5), (12), (13), (15), and (16), it follows that for a building rectangular in plan, of height H and width B, the spectral density of the fluctuating response at a point M is

$$S_a(M, n) = \rho^2 \int_0^B \int_0^B \int_0^H \int_0^H (C_w^2 + 2C_wC_1N(n) + C_\ell^2)\, H^*(M, P_1, n)H(M, P_2, n)$$

$$\bar{v}(z_1)\bar{v}(z_2)S_v^{1/2}(P_1, n)S_v^{1/2}(P_2, n)R(y_1, z_1, y_2, z_2, n)dy_1dy_2dz_1dz_2 \quad (22)$$

In Equation (22), the identities $N(P_{1_w}, P_{2_w}, n) = N(P_{1_\ell}, P_{2_\ell}, n) \equiv 1$, and the notation $N(P_{1_w}, P_{2_\ell}, n) = N(P_{1_\ell}, P_{2_w}, n) = N(n)$ are used.

The mean square value of the dynamic response is

$$\overline{a'^2(z)} = \int_0^\infty S_a(M, n)dn \quad (23)$$

and the maximum probable fluctuating response can be written as

$$a'_{max}(z) = g(z)\overline{a'^2(z)}^{1/2} \quad (24)$$

in which the peak factor is (6)

$$g(z) = [2\ln\nu_a(z)T]^{1/2} + 0.577/[2\ln\nu_a(z)T]^{1/2} \quad (25)$$

T = duration of wind loading and

$$\nu_a^2(z) = \int_0^\infty n^2 S_a(M, n)dn/\overline{a'^2(z)} \quad (26)$$

The mean response may be written in terms of generalized masses and forces as (19)

$$\overline{a(z)} = \frac{1}{2}(C_w + C_\ell)\rho B \sum_r \frac{\mu_r(z) \int_0^H \bar{v}^2(z)\mu_r(z)dz}{4\pi^2 n_r^2 \int_0^H m(z)\mu_r^2(z)\, dz} \quad (27)$$

If the contribution of the higher modes of vibration can be neglected, it is convenient to write the mean square value of the response as, approximately, the sum of the "background" and a "resonant" response (6, 24, 25). It follows then from Equations (22) and (23),

$$\overline{a'(z)}^2 \simeq \rho^2 \mu_1^2(z)(B + K)/16\,\pi^4 n_1^4 M_1^2 \tag{28}$$

in which the quantities B and K, which are proportional to the background and resonant response, respectively, have the expressions

$$B = \int_0^\infty \left[\int_0^B \int_0^B \int_0^H \int_0^H I_a(y_1, y_2, z_1, z_2, n)\, dy_1 dy_2 dz_1 dz_2\right] dn \tag{29}$$

$$K = \frac{\pi n_1}{4\beta_1} \int_0^B \int_0^B \int_0^H \int_0^H I_a(y_1, y_2, z_1, z_2, n_1)\, dy_1 dy_2 dz_1 dz_2 \tag{30}$$

$$I_a(y_1, y_2, z_1, z_2, n) = [C_w^2 + 2C_w C_\ell N(n) + C_\ell^2]\mu_1(z_1)\mu_1(z_2)\bar{v}(z_1)\bar{v}(z_2)$$
$$S_v^{1/2}(P_1, n) S_v^{1/2}(P_2, n) R(y_1, y_2, z_1, z_2) \tag{31}$$

Numerical integrations carried out using the computer program briefly described in Ref. 19 show that the approximation involved in Equation (28) is of the order of 1%.

The total, maximum deflection in the alongwind direction is

$$a(z) = [1 + g(z)\, \overline{a'^2(z)}^{1/2}/\bar{a}(z)]\, \bar{a}(z) \tag{32}$$

The quantity between brackets in Equation (32) is known as the gust response factor. The equivalent static load is then the product of the mean load and the gust response factor.

BASIC FEATURES OF PROCEDURES FOR COMPUTING ALONGWIND RESPONSE

The framework described in the preceding section will now be used to discuss certain procedures that have been proposed for the calculation of alongwind response.

Procedure Described in the A58.1 Standard (1)

The mean wind speeds specified for design purposes by the A58.1 Standard correspond to 50- and 100- year mean recurrence intervals based on Type II probability distributions of the largest values. In the calculations, hourly means are used, which can be easily obtained if the fastest-mile speeds are known (24). The mean pressures on both the windward and the leeward sides are proportional to the square of the mean speeds, which are assumed to obey the power law. The pressure coefficients are $C_w = 0.8$ and $C_\ell = -0.6$ or $C_\ell = -0.5$ (for $H/B \geq 2.5$ or $H/B < 2.5$, respectively). The wind spectra are assumed to be invariant with height. As pointed out previously, this assumption results in overestimates of the dynamic part of the response. The acrosswind correlation coefficient is essentially similar to that given by Equation (21). The alongwind correlation coefficient is assumed to be

$$N(P_{1_w}, P_2, n) = \frac{1}{\xi} - \frac{1}{2\xi^2}(1 - e^{-2\xi}) \tag{33}$$

in which $\xi = 3.85\, n\Delta x/\bar{v}$, Δx is the smaller of the distances 4B or 4H and $\bar{v} = \int_0^H \bar{v}^2(z)\, dz/H$. Although, by definition, $N(P_{1_w}, P_{2_w}, n) \equiv N(P_{1_\ell}, P_{2_\ell}, n) \equiv 1$, it is implicit in this procedure that these quantities are both equal to $N(P_{1_w}, P_{2_\ell}, n)$ and, as shown in Ref. 17, this results in underestimates of the dynamic part of the response. A value of the peak factor $g(z) = 3.0$ is used, rather than the more correct value given by Equation (25) which,

for T = 3600 s, is usually g(z) = 3.4 - 4.0. The contribution of the higher modes of vibration is not taken into account. As will be shown subsequently, in most cases of practical interest this contribution may be neglected.

Procedure Described in the National Building Code of Canada (5, 11)

For design purposes, the NBC specifies mean speeds averaged over one hour and corresponding to 30- and 100-year mean recurrence intervals based on Type I probability distributions of the largest values (7). A statistical analysis carried out by the writers of 30 extreme wind records taken over periods of 20 to 45 years showed that these speeds are approximately 6% lower than those specified by the A58.1 Standard. Since the mean response is proportional to the square of the mean speeds, the corresponding difference between the respective mean responses is about 12%. The mean pressures on the windward side are proportional to the square of the mean speeds, which are assumed to obey the power law, except that in the lowest 30 ft. (9.15 m) in open terrain and 100 ft. (30.5 m) in urban terrain the mean pressures are assumed to be uniformly distributed (11). A pressure coefficient $C_w = 0.8$ is used. The mean pressures on the leeward side are assumed to be distributed uniformly and are proportional to the square of the mean speed at an elevation H/2, where H is the building height, with $C_\ell = -0.5$. (This assumption results in a further increase of the difference between mean responses calculated by Refs. 1 and 11). The same expression for the wind spectrum and essentially the same expression for the acrosswind correlation coefficient as in the A58.1 Standard are used. Thus, in this procedure, the variation of the spectrum with height is not taken into account and, correspondingly, overestimates of the dynamic response result. The alleviating effect of the alongwind correlation is also not taken into account, i.e., the assumption $N(P_{1_w}, P_{2\ell}, n) \equiv 1$ is implied, which results in further overestimates of the dynamic response (17). Equation (25) is used to obtain the peak factor and the higher vibration modes are not taken into account.

Vicker's procedure is essentially similar to that of Ref. 11, over which it has the advantage of being more flexible in that it permits the variation of certain parameters (decay coefficients C_y, C_z in Equation (21) and an exponent defining the modal shape). The peak factor is assumed to be g(z) = 3.5.

Procedure Based on Refs. 18 and 19

In this procedure the mean wind speeds are described by the logarithmic law (Equation (17)), and the variation of the wind spectrum with height is taken into account as shown in Ref. 19. Between the elevation $(z_d + 10)$ meters and the top of the building the mean pressures are assumed to be proportional to the square of the mean speeds. In the lowest $(z_d + 10)$ meters, the pressures are assumed to be uniformly distributed and to have the same value as at elevation $(z_d + 10)$. The pressure coefficients assumed in the calculations presented in this paper are $C_w = 0.8$ and $C_\ell = -0.5$. In view of the uncertainty regarding the actual probability distributions of extreme wind speed (7), as well as the optimum recurrence intervals to be used in structural design, calculations were carried out using mean speeds specified by both the A58.1 Standard and the NBC. The peak factor was assumed to be given by Equation (25), and the acrosswind correlation coefficient given by Equation (21) was used. In computing the background response it was assumed conservatively that $N(P_w, P_\ell, n) \equiv 1$. In computing the resonant response, the assumption $N(P_w, P_\ell, n_1) = 0.$, in which n_1 = natural frequency in the fundamental mode was used. Alternatively, in computing the resonant response it was assumed that Equation (33) is valid. The differences between total response calculated using these two assumptions turned out to be insignificant (0-3%).

In the expression for the wind profiles, the values $z_o = 0.07$ m, $z_d = 0$, and $z_d = 0.8$ m, $z_d = 21$ m for open and urban terrain, respectively, were used in calculating the gust factors and the deflections presented in the following. To verify the extent to which the response might be sensitive to variations of the roughness parameters, the values $z_o = 1.2$ m, $z_d = 10$ m were also used for urban terrain as noted by Pasquill (15), experimental results suggest that in urban terrain, as wind speed increases, z_o increases and z_d decreases, possibly because the air stream "penetrates" more deeply between buildings. The results obtained using these values differed in all cases by less than 3% from the results presented herein.

The effect upon the structural response of the possible variation of the peak similarity coordinate f_{pk} was also verified. The dynamic response was calculated using Equation (19) (to which there corresponds $f_{pk} = 0.033$), as well as alternative expressions for the spectra (Equations (5), (9), (10) of Ref. 19) in which f_{pk} appears as a parameter. The ratios of the root mean square values of the fluctuating response $[a'(h)^2]^{1/2}_{f_{pk}}/[a'(h)^2]^{1/}_{0.}$ (where the numerator is based on Equations (5), (9), (10) of Ref. 19 and the denominator is based on Equation (19)), were calculated in the case $v_h = 26.8$ ms^{-1} (v_h = wind speed at 30 ft. above ground in open terrain) for the typical buildings described in the following section of this paper. For $f_{pk} = 0.01$, this ratio was found to be approximately one in all cases. In the case of the 365 m tall building, the ratio was about .95 for $f_{pk} = 0.1$ and .93 for $f_{pk} = 0.19$. In the case of the 150 m tall building, the ratio was about .93 for $f_{pk} = 0.10$ and .92 for $f_{pk} = 0.19$. In the case of the 45 m tall building, the ratio was about .85 for $f_{pk} = 0.1$. It is noted that, for $H < 45$ m, on average, $f_{pk} < 0.1$. Equation (19), which is shown by these results to be moderately conservative, was, therefore, used in calculating the values of the dynamic response presented in this paper.

For the three typical buildings described subsequently, the contribution to the dynamic response of the second and third modes of vibration was calculated. It was found that if, as was assumed in the calculations presented herein, the natural frequencies in the second and third modes are approximately three and six times higher than the fundamental frequency, respectively, the contribution of the higher modes to the response is insignificant.

ANALYSIS OF NUMERICAL RESULTS

For the purpose of comparing the procedures examined in this paper, the gust response factor and the maximum alongwind deflections were calculated for three typical tall buildings previously analyzed by Vickery (25). The geometric, as well as the mechanical, properties of the buildings are shown in Table 1. In all cases, an average building weight of 1,500 N/m^3 was assumed. For steel structures, both the A58.1 Standard and the NBC suggest a damping ratio $\beta_1 = 0.01$. This ratio was used in calculating both gust response factors and maximum alongwind deflection. In addition, gust factors were calculated assuming higher damping ratios (including mechanical and aerodynamic damping). For $\bar{v}_h = 26.8$ ms^{-1}, these ratios were assumed to be the same as used in Ref. 25. For $\bar{v}_h = 40$ ms^{-1} the damping ratios were increased with respect to those of Ref. 25 by amplifying their aerodynamic part in proportion with the wind speed, as shown in Ref. 26. The results of all the calculations are given in Tables 1 and 2.

It can be seen from Table 1 that the gust factors computed in accordance with the A58.1 Standard are in all cases lower than those determined on the basis of the NBC, the differences ranging from about 15% or more in the case of the 45 m tall building in open terrain to almost 100% in the case of the 365 m tall building in urban terrain. The values of Column (4) were calculated on the basis of improved models of the mean profiles, of the wind spectra and of the alongwind pressure correlations (17, 18, 19). If these values are regarded as being correct (even though, as shown previously in this paper and in Ref. 19, they are likely to be slightly conservative), then it may be stated that (1) the values of the gust factors (Equation (32)) based on the A58.1 Standard are low, by amounts ranging from 1% in the case of the 365 m tall buildings in open terrain to 20% in the case of the 150 m tall building in urban terrain, and that (2) the values of the gust factors based on the NBC are high, by amounts ranging from 1% in the case of the 45 m tall building in open terrain to 63% in the case of the tall building in urban terrain.

The differences between the gust factors obtained by the various procedures described in the preceding section are due primarily to the respective assumptions regarding the alongwind pressure correlations and the expression for the wind spectrum. The alongwind

correlation model used in the NBC results in an overestimate, whereas the model used in the A58.1 Standard results in an underestimate of the dynamic part of the response. The assumption used in both Refs. 1 and 11 that the spectrum is invariant with height results in overestimates of the response, which are negligible in the case of lower structures but become substantial in the case of very tall structures. In the case of the NBC, these overestimates are added to those due to the assumptions regarding the alongwind correlation effect. In the case of the A58.1 Standard, the deviation from the actual value of the response due to the assumption that the spectra are invariant with height and the deviation due to the assumption $N(P_{1_w}, P_{2_w}, n) = N(P_{1_\ell}, P_{2_\ell}, n) < 1$ are of opposite signs. Their sum is in most cases negative, as follows from the comparison between Columns (1) and (4).

It can be seen from Table 2 that the mean response determined in accordance with NBC is smaller than that based on the A58.1 Standard. This is the case because, first, for a given wind climate the mean wind speeds specified by the NBC are lower than those specified by the A58.1 Standard; secondly, the leeward pressure coefficient given in the NBC is $C_\ell = -0.5$, whereas that specified by the A58.1 Standard for buildings of ratio $B/H \geq 2.5$ is $C_\ell = -0.6$; thirdly, the contribution to the mean response of the leeward pressures is lower in the case of the NBC (in which these pressures are assumed to be uniformly distributed) than in the case of the A58.1 Standard. It is also noted that, assuming equal wind speed conditions, the values of the mean response determined in accordance with the procedures based on Refs. 18, 19, are in most cases slightly larger than those obtained using the A58.1 Standard. This shows that the power law model of the mean wind speeds is slightly unconservative.

For equal wind speed conditions, the difference between values of the total response determined in accordance with Refs. 18, 19 and with the NBC is relatively small in the case of the 45 m and 150 m tall buildings (2%-13%). In the case of the 365 m building in urban terrain, however, this difference is almost 50%. On the other hand, the differences between total response determined in accordance with Refs. 18, 19 and with the A58.1 Standard are larger for the 45 m and 150 m tall buildings (20%-33%) and are smaller for the 365 m tall buildings (6%-18%).

The maximum deflections calculated in accordance with the provisions of the New York City Code (13), the Uniform Building Code (UBC)(22), and the South Florida Code (21) are also included in Table 2.

For a basic design speed of 75 mph and urban terrain, the New York City Code is quite conservative for the 45 m building and somewhat unconservative for the taller buildings (assuming that 50-year mean recurrence interval is appropriate). The Uniform Building Code, which assumes an open country exposure, is extremely conservative for the 45 m building and slightly conservative in the case of the 365 m building. For a basic design speed of 110 mph and open country terrain, the South Florida Code underestimates the response of all three buildings. The Uniform Building Code slightly underestimates the response of the 45 m building and seriously underestimates the response of the 365 m building.

CONCLUSIONS

A comparative analysis of current procedures for evaluating alongwind structural response has been presented. The analysis confirms that considerable discrepancies exist between results obtained using these procedures. For example, in the case of a 365 m tall building in urban terrain the procedure described in the NBC (5, 11) yields values of the dynamic part of the response, of the gust factor, and of the total maximum deflection which are, respectively, three times, twice, and 1.6 times larger than those based on the A58.1 Standard (1). The basic assumptions used in the various procedures have been examined and their shortcomings have been pointed out. An improved procedure, based on Refs. 18, 19, has been described. Numerical calculations were carried out, based on this, as well as on the other procedures investigated. Typical buildings of 365 m, 150 m, and 45 m height, previously analyzed by Vickery, were used as case studies. For purposes of comparison, the results obtained by the procedure based on Refs. 18, 19 were calculated

using the probabilistic definitions of design wind speeds specified in the A58.1 Standard and in the NBC. The question of these definitions is, however, beyond the scope of this paper. Assuming that these definitions are acceptable, the results of the calculations showed that the procedure described in the A58.1 Standard was unconservative in most cases. On the other hand, the procedure described in the NBC was slightly unconservative for the 45 m buildings and was over conservative for buildings of 150 m and 365 m height. Thus, while in certain cases the procedures described in both the A58.1 Standard and the NBC may yield reasonable results, their fundamental shortcomings may be the cause of considerable underestimates or overestimates of the alongwind structural response. The writers believe, therefore, that the use of the procedure based on Refs. 18, 19, which incorporates recently developed, improved models of the mean wind profiles, the wind spectrum and the pressure correlation in the alongwind direction, and which is described in the body of the paper, is justified in the case of structures in the design of which the wind loading is a major consideration.

REFERENCES

1. "American National Standard A58.1 - Building Code Requirements for Minimum Design Loads in Buildings and Other Structures," American National Standards Institute, New York, New York, 1972.

2. Baines, W.D., "Effects of Velocity Distribution on Wind Loads and Flow Patterns on Buildings," Proceedings, Wind Effects on Buildings and Structures, Teddington, 1963, Her Majesty's Stationery Office, London, 1965.

3. Batchelor, G.K., "The Theory of Homogeneous Turbulence," Cambridge University Press, Cambridge, England, 1953.

4. Blackman, R.B., and Tukey, J.W., "The Measurement of Power Spectra from the Point of View of Communication Engineering," Dover Publications, Inc., New York.

5. "Canadian Structural Design Manual," Supplement No. 4 to the National Building Code of Canada, National Research Council, Ottawa, 1970.

6. Davenport, A.G., "Gust Loading Factors," Journal of the Structural Division, ASCE, Vol. 93, No. ST3, Proc. Paper 5255, June 1967, pp. 11-34.

7. Davenport, A.G., "The Dependence of Wind Loads on Meteorological Parameters," Proceedings, Wind Effects on Buildings and Structures, Vol. I, Ottawa, 1967, University of Toronto Press, Toronto, 1968.

8. Kao, K.H., "Measurements of Pressure/Velocity Correlation on a Rectangular Prism in Turbulent Flow," Engineering Science Research Report BLWT-2-20, University of Western Ontario, London, Canada, 1971.

9. Lam Put, R., "Dynamic Response of a Tall Building to Random Wind Loads," Proceedings, International Conference on Wind Effects on Buildings and Structures, Tokyo, Japan, 1971, pp. III - 4.1 - 11.

10. Lumley, J.L., and Panofsky, H.A., "The Structure of Atmospheric Turbulence," John Wiley and Sons, 1964.

11. National Building Code of Canada, National Research Council, Ottawa, 1970.

12. Newberry, C.W., Eaton, K.J., and Mayne, J.R., "Wind Loading of a Tall Building in an Urban Environment," Building Research Station, Garston, Watford, England, 1968.

13. "New York City Building Code," Local Law No. 76 of the City of New York, New York, New York, 1969.

14. Owen, P.R., "Buildings on the Wind," Quarterly Journal of the Royal Meteorological Society, Vol. 97, 1971, pp. 396-413.

15. Pasquill, F., "Wind Structure in the Atmospheric Boundary Layer," Philosophical Transactions of the Royal Society of London, A., 269, 1971, pp. 439-456.

16. Robson, J.D., "An Introduction to Random Vibration," Elsevier Publishing Company, 1964, p. 91.

17. Simiu, E., "Gust Factors and Alongwind Pressure Correlations," Journal of the Structural Division, ASCE, Vol. 99, No. ST4, Proc. Paper 9686, April, 1973, pp. 773-783.

18. Simiu, E., "Logarithmic Profiles and Design Wind Speeds," Journal of the Engineering Mechanics Division, ASCE, Vol. 99, No. EMS, Proc. Paper 10100, October, 1973, pp. 1073-1083.

19. Simiu, E., "Wind Spectra and Alongwind Structural Response," Meeting Preprint 2086, ASCE Annual and National Environmental Engineering Meeting, October 1973, New York.

20. Simiu, E., "Improved Methods for Determining Wind Profiles and Dynamic Structural Response to Wind," Proceedings, ASCE-IABSE Regional Conference on Tall Buildings, January 1974, Bangkok.

21. "South Florida Building Code," Dade County, Florida, 1970.

22. "Uniform Building Code," International Conference of Building Officials, Whittier, California, 1973.

23. Vaicaitis, R., Shinozuka, M., and Takeno, M., "Response Analysis of Tall Buildings to Wind Loading," Technical Report No. 1, Dept. of Civil Engineering and Engineering Mechanics, Columbia University, July 1973, New York, p. 74.

24. Vellozzi, J., and Cohen, E., "Gust Response Factors," Journal of the Structural Division, ASCE, Vol. 94, No. ST6, Proc. Paper 5980, June 1968, pp. 1295-1313.

25. Vickery, B.J., "On the Reliability of Gust Loading Factors," Proceedings, Technical Meeting Concerning Wind Loads on Buildings and Structures, National Bureau of Standards, Building Science Series 30, Washington, D.C., 1970.

26. Vickery, B.J., and Kao, K.H., "Drag of Alongwind Response of Slender Structures," Journal of the Structural Division, ASCE, Vol. 98, No. ST1, Proc. Paper 8635, January 1972, pp. 21-36.

NOTATION

The following symbols are used in this paper:

A = Area

B = Width of structure

C_M = Added mass coefficient

C_p = Mean pressure coefficient

C_w = Mean pressure coefficient - windward face

C_ℓ = Mean pressure coefficient - leeward face

C_y, C_z = Dimensionless coefficients (defined in text)

$F(t)$ = Stationary random function

H = Height of structure

$H(M, P, n)$ = Mechanical admittance function

$H^*(M, P, n)$ = Complex conjugate of $H(M, P, n)$

M = Denotes a point on the structure

M_r = Generalized mass term

N = Alongwind correlation coefficient

P = Denotes a point on the structure

R = Square root of coherence function

$S(n)$ = Spectral density function

T = Duration time

a = Structural response

f, f_{pk} = Similarity coordinate, peak similarity coordinate

g = Peak factor

m = Mass of structure per unit height

n = Frequency

$\overline{p}$ = Mean pressure

p' = Fluctuating pressure

r = Subscript indicating r^{th} mode

s = Subscript indicating s^{th} mode

t = Time

u_* = Friction velocity

$\bar{v}(z)$ = Mean wind velocity at height z

$v'(z)$ = Velocity fluctuation at height z

z = Height above ground

z_d = Zero plane displacement

z_o = Surface roughness length

β = Damping ratio

Δx = Horizontal separation in the alongwind direction

μ = Modal shape

ν = Effective fluctuation rate

$\xi = 3.85\ n\Delta x/\bar{v}$

1, 2 = Subscripts denoting values of a quantity at points 1, 2

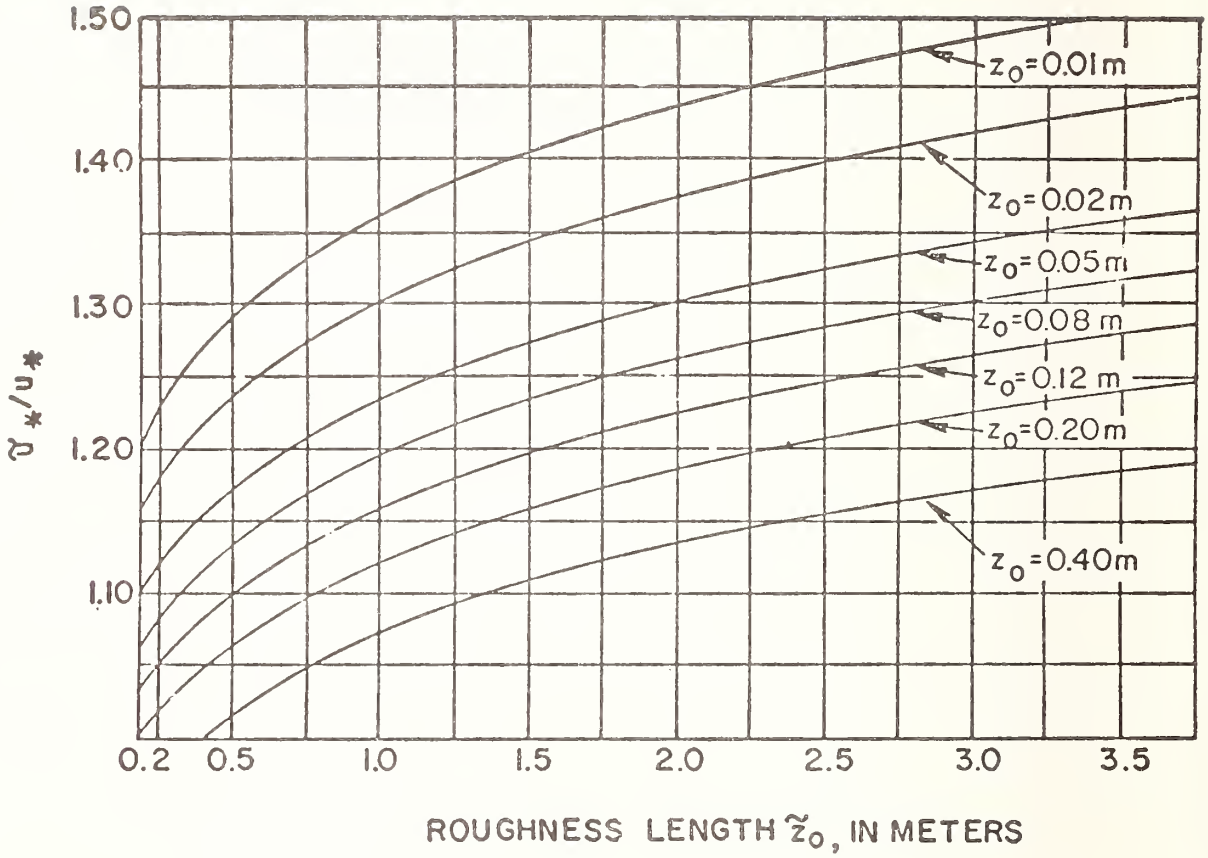

FIG. 1 - Ratios $\tilde{u}_*/u_*$

TABLE 1. - Gust Response Factors

Building	Height meters	Width meters	Depth meters	Fundamental period of vibration sec.	$\bar{v}_h$ meters/second[a]	Terrain	Damping ratios	ANSI A58.1 Ref 1 (1)	NBC of Canada Ref 7 (2)	Vickery Ref 24 (3)	Simiu Refs 18, 19 (4)
1	365	60	45	10	26.8	Open	0.016	1.54	2.25	2.15	1.68
							0.01	1.59	2.56	2.50	1.74
						Urban	0.015	1.55	2.75	2.26	1.89
							0.01	1.59	3.12	2.57	1.96
2	150	61	45	5	26.8	Open	0.015	1.54	2.01	1.97	1.75
							0.01	1.54	2.30	2.20	1.80
						Urban	0.014	1.65	2.55	2.25	2.05
							0.01	1.66	2.75	2.35	2.11
3	45	45	45	1	26.8	Open	0.012	1.59	1.84	1.83	1.77
							0.01	1.59	1.86	1.83	1.78
						Urban	0.011	2.10	2.77	2.67	2.04
							0.01	2.10	2.78	2.67	2.06
1	365	60	45	10	40.0	Open	0.019	1.60	2.45	2.21	1.76
							0.01	1.74	2.97	2.61	1.91
2	150	60	45	5	40.0	Open	0.0175	1.63	2.34	2.27	1.82
							0.01	1.75	2.65	2.59	1.97
3	45	45	45	1	40.0	Open	0.013	1.58	1.91	1.67	1.81
							0.01	1.60	1.94	1.70	1.83

[a]Hourly mean wind speed at 30 feet above ground in open terrain.

TABLE 2 - Maximum Alongwind Deflections (in centimeters)

Building	Height (meters)	Mean Recurrence Interval (years)	Response	New York City and Vicinity (v_{fm}^{50} = 75 mph[h] [1])										South Florida (v_{fm}^{50} = 110 mph[h] [1])					
				Urban Terrain						Open Terrain				Open Terrain					
				ANSI A58.1[d] (1)	NBC of Canada[c] (2)	Simiu[c] (3)	Simiu[d] (4)	NYC Code[a] (5)	UBC[a,b,f] (6)	ANSI A58.1[d] (7)	NBC of Canada[c] (8)	Simiu[c] (9)	Simiu[d] (10)	ANSI A58.1[d] (11)	NBC of Canada[c] (12)	Simiu[c] (13)	Simiu[d] (14)	South Florida Code[a, b] (15)	UBC[a,b,g] (16)
1[j]	365	50[e]	Mean	55	47	53	59	93	117	86	68	77	86	174	139	157	176	344	232
			Dynamic	31	99	51	56			50	106	57	64	128	274	143	160		
			Total	86	146	104	115			136	191	134	150	302	413	300	336		
			Total	119	202	144	159			188	242	186	208	378	518	376	421		
2[j]	150	50[e]	Mean	7.3	7.5	8.6	7.6	18.5	26.2	15.6	13.1	14.9	16.7	31.8	27.2	31.0	34.7	62.3	49.0
			Dynamic	4.2	13.1	9.1	10.1			8.5	16.9	11.9	11.9	23.9	44.8	30.0	33.8		
			Total	12.01	20.6	17.7	19.7			24.1	30.0	26.8	28.6	55.7	72.0	61.0	69.5		
		100	Total	16.7	28.6	24.5	27.2			33.3	31.6	36.4	37.2	69.7	90.0	76.0	85.5		
3[j]	45	50[e]	Mean	.13	.11	.13	.15	.60	.91	.41	.36	.42	.47	.88	.76	.87	.97	1.64	1.75
			Dynamic	.14	.19	.15	.17			.25	.34	.33	.37	.52	.71	.72	.80		
			Total	.27	.30	.28	.32			.66	.67	.77	.84	1.40	1.47	1.59	1.78		
		100	Total	.37	.41	.39	.44			.91	.93	1.04	1.17	1.75	1.84	1.98	2.22		

[a]Total response. [b]No distinction made in these codes between open and urban terrain. [c]Assumed probability distributions of extreme speeds: type I. [d]Assumed probability distributions of extreme speeds: type II. [e]Except for columns (2), (3), (8), (9), (12), (13), in which response to 30-yr wind is shown. [f]25 psf wind pressure - map area. [g]50 psf wind pressure - map area. [h]50-yr fastest-mile wind at 30 ft above ground in open terrain, based on type II probability distribution. [j]Assumed damping ratio: 0.01.

SEISMIC RETROFITTING OF EXISTING HIGHWAY BRIDGES

by

James D. Cooper
Structural Research Engineer
Office of Research
Federal Highway Administration
Washington, D.C.

R. Richard Robinson
Research Engineer

Anatole Longinow
Manager of Structural Analysis
IIT Research Institute
Chicago, Illinois

The retrofitting of existing highway bridges, to provide an added measure of protection against collapse due to earthquake ground motion, is of great importance. This interest heightened in the United States following the San Fernando earthquake of 1971, which caused extensive damage to a number of modern freeway structures.

Some of the specific concepts for retrofitting to be explored include: (1) widening of bearing supports, (2) motion restrainers across hinges, (3) ties across expansion joints, (4) the elimination of expansion joints, and (5) adding ties or reinforcing to existing columns.

The monetary savings, resulting from an effective retrofit program in preventing collapse of structures, would far exceed the cost of the research involved in generating feasible and practical retrofit details.

This is a progress report on research which will result in mathematical techniques to identify the seismically vulnerable bridge details and a catalog of retrofit techniques. Such techniques will permit strengthening of such weak links, in the total structure integrity.

Key Words: Design; earthquakes; highway bridges; retrofitting; soil-structure interaction; structural engineering.

INTRODUCTION

In the San Fernando earthquake of February 9, 1971, numerous bridges were destroyed even though this earthquake was only of moderate magnitude, approximately 6.6 on the Richter Scale. Damages to highways have been estimated at $22.5 million to the State system and $5 million to city and county roads. The chief damage to the State system was the collapse of five overpasses and damage to an additional seven.

The western part of the United States experiences a severe earthquake on the average of every four years and it is reasonable to assume that any future earthquake of moderate to large magnitude can pose a threat to existing bridges unless steps are taken to increase their structural resistance to seismic loading. Consideration is, therefore, being given to developing economically feasible methods for increasing the seismic resistance of existing bridges through retrofitting measures in order to minimize possible future damage.

A report (1)* to the Federal Highway Administration on a reconnaissance survey made on February 12-13, 1971, of the damage to bridges in the San Fernando earthquake contains the following excerpts:

C. Causes of Collapse

The two principal causes of collapse of the high overcrossings are considered to be: (1) large vibratory motions induced in the superstructures by the high intensity vertical and horizontal ground accelerations, and (2) relative ground displacements which may have occurred between the abutment and column supports. It is the opinion of the authors that the former was the major cause of collapse in these particular cases; there is no evidence that relative ground displacements were a contributing factor.

D. Design Considerations

1. Expansion Joints - Collapse of the high overcrossings was initiated by bridge spans falling off their supports at abutments and expansion joints due to excessive displacements of the spans relative to their supports. This type of behavior should be carefully examined and corrective measures should be taken as soon as possible. Full consideration should be given to eliminating expansion joints wherever feasible, to widening bearing supports, and to providing more effective ties across expansion joints.

2. Columns - The failures in the central portion of the shorter stiffer columns were caused by the transverse shear forces, while the end failures in the larger more flexible columns were caused by flexural forces In each case, there was a noticeable lack of transverse column ties which contributed to these failures. Clearly, the design details of columns should be carefully examined, particularly with regard to size and placement of reinforcing bars and ties, and corrective measures should be taken to improve their performance under ultimate loading conditions involving reverse deformation cycles such as occur during major earthquakes.

3. Column Caps - There appears to be a serious lack of reinforcing bars tying column caps into their respective box girder bridge decks. Corrective measures should be taken to improve this design detail.

---

*Numbers in parenthesis refer to references at the end of the paper.

4. Column Foundations - Failures at the base of columns for both types of supports, i.e., single cast-in-place pile and spread footings with driven piles, showed inadequate anchorage of the main reinforcing bars. Corrective measures should be taken in each case so that sufficient anchorage is provided to develop the full strength of the main reinforcing bars.

5. Abutment and Wing Walls - Failures in abutments and wing walls were caused by large dynamic forces transmitted by backfill earth pressures and by seismic forces developed in the bridge decks. The design details of these structures should be re-examined and appropriate corrective measures should be taken to improve their performance characteristics.

The California Division of Highways has already revised some of its designs for new construction. For example, column spiral splices must now be anchored by extending the spiral wire through the column and anchoring it around vertical bars on the opposite side of the column. Another example consists of revisions to the hinge restrainer to increase the pull-apart resistance of the joint.

Following the San Fernando earthquake, California Division of Highway personnel identified 860 vulnerable existing bridges requiring a $20 million program for correcting the most obviously vulnerable structural detail through installation of horizontal motion restrainers at bearing seats and expansion joints. A $5 million program was authorized for the 120 bridges deemed most critical. To date this is the only known attention given to retrofitting existing highway bridges to provide increased seismic resistance.

The objective of the retrofit program is to identify and define through the use of structural analyses and supporting laboratory tests practical techniques and criteria for retrofitting existing bridges to increase their resistance to seismic forces. The following ten concepts for retrofitting based on post-event seismic damage observations on bridges in Alaska, California, and Japan are currently being evaluated.

1. Techniques to wide bearing supports and improve bearing stability.

2. More effective motion restrainers across hinges or more effective ties across expansion joints.

3. Practical means to eliminate existing expansion joints, where feasible, in existing bridges.

4. Methods of restraining bridge slabs from collapsing such as by cabling on to the supporting or an adjacent foundation of the bridge.

5. Practical means to add additional ties or spiral to an existing column.

6. Epoxy pressure grouting of concrete hairline cracks already existing to eliminate discontinuities in the concrete.

7. Practical means to improve the ties of column caps into their respective box girder bridge decks.

8. Develop a practical means of preventing collapse of bridge piers or columns in the event foundation piles disintegrate during an earthquake.

9. Introduction of interface materials between abutments or wind walls and backfill such as expanded polyeurethane or other suitable frangible materials that will cushion the seismic earth pressures.

10. Attaching elastomeric bearing pads to concrete with thioxol or other suitable material to prevent the vibratory displacement of the pads during shaking.

At the conclusion of the retrofit investigation, design details and installation specifications will be developed for those techniques deemed to be practical and cost effective.

SELECTION OF REPRESENTATIVE BRIDGES AND EARTHQUAKE INPUT MOTIONS

Seven representative types of highway bridges from several states situated in seismic Zone 3 regions are being investigated in the study. Initially, State Highway Departments in Alaska, California, Illinois, Massachusetts, Missouri, Montana, New York, and South Carolina participated in the study by selecting representative bridge types for possible use in future stages of the study. Six bridges were selected from those submitted--one each from Alaska, Illinois, Montana, and New York and two from California. Table 1 gives bridge location and description of each of the structures. The seventh structure, an eight-span, curved concrete box girder bridge with three expansion joints located in California, has been incorporated into the study. The 607-foot long interchange connector type bridge is typical of many of the structures located in populated metropolitan areas. This bridge was added to investigate and further develop the concept of bridge hinge restrainer systems.

Given the life of each bridge structure and the soil boring data for each of the seven bridge sites, effective Richter magnitude and hypocentral distances were calculated. Site spectra for ground motions in the horizontal and vertical directions were generated. Statistical relationships between lateral and vertical spectra experienced in past historical earthquakes were utilized. An analysis earthquake including an acceleration, velocity, and displacement versus time history for the horizontal and vertical directions of each bridge site was generated from site spectra.

Table 2 outlines structure locations, type, and region from which seismic input motion has been generated for use in the analysis and development of retrofit concepts.

BRIDGE ANALYSIS COMPUTER PROGRAM

This computer program was developed for the purpose of analyzing the dynamic structural response of highway bridges when subjected to ground motions produced by an arbitrary earthquake. Its specific purpose is to evaluate the merits of various retrofit measures that would be employed in a given bridge for the purpose of eliminating or reducing structural damage. The program is based on the finite element method of structural analysis and models a given bridge as a three-dimensional (space) frame. As such, six degrees of freedom are allowed per node.

The method of analysis employs a nonlinear dynamic response analysis of the structure. An implicit integration solution scheme employing equilibrium checks is used to solve the incremental form of the equations of motion. A tangent stiffness matrix for the complete structure is reassembled at user-defined arbitrary increments of the integration step. This feature, coupled with the equilibrium checks and the stable implicit inegration technique permits one to feasibly obtain solutions to intermediate size problems (up to 1000 degrees of freedom) subjected to long duration loading (up to 50 sec.). The most outstanding feature of the computer code is its ability to model the reduction in load-carrying capacity of a member subjected to relatively small overstressing for cyclic loading. This is a most serious behavior characteristic which is largely responsible for structural component failures, such as reinforced concrete columns. The elastic-plastic yield surface technique usually employed to model beams subjected to overstressing does not readily lend itself to conveniently modeling this behavior, especially for members of complex cross-section subjected to combined thrust and bending loading about two axes.

The computer code treats the nonlinear response of overstressed members by employing a special elastic-plastic beam element that realistically models the behavior in a simple to use, automatic manner, that is particularly adaptable to numerical analysis. Recalling the formal development of a finite element beam model, the constitutive equations of the material enter the analysis through integrals over the beam cross-section which have the form

$$\int_A \sigma(\varepsilon)dA \; ; \; \int_A \sigma(\varepsilon)ydA \; ; \; \int_A \sigma(\varepsilon)zdA \; ; \; \int \sigma(\varepsilon)yzdA$$

where $\sigma(\varepsilon)$ is the stress at any fiber location (y, z) and ε is the associated strain. The strain can be obtained in terms of the extension, ε_o, and the curvatures k_{oy}, k_{oz}.

The method employed in the computer code evaluates these integrals by numerical integration over the cross-sectional area at each stage in the deformation of the structure. The user subdivides the cross-section of each of these beam elements into a finite number of incremental areas. Each of the subdivided areas is specified as a particular type of material, such as concrete or steel, and as such has a certain user defined nonlinear stress-strain behavior. A knowledge of the current strain and the previous stress-strain path for each subdivided area provides the information necessary to determine the current stress and hence evaluate the integrals to compute the current force resultants.

This concept is employed to derive the incremental force-deformation relationships at each of the beam elements two node points (six degrees of freedom per mode). This information is then employed to integrate over the length of the beam to obtain the time-varying tangent stiffness matrix for these elements.

A soil-structure interaction finite element is provided in the program to model the connection of the bridge structure to the ground. This element simulates the connection by employing three translational and three rotational springs and corresponding viscous dampers. The prescribed seismic motion is imposed at the ground node point of the soil-structure interaction finite element. At the user's option, different spring stiffnesses can be employed for the compression and tension translational degrees of freedom. This feature is quite useful for seismic loading, due to the cyclic nature of the imposed motion, since it permits one to use a high stiffness for compression interaction and a low or zero stiffness for tension interaction for simulating a footing on piles or a spread footing.

A nonlinear expansion joint finite element is included to provide the analyst with a means of accurately modeling connections between different spans of the superstructure, superstructure-abutment (or pier) interactions, and hinges. It models the expansion joint gap, includes coulomb friction and variable spring rates to simulate differences in compression and tension resistance either horizontally or vertically. Tie bars can also be modeled in the expansion joint element.

An elastic beam finite element is also provided in the computer code. It is used to model those components of the structure that will not be subjected to severe overstressing and yielding due to the dynamic loading. It is generally employed to model the majority of the superstructure. Shear deformations are optionally included in the elastic beam element stiffness and stress-displacement matrices.

The computer program was tested on the Bahai Overcrossing in California. Plan, elevation, and cross-sectional views of the two-span, four-cell reinforced box girder bridge are shown in Figures 1 and 2. Figure 3 depicts the reinforcing steel and concrete stress-strain relationships after Brown and Jirsa (2). Note that the ultimate stress for the reinforcing steel is rather low. The steel stress-strain curve for this test was selected so that low axial tensile strength in the pier elements could be simulated.

A one-cycle sinusoidal vertical displacement waveform with period of 0.2 seconds and double amplitude of two inches was used as a simple test input wave motion at the base

of Bent No. 2. Selected displacements, bending moments, and axial forces are shown in Figures 4 through 7. The pier elements fail very near the 0.2 second mark, after which time the superstructure deflects downward a very large amount. Computer runs of the seven structures identified previously are currently being carried out to identify failure mechanisms in the structures.

PRELIMINARY RETROFIT CONCEPTS

Retrofit techniques are in the process of being developed for the seven representative bridge types described previously. It is anticipated that the final fixes selected will be valid for use on other similar types of bridges located within seismically active areas.

Table 3 lists controlling items and methods of increasing seismic resistance of six of the seven bridges under investigation. Some initial concepts have been proposed following the review of detail plans of each of the structures. Analysis of each of the structures is currently being made. Analytical results should help identify additional concepts and verify some of the proposed concepts. Standard detail drawings will be made for each of the final retrofit concepts selected for use.

Some of the initial retrofit concepts envisioned to date are shown in Figures 8 through 16. Cost effective evaluations of the concepts described have not been made.

Figure 8 shows a longitudinal section through the end diaphragms of a concrete box girder. Tie bars have been added to limit longitudinal joint separation. This system has been used by the State of California in their retrofit program. A concept for limiting relative displacement at abutments is shown in Figure 9. Vertical uplift can be controlled through the extension of anchor bolts through the bottom flange of a steel girder as shown in Figure 10. An expansion joint restrainer system for steel girder structures is shown in Figure 11. Tie bars pass through end web stiffeners in this scheme. Figure 12 depicts a steel girder hinge restrainer system in which both vertical uplift and motion normal to the plane of the web is controlled. Support bearing area or restriction of girder motion can be achieved through use of concepts depicted in Figure 13.

Use of fibrous polyester concrete for strengthening beams has been investigated. Figures 14 and 15 show how the addition of high strength fibrous polyester concrete improve the strength and ductility of test beams. Figure 16 shows how the use of such a material could be used to enhance the seismic resistance for reinforced concrete bridge columns. Additional concepts are in the development stage and will be fully evaluated during the next year.

Careful analysis must be made following selection of final retrofit concepts. The addition of retrofit hardward may enhance the seismic resistance of a vulnerable bridge component while at the same time detract from the overall dynamic performance of the structure. Such concepts, if any, will be eliminated from further consideration.

SUMMARY

Retrofitting concepts and corresponding implementation methods for general types of highway bridges are currently being investigated to enhance seismic resistance. The study is not being conducted to define fixes that will eliminate all structural damage resulting from large magnitude earthquakes, but rather is intended to provide fixes which will assure that: 1) structures remain in service for use as emergency routes following earthquakes, 2) damage is limited to the extent that the structure can be quickly repaired, and 3) total collapse of structures is avoided.

REFERENCES

1. Penzien, J., Clough, R.W., "Observations on the Damages of Highway Bridge Structures, San Fernando, California. Earthquake, February 9, 1971," report to the Division Structural Engineers, Federal Highway Administration, Sacramento, California, April, 1971.

2. Brown, Russell H. and Jirsa, James O., "Reinforced Concrete Beams Under Load Reversals," ACI Journal, May 1971

3. Fung, G.G., LeBeau, R.J., Klein, E.D., Belvedere, J., and Goldschmidt, A.F., "Field Investigation of Bridge Damage in the San Fernando Earthquake," Preliminary report of the Bridge Department, Division of Highways, State of California, 1971.

4. "Bridge Details Resulting from Experience Gained from Los Angeles Earthquake," California Division of Highways, 1972.

5. The Great Alaska Earthquake of 1964 - Engineering, "Performance of Highway Bridge Foundations," Ross, G.A., et al., National Academy of Sciences, Washington, D.C., 1973.

6. Cooper, James D., "FHWA Research Program for Earthquake Resistant Design of Bridges," Prepared for U.S.-Japan Seminar on Earthquake Engineering with Emphasis on Safety of Reinforced Concrete Structures, Berkeley, California, September 4-8, 1973.

7. "Techniques for Retrofitting Existing Bridges to Reduce Susceptability to Earthquake Damage," Response to FHWA RFP 154, IIT Research Institute, Chicago, Illinois, March 1973.

8. Podolny, W. and Cooper, J.D., "Toward an Understanding of Earthquakes," Highway Focus, FHWA, U.S. DOT, Vol. 6, No. 1, March 1974.

9. Hanson, John M., Wiss, Janney, Elstner and Associates, Inc., letter report to A. Longinow, IIT Research Institute, March 19, 1974.

10. Robinson, R.R. and Cooper, J.D., "Techniques for Retrofitting Existing Bridges to Reduce Susceptibility to Earthquake Damage," 70th Annual Convention, American Concrete Institute, San Francisco, California, April 3, 1974.

11. First Federally Coordinated Program Progress Review, (Meeting), FCP Project 5A. "Improved Protection Against Natural Hazards of Earthquake and Wind," FHWA, U.S. DOT, San Francisco, California, September 1973.

TABLE 1

BRIDGE DESCRIPTION

BRIDGE	DESCRIPTION
1. Montana (county Road Seperation	4 spans, each simply supported: 55', 100', 100', 45' Type IV prestressed concrete girder superstructure with 20 degree skew. Continuous deck integral with abutments. All ends of spans are fixed. 1¼" high fixed steel bearings. Pier cap supported by two 3'-6" diam. columns; columns supported on separate spread footings. Abutment serves as end diaphragm, supported on treated timber piles. Each span has 2 intermediate diaphragms and also end diaphragm over pier.
2. California (Bahia Over-crossing)	2 span, 4 cell reinforced concrete box girder: 86', 102' continuous straight 5'-6" deep superstructure with no shew. Single 3' x 8' column with bent cap in superstructure. Column footing supported on concrete piles, Abutment and wingwalls monolithic with super-structure and supported on concrete piles.
3. California (Ventura Overcrossing)	4 span, 3 cell reinforced concrete box girder: 112'-3", 129', 97', 47'-3". Articulated curved 6'-10" deep superstructure with no skew. Single 6' diameter column with bent cap in superstructure at all intermediate support points (18'-10", 21'-4", 19'-1" ht for columns) Column footings supported in piles. One abutment and wingwalls monolithic with superstructure and supported on concrete piles. Superstructure on 10" high expansion bearings with no hold-doqn at other abutment (adjacent to 47'-3" span). Abutment on concrete piles. One inch joint at hinge filled with asphalt latex, 5" wide bearing through 6 x 4 x 3/4 angles.
4. Illinois (Rt. 24 over Massac Creek)	3 spans, continuous: 46'-5 ½", 58'-1", 46'-5½" 6 rolled W33 beams with 32 degree skew. Spans are E-F-E-E. 14¼" high expansion and 13 3/8" high fixed steel bearings. Continuous non-composite deck slab-1½" open joint at ends with armor. Full width pier on spread footing. Abutment and wingwalls on steel piles.
5. Alaska (Bridge over Lyon and Tin-can Creek)	3 spans, each simply supported: 40', 60', 40'. Rolled W27 and W36 alloy steel beams, no skew. Spans are F-E, F-E, E-F. Discontinuous non-composite deck with open joints and armored ends. 8" high expansion and 1 7/8" high fixed steel bearings. Full width pier on spread footing. Abutments supported on steel piles. Intermediate and end steel diaphragms on all spans (2 int. in 60' span).
6. New York (I-508 over Delaware and Hudson Rail-road)	3 spans, each simply supported: 91'-8", 118', 118'. 6 welded plate girders per span with 60 degree skew. Span are F-E, etc. Discontinuous composite deck slab-1" open joint, ends of slab are armored. 14½" high fixed and expansion steel bearings. No pier cap (girders bear directly on columns, columns transmit load to continuous spread footing). Abutment with pedestals to support girders (combined abutment and wingwalls on spread footing.

TABLE 2

REPRESENTATIVE BRIDGE TYPES, LOCATIONS AND

SEISMIC ENVIRONMENTS FOR RETROFIT STUDY

Bridges Subjected to regional Earthquake in / Actual Bridge Locatn.	Alaska	Northern California	Southern California	California	Illinois	Montana	New York	Bridge Description
Alaska	*			*	*	*	*	Steel girder with Composite Deck
Northern California		*	*					2 span concrete box on column
Southern California		*	*					4 span, curved concrete box on circular piers
Multi-span California				*				8 span, curved concrete box on circular piers
Illinois	*			*	*			3 span steel girder, non-composite deck on wall pier
Montana	*			*		*		4span skew prestress I girders with composite deck on col. bent.
New York	*			*			*	Prestressed I girder on Multiple column bent
TOTAL	4	2	2	5	2	2	2	19

TABLE 3

PROVISIONS FOR INCREASING

SEISMIC RESISTANCE

BRIDGE	CONTROL ITEMS	WAYS OF INCREASING SEISMIC RESISTANCE
1. Montana (County Road Seperation)	Columns and pier cap	Increase transverse shear resistance to improve torsional resistance of superstructure
	Bearings	Hold-down at interior pier caps
	Abutment and footings on piles	Greater longitudinal resistance
2. California (Bahia Over crossing)	Abutments and column footing on piles	Improve anchorage of pile in cap, abutments need greater longitudinal resistance.
3. California (Ventura Overcrossing)	Hinge	Limit longitudinal movement and prevent transverse and vertical movement.
	Expansion Bearing	Limit separation from abutment and prevent transverse and vertical movement
	Columns	Increase shear resistance and ductility
	Abutments and footings on piles	Improve anchorage of pile in footings; abutments need greater longitudinal resistance
4. Illinois (Rt. 24 over Massac Creek)	Deck joints at abutments	Limit or cushion longitudinal movement and possibly prevent transverse movement
	Abutments on piles	Increase longitudinal resistance
	Bearings	Provide hold-down devices and check transverse resistance
5.. Alaska (Bridge over Lyon and Tin-can Creek)	Deck joints and joint at abutments	Limit or cushion longitudinal movement and prevent transverse movement
	Bearings	Provide hold-down devices, and increase transverse resistance
	Abutments on piles	Greater longitudinal resistance
6. New York (I-508 over Delaware and Hudson Railroad)	Deck joints and joint at abutments	Limit or cushion longitudinal movement and prevent transverse movement.
	Columns	Increase transverse shear resistance to improve torsional resistance of superstricture
	Bearings	Provide hold-down devices and check transverse resistance or re-design bearings and possibly increase area at abutments.

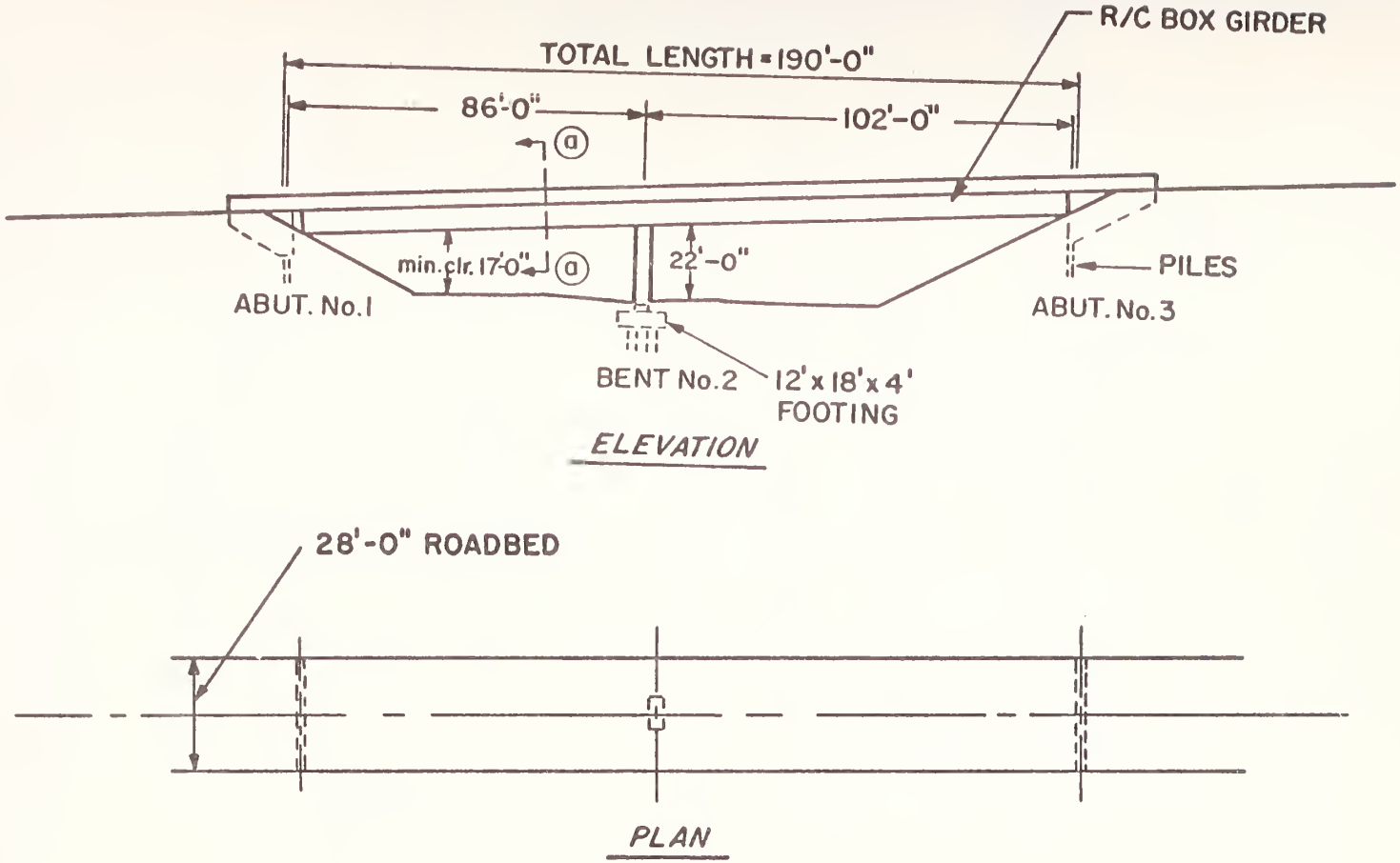

BAHAI OVERCROSSING

FIGURE 1

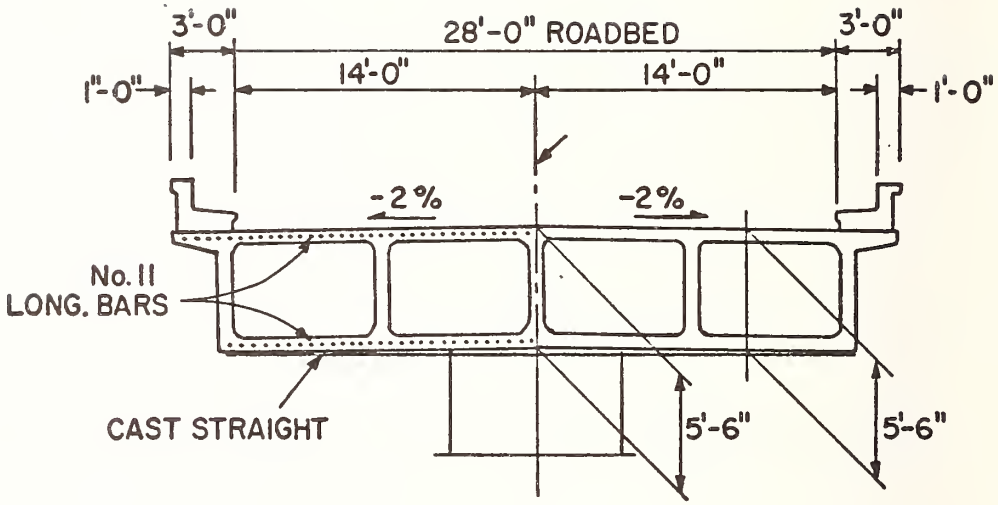

Section a-a

BAHAI OVERCROSSING

FIGURE 2

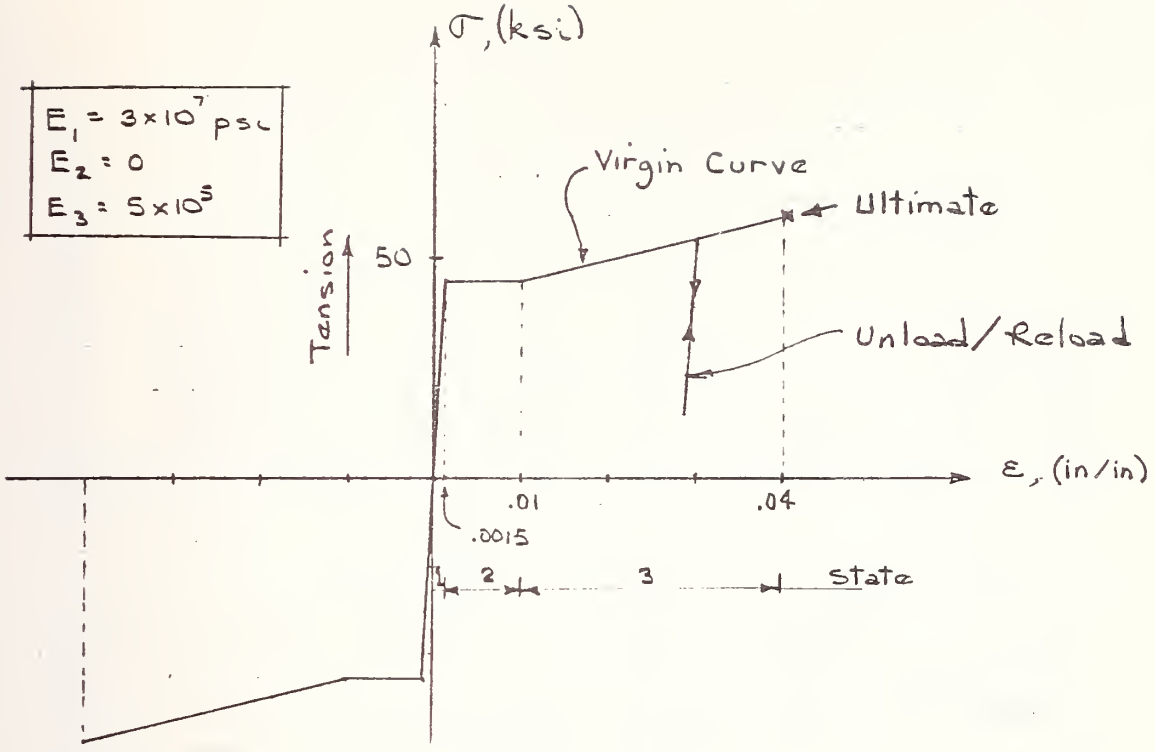

Reinforcing Steel Stress-Strain Variation
(Isotropic Hardening)

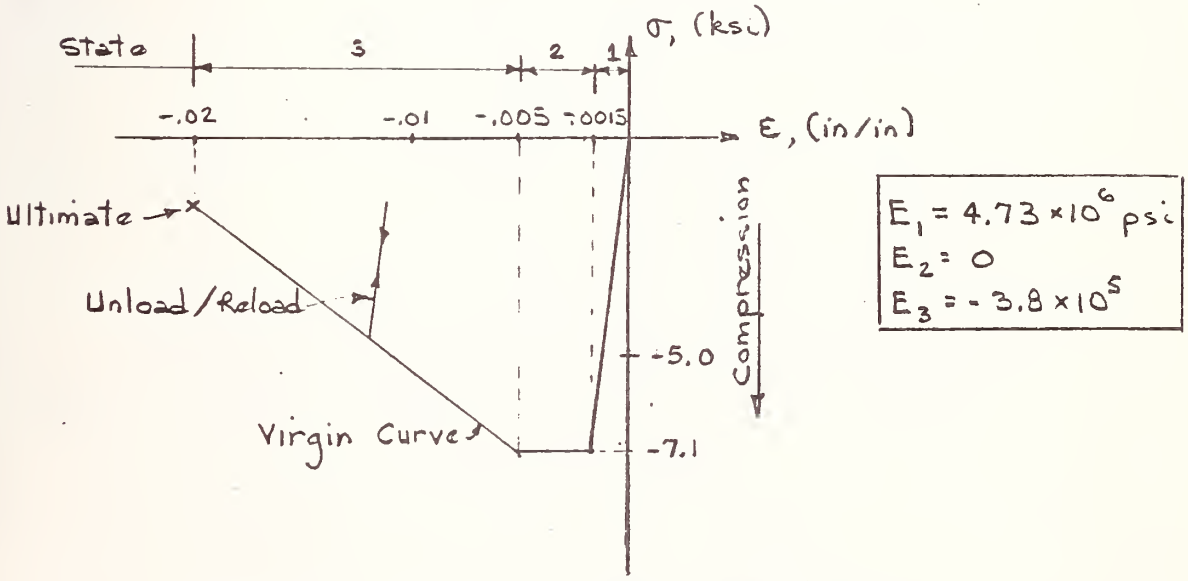

Concrete Stress-Strain Variation
(Isotropic Hardening/Softening, Incapable of Tension)

FIGURE 3

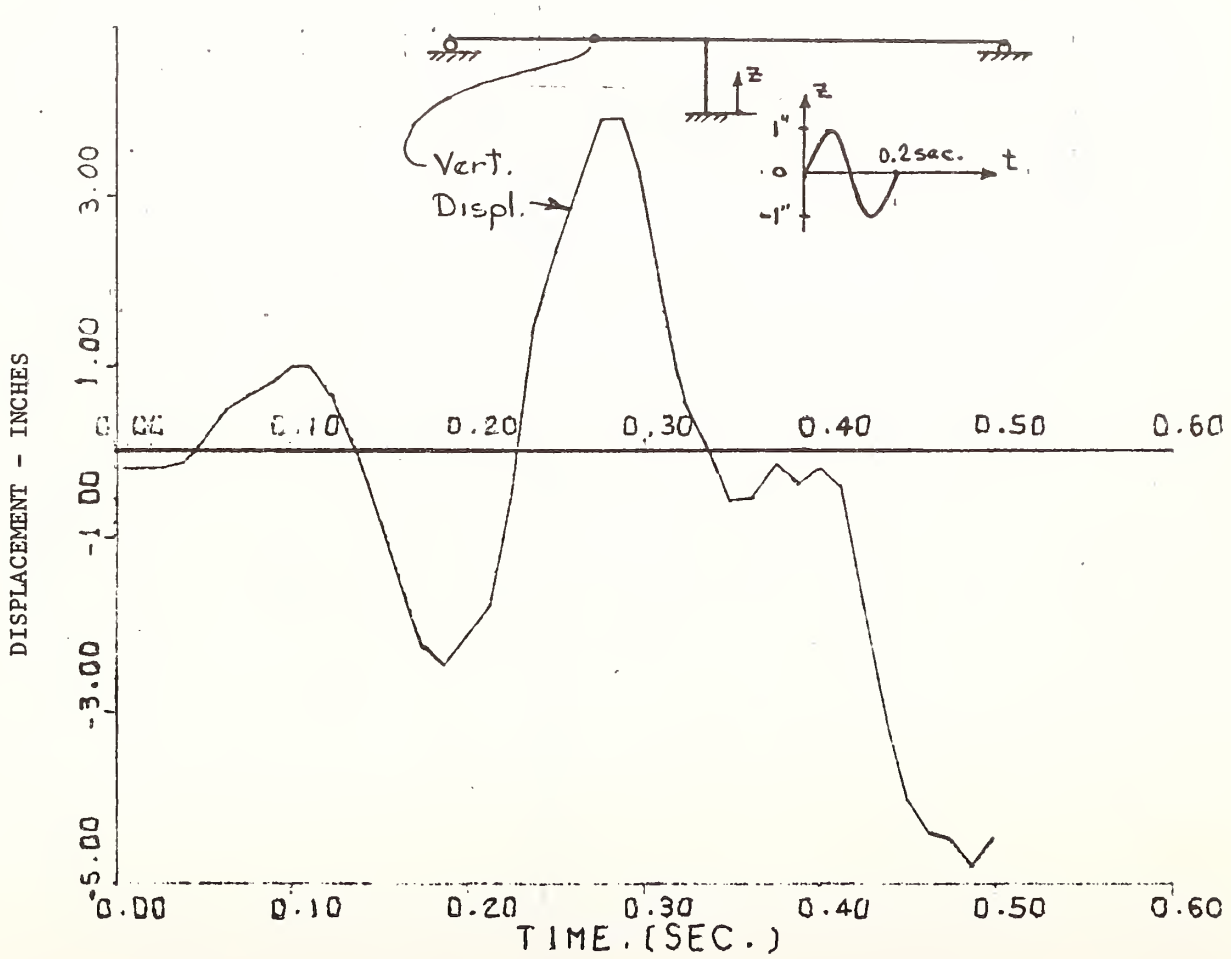

VERTICAL DISPLACEMENT

BAHAI OVERCROSSING

FIGURE 4

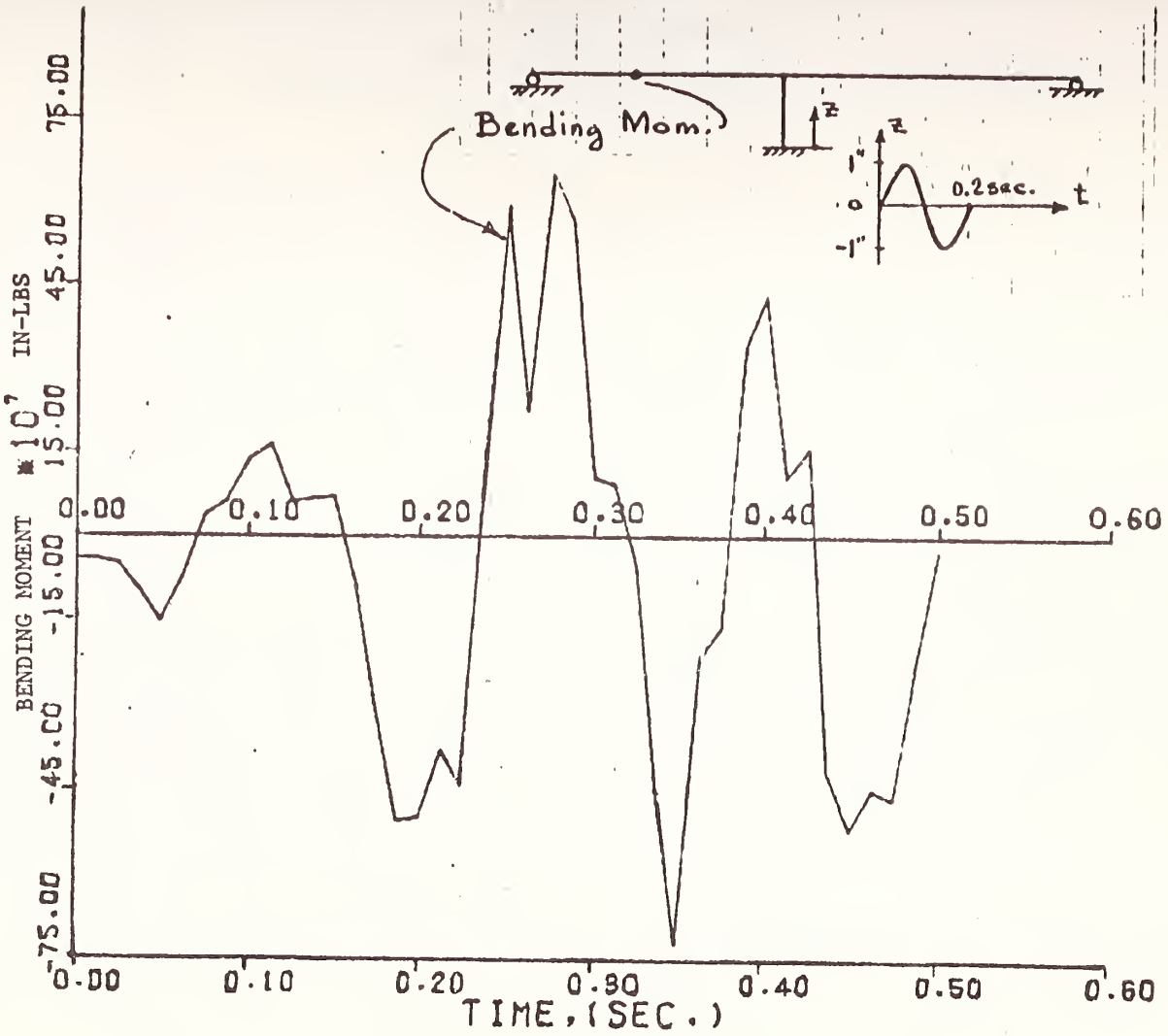

BENDING MOMENT

BAHAI OVERCROSSING

FIGURE 5

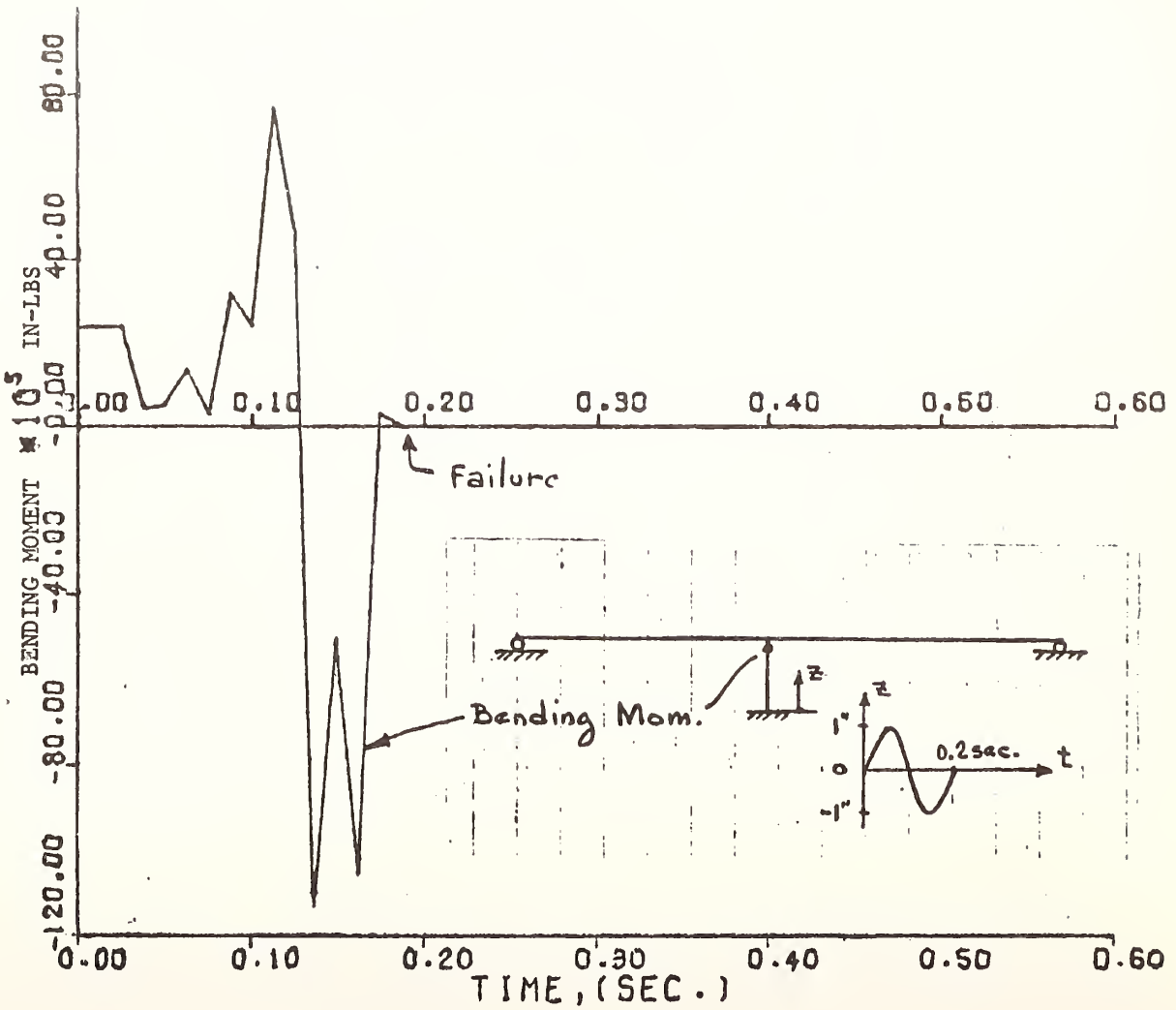

BENDING MOMENT

BAHAI OVERCROSSING

FIGURE 6

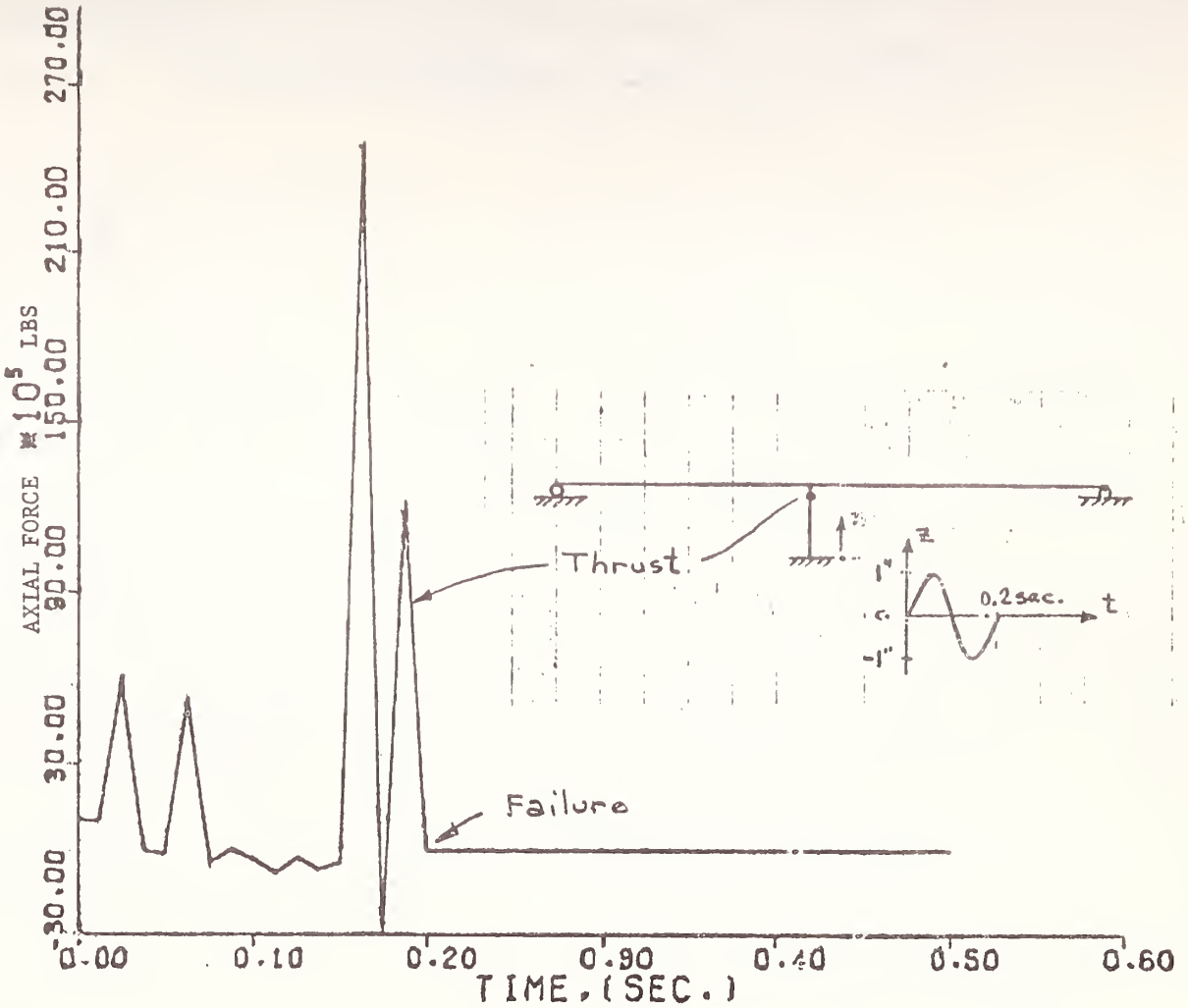

AXIAL FORCE

BAHAI OVERCROSSING

FIGURE 7

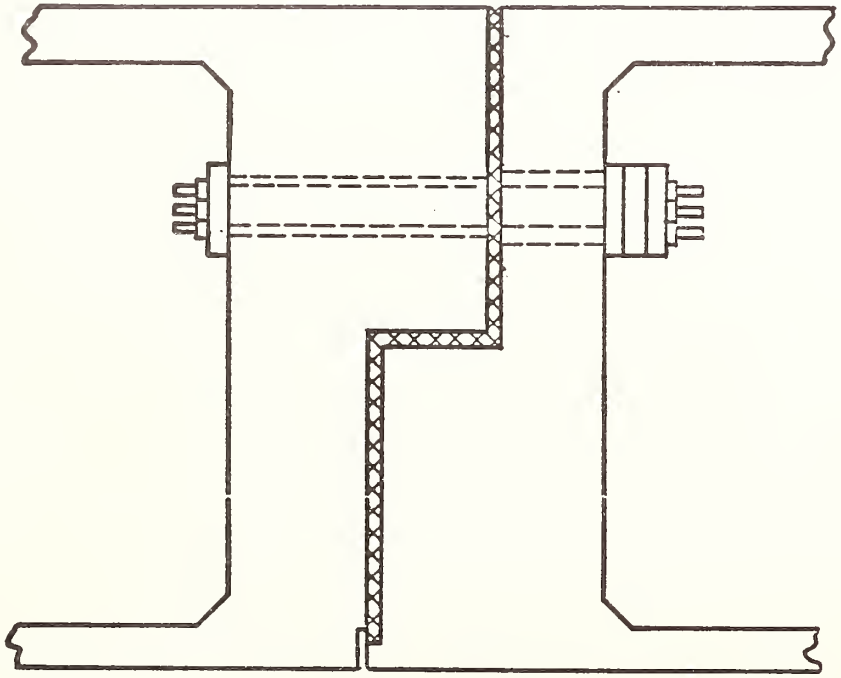

HINGE RESTRAINER - CALIFORNIA

FIGURE 8

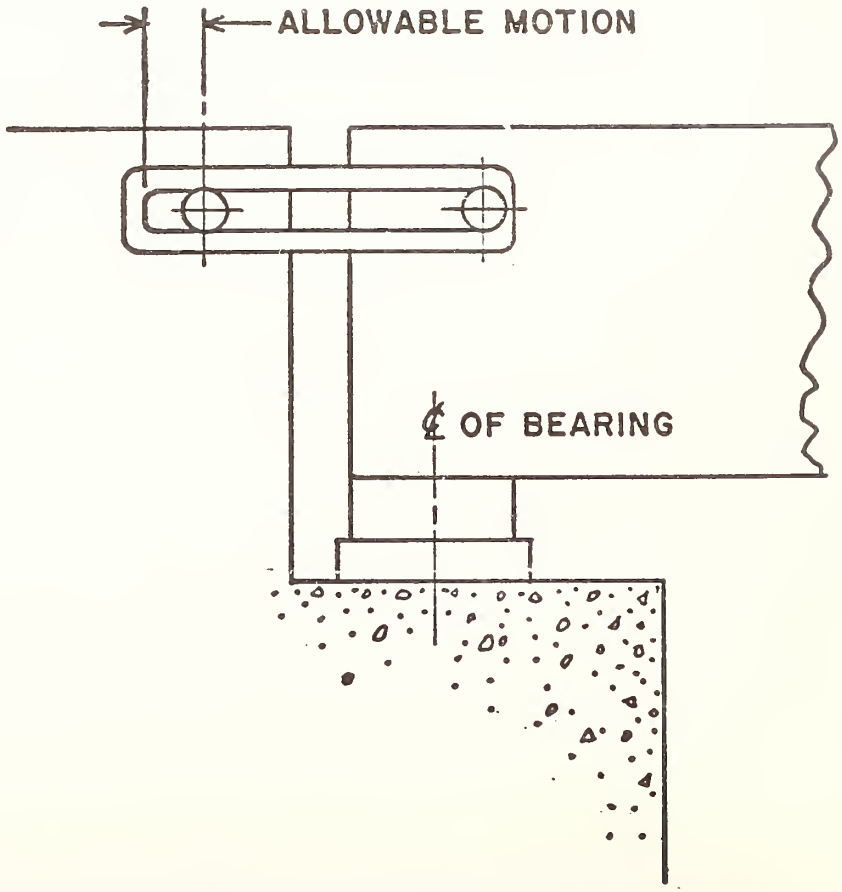

RELATIVE DISPLACEMENT RESTRAINER

FIGURE 9

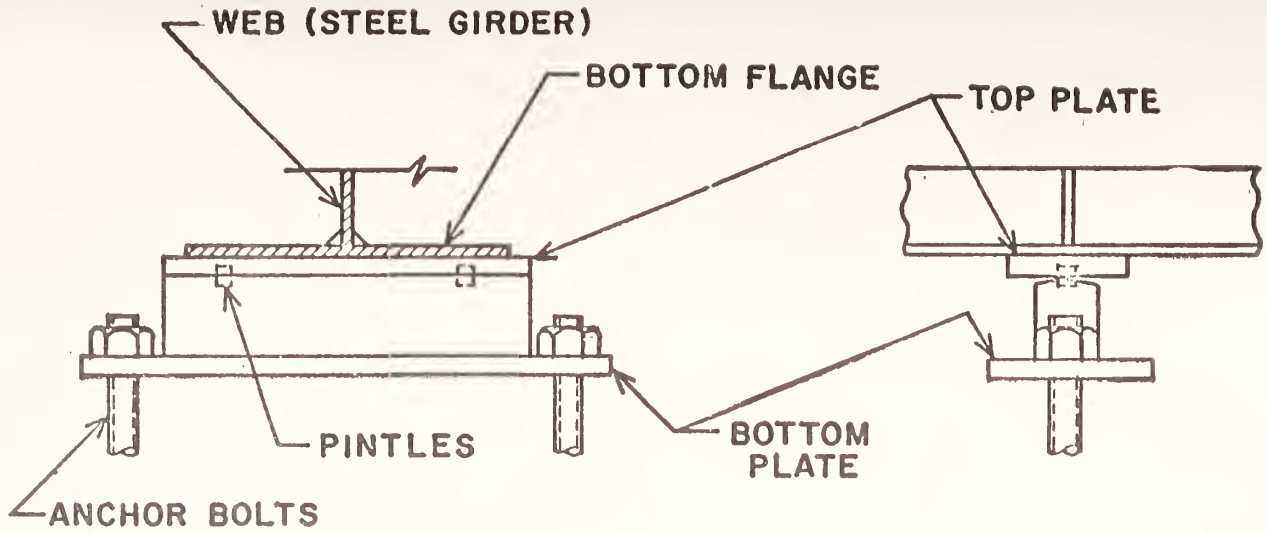

TYPICAL FIXED BEARING

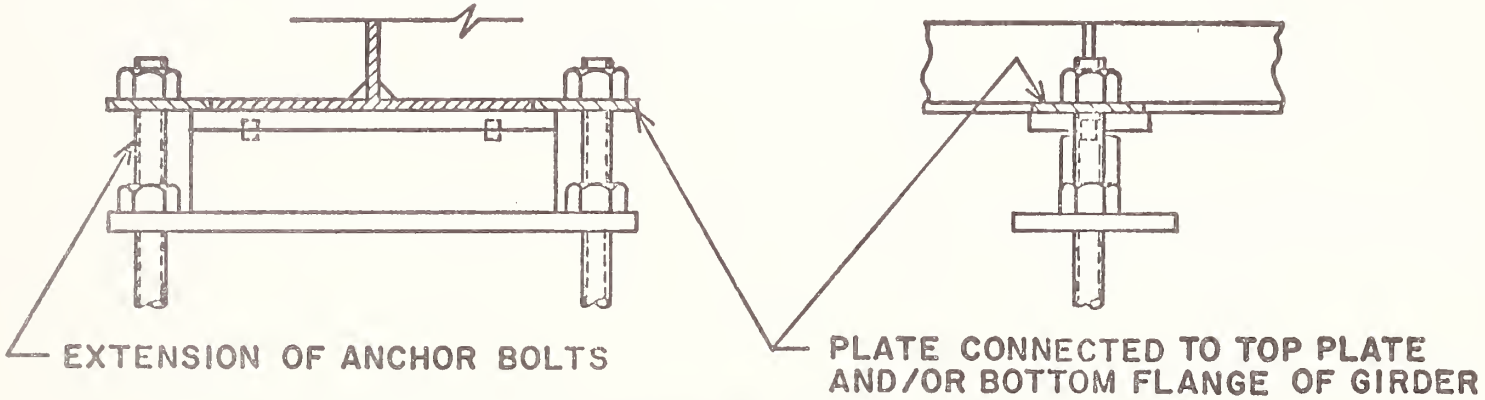

FIXED BEARING WITH MODIFICATION
FOR RESTRAINT AGAINST UPLIFT

FIGURE 10

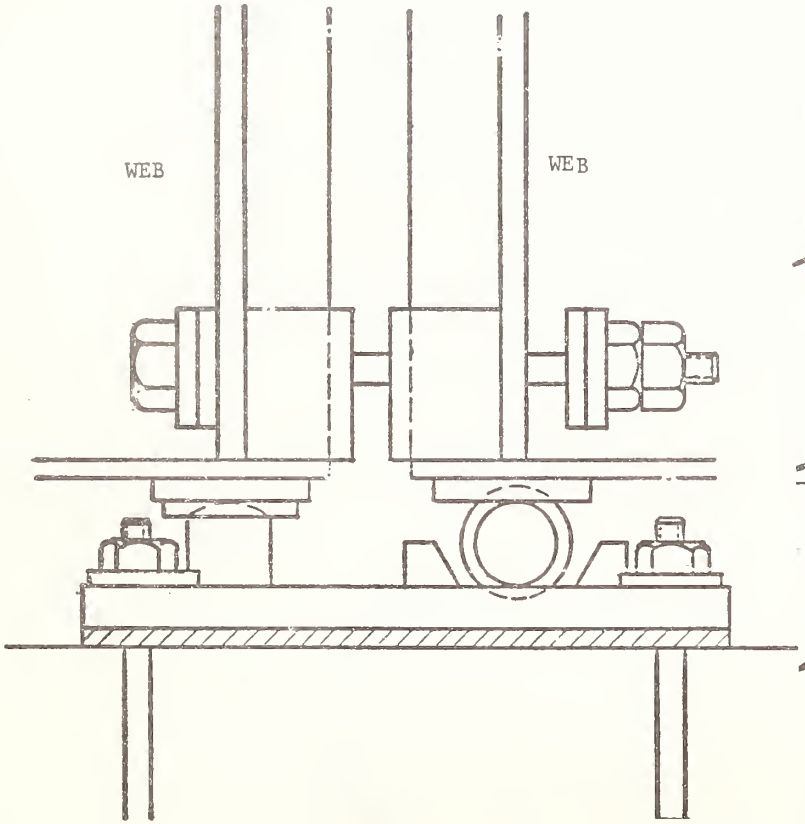

STEEL GIRDER

EXPANSION JOINT RESTRAINER

FIGURE 11

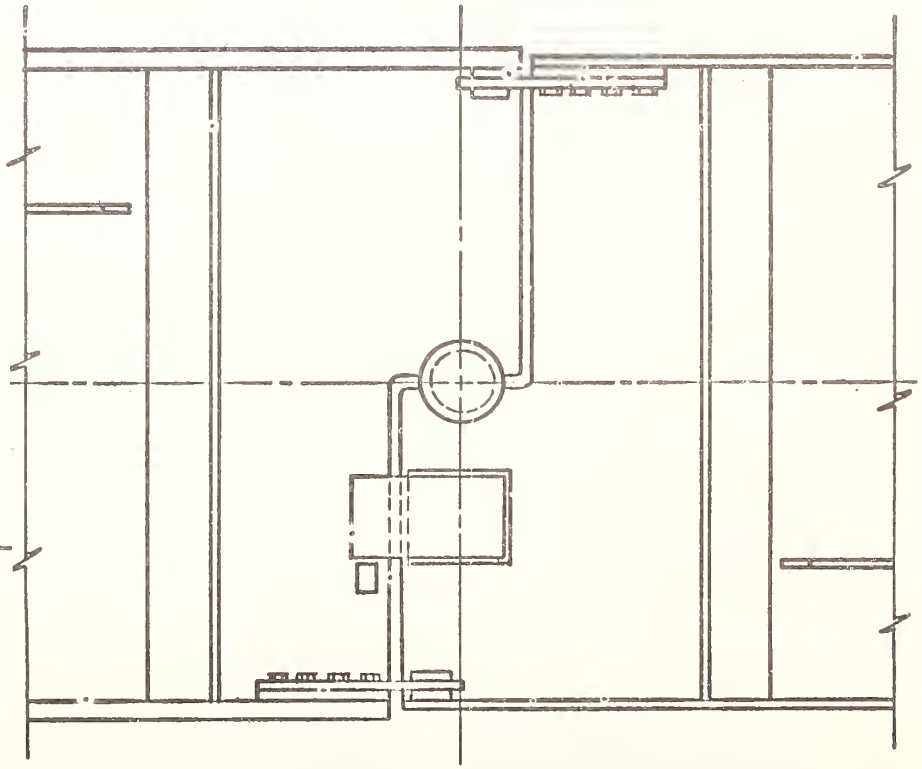

STEEL GIRDER HINGE RESTRAINER

FIGURE 12

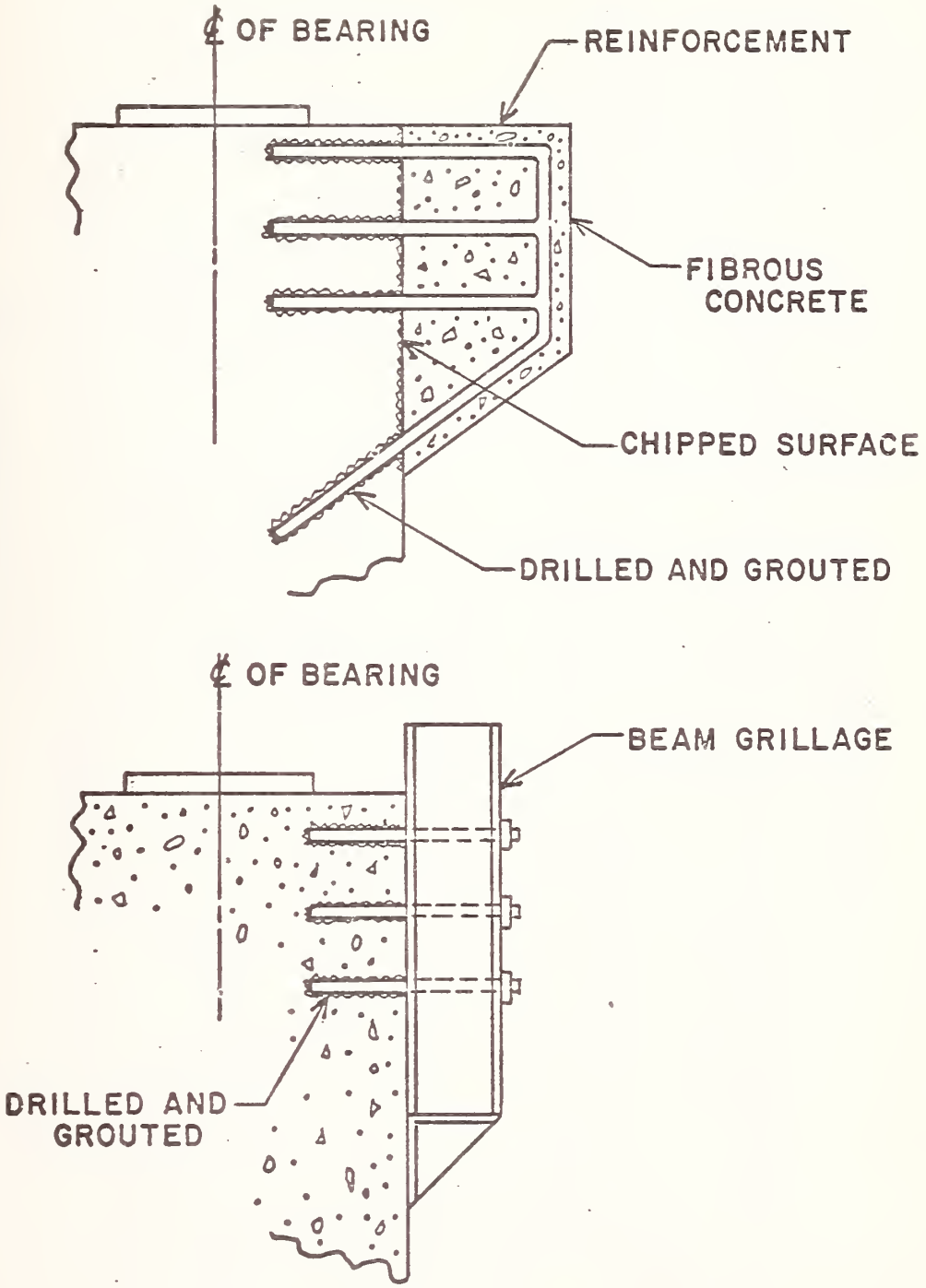

BEARING SEAT EXTENSION AND STOPPER

FIGURE 13

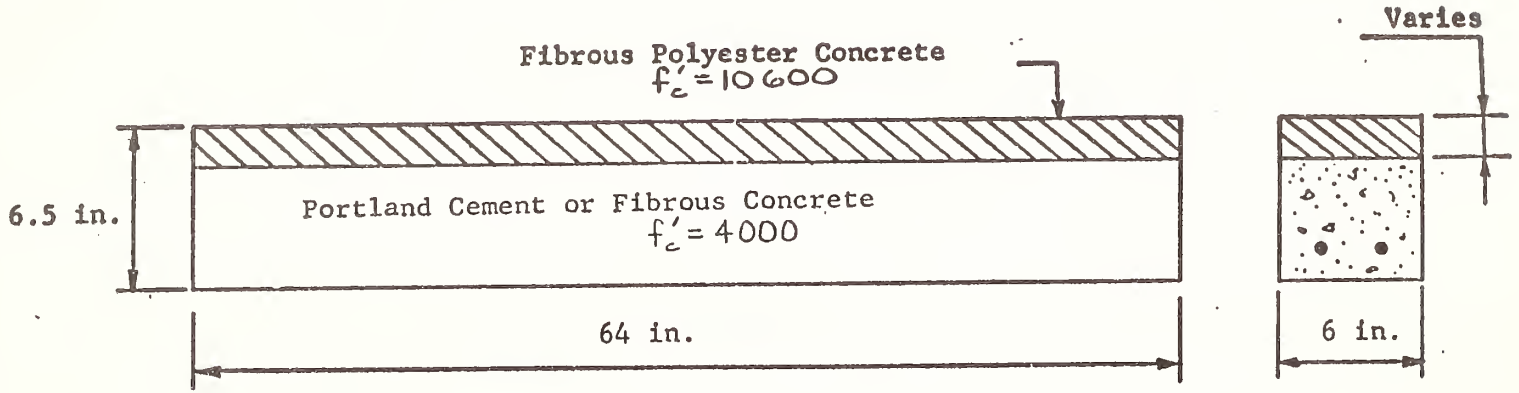

Geometry of Beam Element

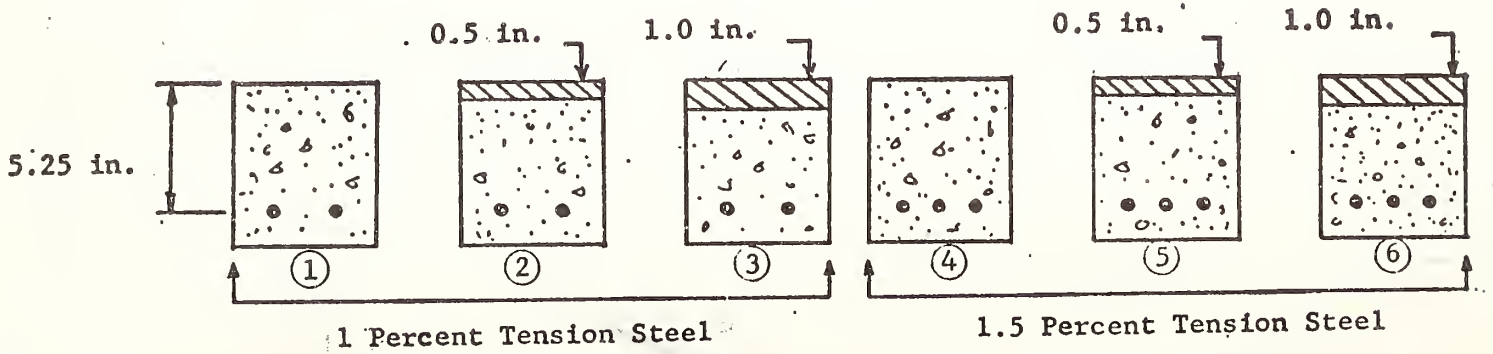

Cross Section Characteristics of Test Elements

FIGURE 14

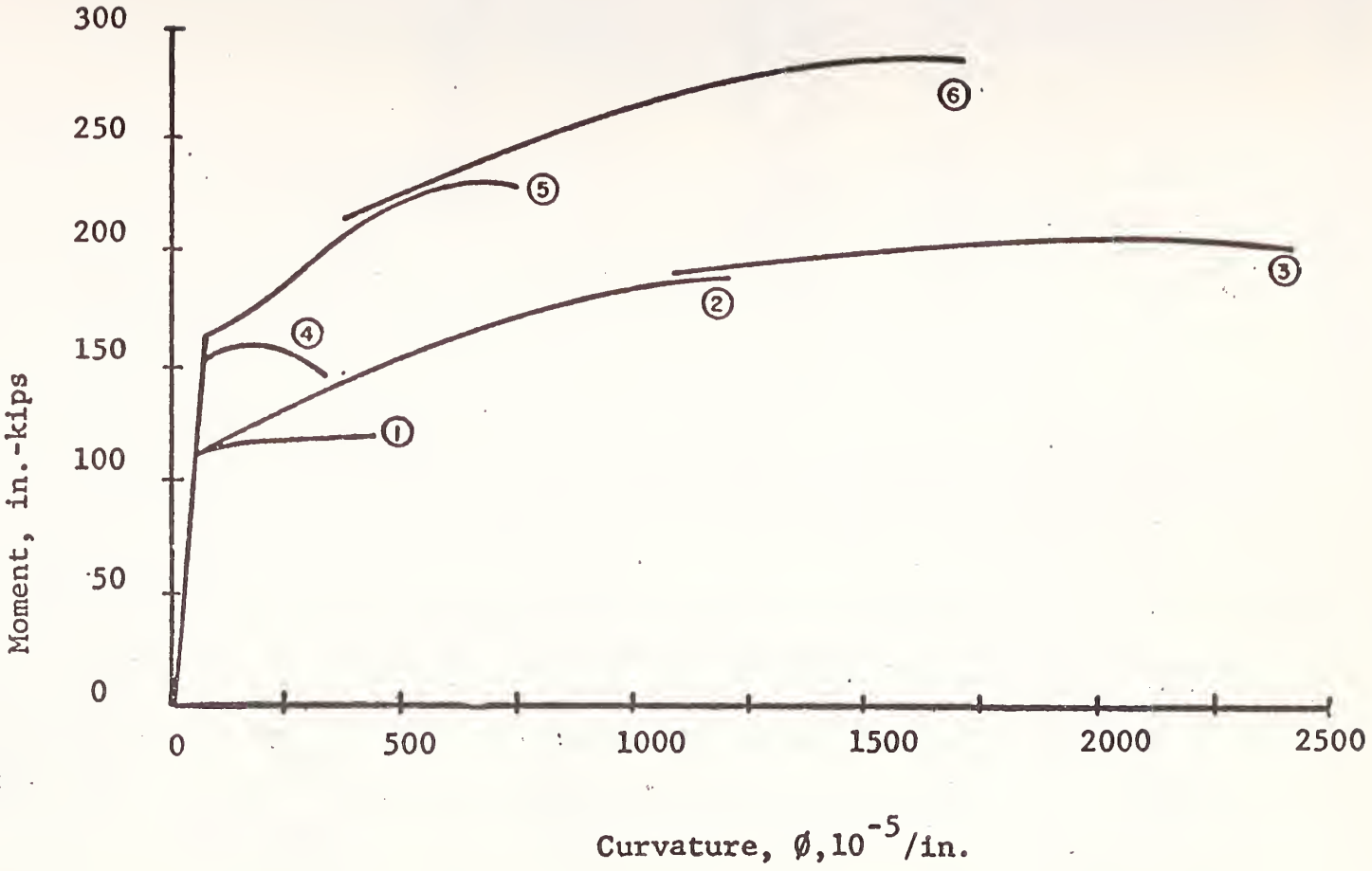

MOMENT-CURVATURE VARIATION
FOR FIBROUS POLYESTER CONCRETE IN COMPRESSION ZONE

FIGURE 15

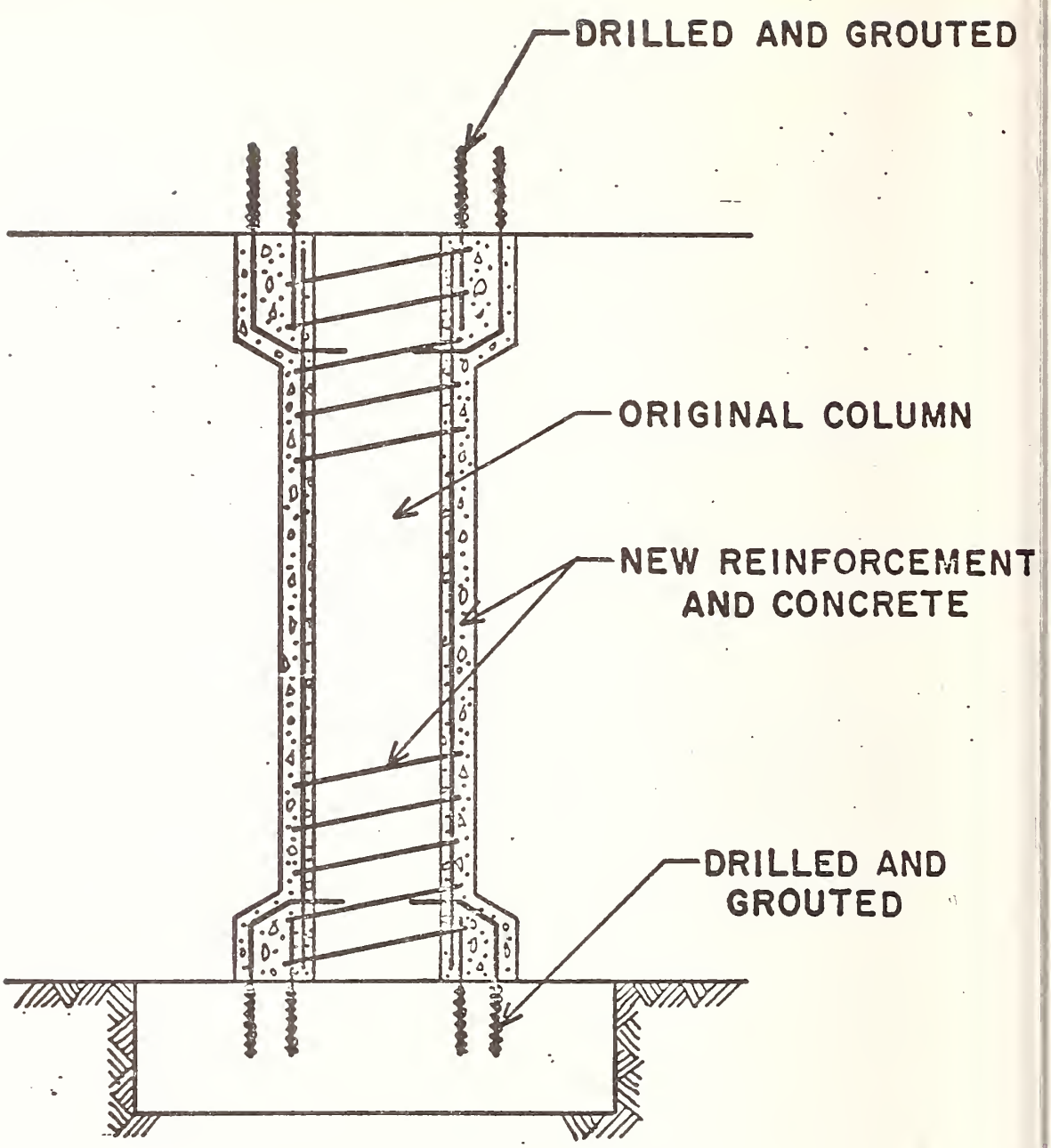

REINFORCED CONCRETE COLUMN STRENGTHENING

FIGURE 16

DYNAMIC TESTS OF STRUCTURES USING A LARGE SCALE SHAKE TABLE

by

Seiichi Inaba

National Research Center for Disaster Prevention

Since 1970, a large scale shake table located at the National Research Center for Disaster Prevention (NRDP) has been widely used for the dynamic testing of structures. This paper presents the results of some of those dynamic tests, using this jumbo earthquake simulator, and the results obtained from some other shake tables operated by other research institutes in Japan.

Key Words: Dynamic tests; earthquake simulator; shake table; structural engineering; tests.

LARGE SCALE SHAKE TABLE OF NRDP

The construction of a large scale shake table located in Japan was proposed in 1964 by many governmental and university researchers after the Niigata Earthquake. The planning, construction, and operation of the shaker was to be by the NRDP, but could be widely used by other researchers throughout the country. The testing of the hydraulic actuators and the design of the table began in 1967. In October, 1968, construction work began in Tsukuba, Ibaraki Prefecture, and was completed in October 1970, with a total cost of 960,000,000 ($3,200,000).

The shake table is a 15 m square horizontal unit which weighs 160 tons. The table can support a 500-ton structural test load, with a horizontal acceleration of 0.55 g. Vertical accelerations of 1.0 g can be imposed on a 200-ton test load, however, the horizontal and vertical motions cannot be applied simultaneously.

The simulator is housed in a steel framed building which is 24 m x 42.5 m in plan and 16 m high. A prestressed concrete foundation supports the shake table, and forms an open box shape. The sides are 2 m thick with an outside dimension of 39 m x 25 m in plan and 9 m deep. The foundation consists of a flat mat and rests on a sand layer where the standard penetration test value is about 30. The total weight of the foundation mass is 12,000 tons. The ratio of the moving mass (table plus test structures) to the foundation is 1:20. Four hydraulic actuators, which have a 90-ton dynamic rating, are provided to drive the table horizontally and four other 90-ton actuators are provided to drive the table vertically. All of these eight actuators have a $\pm$ 30 mm stroke, and are electronically controlled. A moving mass up to a maximum of 660 tons is supported on four balance cylinders during the horizontal drive. The table is constrained in one direction--horizontal or vertical--during motion in the other direction by sixteen guide rollers.

Vibration waves of various forms can also be imposed by a control system simulator, which has a harmonic wave oscillator of sine, rectangular, and triangular wave configurations. A noise generator, using diodes, is equipped to impose random waves and programmed transients of various forms can also be imposed. The programmed seismic input waves must be in the range of the design spectra of the table, with the maximum displacements less than $\pm$ 30 mm for a single amplitude. Programmed displacement analog data are generally used as the input signals. If a low frequency range of acceleration is used, a large displacement can be realized, however, the frequency has less influence on the magnitude of the acceleration. The programmed data comes from motion accelerograph data, which is digitized and then the digital displacement data is obtained by double integration using a computer; the data are then filtered in the range of maximum displacements. This digitized displacement data is then transferred electronically to analog data and a displacement input curve is stored in the data recording system. This displacement curve is then imposed as input signals to the simulator.

The hydraulic power system is composed of a main and subsystem. The main hydraulic system drives the four actuators, using 24,000 liters of oil at 210 kg/cm^2 pressure from thirteen pumping units. A sub-hydraulic system consisting of four pump units drives the following units: twelve hydraulic bearings, four universal joints between the table and actuators, and sixteen guide roller bearings by using 9,600 liters of oil at a pressure of 75 or 140 kg/cm^2. Seventeen pumping units are used in total with each pumping unit being driven by a 150 KVA motor. The capacity of the electric power system to supply the large scale shake table is 2,900 KVA and the entire electrical transformer station is equipped to supply 66,000 Volts.

Figure 1 shows the maximum capacity characteristics of the shake table, in conjunction with test results as obtained without use of a test structure. Figure 2 shows the frequency characteristics of the shake table during horizontal motion of a 100-ton structure. Figure 3 shows the frequency characteristics during vertical motion without a test load. Figure 4 gives the El Centro earthquake displacement and acceleration of the shake table when the El Centro earthquake input characteristics are imposed into the control system. During the fiscal year 1973, the shake table had a total running time of approximately 200 hours.

DYNAMIC TESTS CONDUCTED ON THE NRDP SHAKE TABLE

Since the construction of the large scale shake table at the National Research Center for Disaster Prevention in 1970, a number of dynamic tests of structures have been conducted. The structures that have been tested on the table are classified into the following categories: 1) full-scale structures, 2) large size model structures, 3) soil structures, and 4) ground.

The type of dynamic tests performed on these structures are categorized as follows;

1) Problems related to ground and soil structure, such as the river embankment, sandy ground, and liquefaction of saturated sand layers.

2) Problems related to buildings and equipment, such as pre-fabricated housing units and pre-fabricated room-appliance units.

3) Problems related to industrial plants, such as a graphite-pile nuclear power reactor and a sphere tank.

4) Problems related to soil structure interaction, such as foundations of a long span suspension bridge connecting Honshu and Shikoku, a submerged tunnel for a Tokyo Bay highway crossing and undergound pipe lines.

All of these dynamic tests have been conducted at the Earthquake Engineering Laboratory of the National Research Center for Disaster Prevention. Most of these tests have been performed in cooperation with other research institutes and some projects have been supported by non-governmental organizations.

The dynamic tests that have been conducted since October, 1970 are listed in Table 1.

RESULTS OF DYNAMIC TESTS

Dynamic Characteristics of Sandy Soil

A sandy soil system was built by placing the sand in a steel box which was 12 m x 12 m in plan and 1.5 m high. A sinusoidal vibration with a frequency range of 1 to 20 H_z was applied to the sand at maximum accelerations of 0.05, 0.1, 0.2, and 0.4 g in order to determine the resonance characteristics.

Figure 5 shows the resonance curve at 0.05 g with a resonance frequency of 13 H_z.

Figure 6 shows the curve for 0.4 g and a resonance of 10.5 H_z. Acceleration ratios at the resonance frequency at the center of the sand is ten and five. At the resonance point, the acceleration ratio is greatest at the center of the soil. The greater the acceleration the flatter the acceleration ratio becomes throughout the sandy soil.

Dynamic Tests on a River Embankment

Tests on a river embankment constructed of sand, as detailed in Figure 7, were conducted in 1972 and 1973. Various ground water levels were placed in the embankment and then sinusoidal wave vibration tests were conducted in order to find the dynamic characteristics and structural destruction criteria, such as slip failure of the embankment.

An example of a resonance curve for the embankment is shown in Figure 8. Figure 9 gives an example of the acceleration data that was observed. Figure 10 shows the distribution of excess pore water pressure due to the vibration. The results obtained from these dynamic tests will be used to improve present design criteria and design procedures on earthquake resistant embankments.

Liquefaction of Saturated Sandy Soil

Dynamic tests in saturated soil were conducted in 1972 and 1973 in order to determine the characteristics of liquefaction. Figure 11 shows a resonance curve of 0.02 g sinusoidal acceleration, with a resonance frequency of about 10 H_z. Figure 12 shows the change in the excess pore water pressure during and after the vibration of 0.2 g.

These tests were performed relative to the design of a submerged tunnel and its reclaimed land.

LARGE SCALE SHAKE TABLE IN JAPAN

As shown in Table 2, several large scale shake tables for earthquake engineering have been built in Japan. Large or full scale model tests of earth-filled dams, railway embankments, buildings, nuclear power reactors, and electronic equipment for tele-communication systems or computers have been conducted at these facilities.

CONCLUSION

A brief description of earthquake engineering in Japan relative to present simulators and dynamic tests have been presented.

However, these present large scale shake tables and other simulators cannot completely satisfy the requirements of table size, displacement, maximum test weight, control system, etc. needed by researchers concerned with earthquake engineering. Therefore, researchers of the Science and Technology Agency and NRDP are planning and studying the technical feasibility of large scale shake tables. One such simulator under consideration has a table 6.0 m x 6.0 m in size, with a horizontal and vertical motion driven simultaneously up to ± 150 mm. Another simulator being studied has a table size of 30 m x 30 m with a maximum displacement of ± 200 mm and an acceleration of 0.5 g and a test loading of 1,000 t. The problems involved in designing such vibration test tables are difficult to solve, and it is, therefore, hoped that an exchange of information on earthquake simulators and dynamic tests of structures between our two countries can meet the challenge.

TABLE 1

Test Structure	Weight	Year	Cooperating Institute of Sponsor*
Prefabricated house unit	40t	November 1970	Building Research Institute (BRI)
Sand ground	400t	January 1971	
Graphite-pile reactor	30t	July 1971	BRI
River embankment	300t	September 1971	Public Works Research Institute (PWRI)
Submerged tunnel	5t	November 1971	PWRI
Suspension bridge, pier, and foundation	10t	December 1971	Honshi-Shikoku Connecting Bridge Cooperation* (HSCBC)
Sphere tank	30t	February 1972	BRI Research Institute for Pollution and Resources (RIPR)
Sand ground	5t	May 1972	
High-rise building	1t	July 1972	
Sand ground	400t	August 1972	
River embankment	200t	September 1972	PWRI
Liquefaction of saturated sand ground	200t	October 1972	PWRI
Submerged tunnel	10t	November 1972	PWRI
Suspension bridge, pier, and foundation	10t	December 1972	HSCBC*
Prefabricated room appliances units	25t	February 1973	Japan Combustion Appliances Inspection Association*
Sphere tank	30t	February 1973	BRI, RIPR
Sand ground	300t	June 1973	
Underground pipe	300t	June 1973	
River embankment	100t	July 1973	PWRI
Liquefaction of saturated ground	200t	September 1973	PWRI
Suspension bridge foundation and ground	25t	November 1973	HSCBC*
Oil tank	3t	February 1974	Nippon Kokan*
Underground pipe	300t	March 1974	

TABLE 1 (Continued)

Planned Tests

Test Structure	Weight	Year	Cooperating Institute or Sponsor*
Nuclear reactor	10t	June 1974	Hitachi*
Earthquake-free structure system	30t	July 1974	Fujita Corporation*
Reclaimed land	200t	September 1974	PWRI
Submerged tunnel	3t	November 1974	PWRI
Suspension bridge foundation and ground	400t	December 1974	HSCBC*
Steel frame with brace	30t	February 1975	BRI

TABLE 2

Institute	Drive System	Table Size	Table Weight	Test Weight	Frequency Range	Acceler-ation	Displace-ment	Actuator Force	Foundation Weight
National Research Center for Disaster Prevention	Hydraulic	6m×6m	160t	500t(H) 200t(V)	DC-50 H_z	0.55g(H) 1.0 g(V)	±30 mm	360t	12000t
Central Institute of Electric Power Industry	Hydraulic	6m×6.5m	25t	120t	0.1-20H_z	0.4 g	±50 mm	60t	4000t
Railway Technical Research Institute	Hydraulic	10m×2m×3.2m Box	22t	78t	0.1-20H_z	0.4 g	±30 mm	40t	950t
Mitsubishi Heavy Industry	Hydraulic	6m×6m	21t	100t	0.1-50H_z	1.0 g	±50 mm	100t	
Tokyo University	Hydraulic Springs	10m×2m×2m	35t	135t	1.0-5 H_z		±100 mm	20t	1200t
Obayashi Corporation	Hydraulic	3m×4m	5t	20t	DC-50 H_z	1.0 g	±100 mm	15t	225t
Kyoto University	Hydraulic Electric	3m×3m×2.5m×2.5m		12t 8t	0.1-30H_z 1-200 H_z	0.5 g 0.5 g	±50 mm ±50 mm	6t 4t	
Telecommunication Research Institute	Hydraulic	3m×3m	5t	10t	0.1-50H_z	1.0 g	±100mm(H) ±120mm(V)	15t	1000t
Port and Harbor Research Institute	Electric	5.5m×2m×1.5m(H)	8t	16t	0.2-50H_z	0.5 g	±50 mm	12t	255t

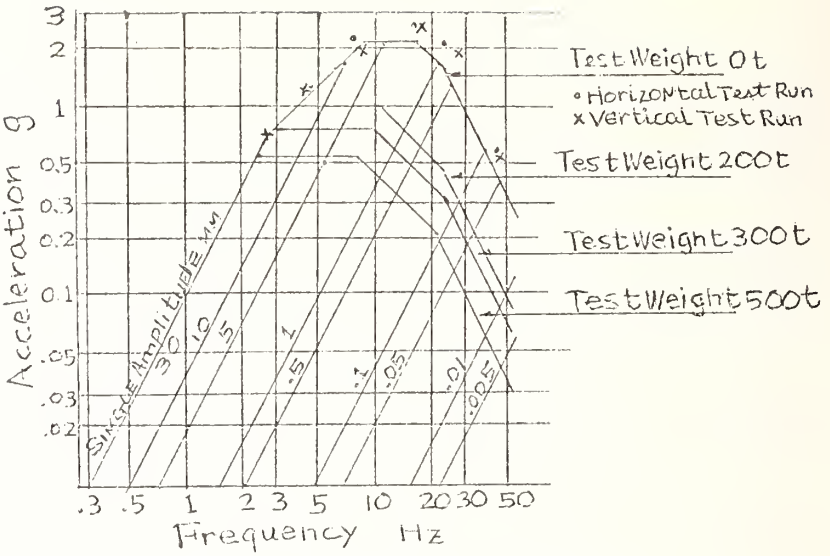

Fig. 1 Capacity Characteristics

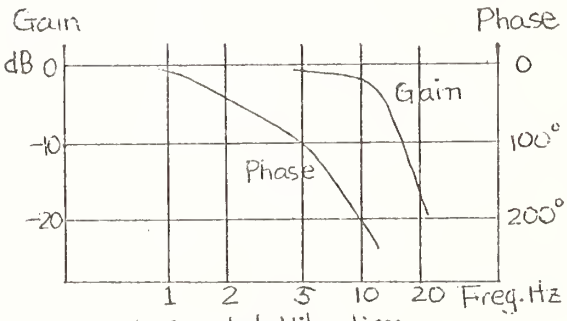

Horizontal Vibration
Test Weight 100t

Fig. 2 Frequency Characteristics

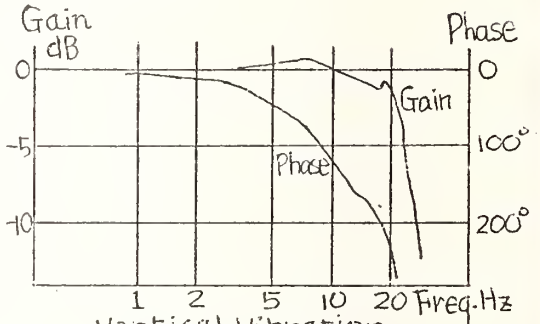

Vertical Vibration
Test Weight 0t

Fig. 3 Frequency Characteristics

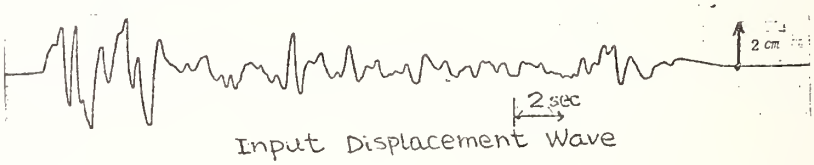

Input Displacement Wave

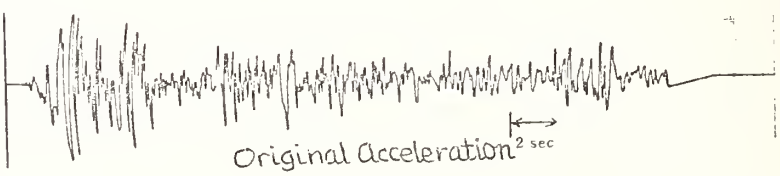

Original Acceleration

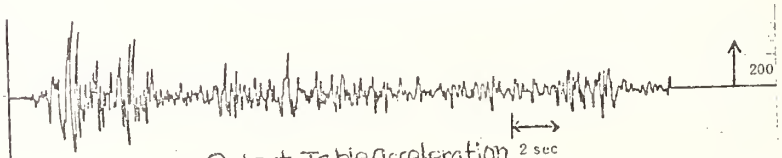

Output Table Acceleration

Fig. 4 Earthquake Wave (El Centro 1940)

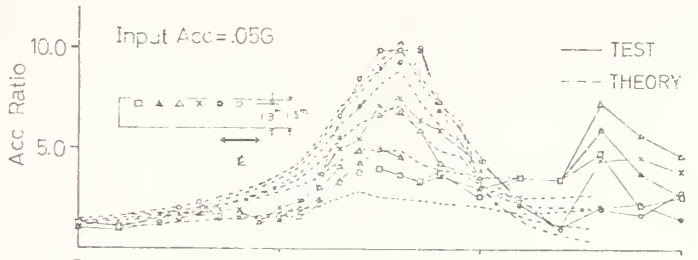

Fig5 RESONANCE CURVE

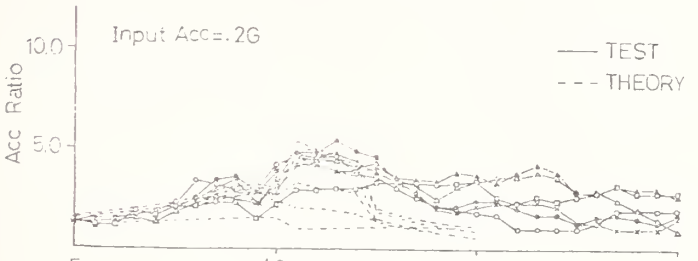

Fig6 RESONANCE CURVE

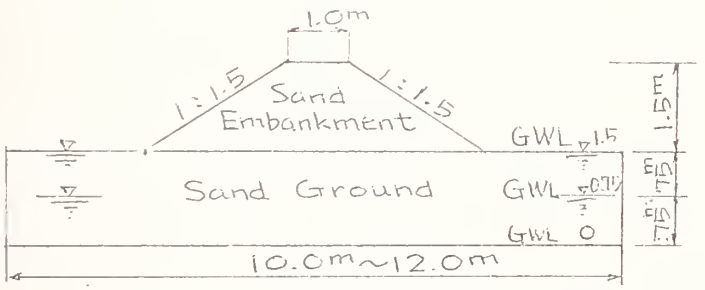

Fig 7 Model River Embankment

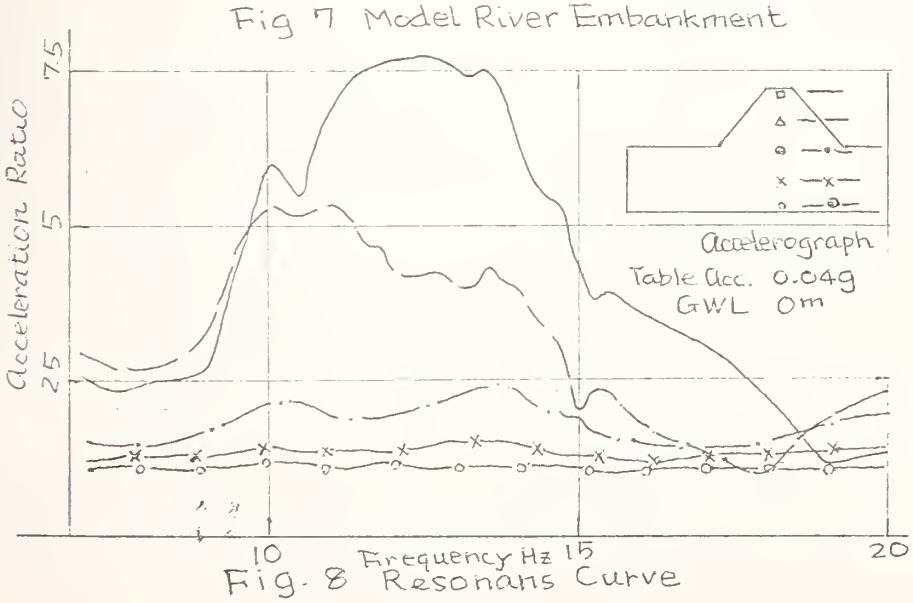

Fig. 8 Resonans Curve

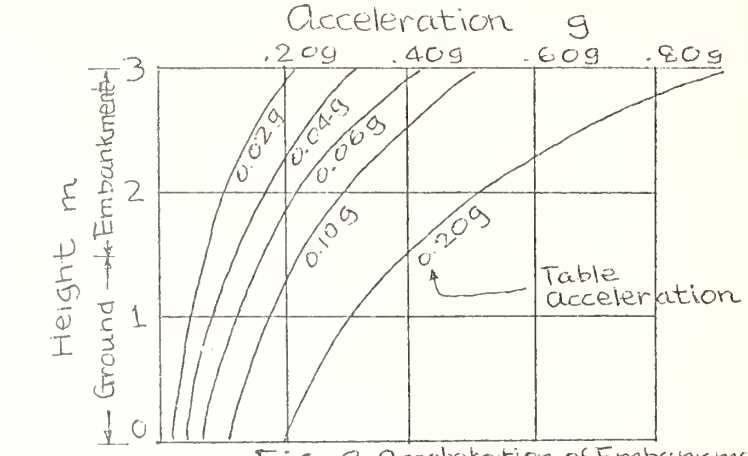

Fig. 9 Acceleration of Embankment

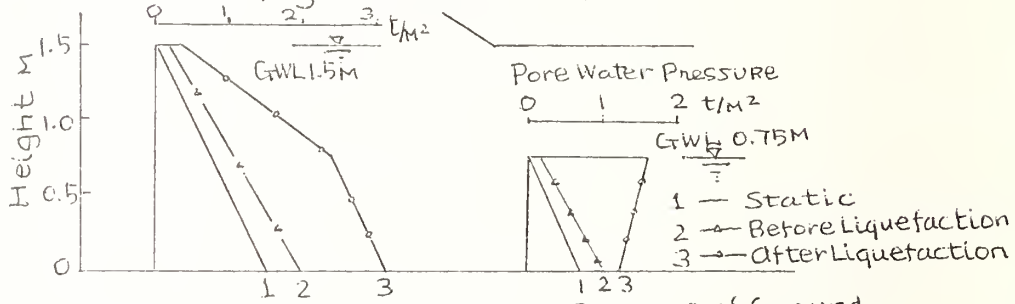

Fig. 10 Pore Water Pressure of Ground

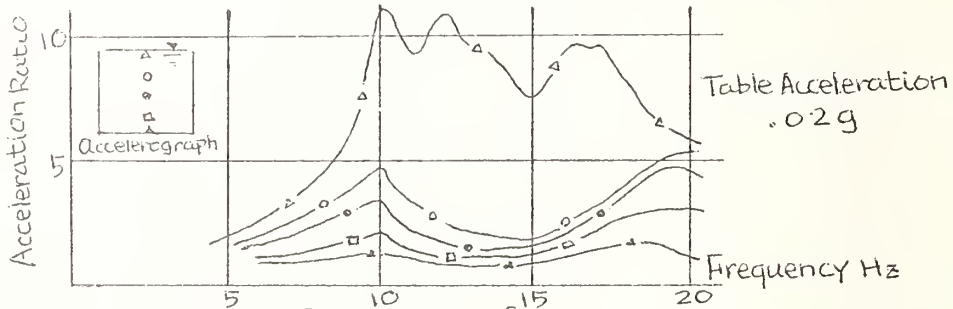

Fig 11 Resonance Curve

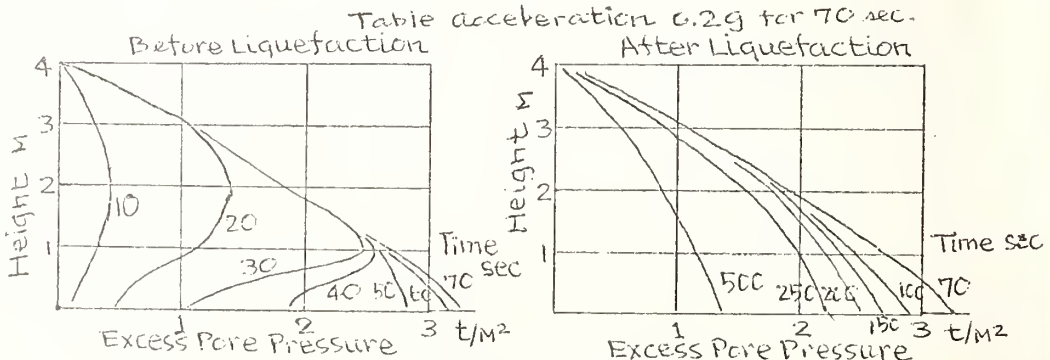

Fig. 12 Excess Pore Water Pressure

A METHODOLOGY FOR EVALUATION OF EXISTING BUILDINGS AGAINST EARTHQUAKES, HURRICANES AND TORNADOES

by

H.S. Lew
and
C.G. Culver

Center for Building Technology
Institute for Applied Technology
National Bureau of Standards
Washington, D.C. 20234

A methodology is presented for evaluation of existing buildings to determine the risk to life safety from natural hazard conditions and to estimate the amount of expected damage. Damage to structural building components resulting from the extreme environments encountered in earthquakes, hurricanes, and tornadoes is considered. The methodology has the capability of treating a large class of structural types including braced and unbraced steel frames, concrete frames with and without shear walls, bearing wall structures, and long-span roof structures. Three independent but related sets of procedures for estimating damage for each of the natural hazards are included in the methodology. The first set of procedures provides a means for qualitatively determining the damage level on the basis of data collected in field surveys of the building. The second set utilizes a structural analysis of the building to determine the damage level as a function of the behavior of critical elements. The third set is based on a computer analysis of the entire structure. All three sets of procedures are based on the current state-of-the-art. The procedures are presented in a format which allows up-dating and refining.

Key Words: Buildings; damage; disaster; dynamic analysis; earthquakes; hurricanes; natural hazards; structural engineering; tornadoes, wind.

INTRODUCTION

Background

Much of the loss of life and property in the United States from natural hazards such as earthquakes, hurricanes, and tornadoes results from the inadequate performance of buildings in response to these extreme natural environments. Past observations have shown, however, that buildings properly designed, detailed, and constructed can withstand these environments. This involves realistic assessment of the forces produced by the environment, proper distribution of these forces to structural and nonstructural building components and providing the necessary resistance to these components in the design process, and continual inspection during construction to insure the design is correctly executed in the field.

Improved building practices incorporating new knowledge relative to natural environments and the performance of buildings will serve to mitigate future losses. Continued updating of building codes and standards, taking into account the latest research findings and experiences gained from past performance of buildings, is one aspect of improved practice. Improved practices, however, apply only to future construction. They do not affect existing buildings. The response of an existing building to an extreme natural environment will reflect the performance level inherent in the codes, standards, and construction practices in existence at the time of design and construction. During the life of the building, building practices continually improve reflecting the advancement of the state of knowledge. Thus, the margin of safety changes from that assumed at the time of design as the state of knowledge and building practices advance. Deterioration during the service life of the building also affects the margin of safety. The need exists, therefore, to continually evaluate buildings with respect to the potential hazard they pose when subjected to extreme natural environmental conditions. Following such an evaluation, appropriate rehabilitation or abatement procedures may be initiated to mitigate unacceptable hazards.

Following the 1971 San Fernando earthquake, several programs aimed at evaluating the hazard posed by existing buildings in the event of an earthquake have been initiated. Most of these programs are similar in nature, however, each uses a somewhat different method of evaluation. Furthermore, since these methods involve evaluating buildings in accordance with the requirements reflected in current building codes, they do not provide an indication of the level of risk of explicit levels of building performance in terms of life safety, protection of property, and maintenance of vital functions. They also do not provide an estimate of the amount of building damage to be expected.

This report presents a methodology for survey and evaluation of existing buildings to determine the risk of life safety under natural hazard conditions and estimate the amount of expected damage.

Scope of the Methodology

The natural hazard loading conditions considered in this methodology are those encountered in earthquakes, hurricanes, and tornadoes. While the source mechanism is different for each of these geophysical processes, they all impose dynamic loading. Existing historical seismic and meteorological data are used in the methodology for determining the magnitude of recurrence interval for these hazard loadings. For earthquakes, recorded seismic data were used for determing expected ground motion. For wind loading, annual extreme wind speeds for specific mean recurrence intervals are used.

The types of structures considered include braced and unbraced steel frames, concrete frames, shear wall structures, combination frame and shear wall structures, bearing wall structures, and long-span roof structures. Although no specific limitations are imposed on application of the methodology, it is intended for buildings with substantial occupancy, i.e., fifty or more people. One- and two-story residential buildings, therefore, are not considered.

Three sets of evaluation procedures were included in this methodology, each set representing a different level of analytical sophistication. Hereafter, these three sets are referred to as the Field Evaluation Method, the Approximate Analytical Method, and the Detailed Analytical Method.

In the Field Evaluation Method buildings are evaluated on a qualitative basis in terms of structural characteristics, structural configuration, and the degree of deterioration of the building. Information on these are obtained from a field survey. This method provides a rapid, inexpensive means for identifying clearly hazardous structures or potentially hazardous ones requiring a more detailed analysis to estimate damage.

In the Approximate Analytical Method buildings are evaluated in terms of the behavior of critical structural members. The procedure requires an analysis of the structure to identify critical members and determine the stress level induced in these members by the extreme environments. A set of building plans, specifications, and construction drawings are needed to obtain the necessary data required to perform the analysis.

In the Detailed Analytical Method the damage level is evaluated on the basis of the energy capacity of the structure. This procedure requires the use of a digital computer program for the evaluation. As in the Approximate Analytical Method, the building data needed for input to the computer program would be obtained from a set of building plans, specifications, and construction drawings.

DAMAGE EVALUATION METHODOLOGY

Field Evaluation Method

The Field Evaluation Method can be used where evaluation results do not need to be refined. This method is particularly applicable if building plans are not available.

Earthquake

For earthquake, a qualitative evaluation of building is made based on a combined effect of structural type, vertical resisting elements, and horizontal resisting elements. Based primarily on the past performance of various types of buildings, relative ratings for these three factors are developed. These are used to determine a basic structural rating which is the basis for determining the building capacity. This is shown schematically in Figure 1.

Ratings for various structural types are to account for past performance and the degree of uncertainty that the building would perform in a manner anticipated for the type. These ratings are based on damage experience and judgment. For instance, moment resisting steel frames would be rated good, whereas unreinforced masonry shear walls would be rated poor.

The vertical resisting elements include shear walls, shear cores, vertical bracings, and columns. In assessing the ratings for the vertical resisting systems, "symmetry", "quantity", and "present condition" of these individual building elements are considered.

The symmetry describes the eccentricity between the center of mass of the structure and the center of stiffness of the vertical resisting elements. Thus, in a building where the only shear walls are the exterior walls with only one opening in the center of the opposite walls, and the building plan is rectangular, the building would be classified as symmetrical. On the other hand, a two-story rectangular structure with nearly solid side and rear walls, but with front wall almost entirely glazed with only four small piers or columns, would be classified as very unsymmetrical.

The quantity refers to the number of vertical resisting elements. If there are many long shear walls, it would be rated good. In the case of moment-resisting frame structures of steel or concrete, both the strength and number of columns are important. For closer spacing of columns, usually about 6 m to 10 m bays, a good rating is given.

The present condition describes wall cracks and other damage. Other damage may be damage caused by deterioration from lactic or tannic acid (frequently found in dairy or slaughterhouse facilities) or from severe popping of concrete caused by the use of reactive aggregates. The degree of damage in such cases can only be estimated by visual observation.

For vertical resisting elements, "quantity" and "symmetry" are combined as one factor. This factor is then combined with "present condition" to obtain the rating for the vertical resisting elements, see Figure 2.

The horizontal resisting elements include diaphragms, premeter beams, and horizontal bracings. The floor or roof systems act as horizontal diaphragms to distribute horizontal forces to the vertical resisting elements, such as shear walls, moment-resisting frames, or braced frames. This diaphragm action is similar to that of a horizontal plate girder spanning between the vertical resisting elements and may be continuous over several supports. In this analogy, the floor itself may be compared to plate girder web, and the marginal beams or walls (chords) compared to plate girder flanges. The floor or roof system, acting as a girder web, is primarily a shear resisting element. The marginal beams or girder flanges (chords) in diaphragm action are primarily subjected to axial loads of tension or compression.

Shears are transferred by the anchorage between floor or roof and the shear walls or frame members. The determination of the adequacy of anchorage or connections involves considerable judgment unless computations are made. For example, where the floor or roof systems are of cast-in-place concrete and are placed integrally with portions of the shear walls or frames, generally a good anchorage with shear transfer capacities can be assumed dependent on the concrete strength, concrete slab thickness and amount and anchorage of reinforcing steel. With metal deck systems, the diaphragm values are dependent on the deck configuration, attachment between units, gage, and attachments to supports.

The capacity of the horizontal resisting system is dependent on either the rigidity of the diaphragm, the anchorage capacity of the diaphragm or horizontal bracings to the vertical resisting system, or the effectiveness of chord members. Thus, the lowest rating of these three factors is considered as the rating for the horizontal resisting system. The rating schemes used to rate the capacity of the horizontal resisting systems are illustrated in Figure 2.

The Basic Structural Rating which describes the capacity of a building to resist the earthquake force is obtained by combining the rating for structural type and the rating for either the vertical resisting system or the horizontal resisting system, whichever provides a lower rating. The rating scheme adopted for this study is illustrated in Figure 3.

Hurricane

Damage to a building is dependent on two basic considerations. One is the effective wind force, usually in terms of pressure, positive or negative. On the other is the resistive capacity of the structure to lateral forces and also to uplift forces on the roof created by the structure's shape.

The same rating scheme used for structural systems in the case of earthquake can be used for wind in the evaluation of a building's ability to resist lateral forces. Because uplift forces are acting simultaneously with the lateral forces, additional factors such as roof anchorage, anchorage to foundation, and internal pressure should also be considered.

The rating of the building is determined by taking the lowest rating of the "Foundation Anchorage" factor, "Roof Anchorage" factor, or the "Basic Structural Rating" as defined in the case of earthquake since these factors affect the building's capacity to resist wind independently.

Tornado

Damage from tornadoes has been most severe to small, light buildings; although tall, flexible, and heavier buildings have sustained some severe structural damage. The most extensive damage to buildings has been to roofs and exterior claddings, including glass. This includes damage from windblown debris. Because the total effects of tornado on a building is not clearly understood at the present time, only a broad categorical rating of buildings, depending upon their types, is possible. In this study, a poor risk rating is given to small and light buildings. A medium risk rating to small, heavy buildings, and to large, multi-story buildings that could be rated high in wind and earthquake resistance. A good rating can only be given to heavy vault-like buildings known to have been designed for tornadoes.

Approximate Analytical Method

The Approximate Analytical Method provides a simplified analytical procedure for evaluation of the building capability to resist natural hazards by determining stress ratios of critical elements of structural elements. These stress ratios are the ratios of the stresses produced by the loading to limiting stresses of the critical building elements.

For the purpose of this evaluation, elastic analyses of building response will be compared with material design capacities. Design stresses will be those designated by material specifications. In the evaluation, buildings are being analyzed, but not designed. Stresses in structural elements will be checked for the combined effects of lateral and vertical loads. Where lateral loads are included, the combined stresses may exeed code working stresses by one-third, except where not permitted in the specifications, with the provision that the stresses resulting from design vertical loads alone will not exceed code design stresses. This method, in general, does not include the use of a dynamic analysis except in special cases.

Earthquake

Any important earthquake resisting element having the highest unit stress as related to allowable design stresses is a critical element to be considered in the evaluation of the structural system. The term "important" element means an element which, if it failed, would seriously reduce the capacity of the structure as a whole to resist lateral forces. Some members would not be critical when deformed beyond their yield level deformations. In other members, yielding may cause an important redistribution of loads. With a multiplicity of well-distributed similar elements, the redistribution of loads would add only a small percentage of stress to adjoining or parallel elements.

In most buildings, the critical elements will be the vertical resisting elements (shear walls or moment resistant frames) and the horizontal resisting elements (diaphragms). This is for earthquake forces acting in the plane of the elements. Earthquake forces normal to a wall are a function of the weight of the wall itself. Where a wall has a long span between floor diaphragms or vertical frame elements, it might be a critical element if its failure would produce collapse of the building as a whole from vertical loads or in-plane lateral forces.

The highest ratio or stress resulting from the required seismic forces (f_e) to the allowable material design stress (f_a) (including 1/3 increase where permitted but deducting capacity required by gravity loads) on any critical element is termed the critical stress ratio f_e/f_a. The critical stress ratio is the indicator for evaluating the seismic resisting capability of the structure. Load factors and ultimate capacities are used for concrete design and for plastic design of structural steel.

Hurricane

Both internal and external pressures must be considered on portions of buildings such as roofs and walls. Corners of walls are exposed to high negative pressures. These corners should be checked.

In determining the response of the building as a whole, the type of diaphragm system must be considered. A stiff diaphragm will distribute horizontal forces to vertical resisting elements in proportion to their relative rigidities. A flexible diaphragm will distribute forces to vertical elements more nearly proportioned to the tributary-exposed wind surfaces.

The usual critical elements for wind resistance are, as in earthquake resistance, the vertical resisting elements (shear walls, braced bays, or moment resistant frames) and the horizontal resisting elements (diaphragms). There is a major difference, however, in that wind forces are applied to exposed surfaces while earthquake forces originate at centers of mass and are proportional to mass. Thus, a lightweight exterior wall might have a relatively small earthquake force normal to the wall but would be exposed to wind forces which are independent of the weight of the wall.

The calculations for the adequacy of the building to resist wind forces can be made using any of the standard analytical procedures. The lateral loading to each story level is determined with positive pressures on the windward side and negative pressures on the leeward side. The path by which these forces are transmitted to the vertical resisting elements is determined and the adequacy of diaphragm or horizontal bracing system to transmit these forces should be evaluated. Lateral forces are applied to the vertical resisting elements at each level and the stresses should be analyzed. The overturning stresses should be checked, including uplift on foundations.

The highest ratio of stress resulting from the wind forces applicable to the site (f_w) to the allowable material design stress (f_a)(including 1/3 increase where permitted but deducting capacity required by gravity loads) on any critical element is termed the critical stress ratio f_w/f_a.

Tornado

For the purpose of evaluation, it will be assumed that a free field wind velocity of 200 miles per hour and a pressure drop of 1.2 psi. Using the formula $P = .0025\ V^2$ to convert velocity to pressure gives P = 100 psf. The 1.2 psi pressure drop is, converting units, equal to a suction or uplift of 172 psf. If it is assumed that tornadoes are similar to other high winds, such as hurricanes, with respect to the relationship of pressures on windward and leeward sides, one finds these coefficients of the velocity pressures to be 0.8 and either 0.5 or 0.6, respectively; depending on the height-width ratio of the building. Thus, the total lateral force on a building subjected to tornadoes for a moderate degree of protection will be 100 x (0.8 + 0.5 or 0.6) = 130 or 140 psf.

There are probably very few buildings that will be undamaged if in the direct path of a strong tornado. The least likely to be severely damaged will be heavy reinforced concrete or reinforced masonry vault-like structures one or two stories in height, with relatively heavy and solid walls. Taller buildings designed to resist hurricanes may have limited damage, but probably will not collapse unless they are of unusual configuration or have large roof overhangs or open sides. Light buildings of wood frame or steel frame and metal sidings have been known to have been torn from their foundations and blown considerable distances. It is possible, however, to provide such light buildings with some resistance to winds by proper anchorage to foundations to the ground to resist uplift.

If a building has been evaluated for wind and given a poor rating, it will be considered to be inadequate to resist tornadoes. The ability of roof systems, designed

only for gravity loads, to resist reversals from uplift need to be evaluated. The wall capacities must be checked for direct horizontal positive and negative force. The floor and roof systems must be checked for adequacy as diaphragms to transmit lateral forces to the vertical resisting elements. Anchorage of walls to footings should be checked for capacity to resist sliding combined with vertical uplift and overturning. The footings themselves should be checked for sliding resistance, uplift, and overturning forces. In checking these the purpose is to determine the ratio of stresses resulting from the imposed tornado loads to the capacity of the structure.

In each of the various resisting systems, such as roof, floors, shear walls, or moment-resisting frames, there may be one or more critical elements which will fail before the other elements. Care must be taken not to derate a building because of one non-important element. Where the failure of such an element would not cause failure of a system, but would only cause minor redistribution of loads, such a member would not be a critical element. The procedure for determining the critical stress ratio is the same that was used in the case for hurricane.

Detailed Analytical Method

This method is based on a modular computer program with each module dealing with a particular aspect of the damageability prediction problem which includes:

1. Environmental Loads
2. Structural Characterization
3. Response Computation
4. Estimation of Potential Damage

For seismic loads, historical and recorded data are used along with the program describing the seismic and wind activity for the entire continental United States, Alaska, and Hawaii. Historically based tornado and hurricane activity for the continental United States is included. With these data, the program will computer, in a probabilistic sense, the specific environment of any given building site in the country. Alternatively, the user may choose to input any of these loads directly.

Structural models of varying complexity can be generated depending on the availability of structural data and the level of effort selected for a particular task. Damage predictions are made on the basis of the building's response to the appropriate loading conditions. Damageability data characterizing the capacity of the building to resist failure must be input by the user. Algorithms for computing damage are based on the assumption that percent damage varies continuously with key response parameters. These key parameters have been selected and are incorporated in the program. The forms of damage distribution curves as functions of response are also built into the program. The user may choose values of the parameters of these functions in accordance with prepared guidelines and exercise his judgment according to the application at hand. A schematic presentation of the computer program is given in Figure 4.

Natural Hazard Loading

Earthquake Loads

Site loads for an earthquake are defined by a ground site response spectrum. This response spectrum reflects an amplification of the hardrock spectrum for the site, which is frequency dependent. The hardrock spectrum is generated in either of two ways. If the risk option is selected, the user must input seismicity data from the Seismic Map provided with the computer program. By further specifying either a return period or building life and probability of non-occurrence, a risk earthquake defined by its Richter magnitude is computed. If the risk option is by-passed, then the user must input a Richter magnitude and a hypocentral distance. In either case,

the computer program computes the maximum hardrock acceleration, velocity, and displacement at the site.

Hurricane Loads

If a wind velocity is generated for the specified site, then a statistical regression analysis is used to compute a mean wind velocity given either a return period or building life and probability of non-occurrence. A standard deviation is also computed and may be used to establish some degree of confidence in the wind velocity selected for analysis. If the user desires, he may alternately choose to input a wind velocity for analysis. As in the case of earthquake, local site conditions modify the wind velocity which is determined on the basis of historical data. For example, free-field wind velocities in large cities are attenuated by the presence of buildings, whereas, on an open prairie, the attenuation is comparatively small as one approaches the ground. Thus, in figuring the wind load on a building, surface conditions are accounted for by specifying a site condition parameter.

Tornado Loads

The probability of being hit by a tornado can be computed from historical data. However, the user must specify a tornado wind velocity. In this case, the static response of the building will be computed and damage assessments made.

Structural Characterization

Three general levels are offered for structural dynamic modeling:

1. A Detailed Model
2. A Story-Stiffness Model
3. An Empirical Model

It is noted that all of the modeling options lead to the same basic dynamic characterization: building natural frequencies and modal displacements.

The three modeling options are illustrated in Figures 5, 6, and 7. If the user selects "Detailed Model" option to generate a detailed stiffness matrix for the structure, then the stiffness matrix is constructed frame by frame, story by story, from top to bottom. Each frame is parallel to the direction of motion in a vertical plane. Stiffness and mass contributions from each frame are superposed in formulating the two-dimensional model of a building. If the user desires "Story-Stiffness Model" option, he must input a story stiffness and story height data for each building story. A total story-stiffness is the sum of the stiffness produced by all columns, partitions, walls, and other lateral force resisting components at that story. If an empirical model is to be generated, then the user must input an estimate of the building's fundamental period and story heights. A straight-line mode is assumed to compute deflections.

Response Computation

Response computations are made for earthquake loads, for tornado and hurricane loads, and for uplift due to wind. Ponding loads are also computed in the long-span roof subroutine.

The response of a building to earthquake ground motion is evaluated by determining the peak modal response in each of the modes (a maximum of six is considered), and combining their contributions to the total response. A damping, a ductility factor, a modal combination scheme, and a value for each story's drift-to-yield are used to compute an effective ductility for the building. An iterative procedure must be used to establish consistent values of damping and response as damping is defined as a function of ductility. While this operation seems to be stable and typically converges in a few cycles (three or four), an upper limit (e.g., six) on the number of interactions is put in and used to transf

control out of the iterative loop in case the computations do not converge to within five percent accuracy. This may only occur when elasto-plastic response is considered.

Inter-story drift, pseudo-velocity, and absolute acceleration are computed for each story. In addition, story forces and shears are computed.

The response of a building to wind is treated as a static problem. The force acting along the building is computed by multiplying the pressure at each story by the tributary story area. For the detailed and story-stiffness models, the inverted stiffness matrix is used to compute deflection of the building. If the empirical modeling option is chosen, the building response is calculated considering the building to be a uniform cantilever beam using a simplified analysis.

Evaluation of Damage

Potential damage to a building which may result from exposure to the environmental loads computed for the building site is evaluated in a damage subroutine. Damage is expressed in percent of total damage on a story-by-story basis. Damage is computed independently for earthquake, hurricane, and tornado. It is segregated into three categories: structural, non-structural, and glass. In the case of structural damage, the damage is further subdivided into damage to frame, walls, and diaphragms.

The key response parameters used to predict damage in each case are outlined below.

Earthquake

a. Structural: Interstory Drift

b. Non-structural: Floor Velocity or Acceleration

c. Glass: Interstory Drift

Wind, Tornado, or Hurricane

a. Structural: Interstory Drift

b. Partitions: Interstory Drift

c. Glass: Direct Pressure

SUMMARY

This report presents a methodology for evaluating the potential damage of buildings due to earthquake and extreme wind including tornado and hurricane. Three independent, but related, sets of procedures are developed. These ranged from a qualitative procedure based on field surveys data to a detailed analytical procedure involving a digital computer program. Historical seismic and meteorological data are used as the basis for establishing environmental loads. Damage estimates are based on empirical correlations between structural response and observed damage coupled with engineering judgment.

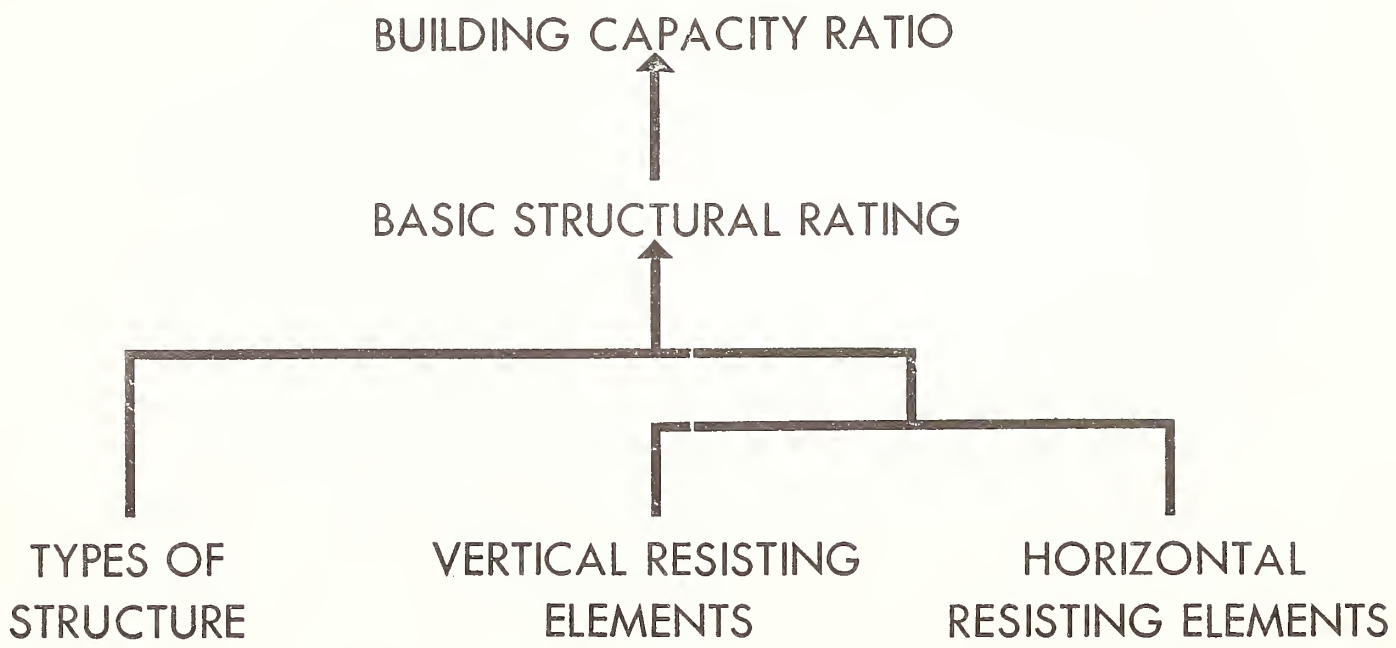

Figure 1. Scheme for Determining Building Capacity

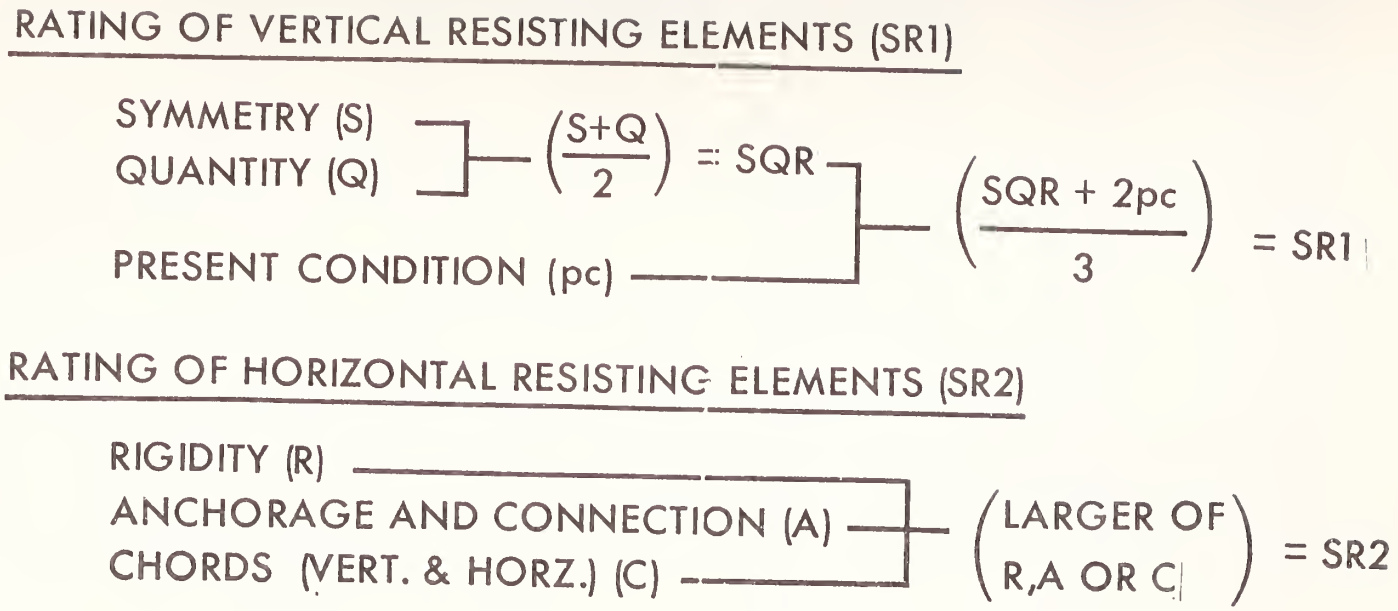

Figure 2. Rating Schemes for Vertical and Horizontal Resisting Elements.

BASIC STRUCTURAL RATING (BSR)

$$BSR = \frac{GR + 2\,(\text{LARGER OF SR1 OR SR2})}{3}$$

RATING OF TYPES OF STRUCTURE (GR)

Figure 3. Scheme for Determining Basic Structural Rating

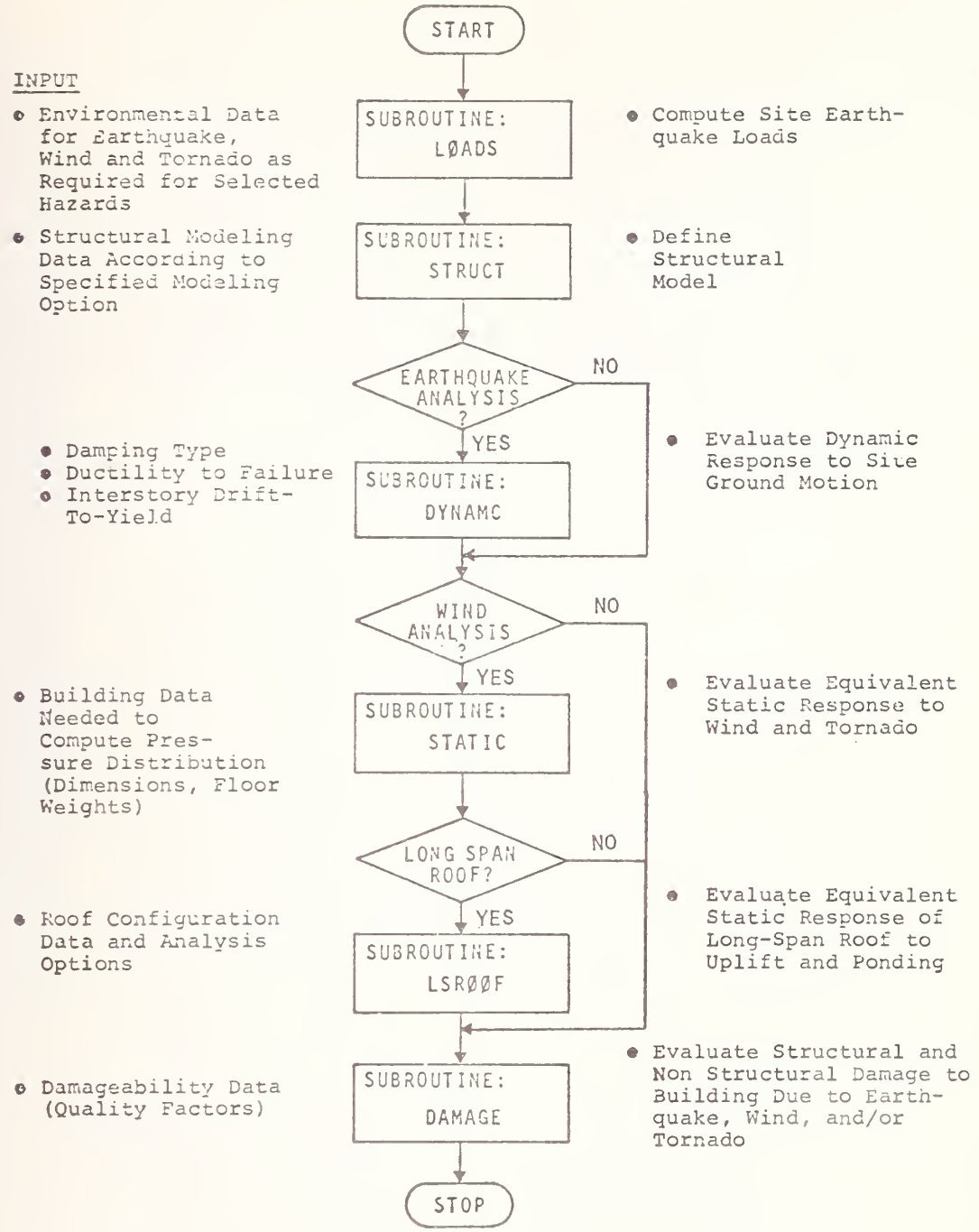

Figure 4. Schematic of Computer Program

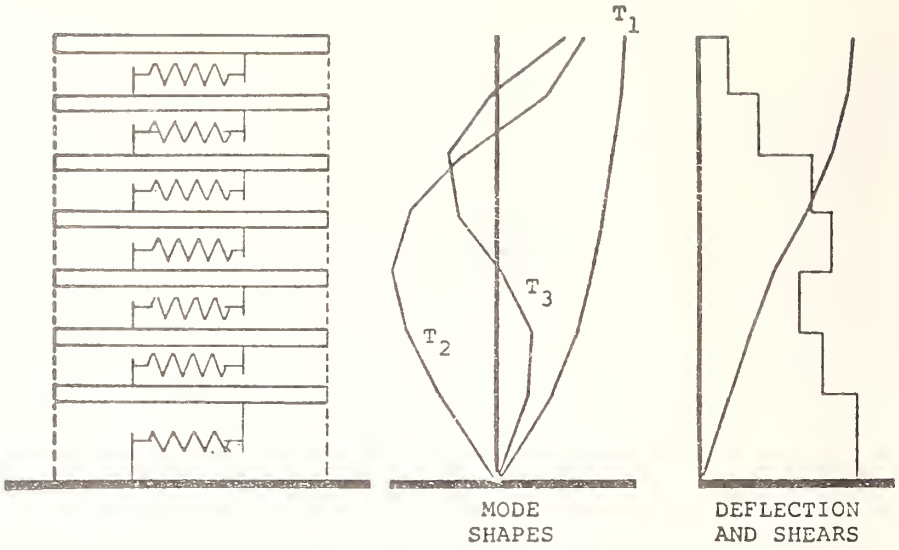

Figure 6. Story Stiffness Model

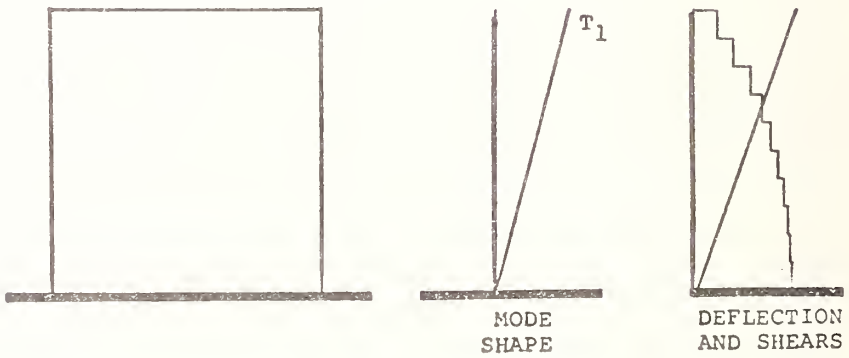

Figure 7. Empirical Model

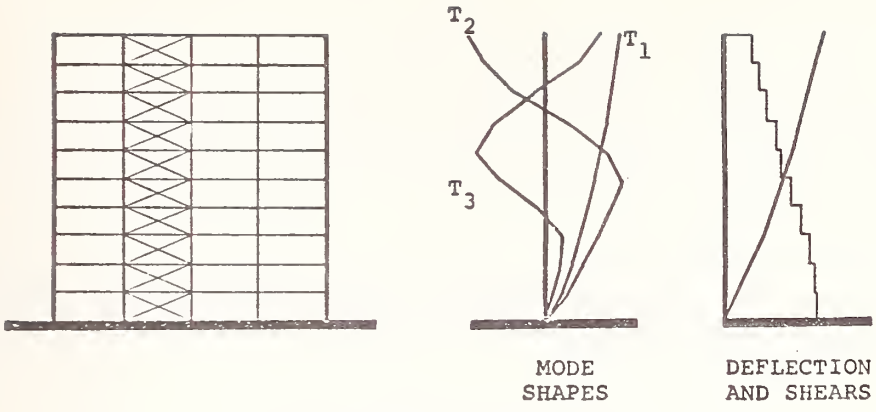

UNBRACED OR BRACED FRAME BUILDING

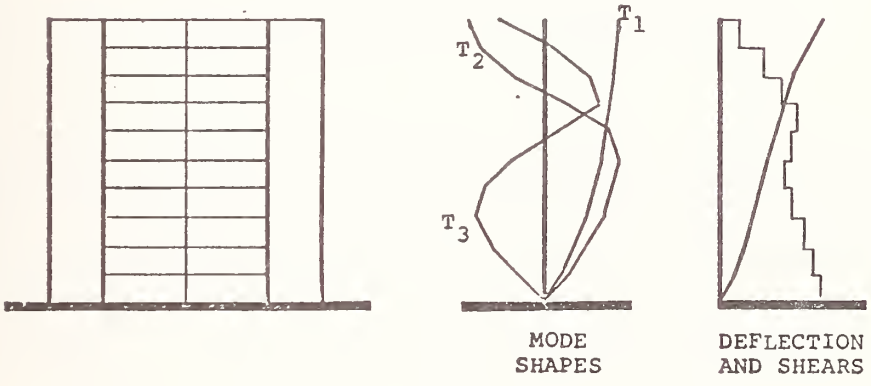

SHEAR WALL OR FRAME AND SHEAR WALL BUILDING

Figure 5. Detailed Frame Model Options

EXPERIMENTAL RESEARCH ON THE ASEISMIC CHARACTERISTIC OF SPHERICAL STEEL TANK FOR LIQUID PETROLEIUM GAS

by

Kiyoshi Nakano
Head of Structural Division
Building Research Institute

Makoto Watabe
Chief of Earthquake Engineering
International Institute Of Seismology And Earthquake Engineering

The results of static and dynamic tests on a spherical steel tank are given in detail. A theoretical technique to explain the "sloshing" effect is presented. A proposal for a safer design procedure to replace the present aseismic design practice is presented.

Key Words: Dynamic analysis; earthquake; seismic design; seismic response; spherical tanks; structural design.

PREFACE

It has recently been pointed out that large tanks containing flammable materials in and around densely populated cities present a dangerous situation for the safety of citizens during severe earthquakes. All people in Tokyo, for instance, would be burnt if all petroleum and liquid petroleum gas in and around Tokyo should catch fire due to an earthquake.

Unfortunately, aseismic design of these tanks has not been adequately developed. Fortunately, research on the aseismic properties of spherical tanks used for liquid butane gas has been conducted by various committees. Recent results on some of this research will be presented herein.

SCOPE OF EXPERIMENTS

The test specimen that was selected consisted of a one-third scale model of a large spherical tank. The dimensions of the test specimen are illustrated in Figure 1. The weight of the test specimen was ten tons and can contain 150 tons of water (88 tons of butane gas). The weight of the test specimen was limited by the capacity of the shake table, details of which are shown in Figure 2.

Initially, the test specimen was subjected to static lateral loading by slightly tilting the specimen, as is shown in Figure 3. This type of loading was expected to give data on the stress distributions in various parts of the specimen and the basic lateral stiffness of the specimen. The location of the strain gages and other measuring devices are described in Figure 4.

The test specimen was then subjected to the dynamic loading. Initially, hand-powered excitations were induced in order to obtain the approximate fundamental period and damping characteristics of the test specimen. Mechanical input forces, using a sinusoidal wave within the range of 0 H_z to 16 H_z, were then applied. Also, forces of actual and simulated earthquake motions, such as the El Centro Earthquake, Hidakasankei Earthquake, randomly modified El Centrol Earthquake, were also applied to the test specimen. The quantity of water, which represents the amount of liquid butane gas, was varied by the following percentages: 0%, 20%, 30%, 50%, 60%, 70%, 80%, 90%, and full. Through this variation in the water content, the complete aspect of the sloshing phenomenon was made clear.

The final stage of the experiment was to induce a failure mechanism by inputing a wave of the modified El Centro Earthquake with 400 gallons of peak acceleration with 85% of the full water capacity.

In order to measure accelerations, ten accelerometers were utilized. To measure relative displacements at the base, transducers were attached between the test specimen and a rigid safety guard. This guard was installed around the test specimen to protect the transducers in case of premature failure. Prior to the dynamic and static tests, tensile forces were induced into the diagonal braces by means of toggle bolts. The tensile strains that were imposed were of the order of 250 μ in./in., the value of which is typical of the strains induced in tanks used in the field.

DISCUSSION OF THE EXPERIMENTAL RESULTS

Static Tilting Test

Figure 5 describes the experimental results from which the lateral stiffness can be computed. Also shown is the calculated load-deformation response. The calculated load-deformation curve and thus, the lateral stiffness was based upon the following assumption.

i) The spherical shell is assumed to be rigid (at Point a shown in Figure 6).

ii) The Point "a" in Figure 6 is assumed to be the center of the connnection between the tubular column and the spherical shell.

iii) Deformation of the members is determined by using a conventional energy method, excluding shear deformations. Surrounding the connection to the tubular column, significant stress concentrations were observed at a distance within three times the thickness of the spherical shell. Using the above area, about four times the yielding strain should be expected when 30% of the total weight is applied as a lateral static loading. Outside of this connection area, the stress concentration effect can be disregarded.

Elastic Dynamic Test

In order to determine the dynamic properties of the test specimen, the following factors must be determined:

i) Characteristic Period

ii) Fraction of Critical Damping

iii) Effective Mass of the Dynamic System

iv) Response to the Earthquake Loading

a) Periods and Damping

When the test structure contains a liquid, the so-called "sloshing phenomenon" (motion of the free surface of the liquid) becomes a common problem and thus the simplified model illustrated in Figure 8 is useful in understanding this complicated behavior. W_f, given in Figure 8, is called the "fixed water"; W_s is called the "effective mass for sloshing"; k_f is the lateral stiffness of the structure; and k_s is the virtual stiffness, all of these parameters characterize the shoshing phenomenon. In this experiment, W_s and W_f are of the same order, however, k_s is much smaller than k_f. Therefore, the two resonance modes appear to be independent and thus the "structural period, T_f" and "sloshing period, T_s" modes will be defined as follows:

$$T_f = 2\pi \sqrt{W_f + W_o/g \cdot k_f}$$

$$T_s = 2\pi \sqrt{W_s/g \cdot k_s}$$

Through a free vibration test, excited by impulse shock and through resonance curves obtained by harmonic excitation from 0 H_z to 16 H_z, periods and fraction of critical damping, as indicated in Table 1, were obtained. The difference in the fraction of damping as obtained from the free vibration and the one obtained from the resonance curve may be due to the powerless performance of the shake table. The damping of the sloshing is extremely small, and almost impossible to state numerically (0.043%).

b) Stiffness and Effective Mass for Sloshing

The lateral stiffness of the structures, as obtained from the static tilting test and by the theoretical calculation, coincides exactly.

The values of W_f and W_s were obtained from the experimental results. Consider the weight of the structure without water to be equal to W_o, the lateral stiffness k_f, the structural period without water T_o, and with water T_f, and the dynamic factor of the structure μ_f. If all of these parameters are known from dynamic tests, then

$$W_f + W_o = (T_f/2\pi)^2 K_f g$$

Therefore, the fraction of fixed water $f(\eta)$ to total water W_w is;

$$f(\eta) = W_f/W_w = \{W_o(T_f/T_o)^2 - 1\}/W_w$$

If we define the dynamic factor of sloshing, without damping, as μ_s, and the base displacement as δ_o and β as $\beta = T_o/T_s$, then;

$$\mu_s = \frac{1}{1 - \beta^2}$$

The shear force or lateral spring F_s in the structure can be expressed as;

$$F_s = K_s \cdot \eta_x \cdot \delta_o$$

Using this value, the dynamic factor of the structure $_f$ can be expressed as;

$$\mu_f = \frac{1}{1 - \beta_f^2} + \frac{k_s \mu_s}{k_f}$$

where $\beta_f = T_o/T_f$.

Noting that $k_s = 4\pi^2/T_s \; W_s/g$ and substituting this relation into the above equation, gives;

$$W_s = \mu_f - \frac{1}{1 - \beta_f^2} \; \frac{k_f T_s^2}{4\pi^2} \; g \; (1 - \beta^2)$$

Using the experimental results and noting that the sum of W_f and W_s equal the total weight W_w, that W_f and W_s are constant and are independent of the amplitude or frequency of the input acceleration, the parameter $f(\eta)$ is obtained as shown in Figure 9.

c) Response to Earthquake Excitations

The linear response of the tank to the modified El Centro Earthquake is tabulated in Table 2. The meaning of "modified" is in relationship to a digital filtering process that is required in order to assume that the maximum displacement of the earthquake is limited within the maximum stroke of the shake table. In this experiment, the maximum displacement was limited to 2.5 cm for a peak acceleration of 400 gallons. When the capacity of the shake table is not sufficient to excite a heavy test specimen, the spectrum ratio between input and output contains a dip along the frequency curve of the structure. Unfortunately, this condition occurred during the testing of the tank structure. Figure 10 shows the response spectrum of the output wave as recorded at the shake table. The deep dip can be seen in Figure 10 during the fundamental structural period. Modification of the earthquake excitation will not improve the response and little can be observed about the sloshing phenomenon.

Dynamic Test of Failure Mechanism

The failure mechanism test was instituted by imposing input of the forms related to the modified El Centro Earthquake (N-S comp.) wave with water content ratios equal to 75% and 85%. Assuming the water content ratio equal to λ_o, the equivalent fixed "liquid" ratio y for λ percent content of liquid butane gas can then be estimated as given in the following procedure;

Assume a density of liquid butane gas equal to $\rho = 0.585$ and a fixed water water ratio $f(\eta)$ for a water content ratio λ_o, then y_o is related by the following expression,

$$\rho\lambda y = \lambda_o y_o$$

From Figure 9, for instance, if y_o is assumed to be 75%, then λ_o is 0.53 and thus λy equals 0.68. Once again from Figure 9, the value of λ and y are 0.915 and 0.74, respectively. By this procedure, it may be understood that 75% of the water content is equivalent to 91.5% of the butane liquid content, in view of the "fixed liquid" weight.

In Figure 11, the relation between the response acceleration and response displacement, as the results of the failure mechanism dynamic test, is shown. Due to the inelastic property of the lateral stiffness beyond the application of 260 gallons, the acceleration and displacement is not linear, but has a multi-linear response which can be predicted theoretically as is illustrated in Figure 11.

Fracture was observed at the connection in the area of the diagonal bracing bars. Almost simultaneously, failure was also observed in the tubular column around the area of the connection to the lateral bracing. No visual failure was seen in the shell sphere at the connection to the tubular column. In Figures 12, 13, and 14, the time history response at various locations are shown. These responses are the displacements and accelerations at the base and at the center of the structure, the strains in the diagonal bracings, and the strains in the shell adjacent to the tubular column connections.

CONCLUSION

Through a series of experiments the following observations have been made;

1) The sloshing behavior can be treated quite exactly by use of a simplified model.

2) The frequency periods for the structure and sloshing are;

$$T_s \text{ (Sloshing period)} = \sqrt{D/g}\ \ \bar{s}(\eta)$$

where

D = Diameter of spherical tank

g = Gravity acceleration

η = Water content ratio

$\bar{s}(\eta)$ = Function of η as shown in Figure 15

In this experiment T_s is expressed

$$T_s = 0.134\ \sqrt{D}\ \ s(\eta)$$

as shown in Figure 15. T_f can be predicted as

$$T_f = 2\pi\ \sqrt{W_f + W_o/g \cdot k_f}$$

where

$W_f = W_w \cdot f(\eta)$

W_o = Weight of steel tank itself

$f(\eta)$ = Function of η as shown in Figure 15

k_f = Structural lateral stiffness as given previously

3) Fraction of Critical Damping

For structural damping, the fraction of critical damping is 0.6%, while for sloshing, the fraction of critical damping is 0.043%.

4) The spherical shell can be assumed to be a rigid body, as indicated by the calculated stiffness and stresses in the diagonal braces.

5) Excitation in the Transverse Direction

About 20% transverse excitation was observed during the last stage of the experiment.

6) Aseismic Coefficient

The yielding shearing force was equivalent to the base shear coefficient (aseismic coefficient) of 1.00. Therefore, if a response dynamic factor is assumed to equal 3.0-4.0, then this type of tank will not be safe when subjected to a peak acceleration equal to or greater than 0.3 g.

7) The sloshing phenomenon was observed during the last stage of excitation.

COMMENT ON THE SAFETY OF THE STEEL SPHERICAL TANKS

In view of the explosive potential of these types of tanks, fracture cannot be permitted during severe earthquake motions. Because fracture of the diagonal bracing does not lead to total collapse of the structure, the load capacity based on that load which induces a yielding lateral force can be used as a design criterion.

In the case of smaller tanks, as was this test specimen, the response dynamic factor to earthquake motions will be about 3.0 to 4.0. If the size of the tank is increased, then the fundamental period will be increased, so the response dynamic factor will be reduced to a value of 2.0-1.0. In this sense, the base shear coefficient should be determined according to the fundmental period. Considering that the reserved strength of these types of tanks is about three times the elastic design strength, the following base shear coefficient (C_B) is appropriate.

$$C_B = 0.45 - 0.6 \qquad T_f \leqq 1.0 \text{ sec.}$$

$$C_B = \frac{0.45 - 0.6}{T_f} + (\text{Effect of Sloshing}) \qquad T_f > 1.0 \text{ sec.}$$

ACKNOWLEDGMENT

This research was supported by the National Science Fund of the Japanese Government supplied by the Science Technology Agency. This research program was carried out by the following committee members;

M. Watabe[2], H. Akiyama[3], Y. Kitagawa[2], H. Murata[2], H. Suzuki[3], Y. Fukazawa[3]

The help extended to us by the staff of the large-scale shake table in Tsukuba is gratefully acknowledge.

---

[2]International Institute of Seismology and Earthquake Engineering

[3]University of Tokyo

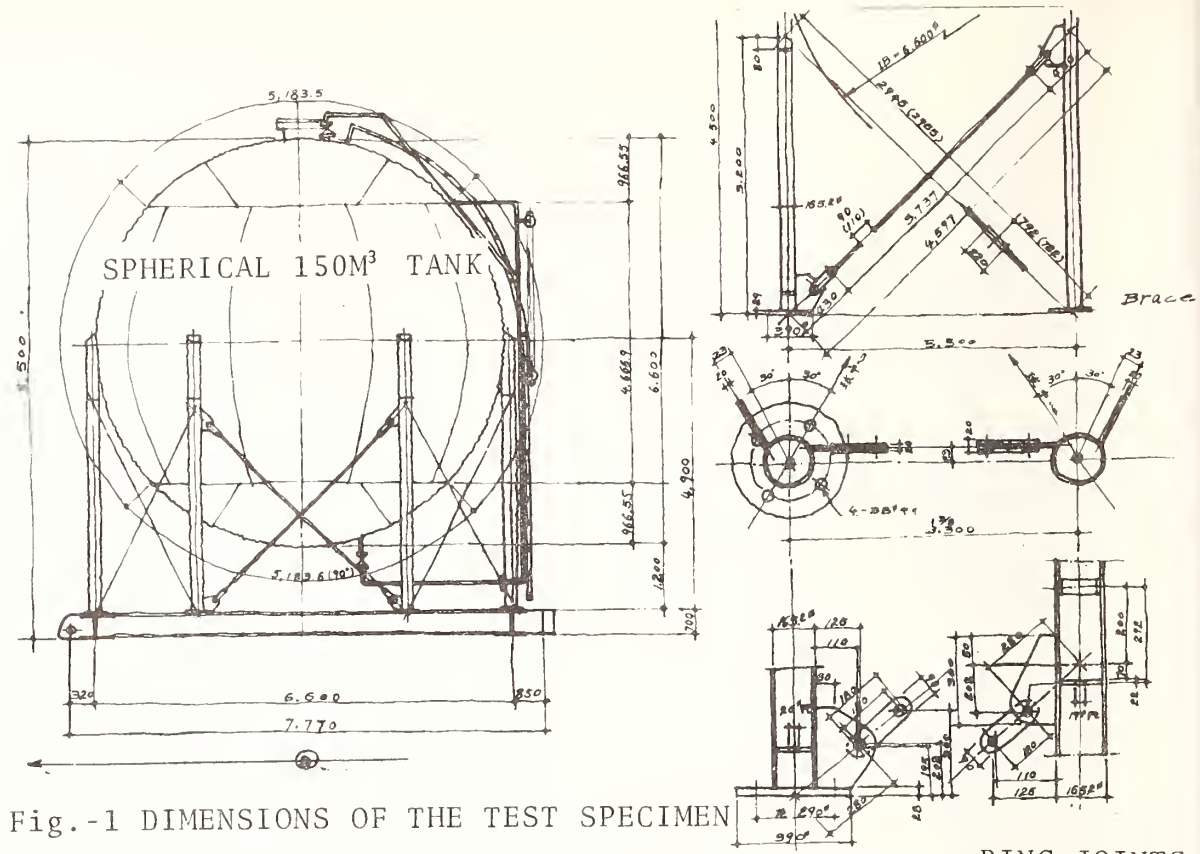

Fig.-1 DIMENSIONS OF THE TEST SPECIMEN

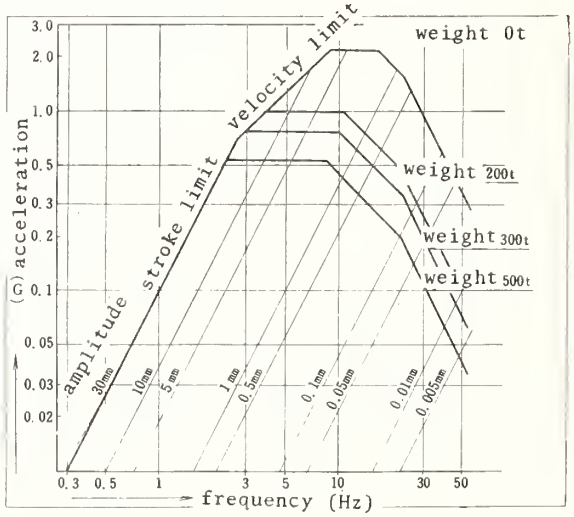

Fig.-2 THE CAPACITY OF THE SHAKING TABLE

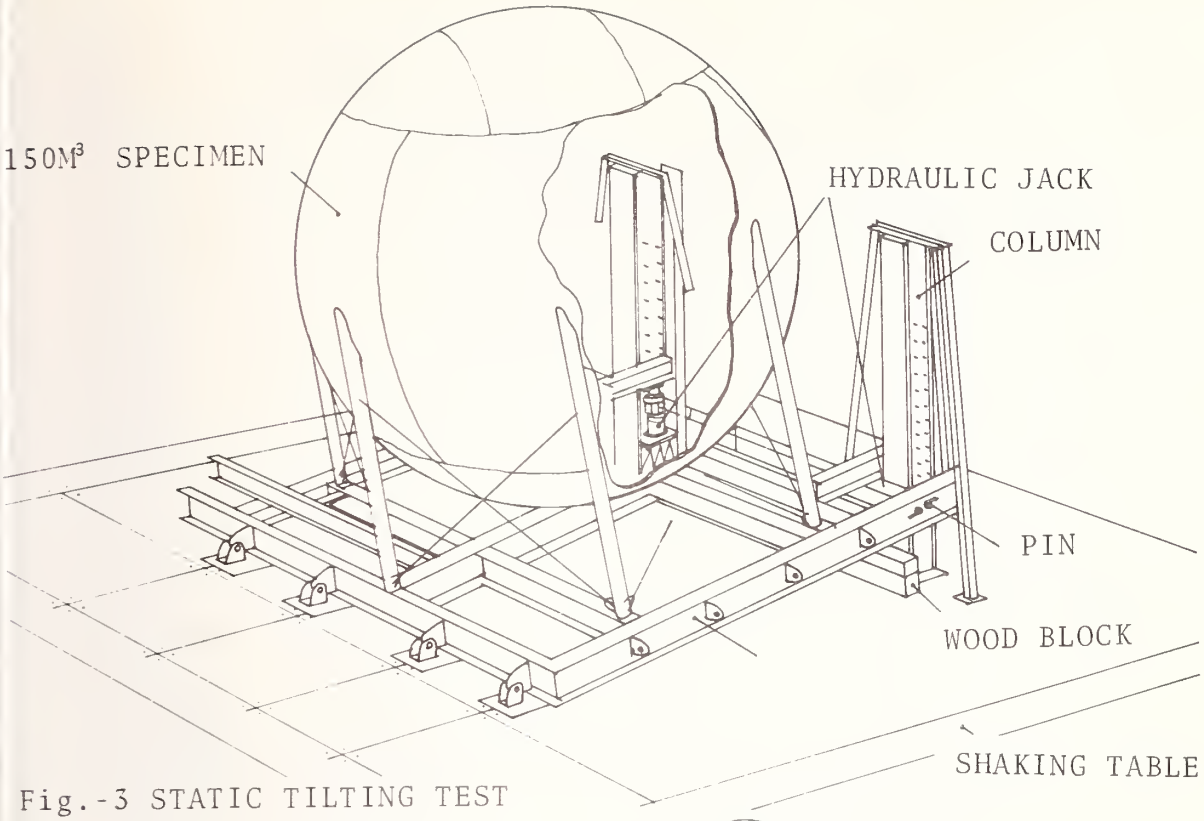

Fig.-3 STATIC TILTING TEST

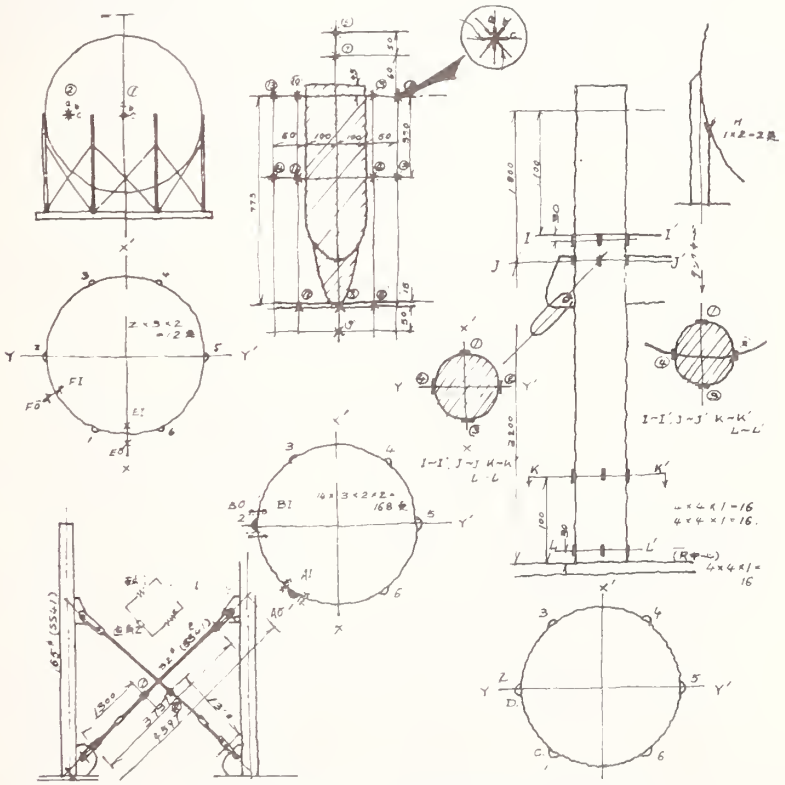

Fig.-4 LOCATION OF STRAIN GAGES

Fig-5

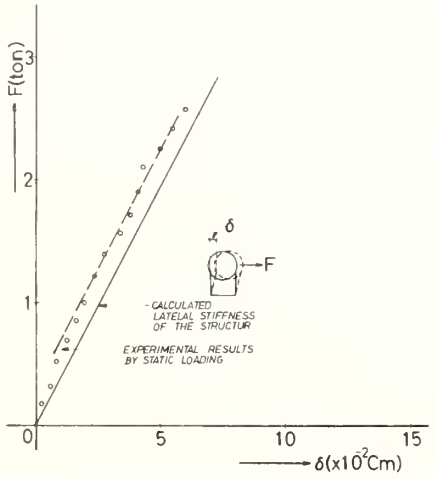

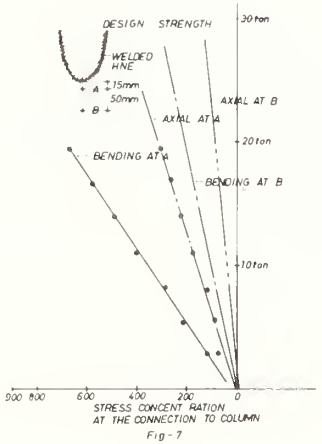

Fig-7

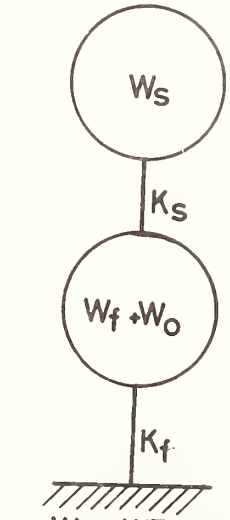

Wo =WEIGHT OF TANK
SIMPLIFIED MODEL

Fig-8

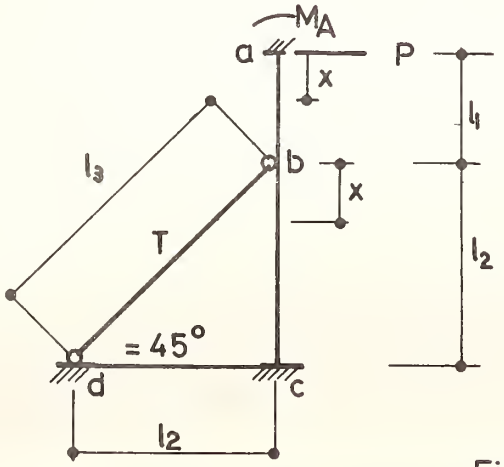

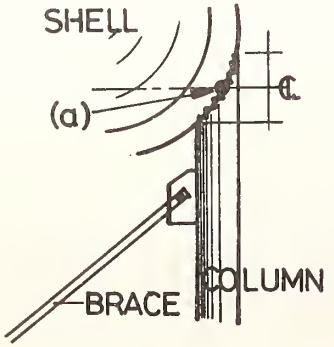

$l_1 = 91.2$ cm
$l_2 = 330.0$ cm
$l_3 = 467.0$ cm

Fig-6

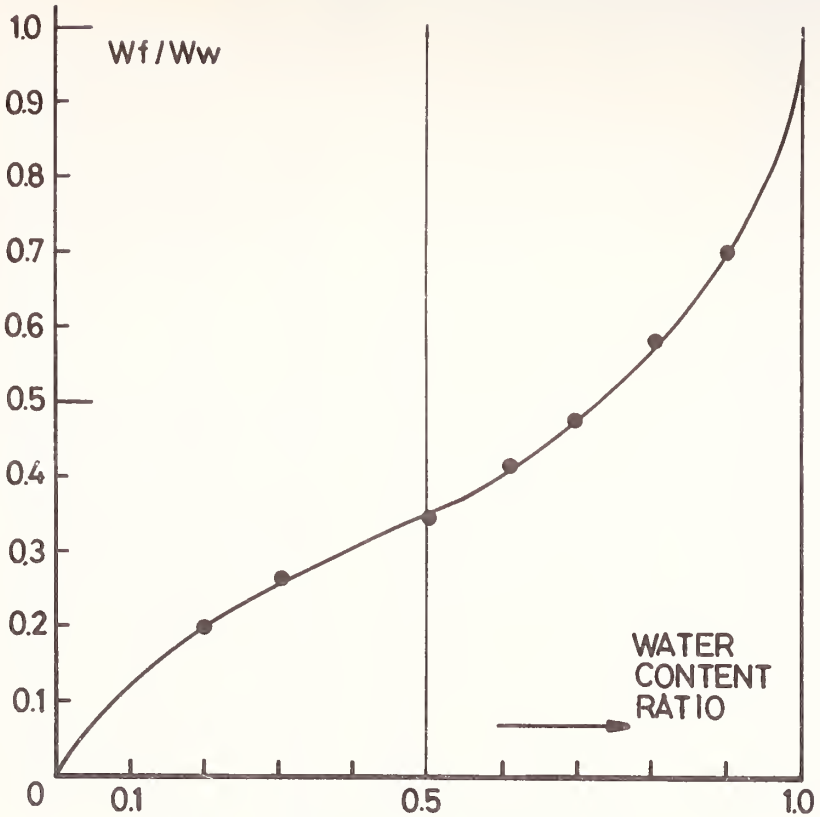

Fig-9 Wf/Ww VS. WATER CONTENT

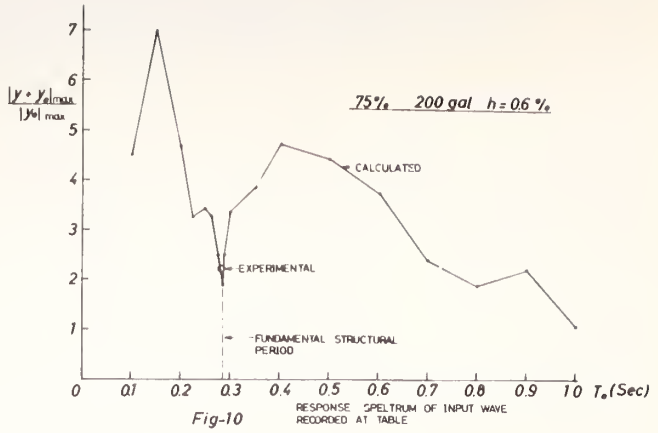

Fig-10

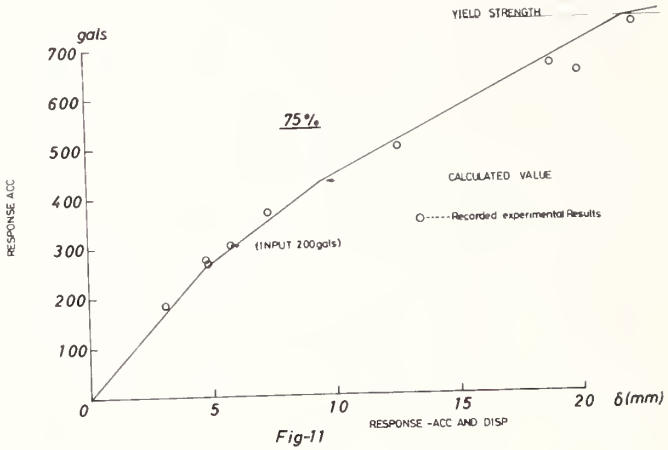

Fig-11

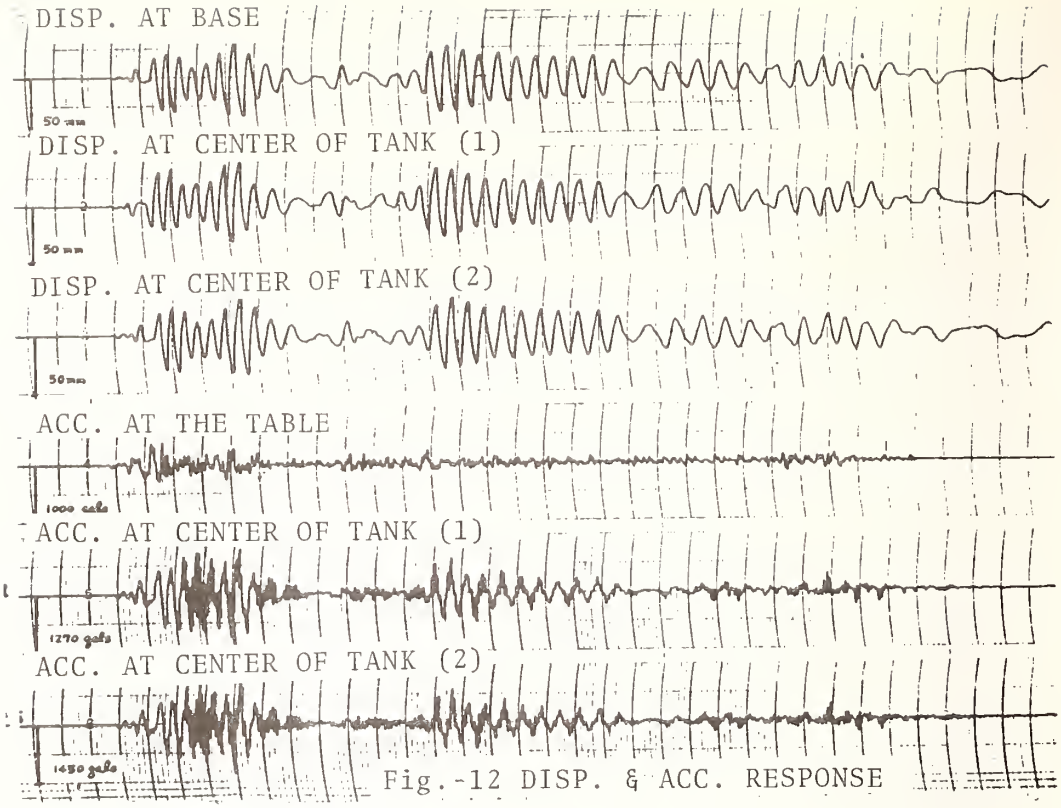

Fig.-12 DISP. & ACC. RESPONSE

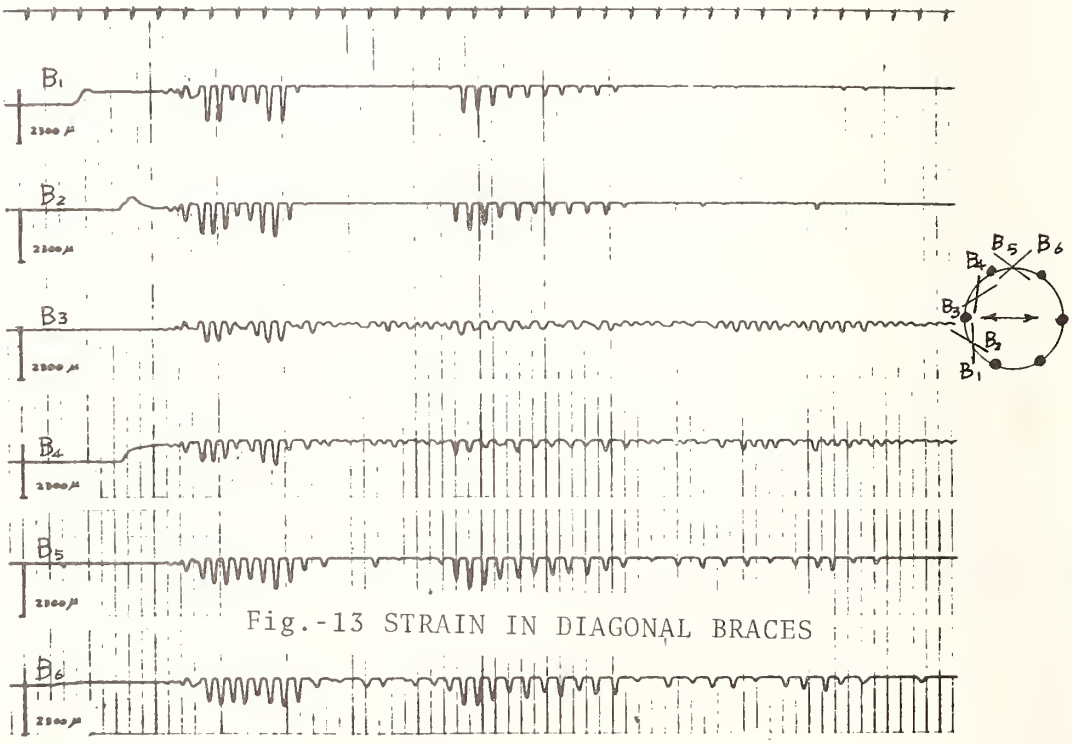

Fig.-13 STRAIN IN DIAGONAL BRACES

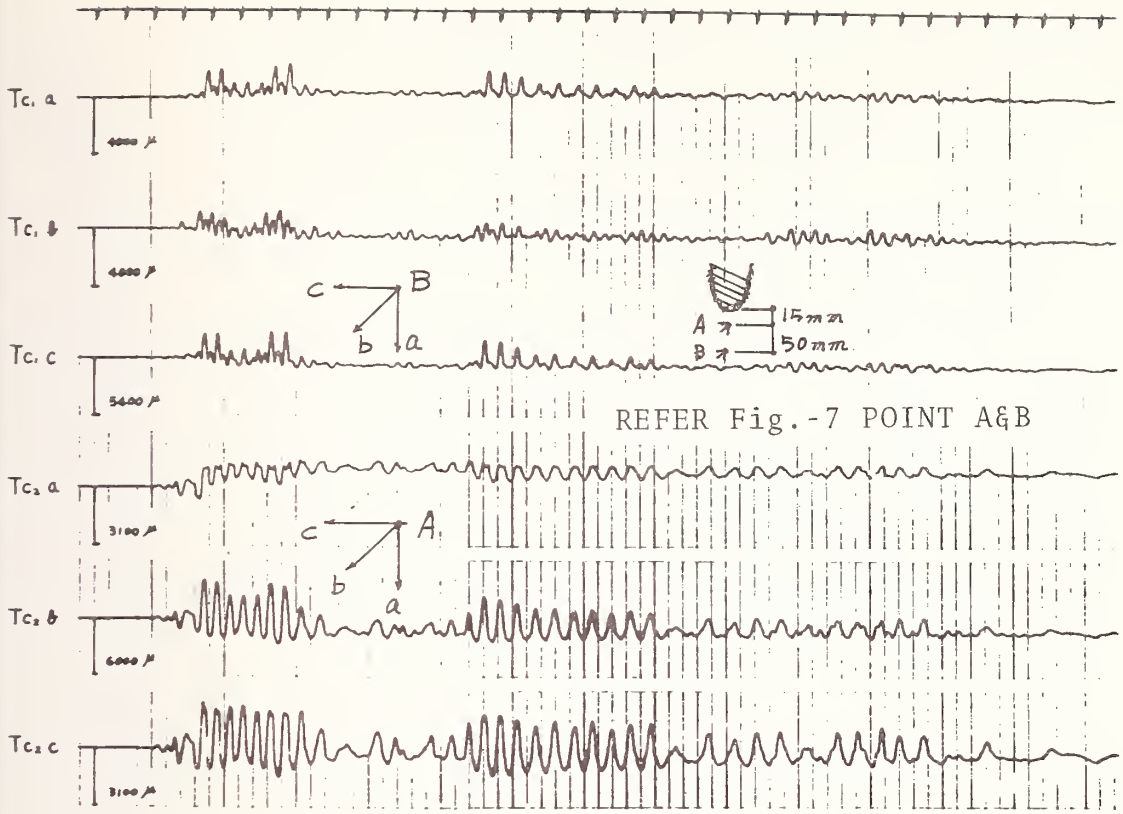

Fig.-14 STRAIN AT COLUMN CONNEC.

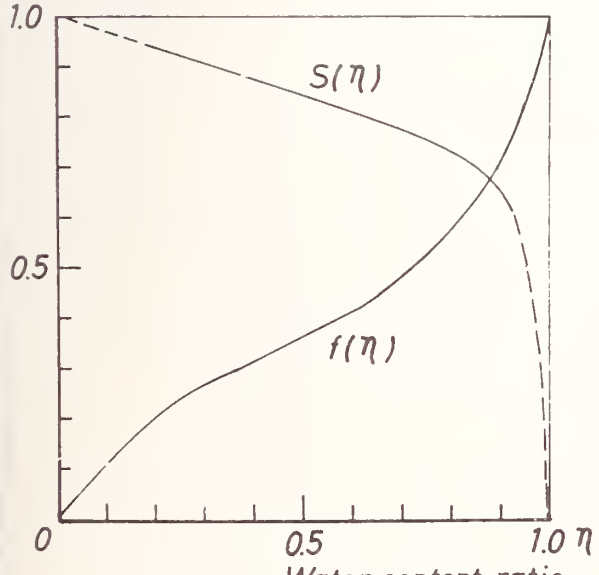

sloshing Ts

$Ts = 0.134\sqrt{D}\, S(\eta)$

$f(\eta) = Wf / Ww$

Ww : Total weight of water

Wf : Fixed water

Free water ratio : $1 - f(\eta)$

$Ws = [1 - f(\eta)]Ww$

Fig-15 Function $S(\eta)$ and $f(\eta)$

Table 1

WATER CONT.	FREE VIBRATION		HARMONIC EXCITATION			
	PERIOD T_f	FRACTION OFDAMPING	PERIOD T_f	FRACTION OF DAMPING	PERIOD T_f	FRACTION OF DAMPING
0%	0.103 sec.	0.6%	0.104 sec.	2.0%	0	———
20%	0.103	0.7	0.131	2.0	3.35 sec.	0.045
30%	0.150	0.7	0.155	3.0	3.15	———
40%	0.165	0.6	———	——	3.05	———
50%	0.190	0.6	0.197	2.5	2.95	———
60%	0.215	0.6	0.228	2.5	2.80	———
70%	0.244	0.4	0.252	2.7	2.65	———
80%	0.280	0.7	0.296	2.7	2.50	———
90%	0.308	0.8	0.336	2.7	2.20	———
100%	0.370	0.5	0.415	2.0	———	———

RESEARCH ON MINIMIZING EARTHQUAKE STRUCTURAL DAMAGE TO SINGLE-FAMILY DWELLINGS

by

William J. Werner, P.E.

Office of Policy Development and Research
Department of Housing and Urban Development

This paper discusses proposed research work to be carried out by the Applied Technology Council of the Structural Engineers Association of California under the sponsorship of the Department of Housing and Urban Development. The objective of the project is to develop a manual of recommended construction practice for earthquake resistive dwellings, for use primarily by builders, building officials, field inspectors, plan checkers, and designers.

The manual is intended to explain the structural behavior of single-family dwellings and townhouses subjected to forces produced by earthquake shocks, illustrate the HUD Minimum Property Standards, building code earthquake requirements and sound practical construction methods and details for the reduction of single family dwelling damage. The paper discusses the need for this research, the various tasks the contractor will perform, and the final products expected to be achieved by the research program.

Key Words: Building codes; construction practices; damage; earthquake; houses; residential dwelling.

Historically, there has been a great deal of interest on the part of the engineering profession in investigating the damage to buildings and other structures as a result of seismic activity. In the United States, as in other countries, disaster teams composed of qualified experts in the field are among the first people at the site following an earthquake or similar disaster. This activity has even been expanded into international cooperation whereby disasters which occur any place in the world are thoroughly investigated.

The results of these investigations can be found in detailed reports which identify the many types of failures which have occurred and, in greater or lesser degree, offer recommendations for prevention of the types of failure observed in the future. The incorporation of these recommendations by professional engineers into buildings for which they have design responsibility, even though perhaps not incorporated into building codes and standards, is by virtue of the professionalism of the engineer as a matter of good engineering practice. This is not always the case in those types of buildings which may not have a professional engineer or architect in responsible charge of the design. This class of building is usually the single family house. It is because of this situation that the Department of Housing and Urban Development has initiated a research program into the area of the reduction and/or prevention of the types of failures observed in single family housing in past earthquakes.

Among the many reports of the effect of past earthquakes, one of the most significant was a study on the performance of single family dwellings in the San Fernando Earthquake of February 9, 1971. This study found that the total financial losses to single family dwellings in the San Fernando area were larger than the financial losses to any other building category in the private sector. Wood frame dwellings generally had increasing damage in the following order: one-story, two-story, and split level. The primary cause of the overall damage to the buildings was attributed to the lack of adequate lateral bracing. The types of dwelling components with the higher damage values were the exterior wall finish, the interior wall finish on the exterior wall, and the interior partition finish. The increase in damageability progresses from the non-brittle finished materials (plywood) to the more brittle materials (stucco, gypsum lath, and plaster, etc.).

In order to attack this problem, the Department of Housing and Urban Development has engaged the services of the Applied Technology Council, which is a nonprofit corporation established in October 1971 by the Structural Engineers Association of California. ATC will embark on a research project, the objective of which will be to develop a manual of recommended construction practices for earthquake resistive single family residential buildings for the use primarily of builders, building officials, field inspectors, plan checkers, and designers. The manual will explain the structural behavior of single family dwellings subjected to forces produced by earthquake shocks, illustrate the Departmental Minimum Property Standards and Building Code Requirements, and further illustrate sound practical construction methods and details for the reduction of structural damage due to earthquakes. The manual will illustrate recommended construction details, architectural layouts, types of construction recommended or to be avoided, and methods of installing mechanical equipment to resist seismic forces. It is intended that the manual be self-explanatory for rapid and clear understanding of the material contained therein.

Several resource documents illustrating single family house failures due to earthquakes will be used by ATC in performing this project which is anticipated to take approximately twelve months for completion. ATC will perform the project in a series of well-defined tasks including: a review of existing damage literature, a review of the HUD/FHA MPS and earthquake code requirements, development of construction details including supplimentary engineering analysis and an educational slide presentation to builder organizations and related groups.

Of primary importance to the UJNR panel on wind and seismic effects is Task 3, which is the development of construction details. ATC will develop typical engineering drawings, illustrations, and details for residential dwellings which are required to resist forces from earthquakes with appropriate descriptions and explanations so that the full intent

of the construction detail may be easily understood by a builder. The construction details will be presented in such a manner that analytical calculations by the user of the manual will not be necessary in order to fabricate the detail. If necessary, such details will be categorized by the earthquake zones in the United States, i.e., 1, 2, or 3. However, it will be required that the details be substantiated by calculations to the extent necessary for the engineering justification of the integrity of the design to resist seismic forces. Typical details will be illustrated for the various types of construction most commonly used in the United States for residential dwellings in seismically active areas including: wood frame with wood siding, wood frame and brick veneer, wood frame and stucco, brick or block masonry, steel and/or aluminum frame with siding and/or masonry veneer and other prevalent conventional combinations of framing materials and building components. Included also will be construction details for basement and slab foundations, the structure of the dwelling, installation of utilities and mechanical equipment, chimneys and fireplaces, attached garages and other architectural and structural components which affect the strength, rigidity, and stability of the dwellings.

In order that this data can be effectively transmitted into the hands of the ultimate users, a slide presentation accompanied by appropriate text material and voice tape will be used to explain the contents of the manual to user groups, such as builders, building officials, and designers. The presentation will be self-explanatory so that it may be presented to the organizations without the need of experts for extensive interpretation. Prior to extensive national exposure, presentations will be made by ATC to home builder organizations, designers, and building officials in Los Angeles, San Francisco, Portland, Oregon, and Seattle, Washington. After these sessions, the slide presentation will be revised as necessary based upon the questions raised by the audience and the appropriate answers which develop from the discussions. The revisions will be such that the presentation becomes self-explanatory so that it may be presented by others without further explanation being required.

While this paper has only dealt with our on-going research activity, the results of which are not yet available, it was felt that it would be of interest to this body in terms of a knowledge of the type of activity which is being sponsored by the Department of Housing and Urban Development in the area of disaster mitigation and loss control. At the next meeting of the U.S.-Japan Panel on Wind and Seismic Effects, we will make available the final reports of this research and present the audio visual program for your further information.

EARTHQUAKE ENGINEERING RESEARCH SUPPORTED BY THE NATIONAL SCIENCE FOUNDATION

by

Charles C. Thiel
Program Manager, Earthquake Engineering
Research Applications Directorate (RANN)
National Science Foundation

A summary of earthquake engineering research work conducted by various researchers throughout the United States under the sponsorship of the National Science Foundation is presented.

Key Words: Earthquake engineering; grant; RANN; sponsorship; structural engineering.

INTRODUCTION

Numerous recent publications attest to the seriousness of the hazard presented by earthquakes to peoples and economies, both of the United States and of the world (e.g., Refs. 1-6). Thus Chapter F (1) asserts, "Earthquakes, of all the natural disasters in this country, can inflict the greatest loss of life and property. Studies have concluded that a repetition of the 1906 San Francisco earthquake could cause billions of dollars of damage, with the potential loss of thousands of lives. They are the most difficult disaster phenomenon to prepare for." Reference 2 reinforces these conclusions by forecasting some $21 billion in earthquake losses for the state of California alone, the period being 1970-2000, under the assumption of no "improvement of existing policies and practices."

The 1969 National Academy of Engineering report (3) has served as a useful basis for recent RANN planning. Its introduction deserves to be quoted at length: "Earthquakes devastate cities, with heavy loss of life, several times each year. A recent example is the Khorasan, Iran, earthquake of September 1, 1968, with over 10,000 lives lost. The United States has been shaken many times by large earthquakes, for example, 1964 Alaska; 1959 Hebgen Lake, Montana; 1949 Seattle, Washington; 1906 San Francisco, California; 1886 Charleston, South Carolina; 1857 Fort Tejon, California; 1811-1812 New Madrid, Missouri; 1755 Cape Ann, Massachusetts. The history of destructive shocks in the United States is very short compared to other seismic regions such as Japan, the Middle East, and India because the country has been inhabited by urban dwellers for only a short time. The growth of population and the development of cities are so recent that it is only during the past 100 years, or so, that the potential for great earthquake destruction has existed. It is evident, however, from past occurrence of earthquakes that the highly seismic regions of the country have a serious earthquake problem, and even the less seismic regions in the central and eastern parts of the country have an earthquake problem which, although less urgent, should not be ignored."

"Public welfare, in many parts of the country, depends on facing the following questions: What intensity of ground shaking may occur? How will existing buildings respond to the ground shaking? How should new buildings and other works of man be constructed so as to minimize earthquake hazards?"

To illustrate the nation's life risk to earthquakes (and infer its property risk), the following table lists the population at varying risk:

Seismic Risk	U.S. Total	California
Zone 0 (Low)	16.1 M (8%)	0
1	115.1 M (57%)	0
2	40.5 M (20%)	2.6 M
3 (High)	30.9 M (15%)	17.3 M

Zone 0 corresponds to no earthquake damage expected; Zone 1 - minor damage expected; Zone 2 - moderate damage expected; Zone 3 - major damage expected. Thus 35% of the U.S. population (71.4 M) are in risk zones 2 and 3, of which 28% are in California. The extent of development in different regions of the country has led to the conclusion that there will be as much damage to residential type structures in the next 200 years east of the Rocky Mountains as west of the Rockies. The destructive potential posed by earthquakes is indeed a national concern.

Within the United States, Earthquake Engineering is a young field. The great San Francisco Earthquake of 1906 has generally been credited with awakening the nation to the disaster potential of the occurrence of quakes in its urban centers. The primary scientific consequence of the 1906 event was the identification and development of seismology as a research area. It was not until the Santa Barbara earthquake of 1925, however, that serious attention became focused on research into seismic design. Prior to this event, the prevailing attitude was that if adequate information were made available to the designer about the phenomenon, he could cope with it directly. The 1933 Long Beach earthquake established earthquake engineering as a legitimate academic and professional research

pursuit and forced the inclusion of earthquake considerations in the building codes of California, and eventually elsewhere.

From NSF's beginning in 1950 to the Great Prince William Sound Alaskan Earthquake of 1964, the Foundation's commitment to the support of earthquake engineering research was limited to a few awards. The Alaskan quake caused extensive damage to modern structures. It caused the NSF to assess its commitment to fund research in the field of engineering. The Engineering Mechanics Program, following this assessment, identified Earthquake Engineering Research as a focused activity within its general disciplinary support of Civil and Mechanical Engineering Research.

One of the new program's first steps was to have a comprehensive report on the state of knowledge and research needs prepared (3). A national conference was held to exchange ongoing research information and establish priorities. The Universities Council on Earthquake Engineering Reserach (UCEER) was formed as a consequence of the latter activity. It acts as a forum for the exchange of ideas in the university community and as a focus for coordination of research.

The first focused program expenditures were in FY 1966. For the next four years, the Mechanics Program maintained an award level of approximately one million dollars annually (see Figure 1). During this period, a major emphasis was placed on developing a research community capable of achieving substantial forward strides in the 1970's. Awards were made to a number of institutions and principal investigators.

The San Fernando Earthquake of February 9, 1971, furnished a major impetus in committing the NSF to vigorous support of Earthquake Engineering Research. About this time, the Foundation initiated its Research Applications Directorate (RANN Program) and included the Earthquake Engineering Program as part of its activities. From its inception to the creation of RANN, Dr. M.P. Gaus was in charge of the Earthquake Engineering Program. Subsequently, the program has been under the direction of Dr. Charles C. Thiel.

The program has grown since becoming a part of RANN from a base level of $2.5 million in FY 1971 to a level of $8.0 million in FY 1974. The program has assumed extensive new research responsibilities during this period. In 1972, major efforts in utilization (Data Base, Information Dissemination, and Technology Transfer) were initiated. In 1973, the basic program was augmented by initiating research in the area of System Response. In 1974, the areas of Implementation Studies and Policy Studies were added to make the program more comprehensive. (See Section 3 for details). Between 1966-1974, the program has made awards to over 100 principal investigators at over 35 institutions. Not listed in these proceedings are the details of the awards during the past three years. Currently, about 65 grants and contracts are active. Although awards have been primarily to universities, we are beginning to use the resources of professional societies, governmental units, and profit making organizations. Subsequent sections describe the specific objectives of the NSF program.

GENERAL PROGRAM OBJECTIVES

The occurrence of an earthquake, or any other natural event, is important only insofar as it affects man and his works. It is the disaster potential of earthquakes that has caused man individually and collectively to seek adjustments to his physical and social environment that decrease his vulnerability. The measurement of vulnerability is related to the potential or realized loss of life (and injury), property damage, and/or disruption of function. While each individual or group will apply a different normative combination of these measures in its decisions, the general objective remains to control the sequences of the event.

As adjustments, one may seek either to change the phenomenon or to alter the response of man and his works to the phenomenon. Possible physical adjustments the decision maker may seek are to:

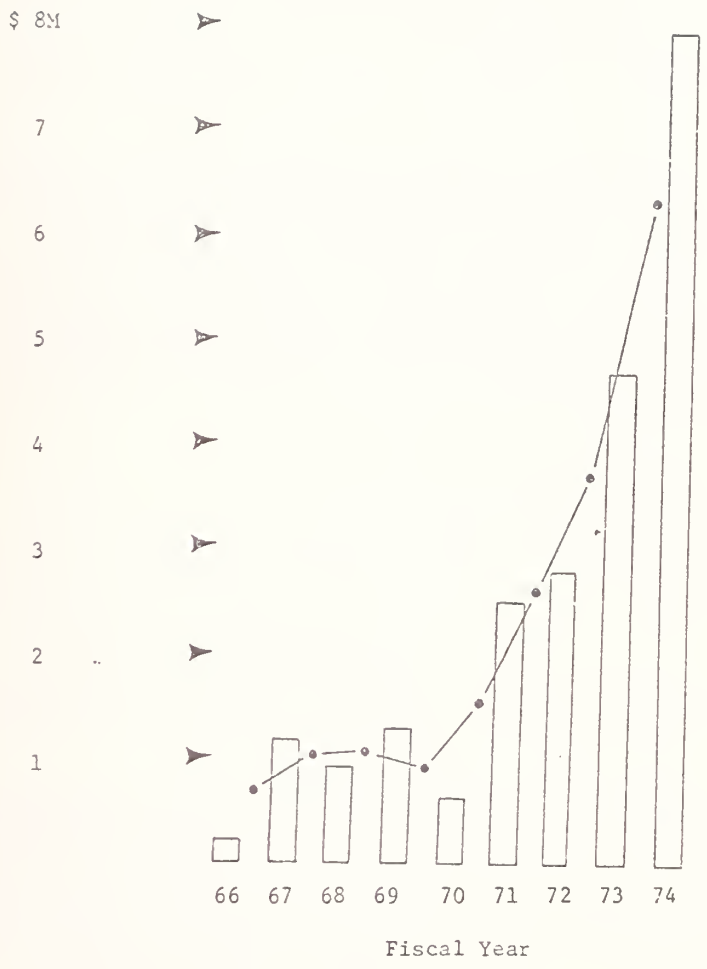

Figure 1 - Earthquake Engineering Program Expenditures, 1966-1974 with center two year moving average

Control the event by prevention or modification of the event

Anticipate the event so that remedial actions may be taken

Identify the seismic potential of areas

Construct facilities so as to perform acceptably during and after the event

Among the possible social adjustments, the decision maker may seek to:

Plan for the warning, response, and recovery to the event

Distribute economic risk

Generate and select alternative physical development plans

Adopt and enforce zoning, construction, and management standards

Clearly the physical and social adjustments depend critically on each other. It must be remembered that adjustments to earthquakes are not made *in vacuo*; there are other considerations in making decisions regarding vulnerability reduction.

Noting the responsibilities of other Federal agencies to develop techniques for earthquake prediction and control (USGS) and noting the types of adjustments given above, four general objectives have been identified to fulfill the overall program objective. The latter is stated first.

RANN Earthquake Program Objective

To develop methods that allow decision makers to control the consequences of earthquake occurrences.

In furtherance thereof, the RANN Program supports research projects leading to:

A.	Design	Development of economically feasible design and construction methods for building earthquake resistant structures of all types.
B.	Land Use	Development of procedures for integrating information on seismic risk with on-going land use planning processes.
C.	Social	Development of an improved understanding of social and economic consequences of individual and community decisions on earthquake related issues.
D.	Implementation	Presentation of program results in forms usable by the affected interest communities to control their vulnerability to earthquakes.

SPECIFIC OBJECTIVES AND PROGRAM ELEMENTS

In order systematically to structure a program over a period of years aimed at achieving the four general objectives, nine program elements have been identified. With each of these elements are associated several specific objectives, which serve as guidelines for developing that element. In the context of the present report, however, particular project descriptions are inappropriate; rather, the program elements serve as categories into which specific research activities can be divided.

It should be noted that this method of structuring earthquake engineering and related fields owes a debt to the NAE Committee report (3). The detailed program breakdown and recommendations prepared by NAE have proved very useful in structuring what follows here.

The nine elements have been framed so as to deal with specific problems in the design, analysis, and synthesis of engineering and scientific knowledge to control the consequences of earthquake, measured by life loss, property loss, and/or function loss.

I. Ground Motion/Data Services

Destructive ground motions resulting from earthquake action are of several different types, including heavy ground shaking, slow or rapid fault slip, subsidence, and landslides. Fundamental to an understanding of any of these damaging phenomena, however, is an accurate knowledge of the actual earthquake ground motion. Fundamental to the validation of structural design and analysis procedures is the actual structural response generated by the ground motion.

The measurement of destructive ground motions in the epicentral region of large earthquakes and the associated response of structures is achieved by placing a network of instruments at a variety of sites where earthquakes are likely to occur. These instruments include both passive and active recording devices. The strong motion accelerograph records the time history of acceleration in three component directions. It begins recording after an acceleration threshold has been exceeded. These instruments are the most generally used and find applications in most types of data gathering. Other active recording systems include pore pressure gauges to measure the liquid pressure in saturated soils, earth pressure gauges to measure the inertial effects of soils usually on a foundation wall, strain gauges, and displacement meters. Among the passive instruments are the seismoscope, a conic pendulum that records motion on a smoked glass, scratch strain gauges and extensometers.

The measurements obtained are directed at achieving three principal objectives:

A. To support the research program by measuring pertinent quantitities to validate, calibrate, and/or formulate theories of earthquake response.

B. To support the designer's need for earthquake motion information at varying geological and seismological sites.

C. To obtain a comprehensive data base to perform microregionalization of earthquake risk areas based on events in the area.

These objectives are both research and operational program related. During FY 1973, NSF assumed responsibility for the Seismological Field Survey. SFS is the principal focus for strong motion instrument networks. Using SFS as its principal agent, the RANN Program will: develop criteria for placing an optimal strong motion recording network; begin the placement of this network by new installations and adjustments to the existing network; develop and place specialized instrument networks to answer specific research needs, e.g., down hole soil response arrays, detailed structure response; develop a qualified products list of existent instrumentation, define characteristics for new instrumentation, and ensure steady improvement of instrument quality, sensitivity, and reliability.

II. Soils Response and Analysis

One of the greatest potential sources of property loss is damage to structures that rest on soils or on foundations which, although adequate to support the structures under ordinary circumstances, might fail during an earthquake. A great potential for life loss resides in the possibility of a dam failure. The following areas represent forms of soil failure under consideration by the program: settlement of cohesionless soils; bearing capacity failure; embankment failure; soil liquefaction; and waterfront bulkhead failures, etc.

The dynamic behavior of a structure during an earthquake depends on the shaking transmitted to it by the surrounding soil. These motions are imparted to the structure through the interaction between its foundation and the supporting soil and/or bedrock and include amplification effects.

The objectives of this element are to:

A. Develop methods to evaluate and control soil failure potentials.

B. Develop analysis and design methods to evaluate and control soil amplification.

C. Develop design and analysis methods to characterize the loadings transmitted to structures through soil-foundation interaction.

III. Structural Response and Analysis

The realization of a structure rests on two complementary activities: analysis, and synthesis and design. Analysis forms the basis for design. The ability to analyze a hypothetical structure and determine the stresses and displacements that would be produced by a specified loading is an essential part of the design process. The more accurately this can be done, the more efficient and economical can be the design and the more reliable the design factor of safety. The analysis of a structure can be exceedingly difficult, first, since ordinary structures are exceedingly complex dynamic systems; second, because the ground motions which the structure will be subjected to during its lifetime are probabilistic; and third, because the construction process leads to a structure which is not precisely known. The analysis of structural response requires knowledge of the full system, including foundations, adjacent soils, and in some cases the properties of adjacent structures.

The objectives for this program element are to:

A. Determine appropriate models for element (e.g., beam, column, plate, etc.) response to strong motion excitation from analytic and experimental studies.

B. Develop digital computer methods of analysis that predict earthquake response of structural systems comparable in complexity to real structures.

C. Validate and calibrate these models by comparison with earthquake measured motions and damage of structural system and elements.

The basic problem of earthquake design is to synthesize the structural configuration; the size, shape, and materials of the structural elements; and the methods of fabrication, so that the structure will safely and economically withstand the action of earthquake ground motions. The object of design is to control the effects of an earthquake on a structure and keep damage within acceptable bounds. A further series of objectives has been determined for this element:

D. Determine the dynamic properties of structures, elements, and materials under conditions of large strains, beyond the yield point and up to failure.

E. Develop reliable, practical, and simplified methods of earthquake design for widely used and special important structures: e.g., low-rise residential, low-rise commercial, school houses, high-rise buildings, dams, bridges, and industrial structures.

F. Thoroughly study structures that failed during an earthquake, as well as those that did not fail, to refine design principles.

G. Develop design and analysis methods for nonstructural elements and mechanical components of structures.

IV. Systems Response

Previous elements of the research program have dealt almost exclusively with localized structures, that is, a single building, dam, etc. The operation of the community during the emergency and recovery periods is dependent on the functioning of utility and public service facilities that function as a system with elements located at many sites in the affected area. The failure of an element can cause the total system to malfunction or be inoperative. Thus the design of system elements must consider the seismic characteristic requirements of the extended system. Both physically connected and non-connected systems are to be investigated. An example of a connected system is fire water distribution (storage, pumping stations, water mains, etc.) while a non-connected system is represented by emergency health care facilities (hospitals, clinics, laboratories, etc.).

The objectives of the element are to:

A. Develop principles of planning and laying out facilities for minimum disruption of operations due to earthquake ground displacements.

B. Develop design procedures for special structures and equipment of each type of utility and public service facility. Among these, ranked in approximate priority order, are:*

1. Fire fighting and emergency transportation
2. Emergency power and communications
3. Hospitals and emergency agencies
4. General communications
5. Water services and sewage disposal
6. Electrical power and natural gas or fuel supplies
7. General transportation facilities

C. Evaluate existing methods of land-use control, such as microzonation, that will allow a community to control its earthquake vulnerability.

V. Coastal and Inland Waterways

An earthquake at sea may generate a tsunami, or tidal wave, that presents a real danger to coastal and island regions of the U.S. The risk posed by tsunamis may best be controlled by land use regulation in vulnerable areas. Verification of the occurrence of a tsunami permits the evacuation of potential affected areas.

If a dam fails, an inundation wave may be generated when the reservoir empties. This wave can cause serious downstream damage. Structuring downstream land use, with this potentiality in mind, can reduce life and property loss. When a reservoir behind a dam is filled, a series of earthquakes often occurs in the vicinity of the impoundment. The incremental risk these quakes cause above the natural risk is at present uncertain.

The objectives of this element are to:

A. Develop methods to verify that an ocean-based earthquake has generated a tsunami.

*Note that nuclear power plants and related facilities, which would otherwise head such a list, are a responsibility of the Atomic Energy Commission.

B. Develop methods to anticipate tsunami run-up in coastal regions.

C. Develop methods to anticipate downstream inundation levels.

D. Determine the incremental seismic risk associated with filling a reservoir and the degree that this risk should be part of the design criteria for the dam.

VI. Technology Transfer

Within the Earthquake Engineering Program, utilization activities have been centralized and formulated as a specific program thrust, to be conducted by a core series of awards rather than distributed as a component in each individual award.

The objectives in this element are to:

A. Maintain a technical reference collection of published reports and papers and unpublished data available to researchers and professionals; to provide for information dissemination.

B. Maintain a software center to archive, document, validate, and distribute computer programs developed for earthquake engineering applications.

C. Consolidate the best knowledge regarding design and analytic methods from current and completed research and professional experience in codes, criteria, and standards for use by professionals and regulatory bodies.

D. Conduct regular conferences and workshops to act as foci for dialogues between the research and professional communities.

E. Conduct post earthquake inspections to obtain engineering data and to identify unfulfilled research needs.

VII. Other

This category includes conference travel, general conference support, advisory committee meetings, program planning, and other activities that do not fit conveniently under one of the above classifications.

VIII. Implementation Studies

Advances in civil engineering methods are implemented through two types of actions: individual professional application; and adoption by regulatory/enforcement agency. The latter process is primarily political, while the former is educational. The structuring of the flow of technological developments from research to implementation is a particularly arduous one, involving a vast complex of institutions, special interest groups, and secondary agendas. The way in which this process works is not well understood. An understanding of the process is a first step in structuring a methodology to foreshorten the period from research to practice.

The objectives of this program element are to:

A. Develop an understanding of the implementation process.

B. Develop a methodology to program the education of professionals, using suitable aids, to the best earthquake engineering practice.

C. Develop a strategy of program results to be processed through the community into regulatory and enforcement agency regulations in a timely fashion.

D. Advocate the accomplishment by public and private groups of the developed plan.

The accomplishment of these goals will have far reaching implications on several RANN programs. Indeed, the incorporation of earthquake engineering reserach results is but a small part of the problem of moving technical innovations into building practices. The same basic methodology is applicable to fire safety, energy conservation, building utilities, and novel energy systems such as solar heating and cooling. The program element is beyond the single interests of the Earthquake Engineering Program and, as such, will be considered within the context of the building sciences.

IX. Social and Behavioral Studies

The mitigation of earthquake effects may depend on a variety of actions not directly associated with the assurance of safe structures. The possibilities of earthquake control (or modification) and prediction present different technical methods that may lead to mitigation. Community actions during and following the event may significantly affect the consequences of the quake. Condemnation and redevelopment attitutdes, insurance programs, and economic assistance may markedly affect the communities' vulnerability to future events. With a view to filling important gaps in our understanding of earthquakes as they impact man and his social environment, research in the social and behavioral sciences, and in economics, will be undertaken to:

A. Develop policy alternatives for the community to provide emergency rescue, recovery, and redevelopment services.

B. Develop policy alternatives for the dissermination of earthquake warnings.

C. Assess the consequences of technical developments and policy alternatives on the achievement of disaster mitigation.

SPECIFIC RESEARCH PROGRAMS

The National Science Foundation has supported a wide spectrum of research on earthquake hazard reduction. Rather than detail the specific character of these projects, Appendix A presents the titles, performer, and institution for each project initiated in the past three years.

Two recent projects warrant specific highlighting.

These have as their objective the development of improved earthquake design criteria, standards, and codes. The first of these projects is a test of the practical design feasibility of new code procedures and assumptions, plus an evaluation of the economic consequences of such a "new code."

The project has four chief objectives:

Draft a set of design rules based on a "design spectrum" type of code;

Apply these rules to the redesign of several types of existing buildings in order to evaluate their applicability by example;

Make a preliminary assessment, as part of a literature survey, of methods by which such a code could include consideration of variations in regional seismicity, proximity of known active faults, and soil amplification and topographic effects of local site conditions; and,

Make a preliminary evaluation of the economic and performance effects of such proposed changes on the example buildings.

The work statement of this project divides the accomplishment of the above objectives into two separate phases. Phase I covers the establishment of the design rules and the effect-evaluation procedures. The application of the rules, the literature survey, and the actual evaluation of economic and performance effects will be achieved in Phase II. Fortunately, some of the existing buildings to be studied have been subjected to special studies as a result of the 1971 San Fernando earthquake. These special studies will prove useful in the Phase II evaluation of the Phase I design rules.

In this study, the lateral force resistance systems of eleven existing buildings (see Table 1) of varying structural types and heights are to be redesigned for the effects of a dual-earthquake criterion: Specifically, a damaged threshold spectrum, and a collapse threshold spectrum. Current applicable portions of the 1973 Uniform Building Code and the SEAOC Code are to be employed, with the exception that earthquake loading and related deformations are to be computed by the use of the dual spectra. Damping and ductility values have been assigned which are considered to be within certain assumed capabilities of each type of structure being studied. Each of the eleven buildings contains a valid lateral force resisting system within the K-factor categories of the current SEAOC Code. Each is reasonably regular in plan and elevation, therefore, the problems of torsional racking, setback response, and soft-story effects will not be significant in the analyses of these particular buildings. (These problems are recognized as important, however.) The project is nearing completion.

The second project builds upon the first. It is just beginning and will not be completed until late 1975. The objective, simply stated, is to develop a new set of provisions for the SEAOC Lateral Force Requirements. The current criteria are based on the technology of the 1950's with minor updating in subsequent revisions. This study entails carrying out a comprehensive program of updating and revising the present SEAOC seismic requirements so that it will be applicable throughout the United States based upon the latest state-of-the-art of earthquake engineering and construction practices. The format of the seismic provisions will be augmented to include provisions for other natural meteorologically caused phenomena such as hurricanes, tornadoes, and wind storms. The format will follow existing building codes so that it can be codified, adopted, and promulgated by various groups writing and implementing code provisions. The new seismic provisions will be comprehensive and written with a national perspective. Provisions concerning the code will include all aspects of building and applicable geotechnical practices for mitigation of losses from earthquakes and earthquake related geologic hazards. The specifications will be based on goals and objectives developed from a performance criteria to be clearly set forth in the provisions so that appropriate regulatory bodies can recognize the level of risk associated with the various code provisions. It will be a balanced statement with proper consideration of low-rise (one to three stories), intermediate-rise (four to six stories), and high-rise (over six stories) as well as other nonbuilding type structures. Provisions for nonengineered buildings and engineered buildings will be included. Recognition will be given for different construction practices and different use of materials throughout the United States. The provisions will be stated in simple terms to the fullest extent possible consistent with the goals of the code, the state-of-the-art and practice to produce these objectives, and the complexities of the earthquake phenomenon. The provisions will set forth the loading criteria and performance (resistance) criteria with recommended methods of design and analysis consistent with the seismicity of the site, the importance of the structure, the type of construction, and height of the structure.

It will include where feasible, provisions for considering, within the framework of earthquake engineering, various facets such as architectural configurations, contract documents, construction team, quality control, supervision and inspection as well as structural analysis and design.

It will be comprehensive in scope and will be developed after consideration of many provisions not included or adequately covered in the present seismic codes. Evaluation of the state of the knowledge, art and practice relating to each provision will be used to make recommendations for their inclusion in the code. Among such elements are the following:

TABLE 1

BUILDINGS TO BE REDESIGNED IN THE SEISMIC CODE EVALUATION STUDY

Building 1	Five stories plus basement Ductile reinforced concrete frame
Building 2	Nineteen stories plus four levels basement parking Steel frame, moment resistant in one direction, Braced in the other direction
Building 3	Ten stories Semi-ductile reinforced concrete frame in one direction, Shear wall in the other direction
Building 4	Fourteen stories Shear walls on both major axes of building
Building 5	Six stories Shear walls are non-load bearing
Building 6	Two stories Steel frame with vertical bracing system
Building 7	Two stories Concrete block masonry, bearing and shear walls
Building 8	Nine stories Reinforced concrete, shear wall
Building 9	One story Tilt-up, plywood diaphragm, re-entrant corner
Building 10	Two-story school Moment resistant steel frame
Building 11	One-story school Brick masonry, plywood diaphragm

1. Goals for structural and non-structural damage.

2. Post-earthquake factors, importance factors, and other socio-economic considerations.

3. Various loading and analysis methodologies and when they should be used: equivalent static force approach, elastic single degree of freedom and multidegreee of freedom modal superposition response spectral analysis, elastic and inelastic time history response analysis and deterministic and probabilistic rock and ground motions.

4. Seismicity, probability consideration of various design earthquakes, seismic risk, and seismic zone concepts.

5. Design earthquake criteria based on dual performance for the moderate design earthquake and the severe design earthquake based on maximum credible earthquake.

6. Geologic, topographic, soil and other site condition influences on ground motion.

7. Basic realistic levels of ground motion to represent the design earthquake at a site of average exposure having no unusual soil conditions.

8. Influence of soil conditions on intensity of ground shaking in terms of displacement, velocity, and acceleration.

9. Soil structure interaction, including influence of the structure on the ground motion and the influence of ground motion on the structural response.

10. Structural system damping, ductility and stability including P-delta effects.

11. Relative performance criteria of structural systems and materials with particular attention to brittle material behavior and elasto-plastic response.

12. Realistic deterministic ultimate design stresses, load factors, and resistance factors for all materials.

13. Specific criteria to be used for dynamic analysis and design.

14. Drift limitations consistent with realistic response to strong earthquakes.

15. Vertical acceleration criteria.

16. Shear wall frame interaction provisions.

17. Hazardous and earthquake damaged buildings and their rehabilitation and reconstruction.

18. Seismic design requirements for mechanical, electrical elevator and other building "life-safety" systems.

REFERENCES

1. Office of Emergency Preparedness, Executive Office of the President, Disaster Preparedness, 3 Vols. Report to the Congress, January 1972, U.S. Govt. Printing Office, Washington, D.C., 1972.

2. Alfors, J.T., J.L. Burnett, and T.E. Gay, Jr., Urban Geology, Master Plan for California, Bulletin 198, California Division of Mines and Geology, Sacramento, 1973.

3. National Academy of Engineering Committee on Earthquake Engineering Research, Earthquake Engineering Research, published by NAS, Washington, D.C., 1969.

4. Seismology: Responsibilities and Requirements of a Growing Science, Parts I and II, National Academy of Sciences, 1969.

5. Federal Council of Science and Technology, Office of Science and Technology, Executive Office of the President, Proposal for a Ten-Year National Earthquake Hazards Program, U.S. Govt. Printing Office, Washington, D.C., 1966.

6. Office of Science and Technology, Executive Office of the President, Earthquake Prediction, a Proposal for a Ten-Year Program of Research, U.S. Govt. Printing Office, Washington, D.C., 1964.

Appendix A which lists NSF earthquake engineering awards in 1972-1974 is not included herein. The list may be obtained from the author.

THE WIND ENGINEERING PROGRAM

by

M.P. Gaus
Head, Engineering Mechanics Section
National Science Foundation
Washington, D.C. 20550

A summary of wind engineering research work conducted by various researchers under the sponsorship of the National Science Foundation is presented.

Key Words: Research programs; sponsorship; wind engineering.

WIND ENGINEERING

Wind engineering is concerned with the interaction between wind and either engineered facilities or natural systems which are located in the boundary layer of the atmosphere or roughly from ground surface to as much as 800 meters in elevation. It is precisely in this boundary layer where the average citizen conducts his daily affairs, where we construct most of our facilities, and discharge the gaseous effluent of our modern technological society. From an engineering viewpoint this boundary layer is virgin territory with a dearth of utilizable information for design or solution of problems. Unfortunately, little assistance is obtained from meteorological studies which tend to concentrate on higher elevations.

The Wind Engineering Program presently identifies needed research studies in sixteen categories. Some of these are oriented toward generating or collecting the basic information required for the development of wind design, analysis, and simulation methods. Others are oriented toward providing general information of use to practitioners and for improvement of codes and regulations and in planning procedures. The remainder are oriented toward economic and people problems which are an important component of engineering problems. At the present time, research is or has been supported which related to about twelve of the categories. At the present level of activity, however, the amount of effort in a number of these categories is rather token.

Shortly after the Wind Engineering Program was proposed, a series of intense tornadoes converged on the city of Lubbock, Texas, causing extreme damage to the city. Within hours after the tornado struck a combined team of engineers and meteorologists was dispatched to collect perishable information. This was followed up through grants to Texas Tech University and the Institute for Storm Research, University of St. Thomas to reconstruct from this information details of the wind and pressure differential loads and missile effects caused by the tornado. The resulting information, published in several reports, has provided for the first time a factual and reliable base of information regarding the actual effects of an intense tornado from an engineering viewpoint. The results indicate that the wind velocities which must be used in design are only about 1/2 to 1/3 of those which had been claimed by meteorologists and make tornado resistant design feasible for many structures. Other tornado studies in progress include an experimental program at Catholic University in which special vortex tunnels are being used to measure pressure distributions, forces, and moments on various types of buildings as on intense vortex passes; a study at the Los Alamos Scientific Laboratory to develop numerical analysis of tornado wind loads related to various flow variables; a study at Tulane University on prester tornadoes; and a study at George Washington University which is looking into the relationship between different terrain conditions and the wind loadings of ground structures inside intense tornadoes.

Another wind problem concerns the failure of glass, shingles, cladding, or isolated components due to wind. The yearly damage due to such effects is quite widespread and substantial, but is perhaps most dramatically illustrated by the much publicized difficulties of the new John Hancock Mutual Life Insurance Company Building in Boston, Massachusetts. Although wind tunnel studies were made in the design stage for this building, they clearly were not adequate. Instrumentation has been installed in the John Hancock Building by a group from MIT under an NSF grant, with heavy financial participation by the Hancock Insurance Company, to take advantage of this unfortunate situation. This information along with other analytical and experimental studies will probably be instrumental in revising the building regulations in Boston and other cities.

Clearly, wind tunnel testing is required to gain a better understanding of boundary layer aerodynamics and for predicting various effects before construction takes place. A comprehensive program is being conducted at Colorado State University utilizing special long-fetch adjustable roof wind tunnels for simulating natural winds. Problems to be examined include local flow phenomena, local wind pressures and heat transfer rates on building surfaces, dynamic excitation by buffeting, wind speed and gustiness at the pedestrian level and circulation of air pollutants. Although the CSU facilities are currently the best available in the U.S., there are still unresolved questions regarding the scale and

distribution of turbulence, simulation of gustiness, and the validity of the extreme scaling from present wind tunnel sizes to full-scale structures. The latter problem can only be resolved by comparing wind tunnel tests to full-scale observations. The first problem is being studied at Notre Dame University where a feasibility study is being carried out for a large multipurpose boundary layer wind tunnel using an active rather than passive turbulence generation process.

Also of great concern are the environmental wind conditions around buildings. Through grants to Illinois Institute of Technology and Catholic University, studies are in progress on the microclimate of buildings and urban areas. These studies directly relate to pedestrian comfort, concentration of pollutants between buildings or in depressed roadways, and to buffeting and missile problems.

Space does not premit descriptions of other studies in progress on windwave effects, development of new wind instrumentation for field observation, motion perception and tolerance, etc.

Studies just started or scheduled for future action include the instrumentation of full-scale buildings, cooling towers, and other structures to obtain actual measurements of wind effects. These full-scale measurements will be compared to very thorough wind tunnel studies modeling the structures and terrain. Comparisons will be made to determine the accuracy of wind tunnel determinations of wind characteristics, wind loadings, dynamic response, interaction between wind and energy consumption in buildings, performance of cooling towers, effect of wakes, and environmental effects. At the same time, computer software for wind engineering analysis is under further development so that both the tools and supporting data can be made available to practicing engineers.

Also being started are studies of storm-surge and coastal effects in hurricanes and other strong wind storms.

Both industry and state and local governments are being encouraged to participate in the funding of Wind Engineering research programs. Substantial progress has been made in this respect.

In order to coordinate wind research activity and to disseminate information as rapidly as possible, two actions have been taken. The first is the provision of funding for a Wind Engineering Research Council which will serve as a focal point to coordinate university-industry-government wind research, to organize workshops in specific research areas, and to serve as a contact point for information on wind engineering problems. The second is the provision of funding to prepare a wind engineering research digest which will provide up-to-date information on wind research in progress.

The discription of the various grants allocated during July 1973 to June 1974 are not included herein, but may be obtained from the author.

PRELIMINARY REPORT ON PRESENT STATUS AND DEVELOPMENT PROJECT OF VOLCANOLOGICAL OBSERVATION AND RESEARCH IN INDONESIA

by

Akira Suwa
Head, Seismological and Volcanological Laboratory
Meteorological Research Institute
Japan Meteorological Agency
Tokyo, Japan

Indonesia has about 130 active volcanoes and their eruptions are characterized by dangerous violent explosions, nuee ardente, and volcanic mud-flows. The Geological Survey of Indonesia (GSI), Ministry of Mines, has, therefore, been carrying out observations and surveillances of volcanic activities throughout the country.

The Government of Japan, in response to a request from the Government of Indonesia, has decided to give assistance in this field of science in the framework of the Colombo Plan.* The Overseas Technical Cooperation Agency (OTCA), the executing agency for the Government of Japan, has, therefore, dispatched a preliminary survey mission, headed by the author of this report, Akira Suwa, of the Japan Meteorological Agency to Indonesia in 1972.

The mission stayed in Java and Bali from November 22 to December 23, 1972, and visited the Ministry of Mines at Djakarta, the GSI at Bandung, and eight active volcanoes (eleven observatories) in order to study the possible scope of cooperation in Volcanology between Japan and Indonesia. The mission recognized two serious problems in Indonesia: deficiency of experts in volcanology, and shortage of up-to-date volcanological instruments.

Therefore, the recommendation by the preliminary survey mission to both governments was as follows:

1. Dispatch for several years the following Japanese experts to Indonesia;

    a. Instrumental seismologist
    b. Volcano physicist
    c. Volcanological geologist/petrologist

2. Train junior volcanologists of the GSI in Japan.

3. Provide Indonesia with the following instruments;

    a. Seismographs for permanent and temporary observations
    b. Instruments for petrological and mineralogical laboratory

Key Words: Field observation; Indonesia; Japan; technical aid; volcanos.

*Colombo Plan for Technical Cooperation in South and Southeast Asia

OBJECTIVE OF THE JAPANESE PRELIMINARY SURVEY MISSION ON VOLCANOLOGY TO INDONESIA UNDER THE COLOMBO PLAN

The Government of the Republic of Indonesia requested the Government of Japan to provide technical assistance in order to develop a program on volcanological works for the Geological Survey of Indonesia (GSI). (GSI) also asked that a detachment be sent on a preliminary survey mission, which was headed by Akira Suwa, writer of this report. The Overseas Technical Cooperation Agency (OTCA), which is an executing agency of the Government of Japan, sent the preliminary survey mission on volcanology to Indonesia under the Colombo Plan in November, 1972.

The main objectives of the mission were as follows:

1. To investigate the status of Indonesian active volcanoes, the type of volcanological observations, and speak with the officer of GSI.

2. To discuss the problems of such cooperation with the Indonesian authorities.

MEMBERS OF THE PRELIMINARY SURVEY MISSION

(Chief) Mr. Akira Suwa
Head, Seismological and Volcanological Laboratory
Meteorological Research Institute (MRI)
Japan Meteorological Agency (JMA)

(Member) Mr. Masaaki Seino
Seismologist, Seismological Division
Observation Department, JMA

(Member) Mr. Yoshihiro Sawada
Volcanologist, Seismological Division
Observation Department, JMA

ITINERARY OF THE MISSION (NOVEMBER 22 - DECEMBER 23, 1972)

The preliminary survey mission, which stayed in Indonesia for about one month, visited the following offices, observatories, and active volcanoes:

Ministry of Mines at Djakarta

Geological Survey of Indonesia at Bandung

Volcano Tangkuban Prahu and Tangkuban Prahu Volcano Observatory

Volcano Papandajan

Volcano Dieng and Karang Tengah Volcano Observatory

Merapi Central Observatory at Jogjakarta

Volcano Merapi (Central Java) and Babadan Volcano Observatory, Ngepos Volcano Observatory, Selo Volcano Observatory, and Jrakah Volcano Observatory

Volcano Kelud (Crater Lake) and Maragomulyo Volcano Observatory

Volcano Semeru and Argosko Volcano Observatory and Vudakeling Volcano Observatory

Volcano Batur

Volcano Krakatau seen from the west coast of Java Island

Embassy of Japan at Djakarta

Djakarta Office of the OTCA

The itinerary of the mission is as follows:

November	22	(Wednesday)	Tokyo-Hongkong-Singapore-Djakarta.
	23	(Thursday)	Djakarta-Bandung. Visit the GSI.
	24	(Friday)	Visit the Geological Survey of Indonesia.
	25	(Saturday)	Ditto.
	26	(Sunday)	Visit Volcano Tangkuban Prahu and its Observatory.
	27	(Monday)	Visit Volcano Papandajan.
	28	(Tuesday)	Bandung-Jogkakarta.
	29	(Wednesday)	Visit Merapi Central Observatory at Jogjakarta.
	30	(Thursday)	Visit Volcano Dieng and Karang Tehgah Observatory.
December	1	(Friday)	Visit Merapi Central Observatory at Jogjakarta.
	2	(Saturday)	Visit Volcano Merapi. Babadan and Ngepos Observatories
	3	(Sunday)	Visit Volcano Merapi. Selo and Jrakah Observatories
	4	(Monday)	Jogjakarta-Maragomulyo.
	5	(Tuesday)	Visit Volcano Kelud and Maragomulyo Observatory.
	6	(Wednesday)	Maragomulyo-Malang.
	7	(Thursday)	Malang-Volcano Semeru and Argosko Observatory - Djember.
	8	(Friday)	Djember - the Straits of Bali - Denpasar.
	9	(Saturday)	Visit Volcano Agung. Rendang and Budakeling Observatories.
	10	(Sunday)	Visit Volcano Batur.
	11	(Monday)	Denpasar-Jogjakarta.
	12	(Tuesday)	Jogjakarta-Bandung.
	13	(Wednesday)	Visit the Geological Survey of Indonesia.
	14	(Thursday)	Ditto.
	15	(Friday)	Ditto.
	16	(Saturday)	Ditto.
	17	(Sunday)	Bandung-Djakarta.
	18	(Monday)	Visit the Embassy of Japan and OTCA Office at Djakarta.

December 19	(Tuesday)	Write the tentative report of the mission.
20	(Wednesday)	Visit the Embassy of Japan and OTCA Office at Djakarta.
21	(Thursday)	Visit the Ministry of Mines at Djakarta.
22	(Friday)	Visit the west coast of Java Island to see Volcano Krakatau.
23	(Saturday)	Djakarta-Singapore-Hongkong-Tokyo.

VOLCANIC ACTIVITIES IN INDONESIA

The Indonesian archipelago has about 130 active volcanoes, including solfatara fields (ca. 15% of the total of those in the world), as is shown in Figure 1 and Table 1. These volcanoes have provided the people with various kinds of natural resources and beautiful scenery. In general, Indonesia volcanic areas are high in altitude and are densely populated, because the archipelago is located in the torrid zone and the air temperature at the seaside areas is very high all the year round.

Consequently, eruptions of these volcanoes can cause serious loss of human life and property. To make the matters worse, eruptions of the Indonesian volcanoes are characterized by extremely dangerous phenomena, such as catastrophic explosion, nuee ardente (glowing avalanche), and volcanic mud-flow (the so-called "lahar" in Indonesian language). As an example, twelve of twenty most disastrous eruptions* on the earth have taken place in this country, as shown in Table 2. Lahar is divided into two categories: "eruption lahar" and "rainfall lahar". Both types occur frequently at the various volcanoes in Indonesia.

THE OBSERVATION AND SURVEILLANCE OF VOLCANIC ACTIVITIES BY THE GEOLOGICAL SURVEY OF INDONESIA

Before the World War II, the Dutch Government tried to conduct volcanological observations and research and thus mitigate volcanic disasters in this territory. Since their declaration of independence in 1945, the Government of Indonesia has been making similar efforts to develop volcanic research capabilities. The Geological Survey of Indonesia, which belongs to the Ministry of Mines, is in charge of the observation and surveillance of volcanic activities all over the country.

The Volcanological Division of the (GSI) at Bandung, which has sixty members, consists of two sections, and has two teams concerned with special research projects, as shown in Figure 2. The Volcanological Division also has a branch station "Merapi Central Observatory" (the center for volcanological observation and research of Mt. Merapi) at Jogjakarta and 25 volcano observatories at sixteen active volcanoes on nine islands. (see Table 3.) These observatories are manned by a total of sixty members.

Mr. D. Hadikusumo, Head of the Volcanological Division, and Mr. I. Surjo, scientist in charge of the Project for Volcanic Debris Control, came to Japan in 1957 for one year to study volcanology under Prof. T. Minakami of Tokyo University, and the author of this report, at the Japan Meteorological Agency. Many of the other leading members of the Volcanological Division also studied volcanology in Japan during recent years. However, many members working in the volcano observatories have little schooling although they are diligent and faithful workers.

The Volcanological Observation Section not only manages all the volcano observatories, but also conducts temporary observation at various volcanoes (periodical and urgent observations). The Volcanological Research Section is also conducting research on the mitigation of volcanic disasters, and at present the section is primarily engaged in the zoning

of the dangerous area of each volcano, according to three grades of eruption, which are: (see Figure 6 a, b, c, d.)

1. Permanently Off-Limit Zones: Dangerous even in case of minor eruptions, everyone should be outside zone.

2. First Dangerous Zone: Dangerous in case of big eruptions.

3. Second Dangerous Zone: Apt to be attacked by volcanic mud-flows.

At present, there are many inhabitants even in the Permanently Off-Limit Zones, at such active volcanoes as Merapi, Kelud, Semeru, Agung, etc. It is actually very difficult for the authorities to evacuate this zone in the near future.

For instance, Volcano Merapi has about 30,000 inhabitants in the Permanently Off-Limit Zone and a total of 200,000 inhabitants within the three dangerous zones.

Warnings issued by volcano observatories are sent to the inhabitants through the local governments. Warnings and information on the actual state of Volcano Merapi are usually issued by the Merapi Central Observatory. Additional information is also obtained by observatories. However, in case there is an occurrence of an extremely dangerous phenomena, such as nuee ardente and volcanic mud-flow, each observatory warns the public directly by using an alarm-bell or siren. Warnings regarding the occurrence of the so-called rainfall lahar are issued depending on the amount of precipitation (usually over 60 mm/hour).

At Volcano Kelud, the famous tunnels made in 1928 by the Dutch Government as a preventive measure against overflow of the crater-lake water were devastated by mud-flows in 1951 and 1966. They were rehabilitated by the Ministry of Public Works of the Indonesian Government during 1966-68. The Ministry of Public Words has also constructed dams to prevent a mud-flow disaster at some volcanoes, including Mt. Kelud. The Project Team for Volcanic Debris Control of the (GSI) is cooperating closely with the Ministry of Public Works in the above-mentioned works.

FINDINGS AND CONCLUSIONS

All the members of the Preliminary Survey Mission were deeply impressed with the persistent efforts of the Government of Indonesia to prevent various kinds of volcanic disasters. They also admire the adequate and rational orgainzation of volcanological work at the Geological Survey of Indonesia.

However, the Preliminary Survey Mission recognizes the following serious problems:

1) Deficiency of experts in volcanology

The (GSI) has many volcanological observers throughout the country and has many junior volcanologists, however, there are very few senior volcanologists. Indonesia has a few well-trained specialists in the following fields:

(a) Experts in instrumentation on seismographs.

(b) Experts in analyses of the results of volcanological observations.

(c) Experts in petrology with special reference to lahar (volcanic mud-flow).

2) Shortage of up-to-date volcanological instruments.

In order to elucidate the mechanism of underground volcanic activities, various kinds of instrumental observations should be performed. However, at present, even the

seismological observation, which is indispensable in the surveillance of volcanic activities, there are only a few in operation at several active volcanoes. These seismographs are mostly mosaics of parts produced by various companies in various countries in different years. Therefore, it is impossible not only to determine the parameters or characters of volcanic earthquakes, but also to detect most of the minor shocks.

Due to the above-mentioned findings, the Preliminary Survey Mission concludes that the following cooperation between Japan and Indonesia should be carried out as follows:

1) Dispatch the following three Japanese experts to Indonesia for several years:

   a. Instrumental seismologist

   b. Volcano physicist - specialist in analyses of the results of volcanological observation.

   c. Volcanological petrologist - specialist in petrology with special reference to nuee ardante and lahar.

2) Conduct training of these junior volcanologists of the (GSI) at the International Institute of Seismology and Earthquake Engineering (IISEE) in Tokyo.

3) Donate the following volcanological instruments to Indonesia:

   a. Seismographs for permanent and temporary observations.

      As the situation in volcano observatories of the (GSI) is lacking in commercial electric supply, mechanical recording seismographs are recommended. The seismographs should be provided with spare parts.

   b. Instruments for petrological laboratory.

All of the members of the Preliminary Survey Mission will make every effort to realize the above-mentioned cooperation between Japan and Indonesia in the near future. Item 2 is presently in progress.

Table 1. List of the Active Volcanoes of Indonesia including Solfatara Fields (After the Geological Survey of Indonesia)

No.	Name of Volcano	Altitude (m)	Class	No.	Name of Volcano	Altitude (m)	Class
1	PULU WEH	584	+	34	PERBAKTI	1699	+
2	SILAWAIH AGAM	1726	o	35	SALAK	221	o
3	PEUETSAGDE	2780	•	36	GEDEH	2958	•
4	BUR NI GEUREUDONG	2590	+	37	PATUHA	2434	o
5	BUR NI TELONG	2624	•	38	WAJANG WINDU	2181	o
6	GAJOLESTEN	1500	+	39	TANGKUBAN PRAHU	2084	•
7	SIBAJAK	2212	o	40	PAPANDAJAN	2665	•
8	SINABUNG	2460	o	41	KAWAH MANUK	1950	+
9	PUSUK BUKIT	1981	o	42	KAWAH KAMODJANG	1640-1730	+
10	HELATOBA-TARUTUNG	500-1100	+	43	GUNTUR	2249	•
11	BUAL BUALI	1819	+	44	GALUNGGUNG	2168	•
12	SORIKMARAPI	2145	•	45	TELAGA BODAS	2201	o
13	TALAKMAU	2912	o	46	KAWAH KARAHA	1125-1155	+
14	MERAPI	2891	•	47	TJERIMAI	3078	•
15	TANDIKAT	2438	•	48	SLAMET	3432	•
16	TALANG	2896	•	49	BUTAK PETARANGAN	2222	•
17	KERINTJI	3800	•	50	DIÉNG	2565	•
18	SUMBING	2508	o	51	SUNDORO	3151	•
19	KUNJIT	2151	o	52	SUMBING	3371	o
20	BLERANG BERITI	1958	o	53	UNGARAN	2050	o
21	BUKIT DAUN	2467	o	54	MERBABU	3145	o
22	KABA	1952	•	55	MERAPI	2911	•
23	DEMPO	3173	•	56	LAWU	3265	o
24	BUKIT LUMUT BALAI	2055	+	57	WILIS	2563	+
25	MARGA BAJUR	400-1000	+	58	KELUD	1731	•
26	SEKINTJAU BELIRANG	1719	o	59	ARDJUNO-WELIRANG	3339	o
27	BEMATANG BATA	c.a. 1000	+	60	SEMERU	3676	•
28	HULUBELU	1040	+	61	BROMO	2329	•
29	RADJABASA	1281	o	62	LAMONGAN	1669	•
30	KRAKATAU	813	•	63	IJANG-ARGAPURA	3088	o
31	PULOSARI	1346	o	64	RAUNG	3332	•
32	KARANG	1778	o	65	KAWAH IDJEN	2386	•
33	KIARABERES GAGAK	1511	+	66	BATUR	1717	•

Classification of Active Volcanoes:

• Volcanoes with recorded eruptions (1600 A.D.-present)

o Volcanoes in fumarolic stage, no eruptions known (1600 A.D.-present)

+ Solfatara or fumarole fields

No.	Name of Volcano	Altitude (m)	Class	No.	Name of Volcano	Altitude (m)	Class
67	AGUNG	3142	●	99	NILA	781	●
68	RINDJANI	3726	●	100	SERUA	641	●
69	TAMBORA	2851	●	101	MANUK	282	o
70	SANGEANG API	1949	●	102	BANDA API	658	●
71	WAI SANO	903	+	103	UNA UNA	508	●
72	POTJOK LEOK	1675	+	104	AMBANG	1795	o
73	INERI	2245	o	105	SOPUTAN	1784	●
74	INIE LIKA	1559	●	106	SEMPU	1549	o
75	AMBUROMBU	2124	●	107	BATU KOLOK	890	+
	PUI (8° 51'S, 121° 39'E)	371	?	108	TEMPANG	900	+
76	IJA	637	●	109	TAMPUSU	1180	+
77	SUKARIA	1500	+	110	LAHENDONG	780-988	+
78	NDETU NAPU	750	+	111	SARANGSONG	760-770	+
79	KELI MUTU	1640	●	112	LOKON-EMPUNG	1580	●
80	PALUWEH	875	●	113	MAHAWU	1331	●
81	EGON	1703	o	114	KLABAT	1995	o
82	ILI MUDA	1100	o	115	TONGKOKO	1149	●
83	LEWOTOBI LAKILAKI	1584	●	116	RUANG	714	o
84	LEWOTOBI PERAMPUAN	1703	●	117	API SIAU	1748	●
85	LEROBOLENG	1117	●	118	BANUA WUHU	12	●
86	RIANG KOTANG	200	+	119	AWU	1320	●
87	ILI BOLENG	1659	●	120	SUBMARINE VOLCANO		●
88	LEWOTOLD	1319	●	121	DUKON	1087	●
89	ILI LABALEKAN	1486	o	122	MALUPANG WARIRANG	1115	●
90	ILI WERUNG	1018	●	123	IBU	1340	●
91	BATU TARA	748	●	124	GAMKONORA	1635	●
92	SIRUNG	862	●	125	TODOKO	979	o
93	YERSEY		o	126	PEAK OF TERNATE	1715	●
94	EMPEROR OF CHINA	-2850	●		MOTIR (0° 27'N, 127° 24'E)	690	?
95	NIEUWERKERK	-2285	●	127	MAKIAN	1357	●
96	GUNUNK API	282	●	128	UMSINI	2665	●
97	DAMAR	868	●				
98	TEON	655	●				

Table 2. 20 Most Disastrous Eruptions in the World from the View-Point of the Number of Victims

VOLCANO (Location)	Year	Round Number of Victims	Remarks
(1) TAMBORA (Indonesia)	1815	92,000	Including starvation (82,000).
(2) KRAKATAU (Indonesia)	1888	36,000	Mostly by eruption-tsunami.
(3) PELEE (Martinique)	1902	28,000	Nuée ardente attacked a city.
(4) VESUVIO (Italy)	1631	18,000	Violent explosion & lava-flows.
(5) ETNA (Italy)	1169	15,000	Lava-flows destroyed cities.
(6) UNZEN-DAKE (Japan)	1792	15,000	Mostly by eruption-tsunami.
(7) KELUD (Indonesia)	1586	10,000	Mostly by mud-flows (lahar)
(8) ETNA (Italy)	1669	10,000	Lava-flows destroyed cities.
(9) LAKI (Iceland)	1783	10,000	Lava-flows. Including starvation.
(10) MERAPI (Java, Indonesia)	1006	Several thousands	Mostly by pyroclastic materials.
(11) KELUD (Indonesia)	1919	5,000	Mostly by mud-flows (lahar).
(12) GALUNGGUNG (Indonesia)	1822	4,000	Mostly by mud-flows (lahar).
(13) AWU (Indonesia)	1711	3,200	Mostly by mud-flows (lahar).
(14) LAMINGTON (Papua)	1951	3,000	Mostly by nuée ardente.
(15) MERAPI (Java, Indonesia)	1672	3,000	Mostly by nuée ardente.
(16) PAPANDAJAN (Indonesia)	1772	3,000	By pyroclastic materials.
(17) AWU (Indonesia)	1856	2,800	Mostly by mud-flows (lahar).
(18) AGUNG (Indonesia)	1963	2,000	Nuée ardente & mud-flows (lahar).
(19) SOUFRIERE (St. Vincent Is.)	1902	1,600	Nuée ardente & mud-flows (lahar).
(20) AWU (Indonesia)	1892	1,500	Mud-flows (lahar) & nuée ardente.

Table 3. List of Volcano Observatories in Indonesia

Island	(No.) Volcano	Volcano observatory			
		Name of Obs. (Local name)	Distance from the crater (Km)	Seismograph (component)	Commercial electric supply
Sumatra	(14) Merapi	Kotabaru	4	Mechanical (H)	No
	(16) Talang	Batu berjangjang	9	Mechanical (H)	No
Java	(39) Tangkuban Prahu	Tangkuban Prahu	0.1	Electromagnetic (32)	No
	(55) Merapi	Babadan	4	* " (H,Z)	No
		Ngepos	10.5	No	No
		Plawangan	5	Electromagnetic (H,Z)	115V/ 50 cycle
				Mechanical (2H)	
		Deles	5	*Electromagnetic (H,Z)	No
		Selo	5	* " (H,Z)	No
		Jrakah	4.5	No	No
	(50) Dieng	Karang Tengah	1	Mechanical (2H)	No
				Electromagnetic (Z)	
	(58) Kelud	Maragomulys	6	Mechanical (H)	No
	(60) Semeru	Argosko	9	Mechanical (H)	No
		G. Sawur		No	No
		Tawonsongo	9.5	No	No
	(62) Lanongan	G. Meja		No	No
	(65) Kawah Idjen	Paltuding	3	No	No
Bali	(67) Agung	Rendang	12.5	Mechanical (2H)	No
		Budakeling	12	Mechanical (2H)	No
		Batulompeh	14.5	No	No
Sangeang	(70) Sangeang Api	Tawali	9.25	No	No
Flores	(76) Ija	Ende	5	Mechanical (2H)	No
Banda	(102) Banda Api	Colombo	2.5	Mechanical (Z)	No
Sulawesi	(113) Mahawu	Tomohon	3	Mechanical (2H)	No
Sangir	(119) Awu	Bawendego	7	Mechanical (2H)	No
Makian	(127) Makian	Ngofakiaha	3.5	Electromagnetic (H)	No

* Temporary observation. The numbers of the volcanoes in this table are referred to those used in Fig.1 & Table 1.

Fig.1 Distribution of the Active Volcanoes of Indonesia including Solfatara Fields.
(After the Geological Survey of Indonesia)

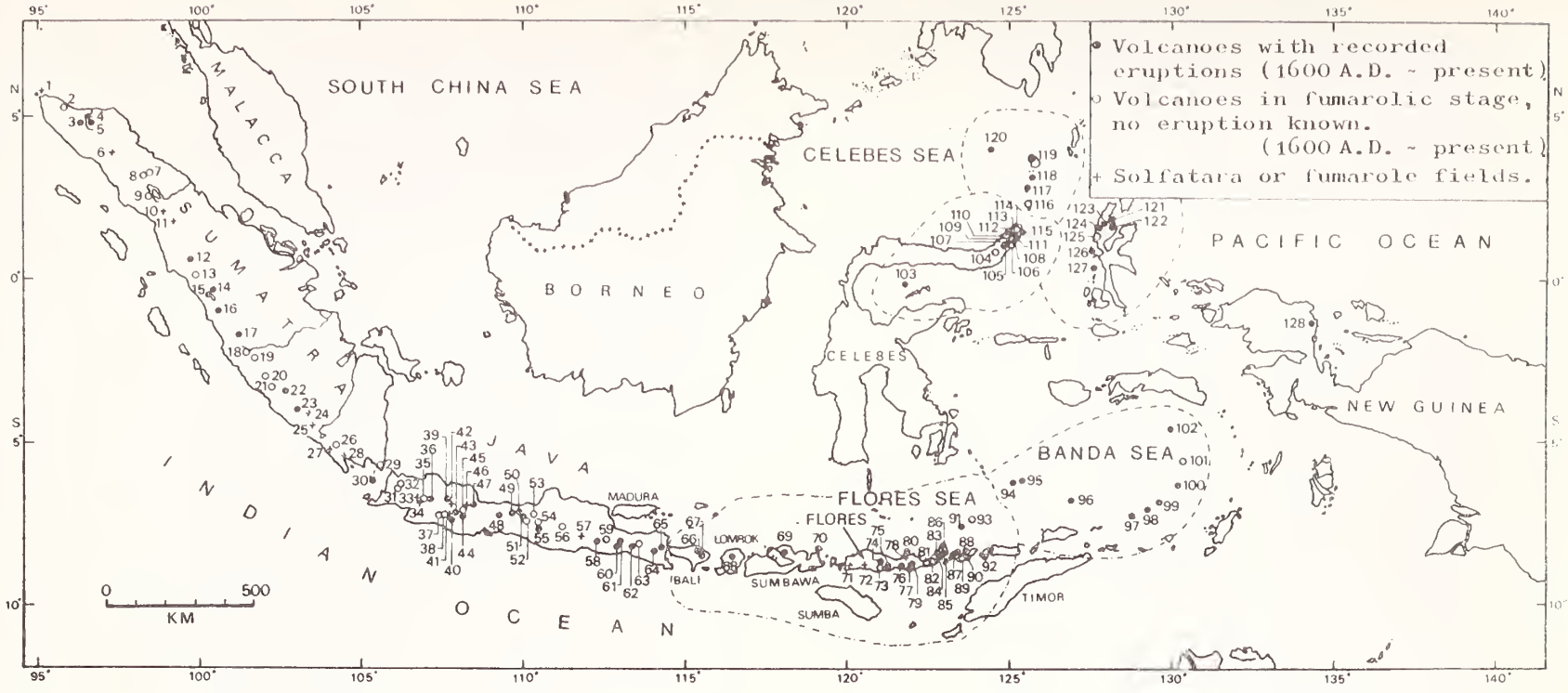

(cf) The numbers of the volcanoes in the map are referred to those used in Table 1.

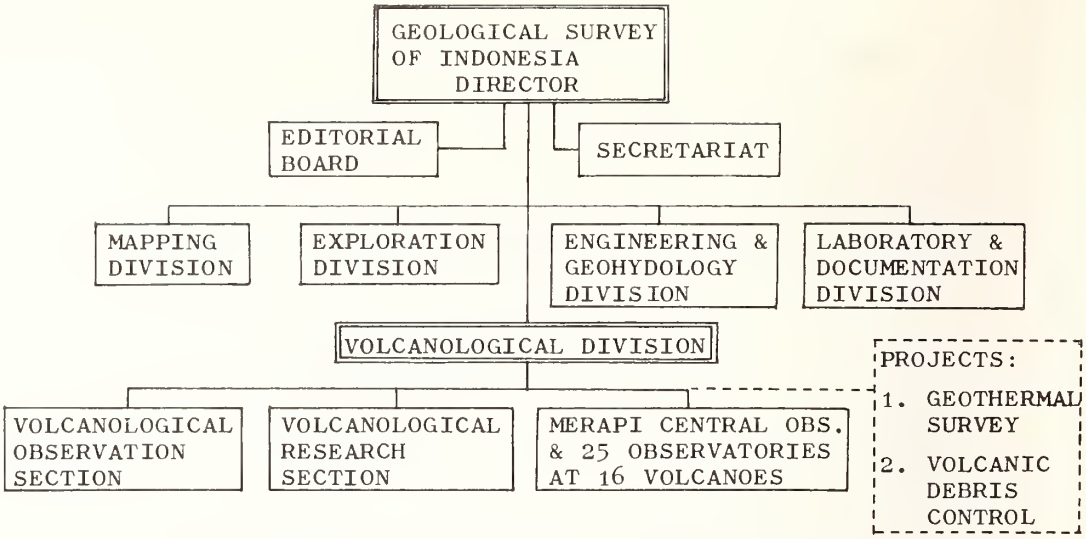

Fig.2 ORGANIZATION CHART OF THE GEOLOGICAL SURVEY OF INDONESIA WITH SPECIAL REFERENCE TO THE VOLCANOLOGICAL DIVISION.

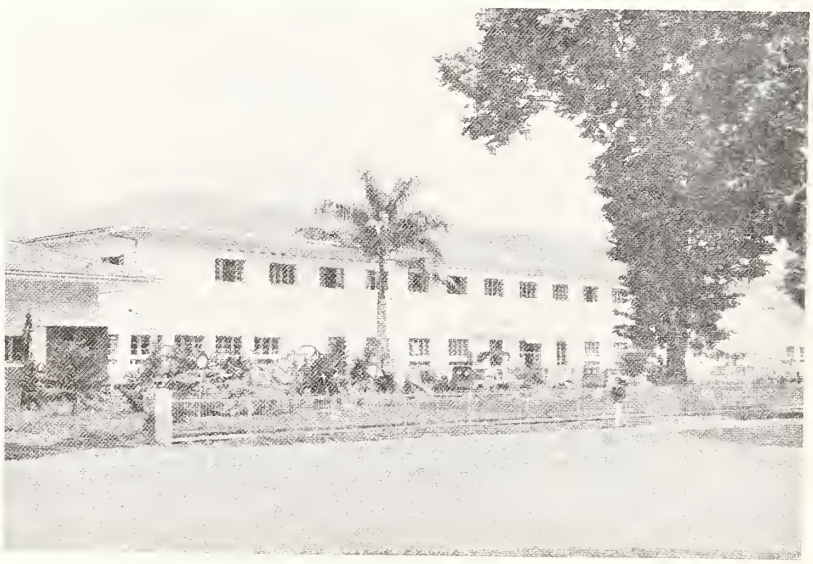

Fig.3 Geological Survey of Indonesia at Bandung.

Fig.4. Members of the Volcanological Observation Section, Volcanological Division, Geological Survey of Indonesia. The left end: Mr. D. Hadikusumo, Head of the Division. The center in the front row: A. SUWA, Chief of the Preliminary Survey Mission, Author of this Report.

Fig.5. Badak Dam, about 10 Km SW of the summit crater-lake of Volcano Merapi. This dam was constructed in 1969 in order to divert mud-flow along the Badak river for the purpose of protecting Blitar City, about 23 Km SW of the summit crater-lake, from the future mud-flows.

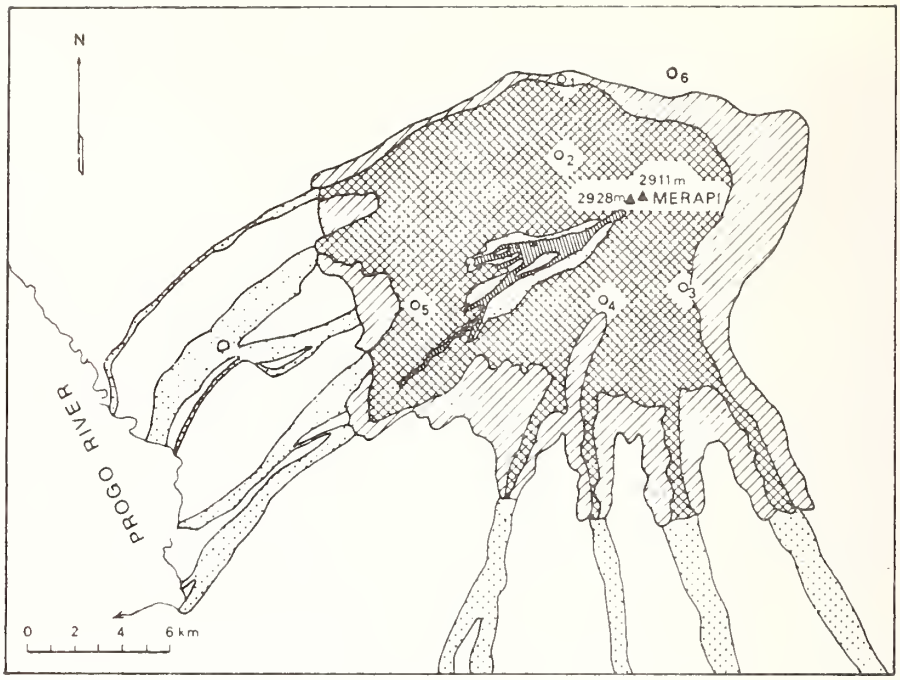

Fig. 6 - a

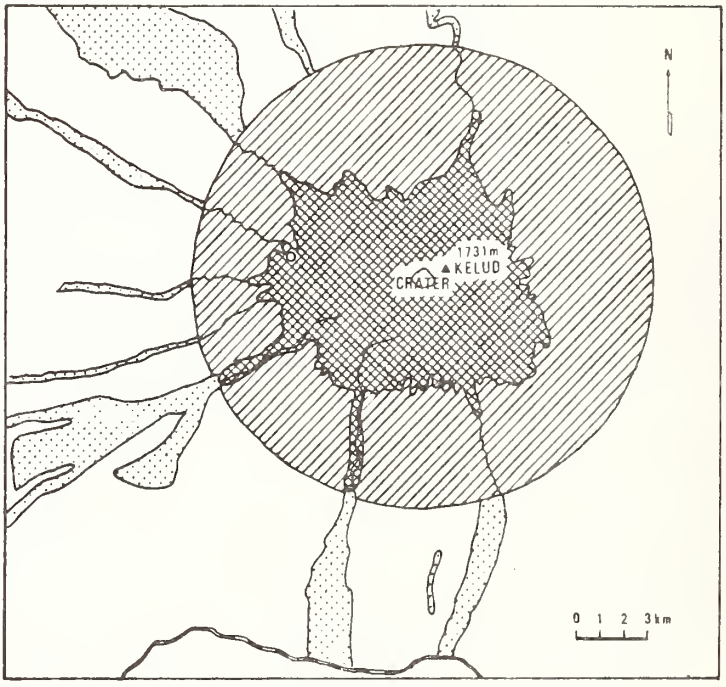

Fig. 6 - b

Fig.6 Maps showing 3 kinds of dangerous zones at representative active volcanoes in Indonesia. The original maps were made by the Geological Survey of Indonesia, but they are reduced & simplified here.

a Volcano Merapi, b. Volcano Kelud
c Volcano Semeru, d. Volcano Agung

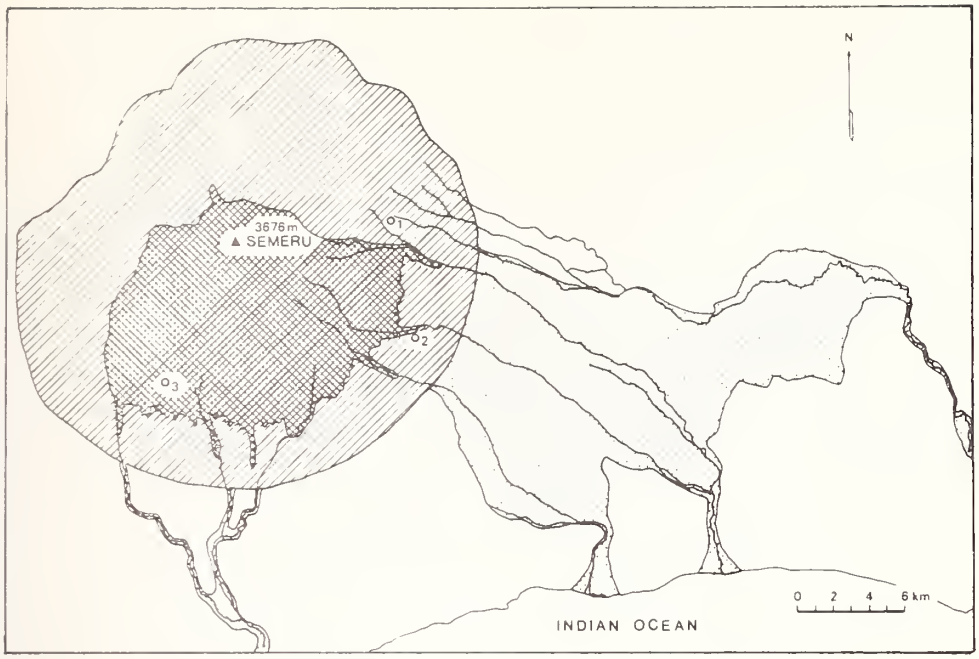
N
3676m
▲ SEMERU
O1
O2
O3
0 2 4 6km
INDIAN OCEAN

Fig. 6 - c

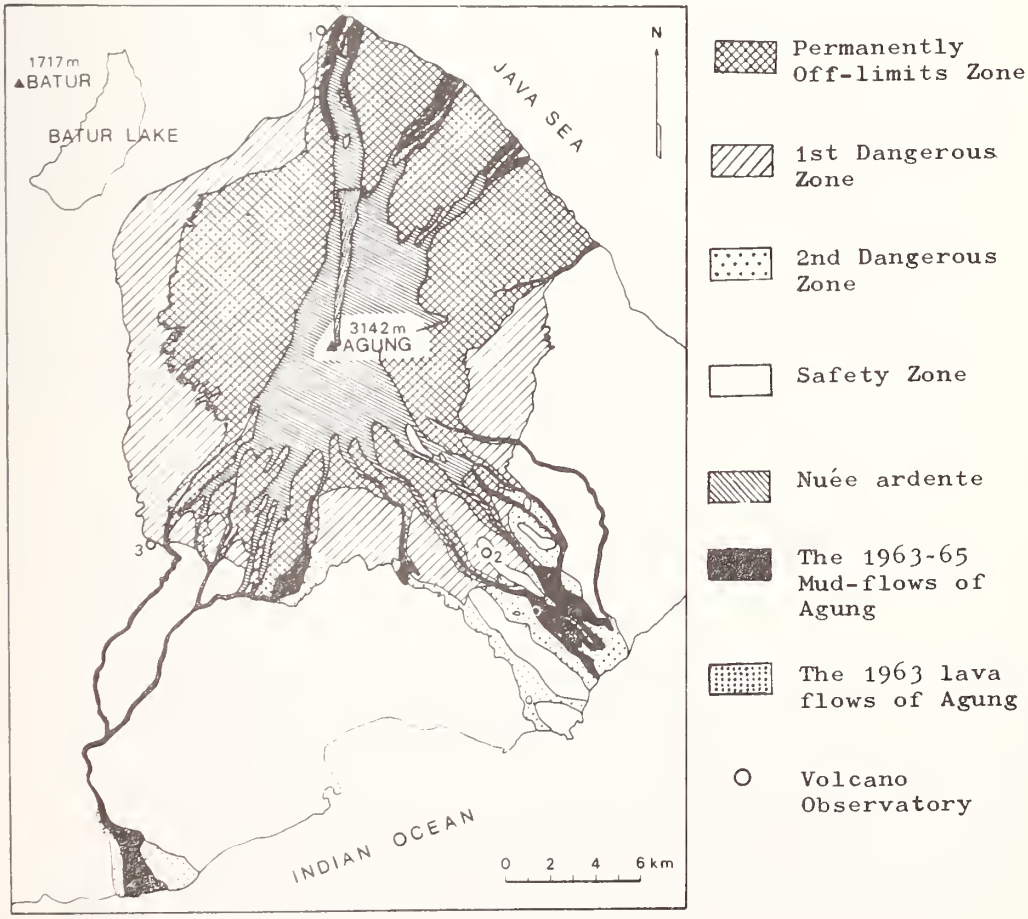
1717m
▲BATUR
BATUR LAKE
JAVA SEA
N
1
3142m
▲AGUNG
3
O2
INDIAN OCEAN
0 2 4 6km
Permanently Off-limits Zone
1st Dangerous Zone
2nd Dangerous Zone
Safety Zone
Nuée ardente
The 1963-65 Mud-flows of Agung
The 1963 lava flows of Agung
Volcano Observatory

Fig. 6 - d

USE OF STABILIZED ADOBE BLOCK AND CANE IN CONSTRUCTION OF LOW-COST HOUSING IN PERU

by

S. G. Fattal

Structures Section
Center for Building Technology, IAT
National Bureau of Standards
Washington, D.C. 20234

A description of the use of adobe block and cane for construction of low-cost housing in seismic areas of Peru is described.

Key Words: Adobe; cane; earthquake; housing; Peru; technical aid.

INTRODUCTION

The May 1970 Peruvian earthquake affected an area of 83,000 square kilometers (7% of Peru's land area) and an estimated population of 1,700,000 (13% of the country's total population). Casualty estimates were 50,000 persons killed and 100,000 persons injured, and loss of material resources was over $500 million. Traditionally, adobe has been, and continues to be, widely used in Peru for housing and other construction. Since a significant number of the structures in the area affected by the earthquake were built of adobe, most of them were destroyed or severely damaged.

In recognition of the need to provide adequate protection against natural disasters, a cooperative program was initiated between financial and technical institutions of Peru and the United States. The primary objective was to develop better quality shelters for low-income occupancy through the use of improved seismic design procedures and construction materials indigenous to Peru. The participants in the cooperative program were:

1) The United States Agency for International Development Mission in Lima, Peru (AID),

2) The Ministry of Housing and the Housing Bank of Peru (MOH,HBP),

3) National University of Engineering in Lima, Peru (NUE),

4) National Bureau of Standards, Washington, D.C. (NBS) and,

5) The International Institute of Housing Construction, California State University, Fresno, California (IIHT).

The program was financially supported by AID and the Peruvian institutions and was implemented in two stages. Stage One consisted of research and testing activities for the development of adequate soil stabilization methods, and establishment of acceptable structural standards for improved seismic-resistant construction. Stage Two consisted of designing and constructing two pilot housing projects, using the improved adobe materials and techniques developed in Stage One, in two selected communities which were affected by the May 1970 Peruvian earthquake.

The two pilot housing projects (one in the coastal town of Nepena, the other in the town of Huaraz located in the highlands) included on-site production of oil-stablized adobe block and the construction of prototype housing units. A major emphasis was placed on training the community in self-help construction methods.

EXPERIMENTAL PROGRAM

All program-related testing was conducted by NUE staff using locally available construction materials and testing specifications prepared by NBS, with IIHT supplying technical documentation, instructional material, and supervisory assistance for the preparation of oil-stablized adobe block masonry.

The experimental work consisted of testing small specimens of masonry in axial compression, diagonal compression, and flexure. Two types of cane (Carrizo and Cana Brava), which were tested in tension, were split longitudinally and used as reinforcement in the stablized block specimens. Load-deformation measurements were obtained by means of dial gages attached to the specimens. The program also included full-scale racking tests on five large-scale walls, direct shear tests on small prisms, pullout tests on cane embedded in cylindrical blocks and miscellaneous other exploratory tests. The NUE tests results were utilized to evaluate strength and stiffness properties for use in the design of the prototype housing units. A summary of conclusions follows:

1) The stablized block specimens developed an average compressive strength of 13 kg/cm^2, an average shear strength at zero axial load, of 1 to 2 kg/cm^2, depending on the type of mortar used, and an initial modulus of elasticity

in compression of 2000 kg/cm^2 which is about 150 times the compressive strength. The tensile strength of unreinforced block was insignificant. These results indicate that oil stablization of adobe block does not appreciably increase or decrease its strength properties. With these low values, it was concluded that adobe construction should be limited to single-story units.

(2) Block stablization with rapid-curing road oil (RC-250) produced superior qualities with regard to waterproofing, abrasion resistance, durability and thermal insulation. The proportion of stabilizer was between one and two percent depending on the quality of soil used.

(3) The two types of cane tested in direct tension developed a tensile capacity of 1000 to 1400 kg/cm^2 and a constant modulus of elasticity of about 200 x 10^3 kg/cm^2 throughout the entire loading range. This was about 150 times its strength and 100 times the initial modulus of elasticity of the block specimens. Tests also indicated that it is difficult or impossible for cane to develop this high tensile capacity in bond with adobe mortar although a significant improvement in bond was effected by using split cane in the pullout tests. Partial loss of bond and local cracking of mortar which was frequently observed was attributed to the expansion of cane by moisture absorption from the surrounding mortar. Stabilization of cane by coating it with a layer of asphalt solution eliminated mortar cracking but it also tended to reduce its bond strength. The effectiveness of split cane as a reinforcing material in stablized wall construction is predicated on its adequate protection against prolonged exposure to adverse environmental conditions such as moisture or insect infestation, and its ability to retain initial bond characteristics.

Research and testing covered many other aspects of housing construction, including foundations, roofing systems, floor surfaces, paints, and other finishes. For example, the newly-developed stablized soil was tested for use as a roofing cover combined with cane, to provide an economic, light, durable, and easily reparable roof cover, offering a high degree of thermal insulation; tiles made with stablized soil, colored or plain, offer an effective and economic solution for floor surfacing; use of stablized soil with gravel in foundations provides adequate protection against exposure to adverse environmental conditions.

DESIGN AND CONSTRUCTION OF PROTOTYPE HOUSING UNITS

The prototype houses were designed and detailed in accordance with well-documented principles of improved seismic construction practice and on the basis of the experimental knowledge acquired in the first stage of the program.

The basic constituents used in the construction of these housing units were stablized soil, stablized block, soil-cement-asphalt mortar, cane (split or whole), and wood. A typical unit consists of a four-room single-story box type structure (fig. 1), with load-bearing walls and partitions of cane-reinforced stablized block masonry construction, and a one-way wood joist roofing system covered with a mat of closely spaced whole cane, laid across the joists, and topped with a 2- to 3-cm layer of stablized soil mixture (fig. 2). Corrugated asbestos cement roof cover is used as a substitute material for cane in regions where cane is scarce. A pair of cross-braces are fastened to the roof joists to help distribute lateral seismic forces through diaphragm action. The floor area is approximately 65 m^2. To help partial deferment of initial costs, a two-room unit of 32 m^2 floor area may be built initially and expanded to full-size at a later date.

The fabrication and curing procedures for the stablized block were in accordance with recommendations developed and documented by IIHT for this program. The blocks were produced by pouring stablized soil into modular wooden forms on flat ground. The forms were then removed and the units were sun-dried for a period of thirty days. Circular cores in the units permitted construction of a single-wythe wall in running bond with the holes aligned to accommodate vertical split-cane reinforcement in both faces and at equal intervals (fig. 3

The size of the block, which was made 38 cm square and 9 cm thick, was governed by the compressive strength requirements of a one-story high wall.

The mortar in wall construction was one of three types used in the tests: M-1, M-2, and M-3. The proportioning of all mortar constituents were made by weight. M-1 mortar consists of soil mixed with two percent Rapid Curing Road Oil, RC-250, and is identified by the symbol S-2. M-2 mortar consists of one part of Portland Cement, ten parts of soil, and one percent RC-250, and is identified by the symbol 1:10-1. M-3 mortar consists of one part cement, six parts soil, four parts sand, and one percent RC-250 and is identified by the symbol 1:(6, 4)-1.

The cane used was one of two types: Carrizo had a hollow core and a hard shell; Cana Brava had a solid fibrous core. Both canes were typically 2 to 3 cm in diameter and 3 mm in shell thickness. They were split longitudinally and were used to reinforce the walls both horizontally and vertically, and to provide connection between the various elements of the system (fig. 3).

The shape of the housing units, the arrangement of walls, partitions, and openings conformed as much as possible to a balanced layout configuration in order to optimize the uniformity of seismic stress distribution (fig. 1). A rectangular plan, with as close a doubly-symmetric configuration as possible, was adopted. Symmetric enclosures of horizontally curved walls used singley or in combination with flat walls were also investigated.

Interior partitions were designed as structural loadbearing walls. This practice helped decrease the roof weight by reducing its span length, and increased the total lateral shear resistance of the system.

The size and spacing of openings were governed by requirements of minimum width of piers flanking adjacent openings or an opening and end of wall, maximum permissible length of lintels spanning across the top of opening, and uniformity of overall layout (fig. 1).

Footings were made continuous under the walls and vertical dowel reinforcement was provided to develop partial continuity with the walls (fig. 4). These dowels were lapped with vertical wall reinforcement for a minimum length of 50 cm. The foundation was cast using specified proportions of cement, stablized soil, gravel, and rock. The width of footing was set at 1.5 times the wall thickness. An 80 cm depth was used, with 20 cm projecting above the ground level.

To the extent that was practical, the sizes of door and window openings were kept to a minimum and provisions were made to equalize the spaces between openings or an opening and the vertical end of wall. Nevertheless, because critical stress conditions under later loads could develop around these openings, it was important to use special reinforcement detailing provisions in these regions. Specially cored half and whole block units were used at both vertical edges of the openings to accommodate vertical cane reinforcement at those locations. The cane was carried through the openings of a ladder-type double joisted lintel and this space was filled with stablized soil mixture. Horizontal cane reinforcement was also provided in the bed joint directly below the sill and carried through beyond the openings on both sides.

Consideration was given to critical stress conditions that could develop at vertical wall-to-wall joints, especially near their top junction where tensile cracking usually begins, and then propagates downward. Special detailing provisions were made to obtain continuity between abutting walls. Such junctions were marked by projections beyond exterior wall surfaces (fig. 3). This was done primarily for two reasons: (a) to give sufficient anchorage length to horizontal cane reinforcement by extending it beyond the common joint area, and (b) to provide for future wall extension. Half block units in alternate courses may be pried loose and removed to permit running bond construction of the wall extension (fig. 3).

The most important seismic consideration in roof design was to provide sufficient in-plane stiffness so that it can adequately transmit lateral forces to the appropriate shear walls through diaphragm action. The roofing scheme (fig. 2) used for the prototype housing units consisted of equally spaced wood joists of rectangular cross-section spanning in one

direction, overlain crosswise with a closely spaced mat of cane mechanically attached to the joists below, and topped with a 2 to 3 cm stablized soil mixture. Diaphragm rigidity was provided by wood cross-braces spanning in the two diagonal directions and were mechanically fastened to the wood joists at all intersecting points. Joists were also provided along the top of the walls. These joists, which formed an integral part of the roof assembly, were to be attached to the walls by mechanical fasteners in order to adequately transfer the horizontal forces to the appropriate shear walls. In addition, all other intersecting wood elements were attached to each other at their functions by using mechanical fasteners (thin nails for attachment of cane mat to joists below were used to minimize the chance of longitudinal splitting of cane). All roof segments, such as the two segments of the doubly-pitched roof, were attached to one another so that the entire roof of the house would act as an integral unit.

CONCLUSIONS

Among the more important features of the model housing units are their improved capacity relative to the traditional adobe house to withstand the action of earthquake forces, and the reduction of cost obtained relative to the cost of conventional construction. This economic breakthrough was achieved by the use of inexpensive construction materials readily available in Peru (soil, cane, lumber, oil derivative), and by the adoption of self-help construction techniques to which the new system is particularly suitable. For instance, the cost of building materials required for the construction of a basic housing unit of 325 sq ft of covered area was the local currency equivalent of 350 dollars, which is about one-third as much as the construction cost of conventional building materials.

Thus far, the results of this experiment have been encouraging and have received official Peruvian recognition. The Peruvian Housing Ministry is presently planning to start a larger housing project in Nepena comprising approximately fifty units. In addition, new building sites for similar projects elsewhere in Peru are presently being selected. The Peruvian Building Code is currently being amended to include new standards and specifications for adobe construction. This will permit insurance companies to place insurance upon improved adobe structures and consequently enable the Peruvian Savings and Loan industry to make mortgage loans to finance such construction.

DIMENSIONAL REQUIREMENTS FOR PROTOTYPE HOUSE

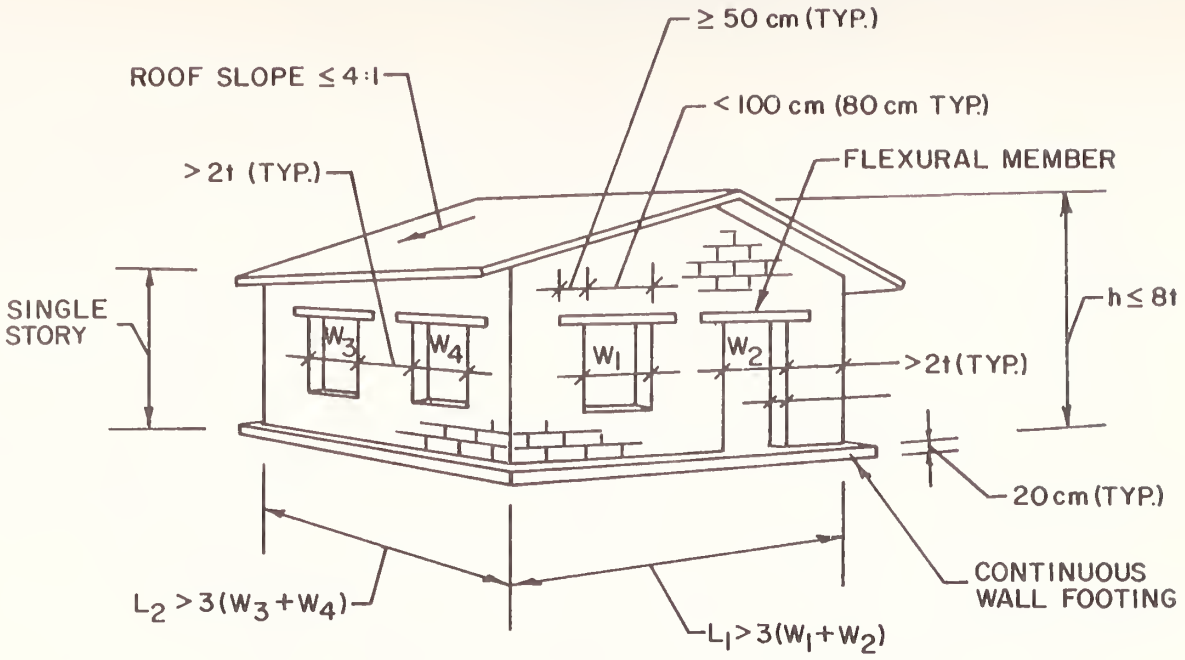

FIGURE 1

ROOFING SCHEME

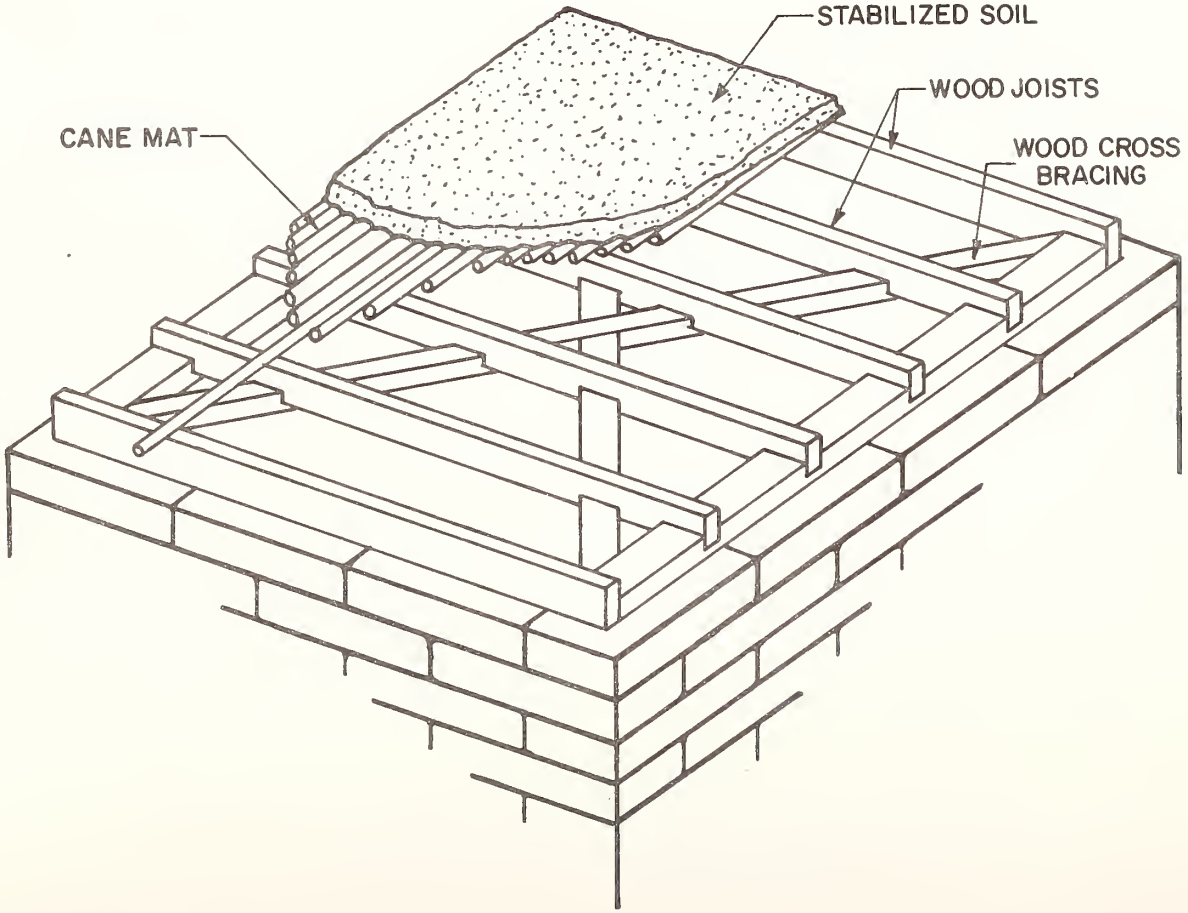

FIGURE 2

WALL-TO-WALL CONNECTION DETAIL

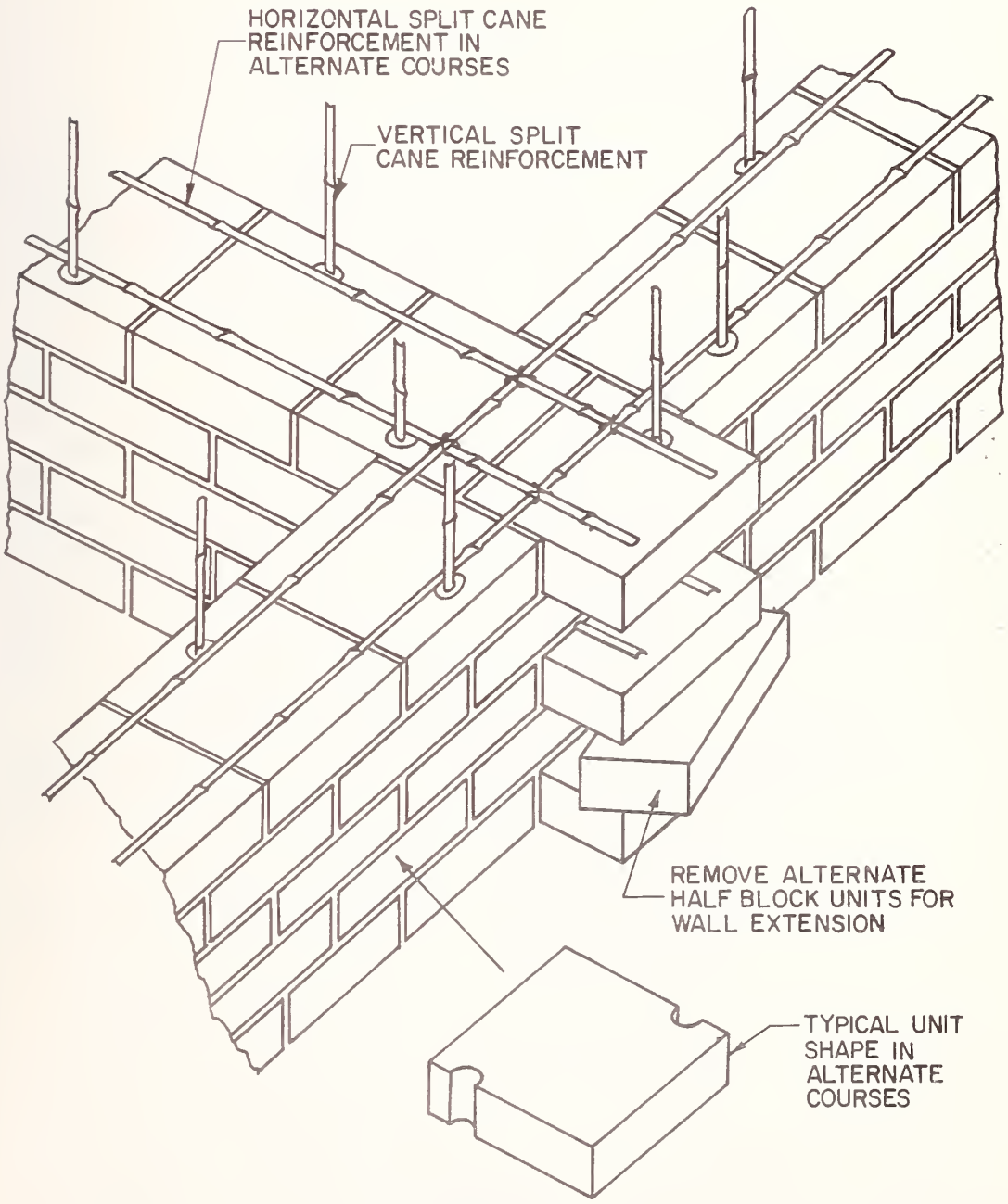

FIGURE 3

REQUIREMENT FOR WALL FOOTINGS

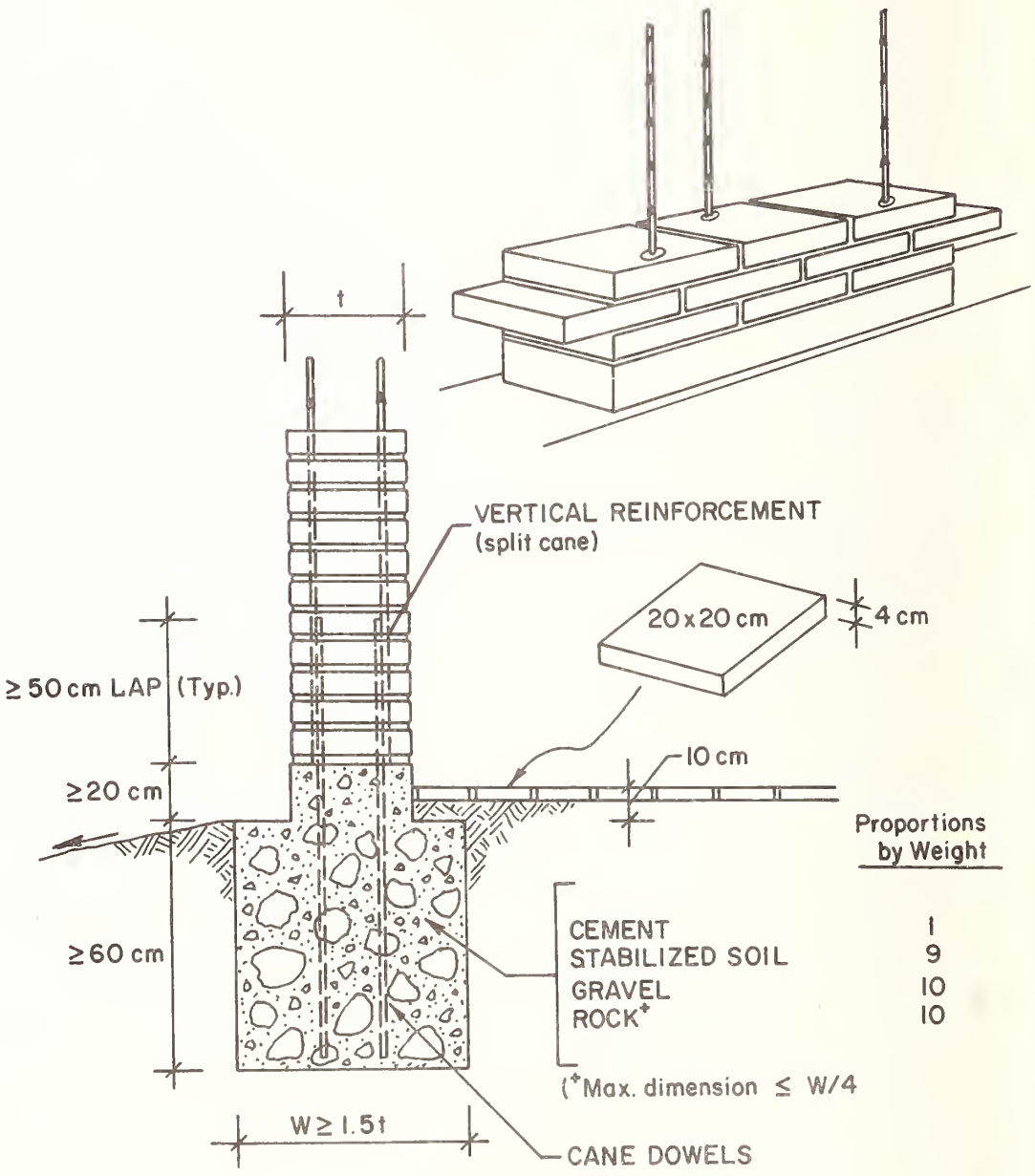

FIGURE 4

A COMMENT ON THE TECHNOLOGICAL AID TO DEVELOPING COUNTRIES

by

M. Nagao
and
Tadayoshi Okubo

Structure and Bridge Division
Public Works Research Institute

This paper describes the technological aid required in developing countries, after a natural disaster, as observed by the writer during surveys of storm and earthquake disasters in these developing countries.

The writer classifies the aid required after a natural disaster into three categories, that is, emergency aid, technological aid, and economic aid. The problems related to the scientific and technological areas in the developing countries after a natural disaster are discussed.

The technological aid is classified into short and long term aid.

Finally, the problems related to the required technological aid are discussed and then the necessary Governmental policy which has been prepared for implementation of a low-cost and disaster resistant housing system is described.

Key Words: Earthquake; Japan; natural disaster; storm; structural engineering; technological aid.

INTRODUCTION

According to the recently developed hypothesis of plate tectonics, every foci of major earthquakes are concentrated in the peripheral zone of the plate and distributed on belts along the peripheries. Most of the countries located near the seismic belts with the exception of Japan, United States, New Zealand, South-European countries, and the U.S.S.R., are developing countries.

Also, damage caused by the world's strongest winds, such as typhoons, cyclones, and hurricanes, occur in the developing countries.

In the past, the writer has gone abroad five times to survey damages caused by natural disasters; in particular, a damage survey of Typhoon "Yoling" in the Philippines in 1970 as a member of UNESCO Survey Mission, the damage survey of the San Fernando Earthquake in the United States, and Bingol Earthquake in Turkey in 1971 as a member of the Japanese Governmental Survey Mission, and the damage survey of the Chili Earthquake in Iran and Managua Earthquake in Nicaragua in 1973. With the exception of the San Fernando Earthquake in the United States, all of the natural disasters mentioned above have taken place in the developing countries. In this paper, the writer will discuss the required technological aid to the developing countries in relation to the natural disasters.

In general, rehabilitation projects performed in the developing countries are apt to take a long time when these countries suffer damages. This is because of the lack of high technological expertese, lack of repair and rehabilitation materials, especially fundamental materials such as steel and cement, and lack of funds and capital necessary to implement the rehabilitation work. Therefore, these countries have requested aid from foreign countries, especially after the disaster.

This kind of aid consists of emergency aid, technological aid, and economic aid.

The emergency aid that has been requested immediately after a natural disaster consists of donations of relief materials such as medicine, clothes, and food. Emergency reconstruction materials, temporary houses, and water filtration apparatus are also requested.

The technological aid consists of dispatching of scientists and engineers to supplement the present technological level of the disaster countries, the offering of instruments for scientific and technological observation and research work, training and education of people in the disaster countries, offering of restoration materials and the recommendations and cooperation on restoration planning. In addition to the above, supplies for the construction industries and life-line systems are included in the technological aid.

The economic aid consists of offering and loan of restoration funds and aid for rehabilitating economic and social damages caused by the disaster.

This paper will deal primarily with the technological aid as supplied to the various countries.

GENERAL SITUATION OF DEVELOPING COUNTRIES

The technological level in developing countries is insufficient and of low caliber. Among the countries the writer visited, there were countries where educational lectures on earthquake engineering and structural dynamics at universities were inadequate. Also, lectures on wind engineering were non-existent. Similar research work in these fields of engineering and design code and standards of wind and earthquake resistant structures together with standards of testing and materials are usually poorly established in the developing countries.

In the developing countries, students who intend to take advanced courses are generally educated in other (developed) countries. However, domestic construction materials,

such as steel and concrete, are meager and most of the materials are imported from the developed countries. Therefore, engineers, who are educated in a developed country where natural disasters such as heavy storms and earthquakes take place, design structures which are based on the wind and earthquake resistant design codes and standards and materials and testing standards of that country and, therefore, prefer to use materials which are imported. Engineers, who are educated in a developed country where natural disasters scarcely occur, design structures based on the design code and standards in the country without considering the effects of natural disasters and prefer to use materials imported from the country where they were educated.

Therefore, in developing countries it is very difficult to establish their own materials and design standards, and together with the economic scale, the existing design system is kept.

When an earthquake disaster takes place in one of these countries, the following difficulties occur:

(1) Because seismic observation stations are not existant or sparcely located, the location of epicenter, focal depth, and magnitude of earthquake cannot be estimated.

(2) Because there is almost no observation and research on the tectonic movement, the cause and mechnism of the earthquake cannot be determined.

(3) There are few skilled engineers who can judge seismic intensities and estimate isoseismals. Especially in the case of shallow earthquakes directly under a populated city, distribution of isoseismals is complicated and difficult to estimate.

(4) In most cases, there are no strong motion accelerograms and the characteristics of ground acceleration and time duration are not clarified.

(5) Data on ground conditions is scarce and the estimations of the amplification of the seismic motion of the ground condition, the relationship between damage, and the ground condition is difficult.

(6) Because there are no standards for materials and construction methods and because laborers are not skilled, the quality of the structures is not uniform and the estimation of structural resistivity is difficult.

(7) The cause of structural damages is not accurately analyzed.

(8) The estimation of the bearing capacity, safety of damaged structures, and the selection of the restoring method are difficult.

(9) Lack of risk analysis of earthquake causes trouble in the establishment of restoration planning and of earthquake resistant design standards.

(10) Materials for emergency temporary structures and resoration are difficult to obtain, therefore, the reconstruction work is difficult to initiate.

However, storms are frequently accompanied by torrential rains, therefore, the following difficulties take place:

(1) The meterorological observatories are sparcely distributed, therefore, the path of the tropical cyclone, maximum wind velocity, and regional distribution of wind velocity are not known.

(2) There are few engineers skilled in the analysis of storm damage of structures, therefore, the estimation of the actual wind loads based on the mode of damage is difficult to determine.

(3) Anemometers are not installed, therefore, the vertical profile and time variation of the wind speed is not known.

(4) Because many of the rivers become wild, the damages to structures are due to both storms and floods.

(5) There is a lack of estimation on the return of strong winds, thus causing troubles on the establishment of the restoration planning of wind resistant design standards.

In addition to the above, difficulties similar to Items (6), (7), (8), and (10), relative to earthquake hazards, also take place.

TECHNOLOGICAL AID

The technological aid that is carried out for supplementing the difficulties mentioned in the previous section and is required for saving life and property of people in the developing country will now be described.

The technological aid is classified into a short-term aid, which is carried out immediately after the disaster, and a long-term aid, which is carried out during a restoration period and consists of supplying specialists and materials.

The first of the short-term technological aids is the dispatch of specialists consisting of;

A. Seimologist, geologists, geophysicists, soil and foundation engineers, structural engineers (building, bridge, dam), and members of a fire brigade in case of earthquake damage;

B. Meteorologist, climatologist, structural engineers (building, bridge) and power transmission system, soil and foundation engineers, and river engineers in case of wind and flood damage.

These specialists are supposed to carry out the following tasks in cooperation with their counterparts in the developing country.

1. In the field of earthquake hazards,

   Observation and measurement of crustal alteration and ground rupture caused by the earthquake.

   Analysis of the mechanism of earthquakes and dynamic characteristics of ground layers by observing aftershocks.

   Estimation of the location, magnitude, and geotectonical cause of the main shock and the estimation of the seismicity of the area in the future.

   Observation of the ground accelerations of strong aftershocks by strong motion accelerographs.

   Survey of the soil conditions in the damaged area by collecting soil data, sampling and testing of the soil at the sites by simplified sampler, and measuring save velocities.

   Survey of the distribution of seismic intensities in the damaged area.

   Evaluating the local characteristics of structural building types and materials and determining the cause of the structural damage.

   Observation of the dynamic characteristics of the damaged and undamaged structures and ground.

Evaluation of the seismic risk in the area.

2. In the field of storm and flood hazards,

Estimation of the path, maximum wind velocity, traveling velocity of the tropicl cyclone, and the vertical profile of the wind velocity.

Evaluating the local characteristics of the structural building types and materials and determining the actual wind loads and cause of damage.

Estimation of the distribution of rainfall, maximum flood discharge, and other hydrological data.

Proposes a plan for river improvement and flood control.

3. In the field common to earthquake and storm hazards,

Draft a code, standards, and system for insuring structural safety against natural disasters.

Draft guidelines on estimation of the safety of damaged structures, methods of repair, and reconstruction work, and a principle for restoring the damaged cities.

Establishment of future technolgoical aids necessary for the disaster country.

In order to implement these surveys and works, it is necessary to send specialists with the necessary instruments after the disaster; also to offer some of the instruments which can be left to continue effective observations and measurements.

The long-term technological aid consists of (1) recommendation and cooperation in the area of restoration planning, re-education of the engineers in the developing country and guidance on the establishment of standards and systems for securing structural safety against natural disasters by sending specialists for a long period, (2) acceptance and education of trainees from the disaster country, (3) offering of contruction materials necessary for restoration, and (4) technological cooperation on the industrial facilities of fundamental construction materials.

PROBLEMS OF TECHNOLGOICAL AID

The technological aid from Japan to the developing countries is made possible by Governmental grants. The problems involved in implementing such grants are as follows.

Problems in the Process of Determining Technologic Aid

(1) Generally social disorder and confusion take place in the damaged area of the developing countries, thus sending foreign teams to survey the damage may be rejected. Thus, before sending a survey mission, an outline of the technological aid other than the damage survey should be determined so as to permit a broader activity of mission, as outlined.

(2) The effects of the recommendations of the emergency survey mission are increased when the dispatch of the mission is immediate and the amount of the aid is large. It is, therefore, desirable to dispatch the mission as soon as possible.

In the 1972 Managua Earthquake, survey teams from the United States and Mexico visited the city within three days after the earthquake and started the survey work. In the case of our country, it takes at least five days for the clearance of passport and visa, which may result in delaying the start of the survey work.

(3) When the dispatch of the survey mission is accompanied by other technological aid, the mission is welcomed by the disaster country. Because of the confusion in the disaster country, immediate communication will be difficult, but acceptance of the mission will commence.

After the earthquake, Managua was declared an open city, and as a result, immigration clearance was omitted. There was a complaint as to why Japan hadn't sent emergency relief teams, including medical teams, immediately after the earthquake. Also, when our mission visited General A. Somoza, President of the National Emergency Committee, he showed his deep interest in aid from Japan.

(4) Instruments and materials necessary for the survey work should be previously prepared and carried by the survey mission.

After the Managua Earthquake, survey teams from the U.S. and Maxico carried their instruments to the site and carried out their observations and testing. These instruments should be supplied by the organizations to which the specialists belong and should be carried by them to the disaster area. It is also desirable to send emergency relief materials, such as medicine, medical instruments, clothes, food, and emergency temporary houses required by the victims. These emergency relief materials should also be reserved in case of domestic disasters.

(5) The survey mission should be furnished with sufficient funds to pay for necessary expenses to conduct the survey, such as purchasing data, hiring cabs, and interpreters, etc.

Problems on the Damage Survey

(1) Even in case of domestic disasters, survey teams must bear some inconveniences such as lack of food, potable water, and hotels in the devastated area. In the case of natural disasters in the developing countries, these inconveniences will be doubled due to differences in living habits. The writer has had experience in lodging in a tent and a room of an office building in the course of conducting a damage survey in developing countries. In the damaged area, the survey team must bear the living conditions the residents bear.

(2) The experts should understand at least one foreign language common in the damaged area. In the developing country to find people who can understand a foreign language, especially in the area apart from the center of administration and culture, is difficult. Without understanding the foreign language, no communication can be carried out between the people of the victim country and the technological aid. Because the objective of each expert differs in carrying out the survey work, understanding of a foreign language by each expert is indispensable.

(3) Experts must be patient if necessary materials cannot be obtained. In the developing country under military administration, it happens that even a map cannot be obtained, much less drawings of damaged structures. In such a case, the ability to communicate with the people of the victim country will cause a difference in the results of the survey and the effectiveness of aid.

Problems of Long-Term Dispatch of Experts

A system of long-term dispatch of experts should be arranged. Usually, a long-term dispatch of experts is requested from developing countries at the occasion of the emergency survey. However, in our country, quite a few experts want to stay longer in a foreign country. On the other hand, there is no sabbatical leave system at the universities. Therefore, the technological aid is sometimes interrupted, although the long-term dispatch of experts is eagerly requested by the developing countries. Reconsideration by both governmental organization and experts is requested.

CONCLUDING REMARKS

Most of the technological aid to the developing countries is carried out as part of a Governmental policy in Japan. However, natural disasters take place without warning; therefore, a system of technological aid on natural disasters in the developing countries must be prepared and established previously by the Government.

According to the writer's experience, damages in the developing countries are characterized by the following.

Damage of buildings, especially residential houses, is dominate; damage of public works is not as severe.

Collapse of residential houses causes a great loss of life.

Most buildings are built of local materials and by local methods of construction, and therefore, lack the resistivity against disasters and are apt to collapse.

Residential house construction is hard to change because of ample labor power and retention of their traditions. These houses are constructed of materials easy to obtain, are easily built and have good insulation capacity, but possess low resistivity against natural disasters. Therefore, in these countries, the development of low-cost houses of ample resistivity and heat insulation capacity is needed. A study and development of such a low-cost house is also necessary in Japan.

*U.S. GOVERNMENT PRINTING OFFICE: 1976 210-801/200 1-3

NBS-114A (REV. 7-73)

U.S. DEPT. OF COMM. BIBLIOGRAPHIC DATA SHEET	1. PUBLICATION OR REPORT NO. NBS SP-444	2. Gov't Accession No.	3. Recipient's Accession No.

4. TITLE AND SUBTITLE

The Proceedings of the Sixth Joint Meeting of the U.S. - Japan Panel on Wind and Seismic Effects

5. Publication Date: April 1976

6. Performing Organization Code

7. AUTHOR(S)
H. S. Lew, Editor

8. Performing Organ. Report No.

9. PERFORMING ORGANIZATION NAME AND ADDRESS

NATIONAL BUREAU OF STANDARDS
DEPARTMENT OF COMMERCE
WASHINGTON, D.C. 20234

10. Project/Task/Work Unit No.

11. Contract/Grant No.

12. Sponsoring Organization Name and Complete Address *(Street, City, State, ZIP)*

National Bureau of Standards
Department of Commerce
Washington, D.C. 20234

13. Type of Report & Period Covered: Final

14. Sponsoring Agency Code

15. SUPPLEMENTARY NOTES

Library of Congress Catalog Card Number: 76-608055

16. ABSTRACT *(A 200-word or less factual summary of most significant information. If document includes a significant bibliography or literature survey, mention it here.)*

The Sixth Joint Meeting of the U.S. - Japan Panel on Wind and Seismic Effects was held in Washington, D.C., on May 15-17, 1974. The proceedings of the Joint Meeting include the opening remarks, the program, the formal resolutions, and the technical papers. The subject matter covered in the papers includes extreme winds in structural design; assessment and experimental techniques for measuring wind loads; dynamics of soil structures and ground response in earthquakes; structural response to wind and earthquakes and design criteria; disaster mitigation against natural hazards; and technological assistance to developing countries.

17. KEY WORDS *(six to twelve entries; alphabetical order; capitalize only the first letter of the first key word unless a proper name; separated by semicolons)*

Bridges; buildings; codes; disaster; dynamic analysis; earthquakes; modeling; soils; structural response; volcanoes; and wind.

18. AVAILABILITY

[XX] Unlimited

[ ] For Official Distribution. Do Not Release to NTIS

[X] Order From Sup. of Doc., U.S. Government Printing Office Washington, D.C. 20402, SD Cat. No. C13.10:444

[ ] Order From National Technical Information Service (NTIS) Springfield, Virginia 22151

19. SECURITY CLASS (THIS REPORT): UNCLASSIFIED

21. NO. OF PAGES: 462

20. SECURITY CLASS (THIS PAGE): UNCLASSIFIED

22. Price: $5.80

NBS TECHNICAL PUBLICATIONS

PERIODICALS

JOURNAL OF RESEARCH reports National Bureau of Standards research and development in physics, mathematics, and chemistry. It is published in two sections, available separately:

• Physics and Chemistry (Section A)

Papers of interest primarily to scientists working in these fields. This section covers a broad range of physical and chemical research, with major emphasis on standards of physical measurement, fundamental constants, and properties of matter. Issued six times a year. Annual subscription: Domestic, $17.00; Foreign, $21.25.

• Mathematical Sciences (Section B)

Studies and compilations designed mainly for the mathematician and theoretical physicist. Topics in mathematical statistics, theory of experiment design, numerical analysis, theoretical physics and chemistry, logical design and programming of computers and computer systems. Short numerical tables. Issued quarterly. Annual subscription: Domestic, $9.00; Foreign, $11.25.

DIMENSIONS/NBS (formerly Technical News Bulletin)—This monthly magazine is published to inform scientists, engineers, businessmen, industry, teachers, students, and consumers of the latest advances in science and technology, with primary emphasis on the work at NBS. The magazine highlights and reviews such issues as energy research, fire protection, building technology, metric conversion, pollution abatement, health and safety, and consumer product performance. In addition, it reports the results of Bureau programs in measurement standards and techniques, properties of matter and materials, engineering standards and services, instrumentation, and automatic data processing.

Annual subscription: Domestic, $9.45; Foreign, $11.85.

NONPERIODICALS

Monographs—Major contributions to the technical literature on various subjects related to the Bureau's scientific and technical activities.

Handbooks—Recommended codes of engineering and industrial practice (including safety codes) developed in cooperation with interested industries, professional organizations, and regulatory bodies.

Special Publications—Include proceedings of conferences sponsored by NBS, NBS annual reports, and other special publications appropriate to this grouping such as wall charts, pocket cards, and bibliographies.

Applied Mathematics Series—Mathematical tables, manuals, and studies of special interest to physicists, engineers, chemists, biologists, mathematicians, computer programmers, and others engaged in scientific and technical work.

National Standard Reference Data Series—Provides quantitative data on the physical and chemical properties of materials, compiled from the world's literature and critically evaluated. Developed under a world-wide program coordinated by NBS. Program under authority of National Standard Data Act (Public Law 90-396).

NOTE: At present the principal publication outlet for these data is the Journal of Physical and Chemical Reference Data (JPCRD) published quarterly for NBS by the American Chemical Society (ACS) and the American Institute of Physics (AIP). Subscriptions, reprints, and supplements available from ACS, 1155 Sixteenth St. N. W., Wash. D. C. 20056.

Building Science Series—Disseminates technical information developed at the Bureau on building materials, components, systems, and whole structures. The series presents research results, test methods, and performance criteria related to the structural and environmental functions and the durability and safety characteristics of building elements and systems.

Technical Notes—Studies or reports which are complete in themselves but restrictive in their treatment of a subject. Analogous to monographs but not so comprehensive in scope or definitive in treatment of the subject area. Often serve as a vehicle for final reports of work performed at NBS under the sponsorship of other government agencies.

Voluntary Product Standards—Developed under procedures published by the Department of Commerce in Part 10, Title 15, of the Code of Federal Regulations. The purpose of the standards is to establish nationally recognized requirements for products, and to provide all concerned interests with a basis for common understanding of the characteristics of the products. NBS administers this program as a supplement to the activities of the private sector standardizing organizations.

Federal Information Processing Standards Publications (FIPS PUBS)—Publications in this series collectively constitute the Federal Information Processing Standards Register. Register serves as the official source of information in the Federal Government regarding standards issued by NBS pursuant to the Federal Property and Administrative Services Act of 1949 as amended, Public Law 89-306 (79 Stat. 1127), and as implemented by Executive Order 11717 (38 FR 12315, dated May 11, 1973) and Part 6 of Title 15 CFR (Code of Federal Regulations).

Consumer Information Series—Practical information, based on NBS research and experience, covering areas of interest to the consumer. Easily understandable language and illustrations provide useful background knowledge for shopping in today's technological marketplace.

NBS Interagency Reports (NBSIR)—A special series of interim or final reports on work performed by NBS for outside sponsors (both government and non-government). In general, initial distribution is handled by the sponsor; public distribution is by the National Technical Information Service (Springfield, Va. 22161) in paper copy or microfiche form.

Order NBS publications (except NBSIR's and Bibliographic Subscription Services) from: Superintendent of Documents, Government Printing Office, Washington, D.C. 20402.

BIBLIOGRAPHIC SUBSCRIPTION SERVICES

The following current-awareness and literature-survey bibliographies are issued periodically by the Bureau:

Cryogenic Data Center Current Awareness Service

A literature survey issued biweekly. Annual subscription: Domestic, $20.00; foreign, $25.00.

Liquefied Natural Gas. A literature survey issued quarterly. Annual subscription: $20.00.

Superconducting Devices and Materials. A literature survey issued quarterly. Annual subscription: $20.00. Send subscription orders and remittances for the preceding bibliographic services to National Bureau of Standards, Cryogenic Data Center (275.02) Boulder, Colorado 80302.

Electromagnetic Metrology Current Awareness Service Issued monthly. Annual subscription: $24.00. Send subscription order and remittance to Electromagnetics Division, National Bureau of Standards, Boulder, Colo. 80302.

U.S. DEPARTMENT OF COMMERCE
National Bureau of Standards
Washington, D.C. 20234

OFFICIAL BUSINESS

Penalty for Private Use, $300

POSTAGE AND FEES PAID
U.S. DEPARTMENT OF COMMERCE
COM-215

U.S.MAIL

SPECIAL FOURTH-CLASS RATE
BOOK

AMERICAN REVOLUTION BICENTENNIAL 1776-1976

75 YEARS NBS 1901-1976

1298